

**CONTROLLING FACTORS OF TWO MIDDLE TRIASSIC
CARBONATE PLATFORMS:
LATEMAR AND ROSENGARTEN
(DOLOMITES, NORTHERN ITALY)**

INAUGURAL — DISSERTATION

zur
Erlangung der Doktorwürde
der
Naturwissenschaftlich-Mathematischen Gesamtfakultät
der
Ruprecht – Karls – Universität
Heidelberg

vorgelegt von

Diplom-Geologe Axel Emmerich
aus Heidelberg, Baden-Württemberg

Tag der mündlichen Prüfung: 09.07.2004

Erklärung

- Hiermit erkläre ich, Axel Emmerich (geb. 26.07.1973 in Heidelberg, Baden-Württemberg), an Eides statt, dass ich die vorgelegte Dissertation selbst verfasst und mich dabei keiner anderen als der von mir ausdrücklich bezeichneten Quellen und Hilfen bedient habe.

- Ich, Axel Emmerich (geb. 26.07.1973 in Heidelberg, Baden-Württemberg), erkläre zudem an Eides statt, dass ich an keiner anderen Stelle ein Prüfungsverfahren beantragt habe, dass ich die Dissertation nicht in dieser oder anderer Form bereits anderweitig als Prüfungsarbeit verwendet habe und dass ich sie an keiner anderen Fakultät als Dissertation vorgelegt habe.

Heidelberg, den 27.05.2004

Gutachter: Prof. Dr. Thilo Bechstäd
Geologisch-Paläontologisches Institut
Ruprecht-Karls-Universität Heidelberg
Im Neuenheimer Feld 234
D-69120 Heidelberg
Deutschland

Prof. Peter A. Kukla, Ph.D.
Geologisches Institut der RWTH Aachen
Wüllnerstr. 2
D-52056 Aachen
Deutschland

Für meinen Großvater

Der große Berg ist ein Gebäude ohne
Treppen, ohne Stockwerke, ohne Türen. Das
Wohnzimmer ist der blaue Himmel. In dem
Haus wohnt niemand, alles ist kalt und leer.
Der Besitzer ist taub und stumm wie Steine.
Das Geheul des Windes sind seine einzigen
Worte.

Wenn du nach oben steigen willst, wird das
Haus zum Gefängnis, die unsichtbaren
Gitterstäbe heißen Ehrgeiz.
Erst nach dem Gipfel bist du wieder frei.

Reinhard Karl, 1946-1982

TABLE OF CONTENTS

Zusammenfassung	1	2.4 Sedimentology of the slope- and reef-facies at Latemar	32
Summary	1	2.4.1 Cima Feudo	34
Part 1:		2.4.1.1 Architecture and sedimentology of the slope	34
General introduction	3	2.4.1.2 Sedimentology and general palaeontology of the reef	34
1.1 Introduction	4	2.4.2 Kirchtagweide	35
1.2 Geological setting	6	2.4.2.1 Architecture and sedimentology of the slope	35
1.2.1 Basin fill and geodynamics	6	2.4.2.2 Sedimentology and general palaeontology of the reef	35
1.2.2 Carbonate platform evolution and palaeo biology	8	2.4.3 Erzlahn	36
1.3 Objectives	9	2.4.3.1 Architecture and sedimentology of the slope	36
1.3.1 Facies analysis	9	2.4.3.2 Sedimentology and general palaeontology of the reef	38
1.3.2 Subsidence/numerical basin modelling	11	2.4.4 Schenon	40
1.4 Methods	11	2.4.4.1 Architecture and sedimentology of the slope	40
1.4.1 Palaeontology, sedimentology and stratigraphy	11	2.4.4.2 General palaeontology of the reef	40
1.4.2 Cathodoluminescence	11	2.4.5 Cresta De Do Peniola	40
1.4.3 Stable isotopes	11	2.4.5.1 Architecture and sedimentology of the slope	44
1.4.4 Thermal maturity	11	2.4.5.2 General palaeontology of the slope and reef	46
1.4.5 Fission tracks	12	2.5 Lithofacies and palaeontology	49
1.4.6 Thermal modelling	12	2.5.1 Lithofacies types	49
1.4.7 Numerical basin reverse modelling	15	2.5.2 General content of the reef-facies	49
1.4.8 Sequence stratigraphic forward modelling	18	2.5.3 Biocoenoses of primary reef-builders	49
1.5 Previous research	18	2.5.3.1 B1 – Solenoporacean bafflestones	49
1.5.1 Latemar	18	2.5.3.2 B2 – “Sphinctozoan”-”Tubiphytes”-bind/bafflestones	49
1.5.1.1 Lagoon-facies	18	2.5.3.3 B3 – “Sphinctozoan”-coral-bryozoan-bafflestones	53
1.5.1.2 Slope-facies	18	2.5.3.4 B4 – Scleractinian-framestones	53
1.5.1.3 Reef-facies	19	2.5.3.5 B5 – Microbialites/microbialitic bindstones	53
1.5.2 Rosengarten	19	2.5.3.6 B6 – “Tubiphytes” multisiphonatus-framestones	53
1.5.3 Concarena	20	2.5.4 Biocoenoses of secondary reef-builders	56
1.5.4 Thermal history	20	2.5.4.1 B7 – <i>Olangoelia</i> -bindstones	56
1.6 Discussion and conclusions	20	2.5.4.2 B8 –” <i>Tubiphytes</i> ”-microproblematica-bindstones	58
1.6.1 Facies, palaeontology, platform architecture and diagenesis	20	2.5.4.3 B9 – <i>Bacinella</i> -bindstones	58
1.6.2 Basin evolution and platform evolution	23	2.5.5 Associations of the lagoon	58
1.6.3 Integration of results	25	2.5.5.1 B10 – Lagoonal pack-/grainstones	58
1.7 Outlook	25		
Part 2:			
The reefal margin and slope of a Middle Triassic carbonate platform: the Latemar (Dolomites, Italy)			
Abstract	27		
2.1 Introduction	27		
2.2 Geological setting	28		
2.3 Previous research at Latemar	30		
2.3.1 Lagoon-facies	30		
2.3.2 Slope-facies	31		
2.3.3 Reef-facies	32		

TABLE OF CONTENTS

2.5.6 Palaeo ecology of the reef-facies at Latemar	60	4.3.3 Measurement of vitrinite reflectance (VR _v)	93
2.5.7 Biostratigraphical position of the reef	62	4.3.4 Apatite fission track analysis	94
2.6 Conclusions	64	4.3.5 Workflow of the integrated modelling approach	96
2.6.1 Correlation with other Late Anisian/Early Ladinian reefs of the western Tethys	64	4.3.6 Thermal modelling	96
2.6.2 Controls on slope evolution at Latemar	67	4.3.7 Reverse basin and sequence stratigraphic forward modelling	98
Acknowledgements	68	4.4 Results	101
Part 3:		4.4.1 Thermal modelling	101
Latemar vs. Concarena (Southern Alps): main characteristics of two Triassic carbonate platform margins		4.4.2 Basin reverse modelling	103
Abstract	69	4.4.3 Stratigraphic forward modelling	103
3.1 Introduction	69	4.5 Discussion	105
3.2 Geological setting	70	4.5.1 Controls on platform evolution at Rosengarten	105
3.3 Platform architecture	71	4.5.2 Carbonate production rates	106
3.3.1 Previous research	71	4.5.3 Porosity evolution	107
3.3.2 Latemar	74	4.5.4 Burial/thermal history	107
3.3.3 Concarena	76	4.6 Conclusions	107
3.3.3.1 Bio- and sequence-stratigraphic correlation of the platform	76	Acknowledgements	108
3.3.3.2 Slope architecture	76	Part 5:	
3.4 Margin configuration	78	Basin and carbonate platform development in the SW-Dolomites: Rosengarten and Latemar (Meso-/Cenozoic, Northern Italy)	
3.4.1 Previous research	78	Abstract	109
3.4.2 Latemar	78	5.1 Introduction	109
3.4.3 Concarena	78	5.2 Geological setting	109
3.5 Cementation	80	5.3 Methods	112
3.5.1 Latemar	80	5.3.1 Numerical reverse basin modelling	112
3.5.2 Concarena	82	5.3.2 Apatite fission track analysis	114
3.5.2.1 Lagoon	82	5.4 Platform architecture	114
3.5.2.2 Reef	84	5.4.1 Rosengarten	114
3.5.2.3 Slope	84	5.4.2 Latemar	116
3.5.2.4 Cathodoluminescence	84	5.5 Timescale of platform evolution	119
3.5.2.5 Stable isotopes	85	5.6 Integrated subsidence histories	120
3.6 Conclusions	86	5.6.1 Rosengarten	121
Acknowledgements	87	5.6.1.1 Subsidence history	121
Part 4:		5.6.1.2 t-T history	121
Quantified Carbonate Platform Development: The Rosengarten/Catinaccio transect (Middle Triassic, Dolomites, Italy)		5.6.2 Latemar	124
Abstract	89	5.6.2.1 Subsidence history	124
4.1 Introduction	89	5.6.2.2 t-T history	124
4.2 Geological setting	90	5.7 Discussion	126
4.3 Methods and database	91	5.7.1 Anisian basin development	126
4.3.1 Sedimentological analyses	91	5.7.2 Syn-Schlern (1) basin development	126
4.3.2 Stratigraphy	93	5.7.3 Post-Schlern (1) basin development	127
		5.8 Conclusions	127
		Acknowledgements	128

TABLE OF CONTENTS

References 129
Acknowledgements 141
Appendix

Zusammenfassung

Die Kombination aus Fazies- und Subsidenzanalyse ermöglicht es, die bei der Entwicklung von Karbonatplattformen maßgeblichen Steuerungsfaktoren zuerst zu identifizieren und dann zu quantifizieren. Intrinsische Faktoren wie paläobiologische Evolution sowie extrinsische Faktoren wie Subsidenz- und/oder Akkommodationsänderungen kontrollieren das Wachstum in einem plattform- und beckenweiten Rahmen. Andere beeinflussende Faktoren wie autozyklische Prozesse, Luv-Lee-Effekte, unterschiedliche Nährstoffversorgung, Wellenexposition und Gezeitenströmungen können hierbei ebenfalls von beträchtlicher Bedeutung sein, spielen aber eher eine untergeordnete, lokale Rolle. Subsidenz- und Akkommodationsänderungen sind leicht vom Sedimentarchiv abzuleiten und können auch einigermaßen verlässlich quantifiziert werden. Die restlichen Faktoren sind jedoch ungleich schwieriger zu identifizieren und daher vor allem schlecht quantifizierbar. Dies ist hauptsächlich auf die Überprägung durch Subsidenz- und/oder Akkommodationsänderungen und autozyklische Prozesse sowie die schlechte Überlieferung von Luv-Lee-Effekten, Einflüssen unterschiedlicher Nährstoffversorgung, Wellenexposition oder Gezeitenströmungen zurückzuführen.

Eine vergleichende Faziesanalyse der Plattformabhäng- und Riff-Karbonate des Latemar (oberstes Anis/unterstes Ladin, Dolomiten) und der Concarena (Oberes Ladin/Unteres Karn, Lombardische Alpen) betont den Zusammenhang zwischen Subsidenz, Sedimentation, Faziesassoziationen und Zementation beziehungsweise deren gemeinsame Wichtigkeit für die Entwicklung triassischer Karbonatplattformen. Hohe Karbonatakkumulationsraten beziehungsweise starker Akkommodationszuwachs verhindern in Verbindung mit einem flachen Relief des Riffandes massive frühe Zementation wie das Beispiel des Latemar belegt. Geringe Raten beziehungsweise geringer Akkommodationszuwachs in Verbindung mit einem "walled reef" fördern hingegen massive frühe Zementation wie die letzten Stadien der Concarena Plattform anzeigen.

Eine Kombination aus thermischer Modellierung mit numerischer Rückwärts- und sequenzstratigraphischer Vorwärtssimulation präzisiert mögliche Plattform- und Versenkungs-/ Subsidenzgeschichten des Latemar und Rosengarten. Das heutige Erosionsniveau war mit einer Gesteinssäule von maximal 1100m Mächtigkeit überlagert. Es gibt keinerlei Anzeichen für ein neogenes

Flysch- oder Molasse-ähnliches Stadium in der Beckenentwicklung der SW Dolomiten, wie es zum Beispiel in anderen alpidischen Becken vorhanden ist. Der Subsidenzspurs gegen Ende des Anis respektive der *Reitzi*-Biozone wird am Latemar und Rosengarten mit ähnlichen Subsidenzraten von 800-850m/Ma (Bubnoff) aufgezeichnet. Beide Plattformen konnten mit diesem raschen Akkommodationsanstieg Schritt halten. Sequenzstratigraphische Vorwärtssimulation der Rosengarten Plattform zeigt, dass minimale vertikale Karbonatakkumulationsraten von bis zu 1000m/Ma notwendig sind, um die heute beobachteten Plattform-Beckenübergänge zu erzeugen. Darüber hinaus wird deutlich, dass die Karbonatproduktion von Latemar und Rosengarten Werte (sub)recenter Karbonatplattformen erreicht. Obwohl das Riff des Latemar noch deutliche Charakteristika frühanisischer Riffe der Dolomiten trägt (inkrustierende Mikroproblematika dominieren über Gerüstbildner) und im Vergleich zu späteren Riffen (z.B. Concarena, Ladin/Karn, Lombardische Alpen) wenig diversifiziert ist, ist dies ein weiterer Hinweis dafür, dass sich die Karbonatfabrik nach dem Perm/Trias-Faunenschnitt schon im späten Anis (untere Mitteltrias) komplett erholt haben muss.

Summary

Integrated facies and subsidence analysis enable the identification and quantification of controlling factors on carbonate platform evolution. Palaeo biologic evolution as intrinsic factors, subsidence and accommodation change as extrinsic factors are the most important controlling factors on carbonate platform growth on a platform(and basin)-wide scale. Other factors like auto-cyclic processes, windward-leeward effects, nutrient supply, wave expositions and tidal currents are also important but play a minor, localised role. Whereas subsidence and accommodation change can easily be deduced from the sedimentary record and be quantitatively assessed, the other factors are much more difficult to identify lest quantify due to overprinting and poor preservation potential.

Facies analysis and the comparison of the slope- and reef-facies from Latemar (Upper Anisian/Lower Ladinian, Dolomites) and Concarena (Upper Ladinian/Lower Carnian, Lombardic Alps) stresses the importance and links between subsidence, sedimentation, facies assemblages and cementation throughout the development of Triassic carbonate platforms. High rates of carbonate

accumulation/accommodation increase combined with low topography of the reefal margin prevent massive early cementation at Latemar; low rates during the last stages of the Concarena platform together with a walled reef promote massive early cementation.

Combined thermal, numerical basin reverse and sequence stratigraphic forward modelling constrained burial and subsidence histories of the Rosengarten and Latemar platforms. Vitrinite reflectance and apatite fission track data both argue for a shallow maximum burial. Present day topography was overlain by a maximum thickness of 1100m of overburden. There are no indications for a Neogene flysch or molasse-type setting as inferred from other Alpine basins. The subsidence pulse at the verge of the Anisian (*Reitzi*-zone) is recorded at Latemar and Rosengarten with similar total subsidence rates of 800-

850m/Ma. Both platforms successfully kept up with this rapid increase in accommodation space. Additionally, sequence stratigraphic forward modelling of the Rosengarten platform showed that minimum vertical accumulation rates of up to 1000m/Ma are necessary in order to reproduce observed present day geometries. The carbonate production rates of both platforms reached values of (sub)recent carbonate platforms. Despite the resemblance of the Latemar reef to other early Anisian reefs of the Dolomites (encrusting microproblematica dominating over framebuilding organisms) and the low diversity of faunal elements with respect to slightly younger reefs (e.g. Concarena, Ladinian/Carnian), this adds further evidence to the observation of a full recovery of the carbonate factory already at the Late Anisian (lower Middle Triassic).

PART 1 General Introduction

This project is accompanied by another Ph.D. thesis carried out on the Lombardic Alps by Michael Seeling, University of Heidelberg. Both projects are part of the superimposed goal of assessing and comparing Middle Triassic carbonate platforms in the SW Dolomites and Lombardic Alps in order to determine and to quantify controlling factors on platform growth. Since many platforms in these two areas are dolomitised, the fundamental base of this task has been the comparison and detailed facies analysis of two carbonate platforms with excellent preservation of primary lithofacies as limestone. The first step, the combined work on the Anisian/Ladinian Latemar (SW Dolomites) and the Ladinian/Carnian Concarena (Lombardic Alps) enabled the identification and comparison of controlling parameters on a quantitative base. Additionally, the difference in age of these two platforms allowed for an assessment of reefal development from Late Anisian to Early Ladinian in this part of the W Tethys. The second step has been the individual modelling of subsidence, sedimentary and burial histories of the two platforms and their immediate surroundings (SW Dolomites: Latemar & Rosengarten; Lombardic Alps: Concarena & Monte Pora). The main difference between these two areas is that both experience completely different burial histories from the

Jurassic onwards: (1) the Lombardic Alps are situated in the Lombardy basin whereas (2) the Dolomites are part of the Trento platform comprising the entire central segment of the Southern Alps. Hence, the future aim beyond these two individual projects will be bringing together the modelling results and developing a unified concept of basin evolution in this part of the Tethys. The integration will shed new light on the causes, timing and mechanisms operating on a larger scale and which are responsible for pronounced differential subsidence in this part of the Southern Alps (see Fig. 1.1).

In the course of this project the following articles have been published and form the backbone of this thesis:

PART 2:

Title: The reefal margin and slope of a Middle Triassic carbonate platform: the Latemar (Dolomites, Italy)
 Authors: Axel Emmerich, Valeria Zamparelli, Thilo Bechstädt & Rainer Zühlke
 Status: Accepted by FACIES

PART 3:

Title: Latemar vs. Concarena (Southern Alps): main characteristics of two Triassic carbonate platform margins
 Authors: Michael Seeling, Axel Emmerich, Thilo Bechstädt & Rainer Zühlke
 Status: Submitted to Sedimentary Geology

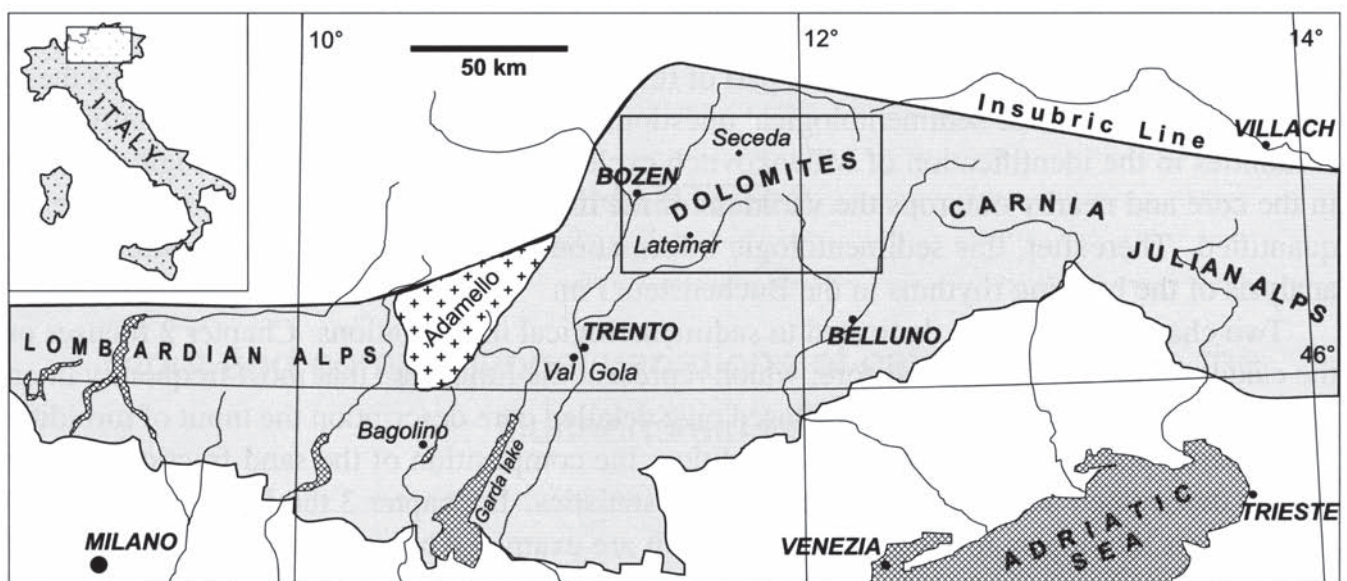


Fig. 1.1 Middle Triassic of the Southern Alps (Northern Italy; from Maurer 2003). Inset to the upper left: location of map area within Italy. Main tectonic lines are sketched. Black rectangle shows outline of palaeogeographic map pictured in Fig. 1.3.

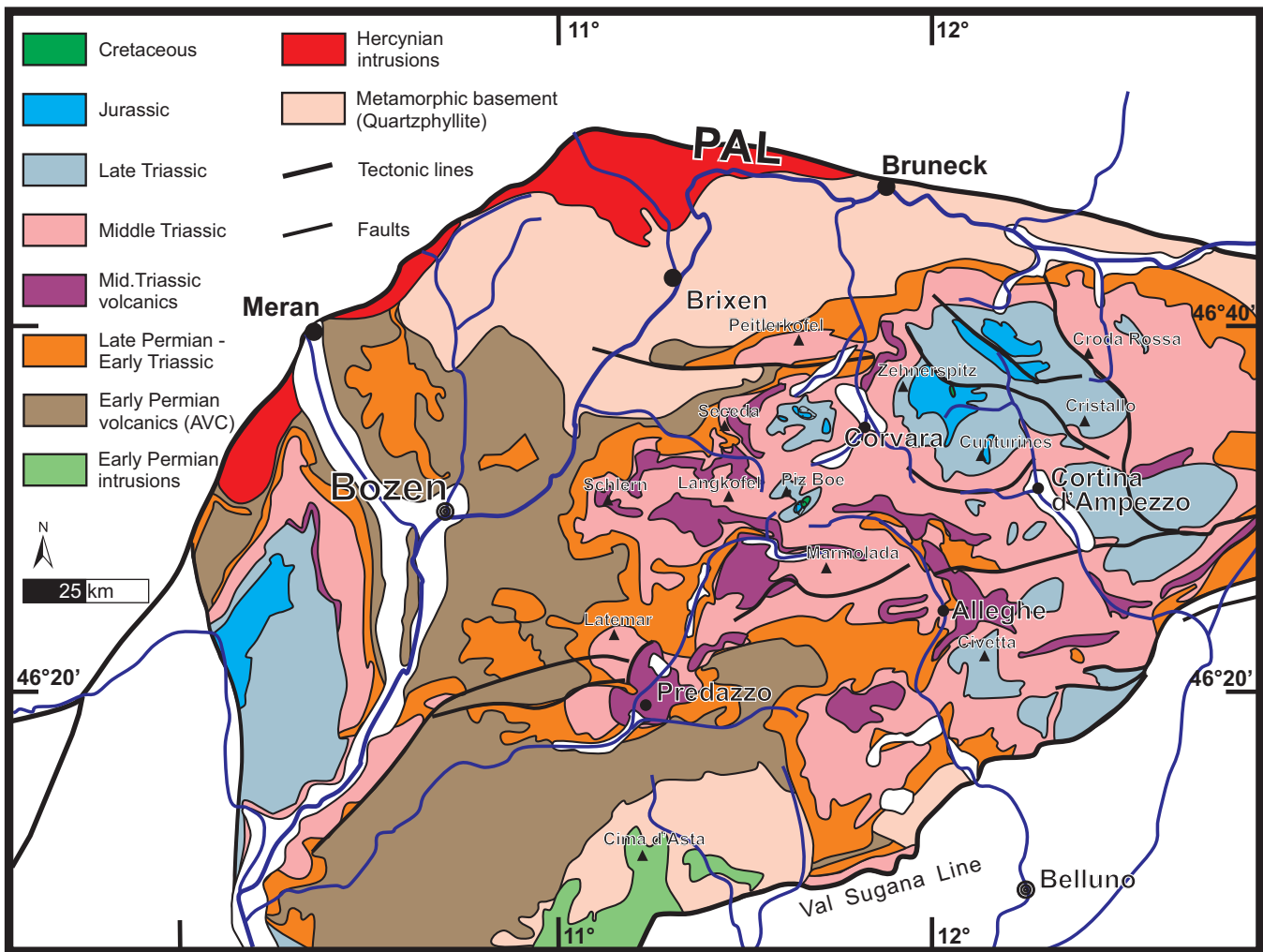


Fig. 1.2 Schematic geologic map of the Dolomites (from Tscherny 2004).

PART 4:

Title: Quantified Carbonate Platform Development: The Rosengarten/Catinaccio transect (Middle Triassic, Dolomites, Italy)

Authors: Axel Emmerich, Robert Tscherny, Thilo Bechstädt, Carsten Bükler, Ralf Littke & Rainer Zühlke
Status: Submitted to IAS Special Publication

PART 5:

Title: Basin and carbonate platform development in the SW-Dolomites: Rosengarten and Latemar (Meso-/Cenozoic, Northern Italy)

Authors: Axel Emmerich, Ulrich A. Glasmacher, Friederike Bauer, Thilo Bechstädt & Rainer Zühlke
Status: Submitted to Sedimentary Geology

1.1 Introduction

The Dolomites of Northern Italy (see. Figs. 1.1 and 1.2) have ever been a study area for carbonate platforms and their reefal communities. Owing to its excellent outcrops, largely absent dolomitisation and early Middle Triassic (Anisian) setting, the Latemar is ideally suited for the study of a reefal community and carbonate platform after the faunal crisis at the Palaeozoic/Mesozoic boundary. Despite their similar excellent preservation – e.g. laterally correlatable platform-basin transitions, seismic-scale outcrops and absent dolomitisation – the Triassic platforms of the Lombardic Alps are far less studied than the Dolomites. Some studies have documented the re-occurrence of Early Anisian reefs after the faunal crisis at the Permian/Triassic boundary (Salomon 1908; Assereto et al. 1965; Unland 1975; Epting et al. 1976; Brack 1984; Gaetani & Gorza 1989; Falletti & De

Donatis 1999). Even less studies have been carried out on the uppermost Anisian to lowermost Carnian re-establishment of rimmed carbonate platforms (Jadoul et al. 1992; Gaetani et al. 1992). The Concarena platform, most recently investigated by Rossetti (1966) and Brack (1984), is one of these uniquely preserved Ladinian/Carnian carbonate platforms. Its lateral facies zonation and occurrence of enigmatic “*Tubiphytes*” in the margin resembles the somewhat older Anisian/Ladinian Latemar platform.

Since Mojsisovics (1879) had termed the word “Über-guss-Schichtung” (i.e. clinostratification), many authors have worked on platform-to-basin transitions of carbonate build-ups in the Dolomites (e.g. Hummel 1928, 1932; Pia 1937; Leonardi 1962, 1967; Bosellini 1984, 1988). The Rosengarten has hereby always served as a refer-

ence model for progradational geometries (e.g. Bosellini and Stefani 1991; Bosellini et al. 1996). However, most approaches of assessing the evolution of carbonate platforms and their respective clinoforms have mainly been of qualitative nature. Quantitative approaches on subsidence development and carbonate production of Middle Triassic platforms in the Dolomites have so far been scarce (Schlager 1981; Doglioni and Goldhammer 1988; Schlager et al. 1991; Maurer 1999, 2000). The age of Middle Triassic platforms in the Dolomites is constrained by coeval basinal sediments (Buchenstein Fm; Brack and Rieber 1993, 1994; see Fig. 1.3). Recently, age-diagnostic air-borne tuff layers in basinal and lagoonal strata were used to synchronise bio-, cyclo- and chronostratigraphy (basinal Buchenstein Fm at Seceda/Geisler Group, W-Dolomites: Mundil et al. 1996; lagoonal Schlern Fm at

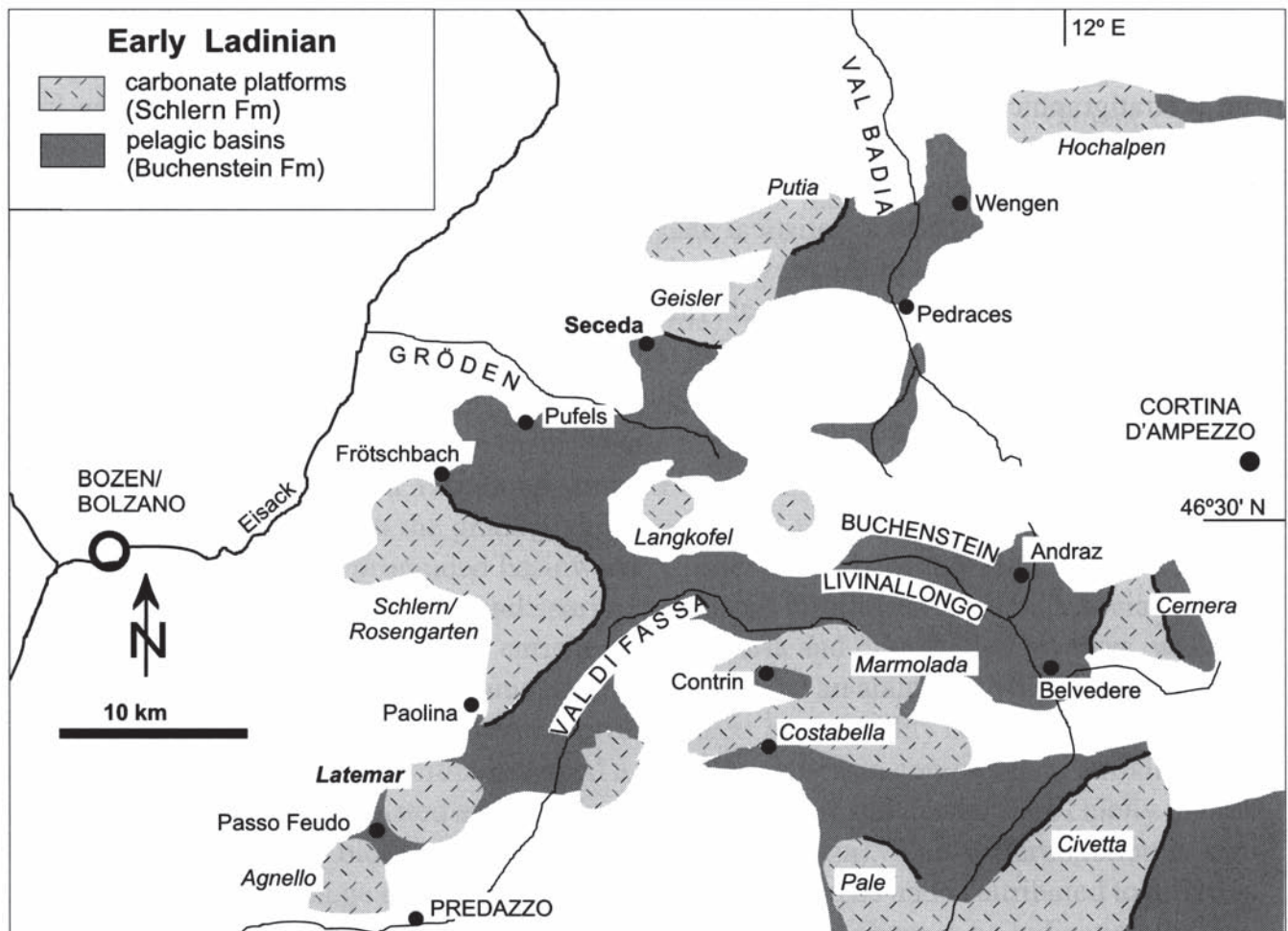
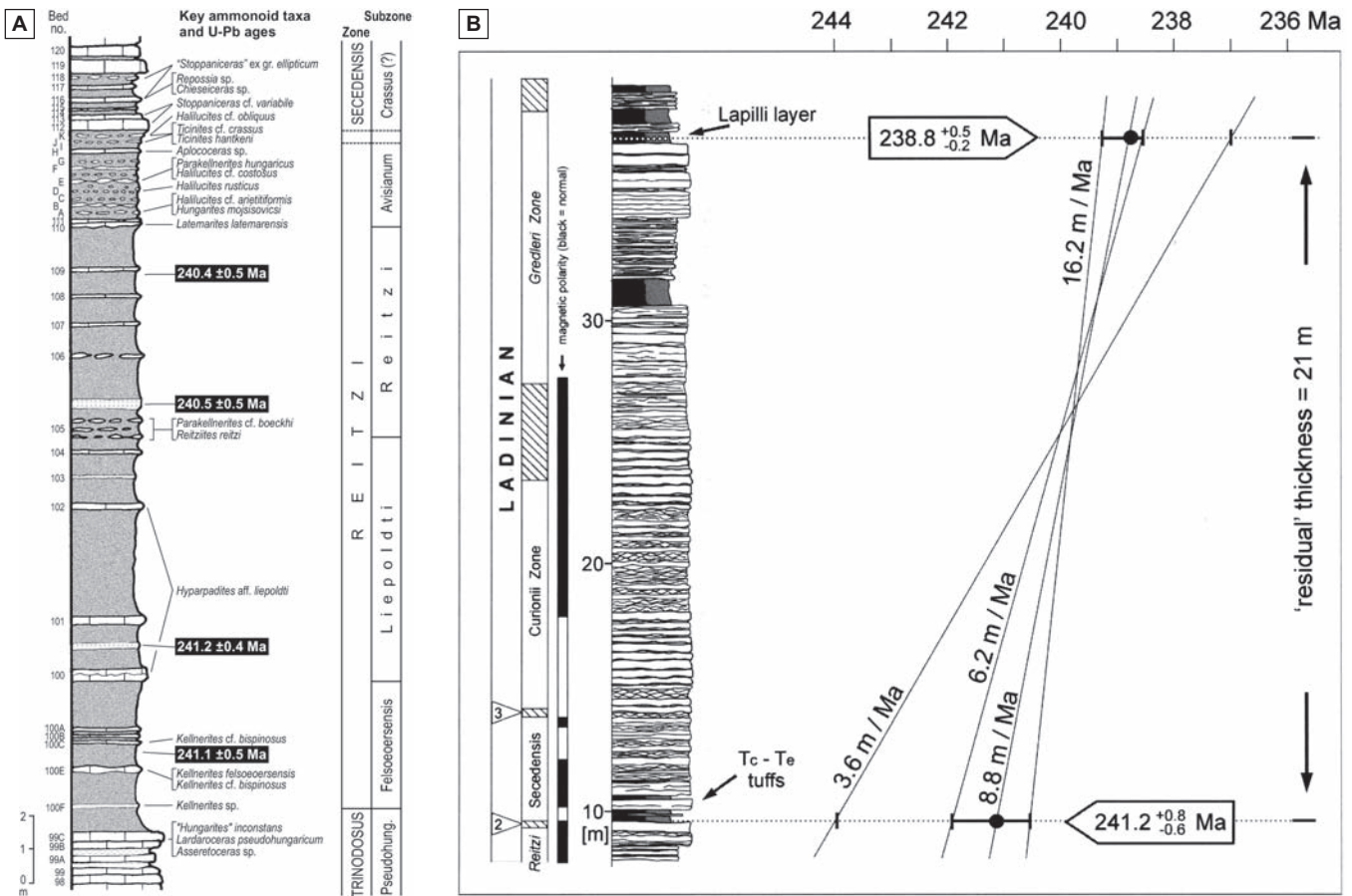


Fig. 1.3 Schematic palaeogeographic map of the Dolomites during the Middle Triassic (Early Ladinian) indicating shallow-water carbonate platforms (Schlern Fm) and coeval basinal sediments (Buchenstein Fm; from Maurer 2003). This distribution of structural highs and lows was however created already in the Middle Anisian.



Figs. 1.4 Bio- and chronostratigraphy of the pelagic Buchenstein Fm.

1.4A Dated ash-layers and key ammonoid fauna within the Plattenkalk Member (lower Buchenstein Fm) of the Balaton Highland (Hungary; Pálffy et al. 2003) illustrating the impressive density of age-diagnostic horizons/intervals within these pelagic sediments.

1.4B Dated ash-layers within the Knollenkalk Member (middle Buchenstein Fm) from the Seceda, Dolomites (after Mundil 1996; from Maurer 2003). The linear regression between the two dated layers indicates a sedimentation rate of av. 8.8m/Ma vs. 3.6m/Ma as derived from time series analysis of the Buchenstein Fm with the assumption of the presence of Milankovitch-cyclicity in certain power spectra (see Maurer 2003).

Latemar, W-Dolomites: Mundil et al. 2003; for locations see Fig. 1.3) providing a unique, high resolution database for numerical basin and carbonate platform modelling (see Figs. 1.4).

1.2 Geological setting

1.2.1 Basin fill and geodynamics

According to Dercourt et al. (1993, 2000) and many earlier authors, the Triassic of the Southern Alps was situated at latitudes of 15-20°N on the western termination of the Tethys. Throughout the Triassic the Dolomites and Lombardic Alps have been situated on the Adriatic Plate. This area represented a highly dismembered passive continental margin with transpressive-transpressive tectonics (Blendinger 1985; Doglioni 1987) and mixed car-

bonate-clastic sedimentation. The Southern Alps of Northern Italy can be subdivided into several parts separated by major tectonic lines of polyphase origin. The Dolomites are located in the centre of the Southern Alps (Fig. 1.1), forming a weakly deformed mountain range east of Bozen. The Lombardic Alps are offset from the Dolomites by the Giudicarie line with major left-lateral offset since the Late Cretaceous (Schönborn 1992).

In the study area in the Dolomites (Fig. 1.2), Early Permian volcanic activity is witnessed by the Atesina Volcanic Complex (AVC). The AVC covers an area of 2000-4000km² and represents a voluminous pyroclastic flow complex with thicknesses between 2000-2500m and subordinate lava flows and intrusions (D'Amico et al. 1980, D'Amico & Del Moro 1988; Barth et al. 1994).

The AVC overlies a Lower Permian erosional unconformity either in direct contact to the Hercynian metamorphic basement – mainly metapelites – or to the Lower Permian Waidbruck conglomerate. The mainly absent deformation of the Dolomites is owed to the rigidity of this underlying magmatic succession. Hence, the SW Dolomites provide a key area for the study of pre-Alpidic basin evolution. The absence of major thrusting enables the assessment of sedimentary and burial history from the Permian onwards.

Sedimentation on the Permian landscape is recorded by the siliciclastic Upper Permian Gröden Fm (“red beds”), followed by evaporites and carbonates of the Bellerophon Fm indicating a relative sea level rise. The long-term transgression of Tethys to the W is further evidenced during the Lower Triassic by sub- to intertidal deposits of the Werfen Fm (Broglia Loriga et al. 1983, 1990). The transition from Scythian to Anisian times (Lower to Middle Triassic) recorded a change in sedimentary characteristics (De Zanche & Farabegoli 1988; De Zanche 1990). Synsedimentary transpressive-transpressive tectonic activity created structural highs and lows along the passive margin leading to so-called facies heteropy (Bechstädt & Brandner 1972). The Anisian also saw the

re-occurrence of carbonate ramps and platforms, with the first ramps made up of simple microbial and algal carbonates (Sarl Fm: Fois & Gaetani 1984; Senowbari-Daryan et al. 1993). Sedimentation on structural highs was recorded by the conglomeratic Richthofen Fm and later by the ramp carbonates of the Contrin Fm whereas more basinal settings were filled with the slightly bituminous Morbiac and Moena Fm (Zühlke 2000). Further tectonic activity enhanced facies heteropy and subsequently carbonate platforms (Schlern Fm 1 sensu Brandner 1991; Schlager et al. 1991; see Fig. 1.3) developed with coeval basinal successions (Buchenstein Fm) indicating water depths of about 800-1000m towards the end of basinal development (Bosellini 1984; Brack & Rieber 1993). Volcanic activities outside the Buchenstein basin lead to the deposition of air-borne ash layers in lagoonal and basinal sediments during Schlern platform development (Callegari & Monese 1964; Cros 1979; Cros & Houel 1983). These volcanic tuff beds represent basin-wide correlatable marker horizons (Brack & Muttoni 2000) and were dated with various methods by many research groups providing chronostratigraphic timelines within basinal and lagoonal sediments (Mundil et al. 1996; Mundil et al. 2003; Pálffy et al. 2003). A high-reso-

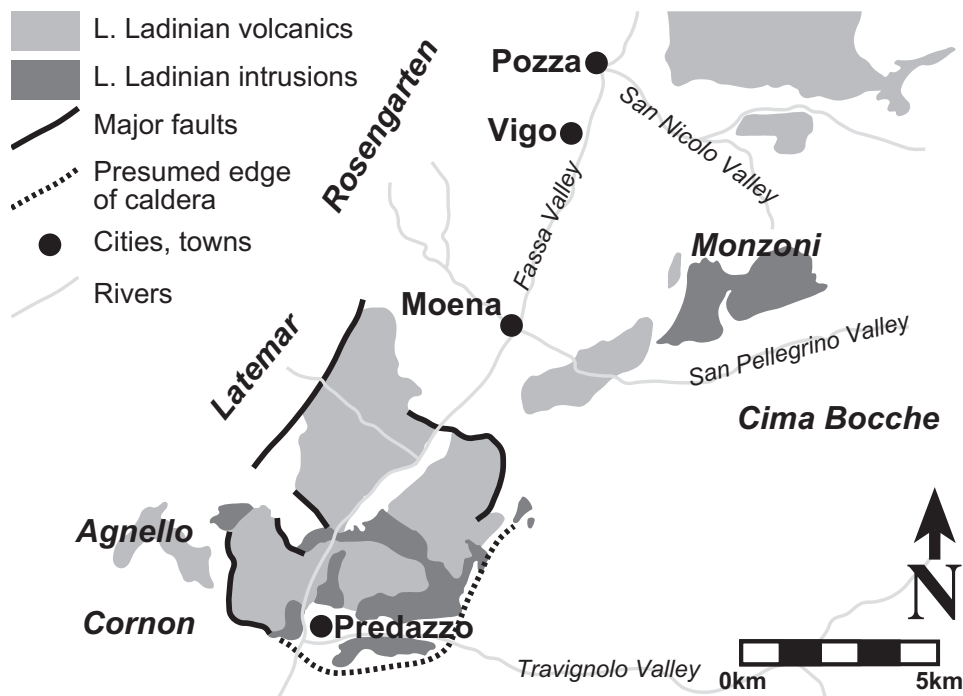


Fig. 1.5 Schematic map of the Middle Triassic (Late Ladinian) magmatism in the area of the volcanic centre at Predazzo/Monzoni. The outline of the caldera having formed after the collapse of the magmatic chamber is well visible (after Doglioni 1987; Bosellini 1991).

lution biostratigraphic subdivision of the Buchenstein Fm (e.g. Brack & Rieber 1993, 1994; Pálffy et al. 2003) further enhances correlation and age assignment (see Figs. 1.4).

Late Ladinian tectonic and volcanic events inside the basin – i.e. Wengen Fm volcanism – ended platform growth by exposing platform tops subaerially and by covering the platforms with lavas and volcanoclastics (Schlern platform; Brandner 1991; Yose 1991) and filling the basins with debris-flows, ashes and lava (Bosellini et al. 1977, 1982). The coeval volcanic complex of Predazzo/Monzoni (Fig. 1.5) formed above the small but deep-reaching fault system of the Trodena/Stava line-Cima Bocche anticline (sinistral transpression creating flower-structures in the basement; Doglioni 1987).

The later basin infills can only be deduced by a comparison with the basin evolution in the eastern parts of Dolomites and the area around Trento. All strata younger than Late Ladinian have been eroded in the study area. Postvolcanic buildups (Schlern Fm 2 – sensu Brandner 1991; Schlager et al. 1991 – or Cassian Dolomite) are of major importance in the eastern Dolomites, thicknesses in the western Dolomites are limited to 50-70m (Schlern; Brandner 1991). Subsequently, Cassian platform tops were subaerially exposed and topographic relief leveled. The Late Carnian Raibl Fm overlies this karstification surface. With the onset of a period of tectonic quiescence a huge carbonate platform developed comprising the entire central segment of the Southern Alps on the Adriatic Plate (Trento platform: Dolomia Principale, Calcari Grigi; Bosellini & Broglio Loriga 1971; Bosellini & Hardie 1985). Jurassic rifting of the continental lithosphere started at the Triassic/Jurassic-boundary (Dercourt et al. 2000), corresponding to ages of around 200Ma according to the new Jurassic time scale after Pálffy et al. (2000). From Middle Jurassic times on, when sea-floor spreading between Adria and Europe began (emplacement of gabbros in the Swiss alps between 160-165Ma; Schaltegger et al. 2002), the Trento platform started subsiding more rapidly and eventually drowned. A phase of deep marine sedimentation began (Ammonitico Rosso Fm; Winterer and Bosellini 1981; Martire 1996; Winterer 1998) and lasted until Late Cretaceous (Marne del Puez Fm; Claps et al. 1991; Antruilles Fm; Stock 1996). Water depths decreased again when the tectonic regime switched from extension to compression and the collision of the Adriatic plate with Europe started with subduction of oceanic crust in the Late Cretaceous (e.g. Hsü

1971; Trümpy 1982; Laubscher and Bernoulli 1982; Dercourt et al. 2000). Upper Oligocene shallow marine conglomerates in the eastern Dolomites witness ongoing continent collision in the Palaeogene (Mair et al. 1996). Fast exhumation of the Southern Alps mainly driven by denudation/erosion is thermochronologically recorded from the Eocene onwards (40-35Ma; e.g. Bernet et al. 2001; Dunkl et al. 2001).

1.2.2 Carbonate platform evolution and palaeo biology

Few studies on reefs in the Dolomites (Fois and Gaetani 1984; Senowbari-Daryan et al. 1993) have investigated the Anisian recovery of carbonate producing organisms from the mass extinction at the end of the Permian where 62% of marine invertebrate families (McKinney 1985) and up to 96% of species (Raup 1979) had been extinguished. All previous studies observe a recovery during the Anisian when many reefal biota (calcisponges, calcareous algae, few microproblematica and few scleractinians) occurred for the first time in the Dolomites again since the P/T crisis. This was confirmed by recent literature (Twitchett 1999) reporting a gradual re-appearance of trace fossils throughout the Lower Triassic of the Dolomites (Werfen Fm) and a complete recovery already in the Uppermost Scythian (top of Werfen Fm). Furthermore, studies from other Triassic reefal locations of the world also indicate a recovery of calci-microbial buildups during the Anisian (for complete discussion and references refer to Flügel 2002).

First carbonate ramps in the Dolomites did not develop until the Early Anisian (Sarl Fm; De Zanche & Farabegoli 1988; Zühlke 2000). The Middle Anisian Dont Fm contained simple reefal mounds only (Fois and Gaetani 1984). Carbonate ramps of Middle/Late Anisian times (e.g. Contrin Fm) were primarily made up of microbial carbonates with very subordinate frame-building organisms only. True frame-builders – i.e. scleractinian corals – were still suffering from the severe faunal crisis at the end of the Permian (scleractinian “reef gap” until the Early/Middle Triassic; Flügel and Stanley 1984; Flügel 1994). Carbonate platforms with highly diversified reefs did not exist prior to the Latest Anisian/Early Ladinian (Schlern Fm).

“Platform” evolution in the Lombardic Alps is recorded from the Early Anisian Dosso dei Morti/Camorelli buildups onward (Unland 1975; Gaetani & Gorza 1989). However, these mud-mounds containing simple microbial

constructions could not keep up with the Pelsonian (Middle Anisian) relative sea level rise recorded in the Lombardic Alps and in parts of the Dolomites (Rüffer & Zühlke 1995; Zühlke 2000). The Early Anisian buildups were subsequently covered with deeper marine deposits (Brack 1984). From Late Anisian until Late Ladinian, the area in the Lombardic Alps experienced deep marine conditions as indicated by the basinal Buchenstein Fm. Carbonate platforms in the Lombardic Alps re-occurred in the Late Ladinian (e.g. Pora, Concarena).

Another reason for the Late Anisian onset of platform development in the Dolomites may lie within the regional lowstand during the Early Triassic (Scythian until earliest Anisian) and clastic input from the south poisoning carbonate producing organisms and inhibiting platform growth. Subaerial exposure (Anisian unconformity) in the westernmost Dolomites restricted carbonate ramps to the central and eastern Dolomites. In the area of the western Dolomites, it took until the Late Anisian when flooding of subaerial structural highs created sufficient accommodation space for carbonate ramp and later platform development (De Zanche and Farabegoli 1988; Rüffer and Zühlke 1995). From the Middle Anisian on into the Late Ladinian, a considerable submarine relief with some emersive parts prevailed in the area of the Dolomites setting the stage for later platform evolution (Bechstädt and Brandner 1970; Blendinger 1985; Doglioni 1987; Zühlke 2000). Subsequently in Middle Anisian to Early Ladinian times, deep marine stagnant basins with fine grained chert- and organic-rich sediments (Sarl Fm, Moena Fm and Buchenstein Fm; see Fig. 1.3) existed alongside shallow marine subtidal carbonate ramps and platforms (Contrin Fm and Schlern Fm). Structural highs of the dismembered carbonate ramp (Contrin Fm) were the nuclei of the Schlern Fm platforms in the Late Anisian (Masetti & Neri 1980; Gaetani et al. 1981). Evolution of most of the platforms in the study area like Schlern, Rosengarten and Monte Agnello and probably also the evolution of the Latemar atoll ended with the extrusion of the Longobardian Wengen Fm volcanics. Hence, the proximity of the volcanic centre at Predazzo/Monzoni (Fig. 1.5) played a crucial role for the platform development in the SW Dolomites. The volcanic centre at Predazzo/Monzoni did control regional subsidence and accommodation development with deep reaching faults (Doglioni 1984) and magmatic updoming as well as terminate platform growth with phreatic eruptions (e.g. Viel 1979a; Viel 1979b; Bosellini et al. 1977, 1982).

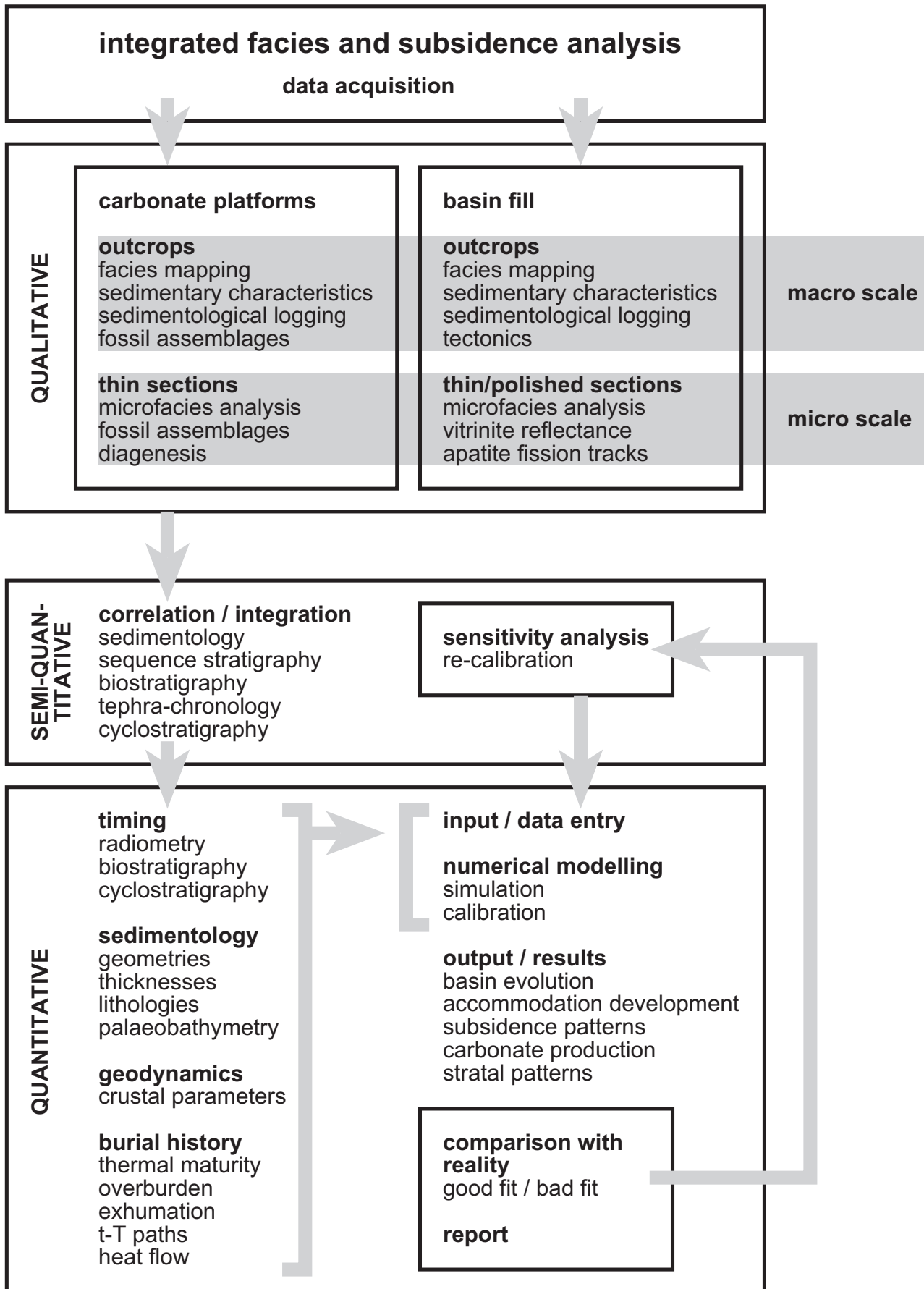
1.3 Objectives

The aims of this project are: (1) to identify control parameters on carbonate platform evolution by comparative facies analysis at two buildups with primary preservation as limestone (Latemar, Dolomites and Concarena, Lombardic Alps); (2) to reconstruct the burial history of Middle Triassic carbonate platform bodies (Latemar and Rosengarten, Dolomites) in order to unravel and quantify their subsidence patterns; (3) to simulate the depositional history of the Rosengarten platform and to quantify carbonate production rates with the help of sequence stratigraphic forward modelling.

This project follows the scheme of data acquisition, processing and interpretation illustrated in Fig. 1.6 (next page). The unique feature of this project is the integration of facies and subsidence analysis in order to unravel sedimentation and burial histories of the studied carbonate platforms. Qualitative studies on macro and micro scale at different carbonate platforms as well as basin fills are integrated/combined by correlation (sedimentology, sequence stratigraphy, biostratigraphy, tephra-chronology and cyclostratigraphy) to serve as input parameters for numerical basin modelling. Quantitative basin analysis begins with the determination of numerical values for timing, sedimentology, geo-dynamics and burial history. This dataset is entered into numerical modelling software like PetroMod™ (IES GmbH, Jülich, Germany) or PHIL™ (Petrodynamics Inc., Houston, U.S.A.) to simulate/verify the conceptual model. If the simulated results do not match reality the conceptual model has to be changed in order to fit calibration parameters (e.g. stratal geometries, thermal maturity).

1.3.1 Facies analysis

The base for this study are new, detailed investigations on the lithofacies and geometries of reef and slope and their relation to the growth characteristics of the platform interior as well as investigations on reefal assemblages. The aim of facies analysis is (1) to identify the processes controlling slope and ultimately platform development, (2) to investigate the possible evolution of faunal assemblages in time and their distribution within the reef of the Latemar and (3) to assess an Anisian/Ladinian age of the reef at Latemar as inferred from the chronostratigraphic framework of the lagoon, (4) to compare the architecture of Latemar and Concarena, and finally (5) to assess the link between massive early ce-



mentation and carbonate accumulation/accommodation increase.

1.3.2 Subsidence/numerical basin modelling

The aim of subsidence/numerical basin modelling within this project is the quantification of the development of the Rosengarten and Latemar platform and the assessment of controlling factors during their evolution. This is realised by an integrated approach of thermal history, reverse basin and forward stratigraphic modelling. Datasets for this numerical basin modelling approach are derived from existing studies and new detailed analyses on allo-/sequence stratigraphy and facies architecture. Thermal maturity and apatite fission tracks from samples of underlying strata are measured in order to assess t-T-paths – i.e. the thermal history – of platform bodies and adjacent basins. A comparison of numerical basin reverse models from the Rosengarten and Latemar platforms allows to verify and constrain evolution and subsidence patterns of these two buildups.

1.4 Methods

The following methods are applied during this study: sedimentological and palaeontological analyses, cathodoluminescence techniques, stable isotope and thermal maturity analyses, fission track analyses on apatites, thermal modelling, numerical basin reverse modelling and sequence stratigraphic modelling.

1.4.1 Palaeontology, sedimentology and stratigraphy

Detailed palaeontological and sedimentological analyses (logging, facies mapping, lateral tracing of physical surfaces, thin sections) are carried out on the complete basin fill with special attention to the carbonate platforms in the study area. Several sections/sedimentological logs cover the entire basin infill from basement (Atesina Volcanic Complex, AVC/Bozener Quarzporphyr; see sections in the appendix) to the basal Schlern Fm. Additional data on the Upper Anisian succession and the Buchenstein Fm were taken from literature (Bosellini and Stefani 1991; Maurer 1999, 2000, 2003; Zühlke 2000). These analyses enable the deduction of vital datasets on thicknesses, lithologies and palaeo water depths. The

latter modelling parameter is based on the integration of all sedimentological evidence from the outcrops (channels, ripples, exposure surfaces, bioturbation etc.) with microfacies analyses of thin sections. Nowadays eroded Middle to Upper Triassic formations are projected from the western and central Dolomites (Schlern and Sella platform), Jurassic strata from the Trento platform, Cretaceous and Tertiary formations from the eastern Dolomites (for a complete list of references, formations and thicknesses see Part 3). Lithology information is combined with published data on chronostratigraphy and palaeo bathymetry. Jurassic palaeo water depths are calculated with a subsidence curve for the Trento platform proposed by Winterer and Bosellini (1981) and Winterer (1998).

1.4.2 Cathodoluminescence

Cathodoluminescence techniques are used to identify different generations of cements. Cathodoluminescence is especially suitable to separate deep burial cements (e.g. zoned blocky calcites; Zeeh & Bechstädt 1994) from early to shallow burial cements (e.g. radiaxial fibrous cements, dog-tooth cement; Zeeh & Bechstädt 1994) and to estimate their volumetric importance with respect to whole rock cementation.

1.4.3 Stable isotopes

In order to obtain information about the isotopic fluid composition during diagenetic cement growth, selected unaltered and homogeneous samples of primary fibrous cements corresponding to early marine diagenesis (Kendall 1985; for discussion see Tucker & Wright 1990) are analysed for their carbon and oxygen isotopic composition.

1.4.4 Thermal maturity

Vitrinite reflectance is the most frequently used parameter in order to assess regional thermal maturity and is furthermore widely used as a calibration parameter for thermal basin modelling. Vitrinite reflectance is determined by microscopic analysis of percentages of light reflected from polished organic particles and calibrated against isotropic standards. The results are given as mean random reflectance (VR_r %), for details on methodology

Fig. 1.6 (previous page) Scheme of data acquisition/processing and modelling illustrating the concept of integrated facies and subsidence analysis.

and measurement see Stach et al. 1982; Taylor et al. 1998). Increasing temperatures during burial or convective/conductive heating produce increasing thermal maturity. Measured VR_r values are converted into burial/heating temperatures with the equation introduced by Barker & Pawlewicz (1986; 1).

$$T = \frac{\ln VR_r + 1.68}{0.0124} \quad (1)$$

$$VR_r = 1.65 VR_{r\text{IMP}} \quad (2)$$

Impregnated sample are corrected with the correction equation by Jacob (1989; 2; with $VR_{r\text{IMP}}$ being the value of the impregnated sample).

1.4.5 Fission tracks

Apatite fission-track (FT) thermochronology is commonly used to determine the magnitude of cooling, exhumation and rock uplift from shallow crustal levels (e.g. Fitzgerald et al. 1995, Tippett and Kamp 1995). The base for this analysis is the time-temperature dependent pres-

ervation of fission tracks. Annealing of fission-tracks is a function of temperature, time and α -radiation damage (Kasuya and Naeser 1988). The amount of α -radiation damage increases with time and with uranium and thorium concentrations in the mineral. Different minerals lose their tracks at different temperatures: (1) Naeser & Faul (1969) describe partial annealing in apatite (apatite partial annealing zone; APAZ) from 50°C to 125°C (see also Fig. 1.7); (2) Tagami & Shimada (1996) discuss a zircon partial annealing zone (ZPAZ) between ~230 °C and 320 °C for a heating duration of about 1Ma. Hasebe et al. (2003) report a lower limit of the ZPAZ at a stable temperature of about 1Ma above 200°C. As vitrinite reflectance analyses revealed a low thermal maturity equivalent to less than 120°C, apatite FT analysis was preferred.

Based on the apatite FT- and geological data, time-temperature paths for samples were calculated using AFTSolve) with the kinetic model after Laslett (1987). The AFTSolve) software is described by Ketcham et al. (2000) in detail. Although the programme attempts to find out of more than 10,000 single t-T paths those best approximating the measured data (“Best Fit”), the primary goal of the programme is to define envelopes (merit value of 0.05 and 0.5) in t-T space containing all paths passing baseline statistical criteria and being conform to user-defined geological constraints. Therefore, the forward modelling procedure of the programme is used to establish segments of the t-T path where monotonic cooling and monotonic heating change. Such constraints are included in the inverse modelling module of the programme. For most of the samples, the t-T constraints are left very wide open.

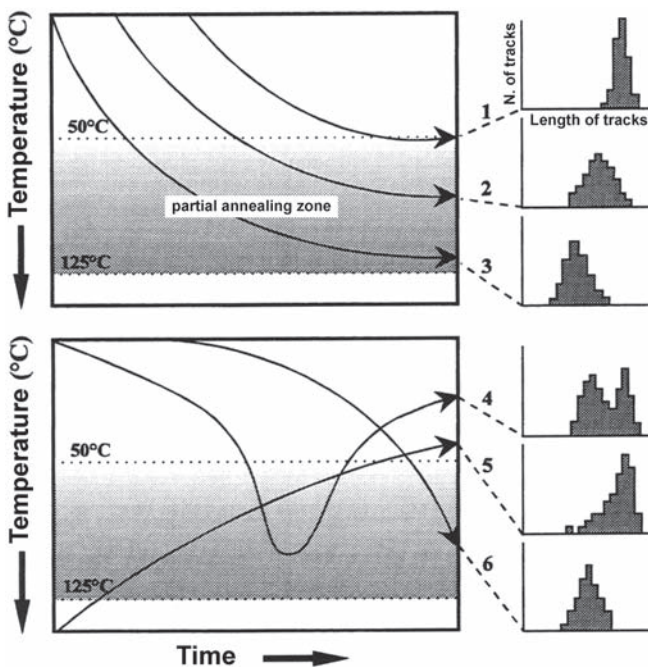


Fig. 1.7 t-T paths and the resulting apatite track length distributions for rocks of varying thermal histories. The upper three models (1-3) show the temperature evolution for progressive burial to different levels in the track annealing zone. The lower distributions (4-6) are the results of different thermal events (after Gleadow et al. 1986; from Petmecky 1998).

1.4.6 Thermal modelling

Thermal modelling is used to simulate the burial and thermal history and the re-construction of the overburden thickness. Simulation is realised with PetroMod™ (IES GmbH, Jülich, Germany). Input parameters (see Part 3 and Appendix 1-3) for numerical models are thickness of stratigraphic units, lithologies, rock physical parameters (e.g. thermal conductivities; see Bükér 1996; see Hertle and Littke 2000 for a more detailed description of the calculation of physical properties of stratified sediment bodies), temperature at sediment-water interface, heat flow at the base of the succession. Subsidence history and temperature field through time are calculated. Burial and heat flow histories are calibrated with meas-

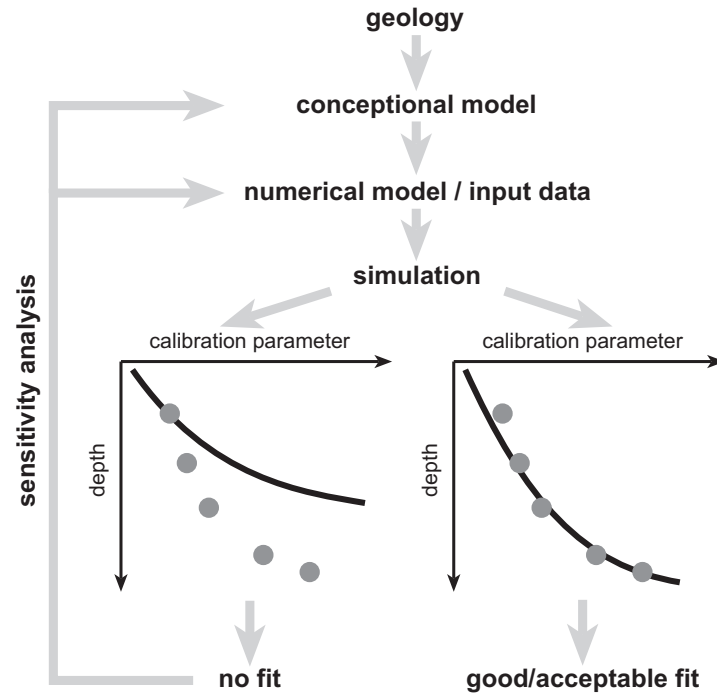


Fig. 1.8 Schematic workflow of basin modelling with e.g. PetroMod. Model-building starts with the deduction of a conceptual model from the geological situation. The numerical model is built according to the data required by the simulator and the objectives. The simulation provides the possibility to check model vs. measured data (calibration parameter; thermal maturity in most cases). If the modelled results do not match the calibration parameters, the conceptual model or the numerical model have to be changed (sensitivity analysis) until an acceptable fit is reached.

ured vitrinite reflectance values (see Fig. 1.8). The model was then fine tuned by modifying heat flow and eroded thicknesses until a satisfactory fit between measured and calculated vitrinite reflectance was achieved. Vitrinite reflectance was calculated using the EASY%Ro-algorithm of Sweeney and Burnham (1990; see also e.g.

Sachsenhofer and Littke 1993; Littke et al. 1994; Leischner 1994; Sachsenhofer et al. 2002). EASY%Ro describes the chemical alteration of vitrinites with increasing temperatures; four reactions occur simultaneously: the release of (1) water, (2) carbon dioxide, (3) higher hydrocarbons and (4) methane. The decrease in

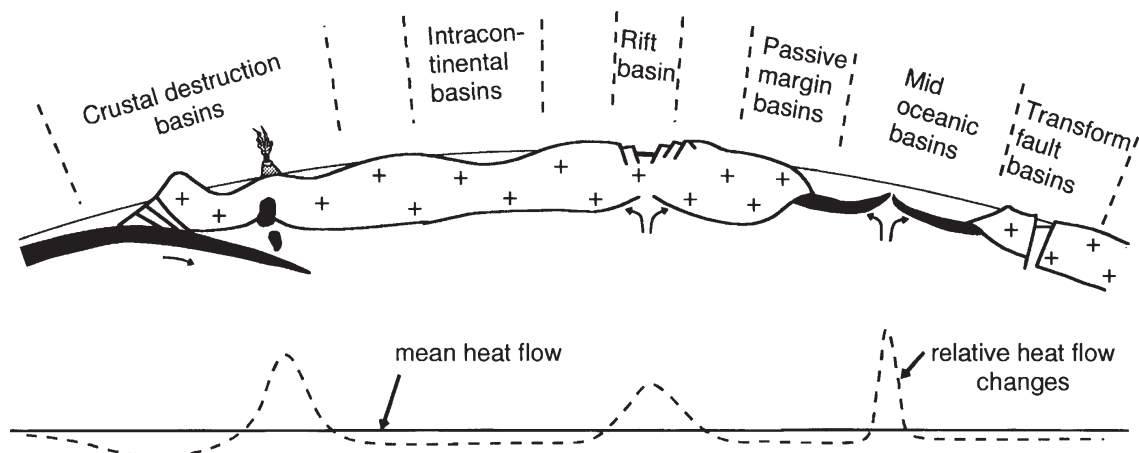
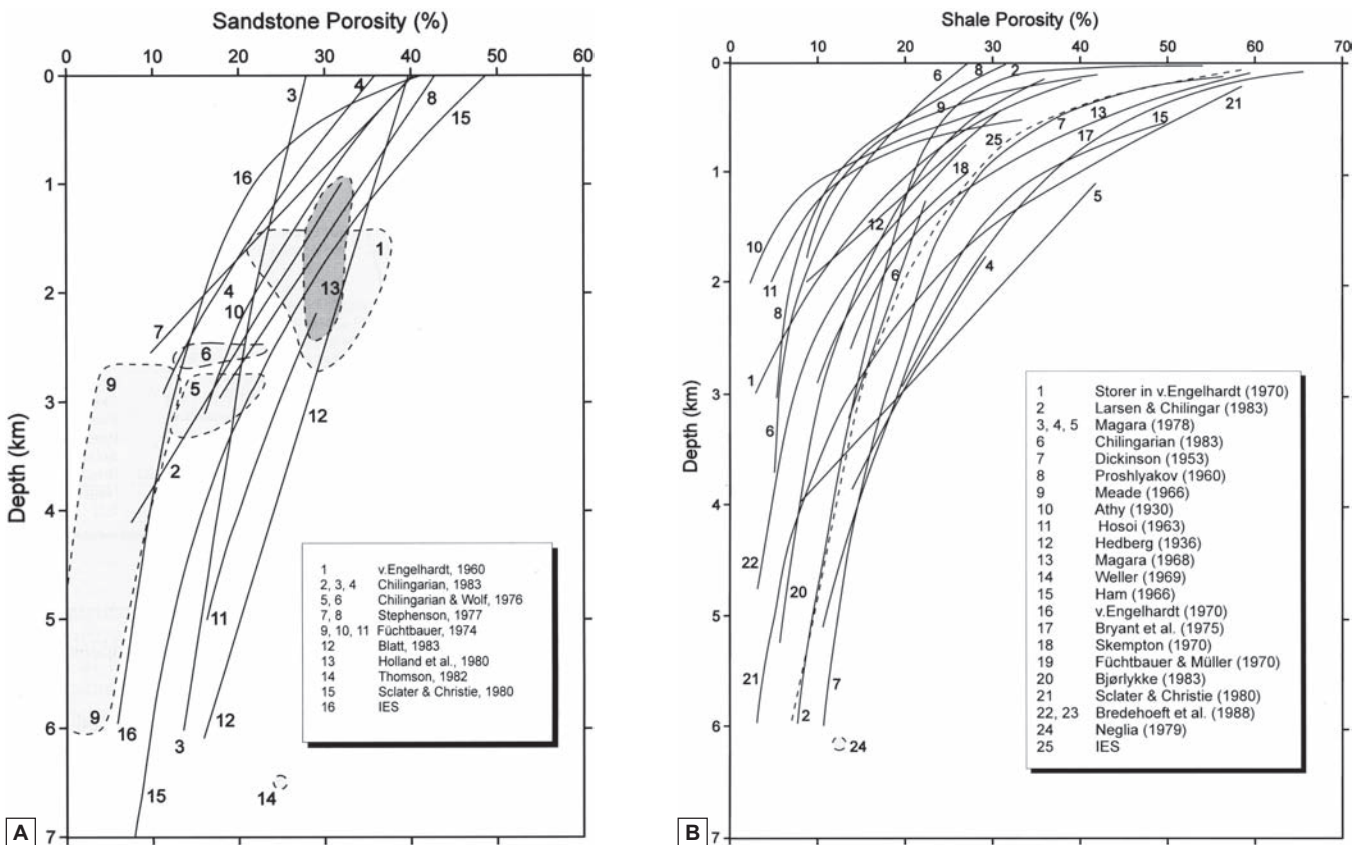


Fig. 1.9 Typical geodynamic settings of basins associated with elevated basal heat flow (indicated by dashed line at the bottom; peaks above solid line indicate elevated heat flow; after Yalcin & Welte 1988).

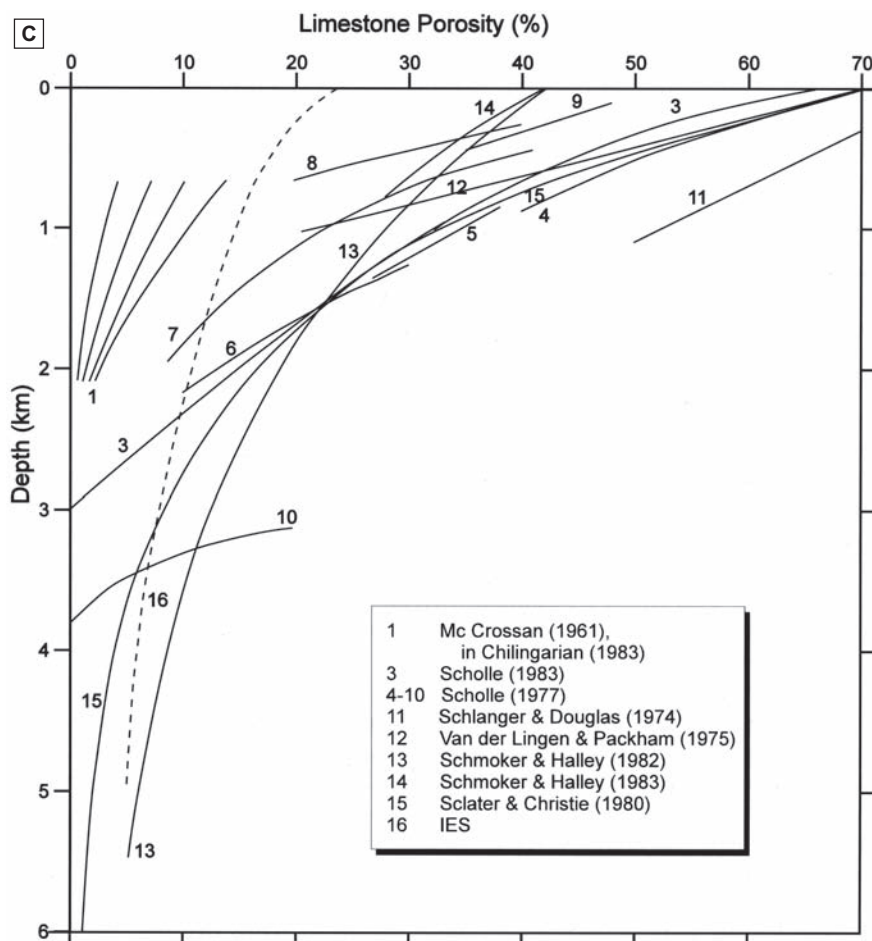
	Mean	Range
Extensional basins		
Active ocean ridges and volcanoes	120	120–205
Active (syn-rift) back-arc basins	85	67–120
Active (syn-rift) rift or passive margin	80	65–110
Thermally subsiding (postrift) rift or passive margin	50	40–65
Compressional basins		
Collisional foldbelt	70	40–97
Ocean trench foreland basin (foothills→margin)	40	40–80
Fore-arc basin unrelated to arc magmatism	35	20–45
Strike-slip basins		
Active strike-slip, deep lithosphere involvement	100	80–120
Active strike-slip, shallow thin-skinned (crustal) extension only	60	50–69
Basement		
Precambrian shield	40	30–55
Oceanic crust (>200 Ma)	35	30–40
Approx. global average heat flow	65	60–70

Table 1.1 Typical heat flow values for sedimentary basins (in mW/m^2 ; after Allen & Allen 1990, from Poelchau et al. 1997).



Figs. 1.10 Porosity-depth curves for three different lithologies with a comparison of the function used by PetroMod (from Wygrala 1989). x-axis: porosity in %; y-axis: depth in km.

1.10A sandstones; **1.10B** shales; **1.10C** (next page) limestones. For original references refer to Wygrala (1989).



these components results in reduction of the H/C ratio in vitrinite and is correlatable with the increase in reflectance (McCartney & Teichmüller 1972; Leischner 1994). The algorithm is based on the Arrhenius-equation and uses a frequency-factor F describing the loss of volatile components.

The crux of thermal modelling is the estimation of palaeo heat flow. Basins can be situated on passive or divergent margins – usually related to the extensional type of basin, on compressive or convergent margins or on transform or strike-slip faults. Each of these positions show characteristic thermal behaviour (Fig. 1.9 and Table 1.1) which can be used to estimate heat flow history associated with basin evolution (Condie 1976; McKenzie 1981; Allen & Allen 1990; Poelchau et al. 1997). The topic of palaeo heat flow estimation is extensively discussed in Yalcin et al. (1997). The applied heat flow history during basin modelling is shown in Part 3.

Compaction is the largely irreversible process of sediment volume reduction due to overburden loading, grain rearrangement, grain solution, etc. Compaction can pri-

marily be described as a function of initial porosity reduction, reduction of solid components plays only a minor role. Bulk compressibility describes compaction as a function of depth. Another important controlling parameter is the ability of the sediment to transmit fluids with increasing pore pressure, i.e. the permeability. In order to model compaction, the general porosity, permeability and compressibility decrease of a given rock volume with depth must be known (Poelchau et al. 1997). The porosity-depth curves for certain lithologies used by PetroMod are compared with other curves from various published sources in Figs. 1.10. The porosity-depth curves used during basin modelling of the Rosengarten transect are shown in Appendix 2.

1.4.7 Numerical basin reverse modelling

Knowing the overall thickness of the basin fill is crucial for numerical basin reverse modelling. Lithology (porosity/permeability) and burial depth chiefly control the amount of compaction during sedimentation and decompaction during reverse modelling (“backstrip-

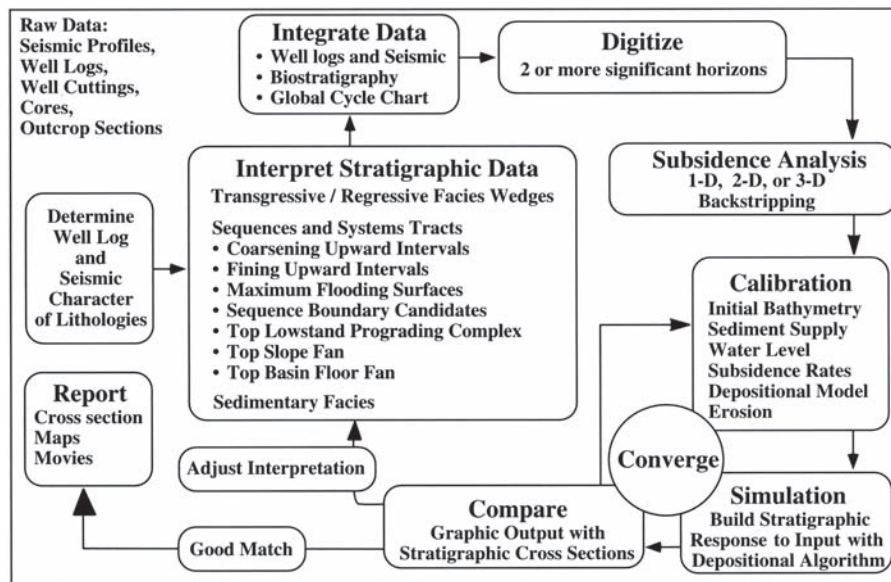


Fig. 1.11 Stratigraphic cross section modelling procedure (from Bowman & Vail 1999).

ping”). Hence, the eroded thickness derived from basin modelling is entered with all other necessary input parameters (see Fig. 1.11) into the basin reverse modelling routine of PHIL in order to determine thermo-tectonic, flexural and compaction induced subsidence rates for forward modelling (see Fig. 1.12A). Numerical reverse basin modeling in this study follows the sequence stratigraphic concept, which considers the creation/destruction of accommodation space (see Fig. 1.12B) and

its infill as the two principal controls on sedimentary systems and basins. Subsidence component, accommodation and sediment flux histories were calculated for each of the time steps identified in the entire basin fill (see Part 3). Basin reverse modelling is running in the opposite direction of sedimentation: the process starts at time t_2 and runs backwards in time to t_0 when all sediment layers have subsequently been removed (“backstripped”). Each timestep (t_0, t_1, t_2) is characterised by a distinct vec-

Lithology	Density (kg/m ³)	Initial Porosity (ϕ_0)	Compaction Rate (r_c)
Quartz Boulders	2650	0.4	0.0001
Quartz Silt Size	2650	0.3	0.001
Quartz Silt/Clay	2650	0.4	0.002
Quartz Sand/Clay	2650	0.4	0.002
Quartz/Silt	2650	0.45	0.0005
Silt/Clay	2750	0.5	0.002
Clay	2750	0.5	0.003
Silt/Coal	2450	0.6	0.008
Clay/Coal	2300	0.85	0.009
Coal	2000	0.92	0.01
Cemented Carbonate	2800	0.45	0.0001
Carbonate Fine Grainstone	2800	0.6	0.001
Carbonate Boundstone	2800	0.6	0.001
Carbonate Coarse Grainstone	2800	0.7	0.002
Micrite	2800	0.7	0.004
Algal Laminates	2800	0.6	0.0005
Dolomite	2900	0.4	0.0001
Gypsum	2330	0.1	0.00001

Table 1.2 Petrophysical parameters used during basin modelling with PHIL (from Bowman & Vail 1999).

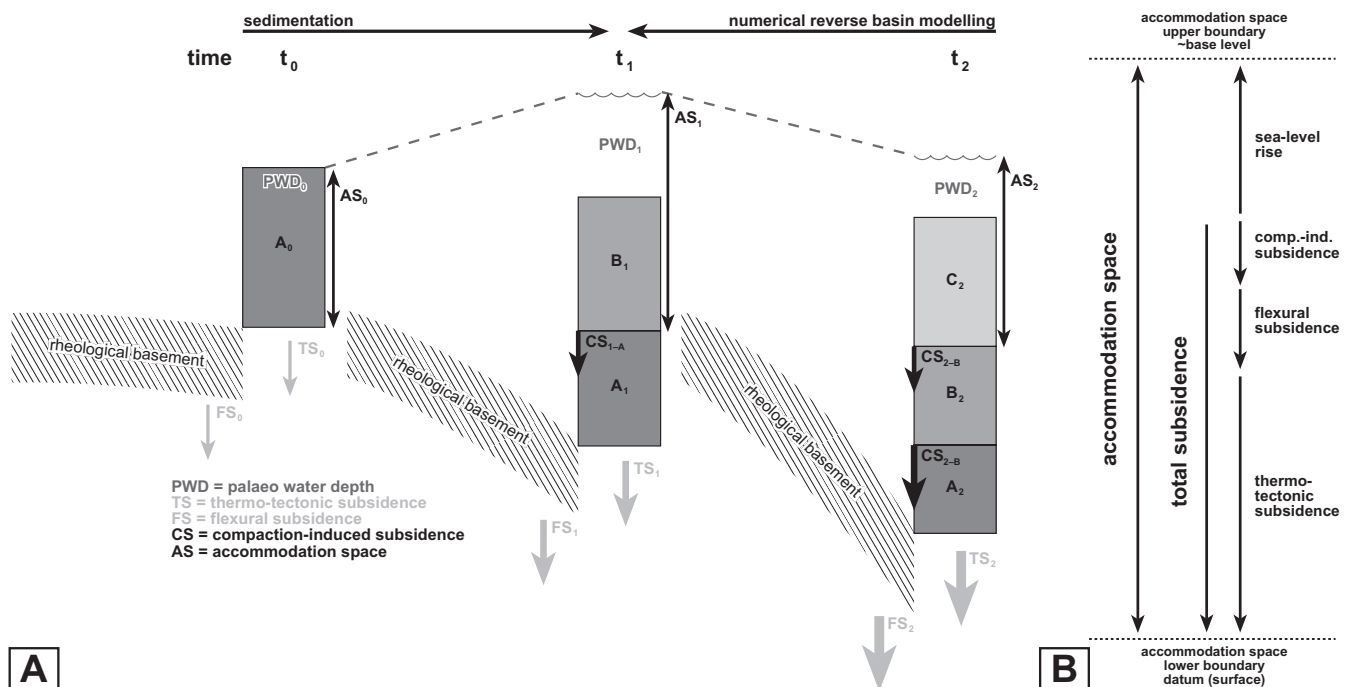
tor of tectonic subsidence (TS_0 to TS_2), flexural (FS_0 to FS_2) and compaction induced subsidence (CS_0 to CS_2) as well as a change in palaeo water depth (PWD_0 to PWD_2). During each step of removal, the hypothetical depth of the basin floor is calculated without being loaded and the current depositional surface is adjusted to pre-defined palaeo bathymetry. Rates are calculated for each time layer with the effects of flexural loading, changes in paleobathymetry, changes in sea level and compaction removed. The flexural backstripping procedure applied in the reverse basin modelling of this study is based on the equations introduced by Turcotte & Schubert (1982, 2002) and Dickinson et al. (1987). The backstripping procedure with the PHIL software has also been described by Bowman & Vail (1999).

$$\phi(z) = \frac{\phi_0}{1 + z * r_c} \quad (3)$$

where ϕ is the porosity, z the depth in metres, ϕ_0 the initial porosity and r_c the compaction coefficient.

The simulator incorporates sediment compaction as function of burial depth. The reverse modelling routine of PHIL requires an initial porosity value averaged throughout the entire basin fill as input parameter. However, the determination of initial porosity of each time step would need detailed diagenetic studies. In the framework of this project it is calculated as an average with the given petrophysical parameters (Table 2) from three sections in the transect: (1) proximal, (2) intermediate and (3) distal (see Appendix 4).

Further input parameters were geometries (measured and projected bed thicknesses), palaeo water depth (derived from facies analysis), depositional ages (see Part 3) and crustal parameters (e.g. effective elastic thickness T_e , plate end boundary distance and density of the mantle). Due to the shortness of the transects (Rosengarten: 6km and Latemar: 4km) and the rigidity of the underlying



Figs. 1.12 The basin reverse modelling process and the concept of accommodation space.

1.12A Schematic sketch of numerical basin reverse modelling. x-axis: time; y-axis: burial depth; stratigraphic units are marked by letters A to C and different greyscales; arrows below the stratigraphic columns illustrate vectors of tectonic and flexural subsidence; arrows at tops of stratal layers indicate compaction-induced subsidence (thick arrow: high subsidence; thin arrow: low subsidence); accommodation space extends from base of topmost layer to base-level. For further explanations refer to the text.

1.12B The four components controlling accommodation space during each timestep. Accommodation space is filled through sedimentary input (see Schlager 1993).

basement (2000-2500m thick Permian AVC), crustal parameters and flexural subsidence play an insignificant role. Nevertheless, recent data on the effective elastic thickness (T_e ca. 20km) of the lithosphere of the Venetian basin (Barbieri & Garcia-Castellanos 2003) was applied. Owing to the short interval of platform evolution – less than 5Ma – 2nd order sea level fluctuations played an insignificant role during accommodation development. 3rd order sea level oscillations (1-3Ma; Duval et al. 1992) have not been considered because their timing and amplitude in the latest Anisian/earliest Ladinian is controversially discussed (Rüffer & Zühlke 1995; Gianolla & Jacquín 1998). Eventual sea level fluctuations are therefore comprised within total subsidence.

1.4.8 Sequence stratigraphic forward modelling

Stratigraphic forward modelling is mainly used to quantify carbonate production rates. The simulation of facies patterns and the identification of processes operating on the platform slope are a minor goal. Input parameters for sequence stratigraphic forward modelling are total subsidence and depth dependant carbonate production rates (“carbonate production curve”). The carbonate productivity functions are normal distribution curves with a specified width and a maximum production at a specified bathymetry (see Part 3). Production is linearly interpolated between the calculated value at low water and zero deposition at high water. Unrestricted traction and fine-grained production will occur on any interface below high water. Shelf-margin production is centered about an optimal location for production with respect to the open basin and exponentially reduced as a function of distance from that location by a specified factor (Bowman & Vail 1999).

$$P_{\text{depth}} = M t R \exp\left(\frac{-(B - D_{\text{mp}})^2}{W^2}\right) \quad (4)$$

where P_{depth} is the production for a cell during the time increment, M is the maximum production rate (in m/Ma), t is time (in Ma), R is a siliciclastic reduction factor, B is the bathymetry (in m) and W the width of the productivity function (in m; from Bowman & Vail 1999). Production rates were adjusted in an iterative process until a best fit with observed, present day geometries was obtained. Bowman and Vail (1999) have described in de-

tail the stratigraphic forward modelling process with the software being used in this project.

1.5 Previous research

1.5.1 Latemar

The Latemar is an atoll-like isolated carbonate platform (Schlern Fm 1; see Fig. 1.3) with a central lagoon surrounded by a marginal reef-rim and platform slope building up from an initially emersive structural high of the Contrin ramp (e.g. Gaetani et al. 1981; Goldhammer and Harris 1989; Egenhoff et al. 1999). Slope sediments of the platform – the slope-facies of the Schlern Fm – interfinger with deep marine deposits of the Buchenstein Fm in the adjacent basins. The platform top was shallow subtidal to shallow intertidal (Gaetani et al. 1981), the adjacent basins reached depths of about 800m to 1000m (Brack and Rieber 1993). The platform top of the atoll-like Latemar platform has a diameter of roundabout 3km and the lagoonal infill consists of at least 720m stacked carbonate deposits with a highly cyclic arrangement (Goldhammer and Harris 1989; Egenhoff et al. 1999; Zühlke et al. 2000; Zühlke et al. 2003).

1.5.1.1 Lagoon-facies

Most of the research has dealt with this cyclic lagoonal interior of the Latemar, the age of which being controversially discussed in literature (e.g. see Hardie and Hinnov 1997; Brack et al. 1997). More recent studies showed that the age of the youngest Latemar strata is Earliest Ladinian and falls within the uppermost *Secedensis* to lowermost *Curionii*-biozone (position of Anisian/Ladinian boundary sensu Brack and Rieber 1993; chronostratigraphy: Mundil et al. 1996; Mundil et al. 2003; bio-/cyclostratigraphy: Brack et al. 1996; Zühlke et al. 2000; Zühlke et al. 2003; Zühlke 2004). As a consequence, the cycle duration of sealevel oscillations causing the microcycle bedding pattern in the lagoon must be significantly shorter than Milankovitch periods (Zühlke et al. 2000, Zühlke et al. 2003; Zühlke 2004). The lagoon-facies can be subdivided in four (Goldhammer and Harris 1989) to six (Egenhoff et al. 1999) units by sequence stratigraphic and/or lithological/microfacial means. This thesis follows the subdivision proposed by Egenhoff et al. (1999; see also Fig. 2.5).

1.5.1.2 Slope-facies

The platform has mainly aggraded during its early evolution (“Lower Edifice”: Gaetani et al. 1981). Goldham-

mer and Harris (1989) observe a rapidly prograding slope during the last stages of platform evolution. This is however not based on direct observations but merely on “the extent of the foreslope” and on the comparison with other (distinctly younger) Ladinian platforms in the Dolomites (Goldhammer and Harris 1989; p.324). Indeed, late stage progradation is a common feature of (Middle to Late) Ladinian platforms in the Dolomites, and might also have happened at Latemar. But the succession preserved at Latemar records Late Anisian to earliest Ladinian times only (see above). In this context, a projection of the evolution of much younger platforms (e.g. Rosengarten/Catinaccio and Schlern/Sciliar) does not seem appropriate. Harris (1994) describes a slope which is not controlled by the high-frequency cyclic rhythms identified in the shallow-water lagoon-facies. However, graded grainstones of the toe-of-slope bypassing the foreslope are reported to be related to times of platform submergence. Slope deposition was mainly episodic and localised with clinofolds originating as slope failures. According to this study, the progradation during the last stage of platform growth is even more pronounced than previously recognised (Harris 1994; p.133).

The studies on the slope of the Latemar by Goldhammer and Harris (1989) and Harris (1994) are in accordance with the so-called “Ladinian model” of Bosellini (1984; see Fig. 2.6A). In this model, the slope prograded over basinal sediments and the lagoonal interior aggraded simultaneously. Continuous and uniform subsidence took place and coeval basins deepened because of their distinctly lower sedimentation rates (Bosellini 1984). This pattern of carbonate sedimentation lead to net deposition on the entire platform-to-basin transition. Hence the slope of the “Ladinian model” is depositional and corresponds to the “slope-apron” facies model sensu Mullins (1983) and Mullins and Cook (1986) where channeling and bypass sedimentation to the toe-of-slope is absent and the deposits on the slope consist of broad, sheet-like debris-flows (see Fig. 2.6B). The original model of Mullins (1983) and Mullins and Cook (1986) requires gentle slopes with an inclination of less than 4°. However, the slopes of most carbonate platforms in the Dolomites reveal steep slopes with clinofolds dipping at 25° to 50° towards the basins.

Another group of authors (De Zanche et al. 1995) reports retrogradation of the platform margin during times of early platform evolution (“Lower Edifice”, equals to Lower Platform Facies/LPF) and aggradation during later

times of platform development. This “anomalous” behaviour – with respect to other platforms in the Dolomites – of the Latemar is thought to be due to the vicinity of the volcanic centre at Predazzo/Monzoni (see Fig. 1.5). According to these authors, the “Lower Edifice” platform growth ended in the Upper Fassanian (i.e. the *Curionii* biozone) where the drowning platform is covered by a “pelagic drape” (De Zanche et al. 1995; p.140). The asymmetry of the platform and its respective margin with steep clinofolds and slump scars on the SW side and more gentle dipping strata on the NW side is attributed by Egenhoff et al. (1999) to windward-leeward effects and different nutrient influx. However, this is contrasting with the concept of a tectonically controlled platform (Doglioni 1984; Bosellini 1989). Emmerich et al. (2000), Emmerich (2001) and Knopp (2002) proposed a more differentiated conception of the slope, where aggradation, progradation and backstepping of the margin can occur simultaneously on the Latemar platform but at different expositions creating different, sometimes even contrasting sedimentological settings.

1.5.1.3 Reef-facies

The reef belt of the Latemar platform has a width of several tens of metres (Gaetani et al. 1981; Goldhammer and Harris 1989) and is mainly made up of microbial crusts (i.e. “*Tubiphytes*” sp.) and syndepositional cements (Harris 1993; Stefani et al. 2001). Recent studies of the reef-facies revealed it to be more complex and diversified than previously assumed (Zamparelli et al. 2001; Emmerich et al. 2002; see Part 2).

The model of Harris (1993) is in tune with previous models of reefs in the Dolomites (e.g. Flügel 1981; Brandner et al. 1991). According to Harris (1993), the reef of the Latemar is laterally consistent and organised in several facies belts – its protagonist “*Tubiphytes*” generally being found in the boundstone facies. Scleractinian corals are rare and form only small mounds on the uppermost foreslope. Hence, the reefal content of the Latemar is generally comparable to other Anisian reefs in the Dolomites, e.g. in the Olango area. The study of Harris (1993) is however based on two outcrops solely, one on the SW side of the Latemar and another one on the western side.

1.5.2 Rosengarten

The Rosengarten is an Anisian/Ladinian carbonate platform with an areal extension of approx. 7x7km. The plat-

form is dissected by several faults, the former outline of the platform top and the thickness of the lagoonal succession is unclear. Bosellini & Stefani (1991) and Maurer (1999, 2000) correlated the lagoonal interior of the Rosengarten at Torri del Vajolet with the lagoonal succession of the Schlern Fm 1 at the neighbouring Schlern platform. At Schlern, lagoonal strata of the Schlern Fm 1 are capped with lava and volcanoclastics indicating a maximum thickness of the pre-volcanic Schlern Fm 1 buildups of approx. 850m (Yose 1991).

The Rosengarten has always been described as a reference model for progradational geometries (Bosellini 1984; Bosellini and Stefani 1991; Bosellini et al. 1996). Bosellini (1984) proposed two main models of carbonate platform progradation in the Dolomites: (1) A “Ladinian” model which is mainly based on the Rosengarten and (2) a “Carnian” model which is mainly based on the Schlern Fm 2 buildups of the eastern Dolomites (see chapter 1.2.1). Both models are characterised by the deepening or shallowing of the respective basin. The distinctive feature of the “Ladinian” model is the more or less horizontal progradation over simultaneously deepening basins due to its slow sedimentation rate. The “Carnian” model describes fast progradation of the carbonate platforms over shallowing basinal strata, i.e. the filling of coeval basins due to a higher rate of sedimentation. Carbonate sedimentation in both models occurs on the entire platform to basin transition, hence their slope is depositional *sensu* Schlager & Ginsburg (1981). Recently, age-diagnostic air-borne tuff layers and biostratigraphically constrained strata in basinal deposits of the Buchenstein Fm were correlated into slope deposits of the Rosengarten platform by Maurer (1999, 2000). This timing of slope progradation and the inferred buildup of the platform top is the base for the numerical basin reverse modelling.

1.5.3 Concarena

Owing to the lack of geometrical models or concepts of facies patterns at the Concarena platform in literature (basic descriptions of platform to basin transitions: Rossetti 1966; Brack 1984) only the established models from the Dolomites were presented in this chapter. Previous research on carbonate “platforms” in this area of the Lombardic Alps mainly focused on the Anisian mudmounds (e.g. Unland 1975; Epting et al. 1976; Brack 1984; Gaetani & Gorza 1989; Falletti & De Donatis 1999).

1.5.4 Thermal history

Some thermal maturity analyses have been carried out on the Late Permian Gröden Fm, but the low density of sample locations in the study area (Buggisch 1978: 2 sample locations; Schulz & Fuchs 1991: 1 sample location; Bielefeld 1998: 3 sample locations) required more detailed sampling. Fission track data has so far only been published on pitchstone glasses from the AVC by Storzer (1970). But sample localities as well as measured ages are widely scattered and it is questionable if ages from the localities are correlatable.

1.6 Discussion and conclusions

1.6.1 Facies, palaeontology, platform architecture and diagenesis

The slope- and reef-facies of the Latemar buildup are far more diversified than previously reported in literature (e.g. Goldhammer and Harris 1989; Harris 1994). The generalised view of the firstly aggrading, then prograding depositional slope at Latemar cannot be confirmed by this study. Contrarily, backstepping of the lagoon by margin failure has mainly been observed during the last stages of platform evolution. Reasons for this behaviour might be accommodation change outpacing a carbonate production rate stretched to its limits. The Concarena platform, in contrast, generally shows initial slight progradation increasing significantly towards late platform development. The regionally observed (W Tethys) relative sea level fall at the Ladinian/Carnian boundary lead in combination with the compartmentalisation of basins and subsequent local development of anoxic conditions to a significant slow-down in accommodation development and decrease in carbonate production.

Latemar’s reef-facies reveals a complex facies pattern, it varies along and across the margin and is rich in encrusting sponges, corals, biogenic crusts and “microproblematica”. Some biota and biocoenoses – e.g. foraminifers (*Abriolina mediterranea*, *Turrioglobina scandonei*) or the “*Tubiphytes*” *multisiphonatus*-biocoenosis - have not been described in the Dolomites before. Biostratigraphic evidence from the uppermost reef-facies confirms existing models of a mainly Anisian age of the outcropping platform. Detailed microfacies and palaeontological investigations at the margins of Latemar (Dolomites) and Concarena (Lombardic Alps) show the importance of “*Tubiphytes*” *multisiphonatus* for the organisation of the reefal communities. Apart from previous findings at Aggtelek (Hungary; Scholz 1972), Hy-

dra (Greece; Schäfer & Senowbari-Daryan 1982, 1983) and Latemar (Italy; this study) the Concarena was identified as the fourth locality where this enigmatic micro-problematicum occurs. Contrastingly to all other locations, “*Tubiphytes*” *multisiphonatus* mounds at Concarena are also part of the reef front to uppermost slope. Additionally, the size and abundance of “*Tubiphytes*” *multisiphonatus* bioconstructions at Concarena exceed all previously described localities such that “*Tubiphytes*” *multisiphonatus* is one of the main constituents of the reefal margin. The so far restricted occurrence of this biota in the central Tethys area might indicate that specific environmental conditions were required for the growth of “*Tubiphytes*” *multisiphonatus*.

The Latemar slope reveals different depositional characteristics at the same time and at different locations. Additionally, a turnover from slope apron via an erosional slope towards a base-of-slope apron was proved on the NE slope (Cresta De Do Peniola, see chapter 2.4.5). Hence it is impossible to establish a generalising model for the entire platform evolution and all expositions. Instead, several trends are visible at Latemar. The slope of the Latemar is strongly asymmetric; steeply dipping clinofolds and erosional characteristics on the SE side are contrasted by more gentle dipping clinofolds and depositional characteristics on the NW side. As the SE side of the Latemar is very close to the Stava Line-Cima Bocche Anticline (Doglioni 1983, 1984), this asymmetry is most likely caused by different rates in tectonic subsidence on the respective sides. Furthermore, it is obvious that sudden tectonic movements along this tectonic line did cause peaks in tectonic subsidence and did consequently trigger giant collapses at the adjacent slope (De Zanche et al. 1995). Retreat of platforms due to tectonic collapses and/or earthquake shocks is a well documented feature of many Tethydan platforms during the Jurassic rifting stages (e.g. Bernoulli 1964; Bosellini 1973; Castellarin et al. 1978; Mutti et al. 1984). The tectonic influence on the slope evolution is further proven by the coeval neptunian dyke in the slope-facies at Cresta De Do Peniola and fissures in the slope NE of Schenon filled with pelicycypods (Brack et al. 1996).

In the case of the Latemar, variations in tectonic subsidence have been the main allocyclic factors for slope evolution. Other parameters like wind and wave directions seem insignificant and/or are being overprinted by variations in tectonic subsidence. Hence, the deduction of a palaeo wind and/or -wave direction as done by Egenhoff

et al. (1999) is not possible. Even more so as the directions were derived from analyses of small restricted areas at the platform top only (Marmolada: Blendinger 1986; Latemar: Egenhoff et al. 1999). The pronounced asymmetry of many platforms in the Dolomites seems to be entirely related to responses to different tectonic settings (Bosellini 1989).

Controlling factors for the development of the carbonate platforms differ strongly from lagoon to slope. Whereas the lagoon is chiefly controlled by non-orbital and orbitally forced small scale sealevel oscillations, the slope reveals to be largely independent from these high-frequency accommodation changes of the platform top (see also Bosellini 1989). The high frequency sealevel oscillations recorded by the platform top are not preserved or recorded by neither the platform slope nor the reef (see Harris 1994). In addition, the reef has been submerged throughout the entire time of platform evolution. This fact rules out sealevel lowstands as causes for the repeated margin collapses.

The slope is a sedimentary environment of episodic and catastrophic events (Coniglio & Dix 1992) destroying any evidence of the accommodation changes as indicated by the lagoonal interior. Therefore, autocyclic processes are of even greater importance for the slope development than for the lagoonal evolution. Cycles of sedimentation-oversteepening-collapse at a platform-wide scale play an important role during slope formation (see also Crevello & Schlager 1980; Mullins et al. 1986). Autocyclic processes such as Blendingers (2001) interpretation of cementation driven self-fracturing of slope sediments were not observed. Fracturing of carbonate sediments took place through movements during re-sedimentation. All blocks from metre to millimetre scale at Latemar are the result of gravity driven brecciation. However, syndepositional cements are locally abundant; but their importance is then restricted to small areas only like in the “*Tubiphytes*” *multisiphonatus* mounds at Erzlahn or in the talus at Schenon. Massive syndepositional cementation as a key factor during the build-up of the margin as assumed by Russo et al. (2000) and Stefani et al. (2001) can be excluded.

The comparison of the two platforms lead to the identification of several boundary conditions for massive early cementation (MEC): (1) Abundant open and connected cavities supplied by e.g. rigid frameworks of reef building organisms or inter-particle space of talus breccias. (2) Effective fluid flow mechanisms like wave activity

in combination with matching platform margin morphology (walled reefs). (3) Low rates of accommodation increase prolonging the time interval of marine phreatic diagenesis (i.e. palaeo water depths ranging from subtidal slope settings to intertidal lagoonal environments).

Owing to the nature of Anisian to Early Ladinian buildups (low growing, encrusting organisms being the main reefal constructor guild and mound-like morphology), MEC is mainly absent in these. Botryoids and large isopachous crusts of radiaxial-fibrous cements are much more likely to develop in the voids of Late Ladinian/Carnian rimmed platforms. The reefal margins of the latter buildups are made up of rigid bioconstructions (e.g. scleractinians) and walled, wave resistant morphology enabling effective fluid flow. According to Ginsburg et al. (1971), James et al. (1976) and Marshall (1986) only seaward margins of walled reefs show MEC related to environmental factors such as high-energy conditions supplying effective pumping of marine fluids. Isolation of primary voids through encrusting organisms and subsequent infill with peloids inhibits MEC.

Accommodation increase is probably the most important boundary condition for MEC as the time interval available for marine phreatic cementation is crucial. If the succession passes quickly through the marine phreatic window primary cavities and voids are much more likely to contain a small amount of cement only. The excellent porosity of many modern hydrocarbon reservoirs in carbonates have been tied to basins during high sea level undergoing rapid subsidence (Moore & Haydari 1993) leaving insufficient time for cementation. It is, however, more precise to link this diagenetic evolution of porosity-prone, MEC-poor platforms to periods of fast sea level rise and/or rapid subsidence (i.e. high rates of accommodation increase). Nevertheless, a certain amount of cementation is necessary in order to counterbalance compaction and to preserve porosity. Leaving burial cementation aside, porosity seems best to be preserved in a certain window of accommodation increase balanced by carbonate production allowing enough cementation to stabilise the platform. Consequently, the link between accommodation change and MEC allows constraining this early diagenetic development to platform types with certain geometries: (1) Aggradational or retrogradational

platforms are unlikely to develop features of MEC. (2) Platforms with progradational characteristics are prone to MEC.

This hypothesis is confirmed if it is tested against other Triassic platforms in the western Tethys area. Boni et al. (1994) and Climaco et al. (1997) describe strikingly similar features from “pathologically prograding” (Bosellini 1989) Upper Triassic platforms of Calabria (Southern Italy). Like at Concarena, the last stages of platform development are governed by slow-down in accommodation increase in combination with anoxic conditions in the basins. Strong similarities also exist with platforms of the Northern Calcareous Alps (Brandner & Resch 1981; Zeeh et al. 1995) where MEC is always linked to progradation and walled reefs.

1.6.2 Basin and platform evolution

The comparison between burial history and subsidence development models of the Rosengarten and Latemar Middle Triassic carbonate platforms allows to constrain quantified platform evolution. Both platforms show similar subsidence patterns during equivalent times of their evolution as unraveled with numerical basin reverse modelling. Hence, the coexistence of structural highs and lows (facies heteropy) in the study area is mainly owed to a pre-platform tectonic development. Differential subsidence ceases during Late Anisian times. The last stage of platform development of the Rosengarten slope where rapid progradation occurs are not recorded neither by the lagoonal succession nor the slope at Latemar. Total subsidence reaches values of 800-850m/Ma during the first stage of aggradational platform evolution at both platforms. These values surpass previous estimates on carbonate production from the Dolomites (Dürrenstein: 230-375m/Ma, Schlager et al. 1991; Rosengarten: 200m/ma, Maurer 1999, 2000) and other areas of the world (see Fig. 1.13). Both platforms – Latemar and Rosengarten – reached the production rates of (sub)recent carbonate platforms (Enos 1991; Schlager 2000; see also Fig. 1.13). As both platforms successfully keep up with this subsidence peak, it is evident that the carbonate factory must have completely recovered from the P/T faunal crisis – despite the “Anisian characteristics” of the reef-facies at Latemar.

Fig. 1.13 (previous page) Carbonate production rates from various locations and periods. x-axis: carbonate production in m/Ma (N.B.: logarithmic plot of x-axis). The calculated values from the Latemar and Rosengarten are minimum vertical carbonate accumulation rates. True production rates might well be higher due to re-deposition and bio-erosion of sediment.

Basin reverse modelling results indicate that the two different intervals of platform evolution at Rosengarten originate from a temporal change in total subsidence. Spatial variations in total subsidence along the 6km transect are insignificant. When total subsidence rates drop to 200-100m/Ma, rapid platform progradation is initiated. The short-spanned subsidence peak recorded at both platforms is closely linked to tectonic movements along the neighbouring Cima Bocche Anticline-Stava Line (approx. 10km to the SE; see Fig. 1.2). The stop in subsidence at Rosengarten is possibly linked to the inflation of the magmatic chamber at Predazzo/Monzoni. Stratigraphic forward modelling quantifies the sediment volumes and influence of sea level oscillations. In order to replicate platform architecture, constant carbonate production rates between 900 and 1000m/Ma – increasing from periplat-form environments to the slope – had to be assumed throughout the existence (< 5Ma) of the Rosengarten platform. Slope progradation from N to S is mimicked by the porosity evolution of the sediment package below the slope (sandstones and shales).

Vitrinite reflectance and apatite fission track analyses are integrated into basin modelling in order to narrow down uncertainties in the modelled regional burial and thermal history. Vitrinite reflectance (VR_r) values in the basal strata (outcrop samples from organic-rich sandstones in the Permian Gröden Fm, marls and limestones of the Permian Bellerophon Fm and Middle Triassic Morbiac Fm) vary between 0.4% VR_r and 0.7% VR_r . This low thermal maturity implies that maximum palaeo temperatures did not exceed 110°C and that eroded strata having overlain present-day topography must have been less than 1100m thick. Maximum temperatures are reached during the Early/Middle Triassic, when high heat flows prevail. Local anomalies in vitrinite reflectance of up to 1.1% VR_r in the SE indicate that the thermal influence of the Predazzo/Monzoni volcanic event (Late Ladinian) neighbouring the Rosengarten area is limited and restricted to its nearest vicinity. The modelled burial history is confirmed by apatite fission track analyses carried out on the Permian Atesina Volcanic Complex (Bozener Quarzporphyr; AVC), the Permian Gröden Fm and the Lower Triassic Werfen Fm. Modelled t-T paths suggest a relatively long burial from Upper Permian times until the end of the Cretaceous and a fast exhumation from the Eocene/Oligocene onward. The area close to the Trodena line and to the volcanic centre of Predazzo/Monzoni has undergone a higher heat flow pulse during

the Late Ladinian and has possibly been buried at shallower levels than the area at Rosengarten. This underlines the localised thermal influence of the Late Ladinian vulcano-thermal event of Predazzo/Monzoni.

Calibration of thermal modelling with vitrinite reflectance and FT-measurements demonstrates that Neogene flysch or molasse-type sediments above present day topography as inferred from other Alpine basins (Massari et al. 1986) did not affect temperature and burial history significantly, i.e. have been either very thin or not present at all. The low thickness of eroded stratigraphy above the Rosengarten transect contrasts with the regional coalification pattern of the eastern Dolomites (unpublished results mainly on Alta Badia area and Sella, see Fig. 1.2). The higher thermal maturity in this area requires either a significantly higher heat flow or higher thicknesses for the eroded Cretaceous overburden. Whereas the latest cooling phase of the eastern Dolomites seems to be similar to that of the Rosengarten area, higher thermal maturity in the eastern and central Dolomites further underline the significance of the Trento platform for the thermal evolution of the western Dolomites.

The time scale set up by Mundil et al. (1996) for the basinal Buchenstein Fm is marginally in accordance with the measured ages from Latemar (Mundil et al. 2003). The duration of the *Secedensis*-zone as derived from the Buchenstein Fm does not allow for a longer microcycle duration than 1.97ka. Numerical basin reverse modelling showed that subsidence patterns of the second stage of platform evolution at Rosengarten are reversed if the *Secedensis*-zone is adapted to a microcycle duration of 4.2ka as derived from time series analysis on the cyclic succession at Latemar (Zühlke et al. 2003; Zühlke 2004). Also, this subsidence pattern would imply that this rapid progradation is not chiefly triggered by a slow-down in total subsidence. However, the *Secedensis*-zone records mainly aggradation followed by rapid progradation from the *Curionii*-zone on. If a yet undetermined factor would have caused progradation in times with an increase in accommodation development (from *Secedensis*- to *Curionii*-zone), the same or another factor must have caused aggradation/hindered progradation in times with a significant slow-down in accommodation development (from *Reitzi*- to *Secedensis*-zone). This is contradictory and seems an unlikely case. Therefore, the correlation of the two time scales for Schlern Fm 1 platform development combined with subsidence modelling results

points out that a maximum microcycle duration of 1.97ka or less for the cyclic succession at Latemar is a more likely scenario.

1.6.3 Integration of results

Both approaches – facies and subsidence analysis – to assess the development of the Rosengarten and Latemar platforms identified the same controlling parameters. Total subsidence is the most important factor for the evolution of slope architecture. The platform top however is additionally governed by sea level fluctuations. The overall platform architecture is mirrored in the subsidence patterns derived from numerical basin reverse modelling. Evolution of reefal fauna seems to be an important factor from a facies point of view but its influence on carbonate productivity is difficult to quantify. On the contrary, constant carbonate production rates from the beginning on at Rosengarten provide sufficient sediment for the observed rapid progradation in its second stage of platform evolution.

The effect of tectonics is visible in slope architecture and subsidence modelling results on various scales: (1) strike-slip tectonics are responsible for the subsidence pulse at the verge of the *Reitzi*-zone, (2) listric normal faulting possibly triggered by earthquakes creates accommodation space on the slope and is accompanied by slumping or collapse of the margin, (3) inflation of magma chambers like at Predazzo/Monzoni promotes progradation through decrease in subsidence/accommodation development.

1.7 Outlook

The SW Dolomites are a key area for the assessment of pre-Alpidic basin evolution. The rigid plate of the Atesina Volcanic Complex/Bozener Quarzporphyr (AVC) and all overlying strata preserved today have escaped extensive overthrusting and folding. Hence, the SW Dolomites provide a view onto almost 300Ma basin history. Further studies will have to concentrate on the regional and local variations in thermal maturity by focusing on vitrinites in sandstones of the Late Permian Gröden Fm. This allows to further constrain uncertainties in existing models. Burial history can subsequently be refined by analysing fission tracks in apatites from the Early Permian AVC and the most prolific horizons within the Early Triassic Werfen Fm. Due to the unique situation of a long burial at constant temperatures of 60°C to 80°C from 150/130Ma to 20/10Ma, the difference in chemi-

cal composition of the apatites is well visible already in the bimodal distribution of track lengths. Whereas chlorine-rich apatites show older ages, fluorine-rich apatites show distinctly younger ages. The AVC of the SW Dolomites might also provide an unequalled study area for the assessment of fission tracks in apatites in general.

In order to homogenise basin-wide time scales, further dating of laterally correlatable physical surfaces is needed. The present situation with different time scales measured at different localities with different methods is unsatisfactory despite the density of published data. Chronological methods applied to the age determination of e.g. ash-layers should in the future be identical. Additionally, future chronological studies will have to consider different diagenetic/thermal histories at the respective sample localities.

Further volcanic ash-layers at Latemar await dating by more precise methods. This might enable the fit of trend lines through its cyclic succession for the determination of min-max sedimentation rates. Additional spectral/time series analyses on the cyclic succession will then allow to assess the duration of the microcycles more precisely. The main goal of future time series analysis of the Middle Triassic in Dolomites must be the integration of spectral analyses from basinal and platform settings. The dogma of the presence of typical Milankovitch-cyclicities within certain power spectra should rather be avoided in order to explain significant frequencies also in lower periods.

The most promising prospect probably provides the planned combination with the work carried out on the Lombardic Alps by M. Seeling. The supposed increase in productivity of the carbonate factory after the faunal crisis at the end of the Permian can be assessed by simulating carbonate production rates at three platforms with different margin configurations: (1) The Early Anisian Dosso dei Morti/Camorelli buildup (Lombardic Alps): mud-mound; (2) the Late Anisian Latemar platform (Dolomites): typical “Anisian” reef with low-growing, encrusting sessile organisms; (3) the Late Ladinian/Early Carnian Concarena/Pora platform: typical “Carnian” walled reef with abundant scleractinians. This synthesis might offer the unique possibility to combine facies and palaeontological studies on reef development with sequence stratigraphic forward modelling in order to quantify carbonate production rates.

PART 2

The reefal margin and slope of a Middle Triassic carbonate platform: the Latemar (Dolomites, Italy)

Abstract

The Latemar is a mainly aggrading platform, but shows repeated backstepping during its development. The behaviour of the slope does not reflect accommodation changes and lateral consistencies of the lagoonal interior, it contemporaneously reveals different, even contrasting depositional characteristics. The slope of the late stage platform evolution corresponds at least partially to the base-of-slope apron model. Controlling factors on slope evolution have been of tectonic (proximity of the Stava Line) and autocyclic (repeated oversteepening) nature. Other factors have been insignificant and/or overprinted.

The reef-facies reveals a complex facies pattern, it varies along and across the margin and is rich in encrusting sponges, corals, biogenic crusts and “microproblematika”. Some biota and biocoenoses - e.g. foraminifers (*Abriolina mediterranea*, *Turriglomina scandonei*) or the “*Tubiphytes*” *multisiphonatus*-biocoenosis - have not been described in the Dolomites before. Biostratigraphic evidence from the uppermost reef-facies confirms existing models of a mainly Anisian age of the outcropping platform.

2.1 Introduction

Since von Richthofen’s discovery of the organic origin of the Triassic carbonate masses (von Richthofen 1860), the carbonate reefs in the Dolomites have been a major study area for carbonate platforms and especially for the research on fossil reefal communities. Owing to the dolomitization of most of the carbonate platforms in the Dolomites, many studies of reefal biocoenoses focused on the so-called “Cipit” boulders; these are reef talus blocks having escaped dolomitization because of erosion and subsequent mass transport to allochthonous positions on toe-of-slope and basin margin areas. Cipit boulders document the composition of the Anisian to Carnian reefs in the Dolomites (e.g. Cuif 1974; Fürsich and Wendt 1977; Biddle 1981; Fois 1982; Brandner et al. 1991; Flügel 1991, Senowbari-Daryan et al. 1993; Russo et al. 1998). Only a few in-situ reefs in the Dolomites have been studied so far (Latemar: Harris 1993;

Marmolada: Blendinger 1986; Mt. Cenera: Fois and Gaetani 1984; complete review on Triassic reefs with a compendium of references in Flügel 2002).

Since the main evidence for the palaeontological composition of Triassic reefs is represented by allochthonous Cipit talus blocks, the study of reefs and platforms in the Dolomites has also focused on carbonate slopes. Many research since von Richthofen (1860) has been carried out on facies patterns and geometries of the platform-to-basin transitions (e.g. Mojsisovics 1879; Hummel 1928; Pia 1937; Leonardi 1967; Bosellini and Rossi 1974; Gaetani et al. 1981; Bosellini 1984; Blendinger 1986; Bosellini and Stefani 1991; Bosellini et al. 1996; Harris 1994; Maurer 2000).

Owing to its excellent outcrops, largely absent dolomitisation and early Middle Triassic (Anisian) setting, the Latemar is ideally suited for the study of a reefal community and carbonate platform after the faunal crisis at the Palaeozoic/Mesozoic boundary. The base for this study are new, detailed investigations on the lithofacies and geometries of the reef and slope and their relation to the growth characteristics of the platform interior as well as investigations on the reef biocoenoses. The aim was (1) to identify the processes controlling slope and ultimately platform development, (2) to investigate the possible evolution of biocoenoses in time and their distribution within the reef and (3) to assess an Anisian/Ladinian age of the reefal biocoenoses as inferred from the chronostratigraphic framework of the

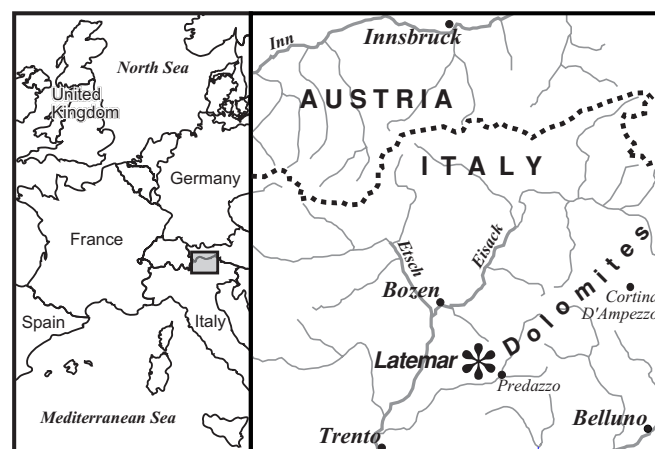


Fig. 2.1A (left) General position of the surroundings of the study area within western Europe (grey rectangle).

Fig. 2.1B (right) Detailed position of the study area within the Southern Alps; the Latemar is marked by an asterisk.

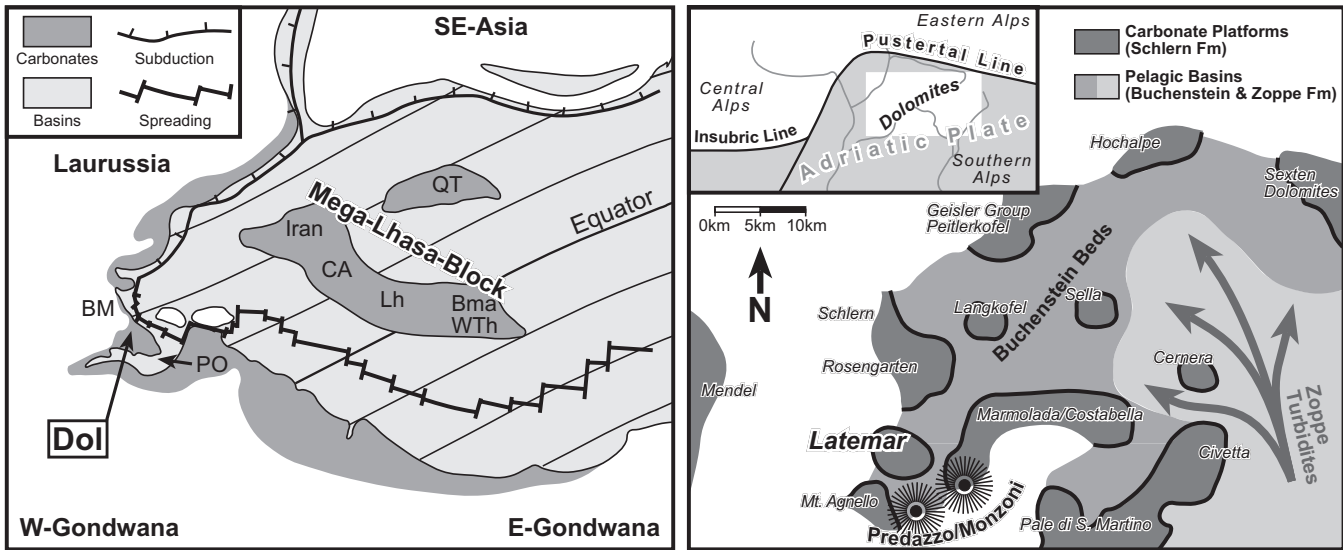


Fig. 2.2A (left) Palaeogeographic map of the western Tethys during the Middle Triassic (Dercourt et al. 1993; Dercourt et al. 2000). Abbreviations: Dol: Dolomites, PO: Pindos-Olonos-Trough, BM: Bohemian Massif, CA: Central Afghanistan, Lh: Lhasa, Bma/WTh: Burma/Western Thailand, QT: Qiantang-Terrane. Legend of map units/symbols in the upper left corner.

Fig. 2.2B (right) Schematic palaeogeographic map of the western Dolomites during the Late Anisian/Early Ladinian (De Zanche and Farabegoli 1988; De Zanche 1990). Legend of lithostratigraphic units in the upper right corner, influx of turbidites into pelagic basins marked by large arrows. Inset: generalised map of the Southern Alps with an indication of major tectonic lines, white rectangle marks the Dolomites.

lagoon. The biotic content of the margin was studied at in-situ reef-facies outcrops as well as in reefal blocks of the slope.

2.2 Geological setting

The carbonate platform of the Latemar is located in the southwestern part of the Dolomites, Northern Italy (see Figs. 2.1) forming a small mountain range west of Bozen/Bolzano with its longest extension from SE to NW of approximately 5km. Primary lithofacies distributions and biocoenoses are very well visible and preserved in the so-called “Latemar limestone” (Gaetani et al. 1981).

Throughout the Triassic the Dolomites have been situated on the Adriatic Plate. This area between former Laurussia and Gondwana represented the eastern margin of a highly dismembered passive continental margin with transpressive-transpressive tectonics and mixed carbonate-clastic sedimentation (Blendinger 1985; Doglioni 1987; Dercourt et al. 1993; Dercourt et al. 2000; see Figs. 2.2).

Few studies on reefs in the Dolomites (Fois and Gaetani 1984; Senowbari-Daryan et al. 1993) have investigated the Anisian recovery of carbonate producing organisms from the mass extinction at the end of the Permian where

62% of marine invertebrate families (McKinney 1985) and up to 96% of species (Raup 1979) had been extinguished. All previous studies observe a recovery during the Anisian when many reefal biota (calcsponges, calcareous algae, few microproblematica and few scleractinians) occurred for the first time in the Dolomites again since the P/T crisis. This was confirmed by recent literature (Twitchett 1999) reporting a gradual re-appearance of trace fossils throughout the Lower Triassic of the Dolomites (Werfen Fm) and a complete recovery already in the Uppermost Scythian (top of Werfen Fm). Furthermore, studies from other Triassic reefal locations of the world also indicate a recovery of calci-microbial buildups during the Anisian (for complete discussion and references refer to Flügel 2002).

First carbonate ramps in the Dolomites did not develop until the Early Anisian (Sarl Fm; De Zanche and Farabegoli 1988; Zühlke 2000). The Middle to Late Anisian Dont Fm contained simple reefal mounds only (Fois and Gaetani 1984). Carbonate ramps of Late Anisian times (e.g. Contrin Fm; see Fig. 2.3) were primarily made up of microbial carbonates with very subordinate frame-building organisms only. True frame-builders - i.e. scleractinian corals - were still suffering from the severe

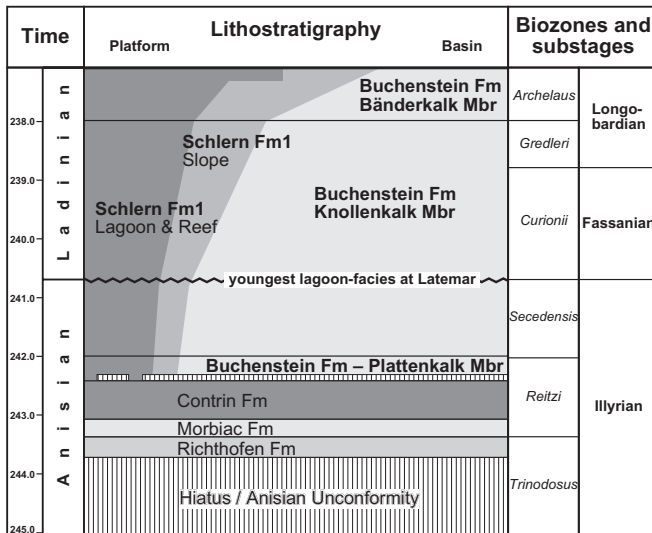


Fig. 2.3 Anisian/Ladinian lithostratigraphic succession and platform-to-basin relationships of the southeastern Dolomites. Formations below the Schlern Fm record a transition from terrestrial environments to carbonate ramp settings. Younger carbonate platforms - e.g. like the neighbouring Rosengarten/Catinaccio (see Fig. 2.2b) - show progradation mainly in the *Gredleri* and *Archelaus* biozone (Maurer 2000). The preserved lagoonal succession at Latemar however reaches only until the basal *Secedensis* zone (as marked by the zig-zag-line; Mundil et al. 2003, Zühlke et al. 2003; see also Fig. 2.5). Timescale after Mundil et al. (1996, 2003) and Lehrmann et al. (2002). Biozones, substages and position of Anisian/Ladinian boundary after Brack and Rieber (1993).

faunal crisis at the end of the Permian (scleractinian “reef gap” in the Early Triassic; Flügel and Stanley 1984; Flügel 1994).

Another reason for the Anisian onset of platform development in the Dolomites may lie within the regional lowstand during the Early Triassic (Scythian until earliest Anisian) and clastic input from the south hindering platform growth. Subaerial exposure (Anisian unconformity, see Fig. 2.3) in the westernmost Dolomites restricted carbonate ramps to the central and eastern Dolomites. In the area of the western Dolomites, it took until the Late Anisian when flooding of subaerial structural highs created sufficient accommodation space for carbonate ramp and later platform development (De Zanche and Farabegoli 1988; Rüffer and Zühlke 1995). Carbonate platforms with highly diversified reefs did not exist prior to the Ladinian (Schlern Fm 1; sensu Brandner 1991; see Fig. 2.3). From the Late Anisian on into the Late Ladinian, a considerable submarine relief with some

emersive parts prevailed in the area of the Dolomites. Middle Anisian transpressive-transpressive tectonics had dismembered the continental shelf in structural highs and lows creating strong regional differences in facies (i.e. facies heteropy; Bechstädt and Brandner 1970; Blendinger 1985; Doglioni 1987; Zühlke 2000). Subsequently in Late Anisian to Early Ladinian times, deepmarine stagnant basins with finegrained chert- and organic-rich sediments (Moena Fm and Buchenstein Fm; see Figs. 2.2b and 2.3) existed alongside shallowmarine subtidal carbonate ramps and platforms (Contrin Fm and Schlern Fm 1). Structural highs of the dismembered carbonate ramp (Contrin Fm) were the nuclei of the Schlern Fm platforms in the Late Anisian (Masetti and Neri 1980; Gaetani et al. 1981).

Evolution of most of the adjacent platforms like Schlern, Rosengarten and Monte Agnello and probably also the evolution of the Latemar atoll ended with the extrusion of the Longobardian Wengen Fm volcanics. Hence, the proximity of the volcanic centre at Predazzo/Monzoni played a crucial role for the platform development in the SW Dolomites (see Fig. 2.2b). The volcanic centre at Predazzo/Monzoni did control regional subsidence and accommodation development with deep reaching faults (Doglioni 1984) and magmatic updoming as well as ter-

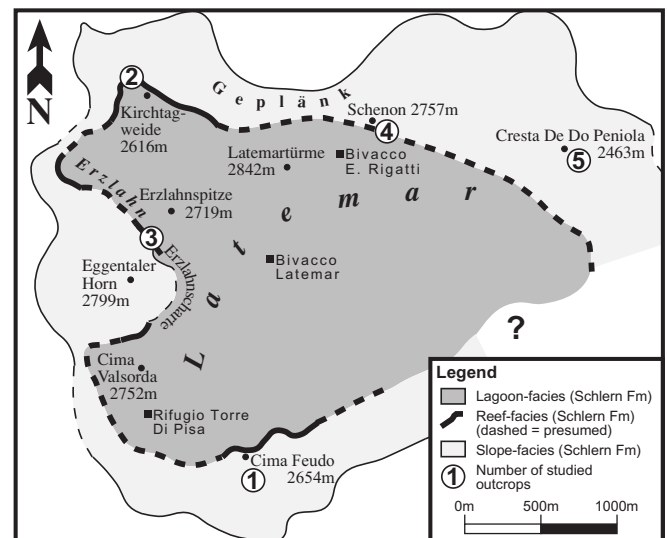


Fig. 2.4 Schematic geologic map of the Latemar; legend of map units in the lower right corner; numbers from 1 to 5 refer to outcrops described in this study (1: Cima Feudo, 2: Kirchtageweide, 3: Erzlahnscharte, 4: Schenon, 5: Cresta De Do Peniola).

minate platform growth with phreatic eruptions (e.g. Viel 1979a; Viel 1979b; De Zanche et al. 1995).

2.3 Previous research at Latemar

The Latemar is an atoll-like isolated carbonate platform (Schlern Fm 1; see Fig. 2.3) with a central lagoon surrounded by a marginal reef-rim and platform slope building up from an initially emersive structural high of the Contrin ramp (e.g. Gaetani et al. 1981; Goldhammer and Harris 1989; Egenhoff et al. 1999). Slope sediments of the platform - the slope-facies of the Schlern Fm - inter-finger with deep marine deposits of the Buchenstein Fm in the adjacent basins. The platform top was shallow subtidal to shallow intertidal (Gaetani et al. 1981), the adjacent basins reached depths of about 800m to 1000m (Brack and Rieber 1993). The platform top of the atoll-

like Latemar platform has a diameter of roundabout 3km (see Fig. 2.4) and the lagoonal infill consists of at least 720m stacked carbonate deposits with a highly cyclic arrangement (Goldhammer and Harris 1989; Egenhoff et al. 1999; Zühlke et al. 2000; Zühlke et al. 2003).

2.3.1 Lagoon-facies

Most of the research has dealt with this cyclic lagoonal interior of the Latemar, the age of which being controversially discussed in literature (e.g. see Hardie and Hinnov 1997; Brack et al. 1997). More recent studies showed that the age of the youngest Latemar strata is Earliest Ladinian and falls within the uppermost *Secedensis* to lowermost *Curionii* biozone (position of Anisian/Ladinian boundary sensu Brack and Rieber 1993; chronostratigraphy: Mundil et al. 1996; Mundil et

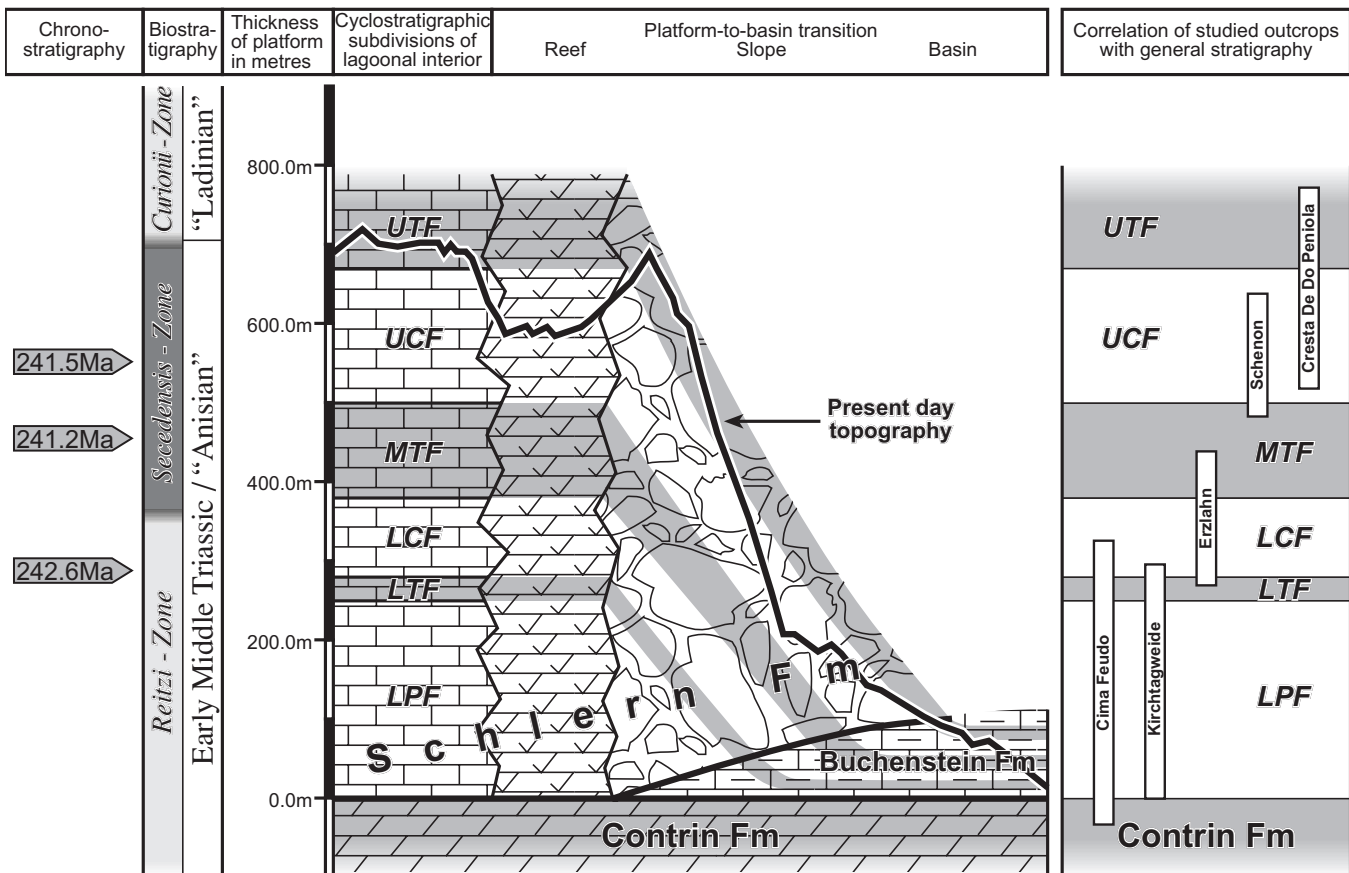


Fig. 2.5 Stratigraphic succession of the Latemar and correlation of studied outcrops; chronostratigraphy of the Latemar succession after Mundil et al. (2003); biostratigraphy and position of Anisian/Ladinian boundary after Brack and Rieber (1993); cyclostratigraphic subdivision of the lagoonal interior after Egenhoff et al. (1999); platform-to-basin transition in the middle of the figure not to scale, vertically exaggerated; correlation of studied outcrops at righthand side. Abbreviations are as follows and are being used in this study accordingly: LPF: Lower Platform Facies, LTF: Lower Tepee Facies, LCF: Lower Cyclic Facies, MTF: Middle Tepee Facies, UCF: Upper Cyclic Facies, UTF: Upper Tepee Facies.

al. 2003; bio-/cyclostratigraphy: Brack et al. 1996; Zühlke et al. 2000; Zühlke et al. 2003). As a consequence, the cycle duration of sea level oscillations causing the rhythmic bedding pattern in the lagoon must be significantly shorter than Milankovitch periods (Zühlke et al. 2000, Zühlke et al. 2003).

The lagoon-facies can be subdivided in four (Goldhammer and Harris 1989) to six (Egenhoff et al. 1999) units by sequence stratigraphic and/or lithological/microfacial means. This paper follows the subdivision proposed by Egenhoff et al. (1999; see Fig. 2.5).

2.3.2 Slope-facies

The platform has mainly aggraded during its early evolution (“Lower Edifice”: Gaetani et al. 1981). Goldhammer and Harris (1989) observe a rapidly prograding slope during the last stages of platform evolution (see Fig. 6a). This is however not based on direct observations but merely on “the extent of the foreslope” and on the comparison with other (distinctly younger) Ladinian platforms in the Dolomites (Goldhammer and Harris 1989; p.324). Indeed, late stage progradation is a common feature of (Middle to Late) Ladinian platforms in the Dolomites, and might also have happened at Latemar. But the succession preserved at Latemar records Late Anisian to earliest Ladinian times only (see above and Fig. 2.5). In this context, a comparison with much younger platforms (e.g. Rosengarten/Catinaccio and Schlern/Sciliar) does not seem appropriate. Harris (1994) describes a slope

which is not controlled by the high-frequency cyclic rhythms identified in the shallow-water lagoon-facies. However, graded grainstones of the toe-of-slope bypassing the foreslope are reported to be related to times of platform submergence. Slope deposition was mainly episodic and localised with clinofolds originating as slope failures. According to this study, the progradation during the last stage of platform growth is even more pronounced than previously recognised (Harris 1994; p.133).

The studies on the slope of the Latemar by Goldhammer and Harris (1989) and Harris (1994) are in accordance with the so-called “Ladinian model” of Bosellini (1984; see Fig. 2.6A). In this model, the slope prograded over basinal sediments and the lagoonal interior aggraded simultaneously. Continuous and uniform subsidence took place and coeval basins deepened because of their distinctly lower sedimentation rates (Bosellini 1984). This pattern of carbonate sedimentation lead to net deposition on the entire platform-to-basin transition. Hence the slope of the “Ladinian model” is depositional and corresponds to the “slope-apron” facies model sensu Mullins (1983) and Mullins and Cook (1986) where channeling and bypass sedimentation to the toe-of-slope is absent and the deposits on the slope consist of broad, sheet-like debris-flows (see Fig. 2.6B). The original model of Mullins (1983) and Mullins and Cook (1986) requires gentle slopes with an inclination of less than 4°. However, the slopes of most carbonate platforms in the Do-

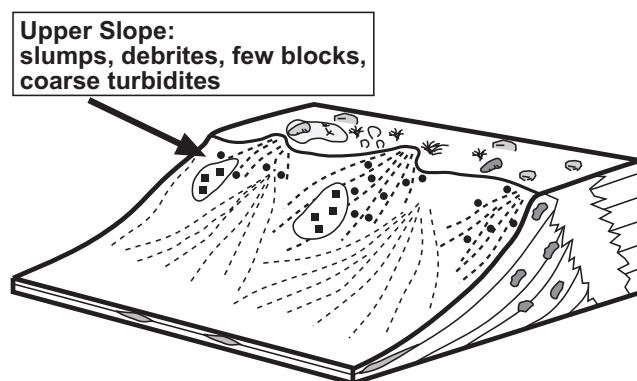
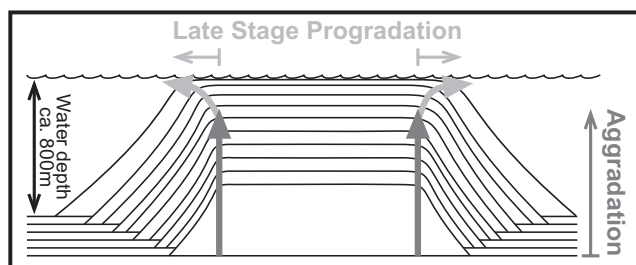


Fig. 2.6A (left) Schematic cross section of the Latemar platform according to Goldhammer and Harris (1989) using Bosellini’s (1984) “Ladinian model” (vertically exaggerated, not to scale). The carbonate platform is mainly aggrading vertically until its last stage of evolution where rapid progradation occurs, e.g. similar to the adjacent Rosengarten platform (for more details see Bosellini and Stefani 1991; Maurer 2000). Flat lying strata in the basin are deposits of the coeval Buchenstein Fm.

Fig. 2.6B (right) Schematic cross section through a carbonate slope corresponding to the type “slope-apron” (vertically exaggerated, not to scale; sensu Mullins, 1983, and Mullins and Cook, 1986). Squares are blocks in slumps, small circles blocks in debrites. Reef and lagoon are roughly sketched.

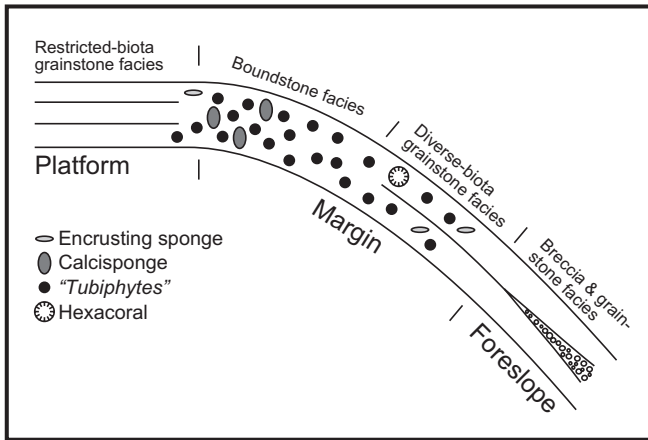


Fig. 2.7 Reef model of the Latemar margin according to Harris (1993; p.39) illustrating topography and biological zonation.

lomites reveal steep slopes with clinofolds dipping at 25° to 50° towards the basins.

Another group of authors (De Zanche et al. 1995) reports retrogradation of the platform margin during times of early platform evolution (“Lower Edifice”, equals to Lower Platform Facies, LPF, in Fig. 2.5) and aggradation during later times of platform development. This “anomalous” behaviour - with respect to other platforms in the Dolomites - of the Latemar is thought to be due to the vicinity of the volcanic centre at Predazzo/Monzoni (see Fig. 2.2). According to these authors, the “Lower Edifice” platform growth ended in the Upper Fassanian (i.e. the *Curionii* biozone) where the drowning platform is covered by a “pelagic drape” (De Zanche et al. 1995; p.140). The asymmetry of the platform and its respective margin with steep clinofolds and slump scars on the SW side and more gentle dipping strata on the NW side is attributed by Egenhoff et al. (1999) to windward-leeward effects and different nutrient influx. However, this is contrasting with the concept of a tectonically controlled platform (Doglioni 1984; Bosellini 1989). Emmerich et al. (2000), Emmerich (2001) and Knopp (2002) proposed a more differentiated conception of the slope, where aggradation, progradation and backstepping

of the margin can occur simultaneously on the Latemar platform but at different expositions creating different, sometimes even contrasting sedimentological settings.

2.3.3 Reef-facies

The reef belt of the Latemar platform has a width of several tens of metres (Gaetani et al. 1981; Goldhammer and Harris 1989) and is mainly made up of microbial crusts (i.e. “*Tubiphytes*” sp.) and syndepositional cements (Harris 1993; Stefani et al. 2001). Recent studies of the reef-facies revealed it to be more complex and diversified than previously assumed (Zamparelli et al. 2001; Emmerich et al. 2002).

The model of Harris (1993) is in tune with previous models of reefs in the Dolomites (e.g. Flügel 1981; Brandner et al. 1991). According to Harris (1993) is the reef of the Latemar laterally consistent and organised in several facies belts (Fig. 2.7) - its protagonist “*Tubiphytes*” generally being found in the boundstone facies. Scleractinian corals are rare and form only small mounds on the uppermost foreslope. Hence, the reefal content of the Latemar is generally comparable to other Anisian reefs in the Dolomites, e.g. in the Olange area. The study of Harris (1993) is however based on two outcrops solely, one on the SW side of the Latemar (Cima Feudo area, location 1 in this study; see Fig. 2.3) and another one on the western side (area around Gamsstallscharte/Forcella dei Camosci, close to location 3 in this study; see also Fig. 2.3).

2.4 Sedimentology of the slope- and reef-facies at Latemar

The database for our study is provided by five outcrops of the reef- and slope-facies at different expositions of the buildup: (1) Cima Feudo, (2) Kirchtageide, (3) Erzlahn, (4) Schenon and (5) Cresta De Do Peniola (see also Figs. 4 and 5). At the first three outcrops, palaeontological investigations were carried out on in-situ reefs, at the latter two on reefal blocks within the slope-facies. The first four locations offer the possibility to study the

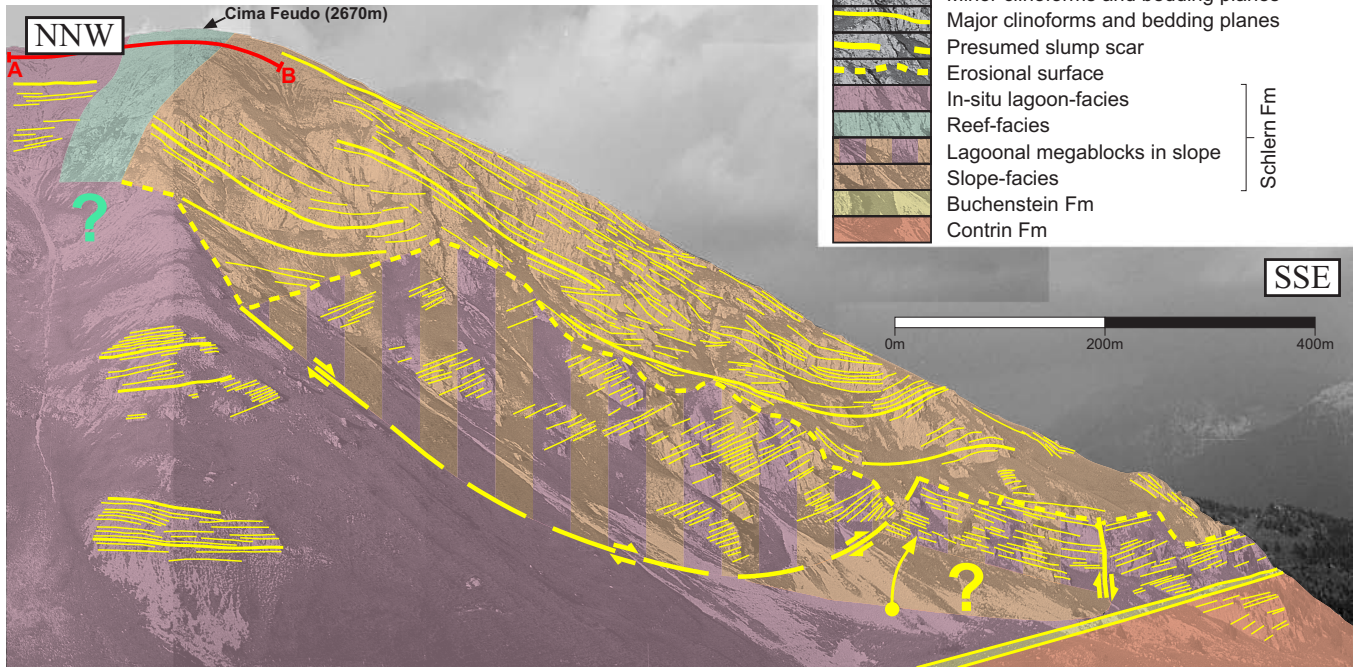
Plate 2.1 (following page) Sedimentology of the slope- and reef-facies at Latemar.

P2.1.1: Panoramic view of the SW flank of Cima Feudo (location 1) with an interpretation of the sedimentary structures. The red line A-B corresponds to the studied reef transect. Legend in the upper right corner.

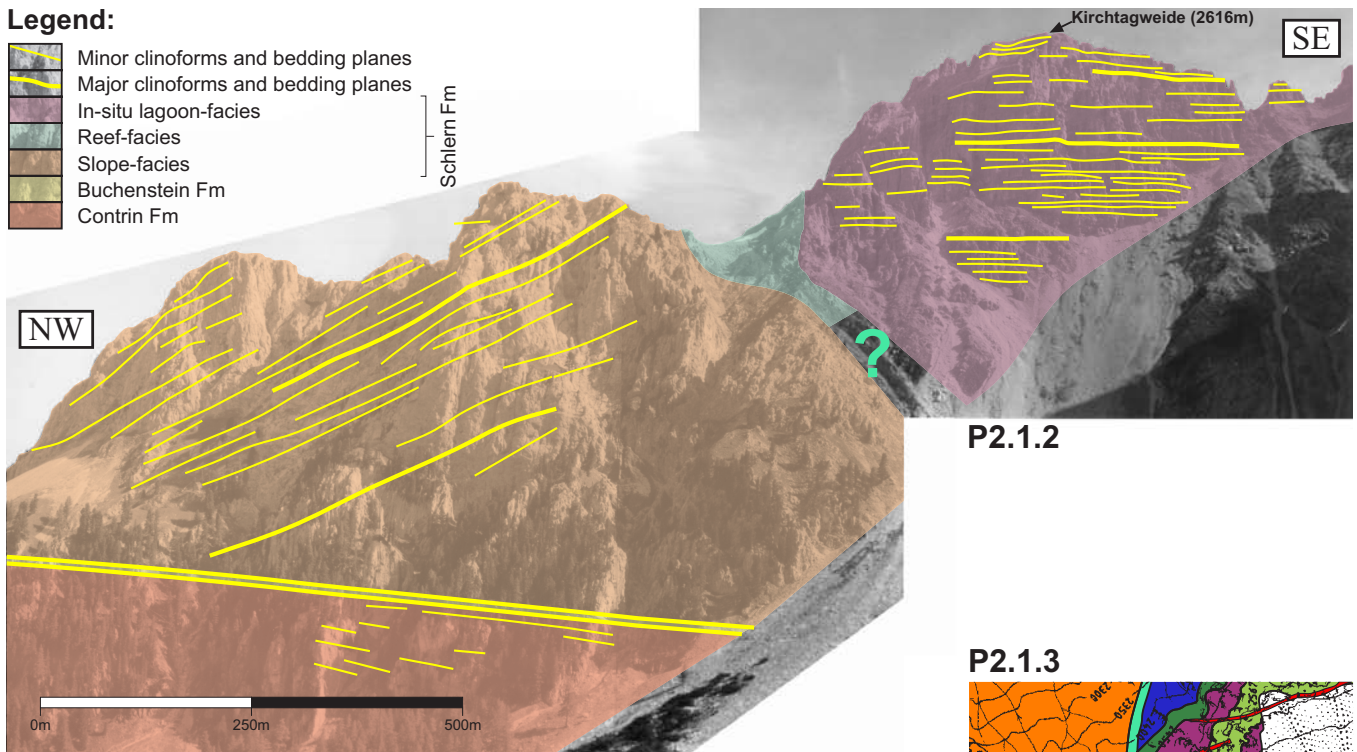
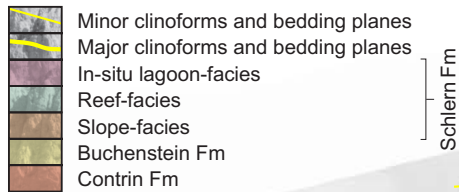
P2.1.2: Panoramic view of the SW flank of Kirchtageide (location 2) with an interpretation of the sedimentary structures. Legend in the upper left corner.

P2.1.3: Geologic map of the reef and its surrounding area at Kirchtageide. Panoramic view in P2.1.2 is from lower left (NW) to upper right (SE). Legend of the geologic map to the left.

P2.1.1



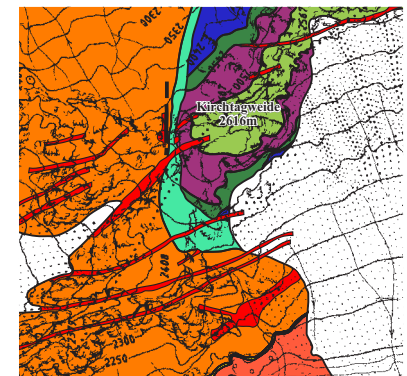
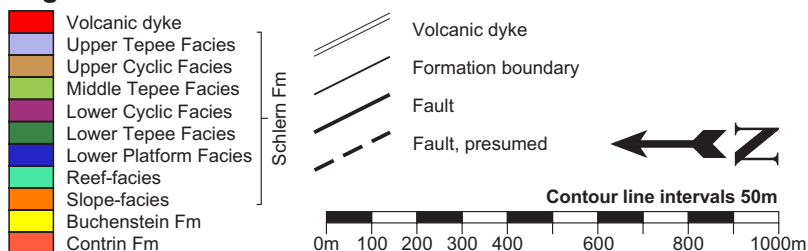
Legend:



P2.1.2

P2.1.3

Legend:



platform-to-basin transition at approx. right angles to the margin. The last locality (Cresta De Do Peniola) provides a transect through the upper slope parallel to the margin. Most of the locations are tectonically undisturbed, hence can be tied into the bio-/chronostratigraphic framework of the cyclic lagoonal succession. The array of all outcrops covers the entire time of platform evolution (see Fig. 2.5). As the reef of the Latemar is to a significant extent part of the uppermost slope, outcrops of the reef-facies are presented within the sedimentological context of the slope.

2.4.1 Cima Feudo

This location in the SW area of the Latemar (see Fig. 2.4) comprises the entire western flank of Cima Feudo - the highest point of the SW ridge of the Latemar - until its summit.

2.4.1.1 Architecture and sedimentology of the slope

This locality offers the unique possibility to trace and correlate clinofolds of the slope from the margin to their termination at the toe-of-slope. Platform evolution at Cima Feudo can be studied from Contrin times on (see Fig. 2.5 and Plate 2.1, P2.1.1). The NNW part of the Cima Feudo platform to basin transition (i.e. on the lefthand side in Plate 2.1, P2.1.1; left of the presumed slump scar) provides insight into an undisturbed stratigraphic succession. The mainly subtidal platform of LPF times - “Lower Edifice” sensu Gaetani et al. (1981) - conformably overlies the Contrin Fm and possibly builds up from a very thin and proximal facies of the Buchenstein Fm. The reefal margin of this early period is not preserved, it is eroded and must have lain outside the pictured area to the SSE where the basin was situated (righthand side in Plate 2.1, P2.1.1).

However, if the flat lying strata are traced from the lagoonal interior (NNW) towards the basin (SSE), they terminate against an antitethically tilted block of lagoon-facies in the centre of the picture (see P2.1.1, large striped area; signature: megablock). The size of the block is considerable, it is approx. 400m thick and 200m wide. In the direction of the palaeo basin (SSE), two additional areas of lagoon-facies are distinguishable by their different dip. The proximal one dips towards the basin (see P2.1.1, small striped area; signature: megablock), the more distal one is horizontally stratified, conformably overlies Buchenstein Fm and seems to be in-situ (see P2.1.1, signature: in-situ lagoon-facies). All three areas

reveal an erosive top and are covered by slope deposits of LTF and LCF times. This facies boundary is relatively distinct and was mapped in the field (see P2.1.1, signature: erosional surface). Reef-facies is - as mentioned above - absent in the lower part of the succession and reappears in the LTF underneath the summit of Cima Feudo.

The buildup phase of the LPF platform at this outcrop continued until a giant failure of the platform flank occurred at the verge from LPF to LTF and removed slope, margin and parts of the lagoon. The downward movement of the lagoonal megablock has a throw of approx. 100m and must have happened alongside a listric fault plane (see P2.1.1, signature: presumed slump scar). As the block moved downward, it crushed the footwall and pushed up another block at its front. Subsequently the platform margin backstepped and re-established itself at the former interior of the platform (see P2.1.1, signature: reef-facies). The interval following this catastrophic event is characterised by the re-establishment of a depositional slope. The giant slump was subsequently buried underneath carbonate slope sediments. Subsequent drowning of the platform and development of a “pelagic drape” (De Zanche et al. 1995; p.140) was not observed. The sheer size of this slump implies that instability of the margin or slope was not the only reason for the collapse of the platform. It was most probably caused by synsedimentary tectonic movement. Anisian faults are known from the Northern Dolomites (Bechstädt and Brandner 1970) and sinistral transpression with deep-reaching faults was ongoing until the Longobardian (Doglioni 1984). The resulting flower structures and domal uplifts were paving the way for the eruption of the Wengen Fm volcanics (Doglioni 1983). Evidence for regional volcano-tectonic activities in the surroundings of the Latemar is the proximity of the volcanic centre of Predazzo/Monzoni having formed above the Stava Line-Cima Bocche Anticline (Doglioni 1984). The observation of a tectonically mutilated platform generally corresponds with De Zanche et al. (1995), although differences exist with respect to mechanisms, size and timing of the backstepping of the LPF platform.

2.4.1.2 Sedimentology and general palaeontology of the reef

Microfacies mapping along a reef transect (length: 300m; line A-B in P2.1.1) at the stratigraphically highest point of Cima Feudo covers the transition from lagoonal inte-

rior across the in-situ margin to the upper foreslope. The transect runs in a single stratigraphic level and is correlatable with the platform of uppermost LTF to lowermost LCF times (see Fig. 2.5).

The transect begins in the lagoon with wacke-/packstones, characterised by the presence of bioclastic material (gastropods, pelecypods), dasycladacean algae, peloids and benthic forams. Among the most abundant foraminifers are Duostominidae, Endotriadidae and Endotebidae (classification sensu Vachard et al. 1994). The proximity of the reef is shown by worm tubes (*Spirorbis* sp.) and reef detritus like fragments of sponges (e.g. *Olangocoelia otti*), “*Tubiphytes*” group and microproblematica like *Plexoramea cerebriformis*, *Bacinella ordinata* and *Baccanella floriformis*. Their abundance increases closer to the reef. “*Tubiphytes*”-rich wackestones are the main indicators of the reefal margin. Forams like *Palaeolituonella meridionalis* and small, micritic worm tubes are present in the central part of the reef-facies. Biogenic crusts together with “*Tubiphytes*” intercalated with boundstones of *Celyphia? minima*, *Deningeria* sp., *Celyphia zoldana* and *Thaumas-tocoelia dolomitica* characterise the reef-facies above the foreslope. An important feature of this reef is the overwhelming abundance of calcisponges (*Solenolmia manon manon*, *Deningeria crassireticulata*, *Meandrostia triasica* and *Follicatena cautica*) which are usually well preserved, as well as the small blocks (or in-situ mounds?) of large, robust scleractinian corals (*Retiophyllia* sp.) at the uppermost foreslope. Microproblematica like *Anisocellula fecunda*, *Bacinella ordinata* and *Baccanella floriformis* are part of the reef-facies at Cima Feudo but not an important reef-builder. The occurrence of small forams like *Turriplomina mesotriasica* indicates the upper part of the slope. Abundant bioclasts (fragments of *Olangocoelia otti*, cephalopods, porostromata and red algae) together with two generations of cement - isopachous and block cement - fill the cavities between the reef talus blocks.

The reef at Cima Feudo reveals a low initial topography and bears no signs of emersion. Our study confirms the model of Harris (1993) at this location although the diversity of biota is greater.

2.4.2 Kirchtageide

This outcrop is located at the northwestern termination of the Latemar and forms a prominent, protruding ridge into the Eggen valley (see Fig. 2.4). The location Kirchtageide

is a tectonically undisturbed transect from the lagoonal interior (summit of Kirchtageide) through a slightly younger reef belt to the coeval toe-of-slope interfingering with basal sediments of the Buchenstein Fm (summit of Bewaller Köpfl, to the NW of the pictured area in Plate 2.1, P2.1.2, for geographical position and geological context please refer to Plate 2.1, P2.1.3). The studied reef-facies correlates with the uppermost LPF to lower LCF.

2.4.2.1 Architecture and sedimentology of the slope

In this transect, slope evolution is recorded from the build-up of the Schlern Fm upon the Contrin ramp. Buchenstein Fm underneath the slope is represented by a very thin (<3m), proximal facies. The slope-facies at Kirchtageide lacks erosional features. Its clinofolds are more or less parallel and display a depositional-type slope. Hence, the slope at this NW exposition of the Latemar corresponds to the Ladinian model of Bosellini (1984) and to the classification slope-apron sensu Mullins (1983) and Mullins and Cook (1986; see also chapter 2.3.2).

2.4.2.2 Sedimentology and general palaeontology of the reef

At least the upper levels of the reef at Kirchtageide show a progradational pattern. Progradation is in the order of 50-100m within the recorded interval of reefal build-up (ca. 300m). The unique feature of the reef-facies



Fig. 2.8 Outcrop photograph of a heavily dolomitised scleractinian framestone at Kirchtageide (location 2). Pen for scale; width of picture ca. 10cm.

at Kirchtage weide is the width of the reef belt (up to 150m) and the abundant presence of scleractinians. The reef itself is entirely dolomitised, no biota are visible apart from the heavily recrystallised branches of corals (*Retiophyllia* sp.?; see Fig. 2.8). The great abundance of corals suggests a well wave-resistant reef rim at this exposition. On its eastern termination, the reef is truncated by a major fault (see Plate 2.1, P2.1.3) before it disappears into the cirque of the “Geplänk” (see Fig. 2.4).

2.4.3 Erzlahn

The so-called Erzlahn is a broad and relatively steep gully with more or less vertical walls on either side located at the NW flank of the Latemar (see Fig. 2.4). The gully follows a postsedimentary, NW-SE trending fault - possibly also a volcanic dyke - dissecting the platform from its margin to the toe-of-slope. Stratigraphic (position of marker horizons) and facial (position of margin) information indicates a negligible displacement along the fault and/or dyke in the order of less than 10m. The fault/dyke in the Erzlahn separates the platform margin in two different blocks with two different sedimentological settings. The gully itself provides access to these two platform-to-basin transitions (see Plate 2.2, Fig. 2.3). The southern block of the fault/dyke is a platform-to-basin transition where the reef belt is missing whereas the northern block displays a transect from lagoon across back-reef margin until reef-front.

2.4.3.1 Architecture and sedimentology of the slope

The slope at Erzlahn corresponds to the upper LCF and lower MTF interval of the lagoonal succession (see Fig. 2.5). The most striking feature of the southern side of the Erzlahn is the missing reef (see Plate 2.2, P2.2.1, and for detailed geographic position please refer to Plate 2, P2.3; legend of geologic map see Plate 2.1, P2.1.3). The direct contact between lagoon- and slope-facies is erosional. Horizontally bedded strata of the lagoon terminate to the NW against a slump scar (slump scar 1 in

P2.2.1) and steeply dipping slope-clinoforms (up until 60°, unit 1 in P2.2.1). Slope unit 1 passes basinwards (NW) into significantly less steep clinoforms (unit 2 in P2.2.1). Unit 1 and unit 2 are both erosionally truncated at their top by an unconformity (slump scar 2 in P2.2.1). This slump scar 2 is conformably overlain by a slope unit with partly antitethic dip (unit 3 in P2.2.1).

Before an erosional event created slump scar 1, a normal platform-to-basin transition with a reef has probably existed. After the event, newly created accommodation space was filled with deposits of slope unit 1, most likely too quick for a stabilising reefal margin to establish. Much of the sediment bypassed the uppermost foreslope and accumulated further downslope (unit 2). Unit 2 is not as steeply stratified as unit 1 and is stabilising the clinoforms of unit 1. But the slope had already reached its maximum of stability, resulting in a second erosional event (slump scar 2) which removed a large quantity of upper slope sediments. Dip measurements in unit 3 above slump scar 2 revealed an inclination of the clinoforms towards the lagoon. This antitethic dip is caused by the listric nature of the slump scar's base. A couple of metres above slump scar 2, clinoforms of the slope are inclined to the basin again and reveal dip values between 5° and 15°. This indicates the re-establishment of a depositional slope after these two erosional events.

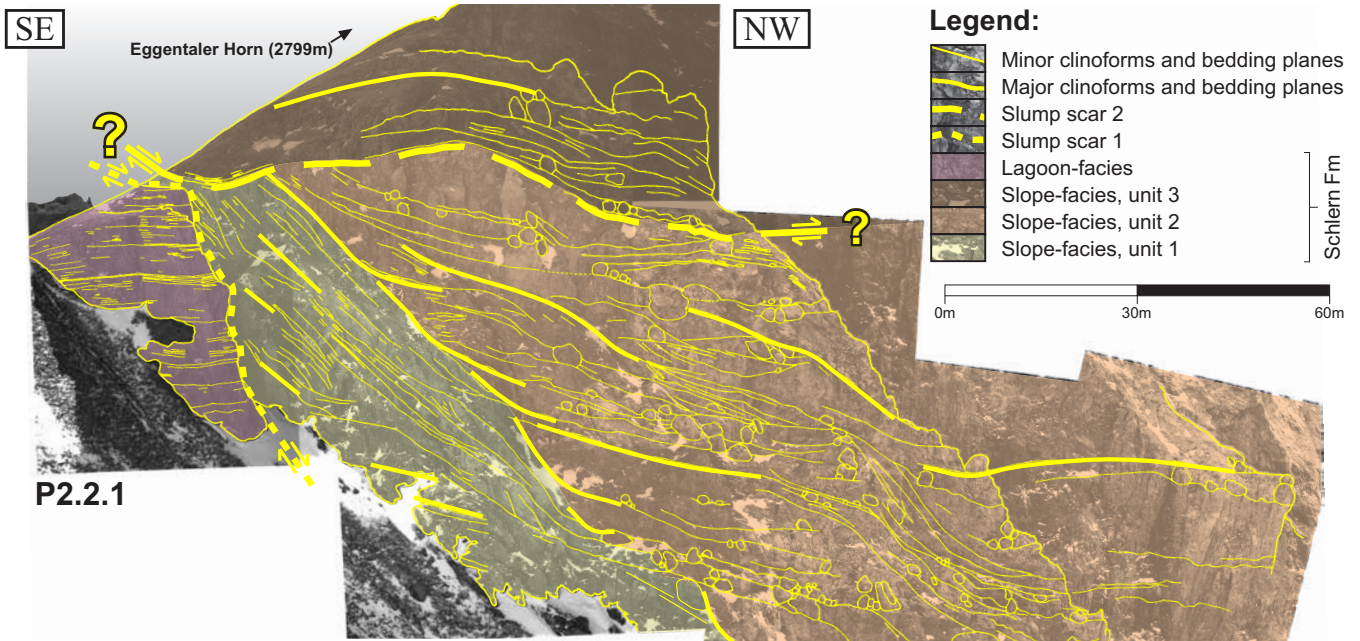
Slump scar 1 corresponds timewise to an onlap of lagoon-facies within the lagoonal interior. The tilting of the entire platform to the SE could have caused the oversteepening of the clinoforms and their subsequent failure in the NW of the platform (Erzlahn, location 3). Similar to the situation at Cima Feudo, the origin of the tilting can be seen in synsedimentary tectonic movements at the nearby Stava Line-Cima Bocche Anticline (i.e. the later volcano-tectonic centre of Predazzo/Monzoni). Major backstepping by margin failure was therefore not only restricted to the SW of the Latemar and LPF/LTF times, it has also occurred on the NW side of the plat-

Plate 2.2 (following page) Sedimentology of the slope- and reef-facies at Latemar.

P2.2.1: Panoramic view of the southern flank of the Erzlahn gully (location 3) with an interpretation of the sedimentary structures of the slope-facies. Legend in the upper right corner.

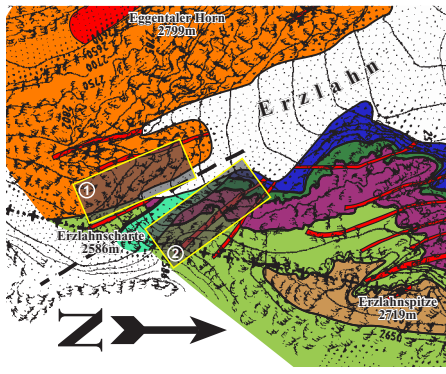
P2.2.2: Panoramic view of the northern flank of the Erzlahn gully (location 3) with an interpretation of the sedimentary structures of the reef-facies. Legend in the lower right corner.

P2.2.3: Geologic map of the Erzlahn area. Both panoramic views of the Erzlahn gully are marked by slightly opaque rectangles (rectangle 1: northern side, P2.2.1; rectangle 2: southern side, P2.2.2). For the legend of the geologic map refer to Plate 2.2.1, P2.1.3.

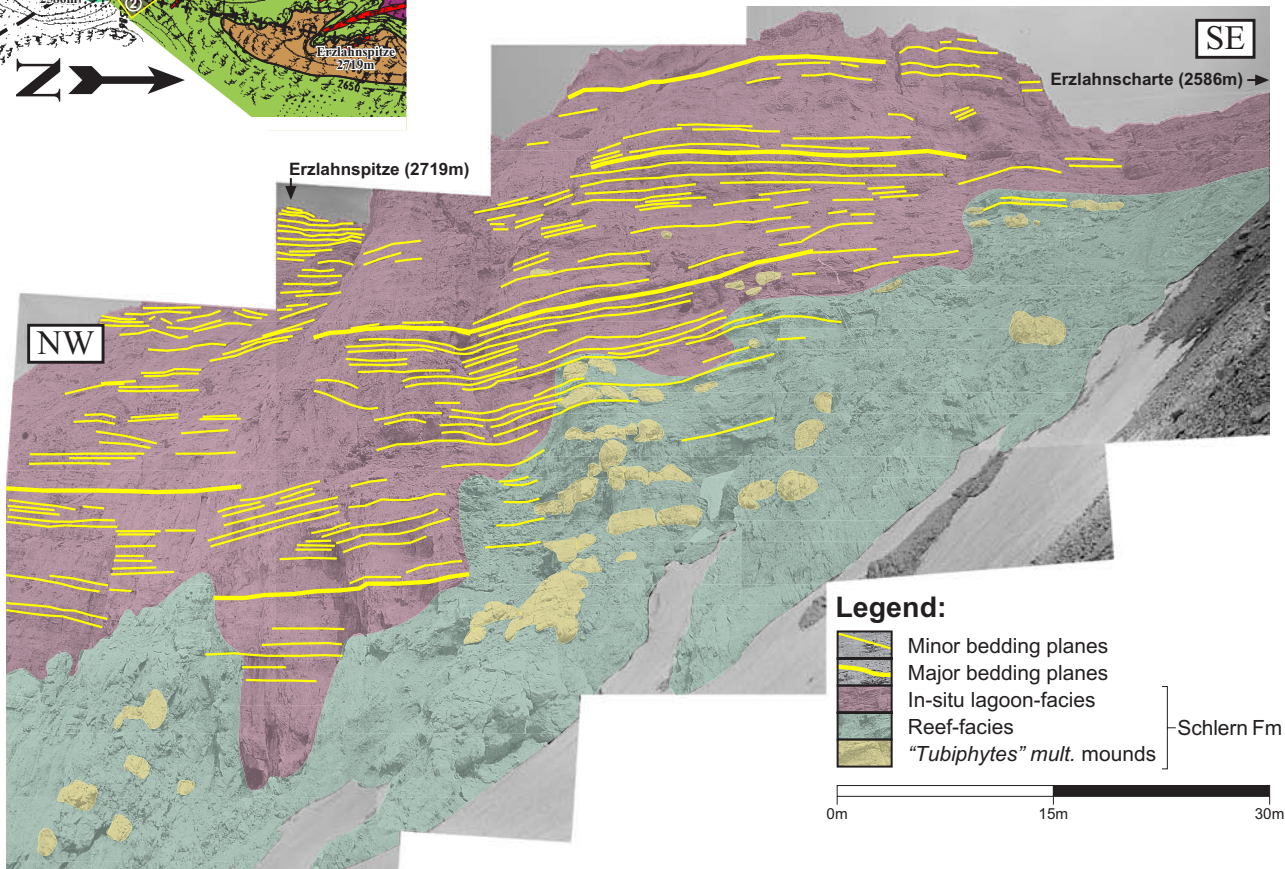


P2.2.1

P2.2.3



P2.2.2



form during the middle part of platform evolution (LCF-MTF). A model of simple aggradation as main platform growth mode until the latest stages of platform evolution is not in line with our observations at these two locations.

4.3.2 Sedimentology and general palaeontology of the reef

The reef at this location is exposed at the northern flank of the Erzlahn gully (see Plate 2.2, P2.2.2, and for detailed geographic position please refer to Plate 2.2, P2.2.3; legend of geologic map see Plate 2.1, P2.1.3) and its SW termination. The reef-facies is easily distinguishable from the adjacent lagoon-facies by the absence of stratification and its slight dolomitisation. The outcrops of reef-facies at Erzlahn are scattered and small; nevertheless, they display features very distinct from all other locations at Latemar.

The reef front is represented by some small patch-reef-like structures made up of large, robust hexacorals - *Retiophyllia* sp. - encrusted with “*Tubiphytes*” and other microbes. These small mounds pass laterally into algae dominated boundstones. The degree of encrustation increases significantly from reef front to reef core (i.e. towards the main outcrop of reef-facies described below and pictured in Plate 2.2, P2.2.2). The centre of the reef is an microbial/algal ridge formed by laminated microbialites. At Erzlahn, this part of the reef-facies is documented in a 20m by 10m wide outcrop. At the northern side of the Erzlahn, the transition from the reef-facies to the lagoon-facies contains mound-like structures sitting on top of indistinct bedding planes. The strata are dipping towards the lagoonal interior - i.e. a depression is situated behind the actual reef (see Plate 2.2, P2.2.2; area in the lefthand half of the panorama underneath Erzlahnspitze). Detailed facies mapping proved the tepee belt to

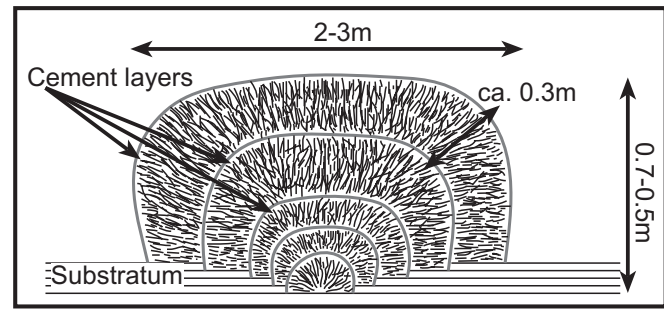


Fig. 2.9 Idealised sketch of “*Tubiphytes*” *multisiphonatus* mounds at Erzlahn (location 3). The entity of the mound is made up of a repetition of several, concentric layers of branches - each one with bush-like ramifications and separated by thin cement layers. Not to scale.

be behind the reefal margin towards the centre of the platform. Like at Cima Feudo and Kirchtage we discussed before, the reef shows no sign of emersion, i.e. the tepee-belt is the bathymetrically highest point of the platform margin. The most interesting feature of the reef at this location is the assemblage of “*Tubiphytes*” *multisiphonatus* mounds (up to 3m wide and 0,7m thick). The framework of these mounds is built up by parallel and/or subparallel branches of “*Tubiphytes*” *multisiphonatus* exclusively. This species forms concentrically growing, bush-like layers with a thickness of 20 to 30cm (for outcrop pictures refer to Plate 2.3.1 and 2.3.2). The organisation of these mounds is shown in Fig. 2.9.

The upright, ramified branches are embedded in coeval sediments (peloids and fragments of algae) and cements (isopachous and block calcite). For the original description of “*Tubiphytes*” *multisiphonatus* the reader is referred to Schäfer and Senowbari-Daryan (1982, 1983). It is obvious that the model of Harris (1993) cannot be applied to the Erzlahn, although confirmed by investi-

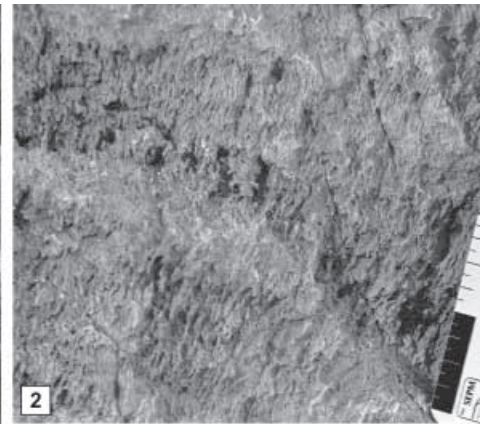
Plate 2.3 (following page) “*Tubiphytes*” *multisiphonatus* mounds at Erzlahn (location 3) and sedimentology of the slope facies at Schenon (location 4).

Fig. 1: Outcrop photograph of a “*Tubiphytes*” *multisiphonatus* mound; the dense network of the “thalli” and multiple layers of radiating “branches” are clearly visible. Location: southern side of Erzlahn (scalebar; lefthand side: subdivisions in inches, righthand side: subdivision in centimetres).

Fig. 2: Detailed outcrop photograph of the same “*Tubiphytes*” *multisiphonatus* mound; “thalli” and the separations between the concentric layers are well visible. Location: southern side of Erzlahn (scalebar: subdivision in inches).

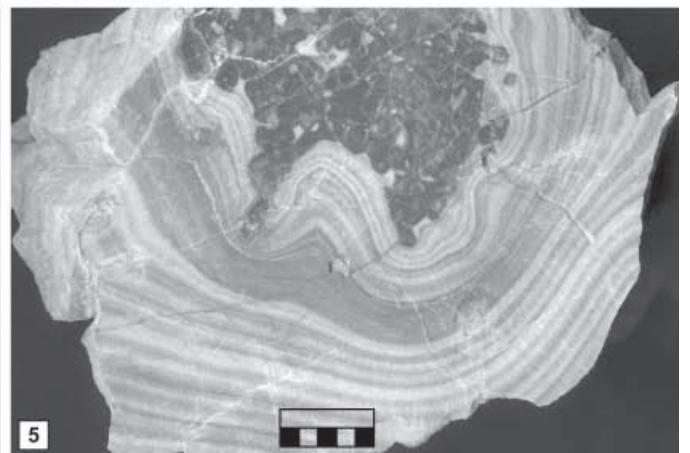
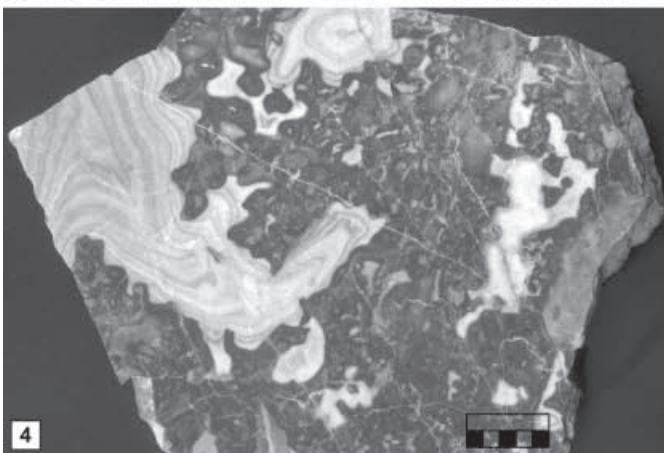
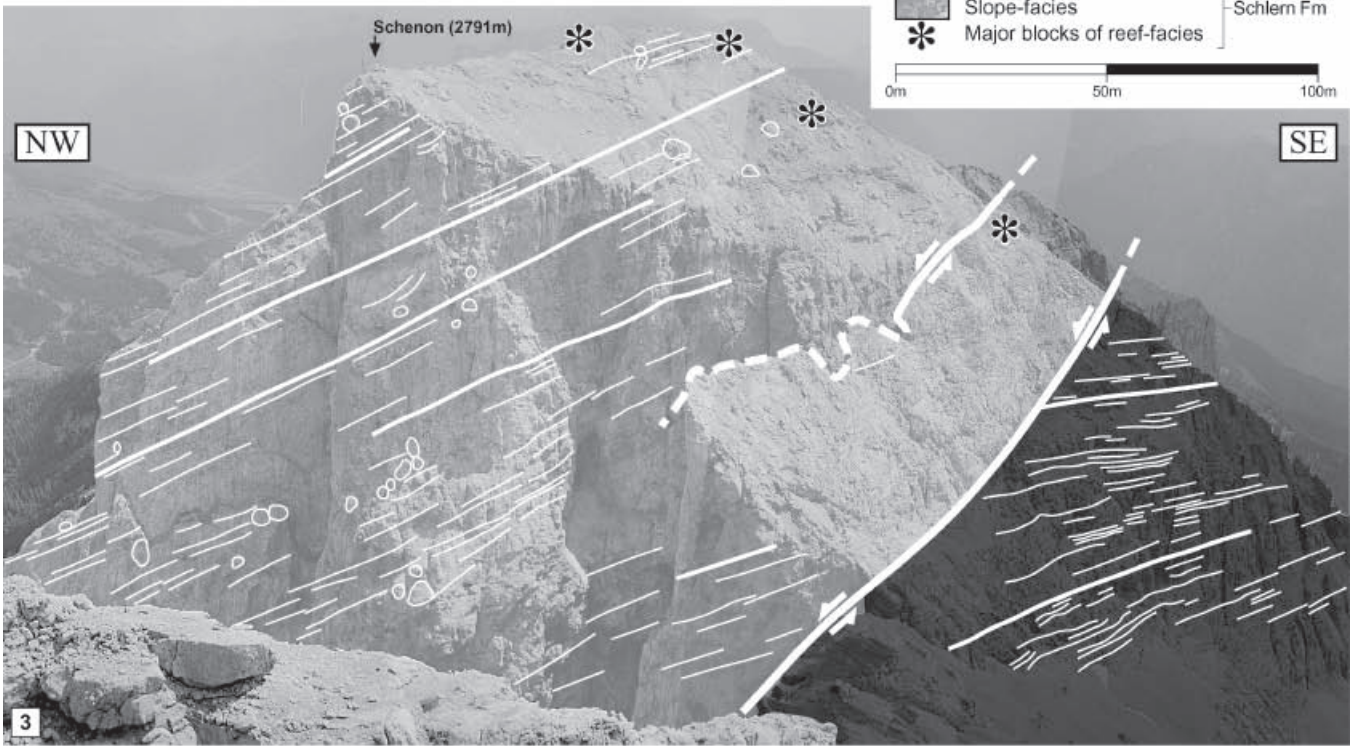
Fig. 3: Panoramic view of the SW face of Schenon with an interpretation of sedimentary and tectonic structures. Legend in the upper right corner.

Fig. 4,5: Photograph of polished slabs from talus blocks at Schenon with cement crusts. Scale bar is 1cm with subdivisions of 2mm.



Legend:

-  Minor clinoforms and bedding planes
 -  Major clinoforms and bedding planes
 -  Major normal faults
 -  Lagoon-facies
 -  Slope-facies
 -  Major blocks of reef-facies
- } Schlern Fm



gations at Cima Feudo. In both areas, the topography is the same, but facies belts and biota differ strongly.

2.4.4 Schenon

The Schenon is one of the highest summits of Latemar's northern ridge (see Fig. 2.4). Its SW vertical face provides insight into the platform development of UCF times (see Plate 2.3.3).

2.4.4.1 Architecture and sedimentology of the slope

At this outcrop, in-situ reef-facies is completely absent. Contrary to the Erzlahn, the contact between the slope and the lagoon is not syndepositional erosional but of postsedimentary tectonic nature. Two major faults dissect the platform at Schenon. They both can be traced for up to one kilometre on either side of the pictured area in Plate 2.3.3.

At this exposition, the preserved slope-facies proves a depositional characteristic of the platform-to-basin transition during UCF times. The clinofolds of the foreslope are subparallel, erosional structures of a larger scale are absent. The preserved slope corresponds to the depositional models proposed by Bosellini (1984) and Harris (1994).

The unique feature of the slope at Schenon is the abundance and size of syndepositional cement crusts (Plate 2.3.4 and 2.3.5). The thickness of these crusts (up to several centimetres) indicates a proximal talus setting for the blocks where fast, high-energy deposition of large blocks and the absence of fine-grained sediments facilitated early cementation and lithification. As the complete platform margin has been eroded after its tectonic destruction, the relation between slope and platform top is unclear. A possible depositional model for the Schenon is proposed in Fig. 2.10.

2.4.4.2 General palaeontology of the reef

Evidence of the reef-facies is found within talus blocks on the upper slope solely. However, the upright position of delicately branched corals (*Margarosmia* sp.) at a few places hints to the possibility of localised in-situ growth of small scleractinian colonies on talus blocks. The setting of a proximal talus fan with resedimented

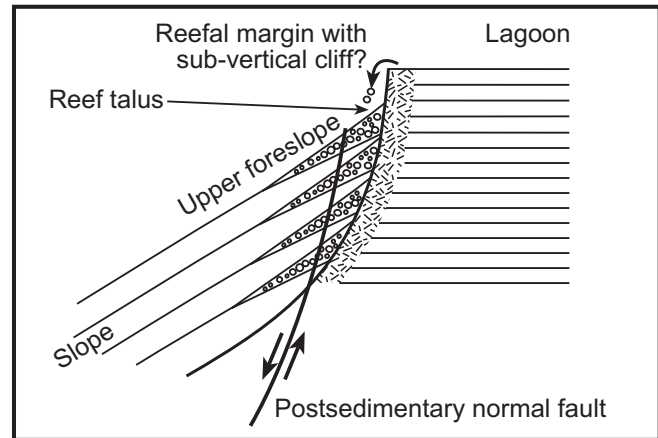


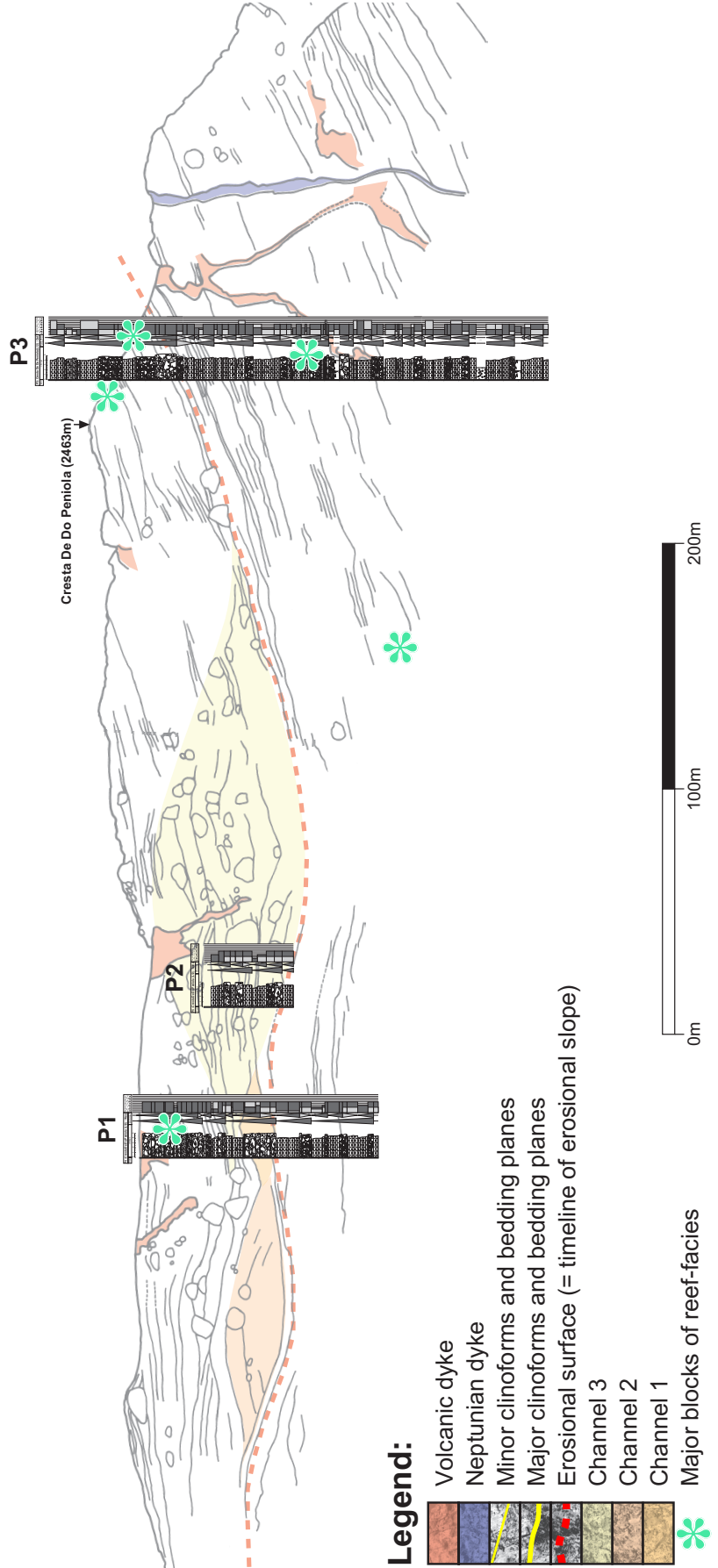
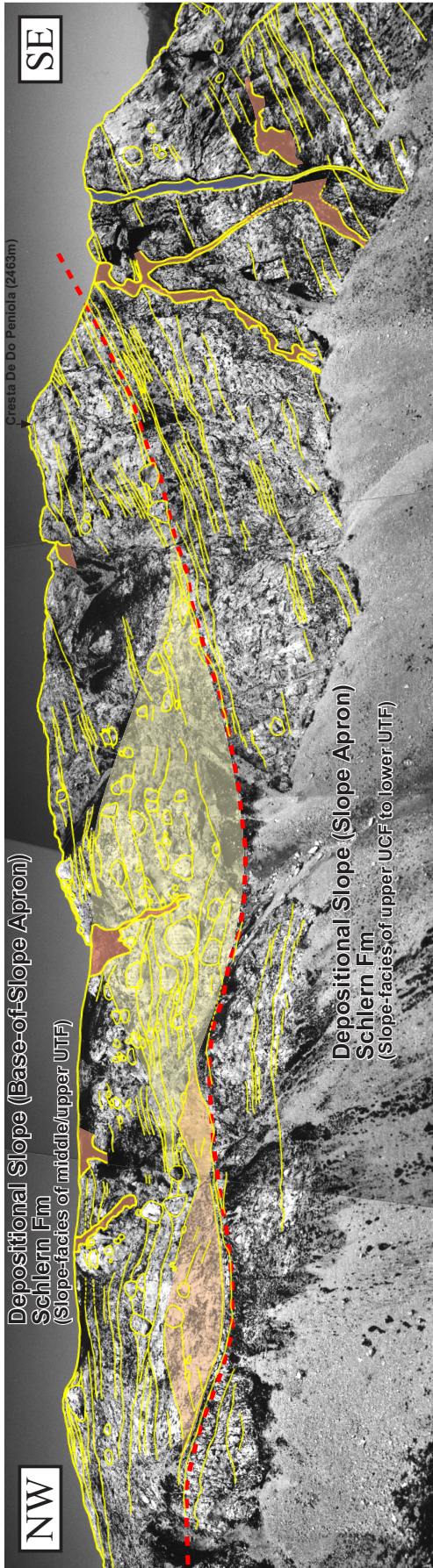
Fig. 2.10 Schematic sketch of a possible margin scenario at Schenon (location 4). Before a postsedimentary normal fault had truncated the margin and juxtaposed slope- and platform-facies, a reefal margin existed. The abundance and size of blocks and cement crusts suggests a proximal talus setting with a steeply cliffed platform margin.

reef-facies is supported by the occurrence of biota from different reef palaeo environments in the same micro-facies. The blocks contain mainly encrusting “sphinctozoan” sponges like *Celyphia zoldana* and *Celyphia minima* as well as *Colospongia catenulata catenulata* and *Follicatena cautica*. The calcisponges are accompanied by fragments of the “Tubiphytes” group and microproblematica (*Plexoramea cerebriformis* and *Radiomura cautica*). Fragments of cryptically growing sessil organisms like *Olangocoelia otti* (sponge, alga?) are associated with fragments of dasyclads (e.g. *Diplopora nodosa*). Forams of the reef and back-reef facies are also abundant, e.g. *Aulotortus? eotriasicus*, *Flatschkoefelia anisica*, duostominids, *Palaeolituonella meridionalis* and Endotebidae. Less common components are echinoid fragments and worm tubes.

2.4.5 Cresta De Do Peniola

This outcrop is located at the NE side of the Latemar atoll (see Fig. 4). The SW flank of the Cresta De Do Peniola was mapped in detail and sampled along three sections. Correlation with basal strata (see Fig. 2.11)

Plate 2.4 (following page) Panoramic view of the SW flank of the Cresta De Do Peniola (location 5) with an interpretation of the sedimentary structures. Note the position of the sections P1 to P3. The neptunian dyke has several thin, crack-like lateral extensions not shown in this panoramic view, parallel to bedding planes of the slope succession. Legend in the lower left corner.



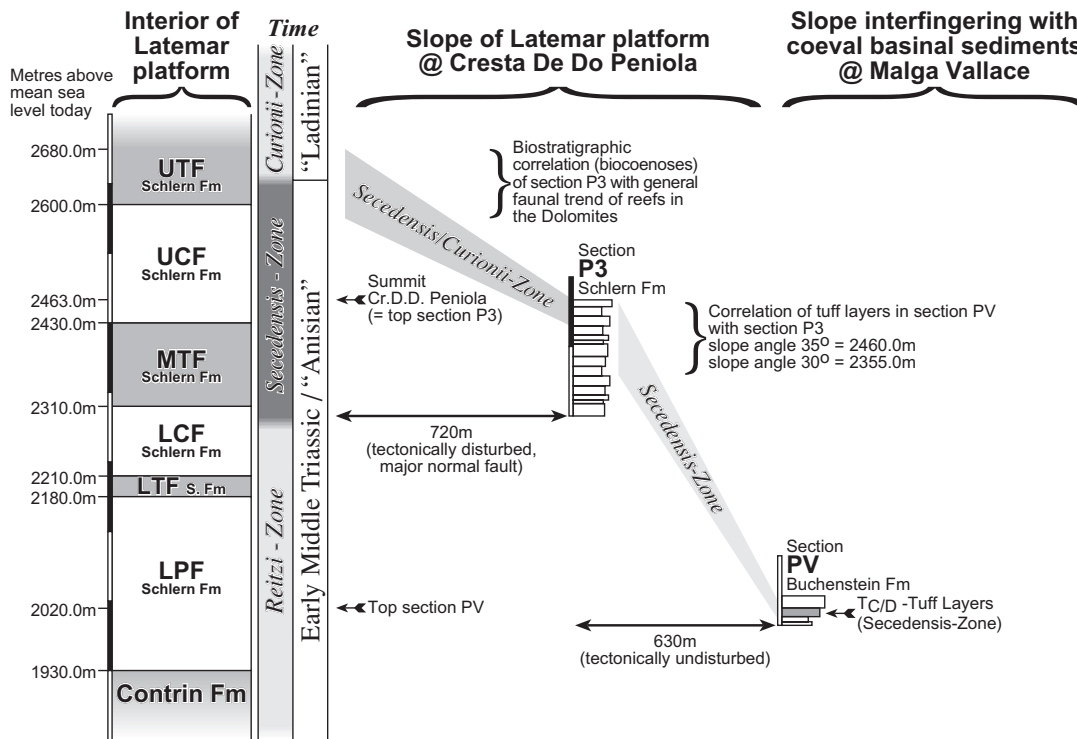


Fig. 2.11 (above) Correlation of a basinal section with section P3 at Cresta De Do Peniola (location 5) and with cyclostratigraphic units of the lagoonal interior. At the location Malga Wallace to the NE in the dip direction of Cresta De Do Peniola, age diagnostic tuff layers (sensu Brack and Rieber 1993) were identified within the Buchenstein Fm; biostratigraphy and position of Anisian/Ladinian boundary after Brack and Rieber (1993).

Correlation was realised by measuring the horizontal and vertical distance between these two sections and the slope angle in section P3. Neither faults with vertical throw nor lateral tectonic movements were observed between these two sections. However, correlation between the lagoonal interior and section P3 is hampered by the presence of a normal fault with unknown displacement. Nevertheless, biostratigraphic evidence from the reef-facies at Cresta De Do Peniola and correlation with the basinal Buchenstein Fm are in accordance and both indicating an age of uppermost *Secedensis*- to lower *Curionii*-biozone, i.e. uppermost UCF to middle UTF platform times.

Plate 2.5 (following page) Anisian reef limestones from the Latemar, Dolomites, Italy: sponges (*Celyphia* sp.) and corals.

Fig. 1. *Celyphia zoldana* Ott, Pisa and Farabegoli. Section through several chambers of an encrusting specimen together with “*Tubiphytes*”-like crusts. (Cresta De Do Peniola, x26)

Fig. 2.-3. *Celyphia zoldana* Ott, Pisa and Farabegoli. Longitudinal section through four chambers of recrystallised specimens. (Cresta De Do Peniola, 2: x9; 3: x13)

Fig. 4. Several chambers of *Celyphia zoldana* overgrown by “*Tubiphytes*”-like crusts and sessil foraminifers. (Cresta De Do Peniola, x10)

Fig. 5.-7. *Celyphia zoldana* Ott, Pisa and Farabegoli. Section through some chambers of recrystallised specimens. The chambers are infilled with calcitic cement and/or sediment (Fig. 5). (5,6: Cresta De Do Peniola, 5: x9, 6: x13; 7: Schenon, x9)

Fig. 8. *Celyphia? minima* Senowbari-Daryan, Zühlke, Bechstädt and Flügel. Longitudinal section through several pear-shaped chambers characterised by ostia with short exauli on the surface of the wall. (Cresta De Do Peniola, x9)

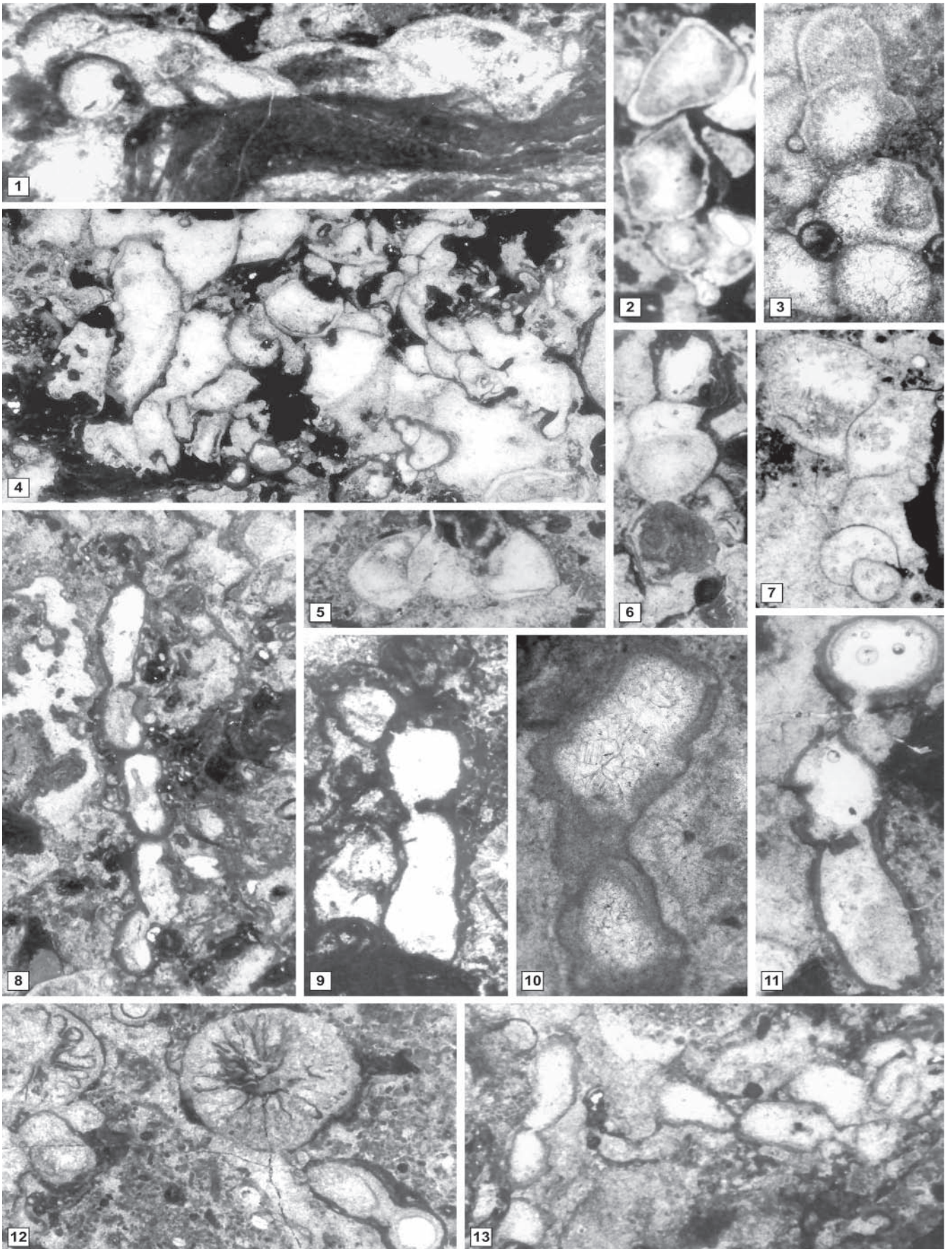
Fig. 9. *Celyphia? minima* Senowbari-Daryan, Zühlke, Bechstädt and Flügel. Section through three chambers. The wall and roof of the chambers are pierced by several pores. According to Senowbari-Daryan et al. (1993, pl.45, Fig 4), the attribution of this sponge to *Celyphia? minima* is not sure and it could probably be a new species. (Cresta De Do Peniola, x13)

Fig. 10. *Celyphia? minima* Senowbari-Daryan, Zühlke, Bechstädt and Flügel. Section through two oval shaped chambers. In the wall of the chambers, large ostia with short exauli are evident. (Cresta De Do Peniola, x16)

Fig. 11. *Celyphia? minima* Senowbari-Daryan, Zühlke, Bechstädt and Flügel. Section through three chambers. (Cresta De Do Peniola, x17)

Fig. 12. Microfacies with corals (*Zardinophyllum* sp.?) and small chambers of sponges cfr. to *C. zoldana*. (Schenon, x13)

Fig. 13. Several specimens of small encrusting sponges cfr. to *Celyphia? minima*. (Cima Feudo, x9)



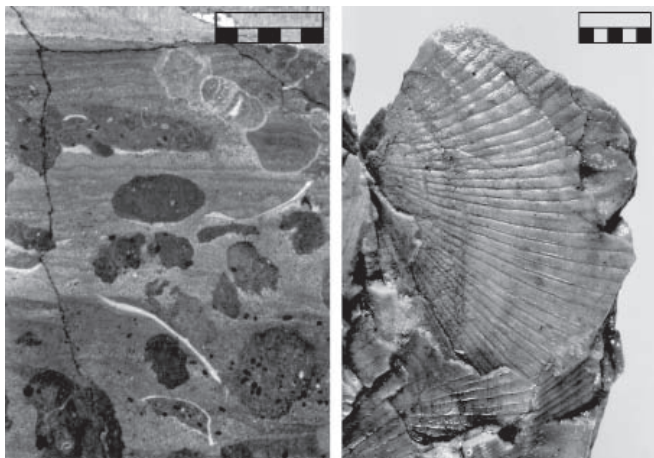


Fig. 2.12A Photomicrograph of a thin section from the neptunian dyke in Cresta De Do Peniola (location 5). Fine-grained peloidal sediments are bioturbated. Ammonoids and microfossils indicate openmarine conditions. Scale bar is 1cm with subdivisions of 2mm.

Fig. 2.12B Shells of *Daonella* sp. in a sample from Cresta De Do Peniola (location 5); scale bar is 1cm with subdivisions of 2mm.

indicates that the top of the section is positioned at the verge from the *Secedensis*- to the *Curionii*-biozone.

2.4.5.1 Architecture and sedimentology of the slope

Three sections at this location (see Plate 2.4 and refer for sections to Figs. 2.13 and 2.14) revealed the presence of an erosional surface separating two different slope types. Whereas the lower part of the slope at Cresta De

Do Peniola is characterised by stacked multiple debris flows and coarse-grained turbidites (lithofacies types 2a/b and 3a/b; see chapter 2.5.1, Table 2.1.), the upper part contains abundant megabreccia (lithofacies types 1 and 2a/b; see chapter 2.5.1, Table 2.1).

The other striking feature of this location is a coeval neptunian dyke dissecting the slope sediments (see Plate 2.4). At three levels, the neptunian dyke has thin (<1m) horizontal, laterally correlatable continuations with sheet-like cement crusts and bioclastic material (radiolarians, cephalopods and *Daonella* sp., see Figs. 2.12A and B) pointing towards openmarine conditions. The infill of the neptunian dyke - red mud-/wackestones - contains small, rare foraminifers indicating an Anisian to Ladinian age and also openmarine conditions. The characterising nanofauna of the dyke is furthermore made up of filaments and small ostracods (see photomicrograph in Fig. 2.12A).

Palaeontological and sedimentological evidence - similar biotic content and lateral correlation - support a common genetic history of the fractures. Especially the presence of *Abriolina mediterranea* is significant evidence for a relationship with reefal associations (Zaninetti et al. 1992). Mechanisms for the synsedimentary opening of the neptunian dyke and its lateral extensions are either extensional tectonics and/or dilatation of slope sediments due to downslope sliding (Winterer et al. 1991; Sarti et al. 2000; Mallarino 2002).

Plate 2.6 (following page) Anisian reef limestones from the Latemar, Dolomites, Italy: *Olangocoelia otti* Bechstädt and Brandner and sponges (sphinctozoans and inozoans).

Fig. 1.-2. A characterising feature of *Olangocoelia otti* Bechstädt and Brandner (sponge or algae?) is the chain-like, in line arrangement of its small chambers surrounding cavities (Fig.1.). However, sometimes *O. otti*-chains are irregularly distributed within the sediment (Fig. 2.). The interior of its chambers is usually infilled with calcite. (1: Cima Feudo, x4; 2: Schenon, x9)

Fig. 3.-5. *Solenolmia manon manon* Münster, a common, large segmented sponge in Anisian to Carnian reef carbonates of the Alpine-Mediterranean region.

Fig. 3. Longitudinal section exhibiting the reticular filling structures and the spongocoel. (Cresta De Do Peniola, x13)

Fig. 4.-5. Longitudinal and oblique sections exhibiting the retrosiphonate spongocoel. In Fig 5., the sponge is overgrown by biogenic crusts. (Cima Feudo, x7)

Fig. 6. *Thaumastocoelia dolomitica* Senowbari-Daryan, Zühlke, Bechstädt and Flügel. Longitudinal section through several barrel-shaped chambers. There is no evidence of pores between roof chambers and vesiculae. (Cima Feudo, x13)

Fig. 7. *Colospongia catenulata catenulata* Ott. Single, monoliliform stem without central tube and porate walls of the chambers. (Schenon, x9)

Fig. 8. *Deningeria* cfr. *crassireticulata* Senowbari-Daryan, Zühlke, Bechstädt and Flügel. (Cima Feudo, x9)

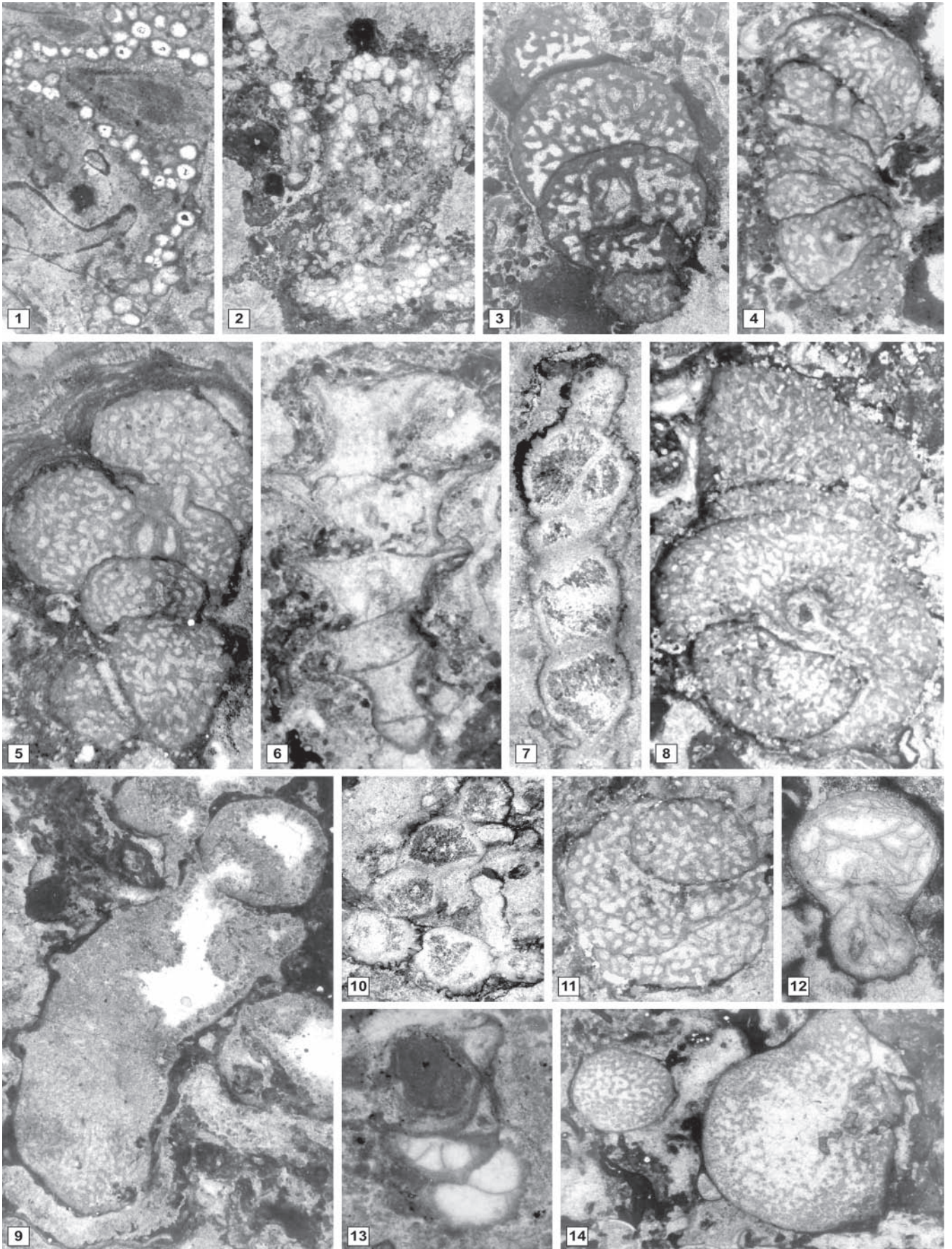
Fig. 9. *Meandrostia triassica* Senowbari-Daryan, Zühlke, Bechstädt and Flügel. (Cima Feudo, x7)

Fig. 10. *Colospongia catenulata catenulata* Ott. (Schenon, x7)

Fig. 11. *Solenolmia manon manon* Münster. (Cima Feudo, x10)

Fig. 12.-13. *Follicatena cautica* Ott. (12: Cima Feudo, x4; 13: Schenon, x4)

Fig. 14. Isolated globular/oval chambers of *Deningeria* sp. (Cresta De Do Peniola, x8)



The lower part of the slope corresponds to the depositional slope type. Sedimentation takes place on the entire platform-to-basin transition; the slope can be classified as “slope apron” sensu Mullins (1983) and Mullins and Cook (1986; see also chapter 2.3.2). The correlatable erosional surface (see Plate 2.4 and Figs. 2.13 and 2.14) forms a timeline of an interval with net erosion on the slope, i.e. corresponds to a stage of an erosional slope. After this interlude, net deposition occurred on the platform-to-basin transition again. In contrast to the interval below the erosional unconformity, a large amount of sediment bypassed the upper slope through two minor and one major channel to the lower slope. Hence this slope - correlatable with middle UTF times - corresponds to the “base-of-slope apron” type sensu Mullins (1983) and Mullins and Cook (1986; see also chapter 2.3.2). Although the main characteristics of the slope at Cresta De Do Peniola are depositional, no indications of progradational patterns of the margin exist for the latest (UTF) stage of platform development. Contrarily, the platform was aggrading or even backstepping as evidenced by the timeline of an erosional slope.

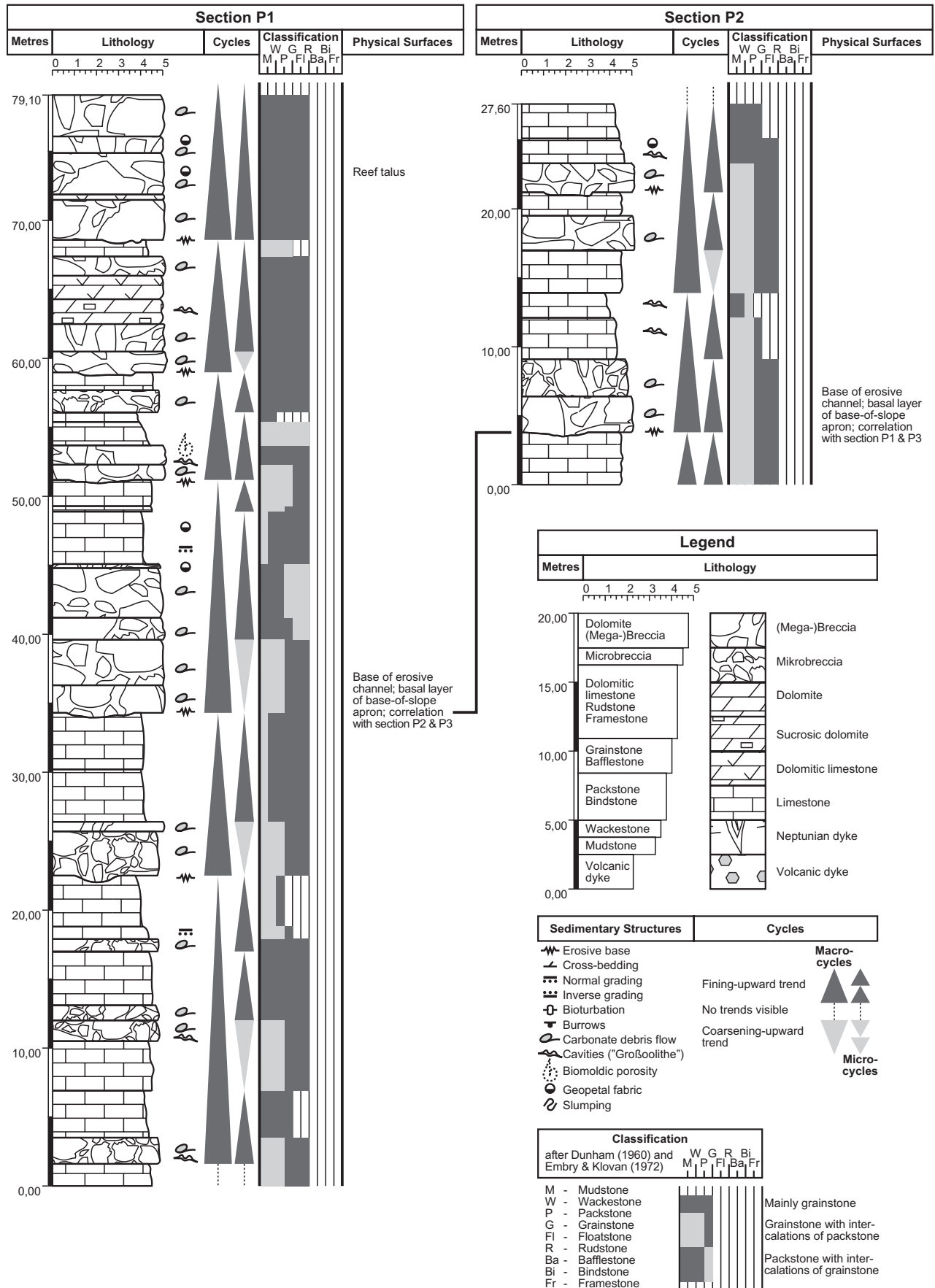
2.4.5.2 General palaeontology of the slope and reef

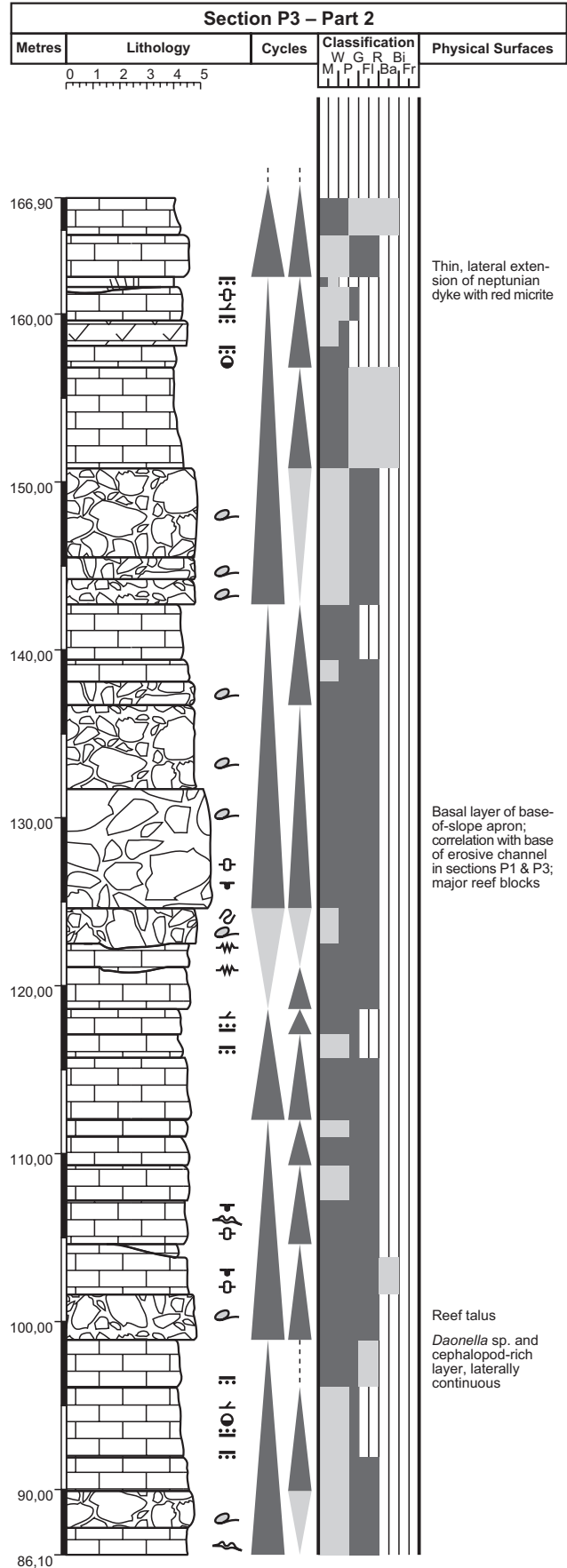
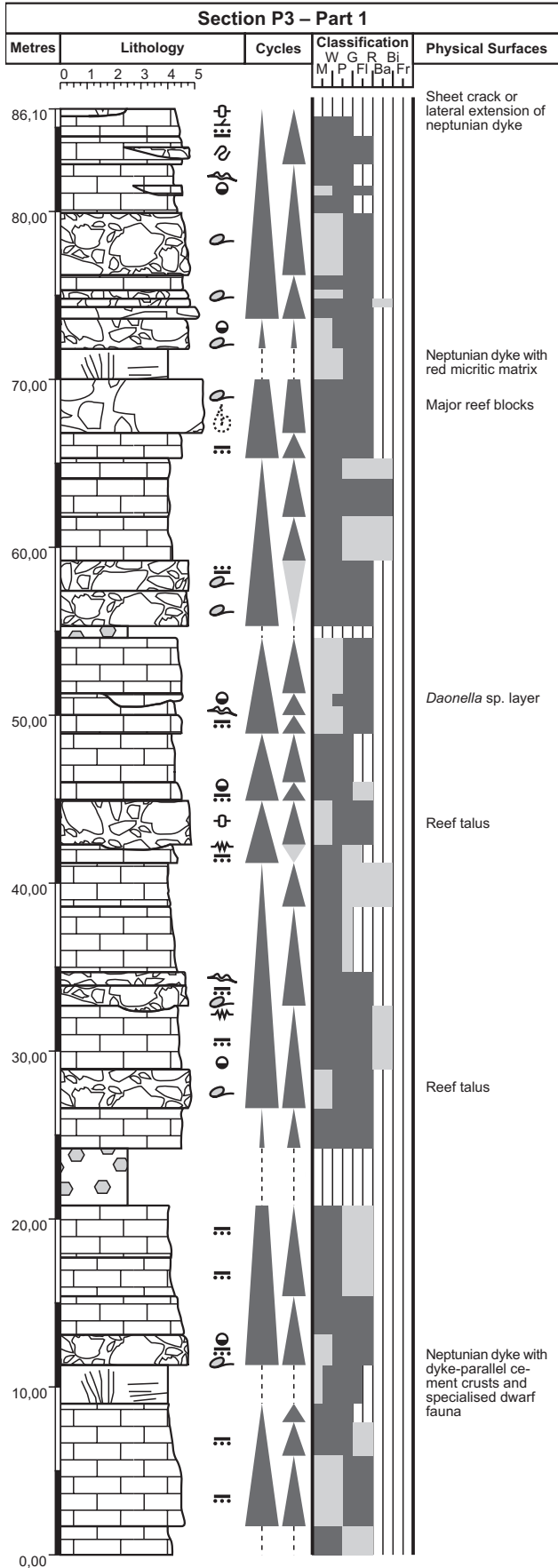
The lower turbiditic and debris flow deposits contain components from both reef and lagoon. Accordingly, there is a broad variety in the biotic spectrum. The sediments of the upper part of Cresta De Do Peniola contain more resedimented material from the slope, but still reveal reefal and lagoonal clasts. In order to define the boundary between these two units more accurate and to track a possible reefal development, three sections at Cresta De Do Peniola were logged (see Plate 2.4 and Figs. 2.13 and 2.14): two sections through the entire succession (P1 and P3) and another one through the channel in the middle of the succession (P2).

Most information on the lower level of the succession comes from P3. Hence, the biotic content of this section is used to describe the basal part of Cresta De Do Peniola. The section starts with turbiditic pack-/wackestones (LF3a/b, see chapter 2.5.1, Table 2.1) containing fragments of grapestones with *Olangocoelia otti* and cavities with isopachous cement. In the following metres, the section cuts through the neptunian dyke. Below the

neptunian dyke, wackestones with encrusting forams (*Bullopore* sp.), fragments of *Olangocoelia otti*, *Plexoramea cerebriformis* and “*Tubiphytes*” sp. occur. The wackestones also contain peloids of the lagoon. The matrix of the neptunian dyke is made up by mud-/wackestones, sometimes red, but always containing fragments of thin pelecypods, foraminifers ostracods, ammonoids and a large amount of coprolites (*Favreina* sp.). The foraminiferal association consists of small porcellaneous (*Ophthalmidium* sp. and *Arenovidalina Chiangchiangensis*), granular (*Krikoumbilica pileiformis*) and hyaline species (*Abriolina mediterranea* and nodosarids). Above the neptunian dyke, the grain size is increasing and the blocks of the basal debris flow contain *Celyphia? minima*, *Olangocoelia otti* and encrusting “*Tubiphytes*”. Forams like Duostominidae and/or Endotebidae and Endotriadidae are also present. The following debris flow with reef talus is made up of blocks with *Baccanella floriformis*, *Bacinella ordinata* and large parts of red algae. The lithoclasts are partially surrounded by *Celyphia zoldana*. The upper part of this fining upward cycle is characterised by *Daonella* sp. levels (see Fig. 2.12B) and serpulids (*Spirorbis* sp.) as well as isopachous cement in cavities. Bryozoan clasts (*Reptonoditrypa cautica*), *Turriglomina mesotriasica* and microproblematica complete the image of a mainly Anisian community. The base of the next turbidite contains fragments of sponges, “*Tubiphytes*” and dasycladaceans. Forams of the back-reef - like *Aulotortus eotriasicus* (see Zaninetti et al. 1994) - are also present. The upper part of this fining-upward microcycle reveals large and little ostracods in blocks, “*Tubiphytes*” together with *Celyphia? minima* and *C. zoldana*, other microproblematica and duostominids. The interval until the erosional unconformity is then characterised by forams as *Palaeolituanella meridionalis*, *Flatschkofelia anisica*, *Turriglomina scandonei* and *Aulotortus eotriasicus*. They occur together with reef detritus like “*Tubiphytes*” bindstones, bryozoans encrusted with *Bacinella ordinata*, as well as lagoonal detritus like dasycladaceans (*Diplopore* sp.), fragments of nautiloids and Porostromata. The basal layer of the base-of-slope apron is very rich in reefal biota. Huge boundstone clasts are made up of *Celyphia zoldana* and *Celyphia? minima*, *Deningeria crassireticulata*,

Figs. 2.13 and 2.14 (following page) Section P1, P2 and P3 through the slope of Cresta De Do Peniola (location 5; for exact position of the sections please refer to Plate 2.4). Legend of the sedimentological logs on Figure 2.13.





“*Tubiphytes*” *obscurus*, biogenic crusts, cerioid hexacorals like *Retiophyllia* sp., red algae (solenopora-ceans), microproblematica (*Plexoramea cerebriformis*) and forams like duostominids and *Endotriada* cfr. *tyrrhenica*. Some of the boundstone clasts are made up entirely of red algae (*Parachaetetes* cfr. *triasinus*) associated with fragments of *Bacinella ordinata* and “*Tubiphytes*” *obscurus*. Forams of the back reef and reef core (*Aulotortus eotriasicus*, *Flatschkofelia anisica*) and large sponges (*Solenolmia manon manon*) continue upward until the lateral extension/sheet crack of the neptunian dyke with red micrite (see Fig. 2.12A).

Sections P1 and P2 reveal similar biota in the lower and middle part, with some other forams like *Reophax/Ammobaculites* but more *Bacinella ordinata*. The uppermost part of these two sections contains “*Tubi-phytes*” *obscurus*, other microproblematica, sponges (*Vesicocaulis oenipontanus*), corals, porostromata, *Bacinella ordinata*, *Celyphia zoldana* and eventually *Ladinella porata* for the first time. A possible temporal trend in reefal evolution has to be rejected as almost the same biocoenoses can be found as well in the lower as in the upper part of the section. It is therefore not possible to clearly distinguish between these two periods of slope evolution. Only a slight development of the faunal associations is visible; e.g. bryozoans are present only in the lower levels, which is also the case for *Olangocoelia otti*. Compared to other outcrops like Cima Feudo or Schenon, the reefal content of the lower levels at Cresta De Do Peniola does not display differences apart from some less abundant components. Even the upper levels at Cresta De Do Peniola reveal only insignificant deviations from the biotic content of other locations.

2.5 Lithofacies and palaeontology

2.5.1 Lithofacies types

Detailed microfacies investigations revealed the lithofacies associations of the slope described in Table 2.1.

2.5.2 General content of the reef-facies

A listing of all biota encountered in the reef-facies at Latemar can be found in Table 2.2 (also refer to Plates 2.5-2.12).

According to the schemes of primary and secondary frameworks of Scoffin and Garrett (1974), Fagerstrom (1987) and Tucker and Wright (1990) our detailed investigation of the reef-facies proved some biocoenoses to be primary (B1 to B7) and others to be secondary

framebuilders (B8 and B9). The secondary framebuilders (encrusting organisms like “*Tubiphytes*” group and *Bacinella ordinata*) are of equal importance for the buildup of the Latemar reef as the primary ones. Secondary framebuilders are associated with all biocoenoses of the reef front.

2.5.3 Biocoenoses of primary reef-builders

The numbering of the biocoenoses is in accordance with their occurrence from reef front (B1) to back reef (B7).

2.5.3.1 B1 - Solenoporacean-bafflestones

Red algae with large branches are the protagonists of this biocoenosis, other components are present to a small extent only. However, this biocoenosis is only of local importance at Latemar’s reef. The solenoporaceans are represented by *Parachaetetes* cfr. *triasinus* and *Solenopora* sp. In some cases they are associated with or encrusted by secondary reef builders like “*Tubiphytes*” *obscurus* (B8), *Bacinella ordinata* (B9), porostromate algae (*Ortonella* sp.) and small encrusting forams (*Flatschkofelia anisica*, *Tolypanmina* sp.).

These delicate baffling organisms show close intergrowth with similarly branching *Margarosmia* sp.-type scleractinians or bryozoans. B1 never occurs together with robust, *Retiophyllia* sp.-framestones. From the palaeo environmental point of view, this biocoenosis is located in the area at the reef front below the mean wave base.

2.5.3.2 B2 - “Sphinctozoan”-“*Tubiphytes*”-bind-/bafflestones

“Sphinctozoan” sponges are the most important primary constituents of the reef-facies at Latemar. Owing to the different growth behaviour of each species, they form both bafflestones and bindstones.

Small segmented sponges are very abundant and mostly encrusting. Together with “*Tubiphytes*” and *Bacinella* they form the framework contributing to the largest part to the growth of the reefal margin. These “sphinctozoan” sponges are equally represented by *Celyphia zoldana* and *Celyphia? minima*, the latter one possibly by two species one of which could be new. In some cases, *Celyphia* is accompanied by *Follicatena cautica*, another encrusting sponge.

Where encrusting “sphinctozoans” are less frequent, large isolated sponges like *Solenolmia manon manon*, *Deningeria* sp., *Colospongia catenulata catenulata*,

Number	Class	Type	Subtype	Description	Number
LF1	Resediments	Megabreccia		Abundance of megablocks (size up to several metres in diameter); grain- and/or mudsupported; neither grading nor bedding, homogeneous mixing.	LF1
LF2a		Calciturbidites	Grainsize 1	Lithoclastic rudstones; mud-free, owing to abundant cement between the clasts transition to microbreccia; angular to well rounded clasts; origin of components: lagoon and reef, clasts of the slope are rare; size of components: few mm to a some cm.	LF2a
LF2b			Grainsize 2	Lithoclastic rudstones with LF4 wackestones (finegrained peloids and bioclastic material) filling inter-particle porosity; mostly grain-supported, sometimes transition towards floatstones; origin of components: lagoon and reef, clasts of the slope are rare; size of components: some mm to a few cm.	LF2b
LF3a			Grainsize 3	Floatstones with bimodal grainsize distribution: finegrained peloids in the matrix (LF4) together with litho- and/or bioclasts up several cm; lithoclasts of LF3a are of the same origin as those of LF2a/b; bioclasts are mainly fragments of "Tubiphytes" sp., others are: peloids, fragments of echinoids, filaments, annelids, fragments of calcareous algae and small cephalopods.	LF3a
LF3b			Grainsize 4	Well sorted grainstones, consisting of peloids solely; very fine-grained, grainsizes ranging from 0.2 to 0.7mm; sometimes cross bedding; often fining-upward trends.	LF3b
LF4		Background sedimentation		Wacke-/packstones with components like small lithoclasts, grapestone/oncoid fragments, fragments of Olangocoelia, peloids, fragments of echinoids and shells; sedimentary characteristics are bioturbation and geopetals; mainly the product of normal background sedimentation on the slope, but also filling interstices in LF1 and LF2a/b.	LF4
LF5		Slumping		Pure mudstones fractured through slumping before lithification; calcitic block and radiaxial-fibrous cements fill interstices; LF5 mudstones contain no components, merely some peloids <<0.5mm.	LF5
LF6	Deposits of openmarine biota		Bioclastic rudstone; bioclastic components are <i>Daonella</i> sp. and small cephalopods solely; bivalve shells are closely packed and stacked one above the other; interstices are filled with cement and sometimes sediment (wackestones with red micrite and fragments of echinoids); geopetals.	LF6	
LF7	Neptunian dykes		Red calcitic mudstones; restricted occurrence of cephalopods and openmarine foraminifers, such as: nodosarids, <i>Abriolina mediterranea</i> and porcellaneous forams (<i>Ophthalmidium</i> sp.); other components are: lithoclasts of the same LF type, finegrained peloids and coprolites (<0.5mm), specialised dwarf fauna (ostracods, micro-filaments); closely packed layers of radiaxial-fibrous cements parallel the walls of the dykes and are often micritised.	LF7	

Table 2.1 List of lithofacies associations of the slope-facies.

Plate 2.7 (following page) Anisian reef limestones from the Latemar, Dolomites, Italy: sponges, corals and algae.

Fig. 1.-3. *Celyphia? minima* Senowbari-Daryan, Zühlke, Bechstädt and Flügel.

Fig. 1. Oblique section through two chambers exhibiting ostia with exauli and pores in the wall. (Cresta De Do Peniola, x13)

Fig. 2. Irregular chamber with evidence of ostia in the wall. (Cresta De Do Peniola, x17)

Fig. 3. Irregular, barrel-shaped chambers with some vesiculae. (Cresta De Do Peniola, x26)

Fig. 4.-6. *Vesicocaulis oenipontanus* Ott.

Fig. 4. Longitudinal section through several oval-shaped, imperforate chambers. The tranverse section provides evidence for the canal-system and the vesiculae. (Cresta De Do Peniola, x9)

Fig. 5.-6. Oblique and tranverse section with canal-system and vesiculae. (Cresta De Do Peniola, x13)

Fig. 7. *?Colospongia* sp. This sponge exhibits numerous pores in the wall as well as ostia. It displays some affinities with the specimen of Plate 1, Fig 9., but has most probably to be described as a new sponge. (Cresta De Do Peniola, x13)

Fig. 8. *?Colospongia* sp. (Cresta De Do Peniola, x9)

Fig. 9.-11. Dasycladacean algae from back-reef limestones.

Fig. 9. *Diplopora* sp.? (Schenon, x9)

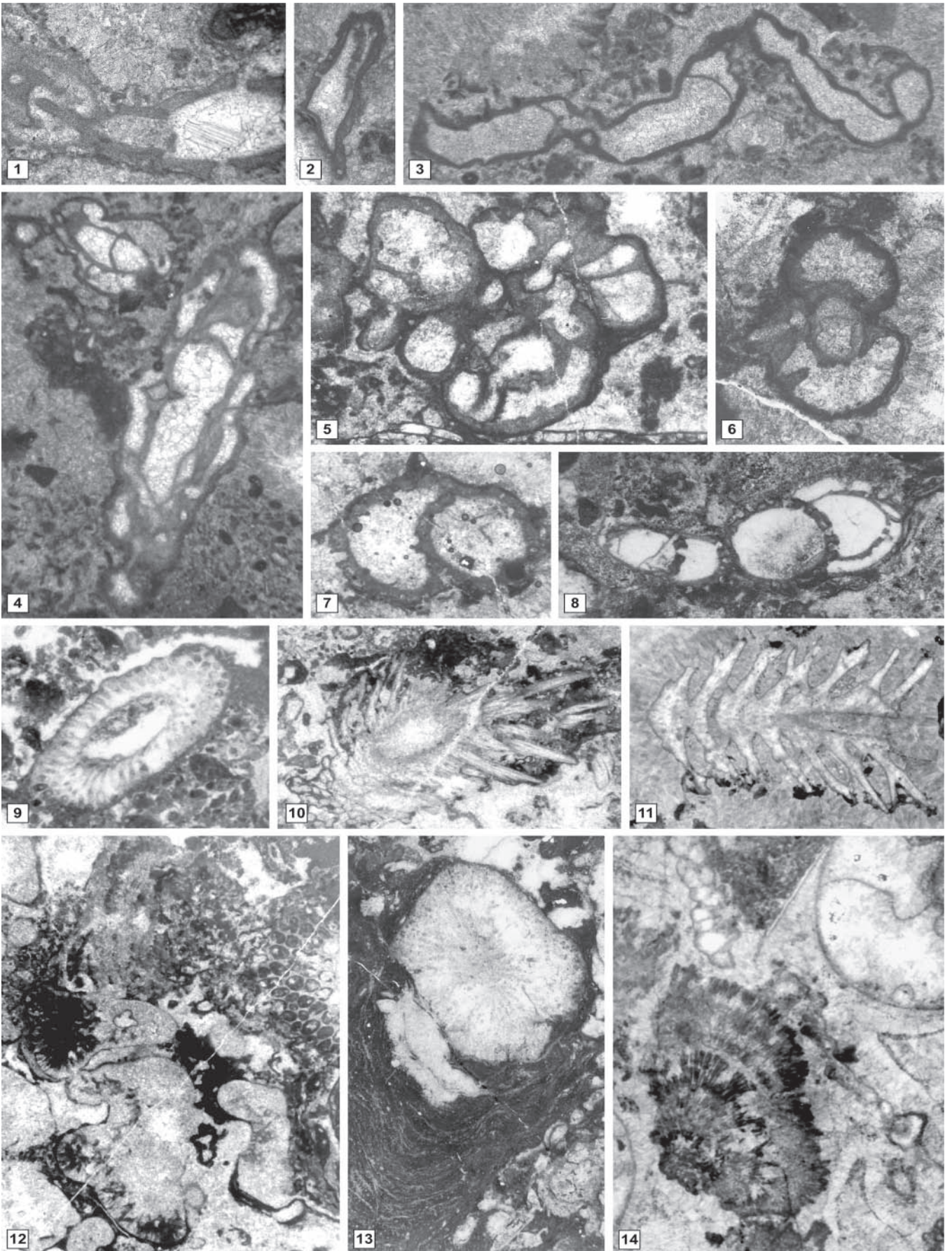
Fig. 10. *Teutloporella peniculiformis?* Ott. (Cresta De Do Peniola, x9)

Fig. 11. *Diplopora nodosa* Ott. (Schenon, x9)

Fig. 12. Coral/bryozoan/"*Tubiphytes*" boundstone microfacies. Irregular thamnasteroid corals together with bryozoa *Reptonoditrypa cautica* and "*Tubiphytes*"-like group fragments. (Cresta De Do Peniola, x13)

Fig. 13. Coral (*Margarosmilia* sp.) surrounded by microbial encrustations. (Cresta De Do Peniola, x9)

Fig. 14. *Olangocoelia*/porostromata floatstone microfacies. This microfacies is rich in fragments of different porostromata, cephalopods and isopachous cements. (Cima Feudo, x9)



"Sphinctozoans"	<i>Celyphia</i> n. sp.?	Senowbari-Daryan, Zühlke, Bechstädt and Flügel 1993	Anisian	
	<i>Celyphia?</i> <i>minima</i>	Ott, Pisa and Farabegoli 1980	Anisian	
	<i>Celyphia zoldana</i>			
	<i>Colospongia</i> sp.			
	<i>Colospongia catenulata catenulata</i>	Ott 1967	Ladinian	
	<i>Deningeria</i> sp.			
	<i>Deningeria crassireticulata</i>	Senowbari-Daryan, Zühlke, Bechstädt and Flügel 1993	Anisian	
	<i>Follicatena cautica</i>	Ott 1967	Ladinian	
	<i>Solenolmia manon manon</i>	(Münster 1941)	Anisian/Ladinian	
	<i>Thaumastocoelia dolomitica</i>	Senowbari-Daryan, Zühlke, Bechstädt and Flügel 1993	Anisian	
Inozoans	<i>Vesicocaulis oenipontanus</i>	(Ott 1967)	Ladinian	
	<i>Meandrostia triassica</i>	Senowbari-Daryan, Zühlke, Bechstädt and Flügel 1993	Anisian	
Sponges?	<i>Olangocoelia otti</i>	Bechstädt and Brandner 1970	Anisian	
Corals	<i>Margarosmia</i> sp.			
	<i>Retiophyllia</i> sp.			
	<i>Zardinophyllum</i> sp.?			
Bryozoans	<i>Reptonoditrypa cautica</i>	Schäfer and Fois 1987	Anisian	
"Microproblematica"	<i>Anisocellula fecunda</i>	Senowbari-Daryan, Zühlke, Bechstädt and Flügel 1993	Anisian	
	<i>Baccanella floriformis</i>	Pantic 1971	Anisian/Ladinian	
	<i>Bacinella ordinata</i>	Pantic 1972	Anisian/Ladinian	
	<i>Ladinella porata</i>	Ott 1968	Ladinian	
	<i>Plexoramea cerebriformis</i>	Mello 1977	Anisian/Ladinian	
	<i>Radiomura cautica</i>	Senowbari-Daryan and Schäfer 1979	Ladinian	
	" <i>Tubiphytes</i> " n. sp.?			
	" <i>Tubiphytes</i> " <i>gracilis</i>	Schäfer and Senowbari-Daryan 1983	Anisian/Ladinian	
	" <i>Tubiphytes</i> " <i>multisiphonatus</i>	Schäfer and Senowbari-Daryan 1983	Anisian/Ladinian	
	" <i>Tubiphytes</i> " <i>obscurus</i>	Maslov 1956	Anisian/Ladinian	
	Dasyclads	<i>Diplopora annulata</i>	Schaffhäutl 1863	Anisian/Ladinian
		<i>Diplopora nodosa</i>	Schaffhäutl 1863	Anisian/Ladinian
		<i>Macroporella</i> sp.		
<i>Teutloporella</i> sp.				
Solenoporaceans	<i>Zornia obscura</i>	Senowbari-Daryan and Di Stefano 2001	Anisian/Ladinian	
	<i>Solenopora</i> sp.			
Porostromata	<i>Parachaetetes</i> cfr. <i>triasinus</i>	Vinassa De Regny 1915	Anisian/Ladinian	
	<i>Ortonella</i> sp.			
	<i>Girvanella</i> sp.			
"Microbial crusts"				
Spongiostromata Auct.				
Foraminifers	<i>Abriolina mediterranea</i>	Luperto 1963	Anisian/Ladinian	
	<i>Arenovidalina chiangchiangensis</i>	Ho 1959	Anisian	
	<i>Aulotortus?</i> <i>eotriasicus</i>	Zaninetti, Rettori and Martini 1994	Anisian	
	<i>Bullopora</i> sp.			
	<i>Diplostromina</i> cfr. <i>astrophimbriata</i>	Kristan-Tollmann 1964	Anisian/Ladinian	
	<i>Duostomina</i> sp.			
	<i>Earlandia</i> sp.			
	<i>Earlandinita</i> sp.			
	<i>Endoteba</i> sp.			
	<i>Endoteba</i> ex gr. <i>obturata</i>	(Brönnimann and Zaninetti 1972)	Anisian/Ladinian	
	<i>Endotriada</i> cfr. <i>tyrrhenica</i>	Vachard, Martini, Rettori and Zaninetti 1994	Anisian/Ladinian	
	<i>Endotriadella</i> sp.			
	<i>Endotriadella wirzi</i>	(Koehn-Zaninetti 1968)	Anisian	
	<i>Flatschkofelia anisica</i>	Rettori, Senowbari-Daryan and Zühlke 1996	Anisian	
	<i>Gaudrinella</i> sp.			
	<i>Krikoumbilica pileiformis</i>	He 1984	Anisian/Ladinian	
	<i>Nodosaridae</i>			
	<i>Lamelliconus</i> ex gr. <i>ventroplanus</i>	(Oberhauser 1957)	Anisian?/Ladinian	
	? <i>Ophthalmidium</i> sp.			
	<i>Palaeolithuonella meridionalis</i>	(Luperto 1965)	Anisian/Ladinian	
	<i>Paraophthalmidium</i> sp.			
	<i>Reophax</i> sp./ <i>Ammobaculites</i> sp.			
	<i>Textularia</i> sp.			
	<i>Tolypammina</i> sp.			
	<i>Trochamminidae</i> sp.			
	<i>Turriglomina</i> sp.			
	<i>Turriglomina mesotriassica</i>	(Koehn-Zaninetti 1968)	Anisian/Ladinian	
	<i>Turriglomina scandonei</i>	Zaninetti, Ciarapica, Martini, Salvini-Bonnard and Rettori 1987	Anisian/Ladinian	
	Worm tubes	<i>Spirorbis</i> sp.		
	Decapod coprolites	<i>Favreina</i> sp.		
Algae incertae sedis	<i>Thaumatoporella</i> cfr. <i>parvovesiculifera</i>	Raineri 1922	Anisian/Ladinian	
Pelecypods	<i>Daonella</i> sp.			
Ammonoids				
Gastropods				
Ostracods				
Echinoids				

Table 2.2 List of biota encountered in the slope- and reef-facies of the Latemar.

Vesicocaulis oenipontanus, *Thaumastocoelia dolomitica* and more seldomly *Meandrostia triassica* form bafflestones. These bafflers are generally surrounded and stabilised by biogenic crusts.

2.5.3.3 B3 - “Sphinctozoan”-coral-bryozoan-bafflestones

In this biocoenosis, encrusting “sphinctozoan” sponges like *Celyphia zoldana*, *Celyphia? minima* and isolated chambers of *Deningeria* sp. are associated with locally abundant hexacorals (*Margarosmilia* sp.) often displaying microboring. The corals are usually covered by biogenic crusts and are very recrystallised. Bryozoans - *Reptonoditrypa cautica* exclusively - play a similar small role. “*Tubiphytes*” *obscurus*, *Bacinella ordinata* and other microproblematica (e.g. *Radiomura cautica*) complete this biocoenosis. Small forams can be found in the trapped (baffled) sediment (duostominids, Endotriadidae, etc.), whereas sessil forams reveal intergrowth with biogenic crusts.

The delicate branches of the scleractinian bafflers are closely spaced, very ramified and associated with encrusting sponges and species of the “*Tubiphytes*” grp.. The high number of septa, the branching growth and the size of the corallites indicate a similarity to *Margarosmilia* sp.. This biocoenosis is not very robust, however it forms large colonies as blocks of this biocoenosis with a diameter of 4m to 5m were encountered on the slope (upper part of Cresta De Do Peniola). Trapped sediment are wacke-/packstones of the lagoon sometimes associated with “*Tubiphytes*” encrustations. Part of this faunal assemblage are also solenoporaceans, revealing microboring and micritisation of surfaces.

2.5.3.4 B4 - Scleractinian-framestones

Generally, corals are primary framebuilders of the bioconstructions at Latemar. Later stages of reef development show the encrustation and overgrowth by secondary framebuilders like algae and/or microbial crusts. The scleractinians of this biocoenosis are mainly characterised by isolated, thick and tall corallites. The corals are less commonly cerioid (branched). A patch reef-like growth is typical, colonies are up to 3m wide and 1m high. These isolated mounds are laterally not continuous and its framestones are very often recrystallised. A low number of septa and a robust nature of the stems points to the identification as *Retiophyllia* sp. (*Retiophyllia* sp. 2 sensu Senowbari-Daryan et al. 1993). The

biggest colonies are found in-situ at Kirchtage weide and in blocks on the slope at Cresta De Do Peniola. In-situ colonies at Cima Feudo and Erzlahn are smaller and the individuals are less robust.

2.5.3.5 B5 - Microbialites/microbialitic bindstones

The framework of this biocoenosis comprises different microbial crusts of cyanobacterial activity. The largest occurrence of B5 is at Erzlahn where the bioconstruction forms an elongated structure (microbial/algal ridge, see chapter 2.4.3.2). Stromatolitic and clotted-thrombolitic fabrics are the vital part of this biocoenosis. Both fabrics reveal a close intergrowth and an equal volumetric percentage. The biogenic crusts reveal different, alternating levels of growth (thrombolitic-stromatolitic) and contain intercalated fragments of cyanobacterial algae like *Girvanella* sp. and sessil forams (nubecularids). Layers of the crusts are quite often replaced by *Baccanella floriformis* on the inside and/or cements on the outside. Seldomly, “*Tubiphytes*” group and *Bacinella ordinata* are part of this symbiotic growth.

However, this assemblage is not very frequent at Latemar compared to its abundance in bioconstructions of other Middle and Upper Triassic reefs in the area of the western Tethys. From the palaeo environmental point of view, this assemblage is generally referred to the reef crest area. In a few cases, B5 occurs together with “*Tubiphytes*” grp. associations also in the upper part of the slope.

2.5.3.6 B6 - “Tubiphytes” multisiphonatus-framestones

This biocoenosis is characterised by the overwhelming presence of “*Tubiphytes*” *multisiphonatus*. Its branches form large colonies of up to 2m width and 0,5m height with different levels/layers of growth (see also Plates 2.3.1 and 2.3.2). The radially growing, slender branches of “*Tubiphytes*” *multisiphonatus* consist of a central tubular channel (“thallus”) and are embedded in a network of micritic filaments. Sometimes peloids are incorporated in the micritic surroundings of the central tubes, sometimes they are part of the sediment between the branches. Longitudinal sections of this framestone reveal the thin, subparallel to parallel “thalli” to be closely associated with large amounts of cements between the branches of a colony. The tubes of “*Tubiphytes*” *multisiphonatus* are sometimes very sinuous (undulated) and not as strictly upright as in the original literature (see Schäfer and Senowbari-Daryan 1983). At least two generations of cement exist; the first generation is usually isopachous

calcite, the second generation block calcite. Oblique and transverse sections show the network of the tubes. Trapped matrix sediment bears irregular fragments of algae (*Thaumatoporella* cfr. *parvovesiculifera*), peloids and seldomly small forams (*Endotriadella* sp.). However, the cement filled “voids” between the “branches” seem to have formed through diagenetic alterations. The bioclastic components incorporated by the micritic filaments around the tubes of “*Tubiphytes*” *multisiphonatus* show abrupt terminations at the “branch”-cement-contact. The outer surfaces of the “branches” are very ir-

regular like having being attacked and destroyed by the cements. This leads to the conclusion that the visible sequence of cements does not reflect primary cementation. Nevertheless, early syn-depositional cements must have played a crucial role during buildup of the mounds; at later stages they might have been pathways for fluid migration and been replaced by secondary cements. 10-20cm thick lenses of small bivalves (1-2cm in diameter; dolomitised; possibly *Daonella* sp.) between the mounds are evidence for a regime of low wave energy. The proximity of the mound-like structures to the lagoon-facies

Location	Aggtelek, Hungary	Hydra, Greece	Latemar, Italy	Concarena, Italy
Formation	Aggtelek Reef Fm (Wetterstein Fm)	Pantokrator Limestone	"Latemar Limestone", reef facies (Schlern Fm)	Esino Fm, reef facies
Author	Scholz (1972)	Schäfer and Senowbari-Daryan (1982, 1983)	this study	M. Seeling (pers. comm. 2003) and this study
Age	Anisian (Early Pelsonian-Upper Illyrian)	Carnian/Norian	Anisian/Ladinian (Middle Illyrian-Earliest Fassanian)	Ladinian/Carnian
Taxa	Hydrozoa	Microproblematica	Microproblematica	Microproblematica
Species	<i>Axopora aggtelekensis</i>	" <i>Tubiphytes</i> " <i>multisiphonatus</i>	" <i>Tubiphytes</i> " <i>multisiphonatus</i>	" <i>Tubiphytes</i> " <i>multisiphonatus</i>
Diameter of central tubes	40-60µm	50-60µm	50µm	40-50µm
Thickness of "branch"	200-400µm (measured from Plate V, p.356)	500-1100µm (measured from Plate 10, p.152)	200-800µm	400-800µm
Length of "branches"	0,3-0,7cm (oblique section?, measured from Plate V, p.356)	"several cm" (Schäfer and Senowbari-Daryan 1983, p.129)	up to 3cm	up to 5cm
Height of bushlike "thalli"	10-15cm	5cm	10-30cm	10-30cm
Maximal dimensions of mound	?	?	height: 70cm; length: 300cm	height: 70cm; length: 300cm
Palaeoposition	"protected parts of the central reef", i.e. transition to back-reef (see p.341)	transition from reef to lagoon (see Schäfer and Senowbari-Daryan 1982, p.155-156; Schäfer and Senowbari-Daryan 1983, p.127)	back-reef	back-reef, transition to the lagoon
Cements	fibrous calcite	?	isopachous calcite around the branches and block calcite	isopachous calcite around the branches and block calcite
Thickness of micritic filaments surrounding central tubes	- ("Coenenchyma", see p.345)	5-10µm	ca. 5 times smaller than central tube (i.e. ca. 10µm)	ca. 5 times smaller than central tube (i.e. ca. 10µm)

Table 2.3 Comparison of “*Tubiphytes*” *multisiphonatus* findings from Scholz (1972) and Schäfer and Senowbari-Daryan (1982, 1983) with the mounds described from Latemar (Dolomites) and Concarena (Lombardy).

Plate 2.8 (following page) Anisian reef limestones from the Latemar, Dolomites, Italy: microproblematica.

Fig. 1.-2. *Bacinella ordinata* Pantic, a common, encrusting microproblematicum together with sponges, algae and bryozoans. (Cresta De Do Peniola, 1: x6; 2: x9)

Fig. 3.-5. “*Tubiphytes*” *obscurus* Maslov, a very abundant organism in the Anisian reef facies of Latemar, generally present with different types of the “*Tubiphytes*” group and other microproblematica. (3: Cresta De Do Peniola, x26; 4: Schenon, x17; 5: Cresta De Do Peniola, x17)

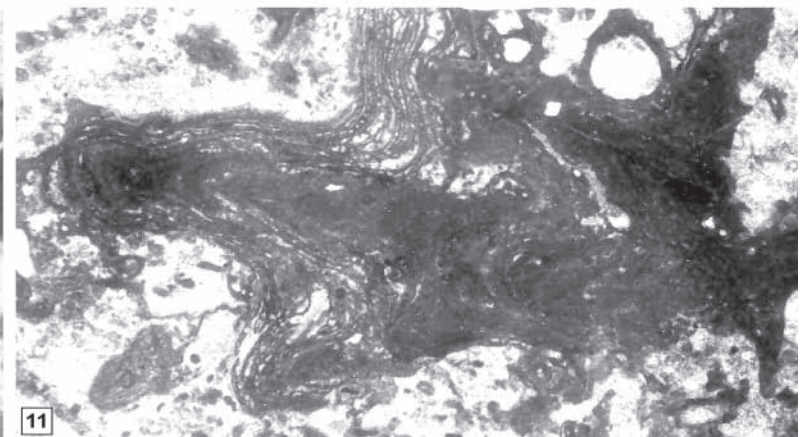
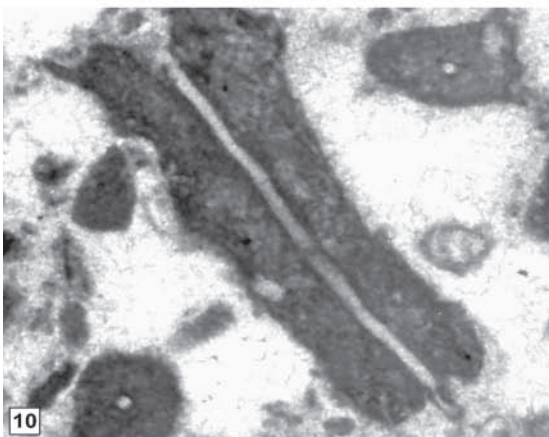
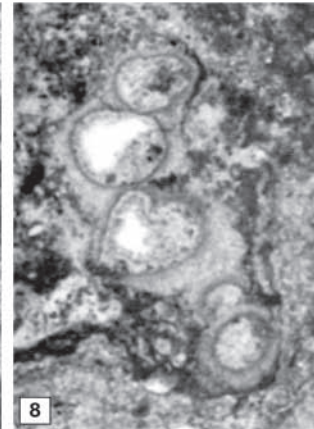
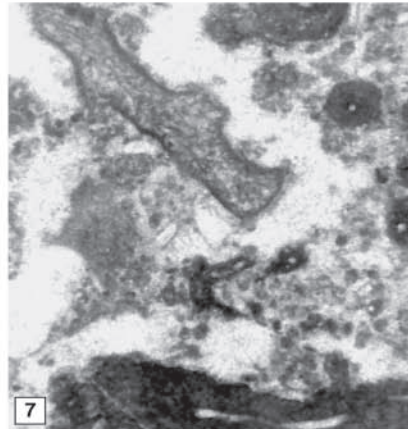
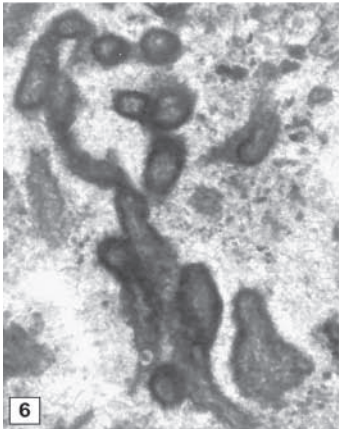
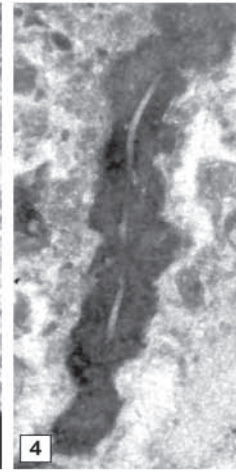
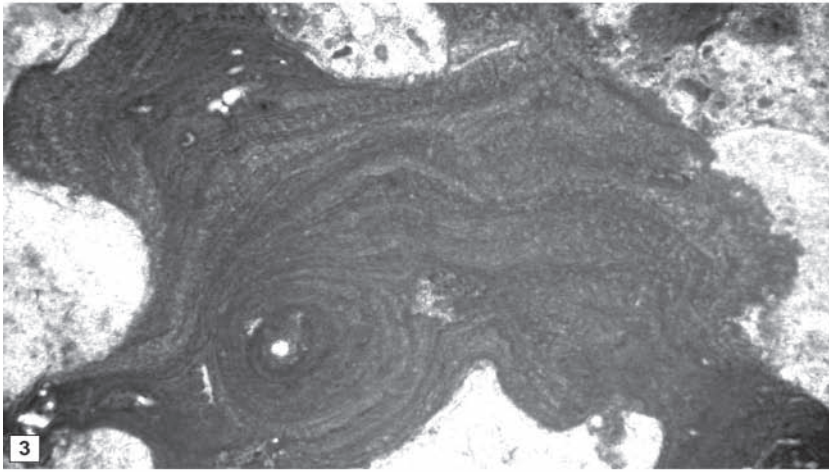
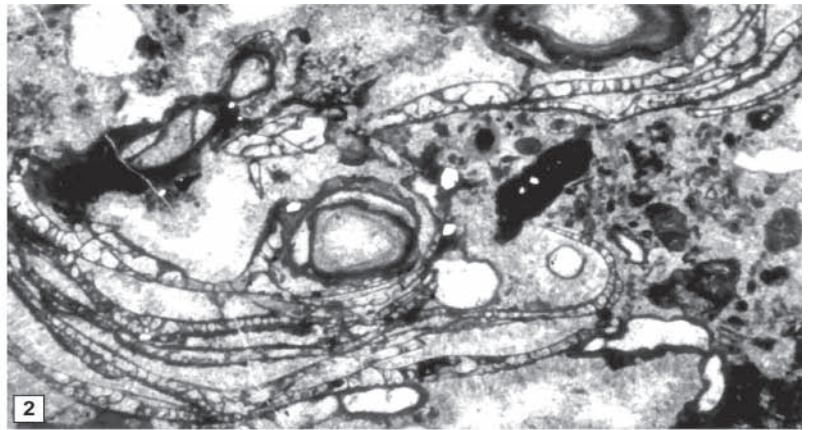
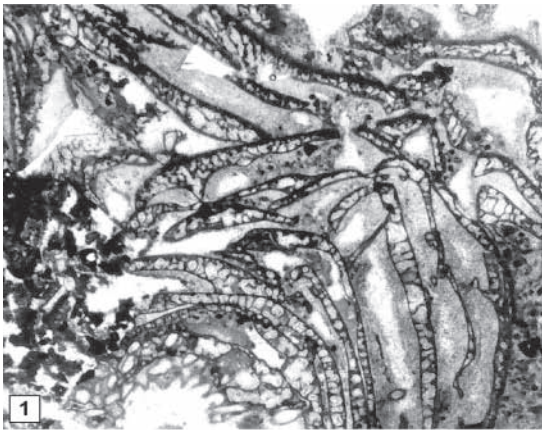
Fig. 6. “*Tubiphytes*” cfr. *carianthicus* Gaetani and Gorza. This specimen seems to be an intermediate, distinguishable form between “*Tubiphytes*” *carianthicus*=*Plexoramea cerebriformis* Mello and “*Tubiphytes*” *obscurus*. (Schenon, x13)

Fig. 7. Association of “*Tubiphytes*” *obscurus* and *Plexoramea cerebriformis* Mello. (Cresta De Do Peniola, x13)

Fig. 8.-9. *Radiomura cautica* Senowbari-Daryan and Schäfer, a rare microproblematicum in the Anisian reef-facies of the Latemar. (8: Cresta De Do Peniola, x13; 9: Schenon, x13)

Fig. 10. Longitudinal and traverse sections of “*Tubiphytes*” *obscurus*. (Schenon, x40)

Fig. 11. Association of “*Tubiphytes*” *obscurus* and microbial encrustations, a very common microfacies of the Anisian reef-facies of the Latemar. (Cresta De Do Peniola, x13)



indicates a sheltered position at the back reef margin. The strata on which the mounds are growing are dipping towards the centre of the Latemar, i.e. a depression (back reef lagoon) existed between the reef and the topographic highest part of the atoll - the tepee-belt (see also chapter 2.5.6).

Our facial and palaeontological investigations allow the deduction of a detailed growth development of the colonies (see chapter 2.4.3.2). Buildup started with several subparallel tubes ramifying towards the end of the first growth stage forming a pillow-like nucleus on which new levels/layers of "*Tubiphytes*" *multisiphonatus* grew. The first, nucleus-like stage is rather small, with some dm in diameter, several cm in height (see chapter 2.4.3.2). The next layers are up to few dm thick. These layers are easily distinguishable in outcrop, whereas in microfacies a separation of layers is not obvious. Here, the bush-like ramification and radial growth of colonies prevail.

"*Tubiphytes*" *multisiphonatus* Schäfer and Senowbari-Daryan (1982, 1983) versus *Axopora aggtelekensis* Scholz (1972):

The microfacial appearance of "*Tubiphytes*" *multisiphonatus* corresponds fully to the description given by Schäfer and Senowbari-Daryan (1983) apart from the undulated nature of its tubes. In the original material from Hydra (Greece), the "thalli" are not sinuous (undulated) but mostly upright. Concerning the outcropping mound, several microfacial features and most importantly the palaeo ecological position, strong affinities exist with the description given by Scholz (1972) of mound-like structures in an Anisian reef (Illyrian) from the Aggtelek

mountains in Hungary. However, Scholz (1972; pp.344-345) attributes the mound-forming colonies to hydrozoans (*Axopora aggtelekensis* Scholz) despite missing tabulae, and interpreted the micritic filaments surrounding the central channels as "coenenchyma" (see Scholz 1972, Plate 2.5). For a comparison of both occurrences please refer to Table 2.3.

A further occurrence of "*Tubiphytes*" *multisiphonatus* mounds is in the Lombardian Alps (M. Seeling, University of Heidelberg, pers. comm. 2003). A comparison between our samples and those from the Lombardian Alps proved both to be identical (see Table 2.3).

2.5.4 Biocoenoses of secondary reef-builders

2.5.4.1 B7 - *Olangocoelia*-bindstones

Olangocoelia otti bindstones are characterised by the crust-like, catenulate arrangement of their small globular or oval chambers around cavities between talus blocks and mostly bioclasts. The cavities are usually filled with synsedimentary isopachous cements. B7 is commonly found as reworked clasts on the slope, scarcely in-situ. It is frequently associated with biota of the platform margin, but also with pelagic organisms (*Daonella* sp. and cephalopods), lagoonal algae (porostromata and dasycladaceans) and/or benthonic foraminifers (duostominids, Endotebidae and Endotriadidae). Porostromata are mainly represented by the *Ortonella* species. Its large thalli fragments are characterised by dark, obvious, linear tubes with a low angle of bifurcation, typical for *Ortonella* sp.. Sessile foraminifers, biogenic crusts and "*Tubiphytes*" group concur to stabilise autochthonous finergrained sediments (LF5) and resedimented litho-

Plate 2.9 (following page) Anisian reef limestones from the Latemar, Dolomites, Italy: "*Tubiphytes*" *multisiphonatus* biocoenosis, biogenic crusts and algae.

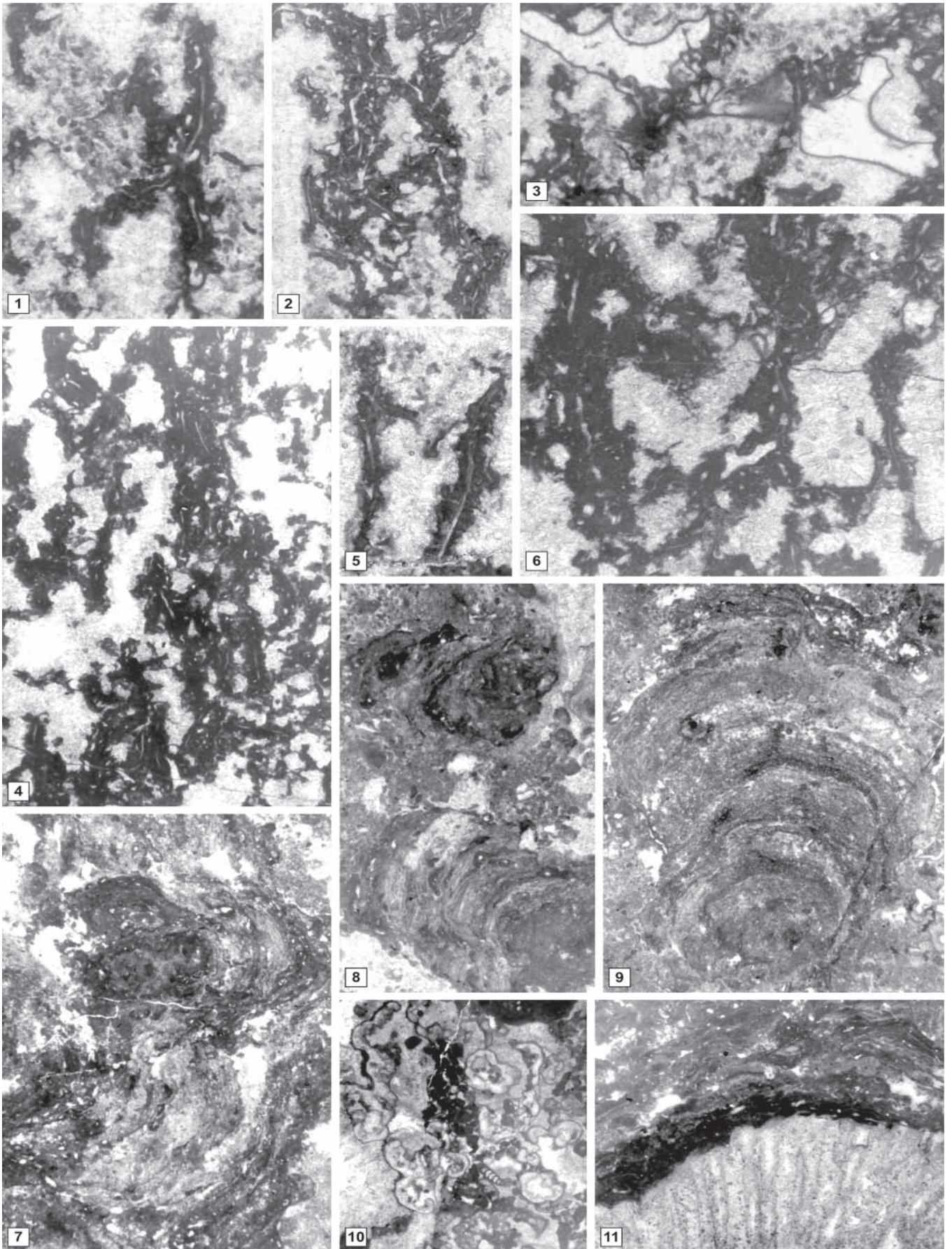
Fig. 1.-2., 4.-6. "*Tubiphytes*" *multisiphonatus* framestone. This biota, firstly described by Senowbari-Daryan and Schäfer (1983), is present on the back-reef margin of the reef belt at Latemar with large colonies, up to 2m wide and 0,5m tall. Corresponding to Senowbari-Daryan and Schäfer's original description (1983), longitudinal sections reveal subparallel to parallel tubes embedded in a network of fine micritic filaments forming erect, slender, ramose "thalli". Large amounts of synsedimentary, isopachous and blocky calcitic cements are present between these "thalli"-like structures of the colonies. (Erzlahn, 1: x9; 2: x6; 4: x5; 5: x9; 6: x17)

Fig. 3. Peloids and algal remains (similar to *Thaumatoporella* cfr. *parvovesiculifera*) in oblique section between the "thalli" of "*Tubiphytes*" *multisiphonatus*. (Erzlahn, x13)

Fig. 7.-9. Biogenic crusts. Bundles of microbial encrustations ("spongiostromata" Auct.) derived from cyanobacterial activity sometimes together with sessile forams. This biocoenosis can also be referred to the stromatolites/microbialites. (Erzlahn, 7: x9; 8: x4; 9: x9)

Fig. 10. *Zornia obscura* Senowbari-Daryan and Di Stefano. This very rare organism (dasyclad?) of the lagoon-facies at Latemar is here associated with fragments of other dasycladacean algae. (Erzlahn, x9)

Fig. 11. Fragment of a coral surrounded by microbial encrustations. (Cima Feudo, x4)



clastic material (LF2). The occurrence of reefal detritus and openmarine cephalopods points to a setting on the uppermost slope. Hence this biocoenosis is found in the lower parts of the Cresta De Do Peniola sections and on the uppermost slope at Cima Feudo and Schenon. At Latemar however, this biocoenosis is only of local and minor importance unlike at other, but slightly older Anisian reefs of the Dolomites where *Olangocoelia otti* is an important reef-builder (Fois and Gaetani 1984; Senowbari-Daryan et al. 1993).

2.5.4.2 B8 - "Tubiphytes"-microproblematica-bindstones

Despite being a secondary reef-builder, this biocoenosis is the most important faunal association at Latemar. Its distribution ranges from the upper slope to the central reef concurring to the stabilisation of carbonate sediments and primary reefal frameworks. B8 is rich in different species of the "Tubiphytes" group ("*Tubiphytes gracilis* in fragments only, "*Tubiphytes obscurus* most frequently and "*Tubiphytes*" sp.) generally associated with biogenic crusts within the framework of biogenic structures. Microproblematica are equally abundant and being mainly represented by *Plexoramea cerebriformis*, *Bacinella ordinata* and only in a few cases - i.e. in the upper parts of the Cresta De Do Peniola sections - by *Ladinella porata*. The "Tubiphytes" group at Latemar's reef is characterised by different, heterogeneous microfabrics. Their common characteristics are circular tubes or central channels in the middle of micritic crusts with undulated laminae or reticular tissue. The smaller species of this biocoenosis is referred to "*Tubiphytes gracilis*", showing a dense network of small and very irregular branches. Sometimes "*Tubiphytes gracilis*" is associated with other encrusting organisms like sessil forams or *Ladinella porata*. In some cases it is not possible to

distinguish between individuals of *Plexo-ramea cerebriformis* and "Tubiphytes" group (for intergrowth of both species see also Enos et al. 1997). Compared to other Anisian reefs in the Dolomites like in the Olang area (Fois and Gaetani 1984; Senowbari-Daryan et al. 1993), "Tubiphytes" group and microproblematica are much more abundant at Latemar.

2.5.4.3 B9 - *Bacinella*-bindstones

This biocoenosis is not a major constructor of the reef-facies but is always assisting in the stabilisation of primary frameworks. Only in some cases, *Bacinella*-bindstones form primary fabrics where their framework is almost exclusively organised by this species. *Bacinella* sp. is heavily encrusting sponges, corals and fragments of the "Tubiphytes" group. Microproblematica are generally of major importance for this biocoenosis. Among the most abundant are the "Tubiphytes" group and *Radiomura cautica*. This faunal assemblage is also associated with bryozoans, bundles of Porostromata as well as some sponges, few dasycladaceans and encrusting sessil forams (nubecularids). The isolated parts of the *Bacinella ordinata* mesh have large, ordinate cells, whereas the dense, encrusting parts (*Bacinella* sp.) reveal closer spaced and less regular cells. The matrix of the boundstones are wacke-/packstones with peloids. Cavities are recrystallised and also covered with *Bacinella* sp.. Duostominids, Endotebidae, fragments of sessil forams and *Palaeolituonella meridionalis* are the most abundant foraminifers of intercalated sediment.

2.5.5 Associations of the lagoon

2.5.5.1 B10 - Lagoonal pack-/grainstones

The pack-/grainstones of the lagoon-facies are part of the reef-facies at the transition from back-reef to tepee-belt (see chapter 2.5.6 and Fig. 2.15). They are full of

Plate 2.10 (following page) Anisian reef limestones from the Latemar, Dolomites, Italy: solenoporacean and porostromate algae, bryozoans and corals.

Fig. 1.-2,4. Nodular to branched thalli of *Parachaetetes* cfr. *triasinus* Vinassa de Regny. Small cells and horizontal elements indicate growth stages. Microboring and presence of microproblematica (*Bacinella* sp.) are typical for these associations. (1: Cresta De Do Peniola, x13; 2: Cresta De Do Peniola, x9; 4: Cresta De Do Peniola, x9)

Fig. 3. *Solenopora* sp. (Cima Feudo, x4)

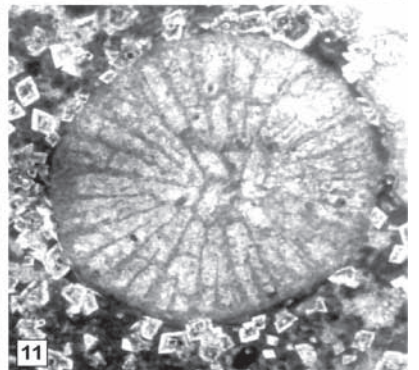
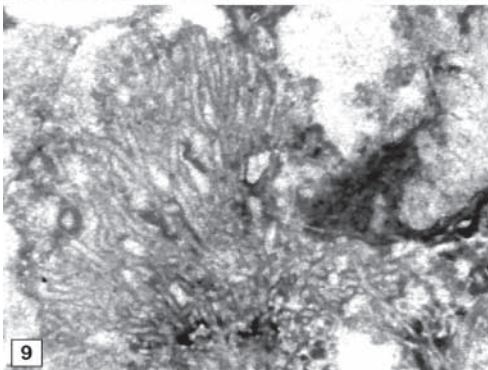
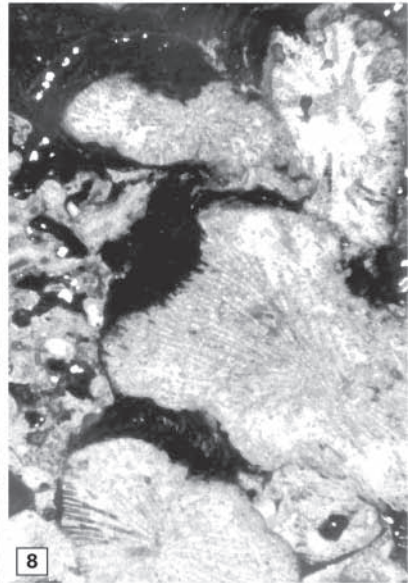
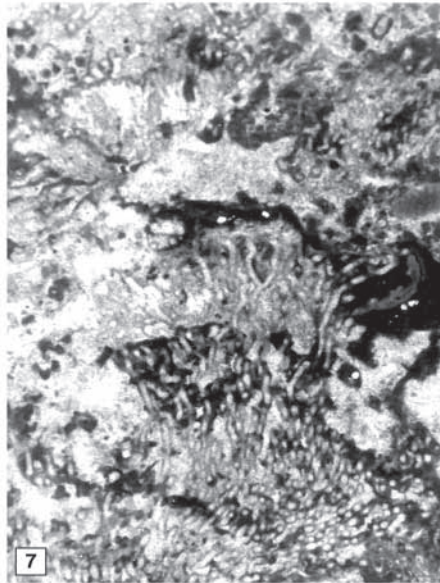
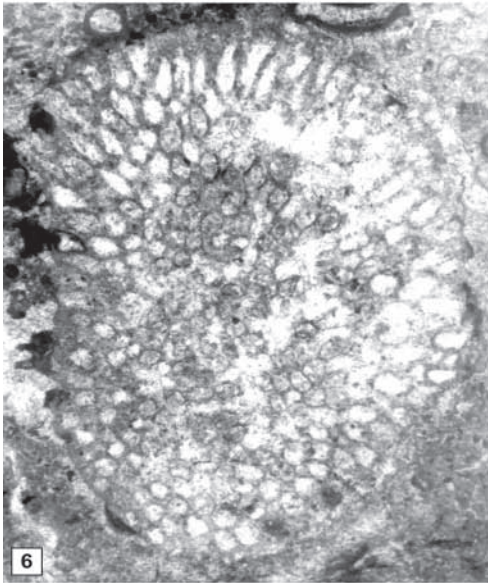
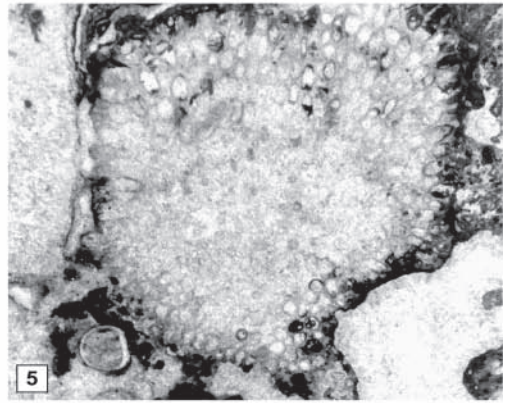
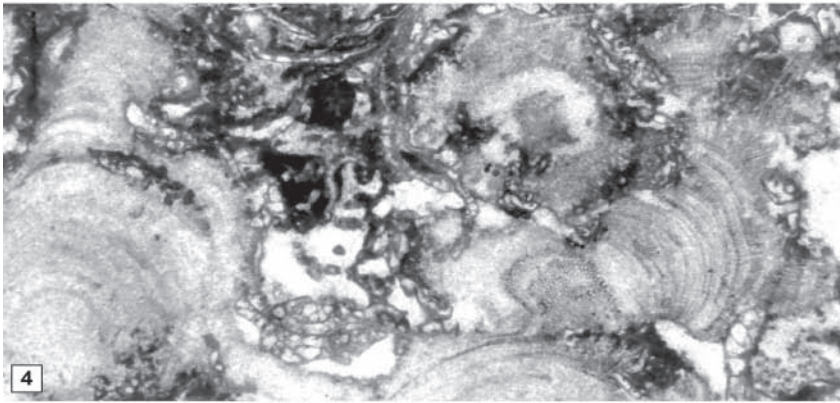
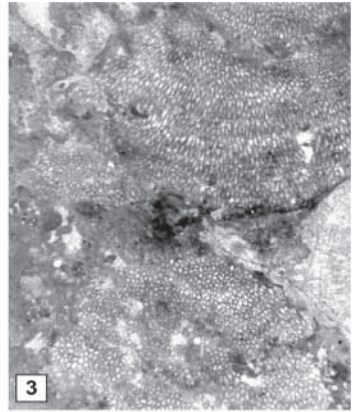
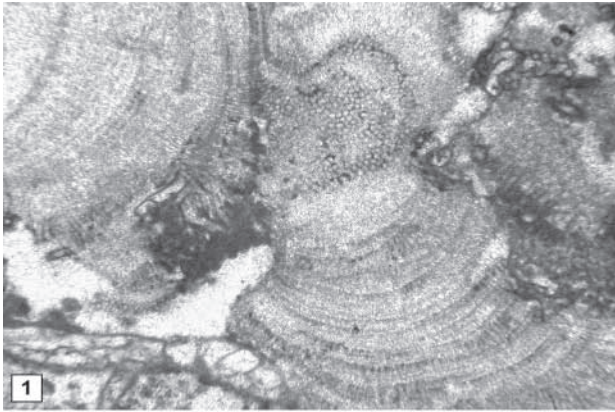
Fig. 5.-6. *Reptonoditrypa cautica* Schäfer and Fois, the only bryozoan found in the Latemar area. On the surface evidence of microboring. (Cresta De Do Peniola, 5: x5; 6: x9)

Fig. 7.,9. Porostromate algae: *Ortonella* sp. (Cresta De Do Peniola, x9)

Fig. 8. Cerioid corals (*Retiophyllia* sp.). (Cresta De Do Peniola, x9)

Fig. 10. Transverse section of a coral with an affinity to *Zardinophyllum* sp.. (Schenon, x4)

Fig. 11. Transverse section of an isolated *Retiophyllia* sp. (Erzlahn, x11)



fragments of dasyclads (*Diplopora nodosa*, *Teutloporella* sp. and *Macroporella* sp.), *Zornia obscura* (probably fragments of dasycladacean algae), benthic forams (autotortids, *Reophax/Ammobaculites* sp.), gastropods, bivalves and worm tubes. The presence of lithoclasts indicates levels of higher energy. In some cases pelagic material (*Daonella* sp. and cephalopods) is washed into the lagoon by storms. For a detailed analysis of lagoonal facies at Latemar refer to Egenhoff et al. (1999).

2.5.6 Palaeo ecology of the reef-facies at Latemar

Our reef model takes into account the relation between faunal associations in each locality and their different palaeo environmental positions (see Fig. 2.15). The majority of the biocoenoses presented in our reef concept are of Anisian or Anisian/Ladinian age, only in a few cases Ladinian biota were observed. The concept of the reef-facies at Latemar consists of a very diversified biotic association being generally correlatable with other localities of Anisian/Ladinian reefs in the Dolomite area (Fois, 1982; Fois and Gaetani, 1984; Brandner et al., 1991; Senowbari-Daryan et al., 1993). However, differences exist in the little abundance of *Olangocelia* sp., in the higher diversification proven by mounds of “*Tubiphytes*” *multisiphonatus* (see P2.2.2, P2.3.1, P2.3.2 and chapter 2.4.3) and the large abundance of micropro-

blematica like “*Tubiphytes*” *obscurus*. The foraminiferal associations also correspond with other Anisian/Ladinian reefs described in literature (e.g. Trifonova and Vaptsarova 1982; Isintek et al. 2000), in particular with the Olang area (Fois and Gaetani 1984; Senowbari-Daryan et al. 1993) with respect to Duostominidae, Endotriadidae, Endotebidae and sessile forms like *Flaschkofelia anisica*. Differences are witnessed by the presence of several genera, like *Turriglomina mesotriasica*, *Turriglomina scandonei*, *Lamelliconus* ex gr. *ventroplanus*, *Aulotortus eotriasicus* and *Abriolina mediterranea*, the latter one found only in the Lagonegro area in Southern Italy and few other reef localities in the world (Zaninetti et al. 1992).

According to the outcrops, three main zones within the reef facies can be defined: (1) reef front, (2) reef crest and (3) back reef. In the reef front, three subzones were distinguished with the help of different biocoenoses (see Fig. 2.15). Those zones inhabiting sediment baffling organisms with a branching growth are situated beneath the mean wave base (biocoenoses B1 to B3; see chapter 2.5.3). They have the least potential of preservation in the geological record due to their delicate forms. Clasts of these biocoenoses are abundant in slope sediments. The base of the branching zone is formed by stabilising algae and is followed by bryozoans, sphinctozoans and

Plate 2.11 (following page) Anisian reef limestones from the Latemar, Dolomites, Italy: foraminiferal associations.

Fig. 1.-5. *Abriolina mediterranea* Luperto. (Cresta De Do Peniola, 1: x105; 2: x130; 3: x150; 4: x90; 5: x90)

Fig. 6.-7. *Arenovidalina chiangchiangensis* Ho. (Cresta De Do Peniola, 6: x90; 7: x33)

Fig. 8.-9. *Turriglomina mesotriasica* Koehn-Zaninetti. (8: Cresta De Do Peniola, x70; 9: Cima Feudo, x90)

Fig. 10. *Turriglomina* sp. (Cresta De Do Peniola, x70)

Fig. 11. *Turriglomina scandonei* Zaninetti, Ciarapica, Martini, Salvini-Bonnard and Rettori. (Cresta De Do Peniola, x70)

Fig. 12. *Aulotortus? eotriasicus* Zaninetti, Rettori and Martini. (Cresta De Do Peniola, x23)

Fig. 13. *Bulloporella* sp. (Cresta De Do Peniola, x17)

Fig. 14. *Aulotortus? eotriasicus* Zaninetti, Rettori and Martini. (Schenon, x26)

Fig. 15. *Lamelliconus* gr. *ventroplanus* Oberhauser. (Schenon, x43)

Fig. 16.-18. *Diploremmina* cfr. *astrofimbriata* Kristan-Tollmann. (16,17: Cresta De Do Peniola, 16: x22; 17: x17; 18: Schenon, x43)

Fig. 19.-20. *Duostomina* sp. (Cima Feudo, 19: x26; 20: x35)

Fig. 21. *Endoteba* ex gr. *obturata* Bronnimann and Zaninetti. (Cima Feudo, x17)

Fig. 22. *Endotriadella* sp. (Cresta De Do Peniola, x17)

Fig. 23. *Endotriada* cfr. *tirrenica* Vachard, Martini, Rettori and Zaninetti. (Erzlahn, x35)

Fig. 24.-26. *Endoteba* sp.. (24,25: Schenon, x35; 26: Cresta De Do Peniola, x35)

Fig. 27.-28. *Endotriadella wirzi* Koehn-Zaninetti. (27: Cresta De Do Peniola, x35; 28: Erzlahn, 26x)

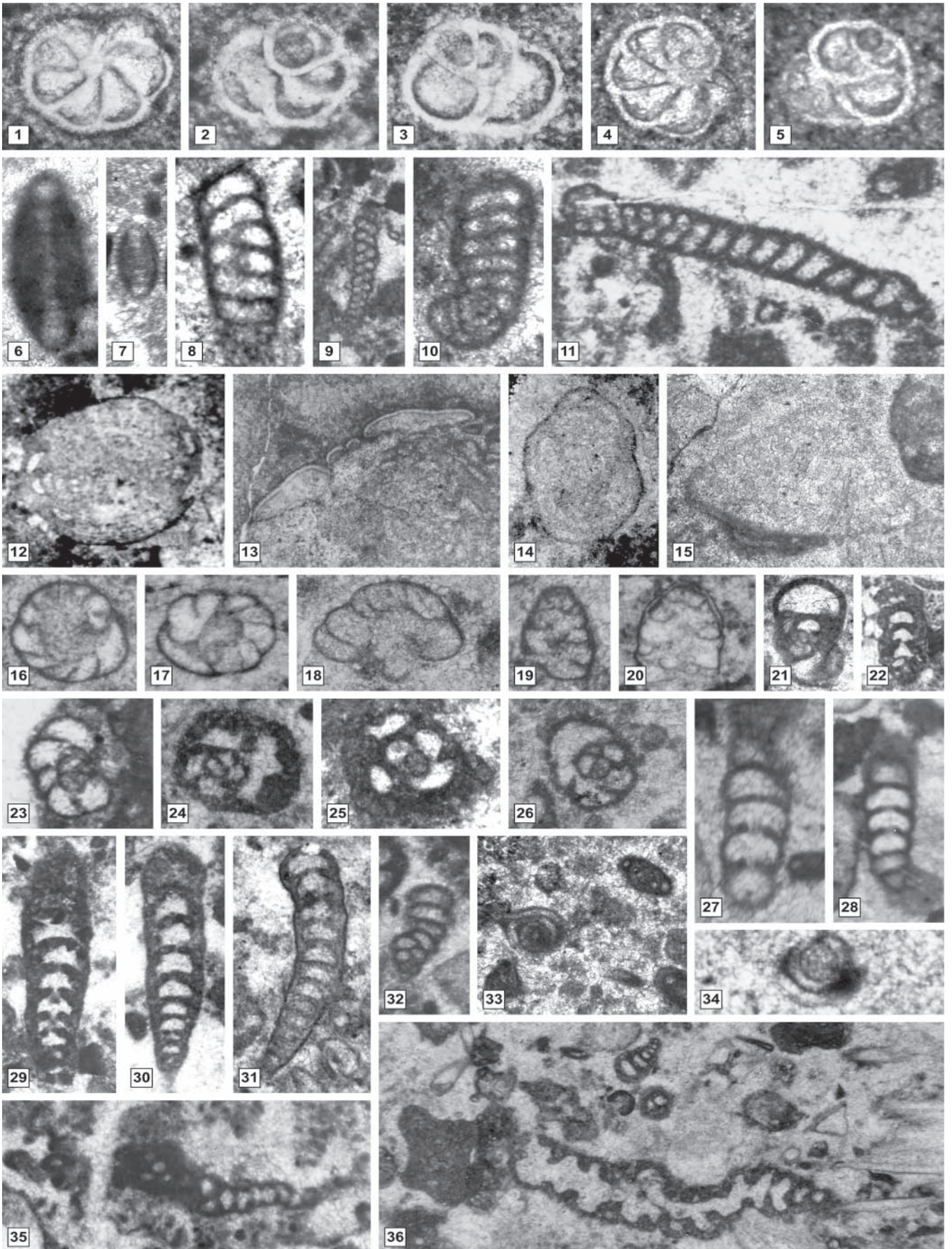
Fig. 29.-31. *Earlandinita* sp. (29: Cresta De Do Peniola, x24; 30,31: Cima Feudo, x24)

Fig. 32. *Gaudrinella* sp. (Schenon, x35)

Fig. 33. *Paraophthalmidium* sp.. (Cresta De Do Peniola, x35)

Fig. 34. ?*Ophthalmidium* sp. (Cresta De Do Peniola, x35)

Fig. 35.-36. *Flaschkofelia anisica* Rettori, Senowbari-Daryan and Zühlke. (Cresta De Do Peniola, 35: x35; 36: x30)



delicate branching corals. The wave resistant constructs of scleractinian framestones are located above the mean wave base and below the surf zone (B4; see also Harris 1993). The reef crest (backbone of the reef) is marked by the microbial/algal ridge withstanding waves and possibly tidal currents (B5; see also Biddle 1981). The transition towards the lagoon is inhabited by patchy mounds of “*Tubiphytes*” *multisiphonatus* (B6) becoming more rare as the lagoon approaches (see also Schäfer and Senowbari-Daryan 1982, 1983; Scholz 1972).

Another unique feature of the reef-facies at Latemar are the lateral variations of its biotic content: (1) The reef at Cima Feudo is characterised by well-preserved sponges. (2) The main feature of the Kirchtage weide reef is the abundant presence of scleractinian corals. (3) So far, Erzlahn is the only occurrence of “*Tubiphytes*” *multisiphonatus* in the reef-facies at Latemar and possibly in the Dolomites. (4) Schenon, however, reveals a similar biotic content of the reef-facies in talus deposits as the in-situ margin at Cima Feudo. (5) Forams of inter-reef sediment and especially microproblematica are abundant at Cresta De Do Peniola; it is also the only “reefal” location with bryozoan mounds. The reasons for these lateral variations within the same reef belt remain unclear as - according to present knowledge - neither palaeo current nor palaeo wind directions at Latemar are the cause for such changes in biocoenoses. Tying these micro-macroscale variations to differences in nutrient influx through synsedimentary volcanic dykes appears too speculative. Even at recent reefs where pronounced micro-macroscale biozonation can be observed directly, the causes for such lateral variation are often obscure (e.g. James and Ginsburg 1979; Zacher 1980; Iryu et al. 1995). Evidence for emersion of the reef-rim is absent, all reefal zones lie within the range of the mean wave base; i.e. the tepee belt is the highest topographical elevation of the carbonate platform (see chapter 2.4.3). Hence high frequency sea level oscillations as recorded by the lagoonal succession did not affect the reefal margin.

2.5.7 Biostratigraphical position of the reef

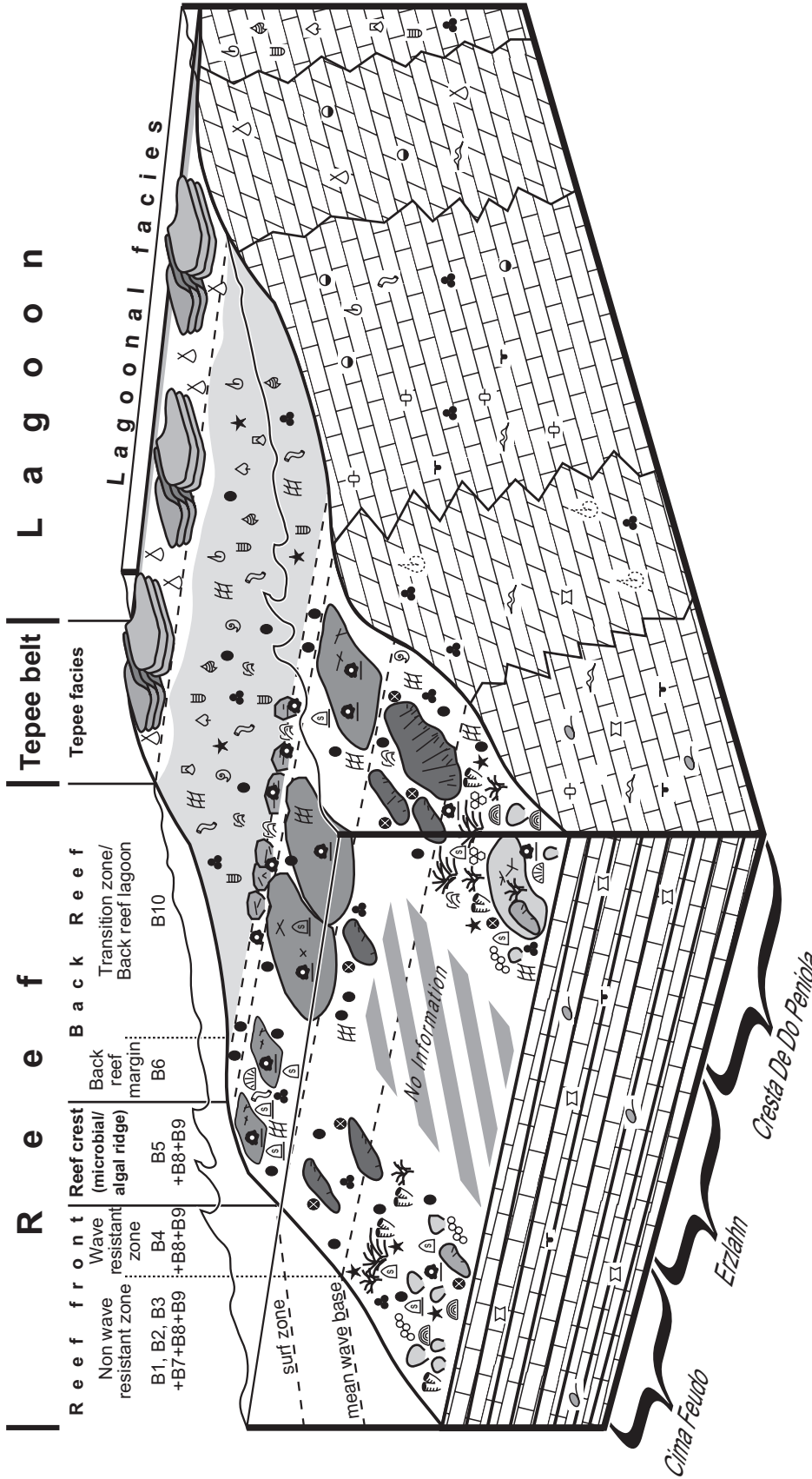
Palaeontologic evidence from the reef-facies points in many ways to a predominantly Anisian age of the entire Latemar platform (see also Table 2.2). Small encrusting “sphinctozoids” like *Celyphia zoldana* and *Celyphia? minima* are generally found in the Anisian and are very common throughout Latemar’s succession, even in the upper part of the sections at Cresta De Do Peniola. The occurrence of age-diagnostic foraminifers throughout the sections at Cresta De Do Peniola until the very top of the Latemar also indicates a mainly Anisian age. Typical Ladinian associations are not present (see Table 2.2; 12 species are Anisian, 21 are Anisian/Ladinian and only 5 are Ladinian). Only at the top of the sections at Cresta De Do Peniola there is a slight increase in abundance of rare sponges, forams and microproblematica which are generally more frequent in Ladinian reefs (like *Colospongia catenulata*, *Solenolmia manon manon*, *Ladinella porata* etc.).

A reefal evolution in the timespan from Lower Platform Facies (LPF) to Upper Tepee Facies (UTF) is not visible as almost the same biocoenoses can be found as well in the younger as in the older part of Latemar’s reef (see also chapter 2.4.5.2). The duration of reefal (i.e. platform) growth has been in the order of one biozone or only slightly more (Brack et al. 1996; Zühlke et al. 2000; Mundil et al. 2003; Zühlke et al. 2003) and thus too short to establish any trends of faunal evolution. The lack of a true evolution of the reef within the timeframe of the platform development supports - together with the general absence of biota indicative of true Ladinian age - the observation by other authors that the Latemar is a short spanned carbonate platform of mainly Anisian age (Brack et al. 1996; Zühlke et al. 2000; Mundil et al. 2003; Zühlke et al. 2003). The topmost succession at Cresta De Do Peniola corresponds to the youngest strata of the lagoon and is consequently Earliest Ladinian (see Fig. 11). Most of the typical Anisian “*Tubiphytes*” group boundstones still occur in this - Earliest Ladinian - inter-

Fig. 15 (following page) Schematic reef model of the Latemar indicating the three main zones (reef front, reef crest and back reef) together with their characteristic biocoenoses (B1-B10). For the biocoenoses B1-B10 refer to chapters 2.5.3-2.5.5.

The reef is always below sea level, the bathymetrically highest point of Latemar’s margin is the tepee belt separating the back reef from the lagoonal interior of the platform (see also Egenhoff et al. 1999). Organisms with more delicate/branching growth are found beneath the mean wave base, whereas the wave resistant zone is mainly marked by corals and algae.

The information for this reef model is derived from three outcrops, Cima Feudo, Erzlahn and Cresta De Do Peniola (from left to right). Each one showing different characteristics; some features - e.g. the “*Tubiphytes*” *multisiphonatus* mounds (Erzlahn) or bryozoans (Cresta De Do Peniola) - were observed at one locality only.



Sedimentary Structures	Lithology	Growth forms	Reefal biota	Other biota/components
<ul style="list-style-type: none"> X Tepees ○ Geopetal fabrics ⊕ Bioturbation ⊖ Burrows ⊗ Cavities ⊙ Biomoldic porosity — Carbonate debris flow 	<ul style="list-style-type: none"> ▨ Dolomite/ dolomitic limestone ▩ Limestone 	<ul style="list-style-type: none"> ⊙ "Stromatolitic" ⊕ Platy or encrusting ⊖ Robust ⊗ Moundlike or small mounds ⊙ Branching – ceroid 	<ul style="list-style-type: none"> ⊙ "Tubiphytes" multisiphonatus ⊕ "Tubiphytes" sp., encrusting ▨ Porostromata ⊖ Solenoporaceans ⊗ Scleractinians, robust ⊙ Scleractinians, ceroid ⊕ <i>Reptonoditrypa cautica</i> (bryozoa) ⊗ Calcisponges ⊙ Calcisponges, encrusting ⊕ <i>Olangocoella otti</i> (sponge?) 	<ul style="list-style-type: none"> ⊙ Bioclasts in general ⊕ <i>Daomella</i> sp. (peleagic bivalve) ⊖ Other bivalves ⊗ Cephalopods ⊙ Gastropods ⊕ Echinoids ⊗ Dasycladaceans ⊙ Microproblematica ⊕ Foraminifers ⊗ Worm tubes ⊙ Plant incrusts (wood) ⊕ Peloids ⊗ Lithoclasts

val of platform growth. Hence, our biostratigraphic data from Latemar's reef is in accordance with the chrono-, cyclo- and biostratigraphical data of the lagoon presented by Zühlke et al. (2000), Zühlke et al. (2003) and Mundil et al. (2003). Additionally, the biotic content (dasyclads: *Diplopora nodosa*, *Zornia obscura*) of the lagoonal strata analysed at some localities further confirms the Late Anisian/Early Ladinian age of the reef. Especially *Zornia obscura* - so far described only from Ticino (Ladinian: "Problematikum 1"; Zorn 1971, 1972), Sicily (Anisian?/Ladinian; Senowbari-Daryan and Di Stefano 2001) and Southern China (Anisian; Bucur, pers. comm. 2003) - indicates the same biostratigraphic position.

2.6 Conclusions

2.6.1 Correlation with other Late Anisian/Early Ladinian reefs of the western Tethys

Compared to other - slightly older - Anisian reefs of the Dolomites as described by Fois and Gaetani (Olang and Mt. Cenera, 1984) and Senowbari-Daryan et al. (Olang, 1993), the Latemar reef reveals significant biotic relations to both areas concerning sponges (e.g. *Celyphia zoldana* and *Olangocoelia otti*), solenoporacean algae, microproblematica (e.g. "*Tubiphytes*" *obscurus* and *Radiomura cautica*) and foraminifers (e.g. duostomionids). But there are also differences with respect to the presence or absence of certain biota and looked at it in detail, the Latemar reef seems considerably more diversified. This feature might partly be due to the fact that investigation on the reef facies in Olang and at Mt. Cenera can mostly be carried out on resedimented blocks in basinal strata influenced by siliciclastic input from the hinterland (basin depths approx. 150m; Zühlke 2000); but the reef does certainly not contain as much "*Tubi-*

phytes" group biota as the locations at Latemar, especially as the Cresta De Do Peniola section.

Strong similarities of reefal margin and slope exist with some Anisian platforms of the eastern Tethys (e.g. Guizhou/China; Enos et al. 1997). There, "*Tubiphytes*" and microproblematica like *Plexoramea cerebriformis* are the main framework elements. In-situ reef-facies is characterised by sponges, various encrusters and cements. Corals play a minor role and display a slender, digitate growth. Retreat of the platform margin is observed from the beginning of platform evolution on, although the scale is different (up to 2.7km margin retreat; Enos et al. 1997).

With respect to the foraminifers in Latemar's reef, coeval, similar assemblages and biofacies are furthermore found in Late Anisian successions in North Bulgaria (Trifonova and Vaptsarova 1982) and Western Turkey (*Palaelituo-nella meridionalis*; Isintek et al. 2000).

As mentioned earlier, the "*Tubiphytes*" *multisiphonatus* findings (originally: hydrozoans; see discussion in chapter 2.5.3.6 and Table 2.3) in the Anisian to Ladinian Wetterstein reef complex in North Hungary by Scholz (1972) indicates a relationship with at least the situation at Erzlahn. The similarity is further amplified by the distinct zonation of the reef at Aggtelek despite its Anisian to Ladinian age as proven by age-diagnostic foraminifers, dasyclads and brachiopods. However, abundant brachiopods and echinoderms are not observed at Latemar.

The most important biotic affinities probably exist with the time equivalent reef described by Scheuber (1990) from the Vicentinian Alps of Northern Italy. The in-situ reef in the area of Recoaro is less diverse than the one described in this study. But the main characteristics are strikingly equal: with respect to the dominating, abun-

Plate 2.12 (following page) Anisian reef limestones from the Latemar, Dolomites, Italy: foraminiferal associations, wormtubes and microproblematica.

Fig. 1. *Tolypammia* sp.. (Schenon, x26)

Fig. 2.-3. *Reophax* sp./*Ammobaculites* sp.. (Cresta De Do Peniola, 2: x17; 3: x13)

Fig. 4. *Textularia* sp.. (Cresta De Do Peniola, x50)

Fig. 5.-14. *Palaelituo-nella meridionalis* Luperto. (5,7,13: Schenon, 5: x45, 7: x30; 13: x40; 6,8,9,10,11,12: Cresta De Do Peniola, 6: x40; 8: x55; 9: x50; 10: x35; 11: x35; 12: x30; 14: Cima Feudo, x40)

Fig. 15.-17. *Lagenina* sp.. (Cresta De Do Peniola, 15: x26; 16: x70; 17: x26)

Fig. 18.-22. Worm tubes (*Spirorbis* sp) and encrusting epibiontes of the reef-facies at Latemar. (18,21,22: Cresta De Do Peniola, 18: x13; 21: x22; 22: x45; 19,20: Cima Feudo, 19: x15; 20: x13)

Fig. 23.-24. *Plexoramea cerebriformis* Mello. (23: Schenon, x45; 24: Cresta De Do Peniola, x45)

Fig. 25.,28. *Baccanella floriformis* Pantic. (Cima Feudo, x17)

Fig. 26. *Anisocellula fecunda* Senowbari Daryan, Zühlke, Bechstädt and Flügel. (Cima Feudo, x50)

Fig. 27. *Ladinella porata* Ott. (Cresta De Do Peniola, x13)

Fig. 29. *Bacinella ordinata* Pantic. (Cima Feudo, x26)



dant “*Tubiphytes*” grp. encrustations, corals are of equally minor importance as reef-building organisms. Foraminiferal assemblages (including *Palaeolituonella meridionalis*) and calcisponge-biocoenoses are similar as well. The observed biological zonations at the Monte Spitz reef seem to parallel the reef at Cima Feudo. Sphinctozoan sponges like *Solenolmia manon manon* in the central reef area together with abundant encrusting microproblematica are copying the situation of Cima Feudo. This image is completed by the presence of *Olangocoelia otti*.

The geographically closest reef is located at the Schlern/Rosengarten platform. But here dolomitisation and scarce in-situ reef-facies hamper an investigation of the primary reefal organisation. The reef as derived from the famous Cipit boulders (e.g. Biddle 1981; Brandner et al. 1991) is slightly younger (Early to Upper Ladinian) than at Latemar. But it displays significant similarities e.g. concerning the abundance of low growing sessile organisms as evidenced by microbial/biogenic crusts and calcareous algae (*Ortonella* sp., *Parachaetetes* sp., *Solenopora* sp. etc.). Hence, the biotic content is generally correlatable with the upper parts of Cresta De Do Peniola or the heavily encrusted microbial ridge at Erzlahn. According to Biddle (1981), these microbial constructs were wave-resistant (see also chapter 2.5.6). The occurrence of many species of corals (e.g. *Margarophyllia* sp., *Proheterastraea* sp. and *Trochastraea* sp.) is not paralleled by Latemar’s reef. Additionally, the foraminiferal assemblage at Schlern/Rosengarten differs completely from the one described in this study.

The Ladinian reef of the Marmolada platform in the western Dolomites - as studied by Blendinger (1986) - is mainly made up of solenoporaceans and species of the “*Tubiphytes*” grp.. Porostromate algae, calcareous sponges and solitary corals play only a minor role. Nevertheless, enormous quantities of reefal debris in slope deposits suggest a considerable productivity of the reef belt. Similar to the location at Schenon, some coralline mounds with upright stems (in-situ position) are resting directly on talus deposits indicating a growth of reefal biota to water depths well below the mean wave base. The Ladinian to Carnian Sass da Putia build-up as described by Fois (1982) provides insight into its reef-facies through basinal “Cipit” boulders like at Schlern/Rosengarten, but also offers the possibility to investigate an in-situ reefal margin. Its reef is in sedimentological and palaeontological terms comparable to the

Latemar. The content in encrusters (“*Tubiphytes*” group and microbial crusts) and microproblematica (*Baccanella floriformis* and *Bacinella ordinata*) is similar and scleractinians (*Margarosmia* sp.) are equally rare.

Ladinian reefs of the Northern Calcareous Alps (e.g. Ruffer and Zamparelli 1997) are more diverse with respect to sponges and algae but show a similar abundance of encrusting “*Tubiphytes*” grp.. In Anisian strata, there are no equivalents of the reefs observed in the Dolomites and its surroundings. Ramps with a low topography prevailed. However, Anisian successions (Steinalm Fm) reveal strikingly similar foraminifers, e.g. *Palaeolituonella meridionalis*, *Arenovidalina chiangchiangensis*, *Abriolina mediterranea* and *Turriplomina mesotriatica*. The occurrence of *C. zoldana* and *C.? minima* together with abundant species of the “*Tubiphytes*” grp. is a real novelty in the studies on reefs in the Dolomites. *Celyphia zoldana* is usually typical for the Anisian, whereas large species of the “*Tubiphytes*” grp. are typical for the Ladinian. As a consequence, this is taken as evidence for an Upper Anisian/Lowermost Ladinian age of the section at Cresta De Do Peniola. Moreover, it is obvious that true boundstones with sponges, corals and “*Tubiphytes*” continue up into the Lower Ladinian. The presence of sponges like *Colospongia catenulata catenulata*, *Solenolmia manon manon* - generally very common in Ladinian communities - and of microproblematica like *Ladinella porata* together with encrusting “*Tubiphytes*” *obscurus* in the upper part of the slope facies further supports the Anisian-Ladinian age of Latemar’s upper level reef sections. *Olangocoelia otti* is encrusting lithoclasts, but it is not a very important part of all biocoenoses. It is generally present in the lower part of the Cresta De Do Peniola section but seems to become more rare towards the Anisian/Ladinian boundary. This sponge/alga? forms oncoidal-like crusts and appears together with other microproblematica on the walls of cavities. It is remarkably rare at Latemar, unlike in other Anisian reefs in the Dolomites e.g. in the Olang area (Fois and Gaetani 1984; Senowbari-Daryan et al. 1993).

Compared to all other reef assemblages in the Dolomites, foraminiferal associations in the Latemar reef are more diversified. Additionally, many genera from Latemar’s reef facies have not been described before in the Dolomites. The majority of agglutinated foraminifers is represented by Duostominidae, Endotriadidae and Endotribidae - commonly found in the lagoonal facies - as well

as by the sessil agglutinated *Flatschkofelia anisica* (Rettori et al. 1996) an important element of the epifauna and typical for the reef facies in the Olang area (Fois and Gaetani 1984; Senowbari-Daryan et al. 1993). Among the most frequent benthonic foraminifers at Latemar are *Paleolituonella meridionalis* and large *Reophax/Ammobaculites* occurring in the central reef as well as in the back-reef. The small species *Turriglomina mesotriatica* appears in the finer-grained sediments of the slope facies according to the ecological distribution proposed by Zaninetti et al. (1990), whereas the larger species *Turriglomina scandonei* - found so far only in the Southern Apennines (Zaninetti et al. 1987) - is also present in the boundstone clasts of the slope.

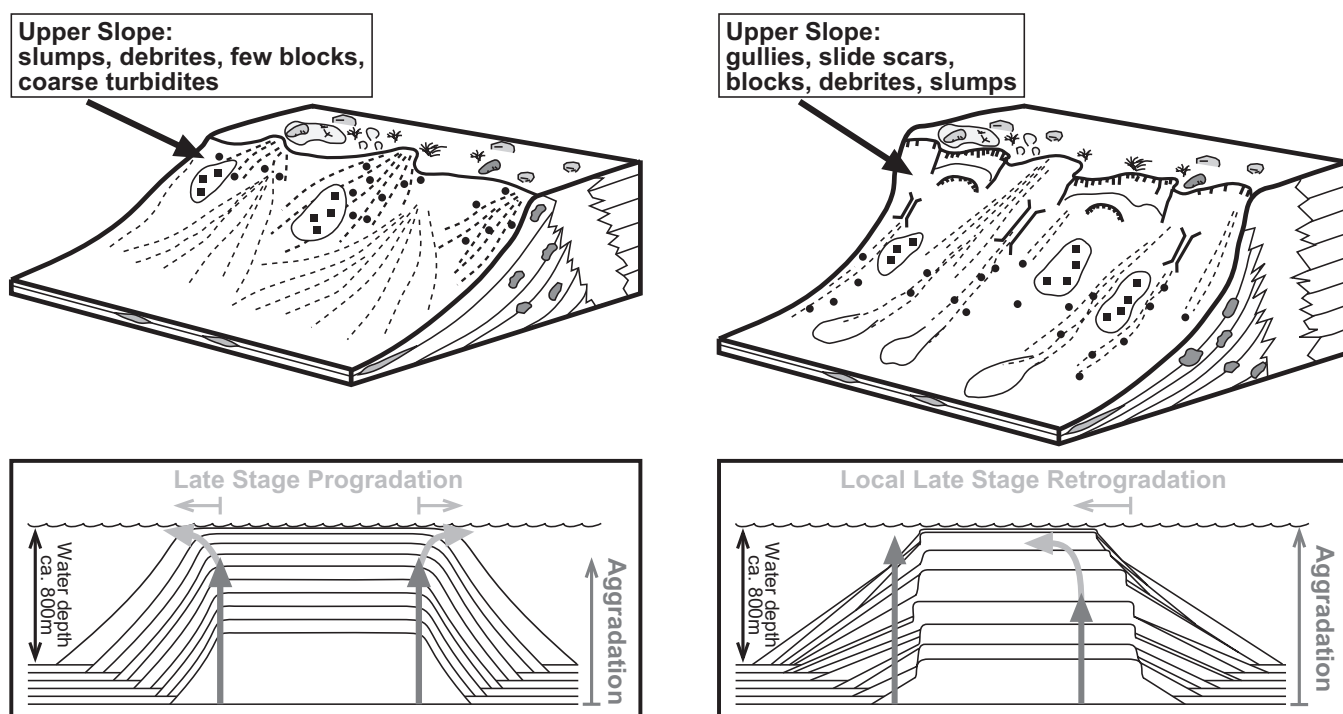
The neptunian dyke at Cresta De Do Peniola contains mudstones with fragments of small nodosarids, well preserved samples of *Abriolina mediterranea*, together with a fine-grained association of *Arenovidalina chianchianensis* and *Ophthalmidium* sp. The occurrence of *Abriolina mediterranea* at Latemar is important for the correlation of Tethylian reefs. Apart from the Anisian?

Ladinian reef facies from the Lagonegro area where it has been firstly described by Zaninetti et al. (1992) the genera of *Abriolina* has yet only been found in the Northern Calcareous Alps (Rüffer and Zamparelli 1997) and probably in Turkey (Middle Triassic) and Southern China (Zaninetti et al. 1992).

2.6.2 Controls on slope evolution at Latemar

The slope- and reef-facies of the Latemar buildup are far more complex than previously reported in literature (see chapter 2.3; e.g. Goldhammer and Harris 1989; Harris 1994). The generalised view of the firstly aggrading, then prograding depositional slope at Latemar cannot be confirmed by this study. Contrarily, backstepping of the lagoon by margin failure has mainly been observed during the last stages of platform evolution (see Figs. 2.16 for a comparison of both models). Reasons for this behaviour might be accommodation change outpacing a carbonate production rate stretched to its limits.

The slope reveals different depositional characteristics at the same time and at different locations. Additionally,



Figs. 2.16 Comparison of the previous model of the Latemar platform (lefthand side, block diagram above and cross section below; vertically exaggerated, not to scale) with the model proposed in this study (righthand side, block diagram above and cross section below; vertically exaggerated, not to scale). The model on the lefthand side corresponds with Bosellini (1984), Goldhammer and Harris (1989; see also chapter 2.1.3.) and Harris (1994). The model on the righthand side - based on Mullins (1983) and Mullins and Cook (1986) - is in accordance with the observations of this study. The latter model allows large quantities of sediment to be bypassed to the toe-of-slope.

a turnover from slope apron via an erosional slope towards a base-of-slope apron was proved on the NE slope (Cresta De Do Peniola, chapter 2.4.5). Hence it is impossible to establish a generalising model for the entire platform evolution and all expositions. Instead, several trends are visible at Latemar. The slope of the Latemar is strongly asymmetric; steeply dipping clinoforms and erosional characteristics on the SE side are contrasted by more gentle dipping clinoforms and depositional characteristics on the NW side. As the SE side of the Latemar is very close to the Stava Line-Cima Bocche Anticline (Doglioni 1983, 1984), this asymmetry is most likely caused by different rates in tectonic subsidence on the respective sides. Furthermore, it is obvious that sudden tectonic movements along this tectonic line did cause peaks in tectonic subsidence and did consequently trigger giant collapses at the adjacent slope (De Zanche et al. 1995). Retreat of platforms due to tectonic collapses and/or earthquake shocks is a well documented feature of many Tethydan platforms during the Jurassic rifting stages (e.g. Bernoulli 1964; Bosellini 1973; Castellarin et al. 1978; Mutti et al. 1984). The tectonic influence on the slope evolution is further proven by the coeval neptunian dyke in the slope-facies at Cresta De Do Peniola.

In the case of the Latemar, variations in tectonic subsidence have been the main allocyclic factors for slope evolution. Other parameters like wind and wave directions seem insignificant and/or are being overprinted by variations in tectonic subsidence. Hence, the deduction of a palaeo wind and/or -wave direction as done by Egenhoff et al. (1999) is not possible. Even more so as the directions were derived from analyses of small restricted areas at the platform top only (Marmolada: Blendinger 1986; Latemar: Egenhoff et al. 1999). The pronounced asymmetry of many platforms in the Dolomites seems to be entirely related to responses to different tectonic settings (Bosellini 1989).

Controlling factors for the development of the carbonate platforms differ strongly from lagoon to slope. Whereas the lagoon is chiefly controlled by non-orbital and orbitally forced small scale sea level oscillations, the slope reveals to be largely independent from these high-frequency accommodation changes of the platform top (see also Bosellini 1989). The high frequency sea level oscillations recorded by the platform top are not preserved or recorded by neither the platform slope nor the reef (see Harris 1994; also refer to chapter 2.1.3). In

addition, the reef has been submerged throughout the entire time of platform evolution. This fact rules out sea level lowstands as causes for the repeated margin collapses.

The slope is a sedimentary environment of episodic and catastrophic events (Coniglio and Dix 1992) destroying any evidence of the accommodation changes as indicated by the lagoonal interior. Therefore, autocyclic processes are of even greater importance for the slope development than for the lagoonal evolution. Cycles of sedimentation-oversteepening-collapse at a platform-wide scale play an important role during slope formation (see also Crevello and Schlager 1980; Mullins et al. 1986). Autocyclic processes such as Blendingers (2001) interpretation of cementation driven self-fracturing of slope sediments were not observed. Fracturing of carbonate sediments took place through movements during re-sedimentation. All blocks from metre to millimetre scale at Latemar are the result of gravity driven brecciation. However, syndepositional cements are locally abundant; but their importance is then restricted to small areas only like in the "*Tubiphytes*" *multisiphonatus* mounds at Erzlahn or in the talus at Schenon. Massive syndepositional cementation as a key factor during the build-up of the margin as observed by Russo et al. (2000) and Stefani et al. (2001) can be excluded.

Acknowledgements

The authors would like to acknowledge Baba Senowbari-Daryan (University of Erlangen, Germany) for palaeontological discussions. Axel Emmerich thanks the "Studienstiftung des deutschen Volkes" (German National Academic Foundation) and the International Postgraduate Programme (University of Heidelberg, Germany) for financial support during fieldwork and travel.

PART 3

Latemar vs. Concarena (Southern Alps): main characteristics of two Triassic carbonate platform margins

Abstract

The comparison of the Triassic carbonate buildups of Latemar (Upper Anisian/Lower Ladinian, Dolomites) and Concarena (Upper Ladinian/Lower Carnian, Lombardic Alps) stresses the importance of “*Tubiphytes*” for the development of Triassic carbonate platforms. The comparison furthermore underlined the influence of carbonate accumulation/accommodation increase and margin topography on massive early cementation. Large mounds – up to 4m in diameter and 1.5m in height – made up exclusively of “*Tubiphytes*” *multisiphonatus* are situated in back reef environments (Latemar and Concarena) and uppermost slope settings (Concarena). This is the first reported occurrence of this “*Tubiphytes*” species outside the type locality on Hydra (Carnian “Pantokrator Limestone”, Greece).

The mainly aggrading Latemar buildup displays no indication for insufficient nutrient supply. The local retreat of the margin is linked to tectonic subsidence at distal areas triggered by downward movements of tectonic blocks along the Stava line in combination with cycles of oversteepening/collapse. The Concarena platform, in contrast, generally shows initial slight progradation increasing significantly towards late platform development. The regionally observed (W Tethys) relative sea level fall at the Ladinian/Carnian boundary lead in combination with the compartmentalisation of basins and subsequent local development of anoxic conditions to a significant slow-down in accommodation increase and decrease in carbonate production. The distinctly contrasting amount of massive early cementation on both platforms underlined the dependence of cementation on carbonate accumulation, accommodation increase and margin topography: High rates of carbonate accumulation/accommodation increase combined with low topography of the reefal margin prevented massive early cementation at Latemar; low rates during the last stages of the Concarena platform together with a walled reef favoured massive early cementation. A peculiar feature of the Concarena platform are cement “mounds” at the transi-

tion from lagoon to back reef in the upper part of the succession. Multiple generations of botryoidal cements associated with organic matter and finally encrusted by isopachous fibrous cements form patchy constructions from decimetre to metre size.

3.1 Introduction

The Dolomites of the Southern Alps provide a key area for the study of Triassic carbonate platform development (e.g. Bosellini 1984; Schlager et al. 1991). Owing to their extensive dolomitisation, the majority of research dealt with platform geometries and sequence stratigraphic interpretation. The study of fossil reefal communities focused either on reef talus blocks having escaped dolomitisation (“Cipit” boulders; e.g. Schlern: Biddle 1981; Brandner et al. 1991; Flügel 1991; Olang area: Bechstädt & Brandner 1971; Fois 1982; Senowbari-Daryan et al. 1993; Sella: Russo et al. 1998) or on a few in-situ mounds preserved in primary lithofacies (Mt. Cenera: Fois & Gaetani 1984; Marmolada: Blendinger 1986; Latemar: Harris 1993; see also Part 2). Among these, the Anisian/Ladinian Latemar most beautifully reveals primary reefal fossil assemblages, geometries of reef and slope and growth characteristics of the entire platform (position of Anisian/Ladinian boundary after Brack & Rieber 1993).

Despite their similar excellent preservation – owing to laterally correlatable platform-basin transitions, seismic-scale outcrops and absent dolomitisation - the Triassic platforms of the Lombardic Alps are far less studied than the Dolomites. Some studies have documented the re-occurrence of Early Anisian reefs after the faunal crisis at the Permian/Triassic boundary (Salomon 1908; Assereto et al. 1965; Unland 1975; Epting et al. 1976; Brack 1984; Gaetani & Gorza 1989; Falletti & De Donatis 1999). Even less studies have been carried out on the uppermost Anisian to lowermost Carnian re-establishment of rimmed carbonate platforms (Jadoul et al. 1992; Gaetani et al. 1992). The Concarena platform, most recently investigated by Rossetti (1966) and Brack (1984), is one of these uniquely preserved Ladinian/Carnian carbonate platforms. Its lateral facies zonation and occurrence of enigmatic “*Tubiphytes*” in the margin resembles the somewhat older Anisian/Ladinian Latemar platform.

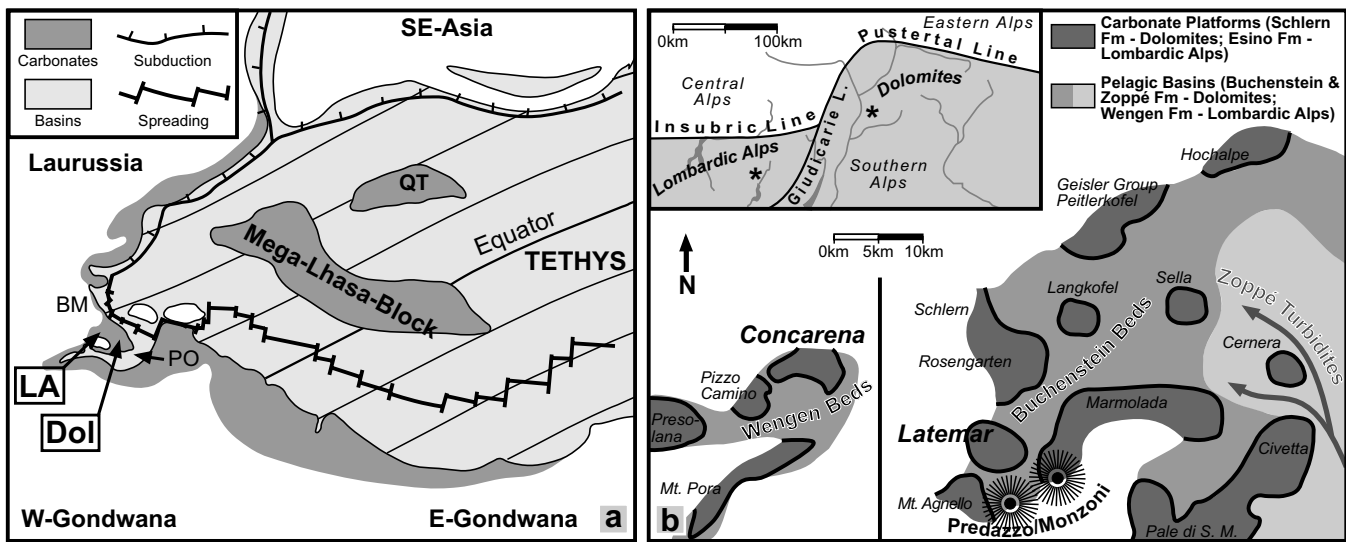


Fig. 3.1A Simplified palaeogeographic map of the western Tethys during the Middle Triassic (after Dercourt et al. 1993, 2000). Abbreviations: LA Lombardic Alps; Dol Dolomites; BM Bohemian Massif; PO Pindos-Olonos trough; QT: Qiantang-Terrane. Legend of map units/symbols in the upper left corner.

Fig. 3.1B Schematic map illustrating platform-basin relationships of the western Dolomites during the Late Anisian/Early Ladinian (De Zanche & Farabegoli 1988; De Zanche 1990) and of the Lombardic Alps during the Ladinian/Carnian (this study). Legend of lithostratigraphic units in the upper right corner, influx of siliciclastic/volcaniclastic turbidites into pelagic basins marked by large arrows. Inset: generalised map of the Southern Alps with an indication of major tectonic lines, asterisks mark the areas of study.

The aim of this study is (1) to compare the architecture of both platforms, (2) to investigate lithofacies and zonation of reef fossil assemblages along transects through the reef belts and (3) to assess the link between massive early cementation and carbonate accumulation/accommodation increase.

3.2 Geological setting

According to Dercourt et al. (1993, 2000) and many earlier authors, the Triassic of the Southern Alps was situated at latitudes of 15–20°N on the western termination of the Tethys (Fig. 3.1A). This area represented a highly dismembered passive continental margin with transpressive-transpressive tectonics (Blendinger 1985; Doglioni 1987) and mixed carbonate-clastic sedimentation. The Southern Alps of Northern Italy can be subdivided into several parts separated by major tectonic lines of poly-phase origin (see inset in Fig. 3.1B). The Dolomites are situated in the centre of the Southern Alps, forming a weakly deformed mountain range east of Bozen with the Latemar being located in its south-western part. The Lombardic Alps are offset from the Dolomites by the Giudicarie line with major left-lateral offset since the Late Cretaceous (Schönborn 1992).

After the Permian/Triassic faunal crisis, first carbonate buildups in the Southern Alps re-appeared in the lowermost Anisian (Flügel 1982; Fois 1982; Gaetani & Gorza 1989). Middle to Late Anisian strata in the Northern Dolomites were still characterised by simple reefal mounds (Olang area: Fois & Gaetani 1984; Senowbari-Daryan et al. 1993) whereas larger carbonate banks like the Camorelli Limestone developed during the Early to Middle Anisian in the Lombardic Alps (Gaetani & Gorza 1989). Investigations on the biofacies of these buildups have shown various, diversified communities with calcisponges, blue-green algae, bryozoans, solenopora-ceans, scleractinian corals and microproblematics (“*Tubiphytes*” Grp. among others). The re-occurrence of microbial carbonates is a significant feature of Anisian buildups. True frame-building organisms, like scleractinian corals are rare. Higher diversified reef communities developed since the Late Anisian (Latemar: see Part 2). Ladinian/Carnian evolution recorded a return of walled reefs with the principal guild being scleractinians (Flügel 2002), capable of resisting wave energy. Owing to its primary lithofacies, the succession at Latemar has also been termed “Latemar limestone” (Gaetani et al. 1981) in order to pronounce its difference

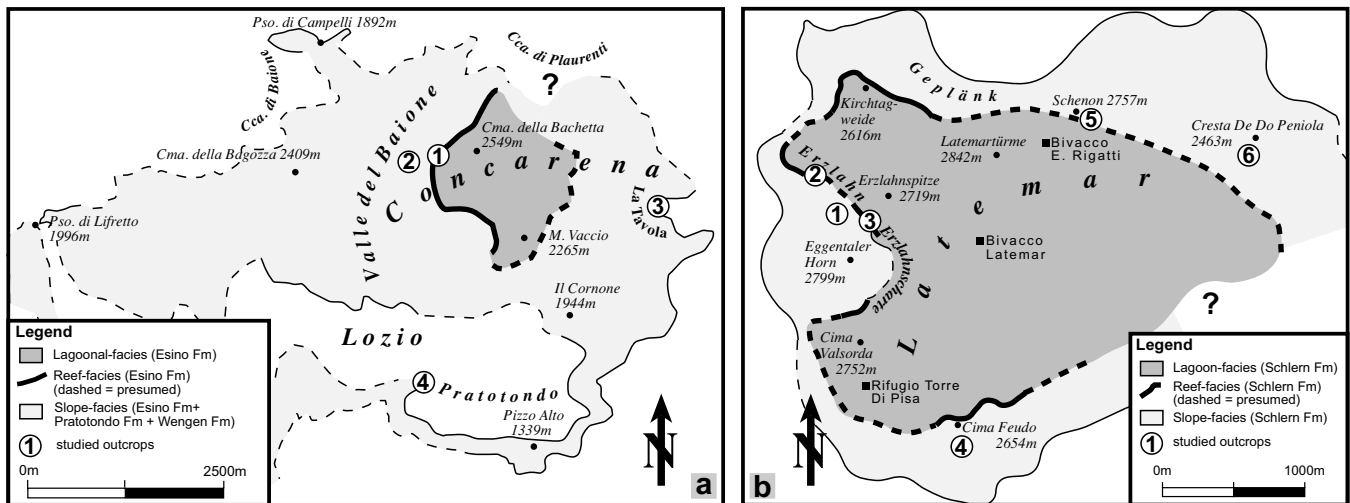


Fig. 3.2A Schematic geologic map of the Concarena; legend of map units in the lower right corner; numbers from 1 to 4 refer to outcrops described in this study (1: Cima della Bacchetta, 2: Valle del Baione, 3: La Tavola, 4: Pratotondo).

Fig. 3.2B Schematic geologic map of the Latemar; legend of map units in the lower right corner; numbers from 1 to 3 refer to outcrops described in this chapter (1: Eggentaler Horn, 2: Erzlahn, 3: Erzlahnscharte) whereas 4 to 6 refer to locations from part 2 (4: Cima Feudo, 5: Schenon, 6: Cresta De Do Peniola).

from the other coeval build-ups of the dolomitic Schlern Fm (e.g. Schlern, Rosengarten etc.; see Fig. 3.1B), which have been further subdivided (see below). The atoll-like Latemar consists of a central lagoon with a diameter of approx. 3km and at least 720m highly cyclic carbonate deposits, a marginal reef rim and a platform slope building up from an initially emersive structural high of the Contrin ramp (e.g. Masetti & Neri 1980; Goldhammer & Harris 1989; Egenhoff et al. 1999; Zühlke et al. 2003; for a sketch map refer to Fig. 3.2B). The slope-facies of the Latemar (Schlern Fm I) is interfingering with the basinal Buchenstein Fm indicating maximum water depths of about 800-1000m (Bosellini 1984; Brack & Rieber 1993). Evolution of the first generation of platforms (Schlern Fm I) in the Dolomites ended with the extrusion of the Longobardian Wengen Fm volcanics (see stratigraphic column in Fig. 3.3) – one source among others being the volcanic centre at Predazzo/Monzoni (e.g. Viel 1979a, 1979b; De Zanche et al 1995; for location of the volcanic centre see Fig. 1b). From the Late Ladinian into the Carnian, a second generation of larger carbonate platforms (e.g. Sella, Peitlerkofel, Geisler, Tofana: Schlern Fm II and Cassian Dolomite) existed in the Eastern Dolomites (Bosellini 1984).

The carbonate platform of the Concarena crops out in Val Camonica north of Brescia (see small inset in Fig. 3.1B) its dimensions being comparable to the Latemar

(Figs. 3.2A and B). Primary lithofacies distribution of the clinostratified platform slope, fossil assemblages of the marginal reef rim and the cyclic arrangement of the at least 800m thick lagoon are preserved in the so-called “Esino limestone” (v. Hauer 1855). The onset of Esino Fm carbonate platforms is observed in the Val Brembana area (Jadoul et al. 1992, Fantini Sestini 1996) and in the northern surroundings of the Grigna (Gaetani et al 1992, 1998, Landra et al. 2000) characterised by a Late Anisian to Early Ladinian fauna. Comparable to the Dolomites, the carbonate platforms mainly interfinger with the Buchenstein Fm (see stratigraphic column in Fig. 3.3). A later stage of Esino Fm carbonate platforms starting in Ladinian times crops out in the Pizzo Camino/Concarena mountain range. This platform shedded carbonate debris into adjacent Wengen age basins. Stratigraphically higher parts of these carbonate platforms have to be attributed to the Early Carnian (Balini et al. 2000; see also Fig. 3.3).

3.3 Platform architecture

3.3.1 Previous research

Bosellini (1984) proposed two main models of carbonate platform progradation in the Dolomites, the “Ladinian” and the “Carnian” model characterised by the deepening or shallowing of the respective basin. The distinctive feature of the “Ladinian” model is the more

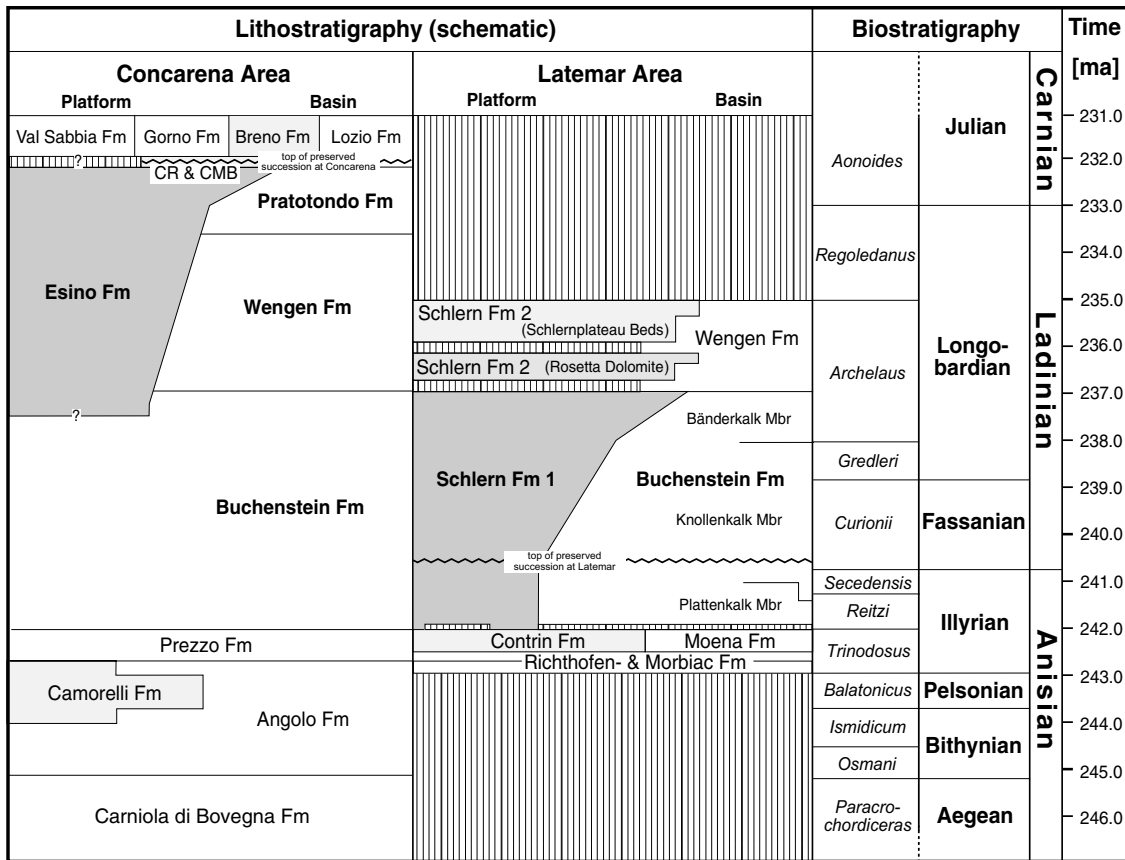


Fig. 3.3 Middle Triassic lithostratigraphic succession and platform-to-basin relationships of the two study areas. The strata overlying present day topographies were projected from immediate surroundings (Latemar area: Rosengarten and Schlern platforms; Concarena area: Mt. Pora platform). The preserved succession at Latemar reaches only until the basal *Curionii* zone (as marked by the zig-zag-line; Mundil et al. 2003, Zühlke et al. 2003). Brack et al. (1996) report the occurrence of younger pelycypods (*Daonella taramellii*; *Daonella longobardica* after Schatz 2000) in neptunian dykes on the slope near Schenon. However, it cannot be excluded that the fossil find does not reflect the true depositional age of the slope at this locality and was contrarily washed into the open cleft during later times. The preserved succession at Concarena reaches until the lowermost Carnian (as marked by the zig-zag-line; Balini et al. 2000). Timescale after Mundil et al. (1996, 2003) and Lehrmann et al. (2002). Biozones, substages and position of Anisian/Ladinian boundary after Brack and Rieber (1993).

or less horizontal progradation over simultaneously deepening basins due to its slow sedimentation rate. The “Carnian” model describes fast progradation of the carbonate platforms over shallowing basinal strata, i.e. the filling of coeval basins due to a higher rate of sedimentation. Carbonate sedimentation in both models occurs

on the entire platform to basin transition, hence their slope is depositional sensu Schlager & Ginsburg (1981). The results of the studies on the slope of the Latemar by Goldhammer and Harris (1989) and Harris (1994) are in accordance with Bosellini’s “Ladinian” model. However, recent studies (Emmerich 2001; Knopp 2002; see also

Plate 3.1 (following page) Platform architecture of the Latemar. Legends on the respective figures; for further explanations refer to the text.

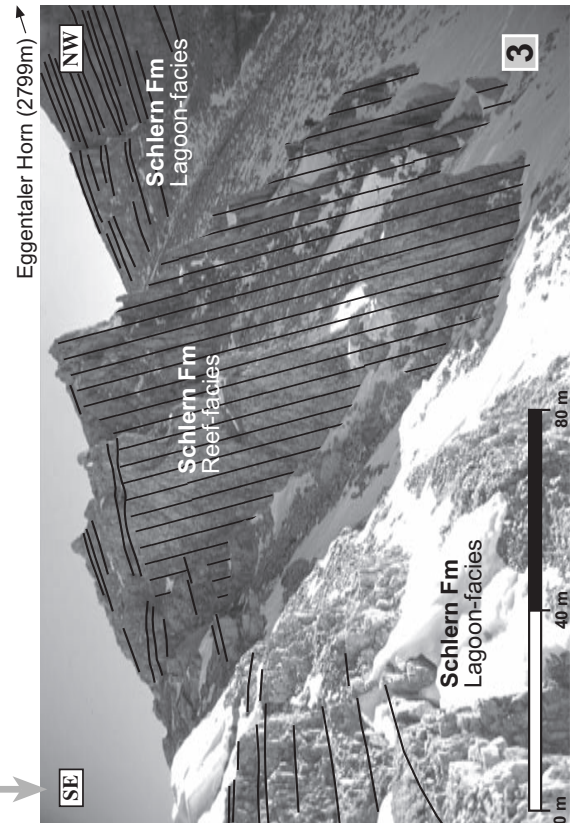
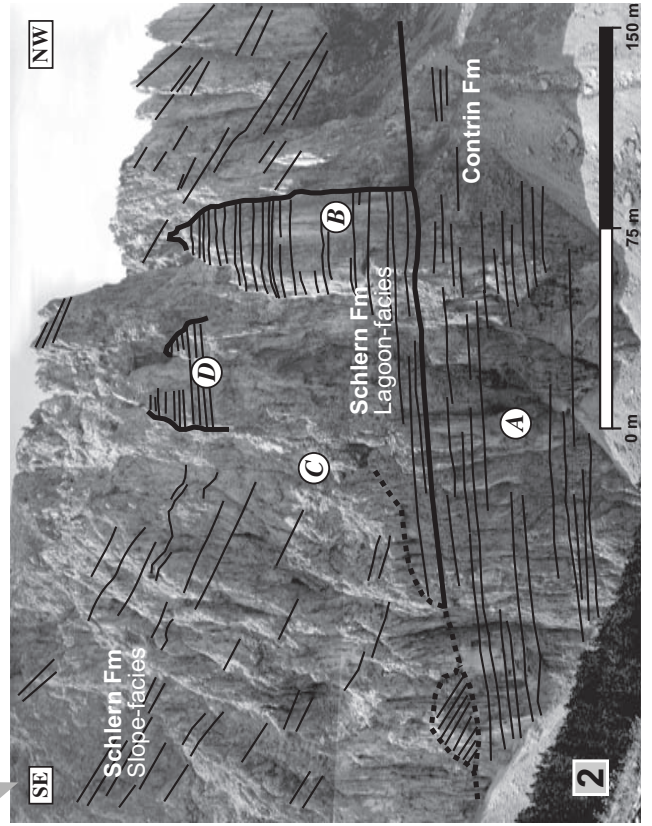
3.1.1: Panoramic view of the SE flank of Eggentaler Horn with an interpretation of sedimentary structures. Letters (A) to (F) correspond to different stages of platform development.

3.1.2: Magnification of the middle part of the Eggentaler Horn transect with an interpretation of sedimentary structures. Letters (A) to (D) correspond to different stages of platform development (see also Plate 3.1.1).

3.1.3: Magnification of the upper part of the Eggentaler Horn transect (i.e. Erzlahnscharte, locality 3 in Fig. 3.2B) with an interpretation of sedimentary structures. The reef-facies displaying massive microbial encrustations is well exposed.



- Minor bedding planes
- Major bedding planes
- Erosional unconformity
- Microbial ridge of reef-facies (Schlern Fm)



Part 2) have proposed a more differentiated concept of the Latemar slope, where – depending on the exposition – aggradation, progradation and backstepping of the margin can occur simultaneously. Even contrasting sedimentological settings (erosional, bypass and depositional sensu Schlager & Ginsburg 1981) were simultaneously present at different expositions.

Owing to the lack of geometrical models or concepts of facies patterns at the Concarena platform in literature (basic descriptions of platform to basin transitions: Rossetti 1966; Brack 1984) only the established models from the Dolomites were presented in this chapter.

3.3.2 Latemar

The description and interpretation of the architecture of the Latemar platform and its platform-basin transitions is exemplarily shown with the Eggentaler Horn transect (locations 1-3 in Fig. 3.2B). Locations 4-6 (see Fig. 3.2B) have comprehensively been discussed in Part 2, hence only a short summary of their main characteristics is presented in this chapter.

The build-up of the lagoon-, reef- and slope-facies of the Schlern Fm at Eggentaler Horn started from an initially emersive part of the Contrin Fm (see area (A) in Plate 3.1.1 and 3.1.2) as indicated by palaeo karst features at the contact of the two formations. Lagoon-facies conformably overlies this boundary and forms an isolated “tower”-like structure (B). The contact to the slope-facies to the left (C) is erosional as displayed by the unconformity cutting right down to the formation boundary between Contrin and Schlern Fm. The slope-facies of area (C) is in turn overlain by lagoon-facies (D). Towards the upper part of the Eggentaler Horn section, lagoon-facies is absent and two units within the slope are distinguishable by the different dip of their clinofolds (areas (E) and (F)). Both units are separated by major erosional unconformities which were mapped around the Erzlahnscharte (see Part 2). The common feature of all platform-basin transitions at Eggentaler Horn is the miss-

ing reefal margin apart from the small area around the Erzlahnscharte (see Plate 3.1.3). Only the central part of the reef-facies characterised by massive microbial encrustations is preserved at this locality (locality 3 in Fig. 3.2B). Hence this area is being referred to as “microbial ridge”.

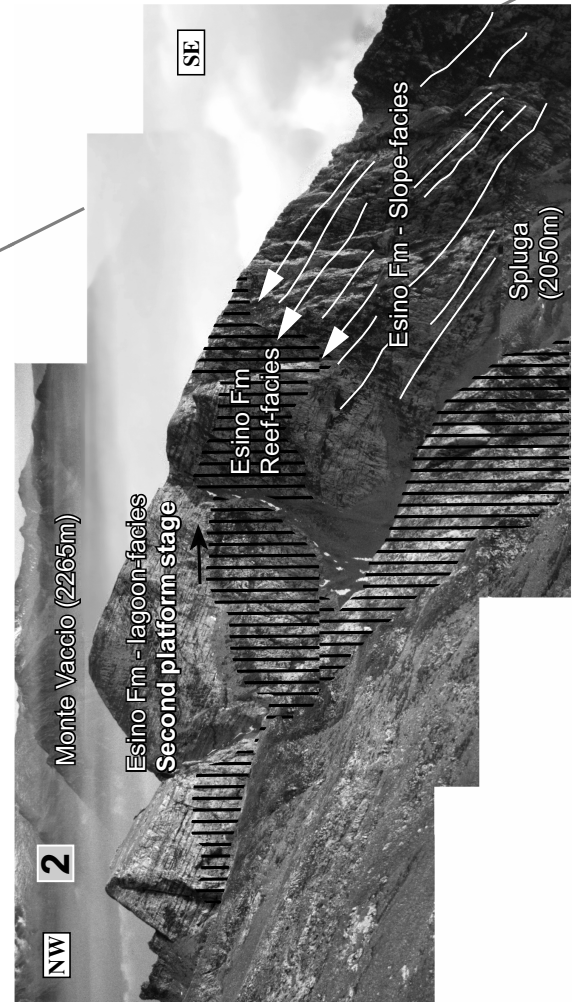
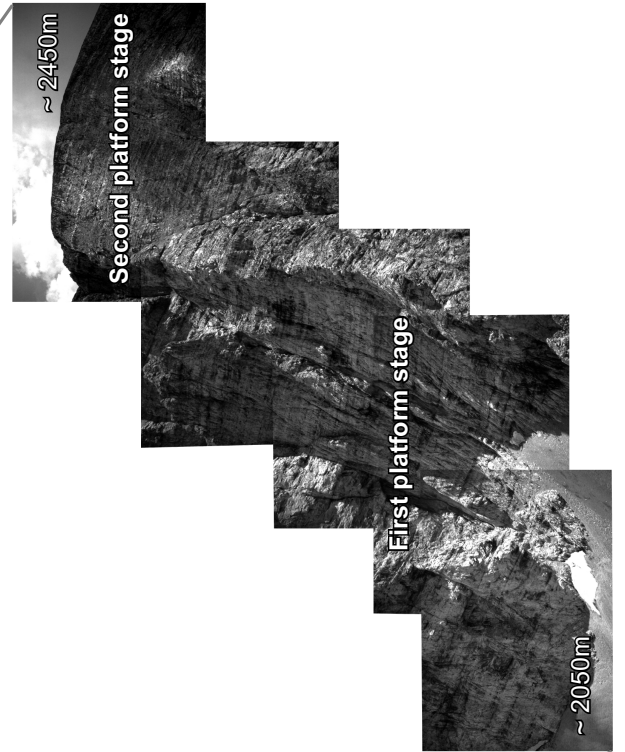
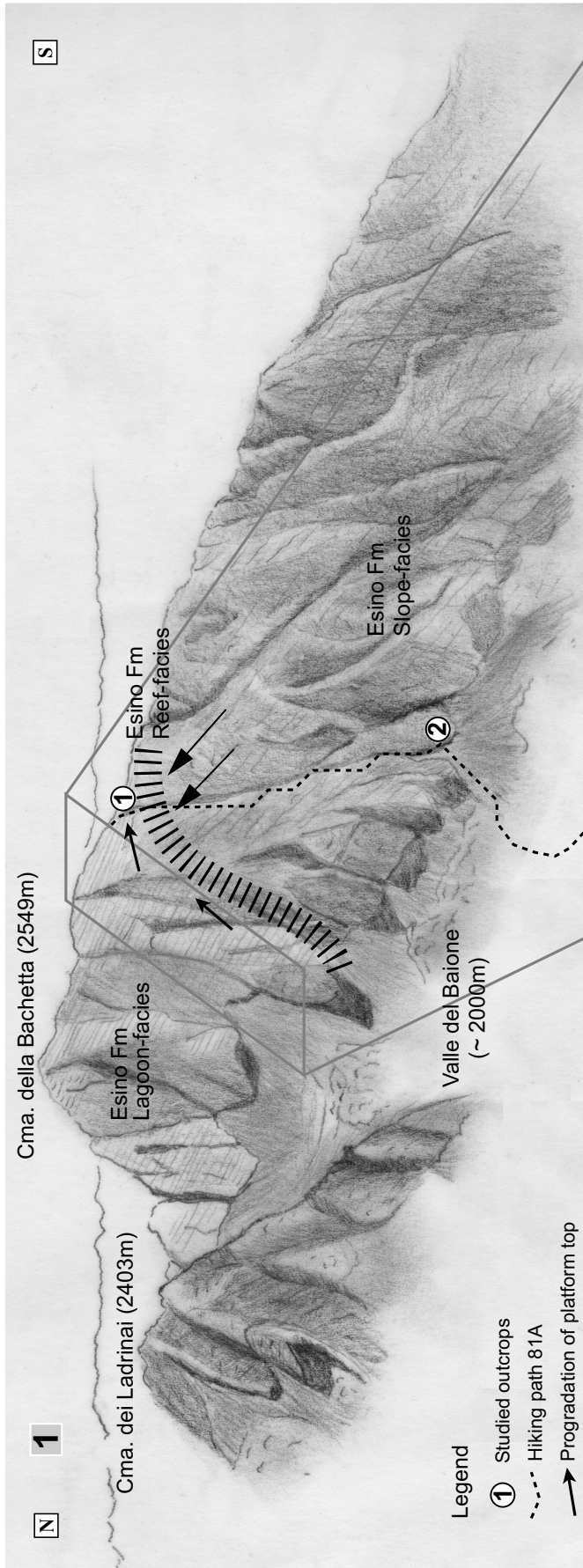
The Eggentaler Horn transect witnesses at least four stages of major collapse of the platform margin which removed large quantities of outer lagoon- and reef-facies and bypassed sediment to the lower slope. The platform margin subsequently backstepped and the slope revealed mainly bypass/erosional characteristics during the development at this exposition. The mechanisms being responsible for these multiple platform margin collapses remain unclear. The most likely seems an interplay of (1) increased tectonic subsidence at distal areas triggered by downward movement of tectonic blocks along the Stava Line to the SE, (2) repeated “cycles” of slope oversteepening and collapse and (3) slope failure controlled by seismic activity (i.e. earthquakes). Other locations from different stratigraphic horizons at Latemar show similar features (e.g. Cima Feudo, location 4; Schenon, location 5; see Fig. 3.2B) where large scale backstepping/erosion occurred on the platform-basin transition. The area to the NE of the Latemar records more depositional characteristics on the slope, but erosional intervals are still common as indicated by a distinct timeline of an erosional slope at Cresta De Do Peniola (location 6; see Fig. 3.2B; see Part 2).

The integration of all sedimentological data from the slope-facies at Latemar points out that the development of the SW, W and WNW parts of the platform has been governed by synsedimentary tectonics. The first platform stage building up directly from the Contrin ramp recorded times of a platform margin with a probably much larger diameter than today as lagoon-facies is unconformably overlain by slope deposits. This early platform retreated due to multiple collapses on the slope, margin and even platform top. Autocyclic processes of collapse-accom-

Plate 3.2 (following page) Platform architecture of the Concarena. Legends on the respective figures; for further explanations refer to the text.

3.2.1: Drawing of the NW flank of Cima della Bacchetta with an interpretation of geometric platform-basin relationships and an indication of studied outcrops. Magnification of the lagoonal succession to the lower right. Note the two distinct stages of lagoonal development.

3.2.2: Panoramic view of the NW flank of the Monte Vaccio area (see also Fig. 2a) with an interpretation of geometric platform-basin relationships. Reefal margin of the second stage of platform evolution – marked by vertical signature – shows pronounced progradation over a depositional slope.



modation fill-oversteepening-collapse together with synsedimentary tectonics resulted in a mainly aggrading platform. These facts together with local retrogradation during the last stages of platform development indicate that the carbonate factory at Latemar was stretched to its limits (see also Part 5).

3.3.3 Concarena

The maximum thickness of the Concarena carbonate platform is preserved in its eastern part (La Tavola area, location 3, see Fig. 3.2A) with a succession of at least 1500m thick slope strata overlapped by later basinal sediments (Pratotondo area, location 4, Lozio shales, see Fig. 3.2A). Approximately 800m of lagoon-facies with shallowing upward cycles are preserved in the north-western part of the platform (Plate 3.2.1). Stacking patterns of 1:5 are common in the lower part of the lagoon where metre-scale, mainly sub- and intertidal cycles are predominant. The upper part of the lagoon is characterised by a distinct decrease of bed and cycle thicknesses (Plate 3.2.1: Valle del Baione view of Cima della Bacchetta; see also small inset in Plate 3.2.1). In this part of the succession inter- to supratidal horizons with tepees, pisoids, vadose and phreatic cements are frequent. Massive early cementation in the lagoon caused early lithification and stabilisation of sediments. An exact differentiation of these two different stages in platform development is difficult as the lagoon-facies records a slow transition between these two intervals.

3.3.3.1 Bio- and sequence-stratigraphic correlation of the platform

Coeval, adjacent basins to the Concarena platform are infilled by two successive formations: Wengen Fm and Pratotondo Fm (Rossetti 1966; Brack 1984; Balini et al. 2000; see Fig. 3.3). The lower part of the Concarena buildup interfingers with the basinal Wengen Fm (uppermost Longobardian; see Fig. 3.3) whereas the upper part intercalates with the Pratotondo Fm (uppermost Longobardian, lowermost Julian; see Fig. 3.3). Balini et al. (2000) locate the Ladinian/Carnian boundary within

the lowermost part of the Pratotondo Fm. Hence, the upper part of the Concarena buildup is lowermost Carnian in age. According to our observations and the biostratigraphic position after Balini et al. (2000), the upper part of the Concarena platform is possibly correlatable with the Car1 sequence sensu Gianolla et al. (1998) or L3 sensu Gaetani et al. (1998). For both authors, these 3rd order sequences are related to a major sea level drop decreasing accommodation development.

3.3.3.2 Slope architecture

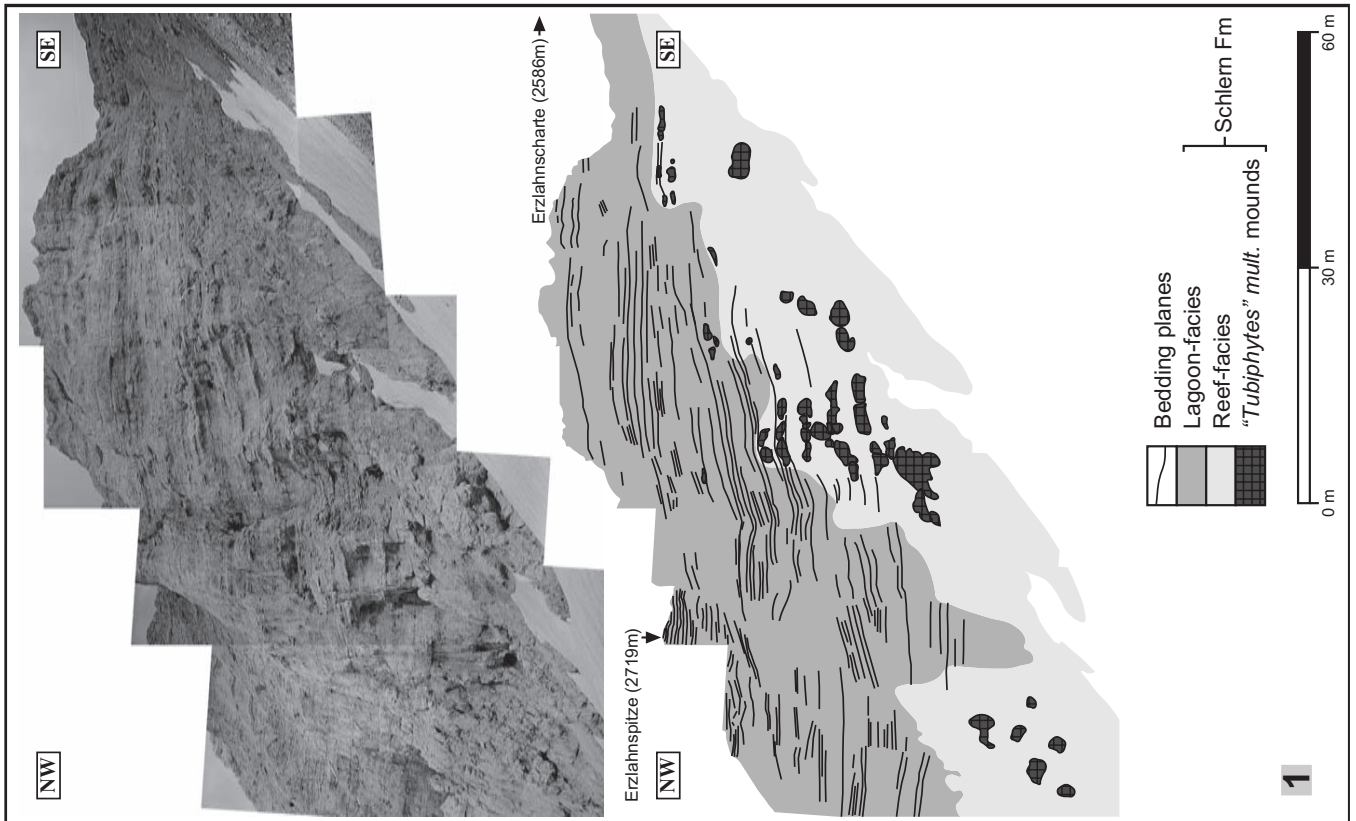
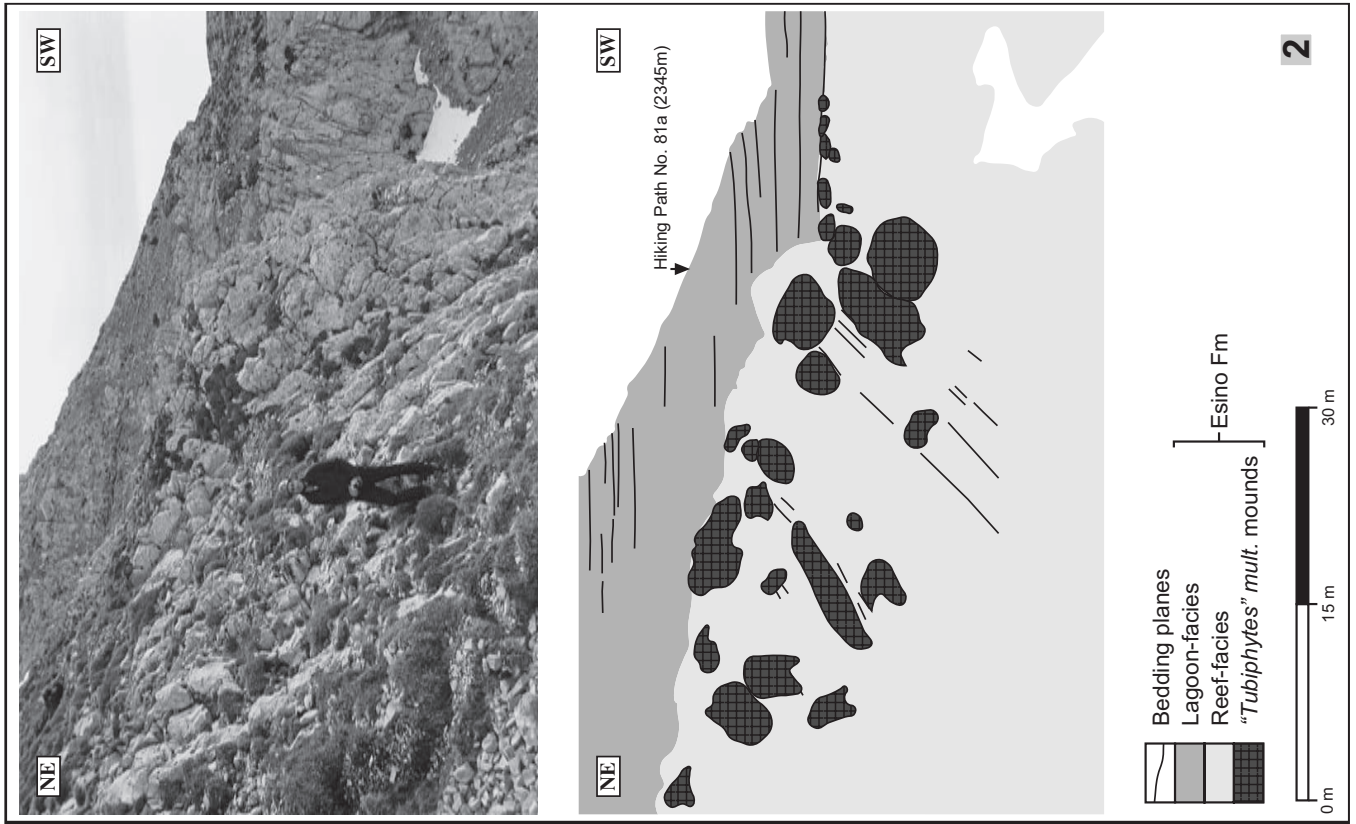
Slope-facies is preserved at all sides of the Concarena buildup: large-scale clinofolds are well visible at the eastern and southern termination of this platform (Plate 3.2.1 and 3.2.2). Moderate progradation occurs in the lower part (first platform stage), whereas the upper part (second platform stage) shows pronounced progradation with a toplap of clinofolds at the platform margin (Plate 3.2.1 and 3.2.2). This progradational pattern is possibly controlled by a change of accommodation space. Ladinian/Carnian boundary sections in the area indicate a relative sea level fall (Gaetani et al. 1998) significantly slowing down the accommodation increase in the Lombardic Basin. The geometries of the platform-basin transition indicate depositional characteristics sensu Schlager & Ginsburg (1981). Uppermost slope facies is ruled by massive early cementation partly comparable to the lagoonal syndepositional cementation. Climbing progradation of megabreccia clinofolds (“Carnian” model) and intercalation with the basinal Wengen Fm (volcaniclastics) characterise the slope-basin relationships in the La Tavola area (eastern termination of Concarena; location 3 in Fig. 3.2A). The thickness and amount of carbonate debris flows increase upward in these adjacent parts of the basins. The relatively high amount of clastic input into the basins and the moderate progradation of slope clinofolds determine the base relationships of the platform in this area.

In the Pratotondo area (southern margin of Concarena; location 4 in Fig. 3.2A) the geometrical configuration of clinofolds is different to the La Tavola area. The slope

Plate 3.3 (following page) “*Tubiphytes*” *multisiphonatus* bioconstructions at Latemar and Concarena. Legends on the respective figures; for further explanations refer to the text.

3.3.1: Panoramic view of the northern side of the Erzlahnscharte (Latemar: location 3) with an interpretation of the sedimentary structures of the reef-facies and indication of the “*Tubiphytes*” *multisiphonatus* mounds.

3.3.2: Panoramic view of the uppermost NW flank of the Cima della Bacchetta (Concarena: location 1) with an interpretation of the sedimentary structures of the reef-facies and indication of the “*Tubiphytes*” *multisiphonatus* mounds.



strata are younger in comparison with La Tavola and flatten out to well bedded, dm-thick, dark limestones (Pratotondo Limestone). Obviously, poorly oxygenated conditions developed, preventing distinct bioturbation. This two-phased evolution of the slope is probably connected to the mentioned change in lagoonal sedimentation (i.e. accommodation space). The combination of the uppermost Ladinian sea level fall with the compartmentalisation of basins (Assereto & Casati 1965; Brack 1984) and subsequent local development of starved basinal conditions decreased carbonate production (extrinsic factors sensu Schlager 1993).

3.4 Margin configuration

3.4.1 Previous research

The reef at Latemar has been the subject of several studies (e.g. Gaetani et al. 1981; Harris 1993) emphasising the importance of microbial encrustations and the similarity to Anisian fossil assemblages. Within its margin, several facies belts were distinguished: (1) back reef, (2) reef crest, (3) reef front and (4) transition to the uppermost slope. Recent research (Part 2) has shown that the biotic content of the reef-facies varies across the reef from uppermost slope to back reef as well as laterally from one locality to another.

Despite its similar primary preservation, the reefal margin of the Concarena has not yet been studied. However, with respect to the Latemar even better outcrop conditions enable the discrimination of facies belts and the lateral tracing of fossil assemblage trends. The following text describes representative transects across the reef.

3.4.2 Latemar

The organisation of the reef at Latemar is exemplarily shown with a description and interpretation of the Erzlahnscharte area (location 3 in Fig. 3.2B, Plates 3.1.3 and 3.3.1). Other locations like loc.s 4–6 (see Fig. 3.2B) have been discussed in Part 2 in detail.

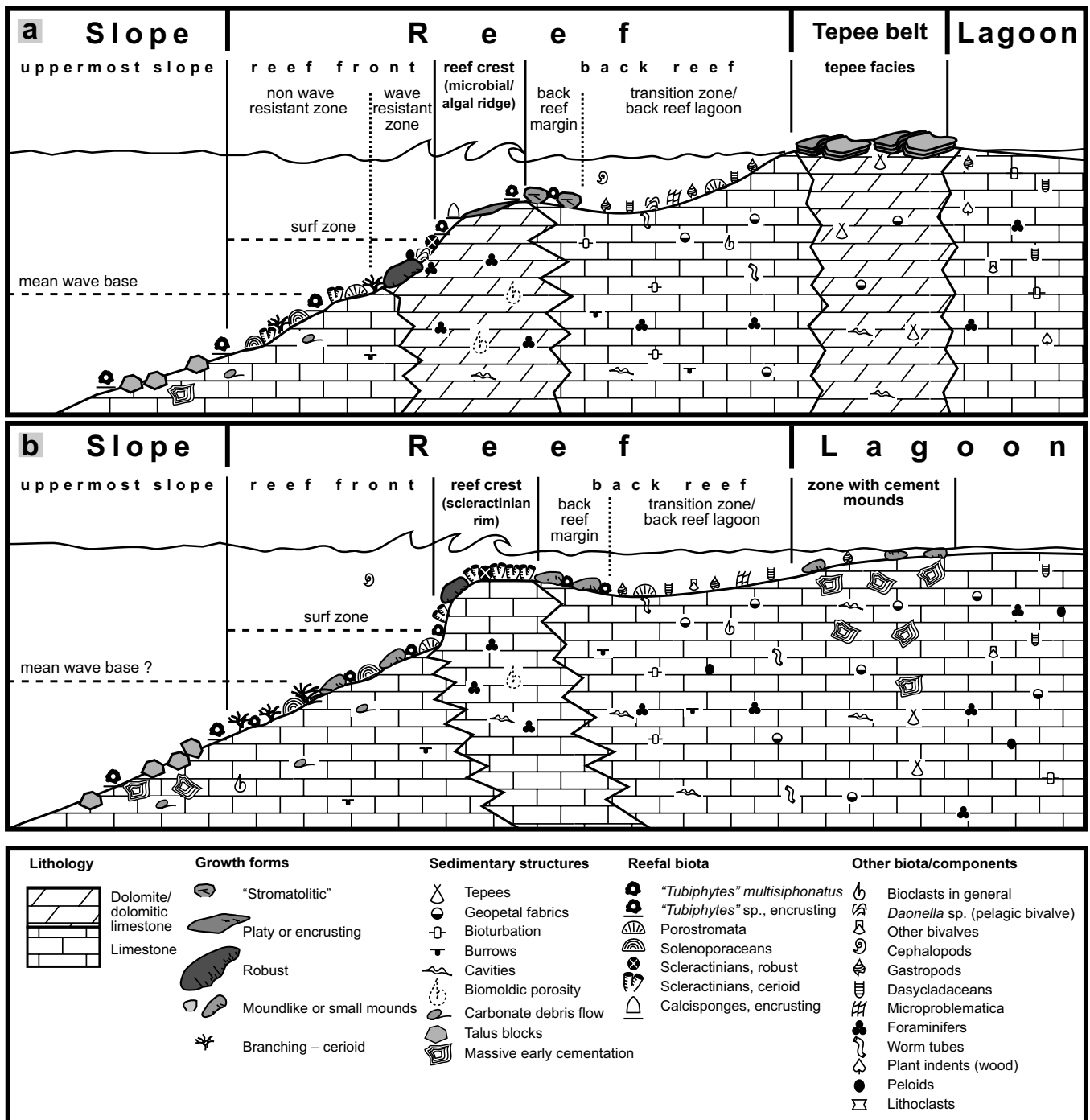
The outcropping parts of the reef-facies at Erzlahnscharte – its width ranging from 20m to 30m – belong to the back reef and reef crest (see Fig. 3.4A). The reef crest displays massive microbial encrustations with minor abundance of scleractinian framestones. The reef reveals a low topography with strata gently sloping towards the centre of the lagoonal platform top and to the upper slope. Evidence for emersion is absent, the reef has always been submerged; the palaeo bathymetrically highest point of the Latemar platform was the tepee belt between back

reef and lagoon (Egenhoff et al. 1999; see Fig. 3.4A). The particular feature of the back reef at this locality is the presence of “*Tubiphytes*” *multisiphonatus* mounds of up to 0.7m in height and 3m in diameter (see Plate 3.3.1). The mounds grew concentrically laterally and upward; “branches” of “*Tubiphytes*” *multisiphonatus* created a mm-wide mesh/framework surrounded by at least two generations of cements, the latter of the two being destructive. Different growth layers are formed by thin cement layers (see Plate 3.4.2). The subparallel to parallel branches consist of one central channel diverging frequently into other, secondary channels surrounded by micritic filaments (see Plate 3.4.5. and 3.4.6). For a more detailed description of the first finding of this species outside its type locality (Hydra, Greece, Carnian “Pantokrator Limestone”) the reader is referred to Part 2. Other reef localities at Latemar (locations 4 to 6; see Fig. 3.2B) show the importance of calcisponges (inozoans, sphinctozoans), Porostromata and Microproblematica for the organisation of the reefal margin.

3.4.3 Concarena

Large parts of the reef crest are exposed around the summit of Cima della Bacchetta (location 1 on hiking path 81A; see Fig. 3.2A, Plate 3.2.1 and 3.3.2). The width of the reef-facies varies between 15 m and 60 m and lacks a uniform geometrical evolution. Similar to the tepee belt at Latemar, a zone of massive cementation is present at the transition from lagoon to back reef. This zone is characterised by mound-like cement structures of considerable size (2–3m across and 1–2m in height). The degree of cementation is decreasing significantly from the lagoon towards back reef settings. Similar to the situation at Latemar, the main features of the back reef at Concarena are “*Tubiphytes*” *multisiphonatus* framestones forming mounds of up to 1.5m height and 4m of lateral extension interfingering with wacke-/packstones of the back reef lagoon. Apart from “*Tubiphytes*” *multisiphonatus* associated with radiaxial fibrous cements forming isopachous crusts (see Plate 3.4.3 and 3.4.4) the only other components are fine-grained bioclasts (e.g. pelecypods, gastropods), peloids, sessile encrusting foraminifers, porostromate algae and micritised worm tubes.

The main difference between Concarena’s and Latemar’s reef is the abundance of scleractinian coralline framestones at Concarena. The scleractinian colonies are up to 3–4m in height and 10m in diameter, interfingering



Figs. 3.4 Schematic reef model of the Latemar and Concarena indicating the three main zones (reef front, reef crest and back reef) and the relationship with the lagoonal succession. Legend in the lower part of the figure. The common feature of both margin models is the *"Tubiphytes" multisiphonatus* zone in back reef settings. Vertical exaggeration, not to scale.

3.4A The reef is always below sea level, the bathymetrically highest point of the Latemar margin is the tepee belt separating the back reef from the lagoonal interior of the platform (see also Egenhoff et al. 1999). Organisms with more delicate/branching growth are found beneath the mean wave base, whereas the more or less wave resistant zone within the surf zone is mainly marked by algae and minor corals.

3.4B The reef is always below sea level, the bathymetrically highest point of the Concarena margin is the lagoon. This is indicated by the geometrical relationship between reef and lagoon and the absence of emersive features at the reef (abundant at the lagoon). The walled, wave resistant zone within the surf zone is marked by corals. The position of the mean wave base is unclear. *"Tubiphytes" multisiphonatus* mounds also occur on the uppermost slope.

together and building a laterally continuous reef rim within the 15m to 60m broad reefal margin. Framestones of this fossil assemblage are characterised by *Margarosmilia* sp.-like corallites with a diameter of up to 15mm. Strong recrystallisation of the corallites prevented an identification of different species. The corals are primary framebuilders of the margin sensu Scoffin and Garrett (1974), Fagerstrom (1987) and Tucker and Wright (1990). Components of the minor trapped sediment are peloids and grains with micritic envelopes, as well as seldomly foraminifers and algae. The scleractinian rim is rich in primary cavities and vugs, lined by radiaxial fibrous cements.

Towards the upper slope, dm-sized talus blocks are increasing in size and abundance. This substratum is mainly stabilised by synsedimentary cement crusts (“Riesenoolithe”/“Evinospongiae”). At Concarena – contrasting to Latemar – “*Tubiphytes*” *multisiphonatus* mounds occur up until the transition to the foreslope. The mounds exhibit the same features as in the back reef environment, the only difference being the presence of possibly two types of “*Tubiphytes*” *multisiphonatus*. One type reveals slender branches and is identical to the *multisiphonatus* species described from the type locality at Hydra (Schäfer & Senowbari-Daryan 1982, 1983) and at Latemar (Part 2). The other one, probably being referred to as a new species of the “*Tubiphytes*” group, displays much thicker and longer “thalli” but reveals the identical internal organisation as described from the other localities – syndepositional cements and parallel to subparallel “branches”.

3.5 Cementation

Triassic carbonate buildups show abundant evidence of early marine diagenesis (e.g. Northern Calcareous Alps:

Brandner & Resch 1981; Eastern Alps: Zeeh et al. 1995; W Lombardic Alps: Frisia-Bruni et al. 1989; SW Dolomites: Russo et al. 2000). The precipitation of these early marine cements in carbonate platforms is a major diagenetic process and plays a key role for stabilisation of the buildup and for the productivity of the carbonate factory.

In the following chapter we refer to the presence or absence of massive early cementation (MEC) as a marine phreatic diagenetic process recorded by isopachous crusts and/or botryoids forming cementstones sensu Wright (1992) in sheltered environments (e.g. primary cavities, inter-reef voids etc.).

3.5.1 Latemar

At Latemar however, massive early cementation (MEC) plays a minor role only as stressed in Part 2. MEC has been observed at one locality on the uppermost slope only where cavities between blocks of a proximal talus fan facilitated the formation of “Evinospongiae”-like crusts (see Plate 3.5.6). The palaeo bathymetrically most elevated part of the Latemar platform – the tepee-belt – which has been emersive during certain periods of platform development (Goldhammer & Harris 1989; Egenhoff et al. 1999) is also governed by early cementation as witnessed by the abundant presence of isopachous radiaxial-fibrous cements and seldomly small botryoids within the central fissure of the tepees (Egenhoff et al. 1999; see also Plate 3.4.3). But the principal characteristics of this facies belt – it is (1) very narrow, (2) not present during all stages of platform evolution and (3) the restriction of cements to the central cavity between the inclined flanks of the tepees – reject a volumetrical importance of cements from this facies zone for the development of the entire platform. However, missing MEC

Plate 3.4 (following page) “*Tubiphytes*” *multisiphonatus* at Latemar and Concarena.

3.4.1: Dense framework of a mound of “*Tubiphytes*” *multisiphonatus* (slender species) on the uppermost slope (Concarena, location 2; scale bar in cm).

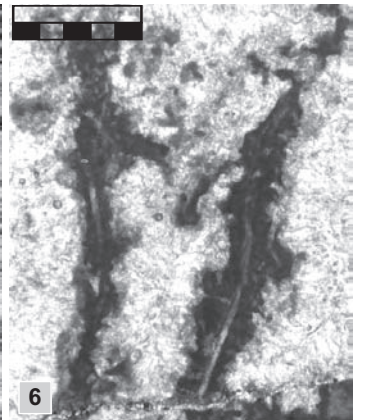
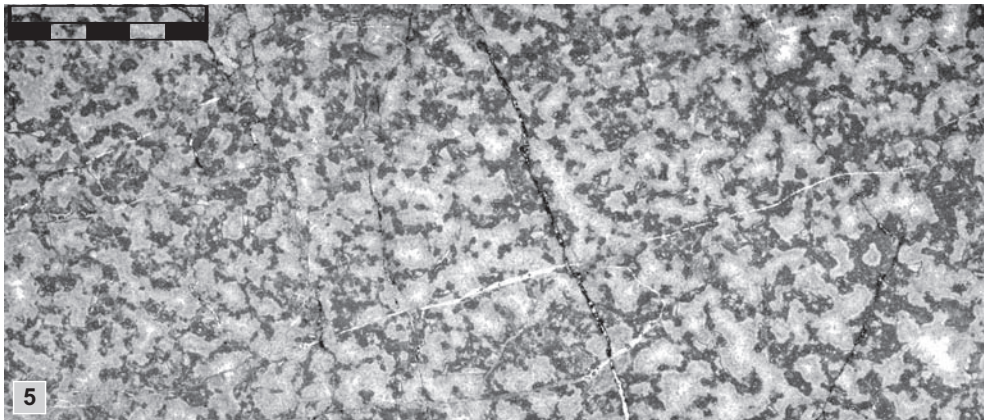
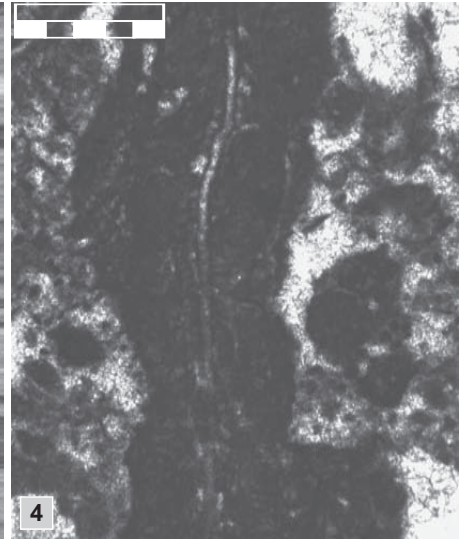
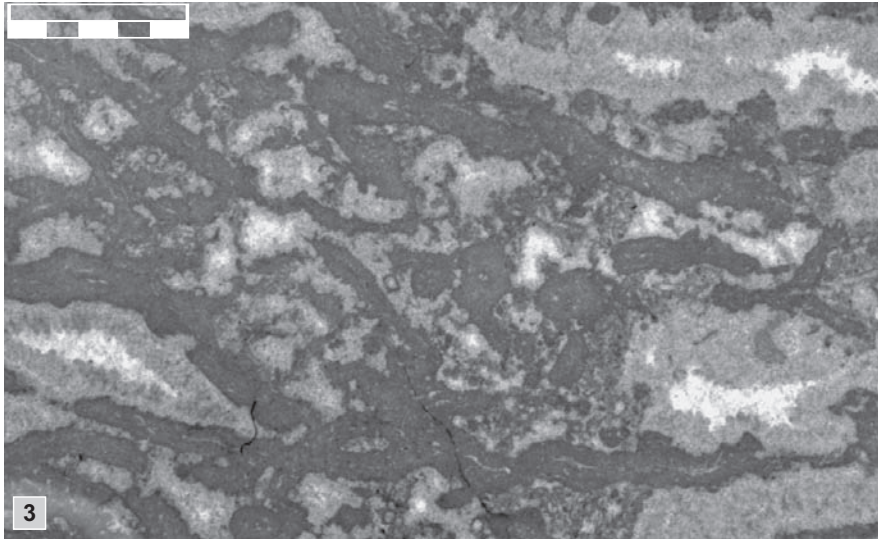
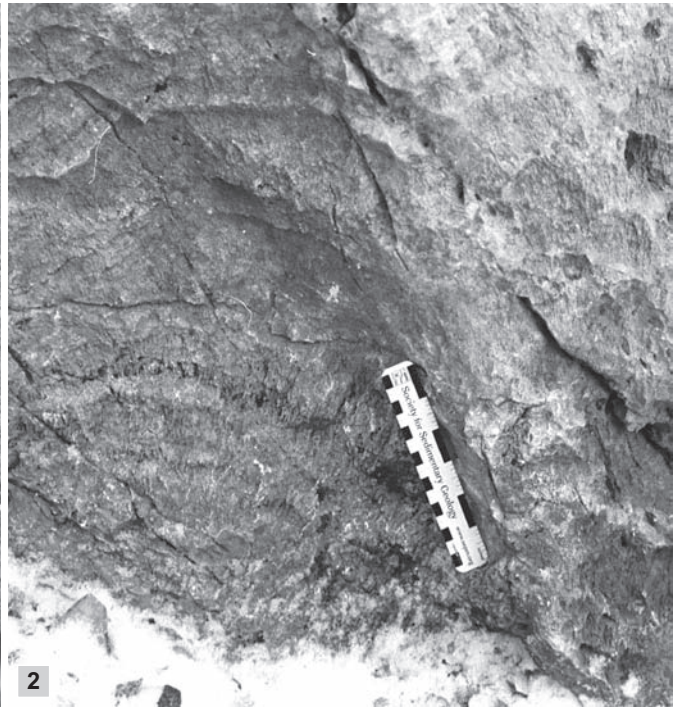
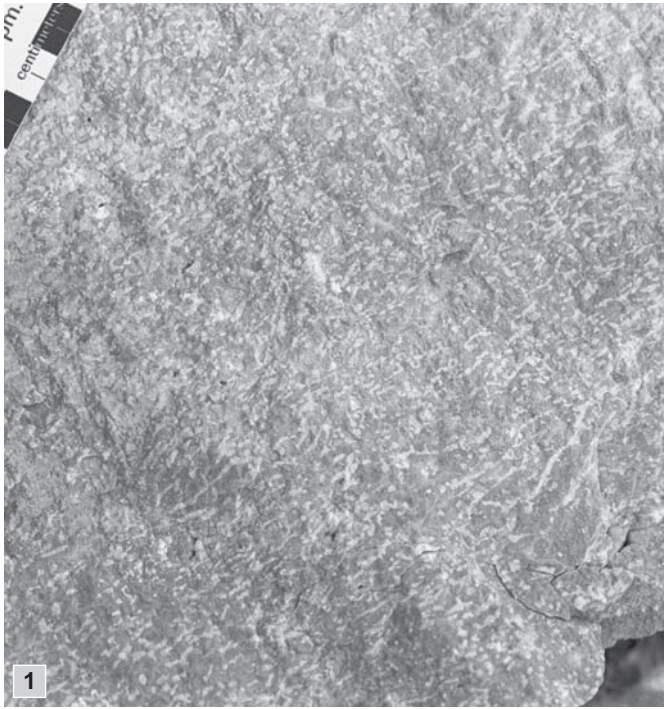
3.4.2: Outcrop photograph of a “*Tubiphytes*” *multisiphonatus* mound. Note the concentric layers separating the radially growing “branches” (Latemar, reef-facies, location 3; scale bar in cm and inches).

3.4.3: Photomicrograph of “*Tubiphytes*” *multisiphonatus* framework (Concarena, reef-facies, location 1; scale bar is 1cm with subdivisions of 2mm).

3.4.4: Photomicrograph of a single “branch” of “*Tubiphytes*” *multisiphonatus*. Note the central channel surrounded by fine micritic filaments (Concarena, reef-facies, location 1; scale bar is 1mm with subdivisions of 200µm).

3.4.5: Photomicrograph of “*Tubiphytes*” *multisiphonatus* framework (Latemar, reef-facies, location 3; scale bar is 1cm with subdivisions of 2mm).

3.4.6: Photomicrograph of two single “branches” of “*Tubiphytes*” *multisiphonatus*. Note the central channel surrounded by fine micritic filaments and the destructive nature of the cements (Latemar, reef-facies, location 3; scale bar is 1mm with subdivisions of 200µm).



at Latemar do not allow for the interpretation of a missing early lithification of the platform margin. Contrastingly, the occurrence of abundant megabreccia at the entire slope and Neptunian dykes at two localities at Latemar stresses the importance of early lithification of the carbonate deposits recording syndepositional tectonic activities because of its brittle behaviour (cfr. Kerans et al. 1986).

One reason for the insignificant abundance of MEC can be seen in the nature of this mainly Anisian reef, made up to a large extent of low growing, encrusting organisms constructing a small reefal margin with few large, isolated void spaces and low topography inhibiting effective fluid pumping. Another cause might be the close relationship between carbonate production and MEC (Lighty 1985). According to this author, high production/accumulation rates prevent MEC. We however suggest expressing this relationship more precisely and to link MEC to a low increase in accommodation (i.e. total subsidence plus sea level rise). Other factors like exposition to marine currents and climate changes are also significant (James & Ginsburg 1979; Playford 1980) but cannot be derived from the platform development. A high rate of accommodation increase shortens the amount of time available for marine phreatic diagenesis – and the formation of typical cements (e.g. botryoids) – as the sediments more quickly reach the window of shallow marine burial diagenesis. As the Latemar reveals very

high rates of total subsidence (see Part 5; Zühlke et al. 2003), it is obvious that MEC must be low.

3.5.2 Concarena

The link between MEC and accommodation development is confirmed by the Concarena case study where MEC is absent during early stages of platform evolution characterised by subtidal/intertidal cycles and moderate progradation. In contrast, the considerable slow-down of carbonate accumulation/accommodation increase and subsequent pronounced progradation towards the last stages of platform evolution (see chapter 3.4.3) leads to the formation of a “cement belt” at the back reef (cfr. Kerans et al. 1986) and of reefal talus consisting of cementstones *sensu* Wright (1992). At Concarena, the distribution of carbonate cements as discussed below follows the zonation of facies belts: (1) the lagoon is characterised by vadose cements indicating frequent subaerial exposure, (2) the transition towards the back reef by botryoids and isopachous crusts, (3) the reef by several generations of marine phreatic cements and (4) the uppermost slope by “Evinospongiae”-like isopachous crusts. All cements of the latter three zones point towards MEC.

3.5.2.1 Lagoon

The uppermost part of the lagoonal succession at Concarena records a complex early, vadose diagenetic

Plate 3.5 Cements at Latemar and Concarena.

3.5.1: Massive early cementation (MEC) at the lagoon in the zone of cement mounds (Concarena, Cima della Bacchetta, scale bar in cm and inches).

3.5.2: MEC at the uppermost slope (Concarena, Cima della Bacchetta, scale bar in cm and inches).

3.5.3: MEC at the lagoon in the zone of cement mounds. Lower part of the mound-like structure is entirely made up of dark botryoids (associated with organic matter?) whereas the upper part contains isopachous crusts exclusively (Concarena, Cima della Bacchetta, scale bar in cm and inches).

3.5.4: Sample from the central cavity between the inclined flanks of tepees showing multiple generations of cement and terra rossa (Latemar, tepee belt, lagoon-facies; scale bar is 1cm with subdivisions of 2mm).

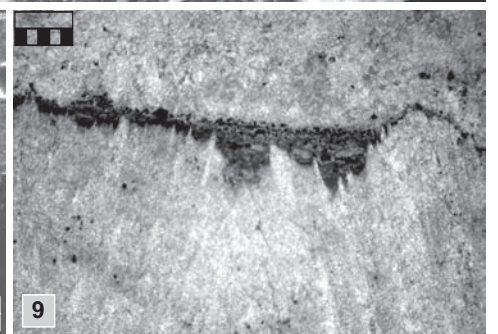
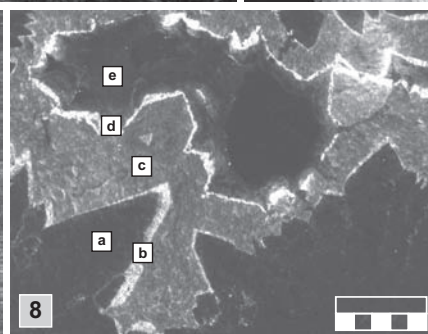
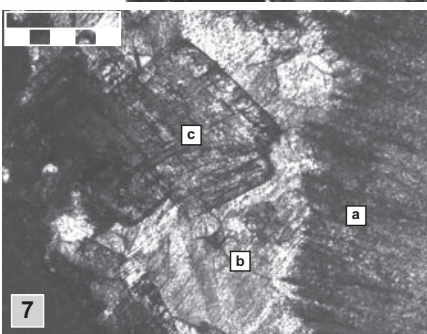
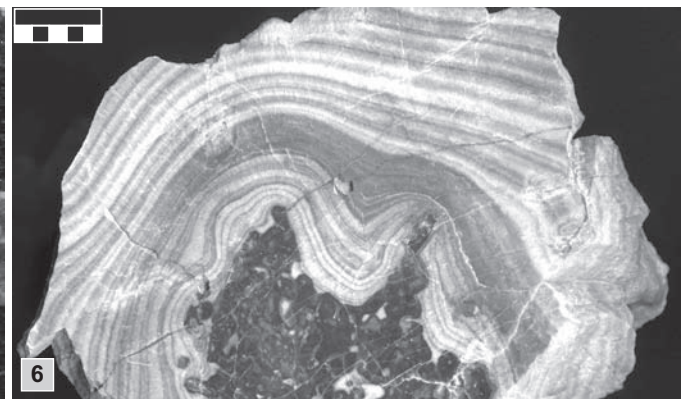
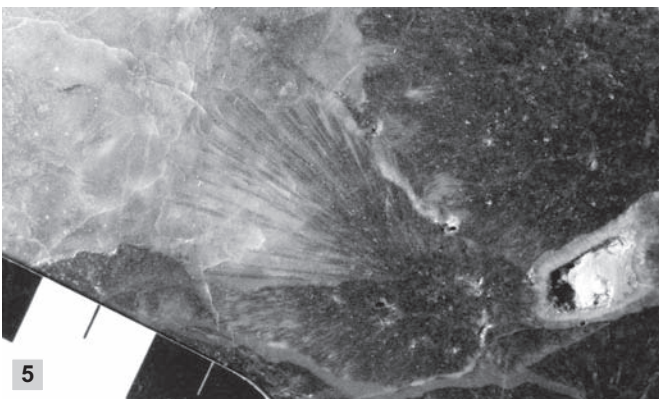
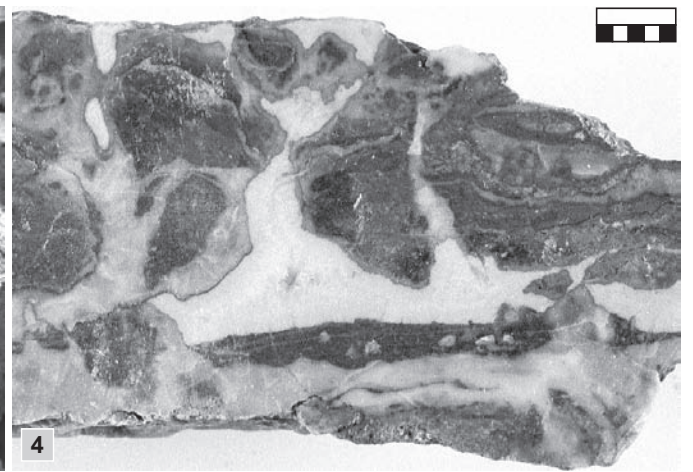
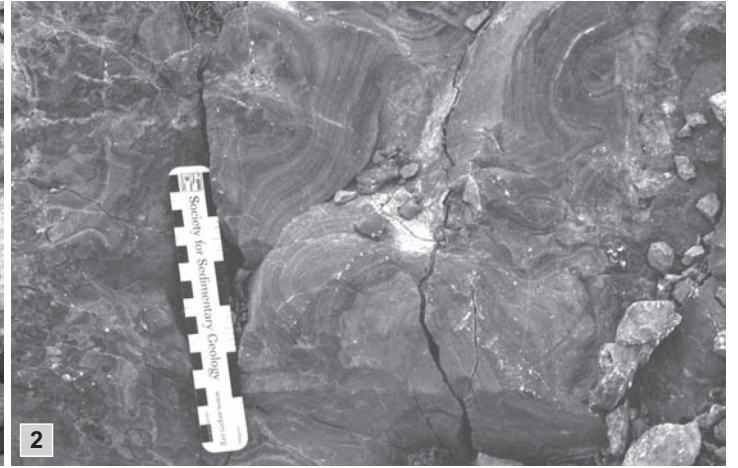
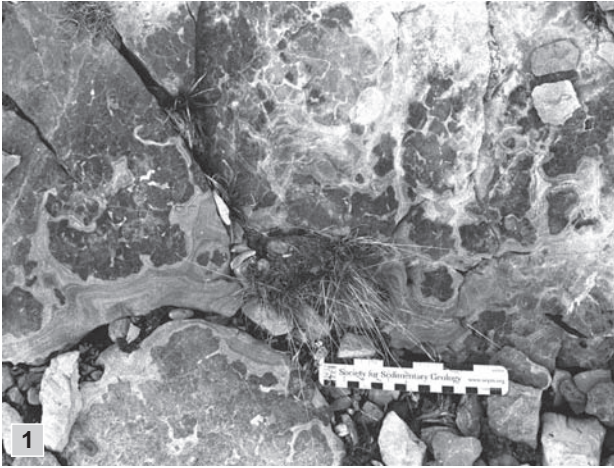
3.5.5: Dark botryoid – approx. 3cm in length – from the zone of cement mounds (Concarena, Cima della Bacchetta, scale bar in cm with subdivision of 5mm).

3.5.6: Photograph of polished slab from talus blocks with isopachous crusts (Latemar, breccia of slope-facies, location 5; scale bar is 1cm with subdivisions of 2mm).

3.5.7: Succession of early and late cements: (a) radiaxial fibrous cement, (b) zoned blocky calcite and (c) saddle dolomite rhomb (Concarena, lagoon-facies, location 1; scale bar is 1mm with subdivisions of 200µm).

3.5.8: Cathodoluminescence image of different stages of shallow to deep burial cements: (a) dog tooth cement, (b) and (d) fringes of bright luminescent cement, (c) and (e) are different generations of blocky calcite (Concarena, slope-facies, location 2; scale bar is 200µm with subdivisions of 40µm).

3.5.9: Botryoidal cement from the lagoon-facies covered by peloids (Concarena, Cima della Bacchetta, scale bar is 1mm with subdivisions of 200µm).



history. Symmetric and asymmetric meniscus cements are common, pisoids, oncoids and dripstone cements are further indicators for inter- to supratidal conditions with frequent exposure. Other diagenetic features are brecciation with infiltration of fine-grained microcrystalline dolomite in a red argillaceous matrix (“terra rossa” Assereto et al. 1977; Mutti 1994) related to near surface processes. Some localities contain botryoids covered by fine-grained peloidal sediment (Plate 3.4.9) pointing towards restricted water circulation within and into the cavity (Lighty 1985). Botryoidal cements show patchy or undulose extinction, a distinct hint to replacement of the former aragonite by calcite.

The striking feature of the transition from the lagoon towards back reef settings are cement arrangements of “mound”-like shape (decimetre to metre size in diameter and height; see Plate 3.5.3). The base of these cement “mounds” is formed by botryoids closely linked to microbial crusts. Isopachous cements massively encrust the dark coloured botryoids (Plate 3.5.1 and 3.5.3). These isopachous crusts are entirely made up of fibrous calcite with alternating light and dark layers indicating syndimentary marine precipitation. The multiple fibrous calcite layers show strong undulose extinction under crossed Nichols and it is possible to distinguish radiaxial fibrous from less common fascicular-optic patterns (Kendall 1985).

3.5.2.2 Reef

With respect to the MEC in all other facies belts, the reefal margin of the Concarena platform reveals the lowest volumetric content of cement. Cementation took mainly place within the “*Tubiphytes*” *multisiphonatus* zone and the scleractinian rim. The “*Tubiphytes*” *multisiphonatus* mounds in the back reef show the same cement history as their counterparts on the Latemar platform (see chapter 3.5.1). The coralline part of the reef exhibits features such as large open cavities, precipitation of small-scale radiaxial fibrous calcite and late blocky calcite inside small vugs and/or coral branches. Like the other facies belts, the reefal margin is also displaying early cementation and later recrystallisation of components.

3.5.2.3 Slope

The occurrence of massive decimetre-sized concentric isopachous crusts is not only restricted to lagoon and back reef areas of the Concarena platform, but is also a

common feature of reef front/uppermost slope settings. The first authors having dealt with similar isopachous crusts in slope environments termed them “Riesenoolith” (v. d. Linth 1853) and/or “Evinospongiae” (Stoppani 1858). For a historical review, the reader is referred to Leuchs (1928) and Russo et al. (2000). The cement layers of the “Riesenoolith”/“Evinospongiae” also contain significant amounts of organic matter, as indicated by the smell of freshly fractured samples. The study of Russo et al. (2000) on the Marmolada slope describes similar cementation and suggests a control on the early diagenetic carbonate precipitation exerted by residual organic matter. However, up to now no detailed studies exist on the origin, biochemical composition and distribution of this material. It therefore remains unclear whether this organic matter represents residues of primary organic material or was mobilised during late burial diagenesis (see Russo et al. 2000). The organic content of the “Riesenoolith”/“Evinospongiae” is highly variable, which might indicate a genetic link to burial induced organic-rich fluid flow. Small vugs in slope deposits are almost entirely filled with radiaxial fibrous calcite.

3.5.2.4 Cathodoluminescence

Cathodoluminescence techniques were used to identify different generations of cements, especially to separate deep burial cements (e.g. zoned blocky calcites; Zeeh & Bechstädt 1994) from early to shallow burial cements (e.g. radiaxial fibrous cements, dog-tooth cement; Zeeh & Bechstädt 1994) in order to estimate their volumetric importance with respect to whole rock cementation. Botryoidal cements – restricted to lagoonal areas – show only patchy luminescence. Radiaxial fibrous cements forming isopachous cement crusts are generally non-luminescent. Shallow burial cements like dog-tooth cement with insignificant or dull luminescence often cover early radiaxial fibrous calcite. They sometimes show multiple, bright luminescing outer rims and are mainly followed by blocky calcite filling most of the remaining porosity and late fractures. This cement stratigraphy corresponds to the scheme of Zeeh (1998) for the Eastern and Southern Alps. A succession of three to five different cements with different luminescence degrees can be observed (Plate 3.5.7 and 3.5.8). In a few cases, red luminescing crystals of deep burial saddle dolomite replaces zoned blocky calcite. Pressure solution is a further common feature of the burial diagenesis and responsible for precipitation of burial carbonate cements, such

as zoned blocky calcite (Zeeh & Bechstadt 1994). Some single saddle dolomite rhombs are partially dedolomitised, as proven by a dark outer – probably iron rich – zone and microfractures (Zeeh et al. 1995; see Table 3.5.7). Observed cross-cut relationships between several deep burial cements and the occurrence of the same cements in younger strata allow to constrain the deep burial diagenesis of the Eastern and Southern Alps to ages younger than Early Cretaceous (Zeeh et al. 1997; Zeeh 1998).

3.5.2.5 Stable isotopes

As mentioned above, isopachous crusts are commonly related to marine fluids precipitated under marine phreatic conditions (Kendall 1985; Boni et al. 1994; Zeeh et al. 1995). In order to obtain information about the isotopic fluid composition during cement growth, selected unaltered and homogeneous samples of primary fibrous cements corresponding to early marine diagenesis (Kendall 1985; for discussion see Tucker & Wright 1990)

were analysed for their carbon and oxygen isotopic composition. $\delta^{13}\text{C}$ values of these early diagenetic cements have an average value of +3.20‰, expressed relative to the V-PDB standard (see Fig. 3.5). The values fit well with other data of Ladinian/Carnian strata (–1‰ to +4‰; e.g. Scherer 1977; Mutti 1994; Zeeh et al. 1997; Veizer et al. 1999; Korte 1999; see Table 3.1) and most likely reflect a marine carbon source. The measured $\delta^{18}\text{O}$ values – having an average of –5.17‰ (expressed relative to the V-PDB standard; see Fig. 3.5) – slightly deviate from calculated and measured oxygen isotope values precipitated from Triassic sea water (–1‰ to –4‰; Frisia-Bruni et al. 1989; Korte 1999; Veizer et al. 1999; expressed relative to the V-PDB-standard; see Table 3.1). This small shift of about one to two permillage points to more negative values probably reflects the higher temperature of buried sea water during shallow burial diagenesis/recrystallisation (Dickson & Coleman 1980). Using the fractionation equation of Hays & Grossman (1991), the observed negative shift in oxygen isotopes

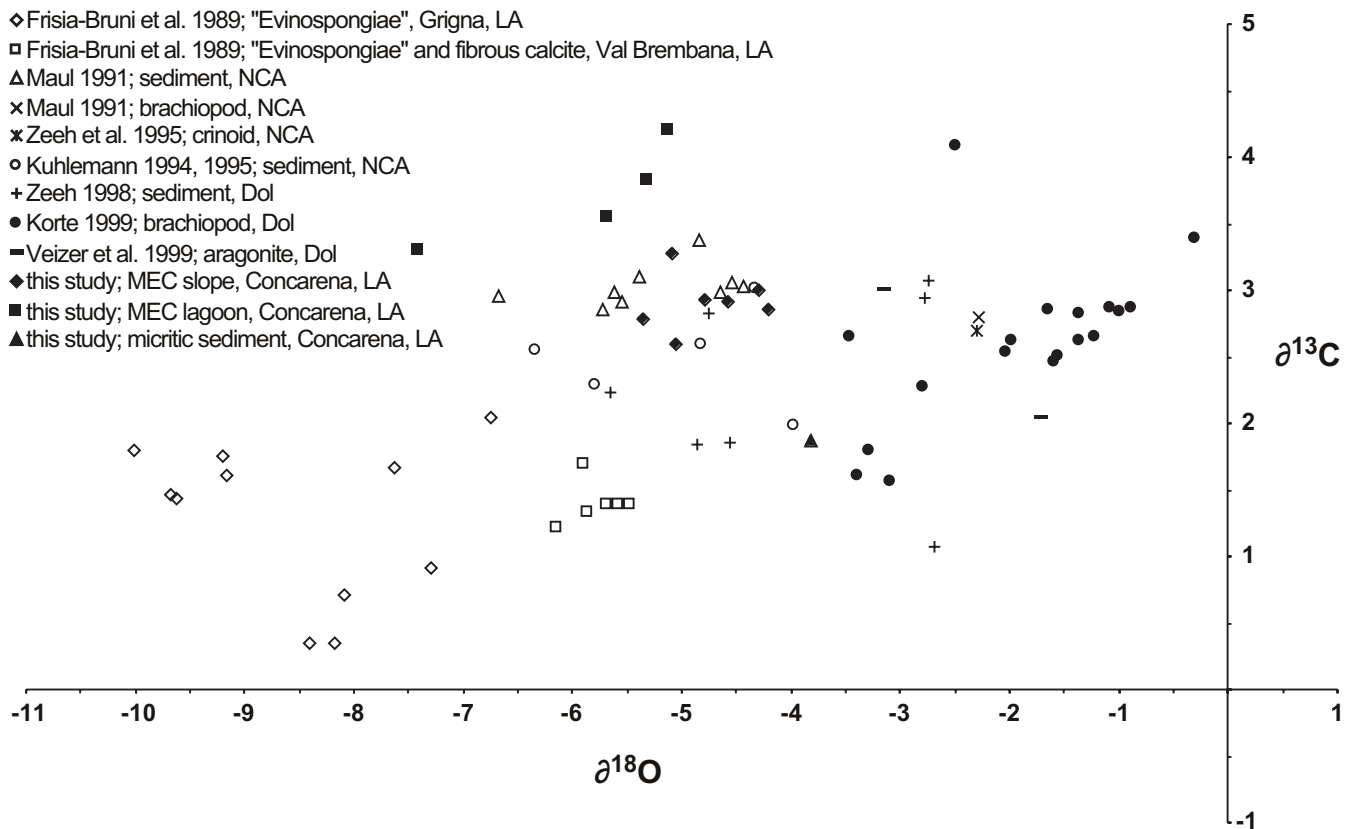


Fig. 3.5 $\delta^{18}\text{O}$ vs. $\delta^{13}\text{C}$ plot of some Middle to Late Triassic carbonates of the Western Tethys. $\delta^{18}\text{O}$ and $\delta^{13}\text{C}$ values are given in ‰. Primary composition of the Triassic seawater is best reflected by brachiopods (–1 to –3‰ $\delta^{18}\text{O}$ and +2 to +3‰ $\delta^{13}\text{C}$). Abbreviations: LA: Lombardic Alps; NCA: Northern Calcareous Alps; Dol: Dolomites.

1	2	3	4	5	6
Sample	$\delta^{18}\text{O}$ (V-PDB)	$\delta^{18}\text{O}$ standard deviation	$\delta^{13}\text{C}$ (V-PDB)	$\delta^{13}\text{C}$ standard deviation	Material
P28.3	-3.81	0.03	1.87	0.02	micritic sediment, distal slope
P28.7	-5.09	0.01	3.28	0.01	radial fibrous cement, slope
P28.8	-4.78	0.01	2.93	0.02	radial fibrous cement, slope
P28.9	-5.06	0.02	2.59	0.01	radial fibrous cement, slope
P28.10	-5.36	0.02	2.78	0.02	radial fibrous cement, slope
P28.11	-4.30	0.02	3.00	0.02	radial fibrous cement, slope
P28.13	-4.57	0.01	2.92	0.01	radial fibrous cement, slope
P28.14	-4.21	0.01	2.85	0.01	radial fibrous cement, slope
P28.15	-7.42	0.02	3.31	0.01	botryoidal cement, lagoon
P28.5	-5.31	0.02	3.82	0.02	radial fibrous cement, lagoon
P28.6	-5.13	0.02	4.20	0.01	radial fibrous cement, lagoon
P28.0	-5.69	0.01	3.55	0.01	radial fibrous cement, lagoon
	-5.17	0.83	3.20	0.47	mean (without sediment)

Table 3.1 $\delta^{18}\text{O}$ and $\delta^{13}\text{C}$ values of samples from the Concarena. The mean of all measurements in the cements is given in the last row. standard deviations are 1s deviations. Column 1: sample ID; column 2: $\delta^{18}\text{O}$ values of the samples in ‰; column 3: standard deviation of the measurements in ‰; column 4: $\delta^{13}\text{C}$ values of the samples in ‰; column 5: standard deviation of the measurements in ‰; column 6: material of the samples.

of the radial fibrous cements indicates temperatures of diagenesis/recrystallisation of about 5°C to max. 10°C higher than the presumed sea water temperature, which lies clearly within the shallow burial realm. In summary, we interpret the concentric isopachous cement crusts to be products of early marine diagenesis having an important influence on the stabilisation of back reef and reef front/upper slope areas. Their isotopic composition was slightly altered during recrystallisation in the shallow burial realm. The botryoids (see Fig. 3.5 and Table 3.1) of the MEC in the lagoon yield isotopically lighter compositions of oxygen owing to meteoric influence.

3.6 Conclusions

Detailed microfacial and palaeontological investigations at the margins of these two Middle Triassic carbonate platforms show the importance of “*Tubiphytes*” *multisiphonatus* for the organisation of the reefal communities. Apart from previous findings at Aggtelek (Hungary; Scholz 1972), Hydra (Greece; Schäfer & Senowbari-Daryan 1982, 1983) and Latemar (Italy; Part 2 and this study) the Concarena was identified as the fourth locality where this enigmatic microproblematicum occurs (for a detailed list refer to Part 2). Contrastingly to all other locations, “*Tubiphytes*” *multisiphonatus* mounds at Concarena are also part of the reef front to uppermost slope. Additionally, the size and abundance of “*Tubiphytes*” *multisiphonatus* bioconstructions at Concarena exceed all previously described localities such that “*Tubiphytes*” *multisiphonatus* is one of the main

constituents of the reefal margin. The so far restricted occurrence of this biota in the central Tethys area might indicate that specific environmental conditions were required for the growth of “*Tubiphytes*” *multisiphonatus*. The comparison of the two platforms lead to the identification of several boundary conditions for MEC: (1) Abundant open and connected cavities supplied by e.g. rigid frameworks of reef building organisms or inter-particle space of talus breccias. (2) Effective fluid flow mechanisms like wave activity in combination with matching platform margin morphology (walled reefs). (3) Low rates of accommodation increase prolonging the time interval of marine phreatic diagenesis (i.e. palaeo water depths ranging from subtidal slope settings to intertidal lagoonal environments).

Owing to the nature of Anisian to Early Ladinian buildups (low growing, encrusting organisms being the main reefal constructor guild and mound-like morphology), MEC is mainly absent in these. Botryoids and large isopachous crusts of radial fibrous cements are much more likely to develop in the voids of Late Ladinian/Carnian rimmed platforms. The reefal margins of the latter buildups are made up of rigid bioconstructions (e.g. scleractinians) and walled, wave resistant morphology enabling effective fluid flow. According to Ginsburg et al. (1971), James et al. (1976) and Marshall (1986) only seaward margins of walled reefs show MEC related to environmental factors such as high-energy conditions supplying effective pumping of marine fluids. Isolation of primary voids through encrusting organisms and subsequent infill with peloids inhibits MEC.

Accommodation increase is probably the most important boundary condition for MEC as the time interval available for marine phreatic cementation is crucial. If the succession passes quickly through the marine phreatic window primary cavities and voids are much more likely to contain a small amount of cement only. The excellent porosity of many modern hydrocarbon reservoirs in carbonates have been tied to basins during high sea level undergoing rapid subsidence (Moore & Haydari 1993) leaving insufficient time for cementation. It is, however, more precise to link this diagenetic evolution of porosity-prone, MEC-poor platforms to periods of fast sea level rise and/or rapid subsidence (i.e. high rates of accommodation increase). Nevertheless, a certain amount of cementation is necessary in order to counterbalance compaction and to preserve porosity. Leaving burial cementation aside, porosity seems best to be preserved in

a certain window of accommodation increase balanced by carbonate production allowing enough cementation to stabilise the platform. Consequently, the link between accommodation change and MEC allows constraining this early diagenetic development to platform types with certain geometries: (1) Aggradational or retrogradational platforms are unlikely to develop features of MEC. (2) Platforms with progradational characteristics are prone to MEC.

This hypothesis is confirmed if it is tested against other Triassic platforms in the western Tethys area. Boni et al. (1994) and Climaco et al. (1997) describe strikingly similar features from “pathologically prograding” (Bosellini 1989) Upper Triassic platforms of Calabria (Southern Italy). Like at Concarena, the last stages of platform development are governed by slow-down in accommodation increase in combination with anoxic conditions in the basins. Strong similarities also exist with platforms of the Northern Calcareous Alps (Brandner & Resch 1981; Zeeh et al. 1995) where MEC is always linked to progradation and walled reefs.

Acknowledgements

The authors would like to express special thanks to V. Zamparelli, University of Napoli (Italy), for the help with reefal biota and Michael M. Joachimski, University of Erlangen (Germany), for the measurement of stable isotopes. We are especially indebted to Flavio Jadoul, University of Milano (Italy), as well as Fabrizio Berra and Gianni Bartolomeo Siletto, Servizio Geologico Regione Lombardia, for introducing us to the field and helping in many respects. Peter Brack, ETH Zürich (Switzerland), indicated his former “playground” Concarena as being worthwhile to compare with the Latemar – he did not tell how distant to walk it is, however. This project has partly been financed by the “Deutsche Forschungsgemeinschaft” (funding M. Seeling; Project Be-641/33), the “Studienstiftung des deutschen Volkes” (funding A. Emmerich) and the International Postgraduate Programme in geosciences at the University of Heidelberg.

PART 4

Quantified Carbonate Platform Development: The Rosengarten/Catinaccio transect (Middle Triassic, Dolomites, Italy)

Abstract

The Middle Triassic (Anisian/Ladinian) Rosengarten platform is characterised by two major stages of platform evolution; the first stage reveals aggradation, the second progradation of the platform margin. Basin reverse modelling results indicate that these two intervals originate from a temporal change in total subsidence. Spatial variations in total subsidence along the 6km transect were insignificant.

During the first stage of platform evolution, high, pulse-like total subsidence rates of up to 820m/Ma led to aggradation. As total subsidence rates dropped to 100m/Ma, platform progradation was initiated. The short-spanned subsidence peak is closely linked to tectonic movements along the neighbouring Cima Bocche Anticline - Stava Line (approx. 10km to the SE).

Stratigraphic forward modelling quantified the sediment volumes and influence of sea level oscillations. In order to replicate platform architecture, constant carbonate production rates between 900 and 1000m/Ma - increasing from periplatform environments to the slope - had to be assumed throughout the existence (< 5Ma) of the Rosengarten platform. The carbonate factory successfully kept up with high accommodation rates of the first stage. Hence it must have had completely recovered from the P/T biotic crisis already at the beginning of platform development in the Upper Anisian. Sea level oscillations played a minor role or have been overprinted by tectonic factors. Slope progradation from N to S is mimicked by the porosity evolution of the sediment package below the slope (sandstones and shales).

Vitrinite reflectance and apatite fission track analyses were integrated into basin modelling to constrain the modelled regional burial and thermal history. Vitrinite reflectance (VR_r) values in the basal strata (outcrop samples from organic-rich sandstones, marls and limestones) vary between 0.4% VR_r and 0.7% VR_r . This low thermal maturity implies that maximum palaeo temperatures did not exceed 110°C and that eroded strata having overlain present-day topography must have been less than 1100m

thick. Maximum temperatures were reached during the Early/Middle Triassic, when high heat flows prevailed. Local anomalies in vitrinite reflectance of up to 1.1% VR_r in the SE indicate that the thermal influence of the Predazzo/Monzoni volcanic event (Late Ladinian) neighbouring the Rosengarten area was limited and restricted to its nearest vicinity. The modelled burial history is confirmed by apatite fission track analyses carried out on Permian sandstones (Gröden Fm). Cooling ages of around 37Ma suggest a relatively long burial from Upper Permian times until the end of the Cretaceous and a fast exhumation from the Eocene/Oligocene onward.

4.1 Introduction

The Dolomites of Northern Italy (see Fig. 4.1) have ever been a study area for carbonate platforms and their reefal communities. Since Mojsisovics (1879) had termed the word “Überguss-Schichtung” (i.e. clinostratification), many authors have worked on platform-to-basin transitions of carbonate build-ups in the Dolomites (e.g. Hummel 1928, 1932; Pia 1937; Leonardi 1962, 1967; Bosellini 1984, 1988). In particular, the Rosengarten has served as a reference model for progradational geometries (Bosellini and Stefani 1991; Bosellini et al. 1996). However, most approaches of assessing the evolution of carbonate platforms and their respective clinofolds have been mainly of qualitative nature. Quantitative approaches on subsidence development and carbonate production of Middle Triassic platforms in the Dolomites have so far been scarce (Schlager 1981; Doglioni and Goldhammer 1988; Schlager et al. 1991; Maurer 1999, 2000). The age of Middle Triassic platforms in the Dolomites is constrained by coeval basinal sediments (Buchenstein Fm; Brack and Rieber 1993, 1994). Recently, age-diagnostic air-borne tuff layers in basinal and lagoonal strata were used to synchronise bio-, cyclo- and chronostratigraphy (basinal Buchenstein Fm at Seceda/Geisler Group, W-Dolomites: Mundil et al. 1996; lagoonal Schlern Fm at Latemar, W-Dolomites: Mundil et al. 2003; for locations see Fig. 4.2) providing a unique, high resolution database for basin modelling. Tephrochronologic correlation of dated tuff layers into slope deposits of the Rosengarten platform was carried out by Maurer (1999, 2000).

The aim of this paper is the quantification of the development of the Rosengarten platform and the assessment of its controlling factors during evolution. This is real-

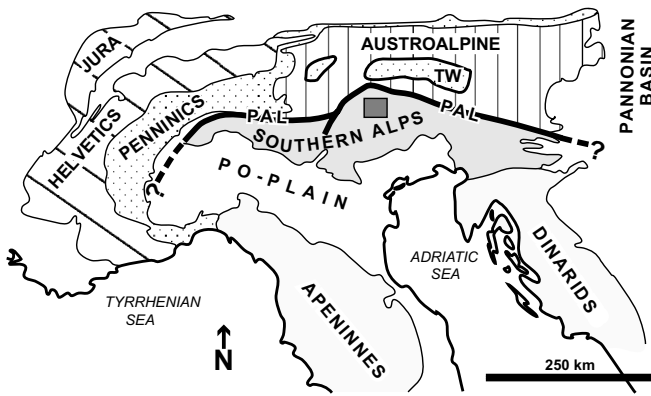


Fig. 4.1 Schematic tectonic map of the Alps. The dark grey rectangle marks the location of the study area. Abbreviations: TW: Tauern window; PAL: Periadriatic lineament.

ised by an integrated approach of reverse basin and forward stratigraphic modelling combined with thermal modelling. Datasets for both modelling approaches were derived from existing studies and new detailed analyses on allo-/sequence stratigraphy and facies architecture, thermal maturity and apatite fission tracks of underlying strata. Another goal of this project has been the investigation of the recovery of the carbonate factory from the faunal crisis at the end of the Permian.

4.2 Geological setting

The southwestern Dolomites (for location within the Alps see Fig. 4.1), are located on the Adriatic Plate between former Laurussia and Gondwana (Dercourt et al. 1993, 2000). Throughout the Triassic, this area was the eastern margin of a highly differentiated passive continental margin with mixed carbonate-clastic sedimentation (Blendinger 1985; Doglioni 1987; Dercourt et al. 1993, 2000). The carbonate factory had suffered from the severe faunal crisis on the verge of the Permian until the Anisian when first carbonate ramps (Early Anisian/Aegean) and small reefal mounds (Early Late Anisian/Pelsonian) developed in the Dolomites (Fois and Gaetani 1984; Senowbari-Daryan et al. 1993). From the Late Anisian on into the Late Ladinian, a considerable submarine relief with local subaerial highs prevailed in the western Dolomites. Middle Anisian transpressive-transpressive tectonics had dismembered the continental shelf creating strong regional differences in facies (i.e. facies heteropy; Bechstädt and Brandner 1970; Blendinger 1985; Doglioni 1987; Zühlke 2000). Deep marine, stagnant basins with fine-grained chert- and or-

ganic matter-rich sediments (Moena Fm and Buchenstein Fm; see Fig. 4.2) existed alongside shallow marine subtidal carbonate ramps and platforms (Contrin Fm and Schlern Fm; see Fig. 4.2). Structural highs of the dismembered carbonate ramp (Contrin Fm) were the future nuclei of the Schlern Fm platforms in the Late Anisian (Masetti and Neri 1980; Gaetani et al. 1981; Bosellini 1989). Evolution of the Ladinian carbonate platforms such as Rosengarten, Schlern and Monte Agnello ended with the extrusion of the Longobardian Wengen Fm volcanics (see Fig. 4.3).

One source of these volcanoclastics, the volcanic centre at Predazzo/Monzoni had formed above a deep reaching fracture zone (Cima Bocche Anticline/Stava Line; see also geological map in Fig. 4.4). Tectonics also played a crucial role in platform development in the SW Dolomites controlling regional subsidence and accommodation development with downward movements along faults and upward movements through magmatic updoming (Doglioni 1983, 1984, 1987). With the creation of pathways for Wengen Fm volcanics, tectonics were also responsible for the termination of platform growth (e.g. Mojsisovics 1879; Viel 1979a; Viel 1979b; De Zanche et al. 1995).

Owing to its excellent, laterally continuous seismic and sub-seismic scale outcrop (see Figs. 4.5), the Rosengarten

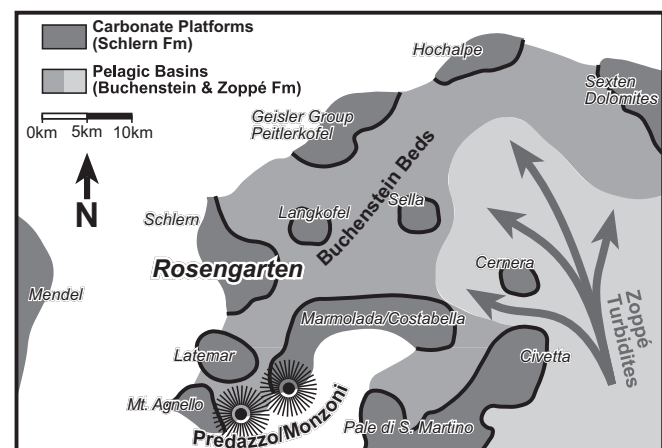


Fig. 4.2 Schematic palaeogeographic map of the Western Dolomites during the Middle Triassic (Late Anisian/Early Ladinian). Legend of lithostratigraphic units in the upper left corner, influx of turbidites marked by large arrows. The volcanic centre of Predazzo/Monzoni in the immediate surroundings of the Rosengarten/Catinaccio platform is sketched with radial lines.

Chronostratigraphy	Platform	Lithostratigraphy	Basin	Detailed Timing of Platform Evolution
236.0		Schlern Fm2 – Schlemplateau Beds	Schlern Fm2 Slope	Biozones: Brack & Rieber (1993, 1994) Radiometry: Mundil et al. (1996, 2003) Correlation: Maurer (1999, 2000)
		Wengen Fm		
237.0		Schlern Fm2 – Rosetta Dolomite	Schlern Fm2 Slope	
		Wengen Fm		
		Schlern Fm 1 – Toplapping Dolomite		
238.0			Buchenstein Fm	top of preserved succession at Rosengarten
			Bänderkalk Mbr	Archelaus
				238.0Ma
				Gredleri
				238.8Ma
239.0		Schlern Fm1 Slope		
		Schlern Fm1 Lagoon & Reef	Buchenstein Fm Knollenkalk Mbr	Curionii
240.0				
241.0				Secedensis
			Buchenstein Fm – Plattenkalk Mbr	241.7Ma
				241.2Ma
242.0			Contrin Fm	Reitzi
			Morbiac Fm	
			Richthofen Fm	
243.0			Hiatus / Anisian Unconformity	Trinodosus

Fig. 4.3 Detailed Anisian/Ladinian stratigraphic succession at Rosengarten/Catinaccio. Zig-zagged line illustrates present day topography. Overlying strata are projected from the Schlern/Sciliar platform (W-Dolomites; see Fig. 4.2) Chronostratigraphy according to Lehrmann et al. (2002) and Mundil et al. (1996, 2003). Biozones and position of Anisian/Ladinian boundary according to Brack and Rieber (1993, 1994). Correlation of age-diagnostic tuff layers from basin to slope according to Maurer (1999, 2000).

Dark coloured arrows in the radiometry column indicate ages from tuff layers in the basinal Buchenstein Fm at Seceda (Geisler Group, W-Dolomites; see Fig. 4.2; Mundil et al. 1996) whereas light grey indicates ages from tuff layers in the lagoonal Schlern Fm at Latemar (W-Dolomites; see Fig. 4.2; Mundil et al. 2003). For uncertainty intervals refer to original literature.

is ideally suited for the study of the geometric development of a carbonate platform and its accumulation/production rates. The platform top of the Rosengarten passes laterally into a platform slope interfingering with basinal sediments. The maximum north- to southward progradation of the Rosengarten slope is approx. 6km. Lagoon-reef- and slope-facies of the buildup are all part of the Schlern Formation, whereas the coeval basinal sediments belong to the Buchenstein Formation. Bio- and chronostratigraphic data (Brack and Rieber 1993, 1994; Mundil et al. 1996, 2003; Maurer 1999, 2000) indicate the onset of platform growth in the upper *Reitzi*-biozone (Anisian; Middle Triassic stages after Brack & Rieber 1993, 1994). According to Maurer (1999, 2000), the slope of the Rosengarten represents five ammonoid biozones (see Fig. 4.5B). During the first two - *Reitzi* and *Secedensis* - biozones of platform existence, aggradation occurs. This first stage of platform evolution is then followed by a second

stage with progradational clinofolds/characteristics. The preserved record of carbonate sedimentation lasts at least until the basal *Archelaus*-zone (Middle/Late Ladinian; Maurer 1999, 2000; see Fig. 4.3 and 4.5B). The maximum thickness of the Rosengarten platform above present day topography can only be inferred by projecting stratigraphical information from the neighbouring Schlern/Sciliar platform (Bosellini and Stefani 1991; see Fig. 4.6). There, 850m of cyclically arranged platform carbonates are partially covered by Wengen Fm volcanics (see Fig. 4.4) preserving the maximum thickness of the Schlern Fm (see Fig. 4.3). Maurer (1999, 2000) calculated compacted carbonate production rates for the first aggradational phase of 200m/Ma increasing during the progradational phase towards the end of Rosengarten's evolution.

The geological evolution from Late Triassic times on can only be derived by studying younger strata in other parts of the Dolomites (e.g. Sella platform, see Fig. 4.2) and Southern Alps. Late Triassic volcanoclastics and carbonates (Wengen Fm, Cassian Fm; Brandner 1991; Mastandrea et al. 1997) filled the basins and with the onset of a period of tectonic quiescence a huge carbonate platform developed. The so-called Trento platform comprised the entire central segment of the Southern Alps on the Adriatic Plate (Dolomia Principale Fm and Calcari Grigi Fm; Leonardi 1967; Bosellini and Broglio Loriga 1971; Bosellini and Hardie 1985; Trevisani 1991; Boomer 2001). From Middle Jurassic times on, the Trento platform started subsiding and eventually drowned. A phase of deep marine sedimentation began (Ammonitico Rosso Fm; Winterer and Bosellini 1981; Martire 1996; Winterer 1998) and lasted until Late Cretaceous (Marne del Puez Fm; Claps et al. 1991; Antruelles Fm; Stock 1996). Water depths decreased again when the tectonic regime switched from extension to compression and the collision of the Adriatic plate with Europe started with subduction of oceanic crust in the Late Cretaceous (e.g. Hsü 1971; Smith 1971; Trümpy 1982; Laubscher and Bernoulli 1982; Hsü 1989; Dercourt et al. 1993, 2000). Upper Oligocene shallow marine conglomerates (Monte Parei Fm) witness ongoing continent collision in the Palaeogene (Cros 1966; Mair et al. 1996).

4.3 Methods and database

4.3.1 Sedimentological analyses

Detailed sedimentological analyses (logging, facies mapping, lateral tracing of physical surfaces, thin sections)

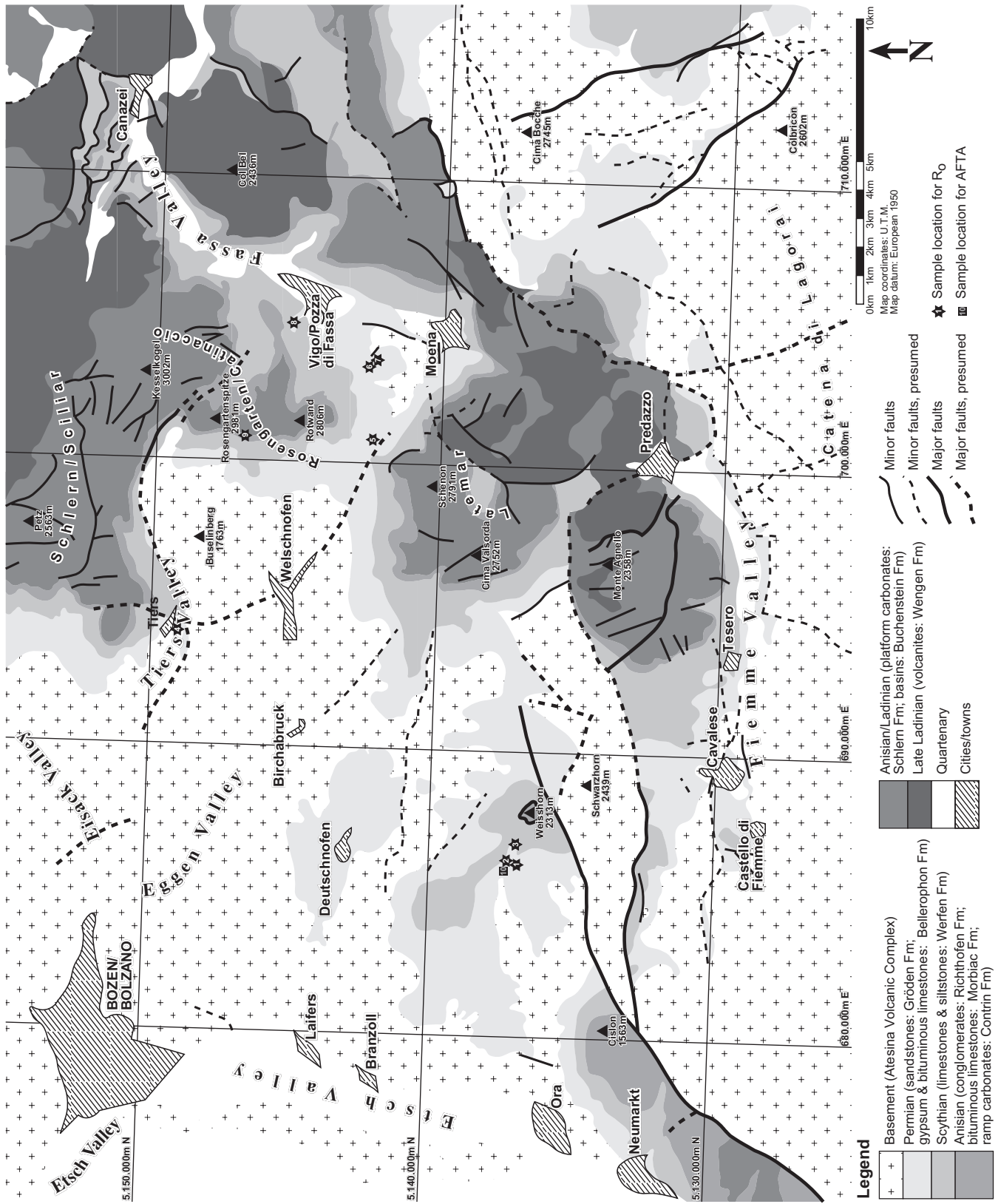
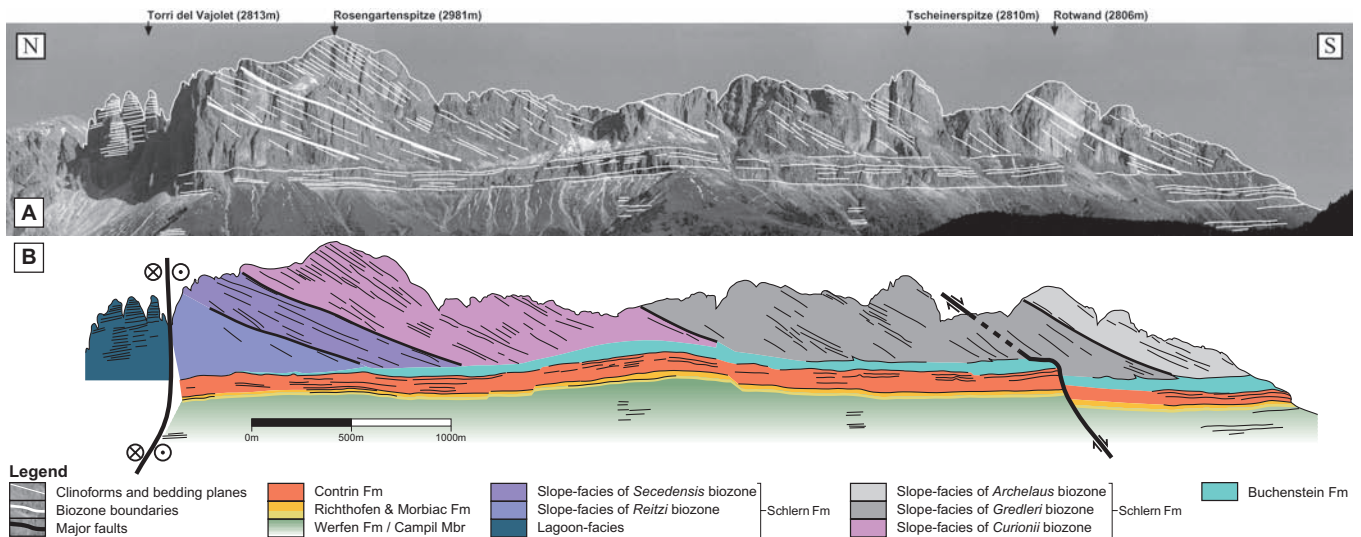


Fig. 4.4 Simplified geological map of the study area and its surroundings. Note the presence of the Cima Bocche Anticline/Stava Line (major faults) and the Late Ladinian Wengen Fm volcanics in the eastern and northeastern part of the area. Legend of the geological map in the lower part. Sample locations for vitrinite reflectance analyses are marked by stars, those for apatite fission track analyses by squares.



Figs. 4.5 Sedimentological interpretation of the Rosengarten platform.

4.5A The Rosengarten platform viewed from the west with an interpretation of stratal lines and clinoforms. Legend in Fig. 4.5B.

4.5B Formations underneath the Rosengarten platform and correlation of carbonate slope deposits with biozones of the basal Buchenstein Fm (according to Maurer 1999, 2000). The transect is tectonically undisturbed, major faults are present at the platform interior only (“Torri del Vajolet”). Legend in the lower part.

have been carried out on the underlying strata of the Rosengarten platform (see Fig. 4.6). Ten sections/sedimentological logs cover the entire basin infill from basement (Permian Atesina Volcanic Complex/Bozener Quarzporphyr) to the basal Schlern Fm. Additional data on the Upper Anisian succession and the Buchenstein Fm were taken from literature (Bosellini and Stefani 1991; Maurer 1999; Zühlke 2000). These analyses were necessary to obtain the vital datasets on thicknesses, lithologies and palaeo water depths. The latter modelling parameter is based on the integration of all sedimentological evidence from the outcrops (channels, ripples, exposure surfaces, bioturbation etc.) with microfacies analyses of thin sections.

4.3.2 Stratigraphy

Upper Triassic formations were projected from the western and central Dolomites (Schlern and Sella platform), Jurassic strata from the Trento platform, Cretaceous and Tertiary formations from the eastern Dolomites (see Table 4.1.). Lithology information was combined with published data on chronostratigraphy (see captions of Table 4.1) and palaeo bathymetry. Jurassic palaeo water depths were calculated with a subsidence curve for the Trento

platform proposed by Winterer and Bosellini (1981) and Winterer (1998). If necessary, thickness of eroded stratigraphic units was adapted to fit the simulated burial history (see chapter 4.3.5).

4.3.3 Measurement of vitrinite reflectance (VR_r)

Vitrinite reflectance is the most frequently used parameter in order to assess regional thermal maturity and is furthermore widely used as a calibration parameter for thermal basin modelling.

Vitrinite reflectance data on five sample locations was previously published (Schulz and Fuchs 1991; Buggisch 1978; Bielefeld 1998). In addition, eleven samples from Upper Permian sandstones (Gröden Fm) to Middle Triassic basinal shaly limestones (Buchenstein Fm) were analysed in this study. Vitrinite reflectance was determined by microscopic analysis of percentages of light reflected from polished organic particles and calibrated against isotropic standards. The results are given as mean random reflectance (VR_r %, for details on methodology and measurement see Stach et al. 1982; Taylor et al. 1998). Only four of our samples - mostly Permian sandstones of the Gröden Fm - contained measurable “vitrinite-like” organic matter (locations are shown in

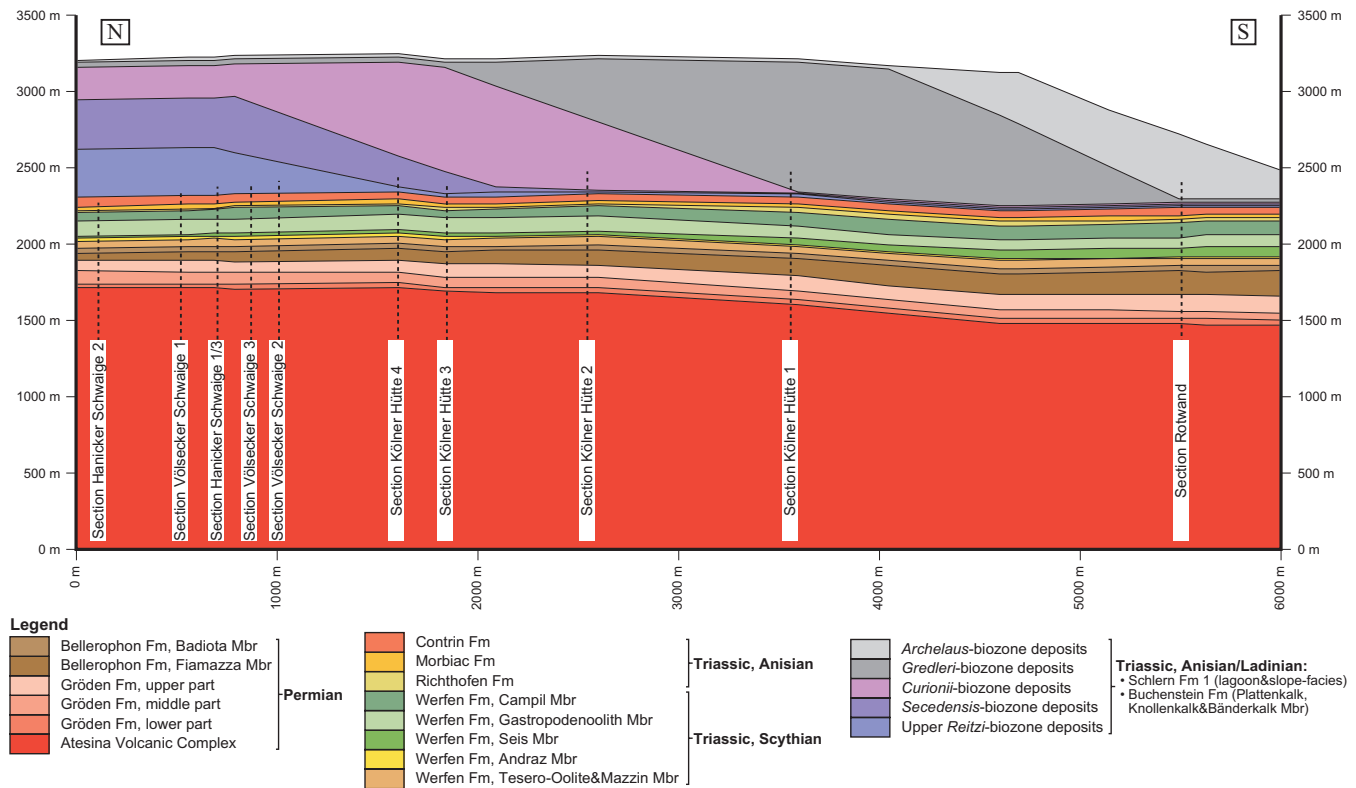


Fig. 4.6 The Rosengarten transect with restored geometries above present day topography (after Bosellini and Stefani 1991; Maurer 1999, 2000) with an overlay of formations, intervals of platform growth (colour legend in the lower part; after Maurer 1999, 2000) and sedimentological sections through the underlying strata of the Schlern Fm. Vertically exaggerated; units of the x-axis are metres along the transect beginning at the platform interior; units of the y-axis are metres above mean present day sea-level.

Fig. 4.4 and data are documented in Table 4.2). Several VR_r values had to be excluded as calibration parameters in thermal history modelling because of altered organic matter and/or statistically insignificant measurements (see also Table 4.2).

4.3.4 Apatite fission track analysis

Apatite fission track (FT) thermochronology is commonly used to determine the magnitude of cooling, exhumation and rock uplift from shallow crustal levels (e.g. Fitzgerald et al. 1995, Tippett and Kamp 1995). Time-

temperature paths for the sample were calculated from the raw data and geologic constraints using the Monte Trax™ software (see Gallagher 1995 for details).

In the strata underlying the Rosengarten platform three samples were collected from different stratigraphic levels within the Permian sandstones (Gröden Fm). Only one sample revealed a sufficient amount of apatites for FT-dating (location in Fig. 4.4; results of FT-dating in Table 4.3).

Table 4.1 (following page) List of formations/timesteps (column 1) applied during modelling with ages at tops of formations/timesteps (column 2), thicknesses (column 3), indication of erosion (timestep erosion, column 4), lithologies (column 5) and palaeo water depths at the sediment water interface (PWD, column 6). The last column (column 7) shows the main references on these formations with respect to the information shown in this table.

The chronostratigraphic framework is derived from the following studies: Permian (Yugan et al. 1997), Triassic (Lehrmann et al. 2002, Mundil et al. 1996, 2001, 2003), Jurassic (Gradstein et al. 1995; Pálffy et al. 2000), Cretaceous (Gradstein et al. 1995), Tertiary (Harland et al. 1989). Strata overlying present day topography were projected from the western and central Dolomites (Middle and Upper Triassic; see also Fig. 4.4), the Trento platform (Jurassic) and eastern Dolomites (Cretaceous and Tertiary).

	1		2		3	4	5		6	7
	Formation / Timestep		Age [Ma]	Thickness [m]	Timestep Erosion		Lithology		PWD [m]	Source / Reference
CRETACEOUS PALAEOCENE	Monte Parei Fm		24.0	90	yes	conglomerate with interbedded sandstone		0	Cros 1966; Mair et al. 1996	
	Hiatus		28.0	-	yes			0	Cros 1966; Mair et al. 1996	
	Antrullies Fm		80.0	70	yes	limestone with interbedded sandstone and clay		1250	Stock 1996	
	Marne del Puez Fm		98.9	60	yes	marl with interbedded fine-grained sandstone		1000	Claps et al. 1991	
	Hiatus		127.0	-	yes			640	Winterer and Bosellini 1981; Winterer 1998	
	Ammonitico Rosso Fm, upper part (RAS)		147.5	10	yes	limestone with interbedded silt		375	Winterer and Bosellini 1981; Martire 1996; Winterer 1998	
	Hiatus		154.0	-	yes			290	Winterer and Bosellini 1981; Martire 1996; Winterer 1998	
	Ammonitico Rosso Fm, middle part (RAM)		155.5	5	yes	limestone with interbedded silt		270	Winterer and Bosellini 1981; Martire 1996; Winterer 1998	
	Hiatus		157.0	-	yes			250	Winterer and Bosellini 1981; Martire 1996; Winterer 1998	
	Ammonitico Rosso Fm, lower part (RAL)		160.0	15	yes	limestone with interbedded silt		210	Winterer and Bosellini 1981; Martire 1996; Winterer 1998	
JURASSIC	Hiatus		167.0	-	yes			120	Winterer and Bosellini 1981; Martire 1996; Winterer 1998	
	Calcarea a Filamenti Fm		169.0	20	yes	limestone		100	Travisani 1991	
	Hiatus		172.0	-	yes			60	Travisani 1991	
	San Vigilio Oolite Mbr		174.0	70	yes	limestone		30	Travisani 1991	
	Calcarei Grigi Fm, Grigno Mbr		178.0	90	yes	limestone		20	Travisani 1991	
	Calcarei Grigi Fm, Roizo Mbr		183.6	85	yes	limestone		15	Bosellini and Broglio Loriga 1971; Travisani 1991	
	Calcarei Grigi Fm, Middle Mbr		190.0	35	yes	limestone		10	Bosellini and Broglio Loriga 1971; Boomer et al. 2001	
	Calcarei Grigi Fm, Lower Mbr		194.5	40	yes	limestone		3	Bosellini and Broglio Loriga 1971; Boomer et al. 2001	
	Dolomia Principale Fm, upper part		200.0	40	yes	dolomite		10	Leonardi 1967; Bosellini and Hardie 1985	
	Dolomia Principale Fm, middle part		207.9	175	yes	dolomite		10	Leonardi 1967; Bosellini and Hardie 1985	
TRIASSIC	Dolomia Principale Fm, lower part		215.8	100	yes	dolomite		3	Leonardi 1967; Bosellini and Hardie 1985	
	Raibl Fm		223.8	40	yes	sandy limestone		8	Leonardi 1967; Dogliani and Goldhammer 1988; Brandner 1991; this study	
	Hiatus		229.9	-	yes			-10	Leonardi 1967; Dogliani and Goldhammer 1988; Brandner 1991; this study	
	Wengen Fm, Schlern Fm 2, Cassian Fm		232.0	100-730	partially	volcanics with limestone boulders, dolomite, shale		0	Brandner 1991; Schläger et al. 1991; Mastandrea et al. 1997; this study	
	Archelex biozone deposits (Schlern & Buchenstein Fm)		237.1	20-400	partially	dolomite		5-800	Brack and Rieber 1993, 1994; Maurer 1999, 2000; this study	
	Greifler biozone deposits (Schlern & Buchenstein Fm)		238.0	18-800	partially	dolomite		5-800	Brack and Rieber 1993, 1994; Maurer 1999, 2000; this study	
	Curtoni biozone deposits (Schlern & Buchenstein Fm)		238.8	12-640	partially	dolomite		5-800	Brack and Rieber 1993, 1994; Maurer 1999, 2000; this study	
	Sacedensis biozone deposits (Schlern & Buchenstein Fm)		240.8	10-300	partially	dolomite		5-600	Brack and Rieber 1993, 1994; Maurer 1999, 2000; this study	
	Reitz biozone deposits (Schlern & Buchenstein Fm)		241.4	10-300	no	dolomite		5-300	Brack and Rieber 1993, 1994; Maurer 1999, 2000; this study	
	Contirin Fm		241.9	40-55	no	dolomite		10	Zühke 2000; this study	
PERMIAN	Morbac Fm		242.5	25	no	marl with interbedded limestone		20	Zühke 2000; this study	
	Richthofen Fm		242.8	7-25	no	conglomerate with interbedded coarse-grained sandstone		-5	Zühke 2000; this study	
	Hiatus		243.2	-	no			-30	Zühke 2000; this study	
	Werfen Fm, Cencenighe Mbr		247.5	80	yes	limestone with interbedded marl		8	Broglio Loriga et al. 1983	
	Werfen Fm, Val Badia Mbr		248.1	80	yes	marly limestone		10	Broglio Loriga et al. 1983	
	Werfen Fm, Campil Mbr		248.7	45-90	partially	fine-grained sandstone with interbedded silt		10	Broglio Loriga et al. 1983; this study	
	Werfen Fm, Gastropodenoolith Mbr		250.0	60-100	no	intercalations of limestone, marl and silt		15	Broglio Loriga et al. 1983; this study	
	Werfen Fm, Seis Mbr		250.6	12-55	no	intercalations of limestone and marl		12	Broglio Loriga et al. 1983; this study	
	Werfen Fm, Andraz Mbr		251.5	12-20	no	sandy dolomite		0	Broglio Loriga et al. 1983; this study	
	Werfen Fm, Tesero-Oolite & Mazzin Mbr		252.0	40-50	no	intercalations of limestone, marl and silt		15	Broglio Loriga et al. 1983; this study	
Bellerophon Fm, Badiola Mbr		253.0	25-35	no	intercalations of limestone and marl		30	Buggisch and Noé 1986; Massari et al. 1988, 1994; Massari and Neri 1997; this study		
Bellerophon Fm, Fiamazza Mbr		253.8	50-150	no	gypsum with interbedded dolomitic marl		2	Buggisch and Noé 1986; Massari et al. 1988, 1994; Massari and Neri 1997; this study		
Gröden Fm, upper part		255.3	65-105	no	silt-rich medium- to fine-grained sandstone		0	Massari et al. 1988, 1994; Massari and Neri 1997; this study		
Gröden Fm, middle part		256.6	45-75	no	silt-rich coarse-grained sandstone		-5	Massari et al. 1988, 1994; Massari and Neri 1997; this study		
Gröden Fm, lower part		258.0	25-35	no	litharenitic sandstone		-10	Massari et al. 1988, 1994; Massari and Neri 1997; this study		
Hiatus		260.0	-	no			-30	Massari et al. 1988, 1994; Massari and Neri 1997; this study		
Alesina Volcanic Complex		267.0	>2000	partially	basement		-200	D'Amico and Del Moro 1988; Barth et al. 1993, 1994; Barth and Mohr 1994		

1	2	3		4	5	6	7	8	9	10
Location	Source / Reference	UTM coordinates		Elevation above s.l. [m]	Formation	Lithology	Vitrinite reflectance VRr [%]	Temperature [°C]	Central Age [Ma]	Mean Track Length [µm]
		x	y							
1	Buggisch 1978	~685800	~5137100	~1500	Gröden Fm, middle part	coarse/medium-grained sandstone	0.73	110		
2	Bielefeld 1998	685800	5137100	1520	Gröden Fm, middle part	coarse/medium-grained sandstone	0.60±0.09	94±11		
3	Schulz & Fuchs 1991	686750	5136900	1650	Gröden Fm, upper part	coarse/medium-grained sandstone	<i>0.88*</i>	<i>125*</i>		
4	Buggisch 1978	693990	5149000	~1000	Gröden Fm, upper part	coarse/medium-grained sandstone	<i>0.8*</i>	<i>117*</i>		
5	Bielefeld 1998	700850	5142350	1760	Gröden Fm, upper part	coarse/medium-grained sandstone	0.67±0.14	103±15		
6	this study	703493	5142526	1600	Gröden Fm, upper part	coarse/medium-grained sandstone	<i>0.9±0.07**</i>	<i>127±6**</i>		
7	this study	703493	5142526	1600	Gröden Fm, upper part	coarse/medium-grained sandstone	<i>1.1±0.14**</i>	<i>143±10**</i>		
8	this study	705014	5145331	1615	Bellerophon Fm, Badiota Mbr	bituminous limestone	0.52±0.02	83±3		
9	this study	700900	5148006	2330	Morbiac Fm	bituminous limestone	<i>0.77±0.02***</i>	<i>114±2***</i>		
10	this study	685780	5137350	1500	Gröden Fm, middle part	coarse/medium-grained sandstone			37.0±4.1	14.11±0.28

Table 4.2 List of vitrinite reflectance data compiled from literature and derived from own analyses as well as apatite fission track analysis. The numbers in the first column correspond to the locations in Fig. 4.3. The source of the data is shown in column 2. UTM coordinates (column 3) and elevations above present day sea-level (column 4) also correspond to the system and map datum used in Fig. 4.3. The formations from which the samples were taken are presented in column 5. The lithology of the samples is shown in column 6. Columns 7 and 8 represent data on thermal maturity. Values in *Italics* in column 7 (thermal maturity) and 8 (palaeotemperature) were not applied during modelling due to the following reasons:

* organic matter not in-situ or altered

** proximity to a volcanic dyke, altered organic matter

*** number of measurements too low, no statistic significance

Palaeo temperature values in column 8 were derived from the measured thermal maturity data (VR_r values in column 7) and calculated after Barker and Pawlewicz (1986). The last columns (9: central age and 10: mean track length) report data from the apatite fission track analysis. For further explanations refer to the text.

4.3.5 Workflow of the integrated modelling approach

The workflow of the integrated modelling approach is illustrated in Fig. 4.7.

Modelling started with the simulation of burial and thermal history and the re-construction of the overburden thickness with PetroMod™ (IES GmbH, Jülich, Germany). Results on the eroded rock column were obtained after calibration of the model by fitting calculated with measured vitrinite reflectance data (see Fig. 4.8).

The eroded thickness derived from basin modelling was entered with all other necessary input parameters (see Fig. 4.7) into the basin reverse modelling routine of PHIL™ (Petrodynamics Inc., Houston, U.S.A.) in order to determine tectonic, flexural and compaction induced

subsidence rates for forward modelling. Then, PHIL's stratigraphic forward modelling module was used to calculate best-fit stratal patterns and sedimentation rates. At the end of this procedure simulated min-max models were ultimately checked against the real world/outcrop data. Calibration of the simulated sedimentation rates and stratal patterns was carried out by visual comparison with geometries along the Rosengarten transect and by measurement of stratal thicknesses.

4.3.6 Thermal modelling

The detailed analysis of the regional thermal maturity (coalification) pattern was combined with basin modelling (PetroMod™) to narrow down uncertainties of thermal boundary conditions (heat flow history) and to quan-

Location	Mineral	No. of Crystals	Track Density ($\times 10^6$ tr cm^{-2})			Age Dispersion ($P\chi^2$)	Central Age (Ma) ($\pm 1\sigma$)	Apatite Mean Track Length ($\mu\text{m} \pm 1$ s.e.) (no. of tracks)	Standard Deviation (μm)
			ρ_s (N_s)	ρ_i (N_i)	ρ_d (N_d)				
10	apatite	20	0.1950 (108)	1.078 (597)	1.144 (7896)	0.00% (89.7%)	37.0±4.1	14.11±0.28 (26)	1.40

Notes:

(i). analyses by external detector method using 0.5 for the $4\pi/2\pi$ geometry correction factor;

(ii). ages calculated using dosimeter glass: CN5 with $\zeta_{\text{CN5}} = 358.8 \pm 12.7$;

(iii). $P\chi^2$ is the probability of obtaining a χ^2 value for ν degrees of freedom where $\nu = \text{no. of crystals} - 1$.

Table 4.3 Details of the apatite fission track analysis of the sample from location 10 (see Fig. 3). For further explanations refer to the text.

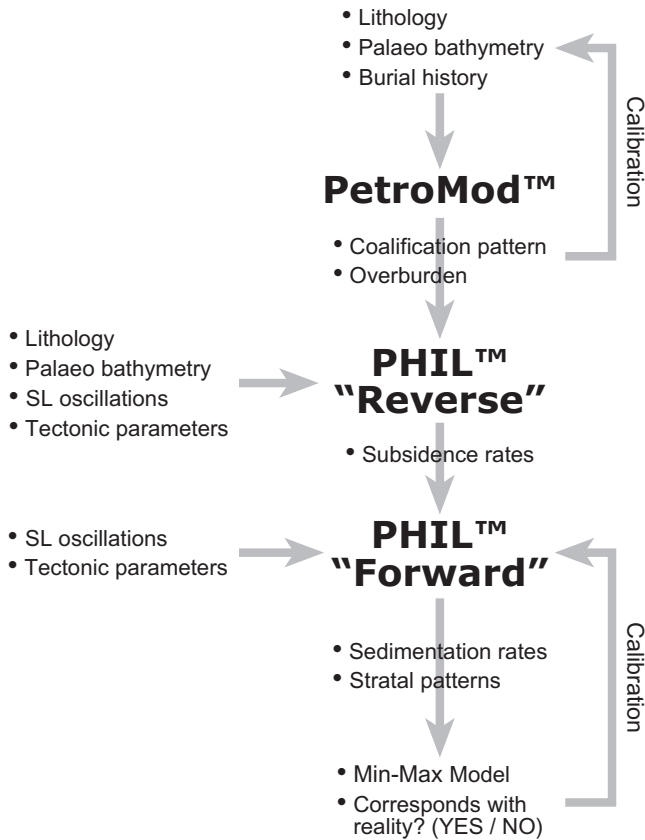


Fig. 4.7 Sketch illustrating the workflow during modelling; workflow starts at the top and ends at the bottom. Input data are arrows towards a simulator (PetroMod™ or PHIL™); output data are arrows pointing away from simulators. For further explanations refer to the text.

tify erosional thicknesses (burial history). This contributes essential knowledge to the geotectonic evolution and the geodynamic interpretation of the Rosengarten transect and the western Dolomites.

Input parameters for numerical models were thickness of stratigraphic units, lithologies (see Table 4.1), rock physical parameters (e.g. thermal conductivities; see Bükér 1996; see Hertle and Littke 2000 for a more detailed description of the calculation of physical properties of stratified sediment bodies), temperature at sediment-water interface, heat flow at the base of the succession (see Fig 4.9A) and palaeo water depths (see Fig. 4.9B).

Subsidence history and temperature field through time were calculated. Burial and heat flow histories were calibrated with measured vitrinite reflectance values (see Fig. 4.8). The model was then fine tuned by modifying heat flow and eroded thicknesses until a satisfactory fit be-

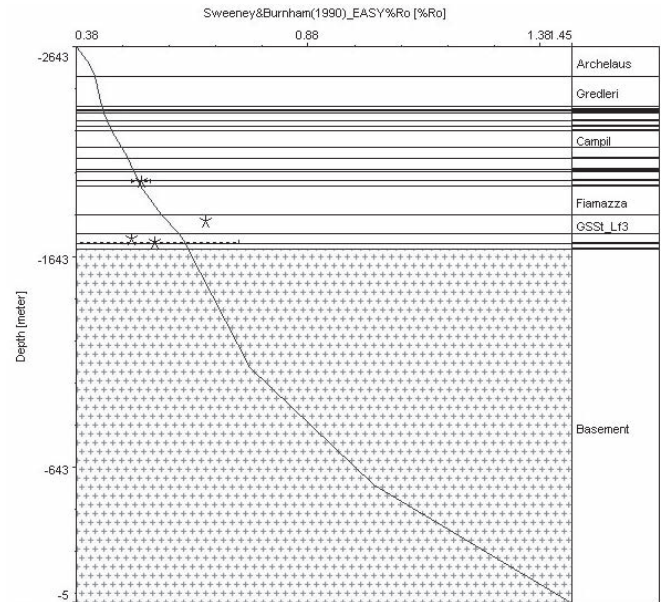


Fig. 4.8 Calibration of the subsidence history at Rosengarten with measured VR_r values (PetroMod). X-axis: vitrinite reflectance in %VR; y-axis: depth in metres (negative values indicate an elevation above present day sea level).

The curve corresponds to the calculated VR_r values of the strata at Rosengarten after the last timestep of subsidence modelling (present day situation). The asterisks mark measured VR_r values (sample locations 1, 2, 5 and 8) with error bars. Formations are indicated at the righthand side.

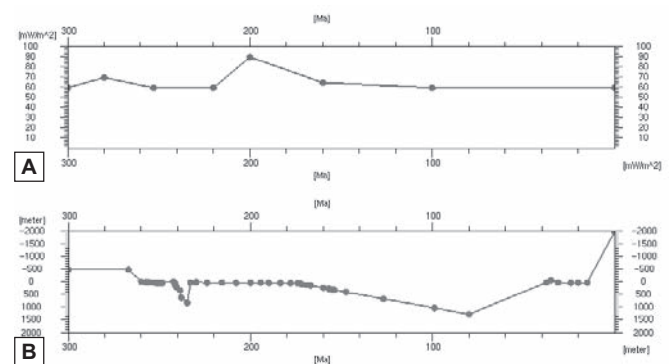
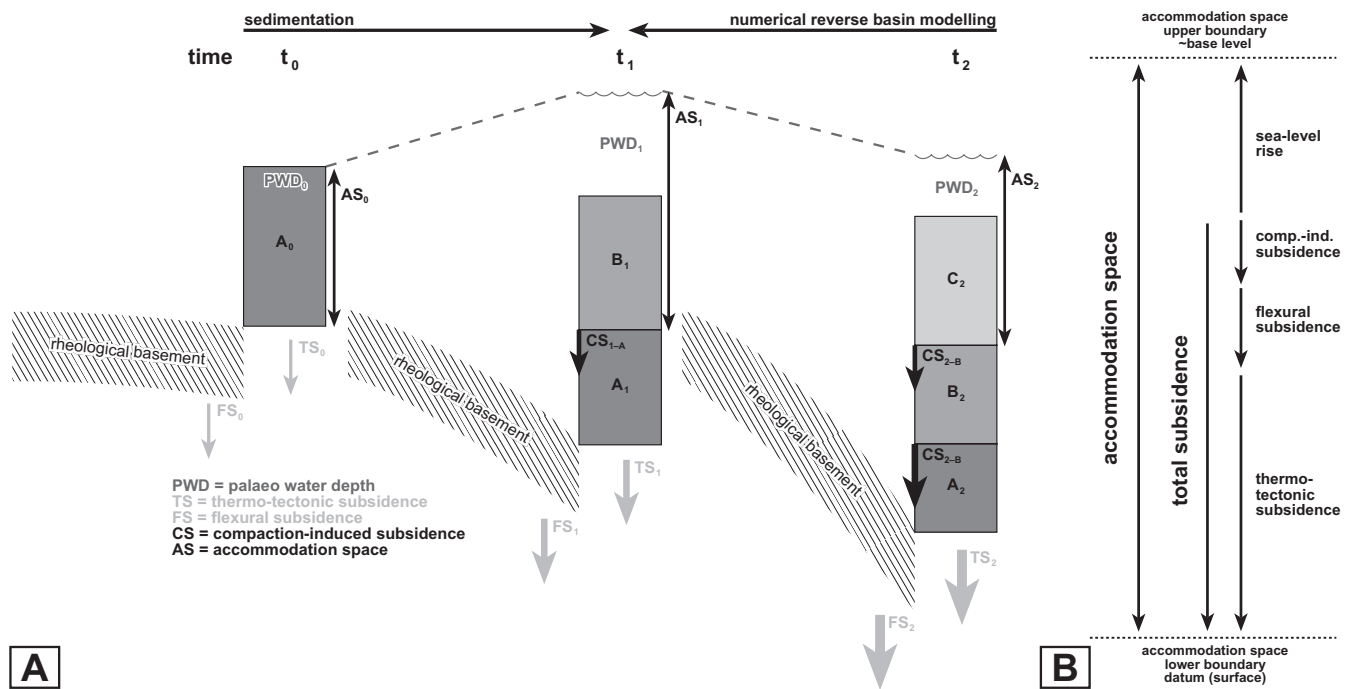


Fig. 4.9 Input data for thermal modelling.

4.9A Heat flow history as applied during modelling with PetroMod. X-axis: time in Ma; y-axis: heat flow in mW/m^2 .

4.9B Palaeo water depth history of the sediment water interface as applied during modelling with PetroMod and Phil. X-axis: time in Ma; y-axis: elevation above mean present day sea level in metres (positive values: water depths below sea level, negative values: elevation above sea level).



Figs. 4.10 Numerical basin reverse modelling.

4.10A Sketch illustrating the basin reverse modelling process (“backstripping”). X-axis: time; y-axis: burial depth; stratigraphic units are marked by letters A to C and different greyscales; arrows below the stratigraphic columns illustrate vectors of subsidence (thick arrow: high subsidence; thin arrow: low subsidence). For further explanations refer to the text.

4.10B The four components controlling accommodation space during each timestep. Accommodation space is filled through sedimentary input (see Schlager 1993).

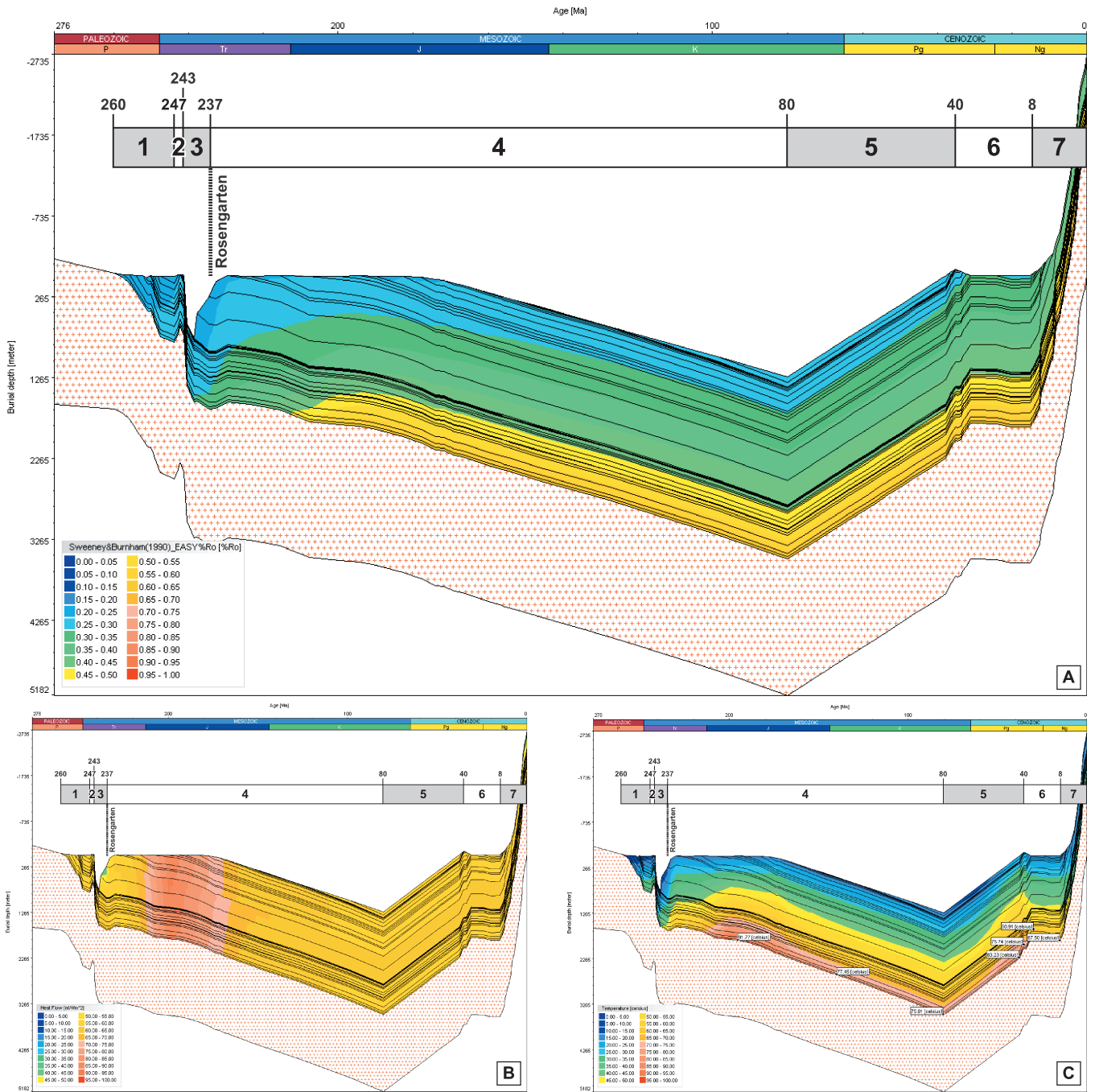
tween measured and calculated vitrinite reflectance was achieved. Vitrinite reflectance was calculated using the EASY%Ro-algorithm of Sweeney and Burnham (1990; see also e.g. Sachsenhofer and Littke 1993; Littke et al. 1994; Leischner 1994; Sachsenhofer et al. 2002; see chapter 4.3.5 and Fig. 4.7).

For more details on thermal modelling with PetroMod™ see Littke et al. (1994), Poelchau et al. (1997), Hertle and Littke (2000) and Littke et al. (2000). Details on the calibration process in fold belts where only outcrop samples are available were published by Noeth et al. (2002).

4.3.7 Reverse basin and sequence stratigraphic forward modelling

Reverse basin modelling (see Fig. 4.12A) was carried out to determine flexural, tectonic and compaction induced subsidence tantamounting to total subsidence. Input parameters were lithology (initial porosity; after Bowman and Vail 1999), geometries (measured and projected bed thicknesses), palaeo water depth (derived from facies analysis) and crustal parameters (e.g. effective elas-

tic thickness T_e , plate end boundary distance and density of the mantle). Owing to the shortness of the transect (approx. 6km) and the rigidity of the underlying basement (2000-2500m thick Permian Atesina Volcanic Complex), crustal parameters and flexural subsidence play a minor role. Nevertheless, recent data on the effective elastic thickness (T_e ca. 20km) of the lithosphere of the Venetian basin (Barbieri and Garcia-Castellanos 2003) was applied. Owing to the short interval of platform evolution – less than 5Ma – 2nd order sea level fluctuations played an insignificant role during accommodation development. 3rd order sea level oscillations (1-3Ma; Duval et al. 1992) have not been considered because their timing and amplitude in the latest Anisian/earliest Ladinian is controversially discussed (Rüffer & Zühlke 1995; Gianolla & Jacquin 1998). Eventual sea level fluctuations are therefore comprised within total subsidence. Numerical reverse basin modeling in this study follows the sequence stratigraphic concept, which considers the creation/destruction of accommodation space (see Fig. 4.12B) and its infill as the two principal controls on sedi-

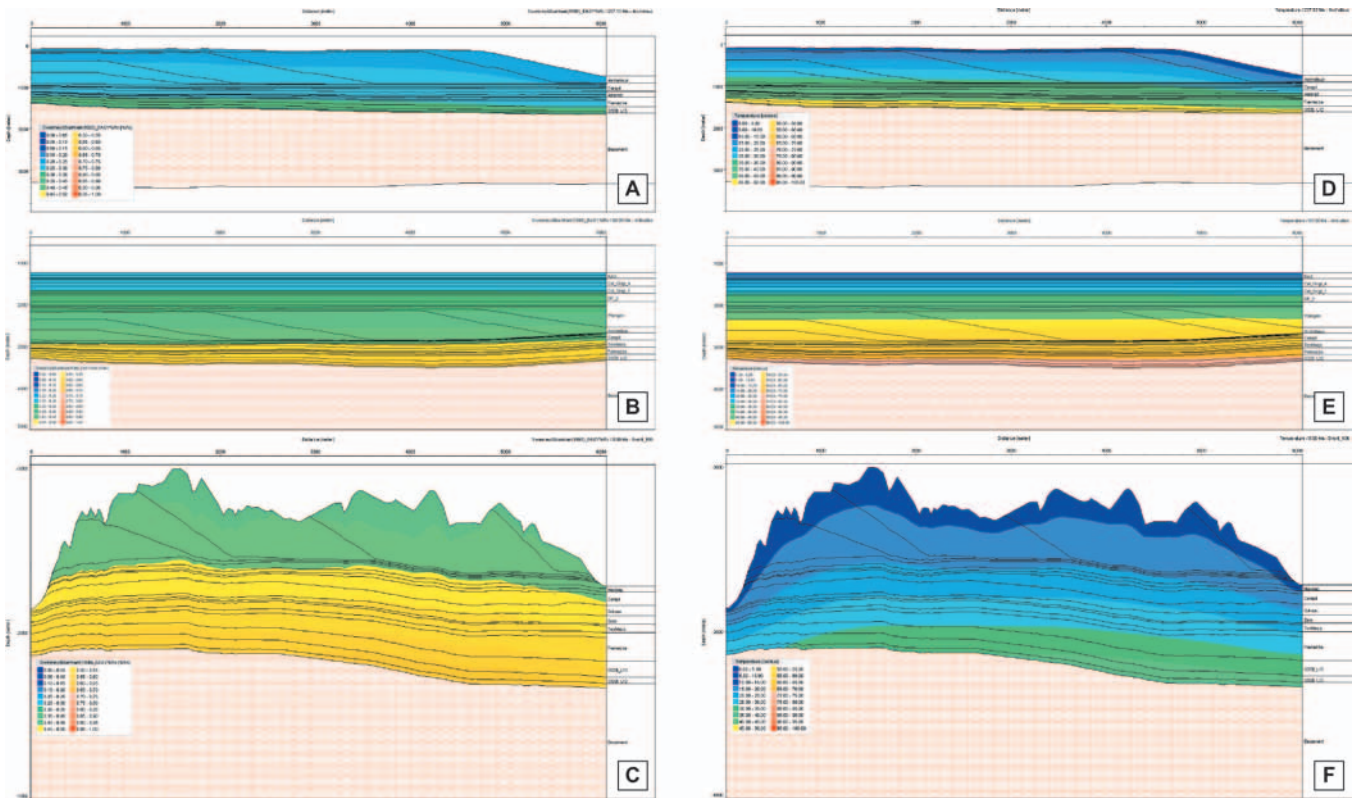


Figs. 4.11 Burial history of a virtual 1D well through the Rosengarten transect (PetroMod). X-axis: time in Ma (abbreviations: P: Permian; Tr: Triassic; K: Cretaceous; Pg: Palaeogene; Ng: Neogene); y-axis: burial depth in metres; black lines are boundaries of timesteps (e.g. formations and their subdivisions). Bar at the top (numbers 1-7) indicates the main stages of basin evolution. Numbers above the bar are ages of respective boundaries according to the timescale applied in this study (see also Table 4.1). The top of preserved stratigraphy at Rosengarten is indicated by a dashed line. For further explanations refer to the text.

4.11A Overlay: calculated vitrinite reflectance [%Rr] indicating the thermal history (legend/colour code to the lower left) of the basin.

4.11B Overlay: heat flow [mW/m²] during basin evolution at Rosengarten (legend/colour code to the lower left).

4.11C Overlay: calculated temperature [°C] indicating the thermal history (legend/colour code to the lower left) with value labels at significant timesteps.



Figs. 4.12 Basin evolution at Rosengarten (PetroMod). X-axis: distance along the transect in metres; y-axis: depth/elevation in metres; formations are indicated at the righthand side; name and age of timestep in the upper right corner. Vertical exaggeration varies; respective legends to the lower left. Increasing temperature during burial and rising basal heat-flow created higher thermal maturity preserved until today. Fig. 4.12C shows the present day situation where maximum thermal maturity is recorded by organic matter in coarse- to medium-grained sandstones of the Permian Gröden Fm (see Table 4.1).

4.12A Overlay: calculated VRr values [%VRr]; timestep after *Archelaus* biozone (Middle Triassic), i.e. after the last stage of platform progradation.

4.12B Overlay: calculated VRr values [%VRr]; timestep after deposition of the Antruilles Fm (Upper Cretaceous), i.e. after maximum burial.

4.12C Overlay: calculated VRr values [%VRr]; present day situation.

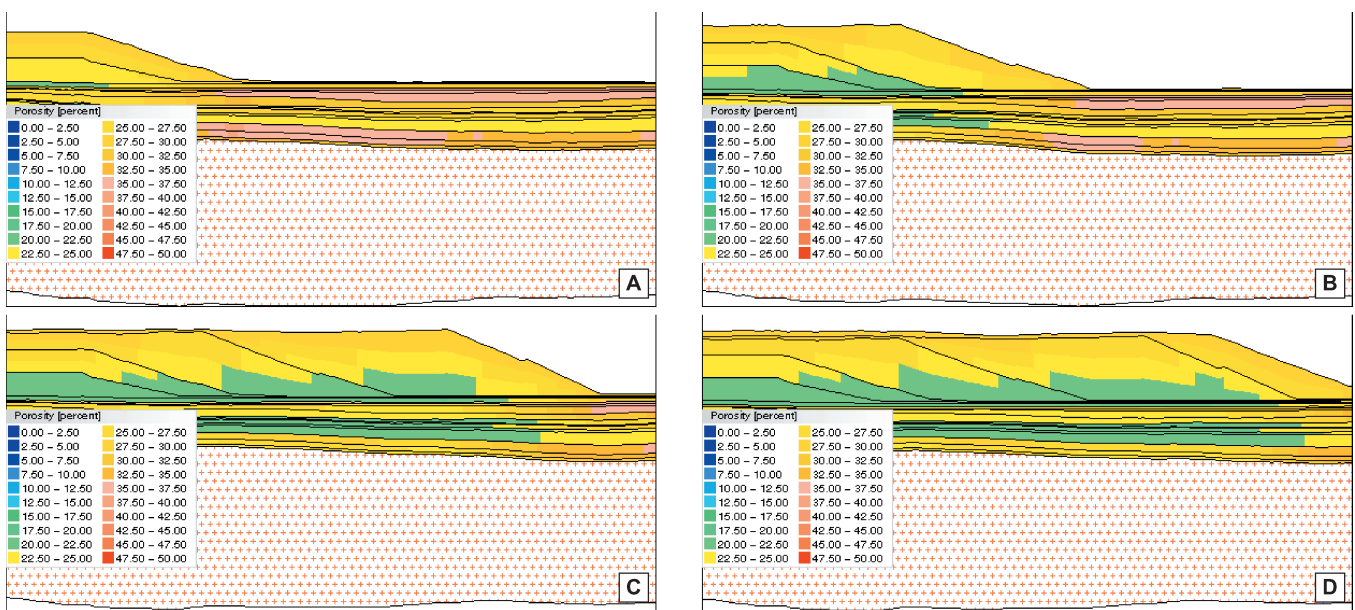
4.12D Overlay: calculated temperature [°C]; timestep after *Archelaus* biozone (Middle Triassic), i.e. after the last stage of platform progradation.

4.12E Overlay: calculated temperature [°C]; timestep after deposition of the Antruilles Fm (Upper Cretaceous), i.e. after maximum burial.

4.12F Overlay: calculated temperature [°C]; present day situation.

mentary systems and basins. Subsidence component, accommodation and sediment flux histories were calculated for each of the time steps identified in the entire basin fill. Basin reverse modelling is running in the opposite direction of sedimentation (see Fig. 4.12A): the process starts at time t_2 and runs backwards in time to t_0 when all sediment layers have subsequently been removed (“backstripped”). Each timestep (t_0 , t_1 , t_2) is characterised by a distinct vector of tectonic subsidence (TS_0 to TS_2), flexural (FS_0 to FS_2) and compaction induced subsidence (CS_0 to CS_2) as well as a change in palaeo water depth (PWD_0 to PWD_2). During each step of re-

moval, the hypothetical depth of the basin floor is calculated without being loaded and the current depositional surface is adjusted to pre-defined palaeo bathymetry. Rates are calculated for each time layer with the effects of flexural loading, changes in paleo bathymetry, changes in sea level and compaction removed. The flexural backstripping procedure applied in the reverse basin modelling of this study is based on the equations introduced by Turcotte & Schubert (1982, 2002) and Dickinson et al. (1987). The backstripping procedure with the PHIL software has also been described by Bowman & Vail (1999).



Figs. 4.13 Modelled porosity evolution during progradation at Rosengarten (PetroMod). X-axis: distance along the transect; y-axis: depth/elevation; overlay: porosity [%]; legends to the lower left. The progradation of the carbonate platform reduces porosity in the underlying strata. For further explanations refer to the text.

4.13A After the *Secedensis* biozone (240.8Ma).

4.13B After the *Curionii* biozone (238.8Ma).

4.13C After the *Gredleri* biozone (238.0Ma).

4.13D After the *Archelaus* biozone (237.1Ma).

4.4 Results

4.4.1 Thermal modelling

Applying a constant heat flow of 60mW/m^2 which is typical for continental crust (see also Allen and Allen 1990) and an increased basal heat flow for an Early Jurassic rifting period, resulted in an appropriate fit with local calibration data (vitrinite reflectance). The increase in heat flow is in accordance with Tethyan geodynamics (see Fig. 4.9A; Hsü 1971; Smith 1971; Dewey et al. 1973; Trümpy 1982; Dercourt et al. 1993, 2000). Furthermore, thermal modelling allowed to constrain the amount of eroded stratigraphy to less than 1100m (see thicknesses in Table 4.1). Both, thermal maturity and apatite fission track data clearly rule out a thick sedimentary cover. This conclusion also implies that there was no extensive Miocene cover during a flysch stadium as projected from other basins in the Alps (Venetian basin; Massari et al. 1986). The VR_r values from the Permian sandstones are too low (see Table 4.2) and the fission track ages (see Table 4.2 and 4.3) indicate temperatures of less than 80°C in the Permian succession from 37Ma on. The latter fact points to a rapid uplift and exhumation of the succession as observed in other areas of the Alps and their surround-

ings (e.g. Berner et al. 2001; Dunkl et al. 2001; Carrapa et al. 2002; Wijbrans et al. 2002).

Burial history plots of 1D sections through the succession did not differ distinctly from proximal (platform interior) to distal (basin) settings. This rather rigid behaviour of the transect is attributed to its shortness of 6km and the rheological behaviour of the Atesina Volcanic Complex underneath (see also chapter 4.3.6). Hence, only one location in the platform interior is presented in the burial history diagrams in Fig. 4.11A-C. Sedimentation on the exposed basement started around 260Ma (see Table 4.1 and Fig. 4.11A), leading to a continuous subsidence to depths of about 800m (stage 1 in Fig. 4.11A). Slight uplift of the succession led to erosion during stage 2 (Anisian unconformity, Fig. 4.11A) and exposed older strata. The third stage (see Fig. 4.11A) was characterised by rapid subsidence until Middle/Late Triassic times. This episode corresponded to the accumulation of the Schlern carbonate platform. It was followed by a long period of steady subsidence (formation of the Trento platform, stage 4 in Fig. 4.11A). Maximum thermal maturity of the transect was possibly reached during the Early Jurassic rifting when basal heat flow

was at a maximum. A value of 90mW/m^2 was assumed in the model (see Fig. 4.11A for burial history plot and Figs. 4.9A and 4.11B for heat flow history). The subsequent burial and subsidence of the Trento platform to deep-marine environments did not increase the thermal maturity significantly as heat flow diminished during this period (see Fig. 4.9A). Maximum burial of the succession was reached during Late Cretaceous times (80Ma; see Figs. 4.11) when the polarity of the tectonic regime

changed from extension to compression (Hsü 1989; Dercourt et al. 1993, 2000). Continuous uplift until about 40Ma (stage 5 in Fig. 4.11A, see corresponding temperatures in Fig. 4.11C) followed by subaerial exposure and erosion of the youngest strata of the succession allowed for a cooling of the basal strata below 80°C as demanded by the FT data (stage 6 in Fig. 4.11A). Deposition of Late Oligocene conglomerates (Monte Parei Fm, stage 6 in Fig. 4.11A) led to short lived subsidence until major

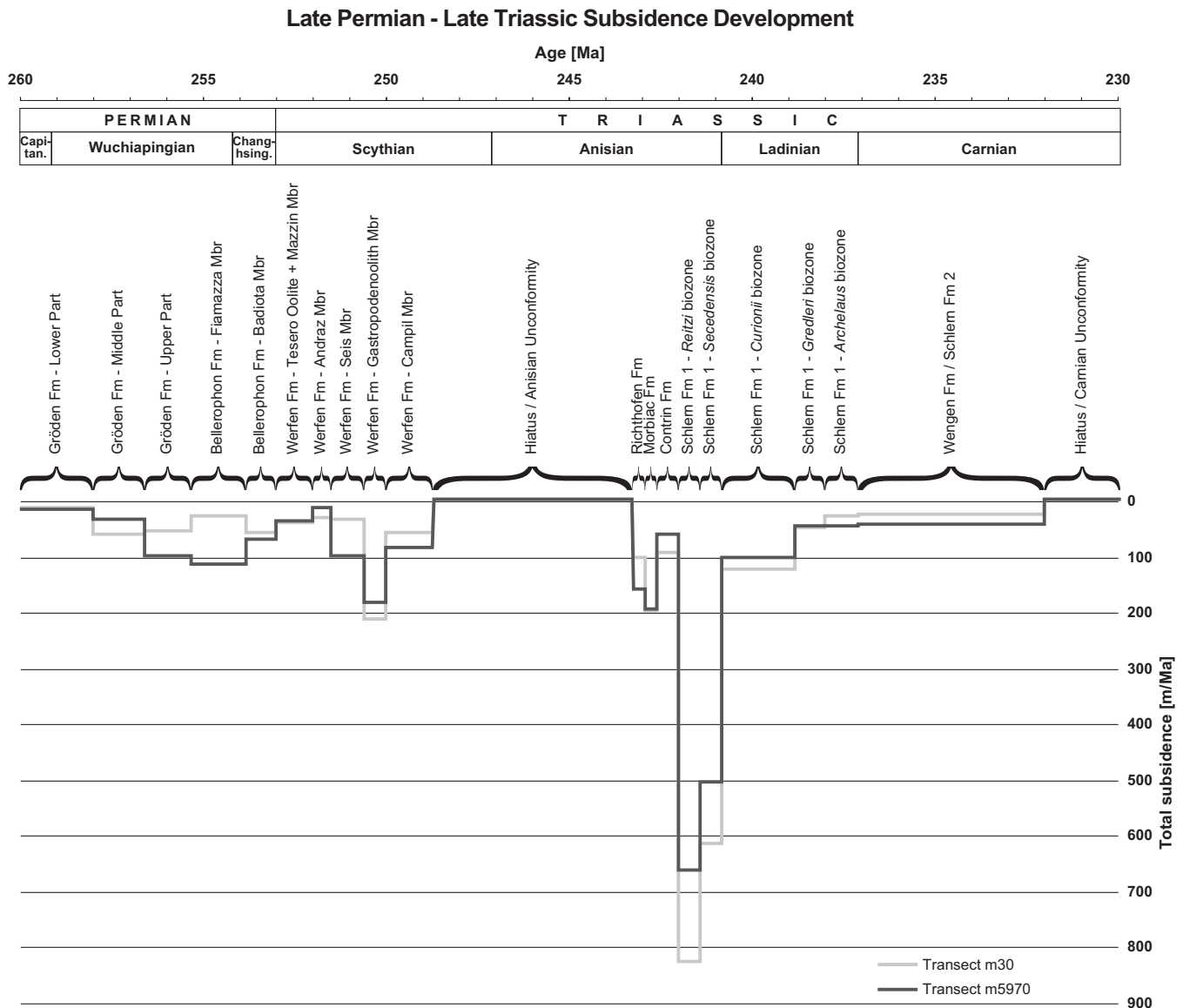


Fig. 4.14 Calculated total subsidence development of the basin at Rosengarten until the extrusion of Wengen Fm volcanics (basin reverse modelling module of PHIL). X-axis: time in Ma; y-axis: subsidence rates in m/Ma. Subsidence was calculated at a proximal (transect metre 30; grey line) and a distal point (transect metre 5970; black line). Differences in total subsidence at proximal and distal settings are mainly attributed to differences in compaction induced subsidence (thicker succession in distal parts). Timescale after Lehrmann et al. (2002), Mundil et al. (1996, 2001, 2003) and Yugan et al. (1997). Permian stages after Yugan et al. (1997), Triassic stages after Brack and Rieber (1993, 1994). For further explanations refer to the text.

uplift occurred from 8Ma onward (stage 7 in Fig. 4.11A). The thermal evolution along the entire transect from Middle Triassic times (A+D) to maximum burial (B+E) and present day (C+F) is illustrated in Figs. 4.12A-F with an overlay of vitrinite reflectance (4.12A-4.12C) and temperature (4.12D-4.12F).

Compaction of footwall strata moves basinward together with the prograding carbonate slope of the Rosengarten platform reducing porosity by its overburden (see Fig 4.13A-D; cf. Hunt and Fitchen 1999; Permian Delaware and Midlands basins, U.S.A.). In order to keep platform tops and basin floors horizontal and to maintain a common gradient of slope deposits throughout all growth stages, water depth maps of up to 800m had to be applied. These palaeo bathymetric values are in accordance with assumptions from Bosellini and Stefani (1991) and Brack and Rieber (1993).

4.4.2 Basin reverse modelling

The basin reverse modelling routine of PHIL (see also Fig 4.10 and chapter 4.3.6) calculates subsidence rates for every gridpoint along the transect. Two sets of subsidence rates are presented in Fig. 4.14, one set from a proximal location within the platform interior (transect m30) and another one from a distal location in the basin (transect m5970). Due to the rigidity of the underlying Permian Atesina Volcanic Complex (>2000m thickness; see also chapter 4.1) and the shortness of the transect, there are no distinct differences in flexural subsidence between a proximal and a distal setting. Differences in total subsidence in the beginning of basin evolution - until the Anisian unconformity - can be attributed to movements along small faults. The differences in total subsidence between a distal and proximal setting on the transect during Late Anisian/Early Ladinian times stem mainly from differences in compaction induced subsidence. Larger amounts of carbonate sediment on proximal areas allow for higher compaction induced subsidence rates.

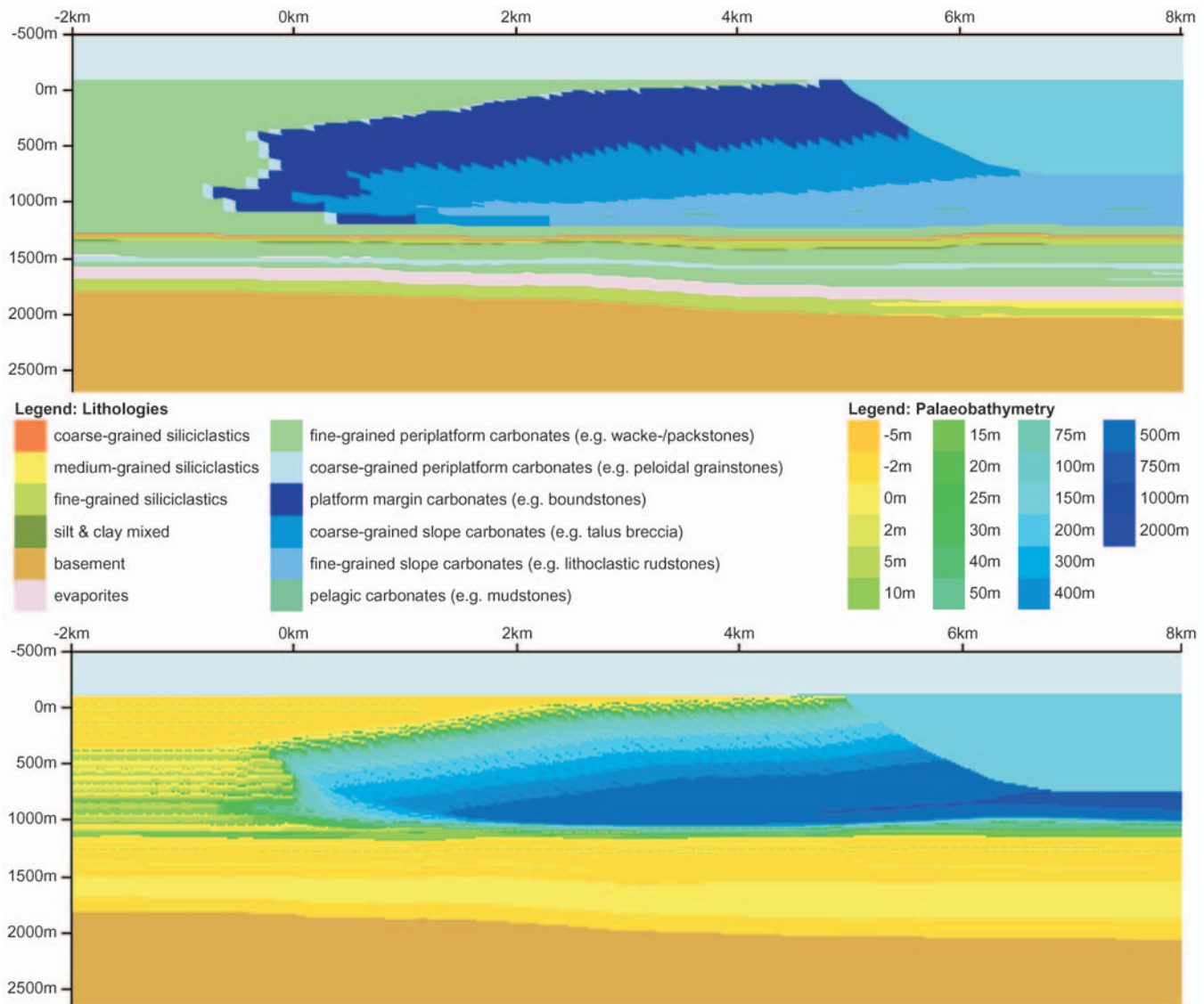
Basin evolution began with the deposition of the Permian Gröden Fm. Subsidence rates are continuously increasing until the Upper Permian Bellerophon Fm. Gypsum and marine intercalations in the upper part of the Gröden Fm and lower part of the Bellerophon Fm witnessed a transgression of the Tethys to the west. Subsidence slowed down towards the Permian/Triassic boundary, when lithofacies changed from basinal, organic-rich limestones (Bellerophon Fm, Badiota Mbr) to shallow ma-

rine oolites (Werfen Fm, Tesero-Oolite Mbr). Subsequent exposure was recorded by the Andraz Mbr. Deepening conditions were evidenced by the mainly carbonate sediments of the Seis and Gastropodenoolith Mbr (both Werfen Fm). The Campil Mbr was deposited under a shallow-marine to peritidal regime; hence the subsidence rates were decreasing again. Exposure from Latest Scythian until Middle Anisian produced a regional unconformity which removed the Cencenighe Mbr, Val Badia Mbr and uppermost parts of the Campil Mbr (Werfen Fm; approx. 160-180m of erosion; see Table 1). Subsidence commenced with the deposition of the Richthofen Fm (conglomerates and evaporites) and increased during Morbiac Fm sedimentation (bituminous limestones and marls). The shallow marine carbonate ramp of the Contrin Fm comprised an interval of decreasing subsidence, before the Anisian drowning unconformity marked a basinwide correlatable subsidence peak with rates of total subsidence of up to 820m/Ma. It decreases slightly to 600-500m/Ma during the *Secedensis* biozone, before subsidence ultimately drops down to values around 100m/Ma (*Curionii* biozone) and less (*Gredleri* and *Archelaus* biozone) and Wengen volcanics terminate platform growth. These high values during the upper *Reitzi* and entire *Secedensis* biozone are responsible for the aggradational behaviour of the Rosengarten platform. As subsidence drops to 100m/Ma, progradational sedimentation patterns develop. As mentioned above, movements along the Cima Bocche Line/Stava Anticline triggered these temporal changes in subsidence (see Part 2).

4.4.3 Stratigraphic forward modelling

In order to adequately simulate the Rosengarten platform with a larger platform interior to the N and a larger basin to the S, the transect had to be extended by two kilometres on each side. Relevant results available from previous modelling steps (thermal modelling, basin reverse modelling) were entered in the stratigraphic forward simulator of PHIL. The sedimentation rates were adjusted until a satisfactory fit was reached with present-day geometries (see also chapter 4.3.5 and Fig. 4.7). Erosion rates were neglected in order to determine minimum decompacted accumulation rates. Carbonate re-distribution to slope and basin was accounted for.

The best fit models are presented in Fig. 4.15 A and 4.15B. Whereas 4.15A shows the modelled transect after the last timestep of platform growth (*Archelaus*



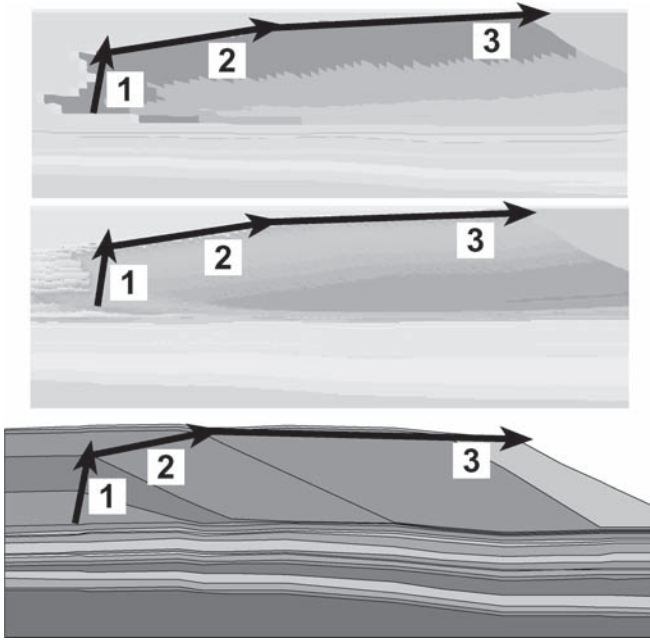
Figs. 4.15 Rosengarten transect as simulated with PHIL after the last timestep of platform progradation (*Archelaus* biozone, 237.1Ma). X-axis: distance along transect in kilometres; y-axis: elevation/depth in metres (negative values: elevation above respective sea-level; positive values: depth below respective sea-level); vertical exaggeration 1x. For further explanations refer to the text.

4.15A Overlay: lithologies. Legend on the lefthand side in the middle. Owing to the similarity in grain-size, fine-grained toe-of-slope deposits (Schlern Fm) have the same colour code as the fine-grained calci-turbiditic deposits of the basinal Buchenstein Fm.

4.15B Overlay: palaeo bathymetry. Legend on the righthand side in the middle. This overlay illustrates the Anisian drowning unconformity, where deep marine sediments of the Buchenstein Fm (dark blue colours) unconformably overlie the shallow marine Contrin Fm (light green colours).

biozone, 237.1Ma) with an overlay of lithofacies, 4.15B shows the same model with an overlay of palaeo bathymetry. The basal strata in Fig. 4.15A such as Gröden Fm (clastics above the basement), Bellerophon Fm (evaporites and carbonates underneath the thin light blue line marking grainstones of the Tesero-Oolite Mbr at the P/T boundary), Werfen Fm (carbonates and clastics un-

derneath the thin red line marking coarse-grained siliciclastics of the Richthofen Fm) and Anisian strata (fine-grained carbonates above the Richthofen Fm) are well visible. From this last timestep on, formation of the Rosengarten platform began. Minor adjustments of the margin back and forth during the first stage of platform development can be neglected due to the separation of



Figs. 4.16 Comparison of the simulated transect with reality. X-axis: distance along transect; y-axis: elevation/depth; vertical exaggeration 1x. For further explanations refer to the text. **4.16A and 4.16B** Details from Fig 4.15A (lithology) and 4.15B (palaeo bathymetry). The 3 different growth stages are marked with arrows and numbers (1: aggradation during *Reitzi* and *Secedensis* biozone; 2: progradation during *Curionii* biozone; 3: rapid progradation during *Gredleri* and *Archelaus* biozone). **4.16C** Detail from reconstructed transect after Bosellini and Stefani (1991) and Maurer (1999, 2000). See also Fig. 4.6. The 3 different growth stages are marked with arrows and numbers (1-3; see above). The last stage of platform development appears to be dipping to the right (south) owing to the dip of the underlying strata.

this short-spanded phase into several discrete time steps. Nevertheless, the aggradational trend is clearly to identify. The overlay with palaeo water depths facilitates the recognition of this first phase (see Fig. 4.16).

The resulting trajectories of the margin are illustrated in Figs. 4.16A and 4.16B. The first stage (1 in 4.16A/B; with a steep, nearly vertical trajectory; present day situation in 4.16C for comparison) is followed by an interval of progradation (2 in Fig. 4.16A/B; with a shallow to intermediate trajectory of the margin) of the *Curionii* biozone until fast progradation occurred during the last stages (3 in Figs. 4.16A/B; very shallow trajectory). A comparison with the conception of the Rosengarten platform according to Maurer (1999, 2000) reveals almost the same arrangement of trajectories (Fig. 4.16C). The initial phase

(1) in the model is a bit shorter whereas the growth stage of the *Curionii* biozone (2) seems a bit longer. This might indicate that the *Curionii* biozone as modelled in this study may in reality have been shorter (i.e. less than the 2Ma) as derived from the chronostratigraphic data of Mundil et al. (1996, 2003). Decompacted carbonate accumulation rates without erosion rates (“production rates”; see Fig. 4.17) increased from lagoon (“periplatform production”) to slope (“platform slope production”). 900m/Ma were applied for periplatform production, 980m/Ma for platform margin production, 1000m/Ma for platform slope production and 50m/Ma for pelagic production (Maurer 2003). The width of the carbonate functions was adapted to recent literature reporting carbonate production on the slope until 200-300m water depths (Kenter et al. 2002; della Porta et al. submitted).

4.5 Discussion

4.5.1 Controls on platform evolution at Rosengarten

The slope of the Rosengarten is characterised by two stages of platform evolution. The initial aggradational phase was followed by a progradational period towards the end of platform development (Bosellini 1984; Bosellini and Stefani 1991; Maurer 1999, 2000). An increase in carbonate production rates during the life-span of the Rosengarten platform can - for several reasons - probably ruled out as a possible explanation for this behaviour. (1) The onset of platform formation is in the Late Anisian. By this time, the carbonate factory in the Dolomites had already fully recovered from the faunal crisis at the P/T boundary as evidenced by Early Anisian reefal communities (Fois and Gaetani 1984; Senowbari-Daryan et al. 1993). (2) The life-span of the Rosengarten platform comprises less than 5 biozones (i.e. 4.7Ma) - an interval which appears to be too short for faunal trends to establish. Changes in intrinsic features (sensu Schlager 2000; i.e. changes of the biotic and abiotic carbonate factory) were not observed. (3) According to Schlager (1999), the production rate of carbonate platforms is much more likely to decrease in the million-year range due to changing environmental factors. (4) The palaeogeographic position of the Adriatic plate is more or less stable, there are no indications for a climatic change (Dercourt et al. 1993, 2000). Temporal changes in tectonic subsidence have to be assumed as driving force for this two-phase growth. A short-lived, pulse-like peak of up to 820m/Ma total subsidence during the *Reitzi* and

Secedensis biozone resulted in an aggrading platform. As soon as the *Curionii* biozone was reached, total subsidence dropped below 100m/Ma resulting in strong progradational pattern of the platform lasting until the termination of platform development through the extrusion of Wengen Fm volcanics.

The subsidence peak of the Late *Reitzi* to Early *Curionii* biozone can be observed throughout the western Dolomites (Rüüfer and Zühlke 1995) and is connected with tectonic movements at the transpressive-transtensive passive continental margin (Bechstädt and Brandner 1972; Doglioni 1983, 1984; Rüffer and Zühlke 1995). As the SE side of the Rosengarten is very close to the Stava Line/Cima Bocche Anticline (approx. 10km; Doglioni 1983, 1984), this two phased growth is most probably caused by tectonic movements and stillstands along this line. Sudden - in the order of 1Ma or less - movements caused peaks in tectonic subsidence (intervals with aggradational clinoforms) whereas during times of tectonic inactivity and/or updoming of the Predazzo magmatic chambers subsidence stopped (intervals with progradational clinoforms).

In the case of the Rosengarten, tectonic subsidence and its variations have been discussed as the major extrinsic (sensu Schlager 1993) factors for platform and slope evolution. Other parameters such as sea level oscillations and palaeo wind or wave directions have been significantly less important and/or heavily overprinted by variations in total subsidence. High frequency sea level oscillations as recorded by the accommodation development of the lagoonal interior at Torri del Vajolet (see Fig. 4.5A) are not preserved or recorded by the development of the platform slope (see Harris 1994; Emmerich et al. 2000). Additionally, sequence stratigraphic forward modelling helped to further constrain the palaeo water depths of the Buchenstein Fm. Best fit simulation shows water depths of up to 800m.

4.5.2 Carbonate production rates

Previous studies on reefal communities and carbonate platforms in the Dolomites (e.g. Fois and Gaetani 1984; Senowbari-Daryan et al. 1993) have stressed the Anisian recovery of reef-builders from the faunal crisis at the end of the Permian where 62% of marine invertebrate families (McKinney 1985) and up to 96% of species (Raup 1979) had been extinguished. New investigations on trace fossil abundance in the Lower Triassic Werfen Fm (see Fig. 4.3) confirmed a gradual re-appearance of

taxa throughout the Lower Triassic of the Dolomites (Werfen Fm) and a complete recovery already in the Uppermost Scythian represented by the top of the Werfen Fm (Twitchett 1999). Additionally, palaeontological studies from other Triassic carbonate platforms around the world also indicate a fast recovery of the calci-microbial carbonate factory (for complete discussion and references see Flügel 2002).

This observation is confirmed by modeled sedimentation rates: up to 1000m/Ma of carbonate sediment had been necessary to keep platform growth up with relative

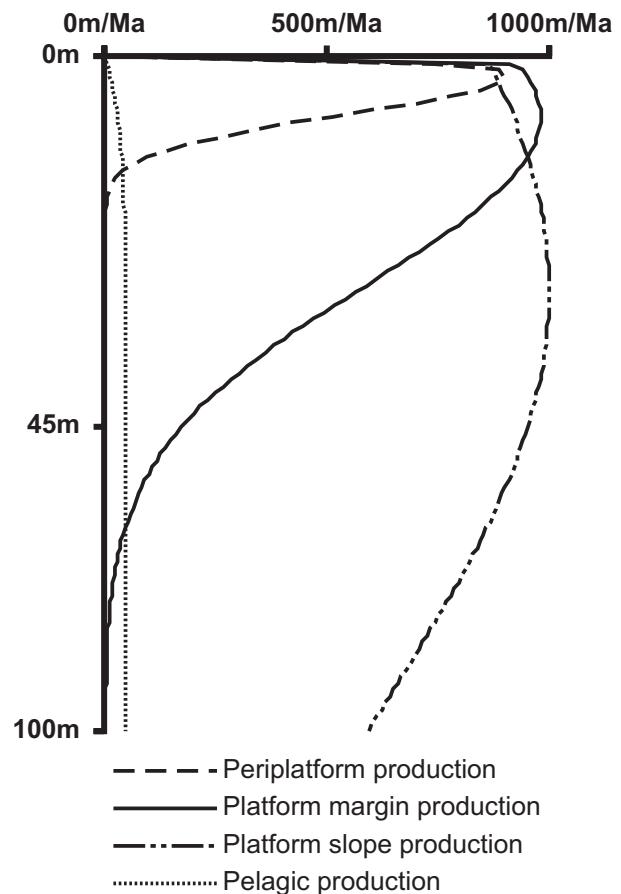


Fig. 17 Carbonate production rates as a function of water depth during simulation with PHIL. X-axis: carbonate production rates in m/Ma; y-axis: water depth in metres. Legend to functions to the bottom.

In order to reproduce present day geometries, the production of the carbonate factory had to be set to values between 900m/Ma and 1000m/Ma. Production increased from periplatform environments (900m/Ma) across the margin (950m/Ma) to the slope (1000m/Ma). Pelagic production (i.e. Buchenstein Fm) was limited to 50m/Ma (see also Maurer 2003). For further explanations refer to the text.

sealevel rise and in order to replicate the progradational clinoforms in our modelling. Carbonate production histories have been kept as simple as possible and erosion was neglected. Thus the modeled rates represent minimum accumulation rates. The best fit with present day geometries was achieved with a constant rate of carbonate accumulation of 900m/Ma to 1000m/Ma from platform margin to upper slope. The carbonate production window (see chapter 4.4.3) reached from shallow subtidal to 200-300m of water depth. This assumption is in accordance with recent studies on carbonate platforms from the Upper Carboniferous of the Asturian and Cantabrian mountains in Spain (Kenter et al. 2002; della Porta et al. submitted).

Previous studies have calculated/estimated 200m/Ma (Rosengarten: Maurer 1999, 2000), 200m/Ma-500m/Ma (Dürrenstein: Schlager 1981; Schlager et al. 1991) and 800m/Ma (n.b.: for the Anisian part of the Latemar succession: Egenhoff et al. 1999) as compacted accumulation rates for Triassic carbonate platforms in the Dolomites. Most of these values are easily surpassed by the ones simulated in this study (up to 1000m/Ma decompacted carbonate sediment production; up to 820m/Ma total subsidence). This adds more evidence to the observation of a complete and rapid recovery of the microbial carbonate-factory some 10Ma after the faunal crisis at the end of the Permian (with respect to the timescale after Mundil et al. 1996, 2001, 2003).

The difference of 80-180m/Ma between total subsidence rates as determined by the basin reverse modelling and the minimum carbonate accumulation rates as assumed in the stratigraphic forward modelling is caused by several reasons. (1) Time steps in basin reverse modelling are much longer than in forward modelling (10^6 - 10^5 vs. 10^3 - 10^2 years). (2) Interferences of total subsidence and sea level rise can lead to higher accommodation rates. (3) Carbonate sediments are re-distributed to the slope, basin and/or out of the transect (debris-flows, calciturbidites). (4) Owing to the small area during the first stages of platform growth, the platform is more prone to drowning than during later stages.

4.5.3 Porosity evolution

The porosity evolution of the underlying strata reflects the platform development of the overlying Schlern Fm. During the last, progradational stage of platform evolution, maximum porosities in the Permian Gröden Fm are preserved in distal, basinal areas (see Figs. 4.13). The

decrease in porosity underneath the slope sediments mimics their progradation; i.e. an area of low porosity is prograding basinwards together with slope deposits. This has implications for shallow hydrocarbon reservoirs in basinal strata below (carbonate) slopes. The migration might thus rather be basinward than in the direction of the platform depending on later compaction by overburden. Basin infilling and deep burial will most probably equalise lateral differences in the underlying strata.

4.5.4 Burial/thermal history

Low VR_r values and short apatite fission tracks point to a long, shallow burial with a relatively thin overburden until the end of the Cretaceous followed by fast uplift/cooling (see Fig. 4.11). Values of VR_r between 0.4% and 0.7% indicate maximum temperatures during burial in the order of 110°C. As illustrated by the burial history plots in Fig. 4.11A-C, maximum temperatures may have been reached already in Middle Jurassic times for which a high basal heat flow of 90mW/m² was assumed.

Uplift occurred from the first collision of oceanic crust on (80Ma; Hsü 1971; Smith 1971; Trümpy 1982; Laubscher and Bernoulli 1982; Hsü 1989; Dercourt et al. 1993, 2000), and fast uplift prevailed from 40Ma onward when the succession moved above the 80°C isotherm. This rapid exhumation/cooling rate is confirmed by recent FT-ages of the Western Alps (Carrapa et al. 2002), as well as by provenance analyses (Dunkl et al. 2001) and ⁴⁰Ar/³⁹Ar dating of white micas from clastic sediments of the Alpine ranges of Europe (Wijbrans et al. 2002). Fast exhumation is mainly driven by fast denudation and subsequent isostatic movement of the upper crust (“steady state exhumation”; Bernet et al. 2001).

4.6 Conclusions

Owing to extensive and high-quality chrono-, bio- and cyclostratigraphic data, the Middle Triassic Rosengarten carbonate platform is an ideal area to assess carbonate accumulation rates after the P/T-crisis and the response of platforms to temporal changes in subsidence. An integrated approach of thermal and stratigraphic modelling revealed that the Rosengarten platform kept successfully up with subsidence rates of up to 820m/Ma and had minimal carbonate accumulation rates of 900-1000m/Ma without taking into account erosion. Both stages of platform growth - firstly aggradation and later progradation - originate in temporal variations in total subsidence.

Calibration of thermal modelling with vitrinite reflectance and FT-measurements revealed that Neogene flysch or molasse-type sediments above present day topography as inferred from other Alpine basins (Massari et al. 1986) did not affect temperature and burial history significantly, i.e. have been either very thin or not present at all. The low thickness of eroded stratigraphy above the Rosengarten transect contrasts with the regional coalification pattern of the eastern Dolomites (unpublished results mainly on Alta Badia area and Sella, see Fig. 4.2). The higher thermal maturity in this area requires either a significantly higher heat flow or higher thicknesses for the eroded Cretaceous overburden. Whereas the latest cooling phase of the eastern Dolomites seems to be similar to that of the Rosengarten area, higher thermal maturity in the eastern and central Dolomites further underline the significance of the Trento platform for the thermal evolution of the western Dolomites.

Acknowledgements

Axel Emmerich thanks the “Studienstiftung des deutschen Volkes” (German National Academic Foundation) and the International Postgraduate Programme (IPP, University of Heidelberg) for financial support during this study. Robert Tscherny acknowledges IES.

PART 5

Basin and Carbonate Platform Development in the SW-Dolomites: Rosengarten and Latemar (Meso-/Cenozoic, Northern Italy)

Abstract

The Rosengarten and Latemar Middle Triassic carbonate platforms show similar subsidence patterns during equivalent times of platform evolution as unraveled with numerical basin reverse modelling. Hence, the coexistence of structural highs and lows (facies heteropy between platforms and basins) in the study area is mainly owed to a pre-platform tectonic development. Differential tectonics ceased during Late Anisian times.

Total subsidence reaches values of 800-850m/Ma during the first stage of platform evolution. As both platforms successfully kept up with this subsidence peak, it is evident that the carbonate factory must have had completely recovered from the P/T faunal crisis. The last stages of platform development of the Rosengarten slope where rapid progradation occurs are recorded neither by the lagoonal succession nor the slope at Latemar.

The area close to the Trodena line and to the volcanic centre of Predazzo/Monzoni has undergone a higher heat flow pulse during the Late Ladinian and has possibly been buried at shallower levels than the area at Rosengarten. This underlines the only local thermal influence of the Late Ladinian volcano-thermal event of Predazzo/Monzoni.

Correlation of time scales of the coeval Buchenstein Fm (basin) and Schlern Fm (platform) as well as subsidence modelling results point to a microcycle duration between 0.9ka and 1.97ka in the cyclic succession at Latemar. Time series analysis on the other hand identifies Milankovitch-cyclicities in larger-order cycle stacking patterns and thus argues for a microcycle duration of 4.2ka.

5.1 Introduction

For several reasons, the Middle Triassic of the Dolomites (Northern Italy) provides an ideal area for basin and stratigraphic modelling: (1) nappe tectonics are absent (e.g. Castellarin & Vai 1982; Doglioni & Castellarin 1985; Doglioni 1987), (2) excellent outcrops of seismic scale (e.g. Bosellini 1988) (3) enable basin-wide corre-

lation (e.g. Brack & Rieber 1993; Brack & Muttoni 2000) and (4) most importantly the Middle Triassic is constrained by a high-resolution bio-, cyclo- and chronostratigraphical dataset (e.g. Brack & Rieber 1993, 1994; Brack et al. 1996; Mundil et al. 1996, 2003; Zühlke et al. 2003). The Rosengarten and the Latemar have both served as reference models for platform development in the Middle Triassic (e.g. Bosellini & Rossi 1971; Gaetani et al. 1981; Goldhammer & Harris 1989; Bosellini & Stefani 1991). Correlation of basin-wide continuous and dated ash layers (Mundil et al. 1996) into slope deposits of the Rosengarten (Maurer 1999, 2000) and dating of ash layers within lagoonal sediments at Latemar (Mundil et al. 2003) set the chronostratigraphic framework for basin modelling at biozone scale. This study aims at (1) comparing the evolution and subsidence patterns of the Rosengarten and Latemar platforms with numerical basin modelling (PHIL; see Bowman & Vail 1999) and (2) assessing t-T-paths – i.e. the thermal history – of these two platforms and its adjacent basins with fission track analyses in apatites.

5.2 Geological setting

In the study area in the Dolomites (Fig. 5.1), Early Permian volcanic activity is witnessed by the Atesina Volcanic Complex (AVC; Fig. 5.2). The AVC covers an area of 2000-4000km² and represents a voluminous pyroclastic flow complex with thicknesses between 2000-2500m and subordinate lava flows and intrusions (D'Amico et al. 1980, D'Amico & Del Moro 1988; Barth et al. 1994). The AVC overlies a Lower Permian erosional unconformity either in direct contact to the Hercynian metamorphic basement – mainly metapelites – or to the Lower Permian Waidbruck conglomerate. The volcanic succession can be subdivided into a lower and an upper group with the upper group mainly containing rhyolitic ignimbrites (e.g. D'Amico et al. 1980; D'Amico & Del Moro 1988; Di Battistini et al. 1988). The coeval Cima D'Asta pluton (CAP) is located to the south of the AVC and is related to the Val Sugana line (see Fig. 5.2; Castellarin et al. 1979; Doglioni 1987). The AVC and CAP magmatites were later overprinted by a Middle to Late Triassic volcanic and hydrothermal event (225-230Ma), resetting isotopic clocks and shifting geochemical signatures significantly (D'Amico et al. 1980; Savelli & Balboni 1984; D'Amico & Del Moro 1988; Barth et al. 1993, 1994).

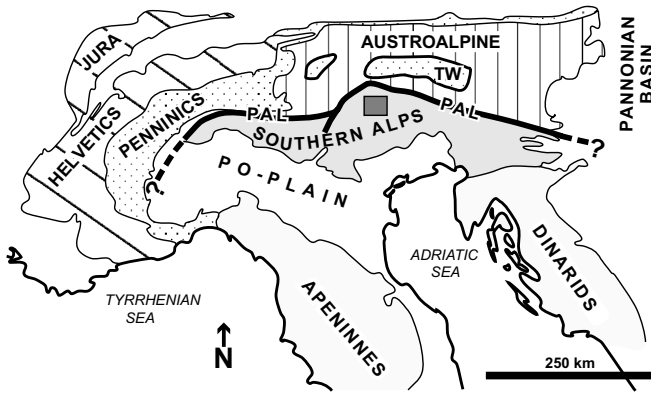


Fig.5.1 Schematic map of major tectonic units in the Alps. The dark grey rectangle marks the location of the study area and its surroundings. Abbreviations: TW: Tauern window; PAL: Periadriatic lineament/Insubric line.

Sedimentation on the Permian landscape is recorded by the siliciclastic Upper Permian Gröden Fm (“red beds”; see Table 5.1), followed by evaporites and carbonates of the Bellerophon Fm indicating a relative sea level rise. The long-term transgression of Tethys to the W is further evidenced during the Lower Triassic by sub- to intertidal deposits of the Werfen Fm (Broglia Loriga et al. 1983, 1990). The transition from Scythian to Anisian

times (Lower to Middle Triassic) recorded a change in sedimentary characteristics (De Zanche & Farabegoli 1988; De Zanche 1990). Synsedimentary transpressive-transpressive tectonic activity created structural highs and lows along the passive margin leading to so-called facies heteropy (Bechstädt & Brandner 1972). The Anisian also saw the re-occurrence of carbonate ramps and platforms, with the first ramps made up of simple microbial and algal carbonates (Sarl Fm: Fois & Gaetani 1984; Senowbari-Daryan et al. 1993). Sedimentation on structural highs was recorded by the conglomeratic Richthofen Fm and later by the ramp carbonates of the Contrin Fm whereas more basinal settings were filled with the slightly bituminous Morbiac and Moena Fm (Zühlke 2000). Further tectonic activity enhanced this facies heteropy and subsequently carbonate platforms (Schlern Fm 1 sensu Brandner 1991; Schlager et al. 1991; see Fig. 5.3 and Fig. 5.4) developed with coeval basinal successions (Buchenstein Fm) indicating water depths of about 800-1000m (Bosellini 1984; Brack & Rieber 1993) towards the end of basinal development. Volcanic activities outside the Buchenstein basin lead to the deposition of airborne ash layers in lagoonal and basinal sediments during Schlern platform development (Callegari & Monese 1964; Cros 1979; Cros & Houel 1983).

	1	2		3	4
	Formation / Timestep	D. age [Ma] from to		Thickness [m]	Lithology
TRIASSIC	Hiatus	232.0	229.9	-	-
	Wengen/Cassian Fm	237.1	232.0	100-730	volcaniclastic deposits with limestone boulders and basinal shales
	<i>Archelaus</i> biozone deposits (Schlern & Buchenstein Fm)	238.0	237.1	20-400	dolomite pinching out to shaly marl
	<i>Gredleri</i> biozone deposits (Schlern & Buchenstein Fm)	238.8	238.0	18-800	dolomite pinching out to shaly marl
	<i>Curionii</i> biozone deposits (Schlern & Buchenstein Fm)	240.7	238.8	12-640	dolomite pinching out to shaly marl
	<i>Secedensis</i> biozone deposits (Schlern & Buchenstein Fm)	242.0	240.7	10-300	dolomite pinching out to shaly marl
	<i>Reitzi</i> biozone deposits (Schlern & Buchenstein Fm)	242.4	242.0	10-300	dolomite pinching out to shaly marl
	Contrin Fm	243.1	242.4	40-55	dolomite
	Morbiac Fm	243.4	243.1	20-30	marl with interbedded limestone
	Richthofen Fm	243.7	243.4	7-25	conglomerate with interbedded coarse-grained sandstone
	Hiatus	247.5	243.7	-	-
	Werfen Fm, Cencenighe Mbr	248.1	247.5	0-30	limestone with interbedded marl
	Werfen Fm, Val Badia Mbr	248.7	248.1	0-45	marly limestone
	Werfen Fm, Campil Mbr	250.0	248.7	45-90	fine-grained sandstone with interbedded silt
Werfen Fm, Gastropodenoolith Mbr	250.6	250.0	60-100	intercalations of limestone, marl and silt	
Werfen Fm, Seis Mbr	251.5	250.6	12-55	intercalations of limestone and marl	
Werfen Fm, Tesero-Oolite, Mazzin & Andraz Mbr	253.0	251.5	70-125	intercalations of limestone, sandy dolomite, marl and silt	
PERM.	Bellerophon Fm	255.3	253.0	75-185	gypsum with dolomitic marl followed by intercalations of limestone and marl
	Gröden Fm	260.0	255.3	135-215	silt-rich coarse-grained sandstone
	Hiatus	267.0	260.0	-	-
	Atesina Volcanic Complex	276.0	267.0	>2000	rhyolitic ignimbrite with subordinate lava flows

Table 5.1 List of Lower Permian, Lower Triassic and Middle Triassic formations/timesteps (column 1) applied during basin reverse modelling with depositional ages (column 2), thicknesses (column 3) and lithologies (column 4). For a complete list of the basin infill until present day refer to part 4. The chronostratigraphic framework was derived from the following studies: Permian: Yugan et al. (1997), Triassic: Lehmann et al. (2002), Mundil et al. (1996, 2001, 2003).

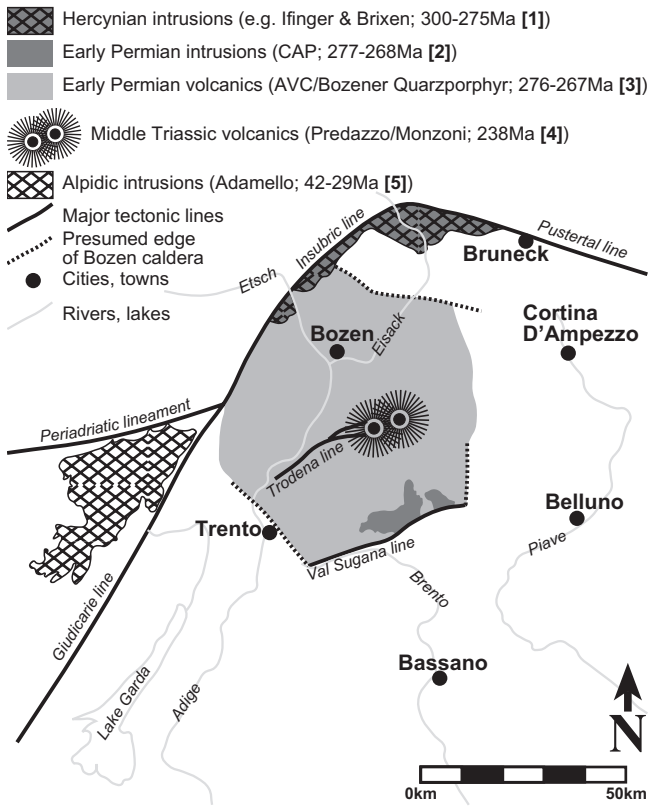


Fig. 5.2 Schematic map of tectonic lines and magmatic and volcanic provinces in the central sector of the Southern Alps illustrating the extent of the Early Permian Atesina Volcanic Complex/Bozener Quarzporphyr (AVC; after Doglioni 1987; D'Amico & Del Moro 1988; Barth et al. 1994). Main magmatic activities –Cima D'Asta (Lower Permian), Predazzo/Monzoni (Middle Triassic) and Adamello (Alpidic) – are linked to suture zones like the Periadriatic lineament/Insubric line, the small but deep-reaching fault system of the Trodena line (Doglioni 1987) or the Valsugana line. Legend to the upper left. Abbreviations: CAP: Cima D'Asta pluton; AVC: Atesina Volcanic Complex. References: [1]: Borsi et al. 1972; Del Moro & Visona 1982; [2]: Borsi et al. 1974; Barth et al. 1994; [3]: D'Amico & Del Moro 1988; Barth et al. 1994; [4]: Borsi & Ferrara 1967; Borsi et al. 1968; [5]: Borsi et al. 1966; Del Moro et al. 1983.

Late Ladinian tectonic and volcanic events inside the basin – i.e. Wengen Fm volcanism – ended platform growth by exposing platform tops subaerially and covering the platforms with lavas and volcanoclastics (Schlern platform; Brandner 1991; Yose 1991) and filling the basins with debris-flows, ashes and lava (Bosellini et al. 1977, 1982). The volcanic complex of Predazzo/Monzoni formed above the small but deep-reaching fault system of the Trodena/Stava line-Cima Bocche anticline (sinistral transpression creating flower-structures in the

basement; Doglioni 1987). The tectonic line also had a major influence on subsidence development of its neighbouring platforms (see Part 2).

The later basin infills can only be deduced by a comparison with the basin evolution in the eastern parts of Dolomites and the area around Trento. All strata younger than Late Ladinian have been eroded in the study area (see Plate 5.1). Postvolcanic buildups (Schlern Fm 2 – sensu Brandner 1991; Schlager et al. 1991 – or Cassian Dolomite) are of major importance in the eastern Dolomites, thicknesses in the western Dolomites are limited to 50-70m (Schlern; Brandner 1991). Subsequently, Cassian platform tops were subaerially exposed and topographic relief leveled. The Late Carnian Raibl Fm overlies this karstification surface. With the onset of a period of tectonic quiescence a huge carbonate platform developed comprising the entire central segment of the Southern Alps on the Adriatic Plate (Trento platform: Dolomia Principale, Calcarei Grigi; Bosellini & Broglio Loriga 1971; Bosellini & Hardie 1985). Jurassic rifting of the continental lithosphere started at the Triassic/Jurassic-boundary (Dercourt et al. 2000), corresponding to ages of around 200Ma according to the new Jurassic time scale of Pálffy et al. (2000). From Middle Jurassic times on, when sea-floor spreading between Adria and Europe began (emplacement of gabbros in the Swiss alps

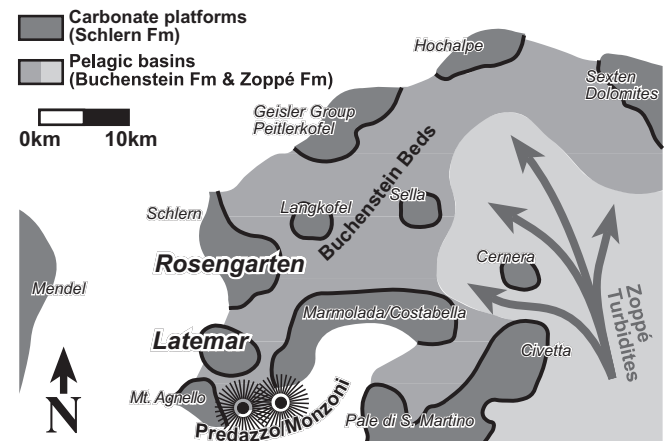


Fig. 5.3 Schematic palaeogeographic map of the Western Dolomites during the Middle Triassic (Late Anisian/Early Ladinian; after De Zanche & Farabegoli 1988; De Zanche 1990). The two carbonate platforms studied here – Rosengarten and Latemar – are marked by large bold letters. Legend of lithostratigraphic units in the upper left corner; influx of siliciclastic Zoppé turbidites marked by large arrows. The volcanic centre of Predazzo/Monzoni in the immediate surroundings of the study area is sketched with radial lines.

between 160-165Ma; Schaltegger et al. 2002), the Trento platform started subsiding more rapidly and eventually drowned. A phase of deep marine sedimentation began (e.g. Winterer and Bosellini 1981; Martire 1996; Winterer 1998) and lasted until the Late Cretaceous (Claps et al. 1991; Stock 1996). Water depths decreased again when

the tectonic regime switched from extension to compression and the collision of the Adriatic plate with Europe started with subduction of oceanic crust in the Late Cretaceous (e.g. Hsü 1971; Trümpy 1982; Laubscher and Bernoulli 1982; Dercourt et al. 2000). Upper Oligocene shallow marine conglomerates in the eastern Dolomites witness ongoing continent collision in the Palaeogene (Mair et al. 1996). Fast exhumation of the Southern Alps mainly driven by denudation/erosion is thermochronologically recorded from the Eocene onwards (40-35Ma; e.g. Bernet et al. 2001; Dunkl et al. 2001).

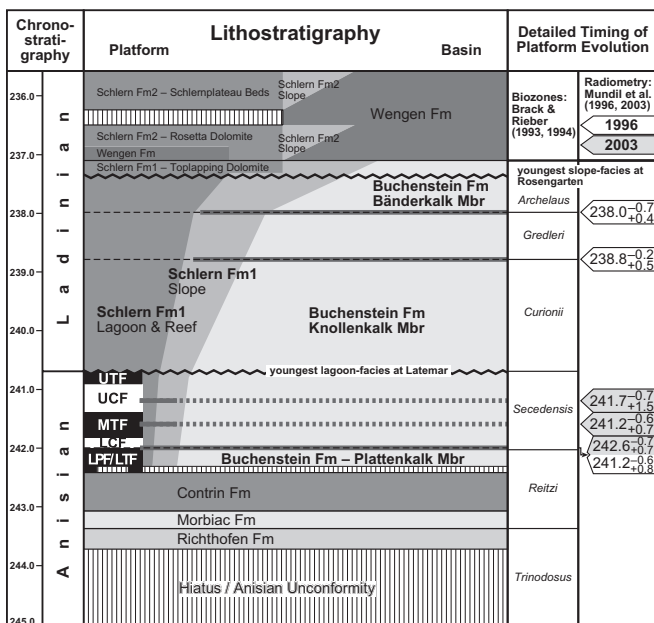


Fig. 5.4 Detailed Anisian/Ladinian stratigraphic succession at Rosengarten and Latemar. Strata of the lagoonal interior of carbonate platforms are to the left, basinal successions to the right. The subdivision of the Latemar lagoon into several facies is depicted with the black and white pattern in the lower left (abbreviations sensu Egenhoff et al. 1999: LPF: Lower Platform Facies; LTF: Lower Tepee Facies; LCF: Lower Cyclic Facies; MTF: Middle Tepee Facies; UCF: Upper Cyclic Facies; UTF: Upper Tepee Facies). The chronostratigraphic subdivision of the Latemar lagoon corresponds to the scheme proposed in this study. The two zig-zagged lines demonstrate present day topographies respectively. Overlying strata are projected from the neighbouring Schlern platform (after Brandner 1991; see Fig. 5.3). The progradation of younger slope deposits at Rosengarten is illustrated with darker colours overlying basinal areas (righthand side). Age-dagnostic tuff layers in the Buchenstein and Schlern Fm are indicated by dark grey lines; the ages of which are to the right (white arrows: ages from Mundil et al. 1996 – Buchenstein Fm at Seceda (Geisler Group), see Fig. 5.3; grey arrows: ages from Mundil et al. 2003 – Schlern Fm at Latemar, see Fig. 5.3). Chronostratigraphy according to Lehrmann et al. (2002) and Mundil et al. (1996, 2001, 2003). Biozones and Anisian/Ladinian boundary according to Brack and Rieber (1993, 1994). Correlation of age-dagnostic tuff layers from the basinal Buchenstein Fm to slope-facies of Schlern Fm according to Maurer (1999, 2000).

5.3 Methods

5.3.1 Numerical reverse basin modelling

Numerical reverse basin modelling in this study follows the sequence stratigraphic concept, which considers the creation/destruction of accommodation space and its infill as the two principal controls on sedimentary systems and basins. Numerical reverse basin modelling was carried out to determine (thermo)-tectonic, flexural and compaction induced subsidence tantamounting to total subsidence (Allen & Allen 1990). Subsidence component, accommodation and sediment flux histories were calculated for each of the time steps identified in the Permian to Late Triassic basin fill (see Table 5.1; for a complete list of time layers up to present-day refer to Part 4). Each time step is characterised by a distinct vector of tectonic subsidence, flexural and compaction induced subsidence as well as a change in palaeo water depth. During each step of removal, the hypothetical depth of the basin floor is calculated without being loaded and the current depositional surface is adjusted to pre-defined palaeo bathymetry. Rates are calculated for each time layer with the effects of flexural loading, changes in palaeo bathymetry, changes in sea level and compaction removed. The flexural backstripping procedure applied in the reverse basin modelling of this study is based on the equations introduced by Turcotte & Schubert (1982, 2002) and Dickinson et al. (1987). The backstripping procedure with the applied software – PHIL™ (Marco Polo Software Inc., Houston, U.S.A.) – has also been described by Bowman & Vail (1999).

Input parameters were lithology (initial porosity; after Bowman and Vail 1999), geometries (measured and projected bed thicknesses), palaeo water depth (derived from facies analysis), depositional ages (see Table 5.1) and crustal parameters (e.g. effective elastic thickness T_e , plate end boundary distance and density of the mantle).

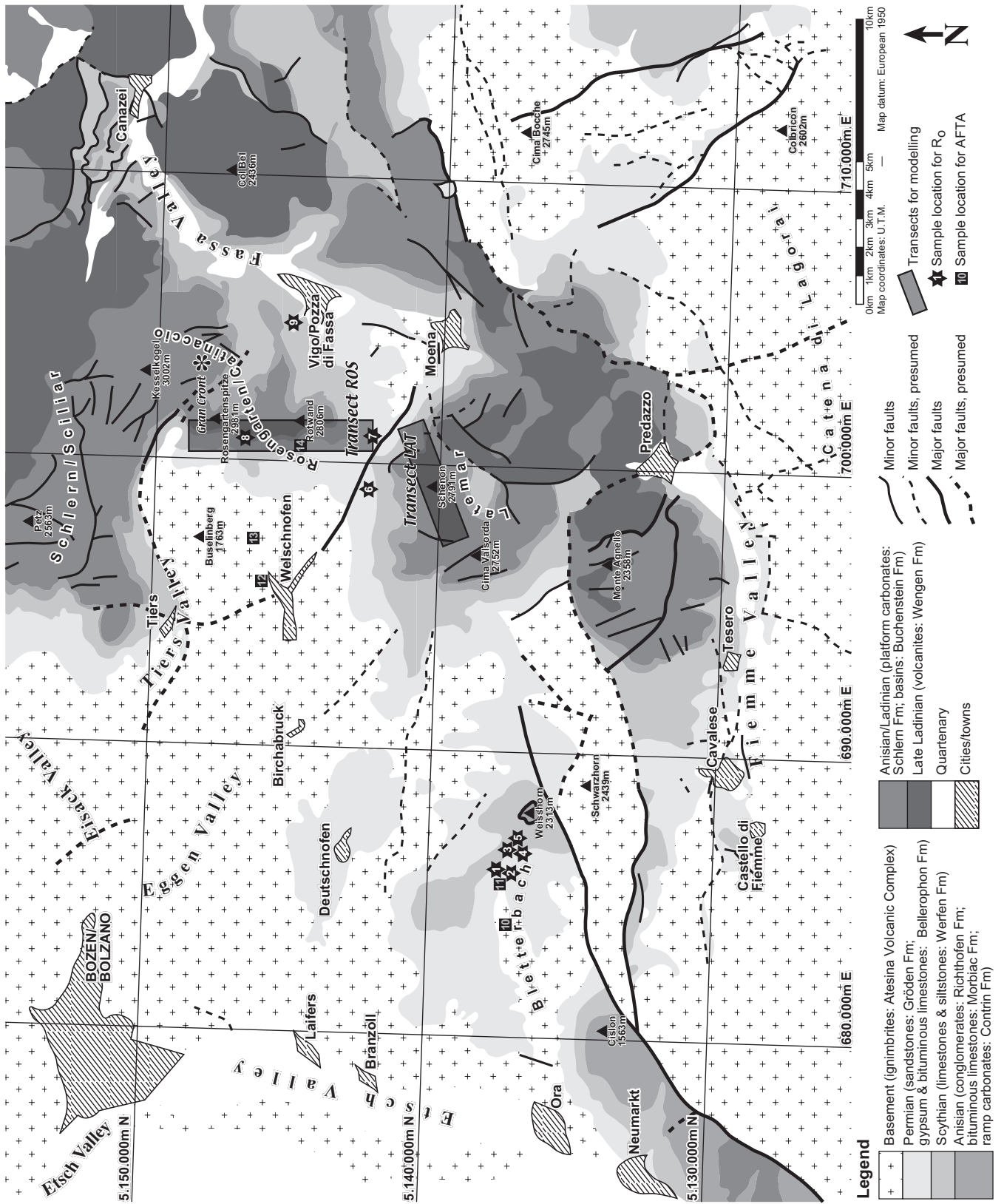


Plate 5.1 Simplified geological map of the study area and its surroundings. Note the presence of the Cima Bocche Anticline/Stava Line (major faults) and the Late Ladinian Wengen Fm volcanics in the eastern and northeastern part of the area. Legend of the geological map in the lower part. Sample locations for vitrinite reflectance analyses are marked by stars, those for apatite fission track analyses by squares. Transects for modelling are indicated by dark transparent rectangles. The sedimentological interpretation of Gran Cront (Rosengarten area) is marked by an asterisk.

Owing to the shortness of the transects (ROS: 6km and LAT: 4km) and the rigidity of the underlying basement (2000-2500m thick Permian AVC), crustal parameters and flexural subsidence play an insignificant role. Nevertheless, recent data on the effective elastic thickness (T_e ca. 20km) of the lithosphere of the Venetian basin (Barbieri & Garcia-Castellanos 2003) was applied. Owing to the short interval of platform evolution – less than 5Ma – and small amplitudes of Middle Triassic sea level change, 2nd order sea level fluctuations played an insignificant role during accommodation development. 3rd order sea level oscillations (1-3Ma; Duval et al. 1992) have not been considered because their timing and amplitude in the latest Anisian/earliest Ladinian is controversially discussed (Rüffer & Zühlke 1995; Gianolla & Jacquin 1998).

5.3.2 Apatite fission track analysis

21 samples of Permian to Triassic age were taken from the study area around Rosengarten and Bletterbach (see Plate 5.1). Only 5 samples revealed a sufficient amount of apatite for FT-dating (Tab. 5.2 and Tab. 5.3). Apatite grain mounts were obtained using standard sample preparation techniques (Grist & Ravenhurst 1992a, b; Glasmacher et al. 1997). FT-ages were determined using the external detector method (Wagner & Van den Haute 1992). Samples were irradiated at the Thetis reactor (Channel No. 16), Ghent, in the presence of three glass neutron dosimeters (CN5) of known uranium content as well as Fish Canyon and Durango apatite age-standards. Apatite was etched in 5 M HNO₃ for 20±1s at 21±1°C and detection mica in 40% HF for 30min at 23°C. Area densities (tracks/cm²) of spontaneous and induced fission-tracks were measured at two 17" TFT screens using an optical microscope (Olympus™ BX 50), an Autoscan® 3D-axis stage with Sony™ external measuring scales, a high resolution F-view II® pelitier-cooled CCD camera of Soft Imaging™ and the latest version of Trakscan®. FT-pooled and weighted mean ages (±1σ error) were calculated applying the IUGS recommended approach of Hurford & Green (1983). The ζ-value of 349±12a/cm² for CN5 was obtained by using Fish Canyon and Durango apatite age-standards. Radial plots were calculated and drawn with the TRACKKEY programme (Dunkl 2002). Confined tracks were measured with a precision of approximately ±0.2µm at 2000x magnification using the same setup as for the determination of track areal density.

Based on the apatite FT- and geological data, time-temperature paths for samples were calculated using AFTSolve® with the kinetic model after Laslett (1987). The AFTSolve® software is described by Ketcham et al. (2000) in detail. Although the programme attempts to find out of more than 10,000 single t-T paths those best approximating the measured data ("Best Fit"), the primary goal of the programme is to define envelopes (merit value of 0.05 and 0.5) in t-T space containing all paths passing baseline statistical criteria and being conform to user-entered geological constraints. Therefore, the forward modelling procedure of the programme was used to establish segments of the t-T path where monotonic cooling and monotonic heating change. Such constraints were included in the inverse modelling module of the programme. For most of the samples, the t-T constraints were left very wide open.

5.4 Platform architecture

The modelled transects are shown on Plate 5.2.1 and 5.2.2 (location of the transects on Plate 5.1). Both transects at Rosengarten and Latemar were selected for the following reasons: (1) almost no tectonics/major faulting involved, (2) maximum number of time indicative marker horizons within the transect and (3) the transects include representative information on the overall evolution of the two buildups.

5.4.1 Rosengarten

The Rosengarten is an Anisian/Ladinian carbonate platform with an areal extension of approx. 7x7km. The platform is dissected by several faults (see Plate 5.1), the former outline of the platform top and the thickness of the lagoonal succession is unclear. Bosellini & Stefani (1991) and Maurer (1999) correlated the lagoonal interior of the Rosengarten at Torri del Vajolet (see Plate 5.2.1) with the lagoonal succession of the Schlern Fm 1 at the neighbouring Schlern platform (see Fig. 5.3 and Plate 5.1). At Schlern, lagoonal strata of the Schlern Fm 1 are capped with lava and volcanoclastics indicating the maximum thickness of the pre-volcanic Schlern Fm 1 buildups (Yose 1991). A projection of these lagoonal strata to the lagoonal interior at Rosengarten yields the reconstruction of the platform top illustrated in Plate 5.2.1.

As described by many authors (e.g. Bosellini 1984, 1988; Bosellini and Stefani 1991; Bosellini et al. 1996; Maurer 1999, 2000), the Rosengarten has served as a reference

1	2	3	4	5	6	7	8	9	10	11	12
Loc.	Reference	Sample no.	UTM coordinates	Elevation	Area	Formation	Lithology	Vitrinite-reflectance VR _r [%]	Temperature [°C]	Central Age [Ma]	Mean Track Length [μm]
			x y	[m]							
1	Buggisch 1978	Bb40	-685800	-1520	BB	Gröden Fm	Coarse – medium grained sandstone	0.73	110		
2	Bielefeld 1998	15e, 15ell	685800	1520	BB	Gröden Fm	Coarse – medium grained sandstone	0.60±0.09	94±11		
3	Bielefeld 1998	Butler2, But	686750	1650	BB	Gröden Fm	Coarse – medium grained sandstone	0.68*	104		
4	Buggisch 1978	Bb, Bb10	686750	1650	BB	Gröden Fm	Coarse – medium grained sandstone	0.62*	97		
5	Schulz & Fuchs 1991	-	686750	1650	BB	Gröden Fm	Coarse – medium grained sandstone	0.88	125		
6	Bielefeld 1998	20a, 20all	698900	1710	LAT	Gröden Fm	Coarse – medium grained sandstone	0.76±0.10	113±10		
7	Bielefeld 1998	N6a, N6b, N6b1	701000	1730	ROS	Gröden Fm	Coarse – medium grained sandstone	0.67±0.14	103±15		
8	Emmerich et al. 2004	070	700900	2330	ROS	Morbac Fm	Bituminous limestone	0.77±0.02**	114±2		
9	Emmerich et al. 2004	belle	705014	1615	ROS	Bellerophon Fm	Bituminous limestone	0.52±0.02	83±3		
10	this study	AE11/PBBQ1	685219	1400	BB	Alesina Volcanic Complex	Rhyolitic ignimbrite			154.2±7.8	12.0±1.3
11	this study	AE12/PBBQ2,3	685679	1450	BB	Alesina Volcanic Complex	Rhyolitic ignimbrite			148.2±7.5	11.9±1.4
12	this study	AE14/UJSO	695807	1275	ROS	Alesina Volcanic Complex	Rhyolitic ignimbrite			84.2±12.7***	10.6±1.5
13	this study	AE18/PPKHQ	697212	1450	ROS	Alesina Volcanic Complex	Rhyolitic ignimbrite			165.6±7.3	9.8±1.6
14	this study	AE10/PRWGAS	701149	2160	ROS	Werfen Fm (Gastropodenoolith Mbr)	Medium – fine grained sandstone			74.7±8.1**	10.8±1.9

Table 5.2 List of vitrinite reflectance data compiled from literature and apatite fission track data from this study. The numbers in the first column correspond to the locations given in Plate 5.1. The source of the data is shown in column 3. UTM coordinates (column 4) and elevations above present day sea level (column 5) also correspond to the system and map datum used in Plate 5.1. Area codes in column 6 are used for quick reference (BB; Bletterbach; LAT; Latemar; ROS; Rosengarten). The formations from which the samples were taken are presented in column 7, their lithology in column 8. Columns 9 and 10 show data on thermal maturity. Palaeo temperature values in column 10 were derived from the measured thermal maturity data (VR_r values in column 9) and calculated after Barker & Pawlewicz (1986). The last columns (11; central age and 12; mean track length) summarise data from the apatite fission track analyses. Errors correspond to 1σ values. For further explanations refer to the text.

* impregnated samples; measured VR_r values corrected according to Jacob (1989)

** number of measurements too low, poor statistic significance

*** samples failed χ²-tests

1	2	3	4	5	6	7	8	9	10	11	12	13	14	15	16
L. no.	S. no.	Elev. [m]	UTM coordinates X Y	Area	Stratigraphy	D. age [Ma]	Lith.	U (std) [ppm]	n	Sp. tracks P _s N _s	Ind. tracks ρ _i N _i	χ ² [%]	age ± 1σ [Ma]	C. t.	M. l. (std) [μm]
10	AE 11	1400	685219 5137373	BB	Alesina Volcanic Complex	276-267 ¹	Qtzporph.	19±5	20	13.599 1339/19.246	1895	96	154.2±7.8	133	12.0±1.3
11	AE 12	1450	685679 5137483	BB	Alesina Volcanic Complex	276-267 ¹	Qtzporph.	18±6	21	12.041 1262/17.737	1859	91	148.2±7.5	134	11.9±1.4
12	AE 14	1275	695807 5145764	ROS	Alesina Volcanic Complex	276-267 ¹	Qtzporph.	17±5	20	6.144 555/16.584	1498	0	84.2±12.7*	26	10.6±1.5
13	AE 18	1450	697212 5146488	ROS	Alesina Volcanic Complex	276-267 ¹	Qtzporph.	40±17	20	30.392 2549/40.026	3357	98	165.6±7.3	62	9.8±1.6
14	AE 10	2160	701149 5144079	ROS	Werfen Fm (Gastropodenoolith Mbr)	250.6-250 ²	Sst.	39±27	31	12.423 747/42.523	2557	0	74.7±8.1*	82	10.8±1.9

Table 5.3 Description of samples for apatite fission track analysis and summary of FT-data. Column 1: sample locations are given by location numbers. Column 2: S. no.: sample number. Column 3: Elev.: elevation of sample location. Column 4: geographic position of the samples corresponding to the system in Plate 5.1. Column 5: Area code of the samples for quick orientation (BB; Bletterbach area; ROS; Rosengarten area). Column 7: D. age: depositional age; 276-267¹: Barth et al. (1994); 250.6-250²: this study. Column 8: Lith.: lithology (Qtzporph.: quartz porphyry; Sst.: sandstone). Column 9: Uranium content of the samples in ppm (ng/g). Column 10: n = number of counted apatite grains. Column 11: r_s = density of spontaneous tracks (x10⁵/cm²) and N_s = number of spontaneous tracks. Column 12: ρ_i = density of induced tracks (x10⁵/cm²) and N_i = number of induced tracks; N_d = 14348 tracks counted on CN-5. Column 13: χ² [%] probabilities of greater values (0: failed). Column 14: ages (154.2±7.8) are calculated as pooled ages using a ζ-value of 349±12a/cm². Ages of two samples, which failed χ²-test were calculated as central ages (74.7±8.1*); see also Fig. 5.8. Column 14: Number of counted tracks; samples with more than 50 measured confined tracks were used for thermal modelling. Column 16: M. l.: mean track length.

model for progradational geometries – the so-called Ladinian model *sensu* Bosellini (1984; see also Seeling et al. this volume). Indeed, the panoramic view of the western side of Rosengarten (see Plate 5.2.1) shows the famous transect where an initial phase of aggradation and/or slow progradation from the upper *Reitzi*- until the *Sedensis*-biozone is followed by rapid progradation during *Curionii*-, *Gredleri*- and *Archelaus*-times (see Plate 5.2.1). At least one other locality – the area around Gran Cront (see Plate 5.1 for location and Plate 5.3 for a panoramic view) – displays completely different sedimentological characteristics. Here, the initial aggradational phase of the *Reitzi*-zone from the western side of Rosengarten is represented by a stage with retrogradation. The platform interior of time (A) – the centre of the lagoon being located in front of Gran Cront (see also Fig. 4b in Maurer 1999) – steps back to the platform interior of time (B). Slope-facies of this stage of platform (B) evolution shows erosional contacts to the lagoonal facies of (A). Slope clinofolds of platform (B) dip to either sides of the platform interior. From stage (B) to stage (C) the platform top is prograding continuously towards the basin. The contact between lagoonal strata of time (C) and coeval slope possibly displays erosional features to the SE of the pictured area indicating margin collapse (below the summit of Gran Cront in Plate 5.3). The area to the NW of Gran Cront (lefthandside in Plate 5.3) is characterised by two sets of clinofolds interfingering with each other – one dipping from stage (B) and (C) towards the basin (slope-facies 1) and another one (slope-facies 2) dipping from the NW towards the platform (B). Whereas the slope-facies 1 undoubtedly belongs to platform (B), the position of the much younger platform interior with slope-facies 2 remains unclear. The most likely source for these progradational clinofolds is the area around the Torri del Vajolet (see Plate 5.1 and Plate 5.2.1) separated from Gran Cront by a major fault. However, it is obvious that parts of the Rosengarten platform like at

Gran Cront showed backstepping characteristics – from time (A) to time (B) – when other parts like the modelled transect of the western side of the Rosengarten displayed aggradation (*Reitzi*-zone in Plate 5.2.1). Furthermore, these backstepping parts of the platform have later been buried by rapidly prograding slope deposits (cf. Plate 5.2.1). Hence the subsidence pattern modelled from the transect in Plate 5.2.1 is valid only for this exposition, other areas of the platform may contemporaneously reveal other sub-sidence/accommodation changes.

5.4.2 Latemar

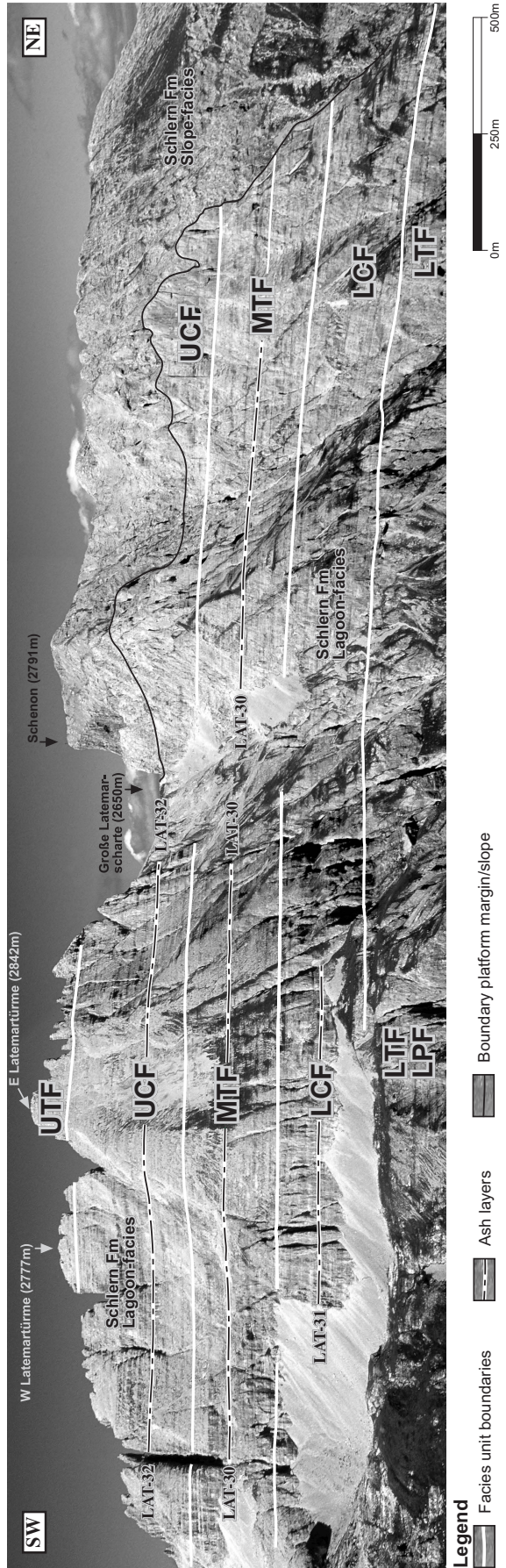
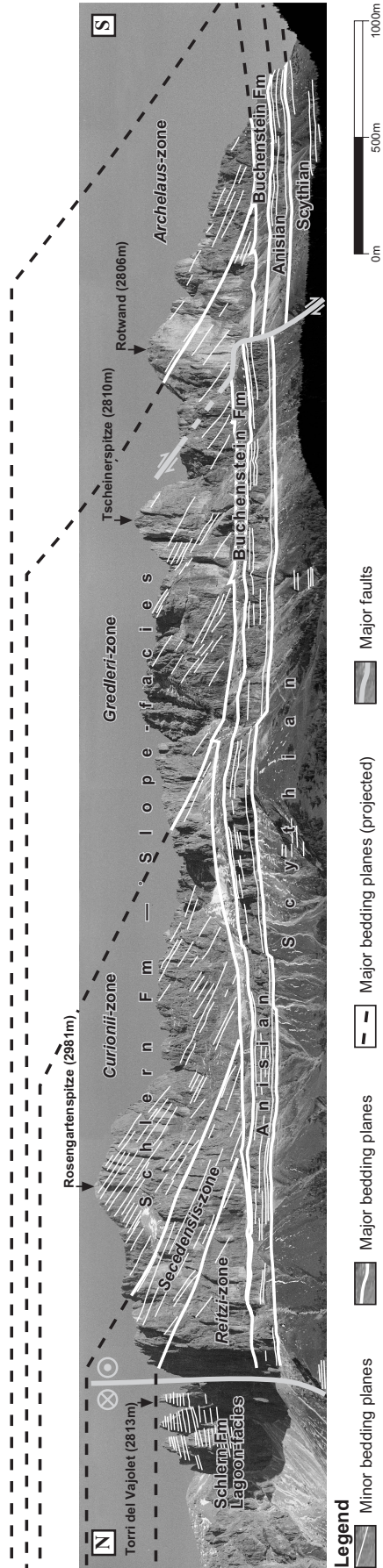
According to Gaetani et al. (1981) the Latemar represents an isolated shallow-marine carbonate platform with a diameter of the platform top ranging from 2.5 to 3.0km. The platform architecture is described in Part 2 and Part 3; thus only a short summary is given in the following text. The preserved lagoon-facies of the Latemar buildup is time-equivalent to the first two biozones recorded in the Rosengarten transect (see Fig. 5.4); a later platform development at Latemar cannot be inferred by the lagoonal interior. Youngest slope deposits are located in the SE where they are covered by volcanics, but the exact biostratigraphic age of this platform slope is unclear and a possible lag between platform growth and extrusion of the volcanics cannot be assessed.

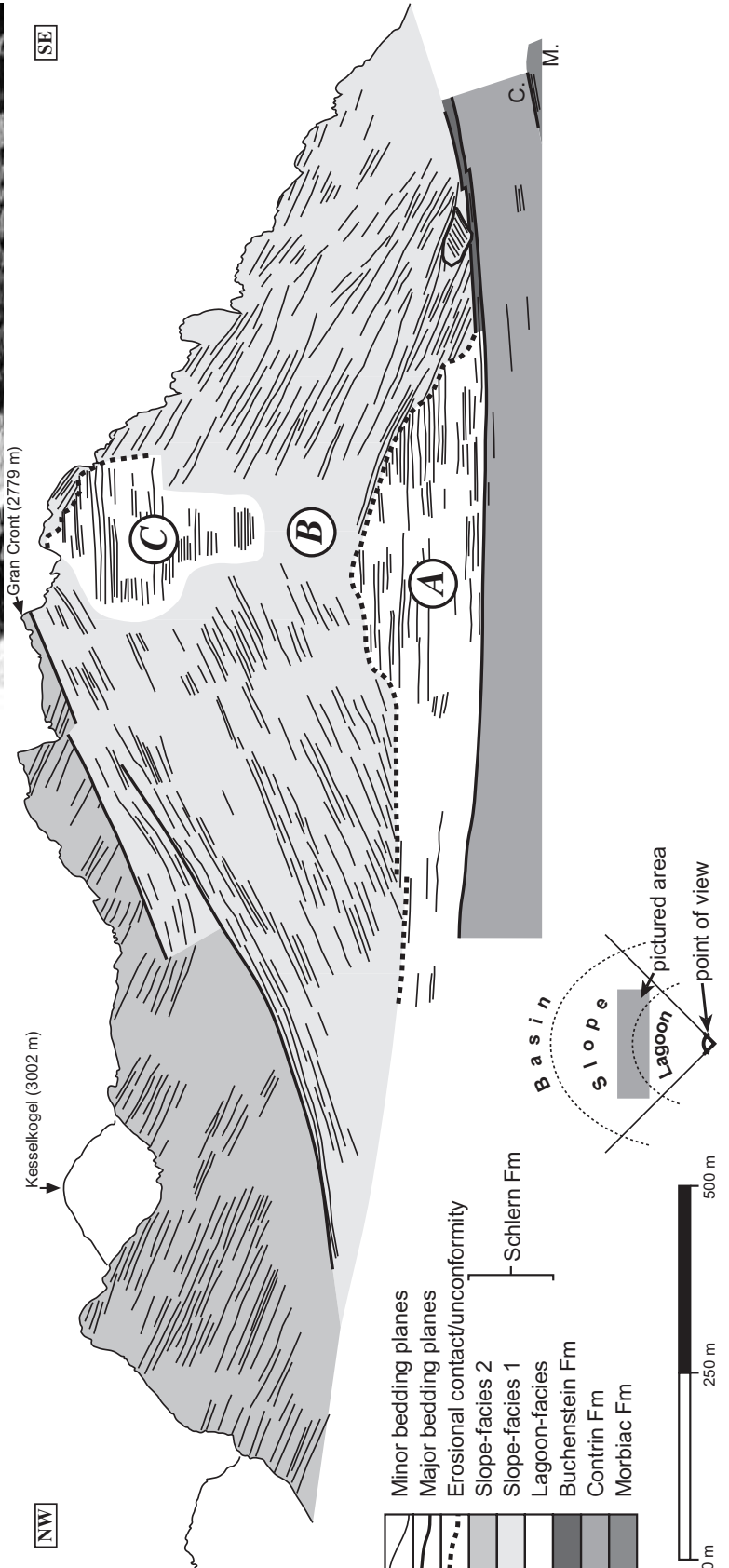
At Latemar, the presence of different coeval platform characteristics with respect to exposition is much more evident than at Rosengarten. Compared to Rosengarten, at Latemar only the first aggradational phase of platform development seems to be preserved (see Fig. 5.4). There are no indications for a later progradational development of the platform. In contrast, our group of authors reports local backstepping of the margin during later stages of platform evolution (Emmerich 2001; Knopp 2002; Part 2) associated with the export of megabreccias to basinal settings.

Plate 5.2 (following page) The modelled transects of Rosengarten and Latemar.

5.2.1: The Rosengarten platform viewed from the west with an interpretation of stratal lines, clinofolds and restored geometries above present day topography (after Bosellini and Stefani 1991; Maurer 1999, 2000). Correlation of carbonate slope deposits with biozones of the basinal Buchenstein Fm according to Maurer (1999, 2000). The transect is tectonically undisturbed, major faults are present at the platform interior only (“Torri del Vajolet”). Legend in the lower part.

5.2.2: The Latemar viewed from the SE with an interpretation of stratal lines, ash layers and facies boundaries (after Zühlke 2004; LPF: Lower Platform Facies; LTF: Lower Tepee Facies; LCF: Lower Cyclic Facies; MTF: Middle Tepee Facies; UCF: Upper Cyclic Facies; UTF: Upper Tepee Facies). Ash layers in the lagoon are marked with a dashed line.





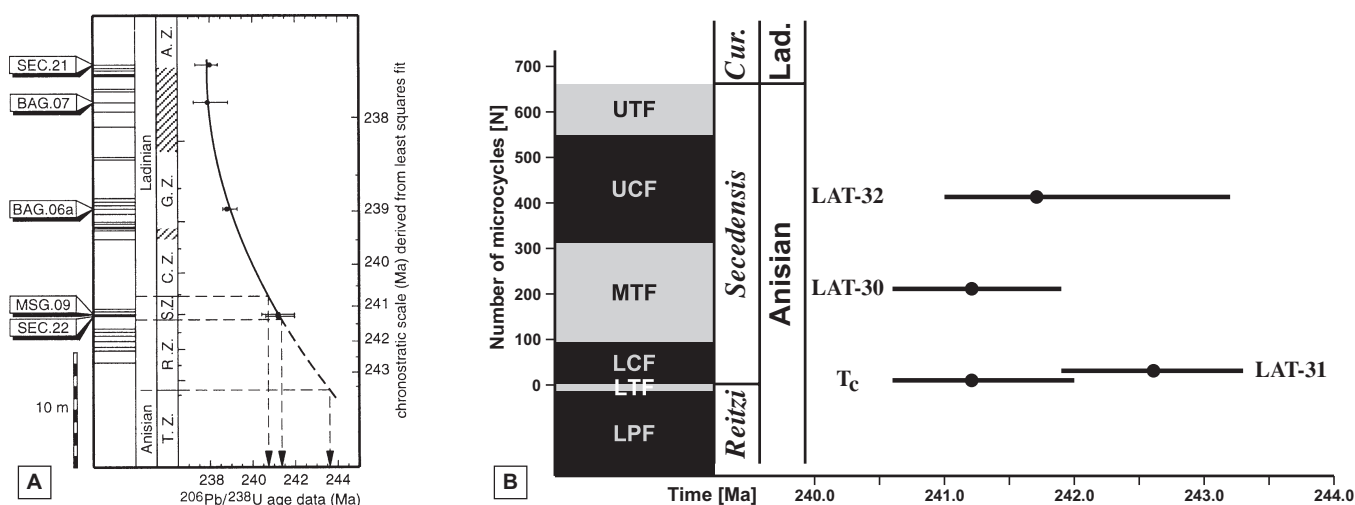


Fig. 5.5 Timescale of the Anisian/Ladinian platform evolution used in this study. For further explanations refer to the text.

5.5A Second-order least-squares fit of age data for the Buchenstein Fm from Mundil et al. (1996; for original figure refer to erratum to Mundil et al. (1996) in EPSL, 143 (1996), p.275). Arrows mark dated volcanic ash-layers within the Buchenstein Fm with corresponding numeric ages. The uppermost age and the lowermost age (SEC.21 and SEC.22) are from the same locality (Seceda) and embrace three biozones, error intervals do not overlap. Abbreviations: MSG: Monte San Giorgio, Lombardic Alps; BAG: Bagolino, Lombardic Alps; SEC: Seceda, Dolomites; T.Z.: *Trinodosus*-zone; R.Z.: *Reitzi*-zone, S.Z.: *Secedensis*-zone; C.Z.: *Curionii*-zone; G.Z.: *Gredleri*-zone; A.Z.: *Archelaus*-zone.

5.5B Correlation of radiometric ages from dated ash horizons with the cyclic succession at Latemar and with the *Secedensis*-zone of Mundil et al. (1996). x-axis is time in Ma, y-axis number of microcycles (averaged from all sections in Zühlke et al. 2003; Zühlke 2004). Stratigraphic column to the left illustrates the lagoonal succession at Latemar (abbreviations after Egenhoff et al. 1999; see also Fig. 5.4). Biozones and position of the Anisian/Ladinian boundary after Brack & Rieber (1993, 1994; abbreviations: Cur.: *Curionii*-biozone; Lad.: Ladinian). The position of ash layers LAT-30 to LAT-32 within the cyclic succession was determined by counting of microcycles.

5.5 Timescale of platform evolution

The challenge of the comparison between these two carbonate platforms was the integration of two different timescales used at both locations (see Figs. 5.5A and 5.5B). At Rosengarten the timing of platform progradation is assessed by tephra-chronologic dating, i.e. the correlation of dated ash layers from basinal settings into the slope, and biostratigraphic constraints (ammonoids, conodonts, pelicycypods). This was realised by Maurer (1999, 2000) who laterally traced basin-wide volcanic marker horizons (previously dated by Mundil et al. 1996, see Fig. 5.5a) and correlated biozones of the Buchenstein Fm (sensu Brack & Rieber 1993, 1994) into the slope of

the Schlern Fm. At Latemar however, timing of evolution of the buildup can be directly assessed from the lagoonal interior avoiding the uncertainties of lateral correlation with basinal strata. Three ash layers were dated by Mundil et al. (2003; see Plate 5.2.2 and Fig. 5.5B) and used by Zühlke et al. (2003) to perform time series analyses on the cyclic succession of the platform. A problem for the integration/correlation of the two time scales – Mundil et al. (1996) vs. Mundil et al. (2003) – might be the fact that they were determined with two different methods. An attempt to reconcile the two time scales is made in Fig. 5.5B. In the Buchenstein Fm, the T_c-tuff marks the beginning of the *Secedensis*-biozone

Plate 5.3 (previous page) Panoramic view of the Gran Cront area (see Plate 5.1) with a sedimentological interpretation. Legend to the lower left. Abbreviations in the lower right: M.: Morbiac Fm; C.: Contrin Fm. Letters (A) to (C) correspond to three different stages of platform evolution. The centre of the Rosengarten lagoon is in front of the pictured area, i.e. slope clinofolds are dipping away from the spectator (see also Fig. 4b in Maurer 1999). The platform interior of time (A) is backstepping towards time (B). Platform (A) shows an erosional contact to clinofolds (slope-facies 1) of platform (B). The lagoonal interior of time (B) is prograding to a more distal position of time (C). Eventually the platform of time (C) is subsequently buried by a rapidly prograding slope from the NW (slope-facies 2).

(Brack & Rieber, 1993) and was dated by Mundil et al. (1996). The boundary between Reitzi- and Secedensis-zone is located within a narrow interval – max. 20 microcycles – at the transition from LTF to LCF based on ammonoid biostratigraphy (Zühlke et al. 2003; Zühlke 2004), therefore the age of $241.2 \pm 0.8 / -0.6$ Ma was placed at the base of the LCF (see Fig. 5.5B). Ash layers LAT-31 and LAT-32 (Mundil et al. 2003) embrace less than one biozone, all ages show considerable overlap of error intervals, i.e. the time interval bracketed by LAT-31 and LAT-32 is shorter than or equal to individual error intervals. However, it is evident that the age of the T_c -tuff of Mundil et al. (1996) is in accordance with the radiometric ages from Latemar lagoon within the given error intervals (see also Mundil et al. 2003).

Zühlke et al. (2003) attribute a duration of \varnothing 1.88 Ma to max. <4.1 Ma to the entire cyclic succession at Latemar. Based on spectral analyses results and a statistical/mathematical goal seek routine for Milankovitch-cyclicities in larger-order cycle stacking patterns, the most probable microcycle period was proposed to be 4.2 ka. However, this result is not in accordance with the timescale set up for the Buchenstein Fm by Mundil et al. (1996) used at Rosengarten. Mundil et al. (1996) proposed a most likely duration of 0.6 Ma for the *Secedensis*-zone by 2nd order least-squares fit of age data to the Buchenstein succession (see Fig. 5.5A). If the age of the base of the *Secedensis*-zone from Mundil et al. (1996) is acknowledged as datum ($241.2 \pm 0.8 / -0.8$ Ma; see Fig. 5b), the average number of microcycles – 660 for the entire cyclic succession (averaged from all logs of Zühlke et al. 2003) – multiplied by the proposed microcycle duration of 4.2 ka would require a topmost age of the *Secedensis*-zone of 238.2 Ma. This projected top would then lie within the *Gredleri*-zone of Mundil et al. (1996) which is constrained by ash layers at the bottom and top ($238.8 \pm 0.5 / -0.2$ Ma and $238.0 \pm 0.4 / -0.7$ Ma respectively). No time would then be left to accommodate the entire *Curionii*-zone. It therefore seems appropriate to calculate a possible duration of the microcycles at Latemar on the base of the timescale of Mundil et al. (1996) rather than on the linear regression between LAT-31 and LAT-32 by Mundil et al. (2003) or the time series analysis of Zühlke et al. (2003). With the calculated time interval of Mundil et al. (1996) for the *Secedensis*-zone (0.6 Ma; see above), the duration of one microcycle of the cyclic succession – comprising of approx. 660 microcycles – at Latemar would be 0.9 ka. If maximum error intervals of

the *Secedensis*-zone (age at base: 242.0 Ma; age at top: 240.7 Ma) are considered, the duration would be 1.97 ka for one microcycle. A microcycle duration between 0.9 ka and 1.97 ka is in accordance with observations on palaeo climate change which reveal a 1.5 ka cyclicality of high precision (e.g. Bond et al. 1997, 2001; Niggemann et al. 2003; Rahmstorf 2003). This sub-Milankovitch cyclicality is attributed to solar irradiation variations causing rhythmic changes in surface hydrography of the oceans as well as possibly deep ocean circulation (Bond et al. 1997, 2001), changes in palaeo humidity (Niggemann et al. 2003) and triggering Dansgaard-Oeschger events (Rahmstorf 2003).

In summary, the maximum microcycle duration of 1.97 ka is in accordance with (1) the timescale of Mundil et al. (1996), (2) radiometric ages from the Latemar (Mundil et al. 2003) and (3) with observations on short-term climate change (e.g. Bond et al. 1997, 2001; Niggemann et al. 2003; Rahmstorf 2003). However, a possible source of uncertainties is the correlation of biozones from lagoonal (Latemar) to basinal (*Seceda*) settings. Furthermore, a maximum microcycle duration of less than 1.97 ka is not in accordance with the spectral analysis of Zühlke et al. (2003) and the identification of typical Milankovitch-periods in certain frequencies of the spectral analysis. Yet, a shorter duration of the microcycles cannot be excluded, further spectral analyses and age datings will be necessary to narrow down these uncertainties. In the following, both time scales of platform evolution are presented.

5.6 Integrated subsidence histories

Results of the modelled subsidence histories were extracted from the lagoonal interior for two reasons: (1) Subsidence patterns from the slope may differ locally whereas subsidence trends of the lagoonal interior are more uniformly distributed. (2) If the subsidence rates at the lagoonal interior are translated into net carbonate accumulation rates, these values reflect the minimum amount of accumulated sediment. In order to assess the later thermal evolution of the platforms, thermal maturity within underlying strata was compiled from literature (sandstones of the Gröden Fm and bituminous limestones of the Bellerophon Fm; see Table 5.1). Furthermore, fission-tracks in apatites from underlying strata (ignimbrites of AVC and sandstones of Werfen Fm; see Table 5.1) were used to determine the timing of heating and cooling. The integration of these datasets enabled a

fairly precise reconstruction of burial history scenarios of the area. Figs. 5.6A and 5.6B show only the details of platform evolution, the older simulated subsidence trends (e.g. Gröden Fm, Bellerophon Fm) were omitted for clarity. Two versions of subsidence trends were calculated: model (A) with the timescale proposed in Table 5.1 corresponding to a microcycle duration at Latemar of 1.97ka (Fig. 5.6A) and model (B) with another dataset corresponding to a timescale taken from Zühlke et al. (2003) optimised for a microcycle duration of 4.2ka (Fig. 5.6B). The main difference between the two models is the longer duration of the *Secedensis*-zone (see chapter 5.5 and Fig. 5.6B). In model (B) the base of the *Secedensis*-zone had to be shifted to older ages in order to correspond to the time-series analysis of Zühlke et al. (2003). Therefore the lower boundary of the *Secedensis*-zone in model (B) does not correspond to the timescale of Mundil et al. (1996). The base of the *Gredleri*- and *Archelaus*-zone had consequently to be shifted to younger ages in order to provide sufficient time for the *Curionii*-zone (within the error intervals of the timescale of Mundil et al. 1996; see age assignments at the x-axis of Figs. 5.6A and 5.6B). However, the relative timing of pre-platform and post-*Gredleri*-zone strata is not affected by the two versions. In model (A) and (B) and both transects (LAT & ROS), sedimentation began after the Anisian unconformity again with the Richthofen Fm, characterised by conglomerates and coarse-grained sandstones. The subsequent increase in total subsidence at both transects (LAT & ROS) indicates the flooding of subaerial highs and development of local basins filled with the marly, slightly bituminous Morbiac Fm. The formation of the Contrin ramp is witnessed by a decrease in subsidence from approx. 200m/Ma to values of around 100m/Ma. As mentioned before, synsedimentary tectonics dismembered the Contrin ramp and the nucleation of Schlern Fm platforms began.

5.6.1 Rosengarten

5.6.1.1 Subsidence history

Model (A) — The regionally observed drop in subsidence at the verge of the Anisian (Rüffer & Zühlke 1995; Zühlke 2000), left only some structural highs where shallow-marine carbonate deposition could develop. The other areas are marked by a drowning unconformity where deep marine, basal sediments (Buchenstein Fm) directly overlie the shallow marine Contrin ramp carbonates. This drop in subsidence is recorded at Rosen-

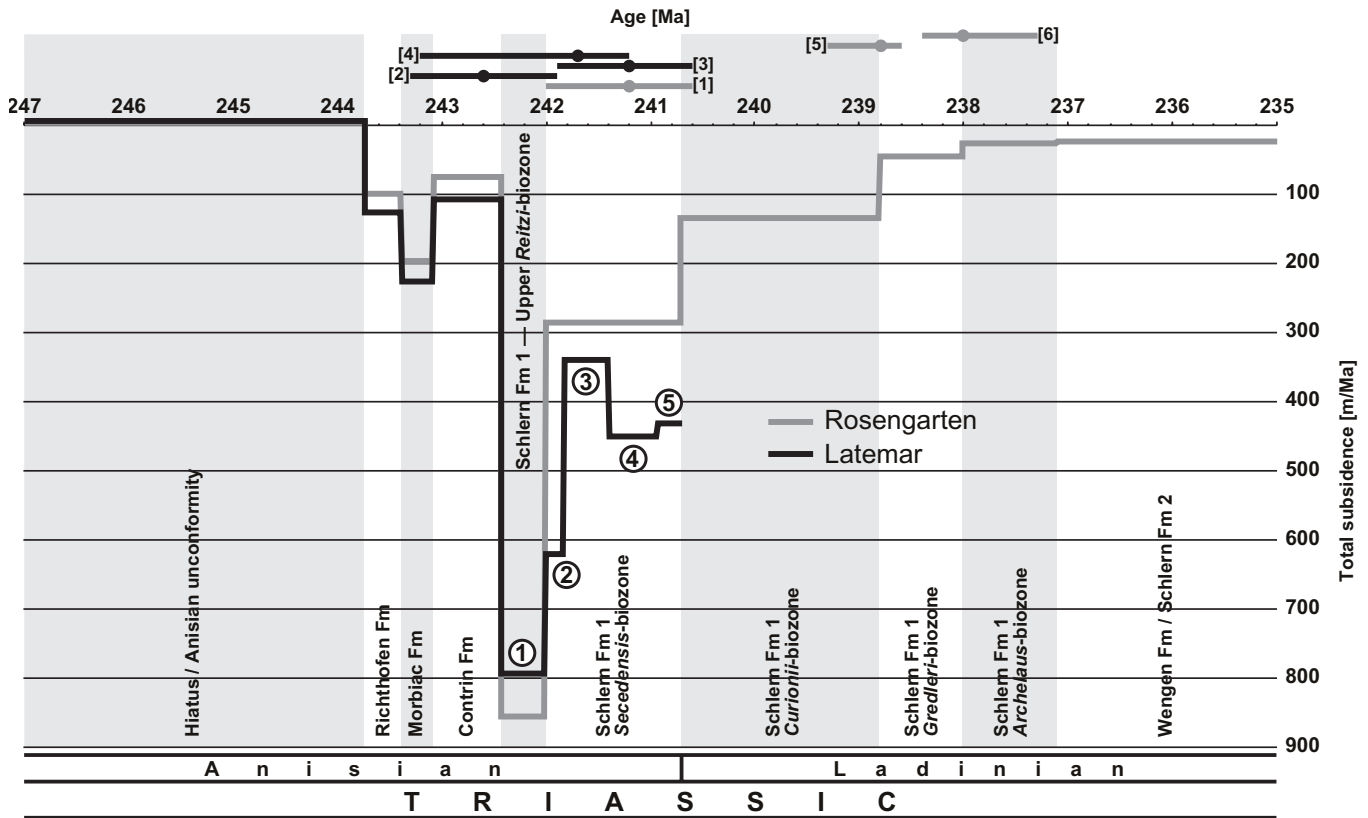
garten by an interval with high – up to 850m/Ma – subsidence in the simulation (*Reitzi*-biozone in Fig. 5.6A) and aggradational geometries in the field (see Plate 5.2.1). During the *Secedensis*-biozone, subsidence decreased significantly to approx. 290m/Ma and slight progradation began. The second stage of platform development with fast progradation was initiated when subsidence in the *Curionii*-biozone decreased even further to values of 130m/Ma. This fast progradation continued until the end of platform evolution as derived from a correlation with the neighbouring Schlern platform (see chapter 5.4.1). At the end of the *Archelaus*-zone, the Rosengarten must have been subaerially exposed and/or covered with Wengen Fm volcanics (cf. Yose 1991).

Model (B) — With the dataset proposed by Zühlke et al. (2003), the subsidence pattern during Schlern times changes significantly. The duration of the *Secedensis*-zone is doubled with respect to model (A), hence the total subsidence rate of this interval is lower than in model (A). Furthermore, the lower boundary of the *Curionii*-zone was shifted to younger ages and consequently subsidence rates increased within this zone with respect to model (A). The subsidence development from the *Secedensis*- to the *Curionii*-zone is reversed, model (B) records an increase in total subsidence from the *Secedensis*- to the *Curionii*-zone. However, as rapid fast progradation from *Curionii*-zone onwards is observed (Maurer 1999, 2000; see Plate 5.2.1), this subsidence pattern would indicate that total subsidence is not the only factor responsible for the rapidly prograding platform margin.

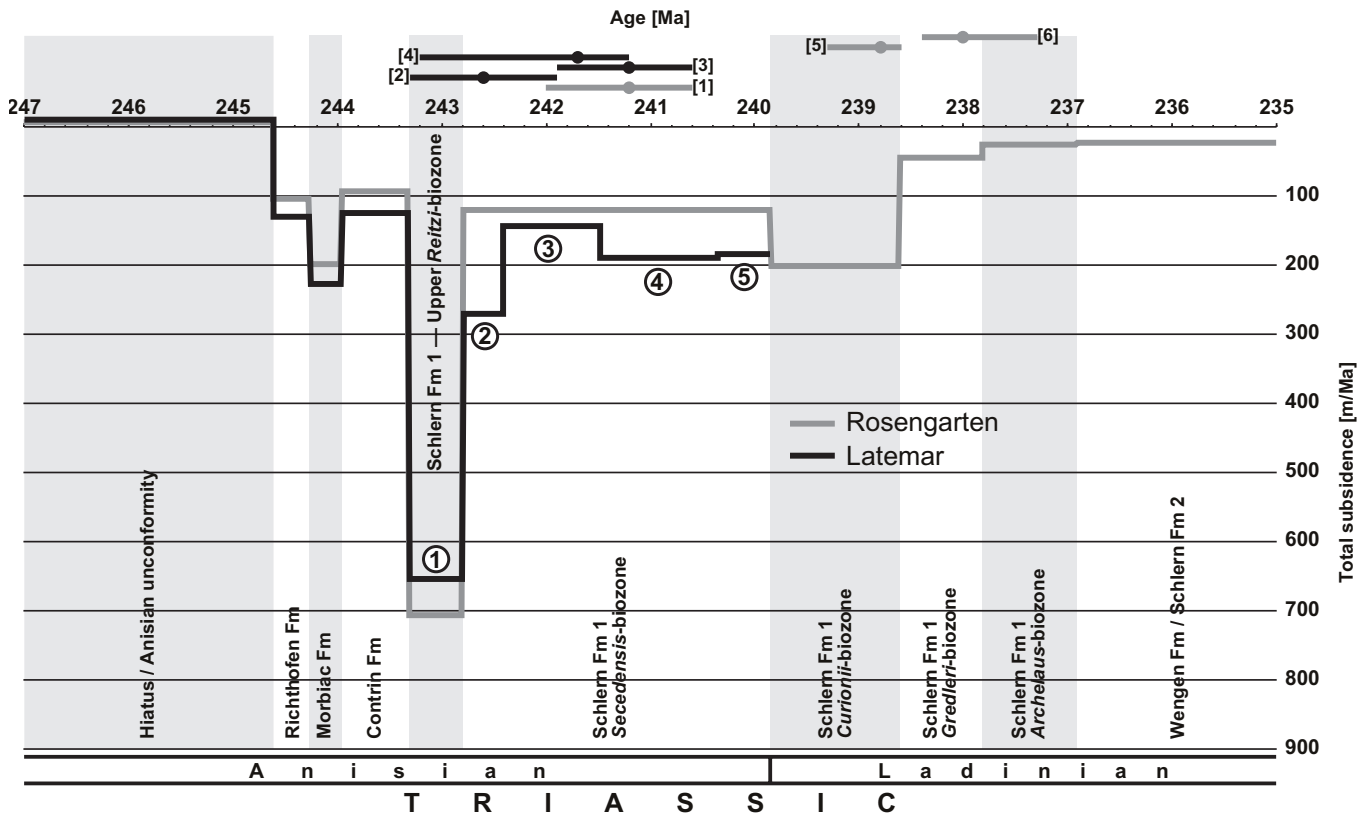
5.6.1.2 t-T history

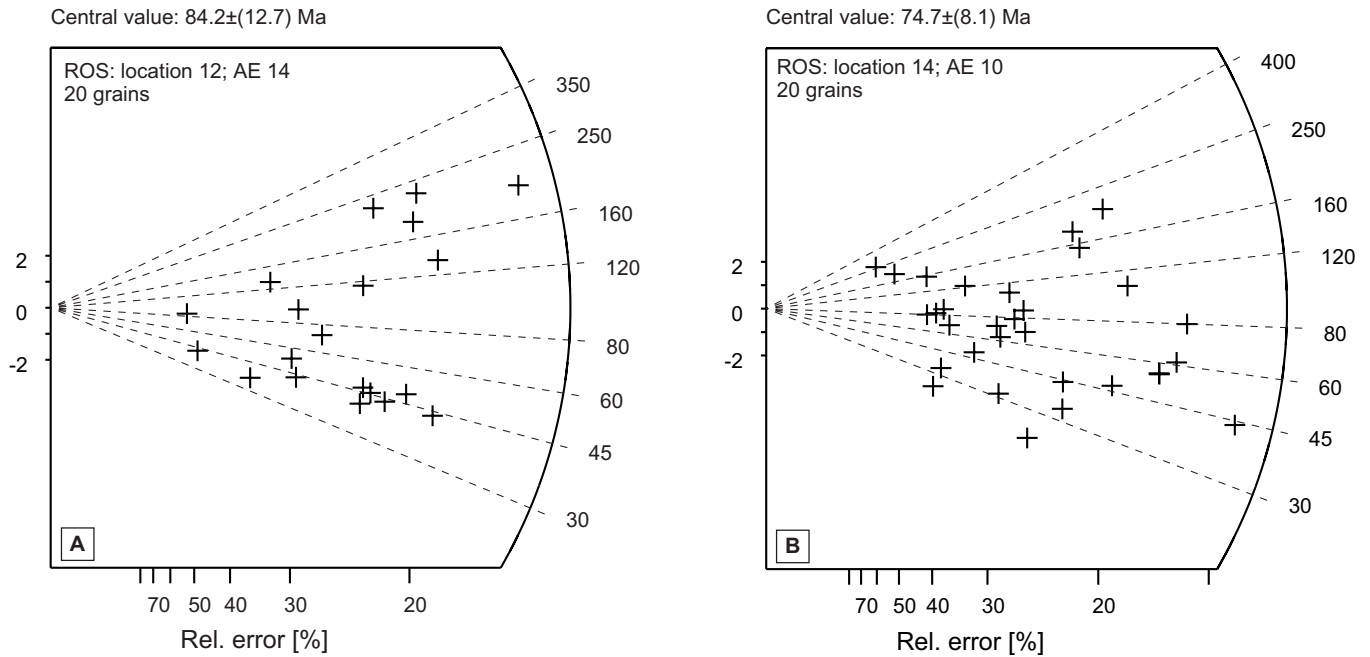
In the Rosengarten area, only one (location 13) of the two Permian quartzporphyry samples revealed a pooled apatite fission-track age of 165.6 ± 7.3 Ma (see Tab. 5.3). The second one (location 12) shows a broad single grain age distribution ranging from 226 ± 45 Ma to 36 ± 13 Ma with a central age of 84.2 ± 12.7 Ma (see Table 5.3 and Fig. 5.7A). Similarly, the apatite grains of a Triassic sandstone of the Werfen Formation (location 14) exhibit a broad single grain age pattern between 260 ± 158 and 22 ± 6 Ma with a central age of 74.7 ± 8.1 Ma (see Table 5.3 and Fig. 5.7B). In both samples, apatite grains with the oldest ages show larger etch pits and track etch channels relative to apatite grains with the youngest ages. As discussed by Donelick (1993), Burtner et al. (1994) and Barbarand et al. (2002), the etch pit size at constant etch-

Subsidence development – 1.97ka per microcycle



Subsidence development – 4.2ka per microcycle





Figs. 5.7 Radial plots displaying apatite FT single grain ages of samples from the Rosengarten having failed the χ^2 -tests. Values to the right are ages in Ma; values to the bottom errors in percent.
7A (left): Location 12; **7B** (right): Location 14 (see also Plate 5.1).

ing conditions is related to the chemical composition of the apatites, especially to their chlorine content. Chlorine-rich apatite grains reveal larger etch pits than fluorine-rich grains (small etch pits). Green et al. (1985, 1986) demonstrated that apatite fission-track ages in the Otway Basin sediments (Australia) could be correlated with the chlorine content. It was observed that for the same thermal history chlorine-rich apatites grains show less annealing of the confined fission tracks than fluorine-rich apatite grains. Therefore, the difference in single grain

ages in samples from the Rosengarten area can be explained by the difference in chemical composition. The mean confined track length in apatite is short, ranging from $9.8 \pm 1.6 \mu\text{m}$ in the Permian quartzporphyry sample to $10.8 \pm 1.9 \mu\text{m}$ in the Triassic Werfen Fm.

The confined track length distribution together with the fission track age of apatite of the Permian quartzporphyry sample (AVC; location 13) was taken to model the individual thermal history (Fig. 5.8A). The AVC formed between 276 and 267 Ma (D'Amico & Del Moro 1988;

Figs. 5.6 (previous page) Calculated total subsidence development of Rosengarten and Latemar platforms until the extrusion of Wengen Fm volcanics after the *Archelaus*-biozone (for stratigraphy see Fig. 5.4). The depicted total subsidence development is extracted from a virtual 1D-well in the lagoonal interior (i.e. proximal position) where subsidence changes reached maximums. x-axis: time in Ma; y-axis: subsidence rates in m/Ma. Timescale after Lehrmann et al. (2002), Mundil et al. (1996, 2001, 2003) and stages after Brack and Rieber (1993, 1994). Chronostratigraphic ages of tuff layers within the Buchenstein Fm are shown above the x-axis. Dark grey colours correspond to ash layers correlated into the Rosengarten slope (see Maurer 1999, 2000), black colours to ash layers from the lagoon-facies of Latemar (see Mundil et al. 2003). Index: [1]: Tc-tuff from Mundil et al. (1996); [2]: LAT-31 from Mundil et al. (2003); [3]: LAT-30 from Mundil et al. (2003); [4]: LAT-32 from Mundil et al. (2003); [5]: base of *Gredleri*-zone from Mundil et al. (1996); [6]: base of *Archelaus*-zone from Mundil et al. (1996); see also Figs. 5.5A and 5.5B. Numbers along the Latemar graph correspond to the following scheme: 1: LPF/LTF; 2: LCF; 3: MTF; 4: UCF; 5: UTF (see Egenhoff et al. 1999).

5.6A (above): Best fit subsidence development with an assumed duration of 1.97 ka per microcycle for the cyclic succession of the Latemar.

5.6B (below): Subsidence development with an assumed duration of 4.2 ka per microcycle for the cyclic succession of the Latemar resulting in a much longer duration of the *Secedensis*-biozone, which then would also be distinctly longer than the other biozones of this interval.

Barth et al. 1994). During one of the eruptions the quartzporphyry sample as part of the AVC cooled rapidly to ambient temperatures (stage 1 in Fig. 5.8A). Since 267Ma the temperature gradually increased up to about 80°C at about 155Ma (stage 2 in Fig. 5.8A). Between 155Ma and about 15Ma the area kept at a constant temperature of about 80°C (stage 3 in Fig. 5.8A). Rapid cooling to surface temperatures started from 15 Ma on due to exhumation of the area during the Alpine orogeny (cf. Bernet et al. 2001; stage 4 in Fig. 5.8A). Assuming a palaeo temperature gradient of ca. 30K/1000m, about 2000m of Meso-/Cenozoic sediments must have covered the Permian erosional unconformity.

5.6.2 Latemar

5.6.2.1 Subsidence history

Model A — At Latemar, platform development started with a similar subsidence trend from the Contrin Fm on. At both platform interiors, a similarly thick LPF-like succession comprises the first stage of platform evolution (Maurer 1999). Initial subsidence during the *Reitzi*-zone – comprising LPF/LTF and partly LCF ((1) in Figs. 5.6A and 5.6B) – of approx. 800m/Ma slightly decreased to values of 620m/Ma towards the base of the *Secedensis*-zone (LCF, (2) in Figs. 5.6A and 5.6B). The *Secedensis*-biozone itself is represented by MTF (3), UCF (4) and UTF (5). During these two time intervals, subsidence approached the values calculated from Rosengarten but was somewhat higher (330-450m/Ma). This is due to much thicker *Secedensis*-zone deposits at Latemar with respect to coeval sediments at Rosengarten (LAT: 455m, Zühlke et al. 2003; ROS: 300m, Maurer 1999, 2000). The slight differences in total subsidence between MTF, UCF and UTF are caused by accommodation changes at the platform top as illustrated by the Fischer plots in Zühlke (2004). The youngest preserved lagoonal strata at Latemar correspond to the uppermost Anisian (Zühlke et al. 2003; Zühlke 2004), unfortunately it is impossible

to assess the platform development until the *Archelaus*-zone like at Rosengarten.

Model (B) — The subsidence peak at the verge of the *Reitzi*-zone slightly lowers to 650m/Ma with respect to model (A). Owing to the longer duration of the *Secedensis*-zone, differences in total subsidence within the cyclic succession level and subsidence rates seem to approach those of the Rosengarten platform. However, ratios between Rosengarten subsidence and Latemar subsidence remain the same.

5.6.2.2 t-T history

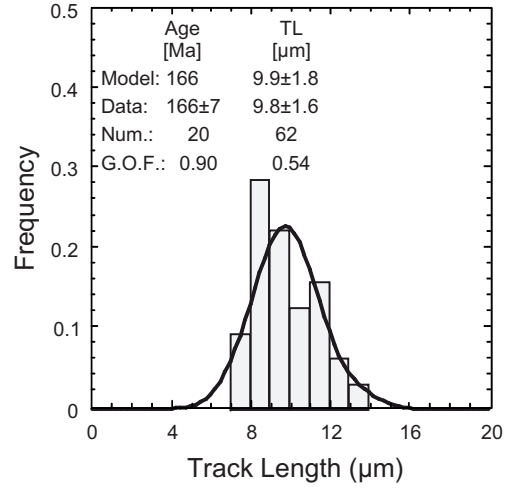
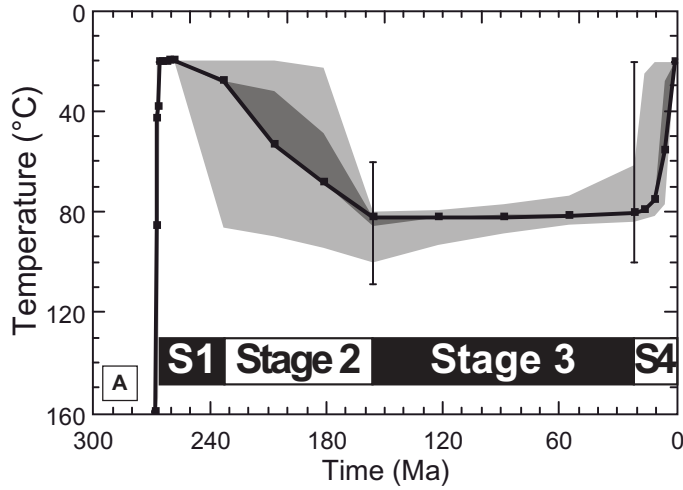
Unfortunately, samples from the immediate surroundings of the Latemar area did not reveal sufficient apatites for fission track analyses. However, as major tectonic features between the Bletterbach and the Latemar area are absent and Latemar and Rosengarten are separated by a major strike-slip fault, the thermochronologic evolution might rather be projected to the Latemar than to the Rosengarten (see Plate 5.1).

In the Bletterbach area, both Permian AVC (rhyolitic ignimbrites) samples (location 10, location 11; see Plate 5.1) revealed pooled apatite fission-track ages of 154.2 ± 7.8 Ma and 148.2 ± 7.5 Ma respectively (Tab. 5.3). The mean confined track length in apatite grains of both samples is longer ($12.0 \pm 1.3 \mu\text{m}$, $11.9 \pm 1.4 \mu\text{m}$) than in the Rosengarten area. The confined track length distribution together with the fission track age of apatite of both Permian quartzporphyry samples (location 10, location 11; see Plate 5.1) were taken to model the individual thermal history (Figs. 5.8B and 5.8C). According to D'Amico & Del Moro (1988) and Barth et al. (1994), the AVC formed between 276 and 267Ma. Similar to the evolution at Rosengarten, the quartzporphyry samples as part of the AVC cooled rapidly to ambient temperatures after the eruptions (stage 1 in Figs. 5.8B and 5.8C). Since 267Ma the temperature gradually increased up to about 110°C at around 200Ma (stage 2 in Figs. 5.8B and

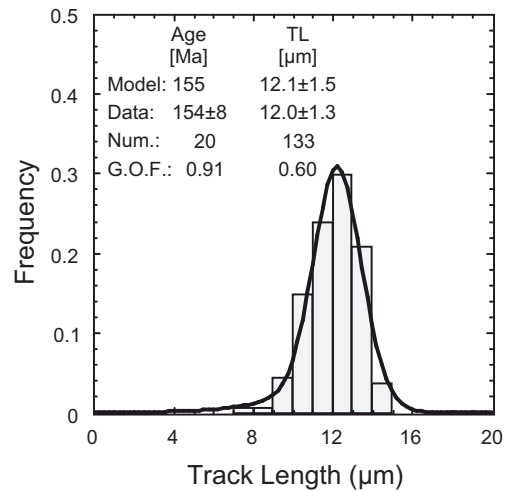
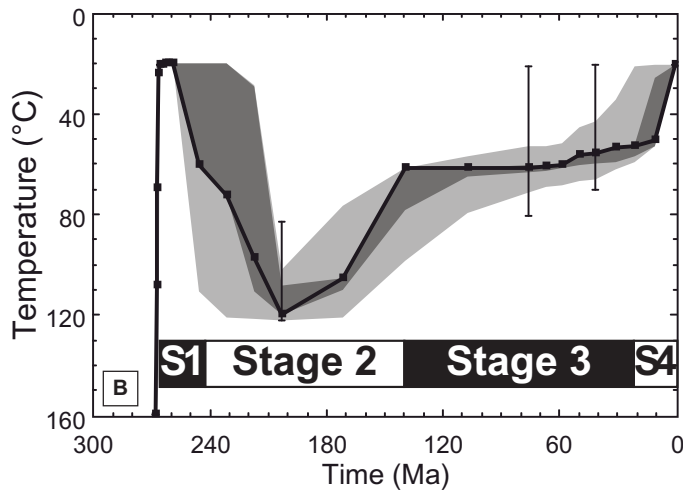
Figs. 5.8 (following page) Results of the thermal modelling with AFTSolve™, displayed in a time (X)-temperature (Y) diagram (left) and frequency distribution (right) of measured confined track length data overlain by a calculated probability density function (best fit) of samples from the Bletterbach (locations 10 and 11) and Rosengarten (location 13). Modelled results in the t-T diagram are indicated by three different reliability levels (light grey envelope: all t-T paths with a merit function value of at least 0.05, middle grey envelope: all t-T paths with a merit function value of at least 0.5, black line: best fit, Ketcham et al. 2000). Independent geological constraints are indicated by vertical brackets. S1 to S4 represent different stages of the modelled t-T path referred to in the text. Abbreviations: AVC: Atesina Volcanic Complex; model: modelled FT-age and modelled mean track length; data: measured weighted mean FT-ages and track length; num.: number of single grains and measured track length; G.O.F.: goodness of fit.

5.8A Location 13, Rosengarten area; **5.8B** Location 10, Bletterbach area; **5.8C** Location 11, Bletterbach area.

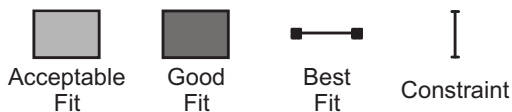
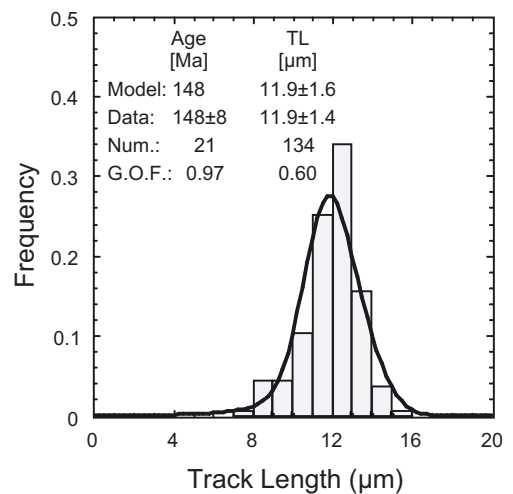
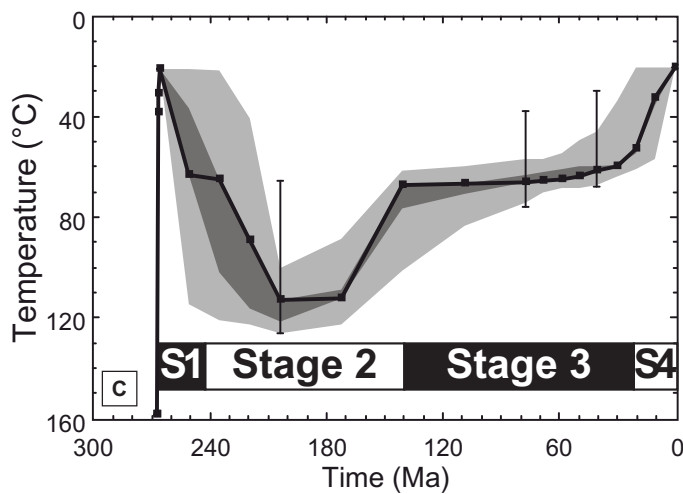
Rosengarten: Location 13; s. no. AE 18; AVC



Bletterbach: Location 10; s. no. AE 11; AVC



Bletterbach: Location 11; s. no. AE 12; AVC



Annealing model: Laslett et al. (1987), Durango

5.8C). At about 240Ma the time-temperature path seems to level for a short time period at a temperature of approx. 70°C. The temperature of about 110°C kept up to approx. 170Ma and decreased to about 70°C at around 150Ma. Up to around 15Ma the temperature kept virtually constant (stage 3 in Figs. 5.8B and 5.8C). Thereafter, rapid cooling to surface temperatures occurred due to exhumation of the area during the Alpine orogeny (cf. Bernet et al. 2001; stage 4 in Figs. 5.8B and 5.8C). In comparison to the regional geological evolution, the pulse of high temperature between 230Ma and 180Ma might be caused by a high heat flow that is related to Upper Triassic to Lower Jurassic rifting in this region. If the temperature gradient was similar to the one in the Rosengarten area, the temperature distribution of approx. 70°C for parts of the Mesozoic and Cenozoic (stage 3 in Figs. 5.8B and 5.8C) might be indicative for about 1600m of sediments.

5.7 Discussion

5.7.1 Anisian basin development

The Anisian pre-platform development in the Dolomites in general and the Rosengarten/Latemar area more specifically was discussed by e.g. Bechstädt & Brandner (1972), Bechstädt et al. (1978), Ruffer & Zühlke (1995) and Zühlke (2000), hence only the main features are summarised: (1) Anisian tectonics exposed large parts of the Dolomites subaerially and dismembered the passive continental margins into different tectonic blocks with different palaeo bathymetric settings (facies heteropy). (2) After the Anisian hiatus, a 2nd order sea level rise led to sedimentation of the Richthofen Fm on flooded subaerial highs. (3) Further sea level rise triggered subtidal to basinal sedimentation (Morbiac Fm). (4) Differential transpressive-transpressive tectonics enhanced facies heteropy – ramps (Contrin Fm) and basins developed (Moena Fm). (5) Facies heteropy initiated the growth of Schlern Fm 1 platforms and the formation of coeval deep-marine basins (Buchenstein Fm).

5.7.2 Syn-Schlern (1) basin development

With onset of Schlern Fm 1 platform growth, differential tectonics ceased in the W Dolomites and the study area experienced similar subsidence patterns despite the platforms being located on two separate structural highs possibly representing two different tectonic blocks. The subsidence peak at the verge of the *Reitzi*-zone is not only recorded in both platforms but also in other areas

of the Dolomites (Ruffer & Zühlke 1995; Zühlke 2000). The subsidence development of both platforms can be divided into two parts. In the first part of platform evolution (until the top of the *Secedensis*-zone), subsidence trends are roughly matching each other. This evolution is matched by platform architecture, where both buildups show aggradational geometries from the top of the Contrin ramp carbonates on. The second stage of platform evolution – where rapid progradation of the slope at Rosengarten occurs – is not preserved in the lagoon-facies at Latemar. Additionally, there are no indications for a progradational phase of the slope. Brack et al. (1996) report ammonoid and pelycypod findings from the E slope at Latemar corresponding to the middle to upper *Gredleri*-zone (faunas L3 and L4 in Brack et al. 1996). These faunal assemblages are however found within allochthonous fissure fills within the slope. Hence, they may not necessarily reflect true ages of deposition of the slope in which the fissures occur, a post-sedimentary influx has to be assumed. Youngest slope deposits interfinger in the eastern part with the *Secedensis*-zone of the Buchenstein Fm (see Fig. 2.11 in Part 2). Palaeontological data of the youngest slope in the E and NE of Latemar indicate an age of Anisian/Ladinian, Anisian fauna is still present in slope-facies corresponding to nowadays eroded lagoon-facies (see Part 2). It therefore can be concluded that probably all the carbonate deposits preserved today at Latemar correspond to a mainly Anisian age (sensu Brack & Rieber 1993, 1994). Due to uncertainties in the distribution and occurrence of biostratigraphically significant fossils or fossil assemblages it can however not be excluded that the youngest slope deposits preserved today correspond to the lowermost Ladinian (i.e. lowermost *Curionii*-zone).

At Rosengarten, three younger biozones of platform evolution are recorded (*Curionii*- to *Archelaus*-zone). The subsidence rates decrease during this interval lead to rapid progradation of the platform margin (see Plate 5.2.1). The main component of total subsidence in the study area is of thermo-tectonic nature. Flexural and compaction induced components are less significant. Furthermore, accommodation development at both platforms is chiefly controlled by the subsiding sediment-water-interface. The influence of sea level fluctuations could not be assessed due to the restrictions pointed out in chapter 5.3.1.

5.7.3 Post-Schlern (1) basin development

The vitrinite reflectance data compiled from literature (see Table 5.2) indicate VR_r values of around 0.6-0.8% for the Bletterbach/Latemar area and 0.5-0.7% for the Rosengarten area. These values indicate maximum burial temperatures of 100-110°C for the Bletterbach area and 90-100°C for the Rosengarten area (calculation after Barker & Pawlewicz 1986). This slight difference is reflected by the simulation of t-T paths with the help of fission tracks in apatites. The Bletterbach area reflects more elevated temperatures – approx. 30K – during an interval ranging from 230Ma to 170Ma (stage 2 in Figs. 5.8A-C), but lower temperatures – approx. 15K – during burial from the Jurassic onwards (stage 3 in Figs. 5.8A-C).

Time-temperature distribution in stage 2 (Figs. 5.8A-C) is pointing towards a higher basal heat flow during Late Triassic/Early Jurassic times. D'Amico et al. (1980), D'Amico & del Moro (1988) and Barth et al. (1993) reported reset ages from the AVC in the area of Predazzo/Monzoni (see Part 2) of 230-225Ma. This age is tied to a hydrothermal event accompanying Late Ladinian magmatism at the volcanic centre of Predazzo/Monzoni. Time-temperature distribution in stage 3 (Figs. 5.8A-C) – lower temperatures during Triassic and Jurassic times at the Bletterbach area – allows two possible explanations: (1) A shallower burial of the Bletterbach area with respect to the Rosengarten block. The amount of overburden can only crudely be estimated (2000m above AVC at Rosengarten and 1600m above AVC at Bletterbach; see chapter 5.6.1 and 5.6.2). However, the estimates from the Rosengarten area roughly correspond to previously published data (see Part 4). (2) The succession at Bletterbach experienced a lower basal heat flow from 130Ma on. The second explanation is considered as unlikely; a higher basal heat flow at Rosengarten over such a long time (130Ma until 20Ma) would surely also have affected the Bletterbach area through convection and/or conduction of heat. Higher thermal maturity values at Bletterbach indicate together with the simulated heat pulse between 230Ma and 170Ma (stage 2 Figs. 5.8A-C) that the influence of the volcanic centre at Predazzo/Monzoni was limited to its nearest vicinity and did not thermally overprint the Rosengarten platform. Another possibility for this slightly elevated thermal maturity would be a higher thermal conductivity of overlying carbonate platform bodies with respect to overlying basinal sediments (pers.

comm. R. Tscherny). Therefore one would expect lower thermal maturity underneath carbonate platforms (e.g. Rosengarten) as beneath shaly basinal deposits (Bletterbach in this case). It is however not possible to assess if the Bletterbach area was covered by basinal or platform sediments.

The chronological resolution of the simulation does not allow to rule out Jurassic rifting as the source for the elevated basal heat flow. This observation would indicate a possible position of the rift system roughly to the SW or W of the area where heat flow has been higher. Due to the proximity of the Insubric lineament to the west (see Fig. 5.2), it is impossible to reconstruct the palaeogeography west of the Adriatic plate (for a review on the Insubric lineament refer to Doglioni 1987). Further studies on thermal maturity and fission tracks in apatites are planned to model the burial history in the W Dolomites and to narrow down the uncertainties in t-T development of the platforms.

5.8 Conclusions

The integrated approach of reverse basin modelling and t-T modelling concurred to assess subsidence patterns of the Rosengarten and Latemar and adjacent areas. Existing studies underlined the importance of the Anisian tectonic development for the two blocks on which these Middle Triassic platforms are located. However, from Schlern times on the area witnessed similar subsidence patterns, differential subsidence had most probably ceased. Both platforms reveal also similar subsidence rates at the beginning of their development, but the last part of their coexistence is not preserved at Latemar. The Rosengarten displays decreasing subsidence rates towards the end of its evolution and hence progrades rapidly over basinal strata.

The time scale set up by Mundil et al. (1996) for the basinal Buchenstein Fm is marginally in accordance with the measured ages from Latemar (Mundil et al. 2003). The duration of the *Secedensis*-zone as derived from the Buchenstein Fm does not allow for a longer microcycle duration than 1.97ka. Numerical basin reverse modelling showed that subsidence patterns of the second stage of platform evolution at Rosengarten are reversed if the *Secedensis*-zone is adapted to a microcycle duration of 4.2ka. Also, this subsidence pattern would imply that this rapid progradation is not chiefly triggered by a slow-down in total subsidence. However, the *Secedensis*-zone

records mainly aggradation followed by rapid progradation from the *Curionii*-zone on. If a yet undetermined factor would have caused progradation in times with an increase in accommodation development (from *Secedensis*- to *Curionii*-zone; see Fig. 5.6B), the same or another factor must have caused aggradation/hindered progradation in times with a significant slow-down in accommodation development (from *Reitzi*- to *Secedensis*-zone; see Fig. 5.6B). This is contradictory and seems an unlikely case. Therefore, the correlation of the two time scales for Schlern Fm 1 platform development combined with subsidence modelling results points out that a maximum microcycle duration of 1.97ka or less for the cyclic succession at Latemar is a more likely scenario.

The observed subsidence pulse at verge of the *Reitzi*-zone corresponds to decompacted vertical carbonate accumulation rates of approx. 800-850m/Ma. These values surpass previous estimates on carbonate production from the Dolomites (Dürrenstein: 230-375m/Ma, Schlager et al. 1991; Rosengarten: 200m/ma, Maurer 1999, 2000). Both platforms – Latemar and Rosengarten – reached the production rates of (sub)recent carbonate platforms (Enos 1991; Schlager 2000). Thus the carbonate factory must have had completely recovered from the Permian/Triassic faunal crisis despite the pronounced “Anisian” nature (low-growing, encrusting organisms) of the respective reefal margins (see Part 2).

The detailed FT analyses in apatites confirmed existing studies on Late Ladinian hydrothermal events in the AVC (D’Amico et al. 1980; D’Amico & del Moro 1988; Barth et al. 1993) and the modelled burial history of the Rosengarten area with a long period of tectonic and sedimentary quiescence from Late Triassic onwards until uplift occurred from the Eocene/Oligocene on as proposed in Part 4.

Acknowledgements

B. Kober, A. Mangini and R. Tscherny are thanked for valuable discussions. This project has partly been financed by “Studienstiftung des deutschen Volkes”, Shell Research B.V. (Fonds: 20702/7800923/9500857) and “International Postgraduate Programme in geosciences at the University of Heidelberg” (funding A. Emmerich).

- Allen, P.A. & Allen, J.R. (1990): Basin analysis, principles and applications. Blackwell Science, London, 451pp.
- Assereto, R. & Casati, P. (1965): Revisione della Stratigrafia Permo-Triassico della Val Camonica meridionale (Lombardia). Riv. Ital. Pal. Strat., 71/4, 999-1097.
- Assereto, R.L.A.M. & Kendall, C.St.G.C. (1977): Nature, origin and classification of peritidal tepee structures and related breccias. Sedimentology, 24, 153-210.
- Balini, M., Germani, D., Nicora, A. & Rizzi, E. (2000): Ladinian/Carnian ammonoids and conodonts from the classic Schilpario-Pizzo Camino area (Lombardy): reevaluation of the biostratigraphic support to chronostratigraphy and paleogeography. Riv. Ital. Pal. Strat., 106/1, 19-58.
- Barbarand, J., Carter, A., Wood, I. & Hurford, T. (2003): Compositional and structural control of fission-track annealing in apatite. Chem. Geol., 198, 107-137.
- Barbieri, C. & Garcia-Castellanos, D. (2003): 2D and 3D subsidence analysis in a complex foreland basin: the Venetian basin (NE Italy). Analogue and numerical forward modelling of sedimentary systems. From understanding to prediction. Utrecht, 9-11 October 2003, Abstracts Volume, 11-12.
- Barker, C.E. & Pawlewicz, M.J. (1986): The correlation of vitrinite with maximum temperature in humic kerogen. In: Paleogeothermics. (Eds. Buntebarth, G. & Stegena, L.) Springer, New York, 79-93.
- Barth, S. & Mohr, B.A.R. (1994): Palynostratigraphically determined age of the Tregiovo sedimentary complex in relation to radiometric emplacement ages of the Atesina volcanic complex (Permian, Southern Alps, N Italy). N. Jb. Geol. Pal., Abh. 192/2, 273-292.
- Barth, S., Oberli, F. & Meier, M. (1994): Th-Pb versus U-Pb isotope systematics in allanite from co-genetic rhyolite and granodiorite: implications for geochronology. EPSL, 124, 149-159.
- Barth, S., Oberli, F., Meier, M., Blattner, P., Bargossi, G.M. & Di Battistini, G. (1993): The evolution of a calc-alkaline basic to silicic magma system: geochemical and Rb-Sr, Sm-Nd and $^{18}\text{O}/^{16}\text{O}$ isotopic evidence from the Late Hercynian Atesina-Cima d'Asta volcano-plutonic complex, Northern Italy. Geochim. Cosmochim. Acta, 57/4, 4285-4300.
- Bechstadt, T. & Brandner, R. (1970): Das Anis zwischen St. Vigil und dem Hohlensteintal (Prager und Olinger Dolomiten, Sudtirol). Festband Geol. Inst., 300-Jahr-Feier Univ. Innsbruck, Innsbruck, 9-103.
- Bechstadt, T., Brandner, R., Mostler, H. & Schmidt, K. (1978): Aborted rifting in the Triassic of the Eastern and Southern Alps: N. Jb. Geol. Pal., Abh., v.156, 157-178.
- Bernet, M., Zattin, M., Garver, J.I., Brandon, M.T. & Vance, J.A. (2001): Steady-state exhumation of the European Alps. Geology, 29/1, 35-38.
- Bernoulli, D. (1964): Zur Geologie des Monte Generoso (Lombardische Alpen). Beitrage zur Geologischen Karte der Schweiz, Neue Folge, Bern, 134pp.
- Bernoulli, D. (1972): North Atlantic and Mediterranean Mesozoic facies – a comparison. In: Initial reports of the Deep Sea Drilling Project, 11, 801-822.
- Berra, F. & Jadoul, F. (2002): Evidence of a “Mid-Carnian” transgression in the western Southern Alps (Lombardy, Italy): stratigraphic and paleogeographic implications. Riv. Ital. Pal. Strat., 108/1, 119-131.
- Biddle, K.T. (1981): The basinal Cipit boulders: indicators of Middle to Upper Triassic buildup margins, Dolomite Alps, Italy. Riv. Ital. Pal. Strat., 86/4, 779-794.
- Bielefeld, D. (1998): Reifebestimmungen an Kohlen des Grodner Sandsteins in Sudtirol (Norditalien). unpubl. Master’s thesis, Geol. Inst. Univ. Cologne, Germany, 87pp.
- Blendinger, W. (1985): Middle Triassic strike-slip tectonics and igneous activity of the Dolomites (Southern Alps). Tectonophysics, 113/1-2, 105-121.
- Blendinger, W. (1986): Isolated stationary carbonate platforms: the Middle Triassic (Ladinian) of the Marmolada area, Dolomites, Italy. Sedimentology, 33, 159-183.
- Blendinger, W. (2001): Triassic carbonate buildup flanks in the Dolomites, Northern Italy: breccias, boulder fabric and the importance of early diagenesis. Sedimentology, 48, 919-933.
- Bond, G., Kromer, B., Beer, J., Muscheler, R., Evans, M.N., Showers, W., Hoffmann, S., Lotti-Bond, R., Hajdas, I. & Bonani, G. (2001): Persistent solar influence on North Atlantic climate during the Holocene. Science, 294, 2130-2136.
- Bond, G., Showers, W., Cheseby, M., Lotti, R., Almasi, P., deMenocal, P., Priore, P., Cullen, H., Hajdas, I. & Bonani, G. (1997): A pervasive millennial-scale cycle in North Atlantic Holocene and glacial climates. Science, 278, 1257-1266.
- Boni, M., Iannace, A., Torre, M. & Zamparelli, V. (1994): The Ladinian-Carnian reef facies of Monte Caramolo (Calabria, Southern Italy). Facies, 30, 101-118.
- Boomer, I., Whatley, R., Bassi, D., Fugagnoli, A. & Loriga, C. (2001): An Early Jurassic oligohaline ostracod assemblage within the marine carbonate platform sequence of the Venetian Prealps, NE Italy. Palaeogeogr. Palaeoclimatol. Palaeoecol., 166, 331-344.
- Borsi, S., D’Amico, C. & Del Moro, A. (1974): Studio radiometrico delle rocce intrusive del massiccio di Cima d’Asta (Trentino). Mem. Soc. Geol. It., 13/1, 145-159.
- Borsi, S., Del Moro, A. & Ferrara, G. (1972): Eta radiometriche delle rocce intrusive del massiccio di Bressanone-Ivigna-Monte Croce (Alto Adige). Boll. Soc. It., 91/2, 387-406.
- Borsi, S. & Ferrara, G. (1967): Determinazione dell’eta delle rocce intrusive di Predazzo con i metodi del Rb/Sr e K/Ar. Miner. Petrogr. Acta, 13, 45-66.
- Borsi, S., Ferrara, G., Paganelli, L. & Simboli, G. (1968): Isotopic age measurements of the M. Monzoni intrusive complex. Miner. Petrogr. Acta, 14, 171-183.
- Borsi, S., Ferrara, G. & Tongiorgio, E. (1966): Rb/Sr and K/Ar ages of intrusive rocks of Adamello and M. Sabion (Trentino, Italy). Earth Planet. Sci. Lett., 1, 55-57.
- Bosellini, A. (1973): Modello geodinamico e paleotettonico delle Alpi Meridionali durante il Giurassico-Cretacico. Sue possibili applicazioni agli Appennini. Accademia Nazionale Lincei, Quaderno, 183, 163-205.
- Bosellini, A. (1984): Progradation geometries of carbonate platforms: examples from the Triassic of the Dolomites, north-

- ern Italy. *Sedimentology*, 31, 1-24.
- Bosellini, A. (1988): Outcrop models for seismic stratigraphy: examples from the Triassic of the Dolomites. In: *Atlas of seismic stratigraphy*, v.2. (Ed.: Bally, A.W.) AAPG Studies in Geology, n.27, 194-203.
- Bosellini, A. (1989) Dynamics of Tethyan carbonate platforms. In: *Controls on Carbonate Platform and Basin Development* (Eds.: Crevello, P.D., Wilson, J.J., Sarg, J.F. & Read, J.F.) SEPM Special Publication No. 44, 3-13.
- Bosellini, A. (1991): Geology of the Dolomites: an introduction. Dolomieu Conference on Carbonate Platforms and Dolomitization, Tourist office, St. Ulrich, Gröden, 43pp.
- Bosellini, A. & Broglio Loriga, C. (1971): I "Calcari Grigi" di Rotzo (Giurassico Inferiore, Altopiano d'Asiago) e loro inquadramento nella paleogeografia e nella evoluzione tettono-sedimentaria delle Prealpi Venete). *Annali dell'Università di Ferrara (Nuova Serie), Sezione IX Scienze Geologiche e Paleontologiche V/1*, 1-61.
- Bosellini, A., Castellarin, A., Doglioni, Guy, F., Lucchini, F., Perri, M.C., Rossi, P.L., Simboli, G. & Sommariva, E. (1982): Magmatismo e tettonica nel Trias delle Dolomiti. In: *Guida alla geologia del Sudalpino centro-orientale*. (Eds.: Castellarin, A. & Vai, G.B.) *Soc. geol. ital.*, 189-210.
- Bosellini, A., Castellarin, A., Rossi, P.L., Simboli, G. & Sommariva, E. (1977): Schema sedimentologico e stratigrafico per il Trias medio della Val di Fassa ed aree circostanti (Dolomiti Centrali). *Giornale di Geologia*, v. 42, 83-108.
- Bosellini, A. & Hardie, L.A. (1985): Facies e cicli della Dolomia Principale delle Alpi Venete. *Mem. Soc. Geol. Ital.*, 30, 245-266.
- Bosellini, A., Neri, C. & Stefani, M. (1996): Geometrie deposizionali e stratigrafia fisica a grande scala di piattaforme carbonatiche triassiche. 78a riunione estiva, Società Geologica Italiana, San Cassiano, Guidebook, 36pp.
- Bosellini, A. & Rossi, D. (1974): Triassic carbonate buildups of the Dolomites, Northern Italy. In: Laporte, L.F. (Ed.) *Reefs in time and space*. SEPM Special Publication No. 18, 209-233.
- Bosellini, A. & Stefani, M. (1991): The Rosengarten: a platform-to-basin carbonate section (Middle Triassic, Dolomites, Italy). *Dolomieu Conference on Carbonate Platforms and Dolomitization Guidebook Excursion C*, Tourist office, St. Ulrich, Gröden, 24pp.
- Bowman, S.A. & Vail, P.R. (1999): Interpreting the stratigraphy of the Baltimore Canyon section, offshore New Jersey with Phil, a stratigraphic simulator. In: *Numerical experiments in stratigraphy: recent advances in stratigraphic and sedimentologic computer simulations*. (Eds.: Harbaugh, J.W., Watney, W.L., Rankey, E.C., Slingerland, R., Goldstein, R.H. & Franseen, E.K.) SEPM Special Publication, 62, 117-138.
- Brack, P. (1984): *Geologie der Intrusiva und Rahmengesteine des Suedwest-Adamello*. Diss. ETH Nr. 7612, Zürich, 253pp.
- Brack, P., Mundil, R., Oberli, F., Meier, M. & Rieber, H. (1996): Biostratigraphic and radiometric age data question the Milankovitch characteristics of the Latemar cycles (Southern Alps, Italy). *Geology*, 24/4, 371-375.
- Brack, P., Mundil, R., Oberli, F., Meier, M. & Rieber, H. (1997): Biostratigraphic and radiometric age data question the Milankovitch characteristics of the Latemar cycles (Southern Alps, Italy). *Reply*. *Geology* 25/5, 471-472.
- Brack, P. & Muttoni, G. (2001): High-resolution magnetostratigraphic and lithostratigraphic correlation in Middle Triassic pelagic carbonates from the Dolomites (Northern Italy). *Palaeogeogr. Palaeoclimatol. Palaeoecol.*, 161, 361-380.
- Brack, P. & Rieber, H. (1993): Towards a better definition of the Anisian/Ladinian boundary: New biostratigraphical data and correlations of boundary sections from the Southern Alps. *Eclogae geologicae Helveticae*, 86/2, 415-527.
- Brack, P. & Rieber, H. (1994): The Anisian/Ladinian boundary: retrospective and new constraints. *Albertiana*, 13, 25-36.
- Brandner, R. (1991): Geological setting and stratigraphy of the Schlern-Rosengarten buildup and Seiser Alm basin. In: *The northern margin of the Schlern/Sciliar Rosengarten/Catinaccio platform* (Eds.: Brandner, R., Flügel, E., Koch, R. & Yose, L.A.) *Dolomieu Conference on Carbonate Platforms and Dolomitization, Guidebook Excursion A*, Tourist office, St. Ulrich, Gröden, 4-16.
- Brandner, R., Flügel, E. & Senowbari-Daryan, B. (1991): Microfacies of carbonate slope boulders; indicator of the source area (Middle Triassic; Mahlknecht Cliff, western Dolomites). *Facies*, 25, 279-296.
- Brandner, R. & Resch, W. (1981): Reef development in the Middle Triassic (Ladinian and Cordevolian) of the Northern Limestone Alps near Innsbruck, Austria. In: *European fossil reef models*. (Ed.: Toomey, D.F.) SEPM Spec. Publ. 30, 203-231.
- Broglio Loriga, C., Goczan, F., Haas, L., Lenner, K., Neri, C., Scheffer, A.O., Posenato, R., Szabo, I. & Makk, A.T. (1990): The Lower Triassic sequences of the Dolomites (Italy) and Transdanubian mid-mountains (Hungary) and their correlation. *Mem. Sci. Geol.*, 42, 41-103.
- Broglio Loriga, C., Masetti, C. & Neri, C. (1983): La Formazione di Werfen (Scitico) delle Dolomiti occidentali: sedimentologia e biostratigrafia. *Riv. Ital. Paleont. Strat.*, 88/4, 501-598.
- Buggisch, W. (1978): Die Grödener Schichten (Perm, Südalpen). *Sedimentologische und geochemische Untersuchungen zur Unterscheidung mariner und kontinentaler Sedimente*. *Geologische Rundschau*, 67/1, 149-180.
- Buggisch, W. & Noé, S. (1986): Upper Permian and Permian-Triassic Boundary of the Carnia (Bellerophon Formation, Tesero Horizon, Northern Italy). *Mem. Soc. Geol. Ital.*, 34, 91-106.
- Büker, C. (1996): Absenkungs-, Erosions und Wärmeflussgeschichte des Ruhr-Beckens und des nordöstlichen Rechtsrheinischen Schiefergebirges. *Berichte des Forschungszentrums Jülich Jül-3319*, 212pp.
- Burtner, R.L., Nigrini, A. & Donelick, R. A. (1994): Thermochronology of Lower Cretaceous source rocks in the Idaho-Wyoming Thrust Belt. *AAPG Bull.*, 78, 1613-1636.
- Callegari, E. & Monese, A. (1964): Il chimismo della "pietra

- verde” degli Strati di Livinallongo (Dolomiti). Contributo allo studio petrogenico della “pietra verde” ladinica. *Stud. Trent. Sci. Nat.*, 41, 45-71.
- Carrapa, B., Wijbrans, J. & Bertotti, G. (2002): Episodic exhumation in the European Western Alps. GSA Annual Meeting, October 27-30, 2002, Denver, Colorado.
- Castellarin, A., Colacicchi, R. & Pratlurion, A. (1978): Fasi distentive, trascorrenze e sovrascorrimenti lungo la Linea Ancona-Anzio, dal Lias medio al Pliocene. *Geologica Romana*, 17, 161-189.
- Castellarin, A., Lucchini, F., Rossi, P., Simboli, G., Bosellini, A. & Somnavilla, E. (1979): Middle Triassic magmatism in the Southern Alps, II.: a geodynamic model. *Riv. Ital. Pal. Strat.*, 85, 1111-1124.
- Castellarin, A. & Vai, G.B. (1982): Introduzione alla geologia strutturale del Sudalpino. In: Guida alla geologia del Sudalpino centro-orientale. (Eds.: Castellarin, A. & Vai, G.B.) *Soc. geol. ital.*, 1-22.
- Claps, M., Masetti, D., Pedrielli, F. & Lucchi Garavello, A. (1991): Analisi spettrale e cicli di Milankovitch in successioni cretache del sudalpino orientale. *Riv. Ital. Pal. Strat.*, 97/2, 153-174.
- Climaco, A., Boni, M., Iannace, A. & Zamparelli, V. (1997): Platform margins, microbial/serpulids bioconstructions and slope-to-basin sediments in the Upper Triassic of the “Verbicaro Unit” (Lucania and Calabria, Southern Italy). *Facies*, 36, 37-56.
- Condie, K.C. (1976): Plate tectonics and crustal evolution. Pergamon Press, New York, 288p.
- Coniglio, M. & Dix, G.R. (1992): Carbonate slopes. In: Facies models: response to sealevel change. (Eds.: Walker, R.G. & James, N.P.) Geological Association of Canada, *Geotext* 1, 349-373.
- Crevello, P.D. & Schlager, W. (1980): Carbonate debris sheets and turbidites, Exuma Sound, Bahamas. *Journal of Sedimentary Petrology*, 50, 1121-1148.
- Cros, P. (1966): Age Oligocène Supérieur d’un poudingue (du Monte Parei) dans les Dolomites centrales italiennes. *Compte Rendu Sommaire des Séances de la Société Géologique de France* 7, 250-252.
- Cros, P. (1979): Relation paléogéographique entre la sédimentation tufacée et les apports terrigènes, Trias moyen et supérieur des Dolomites et des Alpes Carniques. *Riv. Ital. Pal. Strat.*, 85, 953-982.
- Cros, P. & Houel, P. (1983): Repartition and paleogeographical interpretation of volcanoclastic and pelagic sediments of the Livinallongo formation (Italian Dolomites). *Geol. Paläont. Mitt. Innsbruck*, 11, 415-452.
- Cuif, J.P. (1974): Rôle des sclérosponges dans la faune récifale du Trias des Dolomites (Italie du Nord). *Geobios*, 7, 139-153.
- Czurda, K. (1972): Parameter und Prozesse der Bildung bituminöser Karbonate (Bituminöser Hauptdolomit). *Mitt. Ges. Geol. Bergbaustud. Österr.*, 21/1, 235-250.
- D’Amico, C. & Del Moro, A. (1988): Permian and Triassic Rb-Sr dating in the Permian rhyodacitic ignimbrites of Trentino (Southern Alps). *Rendiconti della Società Italiana di Mineralogia e Petrologia* 43, 171-180.
- D’Amico, C., Del Moro, A., Freddo, A. & Pardini, G. (1980): Studio radiometrico delle ignimbriti riolitiche atesine, gruppo superiore. *Rend. Soc. Ital. Miner. Petrol.*, 36/2, 703-716.
- D’Argenio, B., De Castro, P., Emiliani, C. & Simone, L. (1975): Bahamian and Apenninic limestones of identical lithofacies and age. *AAPG Bulletin*, 59/3, 524-530.
- Del Moro, A. & Visona, D. (1982): The epiplutonic Hercynian complex of Bressanone (Brixen, Eastern Alps, Italy). *Petrologic and radiometric data*. *N. Jb. Miner. Abh.*, 145, 66-85.
- Del Moro, A., Pardini, G., Quercioli, C., Villa, I.M. & Callegari, E. (1983): Rb/Sr and K/Ar chronology of Adamello granitoids, Southern Alps. *Mem. Soc. Geol. It.*, 26/1, 285-299.
- della Porta, G., Kenter, J.A.M. & Bahamonde, J.R. (submitted): Depositional facies and stratal geometry of an Upper Carboniferous prograding and aggrading high-relief carbonate platform (Cantabrian Mountains, N Spain). *Sedimentology*.
- Dercourt, J., Gaetani, M., Vrielynck, B., Barrier, E., Biju-Duval, B., Brunet, M.F., Cadet, J.P., Crasquin, S. & Sandulescu, M. (2000): Atlas Peri-Tethys, palaeogeographical maps. CCGM/CGMW, Paris, 24 maps and explanatory notes, 269pp.
- Dercourt, J., Ricou, L.E. & Vrielynck, B. (1993): Atlas Tethys paleoenvironmental maps. Gauthier-Villars, Paris, 307pp.
- De Zanche, V. (1990): A review of Triassic stratigraphy and paleogeography in the eastern Southern Alps. *Boll. Soc. Geol. Ital.*, 109, 59-71.
- De Zanche, V. & Farabegoli, E. (1988): Anisian paleogeographic evolution in the central-western Southern Alps. *Mem. Sci. Geol.*, 40, 399-411.
- De Zanche, V., Gianolla, P., Manfrin, S., Mietto, P. & Roghi, G. (1995): A Middle Triassic back-stepping carbonate platform in the Dolomites (Italy): sequence stratigraphy and biostratigraphy. *Mem. Sci Geol.*, 47, 135-155.
- Di Battistini, G., Bargossi, G.M., Spotti, G. & Toscani, L. (1988): Andesites of the Late Hercynian volcanic sequence in Trentino-Alto Adige (Northern Italy). *Rend. Soc. Ital. Miner. Petrol.*, 43, 1087-1100.
- Dickinson, W.R., Armin, R.A., Beckvar, T.C., Goodlin, S.U., Janecke, R.A., Mark, R.D., Norris, G., Radcliff, G. & Wortman, A.A. (1987): Geohistory analysis of rates of sediment accumulation and subsidence for selected California Basins. In: Cenozoic basin development of coastal California. (Eds.: V.R. Ingersoll & W.G. Ernst), 6, 1-23.
- Dickson, J.A.D. & Coleman, M.L. (1980): Changes in carbon and oxygen isotope composition during limestone diagenesis. *Sedimentology*, 27, 107-118.
- Dogliani, C. (1983): Duomo Medio-Triassico nelle Dolomiti. *Rendiconti della Società Geologica Italiana*, 6, 13-16.
- Dogliani, C. (1984): Triassic diapiric structures in the Central Dolomites. *Eclogae geologicae Helvetiae*, 77/2, 261-285.
- Dogliani, C. (1987): Tectonics of the Dolomites (Southern Alps, northern Italy). *Journ. Struct. Geol.*, 9/2, 181-193.
- Dogliani, C. & Castellarin, A. (1985): A geologic schematic cross-section of the Southern Alps. *Rend. Soc. Geol. Ital.*, 8,

- Suppl. 1, 35-36.
- Dogliani, C. & Goldhammer, R.K. (1988): Compaction-induced subsidence in the margin of a carbonate platform. *Basin Research* 1, 237-246.
- Donelick, R.A. (1993): Apatite etching characteristics versus chemical composition. *Nucl. Tracks Radiation. Meas.*, 21, 604.
- Dunkl I. (2002): Trackkey: a Windows program for calculation and graphical presentation of fission track data. *Computers & Geosciences*, 28, 3-12.
- Dunkl, I., di Giulio, A. & Kuhlemann, J. (2001): Combination of single-grain fission-track chronology and morphological analysis of detrital zircon crystals in provenance studies sources of the Macigno Formation (Apennines, Italy). *Journ. Sed. Res.*, 71/4, 516-525.
- Duval, B., Cramez, C. & Vail, P.R. (1992): Types and hierarchy of stratigraphic cycles. Sequence stratigraphy of European basins: Conference. In: *Proceedings Abstract Volume*, 18-20 May, Dijon, Centre National de la Recherche Scientifique/ Institut Français du Pétrole, Paris. 44-45.
- Egenhoff, S.O., Peterhänsel, A., Bechstäd, T., Zühlke, R. & Grötsch, J. (1999): Facies architecture of an isolated carbonate platform: tracing the cycles of the Latemar (Middle Triassic, Northern Italy). *Sedimentology*, 46, 893-912.
- Emmerich, A. (2001): Der Plattformabhang des Latemar – Fazies und geometrische Entwicklung einer mitteltriassischen Plattform. *Gaea heidelbergensis*, 9, CD-ROM.
- Emmerich, A., Knopp, S., Bechstäd, T. & Zühlke, R. (2000): Development of the margin of Middle Triassic atoll-like buildup: the Latemar, Dolomites, Italy. *Mitt. Ges. Geol. Bergbaustud. Österr.* 43, 40.
- Emmerich, A., Zamparelli, V., Zühlke, R. & Bechstäd, T. (2002): The reef of an Anisian (Middle Triassic) isolated carbonate platform: the Latemar (Dolomites, Italy). 16th International Sedimentological Congress, Abstracts Volume, Rand Afrikaans University, Johannesburg, South Africa, 437-438.
- Enos, P. (1991): Sedimentary parameters for computer modeling. In: *Sedimentary modeling: computer simulations and methods for improved parameter definition*. (Eds.: Franseen, E.K., Watney, W.L., Kendall, C.G.St.C. & Ross, W.) *Kansas Geological Survey Bulletin*, 233, 63-99.
- Enos, P., Jiayong, W. & Yangji, Y. (1997): Facies distribution and retreat of Middle Triassic platform margin, Guizhou province, south China. *Sedimentology*, 44, 563-584.
- Epting, M., Unland, W., Schmidt, K. & Christodoulides, A. (1976): Middle Triassic sediments of selected regions in the Southern Alps (Italy) and their significance for palaeogeographic evolution. *N. Jb. Geol. Pal. Abh.*, 151/1, 1-30.
- Escher v. d. Linth, A. (1853): *Geologische Bemerkungen über das nördliche Vorarlberg und einige angrenzende Gegenden. Neue Denkschriften der allgemeinen Schweizerischen Gesellschaft für Naturwissenschaften*. Vol. 13, 135.
- Fagerstrom, J.A. (1987): *The evolution of reef communities*. John Wiley and Sons, New York, 600pp.
- Fantini Sestini, N. (1996): The Ladinian ammonoids from the Calcare di Esino of Val Parina (Bergamasc Alps, Northern Italy). *PT. 2. Riv. Ital. Pal. Strat.*, 102/2, 211-226.
- Fitzgerald, P.G., Sorkhabi, R.B., Redfield, T.F. & Stump, E. (1995): Uplift and denudation of the central Alaska Range: a case study in the use of apatite fission track thermochronology to determine absolute uplift parameters. *Journ. Geophys. Res.*, 100, 20175-20191.
- Flügel, E. (1982): Evolution of Triassic reefs; current concepts and problems. *Facies*, 6, 297-328.
- Flügel, E. (1991): Environmental analysis of allochthonous carbonate blocks and autochthonous mounds at the northern margin of the Schlern-Rosengarten (Sciliar-Catinaccio) platform. In: *The northern margin of the Schlern/Sciliar - Rosengarten/Catinaccio platform*. (Eds.: Brandner, R., Flügel, E., Koch, R. & Yose, L.A.) *Dolomieu Conference on Carbonate Platforms and Dolomitization, Guidebook Excursion A*, Tourist office, St. Ulrich, Grödenal, 41-55.
- Flügel, E. (1994): Pangean shelf carbonates: Controls and paleoclimatic significance of Permian and Triassic reefs. In: *Pangea: paleoclimate, tectonics, and sedimentation during accretion, zenith, and breakup of a supercontinent*. (Ed.: Klein, G.D.) *GSA Special Paper*, 288, 247-266.
- Flügel, E. (2002): Triassic reef patterns. In: *Phanerozoic reef patterns* (Eds.: Kiessling, W., Flügel, E. & Golonka, J.) *SEPM Special Publication No. 72*, 391-463.
- Flügel, E. & Stanley, G.D. (1984): Reorganization, development and evolution of post-Permian reefs and reef organisms. *Palaeontographica Americana*, 54, 177-186.
- Fois, E. (1982): The Sass da Putia carbonate buildup (Western Dolomites): biofacies succession and margin development during the Ladinian. *Riv. Ital. Pal. Strat.*, 87/4, 565-598.
- Fois, E. & Gaetani, M. (1984): The recovery of reef-building communities and the role of Cnidarians in carbonate sequences of the Middle Triassic (Anisian) in the Italian Dolomites. *Palaeontographica Americana*, 54, 191-200.
- Frisia-Bruni, S., Jadoul, F. & Weissert, H. (1989): Evinosponges in the Triassic Esino Limestone (Southern Alps): documentation of early lithification and late diagenetic overprint. *Sedimentology*, 36, 685-699.
- Fürsich, F.T. & Wendt, J. (1977): Biostratonomy and palaeoecology of the Cassian Formation (Triassic) of the Southern Alps. *Palaeogeogr. Palaeoclim. Palaeoecol.*, 22, 257-323.
- Gaetani, M., Fois E., Jadoul, F. & Nicora, A. (1981): Nature and evolution of the Middle Triassic carbonate buildups in the Dolomites (Italy). *Marine Geology*, 44/1, 25-57.
- Gaetani, M., Gnaccolini, M., Jadoul, F. & Garzanti, E. (1998): Multiorder sequence stratigraphy in the Triassic system of the western Southern Alps. In: *Mesozoic and Cenozoic sequence stratigraphy of European basins* (Eds.: Graciansky, P. C. de, Hardenbol, J., Jacquin, T. and Vail, P. R.) *SEPM Spec. Publ.*, 60, 701-717.
- Gaetani, M., Gnaccolini, M., Poliani, G., Grigniani, D., Gorza, M. & Martellini, L. (1992): An anoxic intraplatform basin in the middle Triassic of Lombardy (Southern Alps, Italy): anatomy of a hydrocarbon source. *Riv. Ital. Pal. Strat.*, 97/3-4,

- 329-354.
- Gaetani, M & Gorza M. (1989): The Anisian (Middle Triassic) Carbonate Bank of Camorelli (Lombardy, Southern Alps) Facies, 21, 41-56.
- Gallagher, K. (1995): Evolving temperature histories from apatite fission-track data. *EPSL*, 136, 421-435.
- Garcia-Mondejar, J. (1988): Aptian-Albian carbonate episode of Basque-Cantabrian Basin, northern Spain. AAPG annual convention with divisions SEPM/EMD/DPA, AAPG Bulletin, 71/5, 558.
- Gianolla, P., De Zanche, V. & Mietto, P. (1998): Triassic sequence stratigraphy in the Southern Alps (Northern Italy): definition of sequences and basin evolution. In: Mesozoic and Cenozoic sequence stratigraphy of European basins (Eds.: Graciansky, P. C. de, Hardenbol, J., Jacquin, T. and Vail, P. R.) SEPM Spec. Publ., 60, 719-747.
- Gianolla, P. & Jacquin, T. (1998): Triassic sequence stratigraphic framework of western European basins. In: Mesozoic and Cenozoic sequence stratigraphy of European basins. (Eds.: Graciansky, P. C. de, Hardenbol, J., Jacquin, T. and Vail, P. R.) SEPM Spec. Publ., 60, 643-650.
- Ginsburg, R.N., Marszalek, D.S. & Schneidermann, N. (1971): Ultrastructure of carbonate cements in a Holocene algal reef of Bermuda. *Journ. Sed. Petrol.*, 41, 472-482.
- Gasmacher, U., Zentilli, M. & Grist, A.M. (1997): Apatite Fission Track thermochronology of Paleozoic sandstones and the Hill-intrusion at the northern part of the Linksrheinisches Schiefergebirge, Germany. In: Advances in Fission-Track Geochronology. (Eds.: Van den Haute & De Corte) Kluwer Academic Publishers, London, 151-172.
- Gleadow, A.J.W., Duddy, I.R. & Lovering, J.F. (1986): Fission track analysis: a new tool for the evaluation of thermal histories and hydrocarbon potential. *APEA Journal*, 23, 93-102.
- Goldhammer, R.K. & Harris, M.T. (1989): Eustatic controls on the stratigraphy and geometry of the Latemar buildup (Middle Triassic), the Dolomites of Northern Italy. In: Controls on Carbonate Platform and Basin Development. (Eds.: Crevello, P.D., Wilson, J.J., Sarg, J.F. & Read, J.F.) SEPM Spec. Publ. 44, 323-338.
- Gradstein, F.M., Agterberg, F.P., Ogg, J.G., Hardenbol, J., Van Veen, P., Thierry, J. & Huang, Z. (1995): A Triassic, Jurassic and Cretaceous time scale. In: Geochronology, time scales and global stratigraphic correlation (Eds.: Berggren, W.A., Kent, D.V., Aubry, M.-P. & Hardenbol, J.) SEPM Spec. Publ. 54, 95-126.
- Green, P.F., Duddy, I.R., Gleadow, A.J.W., Tingate, P.R. & Laslett, G.M. (1985): Fission track annealing: track length measurements and the form of the Arrhenius plot. *Nucl. Tracks*, 10, 323-328.
- Green, P.F., Duddy, I.R., Gleadow, A.J.W., Tingate, P.R. & Laslett, G.M. (1986): Thermal annealing of fission tracks in apatite, 1. A quantitative description. *Chem. Geol.*, 59, 237-253.
- Grist, A.M. & Ravenhurst, C.E. (1992a): Mineral separation techniques used in Dalhousie University. In: Short Course on low temperature thermochronology. (Eds.: Zentilli, M., Reynolds, P.H.). Min. Ass.Can. Short Course V 20, Appendix 2, 203-209.
- Grist, A.M. & Ravenhurst, C.E. (1992b): A step-by-step laboratory guide to fission-track thermochronology at Dalhousie University. In: Short Course on low temperature thermochronology. (Eds.: Zentilli, M., Reynolds, P.H.). Min. Ass.Can. Short Course V 20, Appendix 1, 190-201.
- Haq, B.J., Hardenbol, J. & Vail, P.R. (1987): Mesozoic and cenozoic chronostratigraphy and eustatic cycles. In: Sea-level changes, an integrated approach (Eds.: Wilgus, C.K., Hastings, B.K., Posamentier, H., Van Wagoner, J., Ross, C.A. and Kendall, C.G.St.C.) SEPM Spec. Publ., 42, 71-108.
- Hardie, L.A. & Hinnov, L. (1997): Biostratigraphic and radiometric age data question the Milankovitch characteristics of the Latemar cycles (Southern Alps, Italy). *Comment. Geology* 25/5: 470-471.
- Harland, W.B., Armstrong, R.L., Cox, A.V., Craig, L.E., Smith, A.G. & Smith, D.G. (1989): A geologic time scale 1989. Cambridge University Press, 263pp.
- Harris, M.T. (1993): Reef fabrics, biotic crusts and syndepositional cements of the Latemar reef margin (Middle Triassic), Northern Italy. *Sedimentology*, 40, 383-401.
- Harris, M.T. (1994): The foreslope and toe-of-slope facies of the Middle Triassic Latemar buildup (Dolomites, Northern Italy). *Journal of Sedimentary Research* B64, 2, 132-145.
- Hasebe, N., Mori, S., Tagami, T. & Matsui, R. (2003): Geological partial annealing zone of zircon fission-track system: additional constrains from the deep drilling MITI-Nishikubiki and MITI-Mishima. *Chem. Geol.*, 199, 45-52.
- Hauer, v. R. F. (1855): Curioni's Abhandlung über die Gliederung der Triasgebilde in der Lombardei. *Jb. K. k. geol. R. A.*, 6, 887-896.
- Hays, P.B. & Grossman, E.L. (1991): Oxygen isotopes in meteoric calcite cements as indicators of continental climate. *Geology*, 19, 441-444.
- Hertle, M. & Littke, R. (2000): Coalification pattern and thermal modelling of the Permo-Carboniferous Saar basin (SW-Germany). *Int. Journ. Coal Geol.*, 42, 273-296.
- Hsü, K.J. (1971): Origin of the Alps and the western Mediterranean. *Nature*, 233, 44-48.
- Hsü, K.J. (1989): Time and place in Alpine orogenesis - the Fermor Lecture. In: Alpine tectonics. (Eds.: Coward, M.P., Dietrich, D. and Park, R.G.) *Geol. Soc. London Spec. Publ.*, 45, 421-443.
- Hummel, K. (1928): Das Problem des Fazieswechsels in der Mitteltrias der Südtiroler Dolomiten. *Geologische Rundschau*, 19/3, 223-228.
- Hummel, K. (1932): Zur Stratigraphie und Faziesentwicklung der südalpinen Mitteltrias. *N. Jb. Min. Geol. Pal., Suppl.* 68 B, 403-462.
- Hunt, D. & Fitchen, W.M. (1999): Compaction and the dynamics of carbonate-platform development: insights from the Permian Delaware and Midlands Basins, Southeast New Mexico and West Texas, U.S.A. In: Advances in carbonate se-

- quence stratigraphy: application to reservoirs, outcrops and models (Eds.: Harris, P.M., Saller, A.H. & Simo, J.A.) SEPM Special Publication, 63, 75-106.
- Hurford, A.J. & Green, P.F. (1983): The zeta age calibration of fission track dating *Isotope Geosci.*, 1, 285-317.
- Iryu, Y., Nakamori, T., Matsuda, S. & Abe, O. (1995): Distribution of marine organisms and its geological significance in the modern reef complex of the Ryukyu Islands. *Sedimentary Geology*, 99, 243-258.
- Isintek, I.D., Altiner, D. & Koca, U. (2000): Middle Triassic foraminifera from the type section of the Laleköy Formation (Karaburun Peninsula, Western Turkey): remarks on *Palaeolituonella meridionalis* (Luperto, 1965). *Revue de Paléobiologie*, 19, 191-205.
- Jacob, H. (1989): Classification, structure, genesis and practical importance of natural solid bitumen ("migrabitumen"). *Int. Journ. Coal Geol.*, 11, 61-79.
- Jadoul, F., Berra, F., Frisia, S., Ricchiuto, T. & Ronchi, P. (1992): Stratigraphy, paleogeography and genetic model of Late Carnian carbonate breccias (Castro Formation, Lombardy, Italy). *Riv. Ital. Pal. Strat.*, 97/3-4, 355-392.
- James, N.P. & Ginsburg, R.N. (1979): The seaward marginal Belize barrier and atoll reefs. *IAS Spec. Publ.*, 3, 191pp.
- James, N.P., Ginsburg, R.N., Marszalek, D.S. & Choquette, P.W. (1976): Facies and fabric specificity of early subsea cements in shallow Belize (British Honduras) reefs. *Journ. Sed. Petrol.*, 46, 523-544.
- Kendall, A.C. (1985): Radial-fibrous calcite: a reappraisal. In: *Carbonate Cements*. (Ed.: Schneidermann, N. & Harris, M.T.) SEPM Spec. Publ. 36, 59-77.
- Kenter, J.A.M., van Hoeflaken, F., Bahamonde, J.R., Bracco Gartner, Guido L., Keim, L. & Besems, R.E. (2002) Anatomy and lithofacies of an intact and seismic-scale Carboniferous carbonate platform (Asturias, NW Spain): analogues of hydrocarbon reservoirs in the Pricaspian Basin (Kazakhstan). In: *Paleozoic carbonates of the Commonwealth of Independent States (CIS): subsurface reservoirs and outcrop analogues* (Eds.: Zempolich, W.G. & Cook, H.E.) SEPM Spec. Publ., 74, 181-203.
- Kerans, C., Hurley, N.F. & Playford, P.E. (1986): Marine diagenesis in Devonian reef complexes of the Canning Basin, Western Australia. In: *Reef diagenesis*. (Eds.: Schroeder, J.H. & Purser, B.H.) Springer Verlag, Heidelberg, 357-380.
- Ketcham, R.A., Donelick, R.A. & Donelick, M.B. (2000): AFTSolve: A program for multikinetic modelling of apatite fission-track data. *Geol. Mater. Res.* 2 (1), (electronic: 18 pages, 2 tables, 12 figures). Mineralogical Society of America, Washington, D.C.
- Knopp, S. (2002): Fazies und Geometrien am Plattform-/Beckenübergang einer Mitteltriassischen, isolierten Karbonatplattform: Der Latemar, SW-Dolomiten, Italien. *Gaea heidelbergensis*, 10, CD-ROM.
- Korte, C. (1999): $87\text{Sr}/86\text{Sr}$ -, $\delta 18\text{O}$ - und $\delta 13\text{C}$ -Evolution des Triassischen Meewassers: Geochemische und stratigraphische Untersuchungen an Conodonten und Brachiopoden. *Bochumer Geologische und Geotechnische Arbeiten*, 52, 171pp.
- Kukal, Z. (1971): *Geology of recent sediments*. Academic Press, London, 490p.
- Landra, G., Longoni, R. & Fantoni, R. (2000): Seismic models of two Middle Triassic carbonate platforms from the Southern Alps. *Mem. Sci. Geol.*, 52, 1, 139-163.
- Laslett, G.M., Green, P.F., Duddy, I.R. & Gleadow, A.J.W. (1987): Thermal annealing of fission tracks in apatite, 2. A quantitative analysis. *Chem. Geol.*, 65, 1-13.
- Laubscher, H. & Bernoulli, D. (1982): History and deformation of the Alps. In: *Mountain building processes*. (ed.: Hsü, K.J.) Academic Press, London, 169-180.
- Lehrmann, D., Enos, P., Montgomery, P., Payne, J., Orchard, M., Bowring, S., Ramezani, J., Martin, M., Jiayong, W., HongMei, W., YouYi, Y., Jiafei, X. & Rongxi, L. (2002): Integrated biostratigraphy, magnetostratigraphy and geochronology of the Olenikian-Anisian boundary in marine strata of Guandao section, Nanpanjiang Basin, South China: implications for timing of biotic recovery from the end-Permian extinction. In: *I.U.G.S. Subcommittee on Triassic Stratigraphy*. (Ed.: Piros, O.) STS/IGCP 467 Field Meeting, Veszprém, Hungary, 5-8 September, 2002, 7-8.
- Leischner, K. (1994): Kalibration simulierter Temperaturgeschichten von Sedimentgesteinen. *Berichte des Forschungszentrums Jülich, Jül-2909*, 309pp.
- Leonardi, P. (1962): Il gruppo dello Sciliar e le scogliere coralligene dolomitiche. *Ann. Univ. Ferrara, N.S., sez. IX/3*, 1-83.
- Leonardi, P. (1967): *Le Dolomiti: Geologia dei Monti tra Isarco e Piave*. Manfrini, Rovereto, Vol 1, 1019pp.
- Leuchs, K. (1928): Beiträge zur Lithogenese kalkalpiner Sedimente. *N. Jb. Min. Geol. Paläont., Beilage-Bd. 59B*, 357-408.
- Lighty, R.G. (1985): Preservation of internal reef porosity and diagenetic sealing of submerged early Holocene barrier reef, southeast Florida Shelf. In: *Carbonate Cements* (Eds.: Schneidermann, N. & Harris, P.M.) SEPM Special Publication No. 36, 123-151.
- Litke, R., Büker, C., Hertle, M., Karg, H., Stroetmann-Heinen, V. & Oncken, O. (2000): Heat flow evolution, subsidence and erosion in the Rheno-Hercynian orogenic wedge of central Europe. In: *Orogenic processes: quantification and modelling in the Variscan belt*. (Eds.: Franke, W., Haak, V., Oncken, O. & Tanner, D.) Geological Society Spec. Publ., 179, 231-255.
- Litke, R., Büker, C., Lückge, A., Sachsenhofer, R.F. & Welte, D.H. (1994): A new evaluation of palaeo-heatflows and eroded thicknesses for the Carboniferous Ruhr basin, western Germany. *Int. Journ. Coal Geol.*, 26, 155-183.
- Mair, V., Stingl, V., Krois, P. & Keim, L. (1996): Die Bedeutung andesitischer und dazitischer Gerölle im Unterinntal-Tertiär (Tirol, Österreich) und im Tertiär des Mte. Parei (Dolomiten, Italien). *N. Jb. Geol. Pal., Abh.*, 199/3, 369-394.
- Mallarino, G. (2002): Crisi delle piattaforme carbonatiche e dinamica deposizionale delle piattaforme pelagiche nel Giurassico della Sicilia occidentale. Unpubl. Ph.D. thesis,

- Consorzio di ricerca tra le Università degli Studi di Napoli e Palermo, Palermo, 201pp.
- Marshall, J.F. (1986): Regional distribution of submarine cements within an epicontinental reef system: Central Great Barrier Reef, Australia. In: Reef diagenesis. (Eds.: Schroeder, J.H. & Purser, B.H.) Springer Verlag, Heidelberg, 8-26.
- Martire, L. (1996): Stratigraphy, facies and synsedimentary tectonics in the Jurassic Rosso Ammonitico Veronese (Altopiano di Asiago, NE Italy). *Facies*, 35, 209-236.
- Masetti, M. & Neri, C. (1980): L'Anisico della Val di Fassa (Dolomiti occidentali): sedimentologia e paleogeografia. *Ann. Univ. Ferrara, N.S., sez. IX/7/1*, 1-19.
- Massari, F., Conti, M.A., Fontana, D., Helmold, K., Mariotti, N., Neri, C., Nicosia, U., Ori, G.G., Pasini, M. & Pittau, P. (1988): The Val Gardena sandstone and Bellerophon formation in the Bletterbach gorge (Alto Adige, Italy): biostratigraphy and sedimentology. *Memorie di Scienze Geologiche* 40, 229-273.
- Massari, F., Grandesso, P., Stefani, C. & Jobstraibizer, P.G. (1986): A small polyhistory foreland basin evolving in a context of oblique convergence: the Venetian basin (Chattian to Recent, Southern Alps, Italy). In: Foreland basins (Eds.: Allen, P.A. & Homewood, P.) IAS Spec. Publ., 8, 141-168.
- Massari, F. & Neri, C. (1997): The infill of a supradetachment(?) basin: the continental to shallow-marine Upper Permian succession in the Dolomites and Carnia (Italy). *Sedimentary Geology* 110, 181-221.
- Massari, F., Neri, C., Pittau, P., Fontana, D. & Stefani, C. (1994) Sedimentology, palynostratigraphy and sequence stratigraphy of a continental to shallow-marine rift-related succession: Upper Permian of the Eastern Southern Alps (Italy). *Mem. Sci. Geol.*, 46, 119-243.
- Mastandrea, A., Neri, C. & Russo, F. (1997): Conodont biostratigraphy of the S. Cassiano Formation surrounding the Sella Massif (Dolomites, Italy): Implications for sequence stratigraphic models of the Triassic of the Southern Alps. *Riv. Ital. Pal. Strat.*, 103/1, 39-52.
- Maurer, F. (1999): Wachstumsanalyse einer mitteltriadischen Karbonatplattform in den westlichen Dolomiten (Südalpen). *Eclogae geologicae Helvetiae*, 92, 361-378.
- Maurer, F. (2000): Growth mode of middle Triassic carbonate platforms in the Western Dolomites (Southern Alps, Italy). *Sedimentary Geology*, 134, 275-286.
- Maurer, F. (2003): Bedding rhythms in Triassic basins of the Southern Alps. Ph.D. thesis, Vrije Universiteit Amsterdam.
- McCartney, J.T. & Teichmüller, M. (1972): Classification of coals according to the degree of coalification by the reflectance of vitrinite components. *Fuel*, 51, 64-68.
- McKenzie, D.P. (1981): The variation of temperature with time and hydrocarbon maturation in sedimentary basins formed by extension. *EPSL*, 55, 87-98.
- McKinney, M.L. (1985): Mass extinction patterns of marine invertebrate groups and some implications for a causal phenomenon. *Paleobiology* 11, 227-233.
- Mojisovics, E. (1879): Die Dolomitriffe von Südtirol und Venetien: Beiträge zur Bildungsgeschichte der Alpen. Holder, Wien, 522pp.
- Moore, C.H. & Haydari, E. (1993): Burial diagenesis and hydrocarbon migration in platform limestones: a conceptual model based on the Upper Jurassic of the Gulf Coast in the U.S.A. In: Diagenesis and basin development. (Eds.: Horbury, A.D. & Robinson, A.G.) *Studies in geology*, 36, AAPG, Tulsa, 213-230.
- Mullins, H.T. (1983): Modern carbonate slopes and basins of the Bahamas. In: Platform margin and deepwater carbonates. (Eds.: Cook, H.E., Hine, A.C. & Mullins, H.T.) *SEPM Short Course No. 12*, 4.1-4.138.
- Mullins, H.T. & Cook, H.E. (1986): Carbonate apron models: alternatives to the submarine fan model for paleoenvironmental analysis and hydrocarbon exploration. *Sedimentary Geology*, 48, 37-79.
- Mullins, H.T., Gardulski, A.F. & Hine, A.C. (1986): Catastrophic collapse of the west Florida carbonate platform margin. *Geology*, 14, 167-170.
- Mundil, R., Brack, P., Meier, M., Rieber, H. & Oberli, F. (1996): High resolution U/Pb dating of Middle Triassic volcanics: time-scale calibration and verification of tuning parameters for carbonate sedimentation. *EPSL*, 141, 137-151.
- Mundil, R., Metcalfe, I., Ludwig, K.R., Renne, P.R., Oberli, F. & Nicoll, R.S. (2001): Timing of the Permian-Triassic biotic crisis: implications from new zircon U/Pb age data (and their limitations). *EPSL*, 187, 131-145.
- Mundil, R., Zühlke, R., Bechstäd, T., Brack, P., Egenhoff, S.O., Meier, M., Oberli, F., Peterhänsel, A. & Rieber, H. (2003): Cyclicity in Triassic platform carbonates: synchronizing radio-isotopic and orbital clocks. *Terra Nova* 15, 2, 81-87.
- Mutti, M. (1994): Association of tepees and paleokarst in the Ladinian Calcare Rosso (Southern Alps, Italy). *Sedimentology*, 41, 621-641.
- Mutti, E., Ricci Lucchi, F., Seguret, M. & Zanzucchi, G. (1984): Seismoturbidites: a new group of resedimented deposits. *Marine Geology*, 55, 103-116.
- Naeser, C.W. & Faul, H. (1969): Fission track annealing in apatite and sphene. *J. Geophys. Res.*, 74, 705-710.
- Niggemann, S., Mangini, A., Mudelsee, M., Richter, D.K. & Wurth, G. (2003): Sub-Milankovitch climatic cycles in Holocene stalagmites from Sauerland, Germany. *EPSL*, 216, 539-547.
- Noeth, S., Thomsen, R.O., & Littke, R. (2002): A method for assessing statistical significance and uncertainties for calibration of 1-D thermal basin maturation models. *AAPG Bulletin* 86/3, 417-431.
- Ott, E. (1967): Segmentierte Kalkschwämme (Sphinctozoa) aus der alpinen Mitteltrias und ihre Bedeutung als Riffbildner im Wettersteinkalk. *Abhandlungen Bayerische Akademie Wissenschaften, mathematisch-naturwissenschaftliche Klasse, Neue Folge*, 131, 96pp.
- Ott, E. (1972): Mitteltriadische Riffe der Nördlichen Kalkalpen und altersgleiche Bildungen auf Karaburun und Chios (Aegaeis). *Mitt. Ges. Geol. Bergbaustud. Österr.*, 21/1, 251-

- 276.
- Pálffy, J., Parrish, R.R., David, K. & Vörös, A. (2003): Mid-Triassic integrated U-Pb geochronology and ammonoid biochronology from the Balaton Highland (Hungary). *Journal of the Geological Society, London*, 160, 271-284.
- Pálffy, J., Smith, P.L. & Mortensen, J.K. (2000): A U-Pb and $^{40}\text{Ar}/^{39}\text{Ar}$ time scale for the Jurassic. *Canadian Journal of Earth Sciences*, 37/6, 923-944.
- Petmecky, R.S. (1998): Numerische Simulation der Entwicklungsgeschichte des zentralen Niedersächsischen Beckens unter besonderer Berücksichtigung der Erdgaslagerstätten-Bildung. *Berichte des Forschungszentrum Jülich*, Jül-3567, 242pp.
- Pia, J. (1937): *Stratigraphie und Tektonik der Pragser Dolomiten in Südtirol*. Pia, Wien, 248pp.
- Playford, P.E. (1980): Devonian "Great Barrier Reef" of Canning basin, Western Australia. *AAPG Bulletin*, 64, 814-840.
- Poelchau, H.S., Baker, D.R., Hantschel, T., Horsfield, B. & Wygrala, B. (1997): Basin simulation and the design of the conceptual basin model. In: *Petroleum and basin evolution. Insights from petroleum geochemistry, geology and basin modeling*. (Eds.: Welte, D.H., Horsfield, B. & Baker, D.R.) Springer-Verlag, Berlin, 4-70.
- Rahmstorf, S. (2003): Timing of abrupt climate change: a precise clock. *Geophys. Res. Lett.*, 30/10, 1510.
- Raup, D.M. (1979) Size of the Permo-Triassic bottleneck and its evolutionary implications. *Science*, 206, 217-218.
- Rettori, R., Senowbari-Daryan, B. & Zühlke, R. (1996): *Flatschkofelia anisica* gen. et sp. nov. (Foraminiferida) from the Middle Triassic (Anisian) of Northern Dolomites, Italy. *Riv. Ital. Pal. Strat.*, 102/3, 413-416.
- Rossetti, R. (1966): Considerazioni sui rapporti tra le diverse facies ladiniche nella zona del Pizzo Camino e della Concarena (Brescia nord-occidentale). *Atti dell'Istituto Geologico della Università di Pavia*, vol.17, 124-142.
- Rüffer, T. & Zamparelli, V. (1997): Facies and biota of Anisian to Carnian carbonate platforms in the Northern Calcareous Alps (Tyrol and Bavaria). *Facies*, 37, 115-136.
- Rüffer, T. & Zühlke, R. (1995): Sequence stratigraphy and sea-level changes in the Early to Middle Triassic of the Alps: a global comparison. In: *Sequence stratigraphy and depositional response to eustatic, tectonic and climatic forcing* (Ed.: Haq, B.U.) Kluwer, Amsterdam, 161-207.
- Russo, F., Mastandrea, A. & Neri, C. (1998): The Cipit boulders from the surroundings of the Sella massif. In: *Southern Alps Field Trip Guidebook*. (Eds.: Perri, M.C. & Spaletta, C.) *Ecos VII Giornale di Geologia Special Issue*, 60, 108-115.
- Russo, F., Mastandrea, A., Stefani, M. & Neri, C. (2000): Carbonate facies dominated by syndepositional cements: a key component of Middle Triassic platforms. The Marmolada case history (Dolomites, Italy). *Facies* 42, 211-226.
- Sachsenhofer, R.F. & Littke, R. (1993): Vergleich und Bewertung verschiedener Methoden zur Berechnung der Vitritreflexion am Beispiel von Bohrungen im Steirischen Tertiärbecken. *Zentralblatt Geol. Paläont.* 1992/1, 597-610.
- Sachsenhofer, R.F., Privalov, V.A., Zhykalyak, M.V., Büker, C., Panova, E.A., Rainer, T., Shymanovskyy, V.A. & Stephenson, R. (2002): The Donets basin (Ukraine/Russia): coalification and thermal history. *Int. Journ. Coal Geol.*, 49, 33-55.
- Salomon, W. (1908): Die Adamellogruppe, ein alpines Zentralmassiv und seine Bedeutung für die Gebirgsbildung, Teil I. *Abhandlungen k. u. k. geol. Reichsanstalt*. 21, 433pp.
- Sarg, J.F. (1988): Carbonate sequence stratigraphy. In: *Sea-level changes – an integrated approach*. (Eds.: Wilgus, C.K., Hastings, B.S., Kendall, C.G.St.C., Posamentier, H.W., Ross, C.A., & VanWagoner, J.C.) *SEPM Spec. Publ.*, 44, 63-76.
- Sarti, M., Winterer, E.L. & Luciani, V. (2000): Repeated gravity-controlled fracturing and dilatation of Jurassic limestones over 130m.y. and filling by episodic microturbidity currents of Cretaceous and Palaeogene sediments (Taormina, Sicily). *Mem. Soc. Geol. It.*, 55, 251-260.
- Savelli, C. & Balboni, S. (1984): Determinazioni di età K/Ar di vulcaniti permiane sudalpine. *Miner. Petrogr. Acta*, 28, 243-252.
- Schäfer, P. & Senowbari-Daryan, B. (1982): The Upper Triassic Pantokrator limestone of Hydra (Greece): an example of a prograding reef complex. *Facies*, 6, 147-164
- Schäfer, P. & Senowbari-Daryan, B. (1983): Die Kalkalgen aus der Obertrias von Hydra, Griechenland. *Palaeontographica Abt. B* 185, 4-6, 83-142.
- Schaltegger, U., Desmurs, L., Manatschal, G., Müntener, O., Meier, M., Frank, M. & Bernoulli, D. (2002): The transition from rifting to sea-floor spreading within a magma-poor rifted margin: field and isotopic constraints. *Terra Nova*, 14, 156-162.
- Schatz, W. (2000): *Taxonomie, Palökologie und biostratigraphische Anwendung der Daonellen (Bivalvia) aus der Mitteltrias Europas*. Unpubl. Ph.D. thesis, Universität Zürich, 313pp.
- Scherer, M. (1977): Preservation, alteration and multiple cementation of aragonite skeletons from the Cassian beds (Southern Alps), petrographical and geochemical evidence. *N. Jb. Geol. Paleont., Abh.*, 154, 213-262.
- Scheuber, M. (1990): *Der Spitzkalk von Recoaro (Vicentinische Alpen, Norditalien): Sedimentologie, Paläontologie und Paläogeographie eines mitteltriassischen Ablagerungsraumes*. *Facies*, 23, 57-96.
- Schindel, D.E. (1980): Microstratigraphic sampling and the limits of paleontologic evolution. *Paleobiology*, 6/4, 408-426.
- Schlager, W. & Ginsburg, R.N. (1981): Bahamas carbonate platforms – the deep and the past. *Marine Geology*, 44, 1-24.
- Schlager, W. (1981): The paradox of drowned reefs and carbonate platforms. *Geological Society of America Bulletin* 92, 197-211.
- Schlager, W. (1993): Accommodation and supply: a dual control on stratigraphic sequences. *Sedimentary Geology*, 86, 111-136.
- Schlager, W. (1999): Scaling of sedimentation rates and drowning of reefs and carbonate platforms. *Geology* 27/2, 183-186.

- Schlager, W. (2000): Sedimentation rates and growth potential of tropical, cool-water and mud-mound carbonate systems. In: Carbonate platform systems: components and interactions (Eds.: Insalaco, E., Skelton, P.W. & Palmer, T.J.) Geological Society Spec. Publ., 178, 217-227.
- Schlager, W., Biddle, K.T. & Stafleu, J. (1991): Picco di Vallandro (Dürrenstein) a platform-basin transition in outcrop and seismic model. Dolomieu Conference on Carbonate Platforms and Dolomitization, Guidebook Excursion D, Tourist Office St. Ulrich, Grödenal, 22pp.
- Scholz, G. (1972): An Anisian Wetterstein limestone reef in North Hungary. *Acta Miner.-Petrogr. Szeged* 20/2, 337-362.
- Schönborn, G. (1992): Alpine tectonics and kinematic models of the central Southern Alps. *Mem. Sci. Geol.*, 44, 229-393.
- Schulz, O. & Fuchs, H.W. (1991): Kohle in Tirol: eine historische kohlenpetrologische und lagerstättenkundliche Betrachtung. *Arch. f. Lagerst.forsch. geol. B.-A.*, v.13, 123-213.
- Scofin, T.P. & Garret, P. (1974): Processes in the formation and preservation of internal structure in Bermuda patch-reefs. *Proc. 2nd Int. Coral Reef Symp.*, Brisbane 2: 429-448.
- Senowbari-Daryan, B. & Di Stefano, P. (2001): Middle Triassic dasycladales in Sicily: evidence of an Anisian?-Ladinian carbonate platform. *Acta Geologica Hungarica* 44, 1, 95-109.
- Senowbari-Daryan, B., Zühlke, R., Bechstädt, T. & Flügel, E. (1993): Anisian (Middle Triassic) buildups of the northern Dolomites (Italy): the recovery of reef communities after the Permian/Triassic crisis. *Facies*, 28, 181-257.
- Shinn, E.A., Halley, R.B., Hudson, J.H. & Lidz, B.H. (1977): Limestone compaction – an enigma. *Geology*, 5/1, 21-24.
- Smith, A.G. (1971): Alpine deformation and the oceanic areas of the Tethys, Mediterranean and Atlantic. *Geological Society of America Bulletin*, 82, 2039-2070.
- Stach, E., Mackowsky, M., Teichmüller, M., Taylor, G.H., Chandra, D. & Teichmüller, R. (1982) *Stach's textbook of coal petrology*. Borntraeger, Berlin, 535pp.
- Stefani, M.M., Mastandrea, A.G. & Russo, F. (2001): Massive syndepositional cementation associated with organic matter: a key factor in the depositional dynamics of the Latemar and coeval Middle Triassic carbonate platforms of the Dolomites. In: Abstracts and Programme, 21st IAS Meeting of Sedimentology. (Eds.: Wortmann, U.G. & Funk, H.), Davos, Switzerland, 111.
- Stock, H.W. (1996): Planktonische Foraminiferen aus der Oberkreide der nordöstlichen Dolomiten (Italien). *Revue de Paléobiologie*, 15/1, 155-182.
- Stoppani, A. (1858): Les pétrifications d'Esino ou description des fossils appartenants au dépôt supérieur des environs d'Esino en Lombardie. *Paléont. Lombarde*, 1, Milano, 360pp.
- Storzer, D. (1970): Fission track dating of volcanic glasses and the thermal history of rocks. *EPSL*, 8, 55-60.
- Sweeney, J.J. & Burnham, A.K. (1990): Evaluation of a simple model of vitrinite reflectance based on chemical kinetics. *AAPG Bulletin*, 74, 1559-1570.
- Tagami, T. & Shimada, C. (1996): Natural long-term annealing of zircon fission track system around a granitic pluton. *Journ. Geophys. Res.*, B 101, 11353-11364.
- Taylor, G.H., Teichmüller, M., Davis, A., Diessel, C.F.K., Littke, R. & Robert, P. (1998): *Organic petrology*. Borntraeger, Berlin, Stuttgart, 704pp.
- Terry, C.E. & Williams, J.J. (1969): The Idris 'A' bioherm and oilfield, Sirte Basin, Libya; its commercial development, regional Palaeocene geologic setting and stratigraphy. The exploration for petroleum in Europe and north Africa. *Inst. Petrol.*, London.
- Thomson, D.J. (1982): Spectrum estimation and harmonic analysis. *Proc. IEEE*, 10, 1055-1096.
- Tippett, J.M. & Kamp, P.J.J. (1995): Quantitative relationships between uplift and relief parameters for the Southern Alps, New Zealand, as determined by fission track analysis. *Earth Surf. Process. Landforms* 20, 153-175.
- Trevisani, E. (1991): Il Toarciano-Aaleniano nei settori centro-orientali della piattaforma di Trento (Prealpi Venete). *Riv. Ital. Pal. Strat.*, 97/1, 99-124.
- Trifonova, E. & Vaptsarova, A. (1982): Palaeoecology of Late Anisian foraminifera in part of North Bulgaria. *Geologica Balkanica*, 12, 95-104.
- Triümpy, R. (1982): Alpine palaeogeography: a reappraisal. In: *Mountain building processes* (Ed.: Hsü, K.J.) Academic Press, London, 149-156.
- Tscherny, R. (2004): Zweidimensionale Modellierung der thermischen Evolution und Beckenentwicklung des permomesozoischen Südalpins (Dolomiten) entlang der TRANSALP Traverse. *Dissertation*, Rhein. West. Tech. Hochschule Aachen, in prep.
- Tucker, M.E. & Wright, V.P. (1990): *Carbonate sedimentology*. Blackwell Science, London, 482pp.
- Turcotte, D.L. & Schubert, G. (1982): *Geodynamics - applications of continuum physics to geological problems*. Wiley, New York, 450pp.
- Turcotte, D.L. & Schubert, G. (2002): *Geodynamics*. University Press, Cambridge, 456pp.
- Twitchett, R.J. (1999): Palaeoenvironments and faunal recovery after the end-Permian mass extinction. *Palaeogeog. Palaeoclim. Palaeoecol.*, 154, 27-37.
- Unland, W. (1975): Sedimentary and diagenetic environments of the Dosso dei Morti-Limestone/Giudicarie (Lower and Middle Anisian, Italy). *N. Jb. Geol. Pal., Monatshefte*, v.1975, 54-64.
- Vachard, D., Martini, R., Rettori, R. & Zaninetti, L. (1994): Nouvelle classification des foraminifères. *Endothyroides du Trias*. *Geobios*, 27/5, 543-557.
- Veizer, J., Ala, D., Azmy, K., Bruckschen, P., Bruhn, F., Buhl, D., Carden, G., Diener, A., Ebner, S., Goddard, Y., Jasper, T., Korte, C., Pawellek, F., Podlaha, O. & Strauss, H. (1999): $^{87}\text{Sr}/^{86}\text{Sr}$, $\delta^{18}\text{O}$ and $\delta^{13}\text{C}$ evolution of Phanerozoic seawater. *Chem. Geol.*, 161, 59-88.
- Viel, G. (1979a): *Litostratigrafia Ladinica: una revisione*. Ricostruzione paleogeografica e paleostrutturale dell'area Dolomitico-Cadorina (Alpi Meridionali). I. Parte. *Riv. Ital.*

- Pale. Strat., 85/1, 88-125.
- Viel, G. (1979b) Litostratigrafia Ladinica: una revisione. Ricostruzione paleogeografica e paleostrutturale dell'area Dolomitico-Cadorina (Alpi Meridionali). II. Parte. Riv. Ital. Pale. Strat., 85/2, 297-352.
- von Richthofen, F.F. (1860): Geognostische Beschreibung der Umgegend von Predazzo, Sanct Cassian und Seiser Alpe in Süd-Tyrol. Perthes, Gotha, 327pp.
- Wagner, G.A. & Van den Haute, P. (1992): Fission-Track Dating. Enke Verlag, Stuttgart, 285 pp.
- Wanless, H.R. & Tagett, M.G. (1989): Origin, growth and evolution of carbonate mud banks in Florida Bay. Bulletin of Marine Science, 44/11, 454-489.
- Wartmann, R. & Kantz, P. (1977): Petrographische Untersuchungen an Kohlen und Sandsteinproben aus dem "mittel"-permischen Grödnert Sandstein der westlichen Dolomiten. Archiv Bergbauforschung GmbH; unpubl. Report; Essen, Germany, 8pp.
- Welte, D.H., Horsfield, B. & Baker, D.R. (1997): Petroleum and basin evolution. Springer, Berlin, 535pp.
- Wijbrans, J.R., Carrapa, B. & Von Eynatten, H. (2002): Looking at the Alpine ranges of Europe in the past: $^{40}\text{Ar}/^{39}\text{Ar}$ dating of white micas from clastic sediments tell a tale of provenance and exhumation. GSA Annual Meeting, October 27-30, 2002, Denver, Colorado Abstracts Volume.
- Wilson, J.L. (1975): Carbonate facies in geologic history. Springer-Verlag, Berlin, 471p.
- Winterer, E.L. (1998): Palaeobathymetry of mediterranean Tethyan Jurassic pelagic sediments. Mem. Soc. Geol. Ital., 53, 97-131.
- Winterer, E.L. & Bosellini, A. (1981): Subsidence and sedimentation on Jurassic passive continental margin, Southern Alps, Italy. AAPG Bulletin, 65/1, 394-421.
- Winterer, E.L., Metzler, C.V. & Sarti, M. (1991): Neptunian dikes and associated breccias (Southern Alps and Switzerland): role of gravity sliding in open and closed systems. Sedimentology, 38, 381-404.
- Wright, V.P. (1992): A revised classification of limestones. Sedimentary Geology, 76, 177-185.
- Wygrala, B.P. (1989): Integrated study of an oil field in the southern Po basin, Northern Italy. Berichte Kernforschungsanlage Jülich, Jül-2313, 217p.
- Yalcin, M.N., Littke, R. & Sachsenhofer, R.F. (1997): Thermal history of sedimentary basins. In: Petroleum and basin evolution. Insights from petroleum geochemistry, geology and basin modeling. (Eds.: Welte, D.H., Horsfield, B. & Baker, D.R.) Springer-Verlag, Berlin, 73-167.
- Yalcin, M.N. & Welte, D.H. (1988): The thermal evolution of sedimentary basins and significance for hydrocarbon generation. Bull. Turkish Petrol. Geol., Ankara, 1, 12-26.
- Yose, L.A. (1991): Sequence stratigraphy of mixed carbonate/volcaniclastic slope deposits flanking the Sciliar (Schlern)-Catinaccio (Rosengarten) buildup, Dolomites, Italy. In: The northern margin of the Schlern/Sciliar Rosengarten/Catinaccio platform (Eds.: Brandner, R., Flügel, E., Koch, R. & Yose, L.A.) Dolomieu Conference on Carbonate Platforms and Dolomitization Guidebook Excursion A, Tourist office, St. Ulrich, Grödenal, 17-39.
- Yugan, J., Wardlaw, B.R., Glenister, B.F. & Kotlyar, G.V. (1997): Permian chronostratigraphic subdivisions. Episodes, 20/1, 10-15.
- Zacher, W. (1980): Biozonierung und Sediment-Zusammensetzung in einem phippinischen Saumriff bei Lobo, Batangas. Z. dt. geol. Ges., 131, 793-801.
- Zamparelli, V., Emmerich, A., Bechstädt, T. & Zühlke, R. (2001): The reefal margin and slope of an isolated Mid-Triassic atoll: the Latemar, Dolomites, Italy. In: Abstracts and Programme, 21st IAS Meeting of Sedimentology. (Eds.: Wortmann, U.G. & Funk, H.), Davos, Switzerland, 115.
- Zaninetti, L., Ciarapica, G., Martini, R. & Rettori, R. (1990): Paléocéologie des turriglomines (foraminifères) dans le Trias de l'Apennin méridional (bassin de Lagonegro, Italie). Archs. Sci. Genève, 43/2, 295-305.
- Zaninetti, L., Ciarapica, G., Martini, R., Salvini-Bonnard, G. & Rettori, R. (1987): Turriglomina scandonei, n.sp., dans les calcaires récifaux du Trias Moyen. Revue de Paléobiologie, 6/2, 177-182.
- Zaninetti, L., Rettori, R. & Martini, R. (1994): Aulotortus eotriasicus, n.sp., un nuovo foraminifero del Trias medio (Anisico) delle Dinaridi ed Ellenidi. Boll. Soc. Paleont. Ital., 33/1, 43-49.
- Zaninetti, L., Rettori, R., Martini, R., Cirilli, S. & Ciarapica, G. (1992): Il foraminifero Abriolina Luperto, 1963 (Trias medio, Appennino meridionale): ridescrizione, tassonomia, nuovi dati sulla distribuzione stratigrafica. Revue de Paléobiologie, 11/1, 197-204.
- Zeeh, S. (1998): Karbonatzemente als Indikatoren des Fluid-Flow während der alpinen Orogenese in den Ost- und Südalpen. Gaea heidelbergensis, 5, 168pp.
- Zeeh, S. & Bechstädt, T. (1994): Carbonate-hosted Pb-Zn mineralization at Bleiberg-Kreuth (Austria): compilation of data and new aspects. In: Sediment-hosted Zn-Pb ores. (Eds.: Fontboté, L. & Boni, M.) Springer, Heidelberg, 271-296.
- Zeeh, S., Bechstädt, T., McKenzie, J. & Richter, D.K. (1995): Diagenetic evolution of the Carnian Wetterstein platforms of the Eastern Alps. Sedimentology, 42, 199-222.
- Zeeh, S., Walter, U., Kuhlemann, J., Herlec, U., Keppens, E. & Bechstädt, T. (1997): Carbonate cements as a tool for fluid flow reconstruction: a study in parts of the Eastern Alps (Austria, Germany, Slovenia). In: Basin-wide diagenetic patterns: integrated petrologic, geochemical and hydrological considerations. (Eds.: Montanez, E.P., Greig, J. & Shelton, K.L.) SEPM Spec. Publ., 57, 167-181.
- Zorn, H. (1971): Paläontologische, stratigraphische und sedimentologische Untersuchungen des Salvatoredolomits (Mitteltrias) der Tessiner Kalkalpen. Schweiz. Paläont. Abh., 91, 1-90.
- Zorn, H. (1972): Mikrofazielle Analyse eines mitteltriadischen Riffkomplexes in den Tessiner Kalkalpen. Mitt. Ges. Geol. Bergbaustud. Österr., 21, 123-142.

Zühlke, R. (2000): Fazies, hochauflösende Sequenzstratigraphie und Beckenentwicklung im Anis (mittlere Trias) der Dolomiten (Südalpin, Italien). *Gaea heidelbergensis*, 6, CD-ROM.

Zühlke, R. (2004): Integrated cyclostratigraphy of a model Mesozoic carbonate platform – the Latemar (Middle Triassic, Italy). In: *Cyclostratigraphy – an essay of approaches and case histories* (Eds.: D’Argenio, B., Fisher, A., Premoli Silva, I. & Weissert, H.) *SEPM Spec. Publ.*, 81, in press.

Zühlke, R., Bechstäd, T., Brack, P., Mundil, R. & Rieber, H. (2000): Die Latemar-Kontroverse: neue Daten zur Geometrie, zeitlichen Entwicklung und Interpretation lagunärer Zyklen. *Mitt. Ges. Geol. Bergbaustud. Österr.*, 43, 154.

Zühlke, R., Bechstäd, T. & Mundil, R. (2003): Sub-Milankovitch and Milankovitch forcing on a model Mesozoic carbonate platform - the Latemar (Middle Triassic, Italy). *Terra Nova*, 15/2, 69-80.

Acknowledgements

This project would have been impossible without the support of many people and organisations:

- First of all, I would like to express my sincere thanks to the “Studienstiftung des deutschen Volkes” for financial support throughout the project. Unfortunately, there has been too little time to enjoy and explore all the offers of the Studienstiftung. My mentor – Hans-Günther Sonntag – is thanked for having supported those many applications.
- Funding during the last months of thesis preparation came from Shell Research B.V. (Fonds: 20702/7800923/9500857).
- Thilo Bechstädt, University of Heidelberg, initiated this dissertation by recommending me to the “Studienstiftung des deutschen Volkes”. He further promoted this project by providing financial assistance for field work, for conferences where results were presented and for the last months of thesis preparation. He also had to read and correct loads of manuscripts. Discussions with him contributed to the improvement of the project. The incident with the lightning on top of Latemar surely has “burnt” into my memories!
- Rainer Zühlke, University of Heidelberg, developed an earlier draft of the initial project outline and improved the quality of my presentations and manuscripts by critical reading. He was always open for discussions which helped to ameliorate the quality of my research.
- Valeria Zamparelli, University of Napoli, Italy, introduced me to the fascinating world of Middle Triassic calcareous algae, sponges and microproblematica. I have to express my gratitude for her friendship and hospitality in Napoli, Formia and Bruxelles. ISC 2002 and the field trip to the desert will remain unforgettable experiences.
- Ralf Littke, Technical University of Aachen, always allowed me to use computing facilities and software at his institute and is thanked for assuring me continuous support throughout the project.
- Peter A. Kukla, Technical University of Aachen, refereed the dissertation. I am greatly indebted to his willingness; the completion of the dissertation would otherwise have been significantly delayed.
- Peter Bengtson and Augusto Mangini, both University of Heidelberg, are thanked for their prompt readiness to referee the viva.
- Carsten Büker, now at Shell, learnt me the fundamentals of thermal modelling with PetroMod. He further helped me to add substantially more geology to this project. I am also very grateful for supporting me at one of the most serious crises of the entire project.
- Robert Tscherny, now at IES, took over from where Carsten had finished. He usually was happy to help with any PetroMod problems even if time was running out before congresses. Additionally, Robert always provided free lodging in Aachen. Common field work, IAS 2001 and AAPG 2002 will remain nice memories despite gators on the footpaths in Texas.
- Ulrich A. Glasmacher, MPI für Kernphysik Heidelberg, provided essential and excellent FT data for this project. He is furthermore thanked for giving me useful hints for the preparation of the introductory chapter of this thesis.
- Roswitha Marioth, University of Heidelberg, managed the IPP of Geosciences and enabled funding for many conferences, field work and research travel. She is also thanked for having supported me morally during hard times of the project.
- Michael Seeling, University of Heidelberg, showed me “Unidentified Cementing Objects” on the Concaarena platform. His friendship, the common field work and manuscript preparation were one of the real up-sides of this project.
- Zbynek Veselovsky, University of Heidelberg, readily explained cryptic interfaces and output data of even more cryptic modelling tools. GSA 2002, NGF 2003 and Utrecht 2003 will never be forgotten – especially the stolen slides. The moral support he gave was essential for this project.
- Birgit G. Dietrich, University of Heidelberg, was also part of the “Dream Team” in room 113a. Discussions with her helped to clarify the a.m cryptic modelling tools.
- Florian Maurer, now somewhere in Abu Dhabi, is thanked for having introduced me to the Buchenstein Fm.
- Jörg Grimmer, now at IES, provided me with essential technical support during a very critical phase of manuscript preparation.

- Friederike Bauer, University of Heidelberg, is acknowledged for having worked through an awful lot of samples. Her meticulous sample preparation was the base for the excellent FT analysis.
- In the beginning of each dissertation “old veterans” (sorry guys!) should be consulted. Thomas Müller and Max Neunhöffer helped me a lot to set my objectives (publish or perish!). Max also provided lodging in Aachen and support on mathematical problems.
- Eventually I would like to thank all colleagues from both Aachen and Heidelberg universities whom I forgot to mention.

Last but not least, the entire project would have faltered at some point without the unconditional support from Silke, my family and friends.

Appendix 1 Total thickness plot of Rosengarten transect as entered in PetroMod thermal modelling software and PHIL stratigraphic simulation illustrating restored and projected geometries. x-axis: distance along transect in metres; y-axis: elevation above present day sea level. For a list of timesteps refer to Part 3, Table 3.1. Abbreviations of formations/timesteps: GSst LF1: lower part of Gr den Fm; GSst LF2: middle part of Gr den Fm; GSst LF3: upper part of Gr den Fm; Fiamazza: Fiamazza Mbr of Bellerophon Fm; Bad: Badiota Mbr of Bellerophon Fm; TesMazz: Tesero Oolite and Mazzin Mbr of Werfen Fm; Andraz: Andraz Mbr of Werfen Fm; Seis: Seis Mbr of Werfen Fm; Gasoo: Gastropodenoolith Mbr of Werfen Fm; Campil: Campil Mbr of Werfen Fm; Richthofen: Richthofen Fm; Morbiac: Morbiac Fm; Reitzi, Secedensis, Curionii, Gredleri, Archelaus: lagoon, slope (both Schlern Fm) and basinal deposits (Buchenstein Fm) corresponding to the respective biozone; Wengen: Wengen Fm; Raibl: Raibl Fm; DP1-3: several successions of Dolomia Principale; CalGrigi1-4: several successions of Calcari Grigi; SanVigilio: San Vigilio Oolite; CalFi: Calcare a Filamenti; RAI: Ammonitico Rosso Inferiore; RAM: Ammonitico Rosso Mediore; RAS: Ammonitico Rosso Superiore. Puez: Puez Marls; Antruilles: Antruilles Fm; MonteParei: Monte Parei Conglomerate.

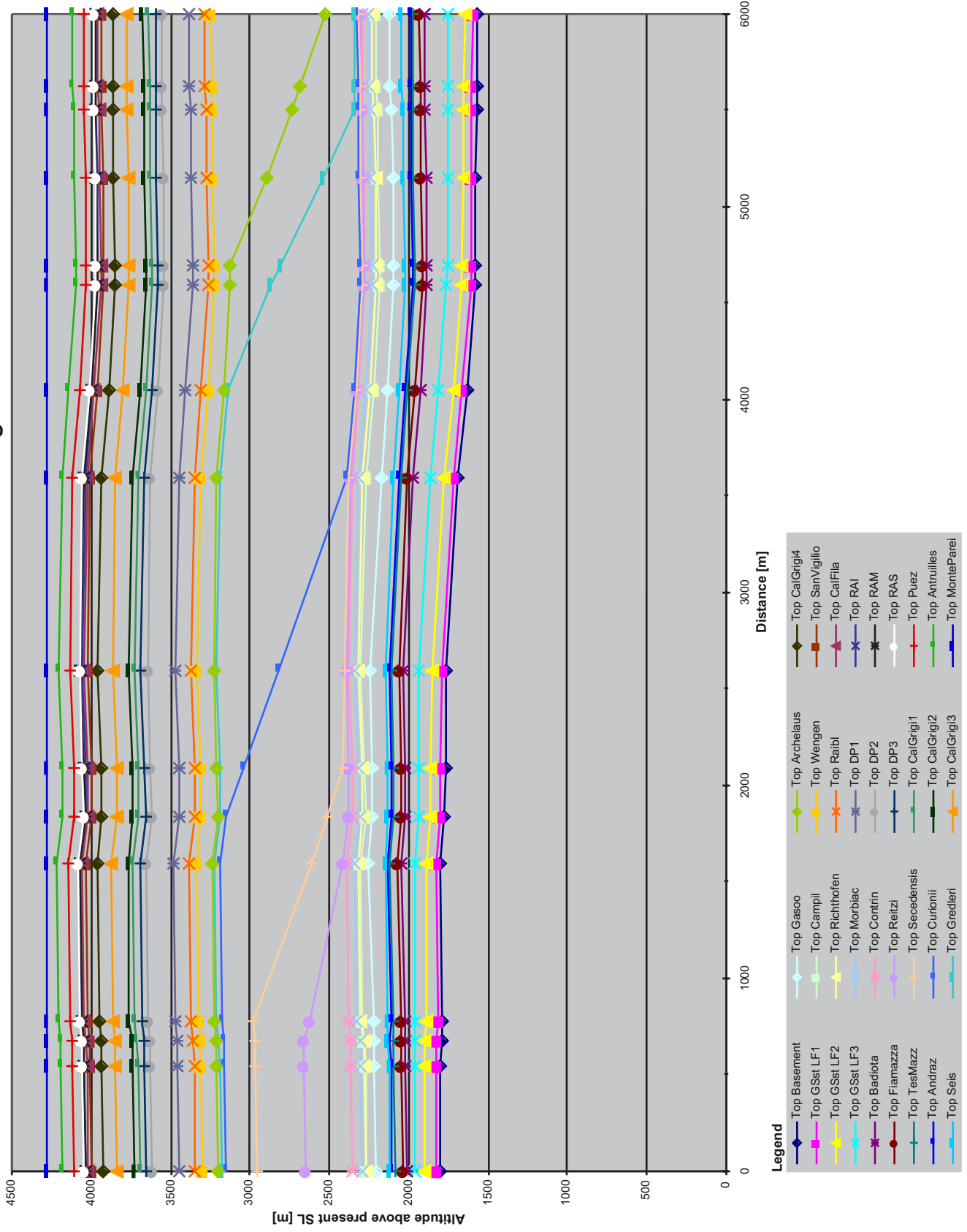
Appendix 2 Porosity depth curves applied during basin modelling with PetroMod. Predefined lithologies were changed to meet the lithologies of the model. The abbreviations correspond to the scheme used in Appendix 1. Other abbreviations: ValBadia: Val Badia Mbr of Werfen Fm; Cencenighe: Cencenighe Mbr of Werfen Fm; Dol: dolomite; Con: Contrin Fm; Sch: Schlern Fm 1; DP: Dolomia Principale; Lst: limestone; CalGri: Calcari Grigi; SVgOo: San Vigilio Oolite; CalFi: Calcare a Filamenti; AmmRosso: Ammonitico Rosso.

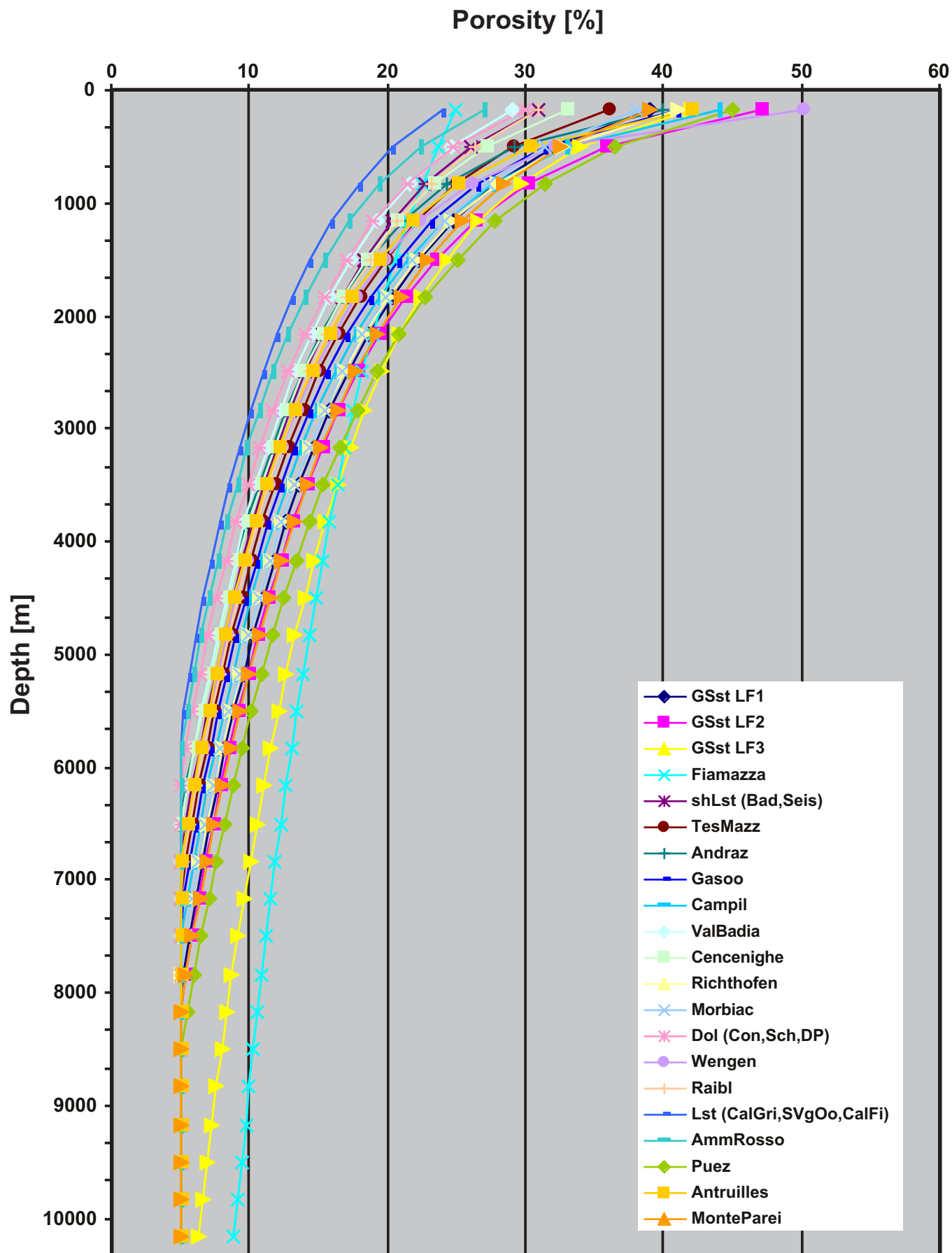
Appendix 3a+b+c+d Petrophysical parameters used during basin modelling with PetroMod. The abbreviations correspond to the scheme used in Appendix 1 and 2.

Appendix 4 Determination of average initial porosity for the numerical basin reverse modelling procedure in PHIL. Portion: portion of thickness of timestep layer with respect to overall thickness; IIP: individual initial porosity, i.e. the sum of this column is the average initial porosity of the entire sedimentary basin fill. Abbreviations correspond to the scheme of Appendix 1 and 2.

Sections B1 to Völsecker Schwaige 2

Total thicknesses transect Rosengarten





	Density kg/m ³	Initial porosity %	Compaction model		Compressibility		Clay content %	Beta factor unitless	e100 unitless	Chem. comp. model Key
			Key	Model	Max 1E-7/kPa	Min 1E-7/kPa				
GSst LF1	2663.1	0.39	Compressibility Model	Compressibility Model	503.6	10	0	0	0	none
GSst LF2	2664	0.47	Compressibility Model	Compressibility Model	1302.6	10	0	0	0	none
GSst LF3	2594.4	0.42	Compressibility Model	Compressibility Model	751.7	6.3	0	0	0	none
Fiamazza	2576.9	0.25	Compressibility Model	Compressibility Model	53.9	4	0	0	0	none
Badiota	2703.1	0.31	Compressibility Model	Compressibility Model	260.1	10	0	0	0	none
TesMazz	2697	0.36	Compressibility Model	Compressibility Model	465.2	10	0	0	0	none
Andraz	2770.4	0.4	Compressibility Model	Compressibility Model	1000	10	0	0	0	none
Seis	2703.1	0.31	Compressibility Model	Compressibility Model	260.1	10	0	0	0	none
Gasoo	2691.7	0.41	Compressibility Model	Compressibility Model	857.6	10	0	0	0	none
Campil	2674.8	0.44	Compressibility Model	Compressibility Model	1191.4	10	0	0	0	none
ValBadia	2705.4	0.29	Compressibility Model	Compressibility Model	216.5	10	0	0	0	none
Cencenighe	2806.2	0.33	Compressibility Model	Compressibility Model	325.8	10	0	0	0	none
Richthofen	2663.9	0.41	Compressibility Model	Compressibility Model	707.2	10	0	0	0	none
Morbiac	2696.2	0.38	Compressibility Model	Compressibility Model	451.1	10	0	0	0	none
Contrin	2836	0.3	Compressibility Model	Compressibility Model	250	10	0	0	0	none
Reitzi	2836	0.3	Compressibility Model	Compressibility Model	250	10	0	0	0	none
Secendensis	2836	0.3	Compressibility Model	Compressibility Model	250	10	0	0	0	none
Curioni	2836	0.3	Compressibility Model	Compressibility Model	250	10	0	0	0	none
Gredleri	2836	0.3	Compressibility Model	Compressibility Model	250	10	0	0	0	none
Archelaus	2836	0.3	Compressibility Model	Compressibility Model	250	10	0	0	0	none
Wengen	2674.8	0.5	Compressibility Model	Compressibility Model	3968.4	10	0	0	0	none
Rabl	2690	0.31	Compressibility Model	Compressibility Model	242.8	10	0	0	0	none
DP1	2836	0.3	Compressibility Model	Compressibility Model	250	10	0	0	0	none
DP2	2836	0.3	Compressibility Model	Compressibility Model	250	10	0	0	0	none
DP3	2836	0.3	Compressibility Model	Compressibility Model	250	10	0	0	0	none
CalGrigi1	2710	0.24	Compressibility Model	Compressibility Model	150	10	0	0	0	none
CalGrigi2	2710	0.24	Compressibility Model	Compressibility Model	150	10	0	0	0	none
CalGrigi3	2710	0.24	Compressibility Model	Compressibility Model	150	10	0	0	0	none
CalGrigi4	2710	0.24	Compressibility Model	Compressibility Model	150	10	0	0	0	none
SanVigilio	2710	0.24	Compressibility Model	Compressibility Model	150	10	0	0	0	none
CalFila	2710	0.24	Compressibility Model	Compressibility Model	150	10	0	0	0	none
RAI	2706.2	0.27	Compressibility Model	Compressibility Model	223.2	10	0	0	0	none
RAM	2706.2	0.27	Compressibility Model	Compressibility Model	223.2	10	0	0	0	none
RAS	2706.2	0.27	Compressibility Model	Compressibility Model	223.2	10	0	0	0	none
Puez	2678.9	0.45	Compressibility Model	Compressibility Model	777.8	10	0	0	0	none
Antruilles	2686	0.42	Compressibility Model	Compressibility Model	1298.9	10	0	0	0	none
MonteParei	2670.2	0.39	Compressibility Model	Compressibility Model	451.7	10	0	0	0	none

Therm. cond. model	Thermal conductivity @20°C		Thermal conductivity @100°C		Thermal conductivity @200°C		Heat capacity @20°C		Heat capacity @100°C		Permeability model		Permeability @5% Porosity		Permeability @75% Porosity	
	W/m/k	W/m/k	W/m/k	W/m/k	W/m/k	W/m/k	kcal/kg/K	kcal/kg/K	kcal/kg/K	kcal/kg/K	Key	Key	log mD	log mD	log mD	log mD
GSst LF1	2.88	2.88	2.57	2.57	2.57	2.57	0.184	0.184	0.218	0.218	Multi-Point Model	Multi-Point Model	-3.28	-3.28	0	0
GSst LF2	2.85	2.85	2.47	2.47	2.47	2.47	0.185	0.185	0.219	0.219	Multi-Point Model	Multi-Point Model	-2.7	-2.7	-0.2	-0.2
GSst LF3	2.28	2.28	2.07	2.07	2.07	2.07	0.223	0.223	0.256	0.256	Multi-Point Model	Multi-Point Model	-6.1	-6.1	-3.4	-3.4
Fiamazza	2.24	2.24	2.04	2.04	2.04	2.04	0.262	0.262	0.287	0.287	Multi-Point Model	Multi-Point Model	-8.57	-8.57	-2.09	-2.09
Badota	2.63	2.63	2.42	2.42	2.42	2.42	0.199	0.199	0.23	0.23	Multi-Point Model	Multi-Point Model	-4.47	-4.47	9.01	9.01
TesMazz	2.5	2.5	2.32	2.32	2.32	2.32	0.201	0.201	0.235	0.235	Multi-Point Model	Multi-Point Model	-4.63	-4.63	6.27	6.27
Andraz	3.02	3.02	2.67	2.67	2.67	2.67	0.202	0.202	0.234	0.234	Multi-Point Model	Multi-Point Model	-3.35	-3.35	9.15	9.15
Seis	2.63	2.63	2.42	2.42	2.42	2.42	0.199	0.199	0.23	0.23	Multi-Point Model	Multi-Point Model	-4.47	-4.47	9.01	9.01
Gasoo	2.42	2.42	2.25	2.25	2.25	2.25	0.201	0.201	0.236	0.236	Multi-Point Model	Multi-Point Model	-4.7	-4.7	5.03	5.03
Campil	2.63	2.63	2.36	2.36	2.36	2.36	0.191	0.191	0.225	0.225	Multi-Point Model	Multi-Point Model	-3.65	-3.65	2.65	2.65
ValBadia	2.7	2.7	2.46	2.46	2.46	2.46	0.198	0.198	0.228	0.228	Multi-Point Model	Multi-Point Model	-4.4	-4.4	10.42	10.42
Cencenighe	3.42	3.42	2.95	2.95	2.95	2.95	0.203	0.203	0.233	0.233	Multi-Point Model	Multi-Point Model	-2.8	-2.8	12.02	12.02
Richthofen	2.8	2.8	2.5	2.5	2.5	2.5	0.186	0.186	0.22	0.22	Multi-Point Model	Multi-Point Model	-3.35	-3.35	0	0
Morbiac	2.45	2.45	2.28	2.28	2.28	2.28	0.203	0.203	0.238	0.238	Multi-Point Model	Multi-Point Model	-4.7	-4.7	4.77	4.77
Contrin	3.81	3.81	3.21	3.21	3.21	3.21	0.202	0.202	0.229	0.229	Multi-Point Model	Multi-Point Model	-2.25	-2.25	15.25	15.25
Reitzi	3.81	3.81	3.21	3.21	3.21	3.21	0.202	0.202	0.229	0.229	Multi-Point Model	Multi-Point Model	-2.25	-2.25	15.25	15.25
Secendensis	3.81	3.81	3.21	3.21	3.21	3.21	0.202	0.202	0.229	0.229	Multi-Point Model	Multi-Point Model	-2.25	-2.25	15.25	15.25
Curtonii	3.81	3.81	3.21	3.21	3.21	3.21	0.202	0.202	0.229	0.229	Multi-Point Model	Multi-Point Model	-2.25	-2.25	15.25	15.25
Gredleri	3.81	3.81	3.21	3.21	3.21	3.21	0.202	0.202	0.229	0.229	Multi-Point Model	Multi-Point Model	-2.25	-2.25	15.25	15.25
Archelaus	3.81	3.81	3.21	3.21	3.21	3.21	0.202	0.202	0.229	0.229	Multi-Point Model	Multi-Point Model	-2.25	-2.25	15.25	15.25
Wengen	2.37	2.37	2.21	2.21	2.21	2.21	0.2	0.2	0.238	0.238	Multi-Point Model	Multi-Point Model	-4.85	-4.85	2.65	2.65
Raibl	2.94	2.94	2.59	2.59	2.59	2.59	0.188	0.188	0.217	0.217	Multi-Point Model	Multi-Point Model	-3.35	-3.35	7.95	7.95
DP1	3.81	3.81	3.21	3.21	3.21	3.21	0.202	0.202	0.229	0.229	Multi-Point Model	Multi-Point Model	-2.25	-2.25	15.25	15.25
DP2	3.81	3.81	3.21	3.21	3.21	3.21	0.202	0.202	0.229	0.229	Multi-Point Model	Multi-Point Model	-2.25	-2.25	15.25	15.25
DP3	3.81	3.81	3.21	3.21	3.21	3.21	0.202	0.202	0.229	0.229	Multi-Point Model	Multi-Point Model	-2.25	-2.25	15.25	15.25
CalGrigi1	2.83	2.83	2.56	2.56	2.56	2.56	0.195	0.195	0.223	0.223	Multi-Point Model	Multi-Point Model	-4.25	-4.25	13.25	13.25
CalGrigi2	2.83	2.83	2.56	2.56	2.56	2.56	0.195	0.195	0.223	0.223	Multi-Point Model	Multi-Point Model	-4.25	-4.25	13.25	13.25
CalGrigi3	2.83	2.83	2.56	2.56	2.56	2.56	0.195	0.195	0.223	0.223	Multi-Point Model	Multi-Point Model	-4.25	-4.25	13.25	13.25
CalGrigi4	2.83	2.83	2.56	2.56	2.56	2.56	0.195	0.195	0.223	0.223	Multi-Point Model	Multi-Point Model	-4.25	-4.25	13.25	13.25
SanVigilio	2.83	2.83	2.56	2.56	2.56	2.56	0.195	0.195	0.223	0.223	Multi-Point Model	Multi-Point Model	-4.25	-4.25	13.25	13.25
CalFila	2.83	2.83	2.56	2.56	2.56	2.56	0.195	0.195	0.223	0.223	Multi-Point Model	Multi-Point Model	-4.25	-4.25	13.25	13.25
RAI	2.75	2.75	2.5	2.5	2.5	2.5	0.196	0.196	0.225	0.225	Multi-Point Model	Multi-Point Model	-4.32	-4.32	11.93	11.93
RAM	2.75	2.75	2.5	2.5	2.5	2.5	0.196	0.196	0.225	0.225	Multi-Point Model	Multi-Point Model	-4.32	-4.32	11.93	11.93
RAS	2.75	2.75	2.5	2.5	2.5	2.5	0.196	0.196	0.225	0.225	Multi-Point Model	Multi-Point Model	-4.32	-4.32	11.93	11.93
Puez	2.47	2.47	2.26	2.26	2.26	2.26	0.199	0.199	0.236	0.236	Multi-Point Model	Multi-Point Model	-4.1	-4.1	-0.62	-0.62
Antruilles	2.62	2.62	2.37	2.37	2.37	2.37	0.195	0.195	0.229	0.229	Multi-Point Model	Multi-Point Model	-3.95	-3.95	5	5
MonteParei	2.7	2.7	2.46	2.46	2.46	2.46	0.191	0.191	0.226	0.226	Multi-Point Model	Multi-Point Model	-3.95	-3.95	-0.27	-0.27

	Permeability		Anisotropy factor		Anisotropy factor		Migration		Crit. oil saturation	Crit. gas saturation	Connate water saturation	Capillary pressure	
	Sandstone model	Permeability Multi-point model	Permeability	log	Thermal conductivity	Saturation	unitless	unitless				unitless	Hg-air
	log mD	Key	log		unitless	unitless	unitless	unitless	unitless	unitless	unitless	unitless	Key
GSst LF1	-2.78	none	1.19	1.12	0.03	0.05	0	0.05	0	0.05	a*porosity+b		
GSst LF2	-1.6	none	1.38	1.18	0.02	0.05	0	0.05	0	0.05	a*porosity+b		
GSst LF3	-0.8	none	1.34	1.2	0.03	0.05	0	0.05	0	0.05	a*porosity+b		
Fiamazza	0	none	0.66	1.06	0.05	0.05	0	0.05	0	0.05	a*porosity+b		
Badiota	0	none	1.1	1.1	0.05	0.05	0	0.05	0	0.05	a*porosity+b		
TesMazz	0	none	1.19	1.12	0.05	0.05	0	0.05	0	0.05	a*porosity+b		
Andraz	0	none	1.46	1.18	0.05	0.05	0	0.05	0	0.05	a*porosity+b		
Seis	0	none	1.1	1.1	0.05	0.05	0	0.05	0	0.05	a*porosity+b		
Gasoo	0	none	1.37	1.16	0.05	0.05	0	0.05	0	0.05	a*porosity+b		
Campil	-0.8	none	1.46	1.18	0.03	0.05	0	0.05	0	0.05	a*porosity+b		
ValBadia	0	none	1.1	1.1	0.05	0.05	0	0.05	0	0.05	a*porosity+b		
Cencenighe	0	none	1.1	1.1	0.05	0.05	0	0.05	0	0.05	a*porosity+b		
Richthofen	-2.35	none	1.28	1.14	0.03	0.05	0	0.05	0	0.05	a*porosity+b		
Morbac	0	none	1.1	1.1	0.05	0.05	0	0.05	0	0.05	a*porosity+b		
Contrin	0	none	1.1	1.1	0.05	0.05	0	0.05	0	0.05	a*porosity+b		
Reitzi	0	none	1.1	1.1	0.05	0.05	0	0.05	0	0.05	a*porosity+b		
Secendensis	0	none	1.1	1.1	0.05	0.05	0	0.05	0	0.05	a*porosity+b		
Curionii	0	none	1.1	1.1	0.05	0.05	0	0.05	0	0.05	a*porosity+b		
Gredleri	0	none	1.1	1.1	0.05	0.05	0	0.05	0	0.05	a*porosity+b		
Archelaus	0	none	1.1	1.1	0.05	0.05	0	0.05	0	0.05	a*porosity+b		
Wengen	0	none	1.66	1.26	0.05	0.05	0	0.05	0	0.05	a*porosity+b		
Raibl	-0.8	none	1.1	1.1	0.03	0.05	0	0.05	0	0.05	a*porosity+b		
DP1	0	none	1.1	1.1	0.05	0.05	0	0.05	0	0.05	a*porosity+b		
DP2	0	none	1.1	1.1	0.05	0.05	0	0.05	0	0.05	a*porosity+b		
DP3	0	none	1.1	1.1	0.05	0.05	0	0.05	0	0.05	a*porosity+b		
CalGrigi1	0	none	1.1	1.1	0.05	0.05	0	0.05	0	0.05	a*porosity+b		
CalGrigi2	0	none	1.1	1.1	0.05	0.05	0	0.05	0	0.05	a*porosity+b		
CalGrigi3	0	none	1.1	1.1	0.05	0.05	0	0.05	0	0.05	a*porosity+b		
CalGrigi4	0	none	1.1	1.1	0.05	0.05	0	0.05	0	0.05	a*porosity+b		
San Vigilio	0	none	1.1	1.1	0.05	0.05	0	0.05	0	0.05	a*porosity+b		
CalFila	0	none	1.1	1.1	0.05	0.05	0	0.05	0	0.05	a*porosity+b		
RAI	0	none	1.19	1.12	0.05	0.05	0	0.05	0	0.05	a*porosity+b		
RAM	0	none	1.19	1.12	0.05	0.05	0	0.05	0	0.05	a*porosity+b		
RAS	0	none	1.19	1.12	0.05	0.05	0	0.05	0	0.05	a*porosity+b		
Puez	-0.6	none	1.1	1.1	0.04	0.05	0	0.05	0	0.05	a*porosity+b		
Antrullies	-0.6	none	1.52	1.22	0.04	0.05	0	0.05	0	0.05	a*porosity+b		
MonterParei	-2.45	none	1.1	1.1	0.03	0.05	0	0.05	0	0.05	a*porosity+b		

	Capillary pressure Hg-air		Capillary pressure Hg-air Parameter B	Capillary pressure Oil @5% porosity Mpa	Capillary pressure Oil @75% porosity Mpa	Capillary pressure Gas @5% porosity Mpa	Capillary pressure Gas @75% porosity Mpa	Radioactive heat microW/m ³	Diffusion coefficient m ² /s	Fracture limit (Lithostatic)%	Fracture curve
	Parameter A	Parameter									
GSst LF1	0	0.22	0.03	0.03	0.03	0.03	0.03	0	1.02	80	none
GSst LF2	0	0.31	0.03	0.03	0.03	0.03	0.03	0	89.57	80	none
GSst LF3	0	5.9	0.68	0.68	0.68	0.68	0.68	0	57.17	0	none
Fiamazza	0	69.41	8.31	8.31	8.31	8.31	8.31	0	30.37	0	none
Badiota	0	8.57	1	1	1	1	1	0	35.17	80	none
TesMazz	0	8.92	1.04	1.04	1.04	1.04	1.04	0	32.56	80	none
Andraz	0	10.08	1.18	1.18	1.18	1.18	1.18	0	36	80	none
Seis	0	8.57	1	1	1	1	1	0	35.17	80	none
Gasoo	0	9.68	1.13	1.13	1.13	1.13	1.13	0	32.17	80	none
Campil	0	1.63	0.19	0.19	0.19	0.19	0.19	0	64	80	none
ValBadia	0	8.57	1	1	1	1	1	0	36.78	80	none
Cencenighe	0	8.57	1	1	1	1	1	0	36.78	80	none
Richthofen	0	0.33	0.04	0.04	0.04	0.04	0.04	0	94	80	none
Morbiac	0	8.57	1	1	1	1	1	0	30.34	80	none
Contrin	0	8.57	1	1	1	1	1	0	40	80	none
Reitzi	0	8.57	1	1	1	1	1	0	40	80	none
Secendensis	0	8.57	1	1	1	1	1	0	40	80	none
Curionii	0	8.57	1	1	1	1	1	0	40	80	none
Gredleri	0	8.57	1	1	1	1	1	0	40	80	none
Archelaus	0	8.57	1	1	1	1	1	0	40	80	none
Wengen	0	14.92	1.74	1.74	1.74	1.74	1.74	0	32	80	none
Rabl	0	1.39	0.16	0.16	0.16	0.16	0.16	0	68	80	none
DP1	0	8.57	1	1	1	1	1	0	40	80	none
DP2	0	8.57	1	1	1	1	1	0	40	80	none
DP3	0	8.57	1	1	1	1	1	0	40	80	none
CalGrigi1	0	8.57	1	1	1	1	1	0	40	80	none
CalGrigi2	0	8.57	1	1	1	1	1	0	40	80	none
CalGrigi3	0	8.57	1	1	1	1	1	0	40	80	none
CalGrigi4	0	8.57	1	1	1	1	1	0	40	80	none
SanVigilio	0	8.57	1	1	1	1	1	0	40	80	none
CalFila	0	8.57	1	1	1	1	1	0	40	80	none
RAI	0	8.92	1.04	1.04	1.04	1.04	1.04	0	39	80	none
RAM	0	1.04	1.04	1.04	1.04	1.04	1.04	0	39	80	none
RAS	0	8.92	1.04	1.04	1.04	1.04	1.04	0	39	80	none
Puez	0	2.18	0.25	0.25	0.25	0.25	0.25	0	49.73	80	none
Antrullles	0	3.54	0.41	0.41	0.41	0.41	0.41	0	51.35	80	none
MonteParei	0	0.55	0.06	0.06	0.06	0.06	0.06	0	84.17	80	none

Proximal										Intermediate										Distal																																																																																																																																																																																																																																																																																																																																																																																																																																																																																																																																																											
Transect KM 0.0										Transect KM 3.6										Transect KM 6.0																																																																																																																																																																																																																																																																																																																																																																																																																																																																																																																																																											
Thickness	Timestep	Portion	IP	Ind. IP	Thickness	Timestep	Portion	IP	Ind. IP	Thickness	Timestep	Portion	IP	Ind. IP	Thickness	Timestep	Portion	IP	Ind. IP	Thickness	Timestep	Portion	IP	Ind. IP																																																																																																																																																																																																																																																																																																																																																																																																																																																																																																																																																							
26.00	GSst Lf1	0.01047	0.39000	0.00408	29.60	GSst Lf1	0.01143	0.39000	0.00446	32.00	GSst Lf1	0.01180	0.39000	0.00460	75.00	GSst Lf2	0.03020	0.42000	0.01269	57.00	GSst Lf2	0.02202	0.42000	0.00925	45.00	GSst Lf2	0.01659	0.42000	0.00697	63.00	GSst Lf3	0.02537	0.36000	0.00913	88.80	GSst Lf3	0.03430	0.36000	0.01235	106.00	GSst Lf3	0.03907	0.36000	0.01407	50.00	Fiamazza	0.02014	0.28000	0.00564	110.00	Fiamazza	0.04249	0.28000	0.01190	150.00	Fiamazza	0.05529	0.28000	0.01548	25.00	Badlota	0.01007	0.51000	0.00513	29.80	Badlota	0.01151	0.51000	0.00587	33.00	Badlota	0.01216	0.51000	0.00620	48.42	TesMazz	0.01950	0.45000	0.00877	43.50	TesMazz	0.01680	0.45000	0.00756	47.00	TesMazz	0.01732	0.45000	0.00780	19.71	Andraz	0.00794	0.36000	0.00286	13.50	Andraz	0.00521	0.36000	0.00188	12.00	Andraz	0.00442	0.36000	0.00159	11.90	Seis	0.00479	0.51000	0.00244	38.10	Seis	0.01472	0.51000	0.00751	56.00	Seis	0.02064	0.51000	0.01053	93.55	Gasoo	0.03767	0.46000	0.01733	71.30	Gasoo	0.02777	0.46000	0.01278	79.00	Gasoo	0.02912	0.46000	0.01339	53.63	Campil	0.02160	0.40000	0.00864	91.50	Campil	0.03535	0.40000	0.01414	79.50	Campil	0.02930	0.40000	0.01172	7.78	Richthofen	0.00313	0.38000	0.00119	25.00	Richthofen	0.00966	0.38000	0.00367	23.20	Richthofen	0.00855	0.38000	0.00325	26.30	Morbiac	0.01059	0.51000	0.00540	25.00	Morbiac	0.00966	0.51000	0.00493	25.30	Morbiac	0.00933	0.51000	0.00476	54.33	Contrin	0.02188	0.40000	0.00875	45.00	Contrin	0.01738	0.40000	0.00695	38.50	Contrin	0.01419	0.40000	0.00568	300.00	Reitzi	0.12082	0.40000	0.04833	11.00	Reitzi	0.00425	0.40000	0.00170	9.50	Reitzi	0.00350	0.40000	0.00140	300.00	Secendensis	0.12082	0.40000	0.04833	8.00	Secendensis	0.00309	0.40000	0.00124	9.50	Secendensis	0.00350	0.40000	0.00140	200.00	Curtonii	0.08054	0.40000	0.03222	12.00	Curtonii	0.00464	0.40000	0.00185	13.00	Curtonii	0.00479	0.40000	0.00192	30.00	Gredleri	0.01208	0.40000	0.00483	799.00	Gredleri	0.30865	0.40000	0.12346	17.50	Gredleri	0.00645	0.40000	0.00258	20.00	Archelaus	0.00805	0.40000	0.00322	20.00	Archelaus	0.00773	0.40000	0.00309	177.00	Archelaus	0.06524	0.40000	0.02610	100.00	Wengen	0.04027	0.52500	0.02114	100.00	Wengen	0.03863	0.52500	0.02028	723.50	Wengen	0.26668	0.52500	0.14001	40.00	Rabl	0.01611	0.58000	0.00934	40.00	Rabl	0.01545	0.58000	0.00896	40.00	Rabl	0.01474	0.58000	0.00855	100.00	DP1	0.04027	0.40000	0.01611	100.00	DP1	0.03863	0.40000	0.01545	100.00	DP1	0.03686	0.40000	0.01474	0.7048	DP2	0.07048	0.40000	0.02819	175.00	DP2	0.06760	0.40000	0.02704	175.00	DP2	0.06450	0.40000	0.02580	0.1611	DP3	0.01611	0.40000	0.00644	40.00	DP3	0.01545	0.40000	0.00618	40.00	DP3	0.01474	0.40000	0.00590	0.1611	CalGrig1	0.01611	0.60000	0.00967	40.00	CalGrig1	0.01545	0.60000	0.00927	40.00	CalGrig1	0.01474	0.60000	0.00885	0.1410	CalGrig2	0.01410	0.60000	0.00846	35.00	CalGrig2	0.01352	0.60000	0.00811	35.00	CalGrig2	0.01290	0.60000	0.00774	0.44229	CalGrig3	0.04429	0.60000	0.02537	105.00	CalGrig3	0.04056	0.60000	0.02434	105.00	CalGrig3	0.03870	0.60000	0.02322	0.03624	CalGrig4	0.03624	0.60000	0.02175	90.00	CalGrig4	0.03477	0.60000	0.02086	90.00	CalGrig4	0.03317	0.60000	0.01990	0.02819	SanVigilio	0.02819	0.60000	0.01691	70.00	SanVigilio	0.02704	0.60000	0.01622	70.00	SanVigilio	0.02580	0.60000	0.01548	0.00805	CalFila	0.00805	0.60000	0.00483	20.00	CalFila	0.00773	0.60000	0.00464	20.00	CalFila	0.00737	0.60000	0.00442	0.00604	RAM	0.00604	0.57000	0.00344	15.00	RAM	0.00579	0.57000	0.00330	15.00	RAM	0.00553	0.57000	0.00315	0.00201	RAM	0.00201	0.57000	0.00115	5.00	RAM	0.00193	0.57000	0.00110	5.00	RAM	0.00184	0.57000	0.00105	0.00403	RAS	0.00403	0.57000	0.00230	10.00	RAS	0.00386	0.57000	0.00220	10.00	RAS	0.00369	0.57000	0.00210	0.02416	Puez	0.02416	0.43500	0.01051	60.00	Puez	0.02318	0.43500	0.01008	60.00	Puez	0.02212	0.43500	0.00962	0.02819	Antrullies	0.02819	0.51000	0.01438	70.00	Antrullies	0.02704	0.51000	0.01379	70.00	Antrullies	0.02580	0.51000	0.01316	0.04169	MonteParei	0.04169	0.41500	0.01730	95.00	MonteParei	0.03670	0.41500	0.01523	161.50	MonteParei	0.05953	0.41500	0.02470	2483.12	TOTAL	1.00		0.45	2588.70	TOTAL	1.00		0.44	2713.00	TOTAL	1.00		0.47	Initial porosity of entire transect					0.45					0.44					0.47				
75.00	GSst Lf2	0.03020	0.42000	0.01269	57.00	GSst Lf2	0.02202	0.42000	0.00925	45.00	GSst Lf2	0.01659	0.42000	0.00697	63.00	GSst Lf3	0.02537	0.36000	0.00913	88.80	GSst Lf3	0.03430	0.36000	0.01235	106.00	GSst Lf3	0.03907	0.36000	0.01407	50.00	Fiamazza	0.02014	0.28000	0.00564	110.00	Fiamazza	0.04249	0.28000	0.01190	150.00	Fiamazza	0.05529	0.28000	0.01548	25.00	Badlota	0.01007	0.51000	0.00513	29.80	Badlota	0.01151	0.51000	0.00587	33.00	Badlota	0.01216	0.51000	0.00620	48.42	TesMazz	0.01950	0.45000	0.00877	43.50	TesMazz	0.01680	0.45000	0.00756	47.00	TesMazz	0.01732	0.45000	0.00780	19.71	Andraz	0.00794	0.36000	0.00286	13.50	Andraz	0.00521	0.36000	0.00188	12.00	Andraz	0.00442	0.36000	0.00159	11.90	Seis	0.00479	0.51000	0.00244	38.10	Seis	0.01472	0.51000	0.00751	56.00	Seis	0.02064	0.51000	0.01053	93.55	Gasoo	0.03767	0.46000	0.01733	71.30	Gasoo	0.02777	0.46000	0.01278	79.00	Gasoo	0.02912	0.46000	0.01339	53.63	Campil	0.02160	0.40000	0.00864	91.50	Campil	0.03535	0.40000	0.01414	79.50	Campil	0.02930	0.40000	0.01172	7.78	Richthofen	0.00313	0.38000	0.00119	25.00	Richthofen	0.00966	0.38000	0.00367	23.20	Richthofen	0.00855	0.38000	0.00325	26.30	Morbiac	0.01059	0.51000	0.00540	25.00	Morbiac	0.00966	0.51000	0.00493	25.30	Morbiac	0.00933	0.51000	0.00476	54.33	Contrin	0.02188	0.40000	0.00875	45.00	Contrin	0.01738	0.40000	0.00695	38.50	Contrin	0.01419	0.40000	0.00568	300.00	Reitzi	0.12082	0.40000	0.04833	11.00	Reitzi	0.00425	0.40000	0.00170	9.50	Reitzi	0.00350	0.40000	0.00140	300.00	Secendensis	0.12082	0.40000	0.04833	8.00	Secendensis	0.00309	0.40000	0.00124	9.50	Secendensis	0.00350	0.40000	0.00140	200.00	Curtonii	0.08054	0.40000	0.03222	12.00	Curtonii	0.00464	0.40000	0.00185	13.00	Curtonii	0.00479	0.40000	0.00192	30.00	Gredleri	0.01208	0.40000	0.00483	799.00	Gredleri	0.30865	0.40000	0.12346	17.50	Gredleri	0.00645	0.40000	0.00258	20.00	Archelaus	0.00805	0.40000	0.00322	20.00	Archelaus	0.00773	0.40000	0.00309	177.00	Archelaus	0.06524	0.40000	0.02610	100.00	Wengen	0.04027	0.52500	0.02114	100.00	Wengen	0.03863	0.52500	0.02028	723.50	Wengen	0.26668	0.52500	0.14001	40.00	Rabl	0.01611	0.58000	0.00934	40.00	Rabl	0.01545	0.58000	0.00896	40.00	Rabl	0.01474	0.58000	0.00855	100.00	DP1	0.04027	0.40000	0.01611	100.00	DP1	0.03863	0.40000	0.01545	100.00	DP1	0.03686	0.40000	0.01474	0.7048	DP2	0.07048	0.40000	0.02819	175.00	DP2	0.06760	0.40000	0.02704	175.00	DP2	0.06450	0.40000	0.02580	0.1611	DP3	0.01611	0.40000	0.00644	40.00	DP3	0.01545	0.40000	0.00618	40.00	DP3	0.01474	0.40000	0.00590	0.1611	CalGrig1	0.01611	0.60000	0.00967	40.00	CalGrig1	0.01545	0.60000	0.00927	40.00	CalGrig1	0.01474	0.60000	0.00885	0.1410	CalGrig2	0.01410	0.60000	0.00846	35.00	CalGrig2	0.01352	0.60000	0.00811	35.00	CalGrig2	0.01290	0.60000	0.00774	0.44229	CalGrig3	0.04429	0.60000	0.02537	105.00	CalGrig3	0.04056	0.60000	0.02434	105.00	CalGrig3	0.03870	0.60000	0.02322	0.03624	CalGrig4	0.03624	0.60000	0.02175	90.00	CalGrig4	0.03477	0.60000	0.02086	90.00	CalGrig4	0.03317	0.60000	0.01990	0.02819	SanVigilio	0.02819	0.60000	0.01691	70.00	SanVigilio	0.02704	0.60000	0.01622	70.00	SanVigilio	0.02580	0.60000	0.01548	0.00805	CalFila	0.00805	0.60000	0.00483	20.00	CalFila	0.00773	0.60000	0.00464	20.00	CalFila	0.00737	0.60000	0.00442	0.00604	RAM	0.00604	0.57000	0.00344	15.00	RAM	0.00579	0.57000	0.00330	15.00	RAM	0.00553	0.57000	0.00315	0.00201	RAM	0.00201	0.57000	0.00115	5.00	RAM	0.00193	0.57000	0.00110	5.00	RAM	0.00184	0.57000	0.00105	0.00403	RAS	0.00403	0.57000	0.00230	10.00	RAS	0.00386	0.57000	0.00220	10.00	RAS	0.00369	0.57000	0.00210	0.02416	Puez	0.02416	0.43500	0.01051	60.00	Puez	0.02318	0.43500	0.01008	60.00	Puez	0.02212	0.43500	0.00962	0.02819	Antrullies	0.02819	0.51000	0.01438	70.00	Antrullies	0.02704	0.51000	0.01379	70.00	Antrullies	0.02580	0.51000	0.01316	0.04169	MonteParei	0.04169	0.41500	0.01730	95.00	MonteParei	0.03670	0.41500	0.01523	161.50	MonteParei	0.05953	0.41500	0.02470	2483.12	TOTAL	1.00		0.45	2588.70	TOTAL	1.00		0.44	2713.00	TOTAL	1.00		0.47	Initial porosity of entire transect					0.45					0.44					0.47																			
63.00	GSst Lf3	0.02537	0.36000	0.00913	88.80	GSst Lf3	0.03430	0.36000	0.01235	106.00	GSst Lf3	0.03907	0.36000	0.01407	50.00	Fiamazza	0.02014	0.28000	0.00564	110.00	Fiamazza	0.04249	0.28000	0.01190	150.00	Fiamazza	0.05529	0.28000	0.01548	25.00	Badlota	0.01007	0.51000	0.00513	29.80	Badlota	0.01151	0.51000	0.00587	33.00	Badlota	0.01216	0.51000	0.00620	48.42	TesMazz	0.01950	0.45000	0.00877	43.50	TesMazz	0.01680	0.45000	0.00756	47.00	TesMazz	0.01732	0.45000	0.00780	19.71	Andraz	0.00794	0.36000	0.00286	13.50	Andraz	0.00521	0.36000	0.00188	12.00	Andraz	0.00442	0.36000	0.00159	11.90	Seis	0.00479	0.51000	0.00244	38.10	Seis	0.01472	0.51000	0.00751	56.00	Seis	0.02064	0.51000	0.01053	93.55	Gasoo	0.03767	0.46000	0.01733	71.30	Gasoo	0.02777	0.46000	0.01278	79.00	Gasoo	0.02912	0.46000	0.01339	53.63	Campil	0.02160	0.40000	0.00864	91.50	Campil	0.03535	0.40000	0.01414	79.50	Campil	0.02930	0.40000	0.01172	7.78	Richthofen	0.00313	0.38000	0.00119	25.00	Richthofen	0.00966	0.38000	0.00367	23.20	Richthofen	0.00855	0.38000	0.00325	26.30	Morbiac	0.01059	0.51000	0.00540	25.00	Morbiac	0.00966	0.51000	0.00493	25.30	Morbiac	0.00933	0.51000	0.00476	54.33	Contrin	0.02188	0.40000	0.00875	45.00	Contrin	0.01738	0.40000	0.00695	38.50	Contrin	0.01419	0.40000	0.00568	300.00	Reitzi	0.12082	0.40000	0.04833	11.00	Reitzi	0.00425	0.40000	0.00170	9.50	Reitzi	0.00350	0.40000	0.00140	300.00	Secendensis	0.12082	0.40000	0.04833	8.00	Secendensis	0.00309	0.40000	0.00124	9.50	Secendensis	0.00350	0.40000	0.00140	200.00	Curtonii	0.08054	0.40000	0.03222	12.00	Curtonii	0.00464	0.40000	0.00185	13.00	Curtonii	0.00479	0.40000	0.00192	30.00	Gredleri	0.01208	0.40000	0.00483	799.00	Gredleri	0.30865	0.40000	0.12346	17.50	Gredleri	0.00645	0.40000	0.00258	20.00	Archelaus	0.00805	0.40000	0.00322	20.00	Archelaus	0.00773	0.40000	0.00309	177.00	Archelaus	0.06524	0.40000	0.02610	100.00	Wengen	0.04027	0.52500	0.02114	100.00	Wengen	0.03863	0.52500	0.02028	723.50	Wengen	0.26668	0.52500	0.14001	40.00	Rabl	0.01611	0.58000	0.00934	40.00	Rabl	0.01545	0.58000	0.00896	40.00	Rabl	0.01474	0.58000	0.00855	100.00	DP1	0.04027	0.40000	0.01611	100.00	DP1	0.03863	0.40000	0.01545	100.00	DP1	0.03686	0.40000	0.01474	0.7048	DP2	0.07048	0.40000	0.02819	175.00	DP2	0.06760	0.40000	0.02704	175.00	DP2	0.06450	0.40000	0.02580	0.1611	DP3	0.01611	0.40000	0.00644	40.00	DP3	0.01545	0.40000	0.00618	40.00	DP3	0.01474	0.40000	0.00590	0.1611	CalGrig1	0.01611	0.60000	0.00967	40.00	CalGrig1	0.01545	0.60000	0.00927	40.00	CalGrig1	0.01474	0.60000	0.00885	0.1410	CalGrig2	0.01410	0.60000	0.00846	35.00	CalGrig2	0.01352	0.60000	0.00811	35.00	CalGrig2	0.01290	0.60000	0.00774	0.44229	CalGrig3	0.04429	0.60000	0.02537	105.00	CalGrig3	0.04056	0.60000	0.02434	105.00	CalGrig3	0.03870	0.60000	0.02322	0.03624	CalGrig4	0.03624	0.60000	0.02175	90.00	CalGrig4	0.03477	0.60000	0.02086	90.00	CalGrig4	0.03317	0.60000	0.01990	0.02819	SanVigilio	0.02819	0.60000	0.01691	70.00	SanVigilio	0.02704	0.60000	0.01622	70.00	SanVigilio	0.02580	0.60000	0.01548	0.00805	CalFila	0.00805	0.60000	0.00483	20.00	CalFila	0.00773	0.60000	0.00464	20.00	CalFila	0.00737	0.60000	0.00442	0.00604	RAM	0.00604	0.57000	0.00344	15.00	RAM	0.00579	0.57000	0.00330	15.00	RAM	0.00553	0.57000	0.00315	0.00201	RAM	0.00201	0.57000	0.00115	5.00	RAM	0.00193	0.57000	0.00110	5.00	RAM	0.00184	0.57000	0.00105	0.00403	RAS	0.00403	0.57000	0.00230	10.00	RAS	0.00386	0.57000	0.00220	10.00	RAS	0.00369	0.57000	0.00210	0.02416	Puez	0.02416	0.43500	0.01051	60.00	Puez	0.02318	0.43500	0.01008	60.00	Puez	0.02212	0.43500	0.00962	0.02819	Antrullies	0.02819	0.51000	0.01438	70.00	Antrullies	0.02704	0.51000	0.01379	70.00	Antrullies	0.02580	0.51000	0.01316	0.04169	MonteParei	0.04169	0.41500	0.01730	95.00	MonteParei	0.03670	0.41500	0.01523	161.50	MonteParei	0.05953	0.41500	0.02470	2483.12	TOTAL	1.00		0.45	2588.70	TOTAL	1.00		0.44	2713.00	TOTAL	1.00		0.47	Initial porosity of entire transect					0.45					0.44					0.47																																		
50.00	Fiamazza	0.02014	0.28000	0.00564	110.00	Fiamazza	0.04249	0.28000	0.01190	150.00	Fiamazza	0.05529	0.28000	0.01548	25.00	Badlota	0.01007	0.51000	0.00513	29.80	Badlota	0.01151	0.51000	0.00587	33.00	Badlota	0.01216	0.51000	0.00620	48.42	TesMazz	0.01950	0.45000	0.00877	43.50	TesMazz	0.01680	0.45000	0.00756	47.00	TesMazz	0.01732	0.45000	0.00780	19.71	Andraz	0.00794	0.36000	0.00286	13.50	Andraz	0.00521	0.36000	0.00188	12.00	Andraz	0.00442	0.36000	0.00159	11.90	Seis	0.00479	0.51000	0.00244	38.10	Seis	0.01472	0.51000	0.00751	56.00	Seis	0.02064	0.51000	0.01053	93.55	Gasoo	0.03767	0.46000	0.01733	71.30	Gasoo	0.02777	0.46000	0.01278	79.00	Gasoo	0.02912	0.46000	0.01339	53.63	Campil	0.02160	0.40000	0.00864	91.50	Campil	0.03535	0.40000	0.01414	79.50	Campil	0.02930	0.40000	0.01172	7.78	Richthofen	0.00313	0.38000	0.00119	25.00	Richthofen	0.00966	0.38000	0.00367	23.20	Richthofen	0.00855	0.38000	0.00325	26.30	Morbiac	0.01059	0.51000	0.00540	25.00	Morbiac	0.00966	0.51000	0.00493	25.30	Morbiac	0.00933	0.51000	0.00476	54.33	Contrin	0.02188	0.40000	0.00875	45.00	Contrin	0.01738	0.40000	0.00695	38.50	Contrin	0.01419	0.40000	0.00568	300.00	Reitzi	0.12082	0.40000	0.04833	11.00	Reitzi	0.00425	0.40000	0.00170	9.50	Reitzi	0.00350	0.40000	0.00140	300.00	Secendensis	0.12082	0.40000	0.04833	8.00	Secendensis	0.00309	0.40000	0.00124	9.50	Secendensis	0.00350	0.40000	0.00140	200.00	Curtonii	0.08054	0.40000	0.03222	12.00	Curtonii	0.00464	0.40000	0.00185	13.00	Curtonii	0.00479	0.40000	0.00192	30.00	Gredleri	0.01208	0.40000	0.00483	799.00	Gredleri	0.30865	0.40000	0.12346	17.50	Gredleri	0.00645	0.40000	0.00258	20.00	Archelaus	0.00805	0.40000	0.00322	20.00	Archelaus	0.00773	0.40000	0.00309	177.00	Archelaus	0.06524	0.40000	0.02610	100.00	Wengen	0.04027	0.52500	0.02114	100.00	Wengen	0.03863	0.52500	0.02028	723.50	Wengen	0.26668	0.52500	0.14001	40.00	Rabl	0.01611	0.58000	0.00934	40.00	Rabl	0.01545	0.58000	0.00896	40.00	Rabl	0.01474	0.58000	0.00855	100.00	DP1	0.04027	0.40000	0.01611	100.00	DP1	0.03863	0.40000	0.01545	100.00	DP1	0.03686	0.40000	0.01474	0.7048	DP2	0.07048	0.40000	0.02819	175.00	DP2	0.06760	0.40000	0.02704	175.00	DP2	0.06450	0.40000	0.02580	0.1611	DP3	0.01611	0.40000	0.00644	40.00	DP3	0.01545	0.40000	0.00618	40.00	DP3	0.01474	0.40000	0.00590	0.1611	CalGrig1	0.01611	0.60000	0.00967	40.00	CalGrig1	0.01545	0.60000	0.00927	40.00	CalGrig1	0.01474	0.60000	0.00885	0.1410	CalGrig2	0.01410	0.60000	0.00846	35.00	CalGrig2	0.01352	0.60000	0.00811	35.00	CalGrig2	0.01290	0.60000	0.00774	0.44229	CalGrig3	0.04429	0.60000	0.02537	105.00	CalGrig3	0.04056	0.60000	0.02434	105.00	CalGrig3	0.03870	0.60000	0.02322	0.03624	CalGrig4	0.03624	0.60000	0.02175	90.00	CalGrig4	0.03477	0.60000	0.02086	90.00	CalGrig4	0.03317	0.60000	0.01990	0.02819	SanVigilio	0.02819	0.60000	0.01691	70.00	SanVigilio	0.02704	0.60000	0.01622	70.00	SanVigilio	0.02580	0.60000	0.01548	0.00805	CalFila	0.00805	0.60000	0.00483	20.00	CalFila	0.00773	0.60000	0.00464	20.00	CalFila	0.00737	0.60000	0.00442	0.00604	RAM	0.00604	0.57000	0.00344	15.00	RAM	0.00579	0.57000	0.00330	15.00	RAM	0.00553	0.57000	0.00315	0.00201	RAM	0.00201	0.57000	0.00115	5.00	RAM	0.00193	0.57000	0.00110	5.00	RAM	0.00184	0.57000	0.00105	0.00403	RAS	0.00403	0.57000	0.00230	10.00	RAS	0.00386	0.57000	0.00220	10.00	RAS	0.00369	0.57000	0.00210	0.02416	Puez	0.02416	0.43500	0.01051	60.00	Puez	0.02318	0.43500	0.01008	60.00	Puez	0.02212	0.43500	0.00962	0.02819	Antrullies	0.02819	0.51000	0.01438	70.00	Antrullies	0.02704	0.51000	0.01379	70.00	Antrullies	0.02580	0.51000	0.01316	0.04169	MonteParei	0.04169	0.41500	0.01730	95.00	MonteParei	0.03670	0.41500	0.01523	161.50	MonteParei	0.05953	0.41500	0.02470	2483.12	TOTAL	1.00		0.45	2588.70	TOTAL	1.00		0.44	2713.00	TOTAL	1.00		0.47	Initial porosity of entire transect					0.45					0.44					0.47																																																	
25.00	Badlota	0.01007	0.51000	0.00513	29.80	Badlota	0.01151	0.51000	0.00587	33.00	Badlota	0.01216	0.51000	0.00620	48.42	TesMazz	0.01950	0.45000	0.00877	43.50	TesMazz	0.01680	0.45000	0.00756	47.00	TesMazz	0.01732	0.45000	0.00780	19.71	Andraz	0.00794	0.36000	0.00286	13.50	Andraz	0.00521	0.36000	0.00188	12.00	Andraz	0.00442	0.36000	0.00159	11.90	Seis	0.00479	0.51000	0.00244	38.10	Seis	0.01472	0.51000	0.00751	56.00	Seis	0.02064	0.51000	0.01053	93.55	Gasoo	0.03767	0.46000	0.01733	71.30	Gasoo	0.02777	0.46000	0.01278	79.00	Gasoo	0.02912	0.46000	0.01339	53.63	Campil	0.02160	0.40000	0.00864	91.50	Campil	0.03535	0.40000	0.01414	79.50	Campil	0.02930	0.40000	0.01172	7.78	Richthofen	0.00313	0.38000	0.00119	25.00	Richthofen	0.00966	0.38000	0.00367	23.20	Richthofen	0.00855	0.38000	0.00325	26.30	Morbiac	0.01059	0.51000	0.00540	25.00	Morbiac	0.00966	0.51000	0.00493	25.30	Morbiac	0.00933	0.51000	0.00476	54.33	Contrin	0.02188	0.40000	0.00875	45.00	Contrin	0.01738	0.40000	0.00695	38.50	Contrin	0.01419	0.40000	0.00568	300.00	Reitzi	0.12082	0.40000	0.04833	11.00	Reitzi	0.00425	0.40000	0.00170	9.50	Reitzi	0.00350	0.40000	0.00140	300.00	Secendensis	0.12082	0.40000	0.04833	8.00	Secendensis	0.00309	0.40000	0.00124	9.50	Secendensis	0.00350	0.40000	0.00140	200.00	Curtonii	0.08054	0.40000	0.03222	12.00	Curtonii	0.00464	0.40000	0.00185	13.00	Curtonii	0.00479	0.40000	0.00192	30.00	Gredleri	0.01208	0.40000	0.00483	799.00	Gredleri	0.30865	0.40000	0.12346	17.50	Gredleri	0.00645	0.40000	0.00258	20.00	Archelaus	0.00805	0.40000	0.00322	20.00	Archelaus	0.00773	0.40000	0.00309	177.00	Archelaus	0.06524	0.40000	0.02610	100.00	Wengen	0.04027	0.52500	0.02114	100.00	Wengen	0.03863	0.52500	0.02028	723.50	Wengen	0.26668	0.52500	0.14001	40.00	Rabl	0.01611	0.58000	0.00934	40.00	Rabl	0.01545	0.58000	0.00896	40.00	Rabl	0.01474	0.58000	0.00855	100.00	DP1	0.04027	0.40000	0.01611	100.00	DP1	0.03863	0.40000	0.01545	100.00	DP1	0.03686	0.40000	0.01474	0.7048	DP2	0.07048	0.40000	0.02819	175.00	DP2	0.06760	0.40000	0.02704	175.00	DP2	0.06450	0.40000	0.02580	0.1611	DP3	0.01611	0.40000	0.00644	40.00	DP3	0.01545	0.40000	0.00618	40.00	DP3	0.01474	0.40000	0.00590	0.1611	CalGrig1	0.01611	0.60000	0.00967	40.00	CalGrig1	0.01545	0.60000	0.00927	40.00	CalGrig1	0.01474	0.60000	0.00885	0.1410	CalGrig2	0.01410	0.60000	0.00846	35.00	CalGrig2	0.01352	0.60000	0.00811	35.00	CalGrig2	0.01290	0.60000	0.00774	0.44229	CalGrig3	0.04429	0.60000	0.02537	105.00	CalGrig3	0.04056	0.60000	0.02434	105.00	CalGrig3	0.03870	0.60000	0.02322	0.03624	CalGrig4	0.03624	0.60000	0.02175	90.00	CalGrig4	0.03477	0.60000	0.02086	90.00	CalGrig4	0.03317	0.60000	0.01990	0.02819	SanVigilio	0.02819	0.60000	0.01691	70.00	SanVigilio	0.02704	0.60000	0.01622	70.00	SanVigilio	0.02580	0.60000	0.01548	0.00805	CalFila	0.00805	0.60000	0.00483	20.00	CalFila	0.00773	0.60000	0.00464	20.00	CalFila	0.00737	0.60000	0.00442	0.00604	RAM	0.00604	0.57000	0.00344	15.00	RAM	0.00579	0.57000	0.00330	15.00	RAM	0.00553	0.57000	0.00315	0.00201	RAM	0.00201	0.57000	0.00115	5.00	RAM	0.00193	0.57000	0.00110	5.00	RAM	0.00184	0.57000	0.00105	0.00403	RAS	0.00403	0.57000	0.00230	10.00	RAS	0.00386	0.57000	0.00220	10.00	RAS	0.00369	0.57000	0.00210	0.02416	Puez	0.02416	0.43500	0.01051	60.00	Puez	0.02318	0.43500	0.01008	60.00	Puez	0.02212	0.43500	0.00962	0.02819	Antrullies	0.02819	0.51000	0.01438	70.00	Antrullies	0.02704	0.51000	0.01379	70.00	Antrullies	0.02580	0.51000	0.01316	0.04169	MonteParei	0.04169	0.41500	0.01730	95.00	MonteParei	0.03670	0.41500	0.01523	161.50	MonteParei	0.05953	0.41500	0.02470	2483.12	TOTAL	1.00		0.45	2588.70	TOTAL	1.00		0.44	2713.00	TOTAL	1.00		0.47	Initial porosity of entire transect					0.45					0.44					0.47																																																																
48.42	TesMazz	0.01950	0.45000	0.00877	43.50	TesMazz	0.01680	0.45000	0.00756	47.00	TesMazz	0.01732	0.45000	0.00780	19.71	Andraz	0.00794	0.36000	0.00286	13.50	Andraz	0.00521	0.36000	0.00188	12.00	Andraz	0.00442	0.36000	0.00159	11.90	Seis	0.00479	0.51000	0.00244	38.10	Seis	0.01472	0.51000	0.00751	56.00	Seis	0.02064	0.51000	0.01053	93.55	Gasoo	0.03767	0.46000	0.01733	71.30	Gasoo	0.02777	0.46000	0.01278	79.00	Gasoo	0.02912	0.46000	0.01339	53.63	Campil	0.02160	0.40000	0.00864	91.50	Campil	0.03535	0.40000	0.01414	79.50	Campil	0.02930	0.40000	0.01172	7.78	Richthofen	0.00313	0.38000	0.00119	25.00	Richthofen	0.00966	0.38000	0.00367	23.20	Richthofen	0.00855	0.38000	0.00325	26.30	Morbiac	0.01059	0.51000	0.00540	25.00	Morbiac	0.00966	0.51000	0.00493	25.30	Morbiac	0.00933	0.51000	0.00476	54.33	Contrin	0.02188	0.40000	0.00875	45.00	Contrin	0.01738	0.40000	0.00695	38.50	Contrin	0.01419	0.40000	0.00568	300.00	Reitzi	0.12082	0.40000	0.04833	11.00	Reitzi	0.00425	0.40000	0.00170	9.50	Reitzi	0.00350	0.40000	0.00140	300.00	Secendensis	0.12082	0.40000	0.04833	8.00	Secendensis	0.00309	0.40000	0.00124	9.50	Secendensis	0.00350	0.40000	0.00140	200.00	Curtonii	0.08054	0.40000	0.03222	12.00	Curtonii	0.00464	0.40000	0.00185	13.00	Curtonii	0.00479	0.40000	0.00192	30.00	Gredleri	0.01208	0.40000	0.00483	799.00	Gredleri	0.30865	0.40000	0.12346	17.50	Gredleri	0.00645	0.40000	0.00258	20.00	Archelaus	0.00805	0.40000	0.00322	20.00	Archelaus	0.00773	0.40000	0.00309	177.00	Archelaus	0.06524	0.40000	0.02610	100.00	Wengen	0.04027	0.52500	0.02114	100.00	Wengen	0.03863	0.52500	0.02028	723.50	Wengen	0.26668	0.52500	0.14001	40.00	Rabl	0.01611	0.58000	0.00934	40.00	Rabl	0.01545	0.58000	0.00896	40.00	Rabl	0.01474	0.58000	0.00855	100.00	DP1	0.04027	0.40000	0.01611	100.00	DP1	0.03863	0.40000	0.01545	100.00	DP1	0.03686	0.40000	0.01474	0.7048	DP2	0.07048	0.40000	0.02819	175.00	DP2	0.06760	0.40000	0.02704	175.00	DP2	0.06450	0.40000	0.02580	0.1611	DP3	0.01611	0.40000	0.00644	40.00	DP3	0.01545	0.40000	0.00618	40.00	DP3	0.01474	0.40000	0.00590	0.1611	CalGrig1	0.01611	0.60000	0.00967	40.00	CalGrig1	0.01545	0.60000	0.00927	40.00	CalGrig1	0.01474	0.60000	0.00885	0.1410	CalGrig2	0.01410	0.60000	0.00846	35.00	CalGrig2	0.01352	0.60000	0.00811	35.00	CalGrig2	0.01290	0.60000	0.00774	0.44229	CalGrig3	0.04429	0.60000	0.02537	105.00	CalGrig3	0.04056	0.60000	0.02434	105.00	CalGrig3	0.03870	0.60000	0.02322	0.03624	CalGrig4	0.03624	0.60000	0.02175	90.00	CalGrig4	0.03477	0.60000	0.02086	90.00	CalGrig4	0.03317	0.60000	0.01990	0.02819	SanVigilio	0.02819	0.60000	0.01691	70.00	SanVigilio	0.02704	0.60000	0.01622	70.00	SanVigilio	0.02580	0.60000	0.01548	0.00805	CalFila	0.00805	0.60000	0.00483	20.00	CalFila	0.00773	0.60000	0.00464	20.00	CalFila	0.00737	0.60000	0.00442	0.00604	RAM	0.00604	0.57000	0.00344	15.00	RAM	0.00579	0.57000	0.00330	15.00	RAM	0.00553	0.57000	0.00315	0.00201	RAM	0.00201	0.57000	0.00115	5.00	RAM	0.00193	0.57000	0.00110	5.00	RAM	0.00184	0.57000	0.00105	0.00403	RAS	0.00403	0.57000	0.00230	10.00	RAS	0.00386	0.57000	0.00220	10.00	RAS	0.00369	0.57000	0.00210	0.02416	Puez	0.02416	0.43500	0.01051	60.00	Puez	0.02318	0.43500	0.01008	60.00	Puez	0.02212	0.43500	0.00962	0.02819	Antrullies	0.02819	0.51000	0.01438	70.00	Antrullies	0.02704	0.51000	0.01379	70.00	Antrullies	0.02580	0.51000	0.01316	0.04169	MonteParei	0.04169	0.41500	0.01730	95.00	MonteParei	0.03670	0.41500	0.01523	161.50	MonteParei	0.05953	0.41500	0.02470	2483.12	TOTAL	1.00		0.45	2588.70	TOTAL	1.00		0.44	2713.00	TOTAL	1.00		0.47	Initial porosity of entire transect					0.45					0.44					0.47																																																																															
19.71	Andraz	0.00794	0.36000	0.00286	13.50	Andraz	0.00521	0.36000	0.00188	12.00	Andraz	0.00442	0.36000	0.00159	11.90	Seis	0.00479	0.51000	0.00244	38.10	Seis	0.01472	0.51000	0.00751	56.00	Seis	0.02064	0.51000	0.01053	93.55	Gasoo	0.03767	0.46000	0.01733	71.30	Gasoo	0.02777	0.46000	0.01278	79.00	Gasoo	0.02912	0.46000	0.01339	53.63	Campil	0.02160	0.40000	0.00864	91.50	Campil	0.03535	0.40000	0.01414	79.50	Campil	0.02930	0.40000	0.01172	7.78	Richthofen	0.00313	0.38000	0.00119	25.00	Richthofen	0.00966	0.38000	0.00367	23.20	Richthofen	0.00855	0.38000	0.00325	26.30	Morbiac	0.01059	0.51000	0.00540	25.00	Morbiac	0.00966	0.51000	0.00493	25.30	Morbiac	0.00933	0.51000	0.00476	54.33	Contrin	0.02188	0.40000	0.00875	45.00	Contrin	0.01738	0.40000	0.00695	38.50	Contrin	0.01419	0.40000	0.00568	300.00	Reitzi	0.12082	0.40000	0.04833	11.00	Reitzi	0.00425	0.40000	0.00170	9.50	Reitzi	0.00350	0.40000	0.00140	300.00	Secendensis	0.12082	0.40000	0.04833	8.00	Secendensis	0.00309	0.40000	0.00124	9.50	Secendensis	0.00350	0.40000	0.00140	200.00	Curtonii	0.08054	0.40000	0.03222	12.00	Curtonii	0.00464	0.40000	0.00185	13.00	Curtonii	0.00479	0.40000	0.00192	30.00	Gredleri	0.01208	0.40000	0.00483	799.00	Gredleri	0.30865	0.40000	0.12346	17.50	Gredleri	0.00645	0.40000	0.00258	20.00	Archelaus	0.00805	0.40000	0.00322	20.00	Archelaus	0.00773	0.40000	0.00309	177.00	Archelaus	0.06524	0.40000	0.02610	100.00	Wengen	0.04027	0.52500	0.02114	100.00	Wengen	0.03863	0.52500	0.02028	723.50	Wengen	0.26668	0.52500	0.14001	40.00	Rabl	0.01611	0.58000	0.00934	40.00	Rabl	0.01545	0.58000	0.00896	40.00	Rabl	0.01474	0.58000	0.00855	100.00	DP1	0.04027	0.40000	0.01611	100.00	DP1	0.03863	0.40000	0.01545	100.00	DP1	0.03686	0.40000	0.01474	0.7048	DP2	0.07048	0.40000	0.02819	175.00	DP2	0.06760	0.40000	0.02704	175.00	DP2	0.06450	0.40000	0.02580	0.1611	DP3	0.01611	0.40000	0.00644	40.00	DP3	0.01545	0.40000	0.00618	40.00	DP3	0.01474	0.40000	0.00590	0.1611	CalGrig1	0.01611	0.60000	0.00967	40.00	CalGrig1	0.01545	0.60000	0.00927	40.00	CalGrig1	0.01474	0.60000	0.00885	0.1410	CalGrig2	0.01410	0.60000	0.00846	35.00	CalGrig2	0.01352	0.60000	0.00811	35.00	CalGrig2	0.01290	0.60000	0.00774	0.44229	CalGrig3	0.04429	0.60000	0.02537	105.00	CalGrig3	0.04056	0.60000	0.02434	105.00	CalGrig3	0.03870	0.60000	0.02322	0.03624	CalGrig4	0.03624	0.60000	0.02175	90.00	CalGrig4	0.03477	0.60000	0.02086	90.00	CalGrig4	0.03317	0.60000	0.01990	0.02819	SanVigilio	0.02819	0.60000	0.01691	70.00	SanVigilio	0.02704	0.60000	0.01622	70.00	SanVigilio	0.02580	0.60000	0.01548	0.00805	CalFila	0.00805	0.60000	0.00483	20.00	CalFila	0.00773	0.60000	0.00464	20.00	CalFila	0.00737	0.60000	0.00442	0.00604	RAM	0.00604	0.57000	0.00344	15.00	RAM	0.00579	0.57000	0.00330	15.00	RAM	0.00553	0.57000	0.00315	0.00201	RAM	0.00201	0.57000	0.00115	5.00	RAM	0.00193	0.57000	0.00110	5.00	RAM	0.00184	0.57000	0.00105	0.00403	RAS	0.00403	0.57000	0.00230	10.00	RAS	0.00386	0.57000	0.00220	10.00	RAS	0.00369	0.57000	0.00210	0.02416	Puez	0.02416	0.43500	0.01051	60.00	Puez	0.02318	0.43500	0.01008	60.00	Puez	0.02212	0.43500	0.00962	0.02819	Antrullies	0.02819	0.51000	0.01438	70.00	Antrullies	0.02704	0.51000	0.01379	70.00	Antrullies	0.02580	0.51000	0.01316	0.04169	MonteParei	0.04169	0.41500	0.01730	95.00	MonteParei	0.03670	0.41500	0.01523	161.50	MonteParei	0.05953	0.41500	0.02470	2483.12	TOTAL	1.00		0.45	2588.70	TOTAL	1.00		0.44	2713.00	TOTAL	1.00		0.47	Initial porosity of entire transect					0.45					0.44					0.47																																																																																														
11.90	Seis	0.00479	0.51000	0.00244	38.10	Seis	0.01472	0.51000	0.00751	56.00	Seis	0.02064	0.51000	0.01053	93.55	Gasoo	0.03767	0.46000	0.01733	71.30	Gasoo	0.02777	0.46000	0.01278	79.00	Gasoo	0.02912	0.46000	0.01339	53.63	Campil	0.02160	0.40000	0.00864	91.50	Campil	0.03535	0.40000	0.01414	79.50	Campil	0.02930	0.40000	0.01172	7.78	Richthofen	0.00313	0.38000	0.00119	25.00	Richthofen	0.00966	0.38000	0.00367	23.20	Richthofen	0.00855	0.38000	0.00325	26.30	Morbiac	0.01059	0.51000	0.00540	25.00	Morbiac	0.00966	0.51000	0.00493	25.30	Morbiac	0.00933	0.51000	0.00476	54.33	Contrin	0.02188	0.40000	0.00875	45.00	Contrin	0.01738	0.40000	0.00695	38.50	Contrin	0.01419	0.40000	0.00568	300.00	Reitzi	0.12082	0.40000	0.04833	11.00	Reitzi	0.00425	0.40000	0.00170	9.50	Reitzi	0.00350	0.40000	0.00140	300.00	Secendensis	0.12082	0.40000	0.04833	8.00	Secendensis	0.00309	0.40000	0.00124	9.50	Secendensis	0.00350	0.40000	0.00140	200.00	Curtonii	0.08054	0.40000	0.03222	12.00	Curtonii	0.00464	0.40000	0.00185	13.00	Curtonii	0.00479	0.40000	0.00192	30.00	Gredleri	0.01208	0.40000	0.00483	799.00	Gredleri	0.30865	0.40000	0.12346	17.50	Gredleri	0.00645	0.40000	0.00258	20.00	Archelaus	0.00805	0.40000	0.00322	20.00	Archelaus	0.00773	0.40000	0.00309	177.00	Archelaus	0.06524	0.40000	0.02610	100.00	Wengen	0.04027	0.52500	0.02114	100.00	Wengen	0.03863	0.52500	0.02028	723.50	Wengen	0.26668	0.52500	0.14001	40.00	Rabl	0.01611	0.58000	0.00934	40.00	Rabl	0.01545	0.58000	0.00896	40.00	Rabl	0.01474	0.58000	0.00855	100.00	DP1	0.04027	0.40000	0.01611	100.00	DP1	0.03863	0.40000	0.01545	100.00	DP1	0.03686	0.40000	0.01474	0.7048	DP2	0.07048	0.40000	0.02819	175.00	DP2	0.06760	0.40000	0.02704	175.00	DP2	0.06450	0.40000	0.02580	0.1611	DP3	0.01611	0.40000	0.00644	40.00	DP3	0.01545	0.40000	0.00618	40.00	DP3	0.01474	0.40000	0.00590	0.1611	CalGrig1	0.01611	0.60000	0.00967	40.00	CalGrig1	0.01545	0.60000	0.00927	40.00	CalGrig1	0.01474	0.60000	0.00885	0.1410	CalGrig2	0.01410	0.60000	0.00846	35.00	CalGrig2	0.01352	0.60000	0.00811	35.00	CalGrig2	0.01290	0.60000	0.00774	0.44229	CalGrig3	0.04429	0.60000	0.02537	105.00	CalGrig3	0.04056	0.60000	0.02434	105.00	CalGrig3	0.03870	0.60000	0.02322	0.03624	CalGrig4	0.03624	0.60000	0.02175	90.00	CalGrig4	0.03477	0.60000	0.02086	90.00	CalGrig4	0.03317	0.60000	0.01990	0.02819	SanVigilio	0.02819	0.60000	0.01691	70.00	SanVigilio	0.02704	0.60000	0.01622	70.00	SanVigilio	0.02580	0.60000	0.01548	0.00805	CalFila	0.00805	0.60000	0.00483	20.00	CalFila	0.00773	0.60000	0.00464	20.00	CalFila	0.00737	0.60000	0.00442	0.00604	RAM	0.00604	0.57000	0.00344	15.00	RAM	0.00579	0.57000	0.00330	15.00	RAM	0.00553	0.57000	0.00315	0.00201	RAM	0.00201	0.57000	0.00115	5.00	RAM	0.00193	0.57000	0.00110	5.00	RAM	0.00184	0.57000	0.00105	0.00403	RAS	0.00403	0.57000	0.00230	10.00	RAS	0.00386	0.57000	0.00220	10.00	RAS	0.00369	0.57000	0.00210	0.02416	Puez	0.02416	0.43500	0.01051	60.00	Puez	0.02318	0.43500	0.01008	60.00	Puez	0.02212	0.43500	0.00962	0.02819	Antrullies	0.02819	0.51000	0.01438	70.00	Antrullies	0.02704	0.51000	0.01379	70.00	Antrullies	0.02580	0.51000	0.01316	0.04169	MonteParei	0.04169	0.41500	0.01730	95.00	MonteParei	0.03670	0.41500	0.01523	161.50	MonteParei	0.05953	0.41500	0.02470	2483.12	TOTAL	1.00		0.45	2588.70	TOTAL	1.00		0.44	2713.00	TOTAL	1.00		0.47	Initial porosity of entire transect					0.45					0.44					0.47																																																																																																													
93.55	Gasoo	0.03767	0.46000	0.01733	71.30	Gasoo	0.02777	0.46000	0.01278	79.00	Gasoo	0.02912	0.46000	0.01339	53.63	Campil	0.02160	0.40000	0.00864	91.50	Campil	0.03535	0.40000	0.01414	79.50	Campil	0.02930	0.40000	0.01172	7.78	Richthofen	0.00313	0.38000	0.00119	25.00	Richthofen	0.00966	0.38000	0.00367	23.20	Richthofen	0.00855	0.38000	0.00325	26.30	Morbiac	0.01059	0.51000	0.00540	25.00	Morbiac	0.00966	0.51000	0.00493	25.30	Morbiac	0.00933	0.51000	0.00476	54.33	Contrin	0.02188	0.40000	0.00875	45.00	Contrin	0.01738	0.40000	0.00695	38.50	Contrin	0.01419	0.40000	0.00568	300.00	Reitzi	0.12082	0.40000	0.04833	11.00	Reitzi	0.00425	0.40000	0.00170	9.50	Reitzi	0.00350	0.40000	0.00140	300.00	Secendensis	0.12082	0.40000	0.04833	8.00	Secendensis	0.00309	0.40000	0.00124	9.50	Secendensis	0.00350	0.40000	0.00140	200.00	Curtonii	0.08054	0.40000	0.03222	12.00	Curtonii	0.00464	0.40000	0.00185	13.00	Curtonii	0.00479	0.40000	0.00192	30.00	Gredleri	0.01208	0.40000	0.00483	799.00	Gredleri	0.30865	0.40000	0.12346	17.50	Gredleri	0.00645	0.40000	0.00258	20.00	Archelaus	0.00805	0.40000	0.00322	20.00	Archelaus	0.00773	0.40000	0.00309	177.00	Archelaus	0.06524	0.40000	0.02610	100.00	Wengen	0.04027	0.52500	0.02114	100.00	Wengen	0.03863	0.52500	0.02028	723.50	Wengen	0.26668	0.52500	0.14001	40.00	Rabl	0.01611	0.58000	0.00934	40.00	Rabl	0.01545	0.58000	0.00896	40.00	Rabl	0.01474	0.58000	0.00855	100.00	DP1	0.04027	0.40000	0.01611	100.00	DP1	0.03863	0.40000	0.01545	100.00	DP1	0.03686	0.40000	0.01474	0.7048	DP2	0.07048	0.40000	0.02819	175.00	DP2	0.06760	0.40000	0.02704	175.00	DP2	0.06450	0.40000	0.02580	0.1611	DP3	0.01611	0.40000	0.00644	40.00	DP3	0.01545	0.40000	0.00618	40.00	DP3	0.01474	0.40000	0.00590	0.1611	CalGrig1	0.01611	0.60000	0.00967	40.00	CalGrig1	0.01545	0.60000	0.00927	40.00	CalGrig1	0.01474	0.60000	0.00885	0.1410	CalGrig2	0.01410	0.60000	0.00846	35.00	CalGrig2	0.01352	0.60000	0.00811	35.00	CalGrig2	0.01290	0.60000	0.00774	0.44229	CalGrig3	0.04429	0.60000	0.02537	105.00	CalGrig3	0.04056	0.60000	0.02434	105.00	CalGrig3	0.03870	0.60000	0.02322	0.03624	CalGrig4	0.03624	0.60000	0.02175	90.00	CalGrig4	0.03477	0.60000	0.02086	90.00	CalGrig4	0.03317	0.60000	0.01990	0.02819	SanVigilio	0.02819	0.60000	0.01691	70.00	SanVigilio	0.02704	0.60000	0.01622	70.00	SanVigilio	0.02580	0.60000	0.01548	0.00805	CalFila	0.00805	0.60000	0.00483	20.00	CalFila	0.00773	0.60000	0.00464	20.00	CalFila	0.00737	0.60000	0.00442	0.00604	RAM	0.00604	0.57000	0.00344	15.00	RAM	0.00579	0.57000	0.00330	15.00	RAM	0.00553	0.57000	0.00315	0.00201	RAM	0.00201	0.57000	0.00115	5.00	RAM	0.00193	0.57000	0.00110	5.00	RAM	0.00184	0.57000	0.00105	0.00403	RAS	0.00403	0.57000	0.00230	10.00	RAS	0.00386	0.57000	0.00220	10.00	RAS	0.00369	0.57000	0.00210	0.02416	Puez	0.02416	0.43500	0.01051	60.00	Puez	0.02318	0.43500	0.01008	60.00	Puez	0.02212	0.43500	0.00962	0.02819	Antrullies	0.02819	0.51000	0.01438	70.00	Antrullies	0.02704	0.51000	0.01379	70.00	Antrullies	0.02580	0.51000	0.01316	0.04169	MonteParei	0.04169	0.41500	0.01730	95.00	MonteParei	0.03670	0.41500	0.01523	161.50	MonteParei	0.05953	0.41500	0.02470	2483.12	TOTAL	1.00		0.45	2588.70	TOTAL	1.00		0.44	2713.00	TOTAL	1.00		0.47	Initial porosity of entire transect					0.45					0.44					0.47																																																																																																																												
53.63	Campil	0.02160	0.40000	0.00864	91.50	Campil	0.03535	0.40000	0.01414	79.50	Campil	0.02930	0.40000	0.01172	7.78	Richthofen	0.00313	0.38000	0.00119	25.00	Richthofen	0.00966	0.38000	0.00367	23.20	Richthofen	0.00855	0.38000	0.00325	26.30	Morbiac	0.01059	0.51000	0.00540	25.00	Morbiac	0.00966	0.51000	0.00493	25.30	Morbiac	0.00933	0.51000	0.00476	54.33	Contrin	0.02188	0.40000	0.00875	45.00	Contrin	0.01738	0.40000	0.00695	38.50	Contrin	0.01419	0.40000	0.00568	300.00	Reitzi	0.12082	0.40000	0.04833	11.00	Reitzi	0.00425	0.40000	0.00170	9.50	Reitzi	0.00350	0.40000	0.00140	300.00	Secendensis	0.12082	0.40000	0.04833	8.00	Secendensis	0.00309	0.40000	0.00124	9.50	Secendensis	0.00350	0.40000	0.00140	200.00	Curtonii	0.08054	0.40000	0.03222	12.00	Curtonii	0.00464	0.40000	0.00185	13.00	Curtonii	0.00479	0.40000	0.00192	30.00	Gredleri	0.01208	0.40000	0.00483	799.00	Gredleri	0.30865	0.40000	0.12346	17.50	Gredleri	0.00645	0.40000	0.00258	20.00	Archelaus	0.00805	0.40000	0.00322	20.00	Archelaus	0.00773	0.40000	0.00309	177.00	Archelaus	0.06524	0.40000	0.02610	100.00	Wengen	0.04027	0.52500	0.02114	100.00	Wengen	0.03863	0.52500	0.02028	723.50	Wengen	0.26668	0.52500	0.14001	40.00	Rabl	0.01611	0.58000	0.00934	40.00	Rabl	0.01545	0.58000	0.00896	40.00	Rabl	0.01474	0.58000	0.00855	100.00	DP1	0.04027	0.40000	0.01611	100.00	DP1	0.03863	0.40000	0.01545	100.00	DP1	0.03686	0.40000	0.01474	0.7048	DP2	0.07048	0.40000	0.02819	175.00	DP2	0.06760	0.40000	0.02704	175.00	DP2	0.06450	0.40000	0.02580	0.1611	DP3	0.01611	0.40000	0.00644	40.00	DP3	0.01545	0.40000	0.00618	40.00	DP3	0.01474	0.40000	0.00590	0.1611	CalGrig1	0.01611	0.60000	0.00967	40.00	CalGrig1	0.01545	0.60000	0.00927	40.00	CalGrig1	0.01474	0.60000	0.00885	0.1410	CalGrig2	0.01410	0.60000	0.00846	35.00	CalGrig2	0.01352	0.60000	0.00811	35.00	CalGrig2	0.01290	0.60000	0.00774	0.44229	CalGrig3	0.04429	0.60000	0.02537	105.00	CalGrig3	0.04056	0.60000	0.02434	105.00	CalGrig3	0.03870	0.60000	0.02322	0.03624	CalGrig4	0.03624	0.60000	0.02175	90.00	CalGrig4	0.03477	0.60000	0.02086	90.00	CalGrig4	0.03317	0.60000	0.01990	0.02819	SanVigilio	0.02819	0.60000	0.01691	70.00	SanVigilio	0.02704	0.60000	0.01622	70.00	SanVigilio	0.02580	0.60000	0.01548	0.00805	CalFila	0.00805	0.60000	0.00483	20.00	CalFila	0.00773	0.60000	0.00464	20.00	CalFila	0.00737	0.60000	0.00442	0.00604	RAM	0.00604	0.57000	0.00344	15.00	RAM	0.00579	0.57000	0.00330	15.00	RAM	0.00553	0.57000	0.00315	0.00201	RAM	0.00201	0.57000	0.00115	5.00	RAM	0.00193	0.57000	0.00110	5.00	RAM	0.00184	0.57000	0.00105	0.00403	RAS	0.00403	0.57000	0.00230	10.00	RAS	0.00386	0.57000	0.00220	10.00	RAS	0.00369	0.57000	0.00210	0.02416	Puez	0.02416	0.43500	0.01051	60.00	Puez	0.02318	0.43500	0.01008	60.00	Puez	0.02212	0.43500	0.00962	0.02819	Antrullies	0.02819	0.51000	0.01438	70.00	Antrullies	0.02704	0.51000	0.01379	70.00	Antrullies	0.02580	0.51000	0.01316	0.04169	MonteParei	0.04169	0.41500	0.01730	95.00	MonteParei	0.03670	0.41500	0.01523	161.50	MonteParei	0.05953	0.41500	0.02470	2483.12	TOTAL	1.00		0.45	2588.70	TOTAL	1.00		0.44	2713.00	TOTAL	1.00		0.47	Initial porosity of entire transect					0.45					0.44					0.47																																																																																																																																											
7.78	Richthofen	0.00313	0.38000	0.00119	25.00	Richthofen	0.00966	0.38000	0.00367	23.20	Richthofen	0.00855	0.38000	0.00325	26.30	Morbiac	0.01059	0.51000	0.00540	25.00	Morbiac	0.00966	0.51000	0.00493	25.30	Morbiac	0.00933	0.51000	0.00476	54.33	Contrin	0.02188	0.40000	0.00875	45.00	Contrin	0.01738	0.40000	0.00695	38.50	Contrin	0.01419	0.40000	0.00568	300.00	Reitzi	0.12082	0.40000	0.04833	11.00	Reitzi	0.00425	0.40000	0.00170	9.50	Reitzi	0.00350	0.40000	0.00140	300.00	Secendensis	0.12082	0.40000	0.04833	8.00	Secendensis	0.00309	0.40000	0.00124	9.50	Secendensis	0.00350	0.40000	0.00140	200.00	Curtonii	0.08054	0.40000	0.03222	12.00	Curtonii	0.00464	0.40000	0.00185	13.00	Curtonii	0.00479	0.40000	0.00192	30.00	Gredleri	0.01208	0.40000	0.00483	799.00	Gredleri	0.30865	0.40000	0.12346	17.50	Gredleri	0.00645	0.40000	0.00258	20.00	Archelaus	0.00805	0.40000	0.00322	20.00	Archelaus	0.00773	0.40000	0.00309	177.00	Archelaus	0.06524	0.40000	0.02610	100.00	Wengen	0.04027	0.52500	0.02114	100.00	Wengen	0.03863	0.52500	0.02028	723.50	Wengen	0.26668	0.52500	0.14001	40.00	Rabl	0.01611	0.58000	0.00934	40.00	Rabl	0.01545	0.58000	0.00896	40.00	Rabl	0.01474	0.58000	0.00855	100.00	DP1	0.04027	0.40000	0.01611	100.00	DP1	0.03863	0.40000	0.01545	100.00	DP1	0.03686	0.40000	0.01474	0.7048	DP2	0.07048	0.40000	0.02819	175.00	DP2	0.06760	0.40000	0.02704	175.00	DP2	0.06450	0.40000	0.02580	0.1611	DP3	0.01611	0.40000	0.00644	40.00	DP3	0.01545	0.40000	0.00618	40.00	DP3	0.01474	0.40000	0.00590	0.1611	CalGrig1	0.01611	0.60000	0.00967	40.00	CalGrig1	0.01545	0.60000	0.00927	40.00	CalGrig1	0.01474	0.60000	0.00885	0.1410	CalGrig2	0.01410	0.60000	0.00846	35.00	CalGrig2	0.01352	0.60000	0.00811	35.00	CalGrig2	0.01290	0.60000	0.00774	0.44229	CalGrig3	0.04429	0.60000	0.02537	105.00	CalGrig3	0.04056	0.60000	0.02434	105.00	CalGrig3	0.03870	0.60000	0.02322	0.03624	CalGrig4	0.03624	0.60000	0.02175	90.00	CalGrig4	0.03477	0.60000	0.02086	90.00	CalGrig4	0.03317	0.60000	0.01990	0.02819	SanVigilio	0.02819	0.60000	0.01691	70.00	SanVigilio	0.02704	0.60000	0.01622	70.00	SanVigilio	0.02580	0.60000	0.01548	0.00805	CalFila	0.00805	0.60000	0.00483	20.00	CalFila	0.00773	0.60000	0.00464	20.00	CalFila	0.00737	0.60000	0.00442	0.00604	RAM	0.00604	0.57000	0.00344	15.00	RAM	0.00579	0.57000	0.00330	15.00	RAM	0.00553	0.57000	0.00315	0.00201	RAM	0.00201	0.57000	0.00115	5.00	RAM	0.00193	0.57000	0.00110	5.00	RAM	0.00184	0.57000	0.00105	0.00403	RAS	0.00403	0.57000	0.00230	10.00	RAS	0.00386	0.57000	0.00220	10.00	RAS	0.00369	0.57000	0.00210	0.02416	Puez	0.02416	0.43500	0.01051	60.00	Puez	0.02318	0.43500	0.01008	60.00	Puez	0.02212	0.43500	0.00962	0.02819	Antrullies	0.02819	0.51000	0.01438	70.00	Antrullies	0.02704	0.51000	0.01379	70.00	Antrullies	0.02580	0.51000	0.01316	0.04169	MonteParei	0.04169	0.41500	0.01730	95.00	MonteParei	0.03670	0.41500	0.01523	161.50	MonteParei	0.05953	0.41500	0.02470	2483.12	TOTAL	1.00		0.45	2588.70	TOTAL	1.00		0.44	2713.00	TOTAL	1.00		0.47	Initial porosity of entire transect					0.45					0.44					0.47																																																																																																																																																										
26.30	Morbiac	0.01059	0.51000	0.00540	25.00	Morbiac	0.00966	0.51000	0.00493	25.30	Morbiac	0.00933	0.51000	0.00476	54.33	Contrin	0.02188	0.40000	0.00875	45.00	Contrin	0.01738	0.40000	0.00695	38.50	Contrin	0.01419	0.40000	0.00568	300.00	Reitzi	0.12082	0.40000	0.04833	11.00	Reitzi	0.00425	0.40000	0.00170	9.50	Reitzi	0.00350	0.40000	0.00140	300.00	Secendensis	0.12082	0.40000	0.04833	8.00	Secendensis	0.00309	0.40000	0.00124	9.50	Secendensis	0.00350	0.40000	0.00140	200.00	Curtonii	0.08054	0.40000	0.03222	12.00	Curtonii	0.00464	0.40000	0.00185	13.00	Curtonii	0.00479	0.40000	0.00192	30.00	Gredleri	0.01208	0.40000	0.00483	799.00	Gredleri	0.30865	0.40000	0.12346	17.50	Gredleri	0.00645	0.40000	0.00258	20.00	Archelaus	0.00805	0.40000	0.00322	20.00	Archelaus	0.00773	0.40000	0.00309	177.00	Archelaus	0.06524	0.40000	0.02610	100.00	Wengen	0.04027	0.52500	0.02114	100.00	Wengen	0.03863	0.52500	0.02028	723.50	Wengen	0.26668	0.52500	0.14001	40.00	Rabl	0.01611	0.58000	0.00934	40.00	Rabl	0.01545	0.58000	0.00896	40.00	Rabl	0.01474	0.58000	0.00855	100.00	DP1	0.04027	0.40000	0.01611	100.00	DP1	0.03863	0.40000	0.01545	100.00	DP1	0.03686	0.40000	0.01474	0.7048	DP2	0.07048	0.40000	0.02819	175.00	DP2	0.06760	0.40000	0.02704	175.00	DP2	0.06450	0.40000	0.02580	0.1611	DP3	0.01611	0.40000	0.00644	40.00	DP3	0.01545	0.40000	0.00618	40.00	DP3	0.01474	0.40000	0.00590	0.1611	CalGrig1	0.01611	0.60000	0.00967	40.00	CalGrig1	0.01545	0.60000	0.00927	40.00	CalGrig1	0.01474	0.60000	0.00885	0.1410	CalGrig2	0.01410	0.60000	0.00846	35.00	CalGrig2	0.01352	0.60000	0.00811	35.00	CalGrig2	0.01290	0.60000	0.00774	0.44229	CalGrig3	0.04429	0.60000	0.02537	105.00	CalGrig3	0.04056	0.60000	0.02434	105.00	CalGrig3	0.03870	0.60000	0.02322	0.03624	CalGrig4	0.03624	0.60000	0.02175	90.00	CalGrig4	0.03477	0.60000	0.02086	90.00	CalGrig4	0.03317	0.60000	0.01990	0.02819	SanVigilio	0.02819	0.60000	0.01691	70.00	SanVigilio	0.02704	0.60000	0.01622	70.00	SanVigilio	0.02580	0.60000	0.01548	0.00805	CalFila	0.00805	0.60000	0.00483	20.00	CalFila	0.00773	0.60000	0.00464	20.00	CalFila	0.00737	0.60000	0.00442	0.00604	RAM	0.00604	0.57000	0.00344	15.00	RAM	0.00579	0.57000	0.00330	15.00	RAM	0.00553	0.57000	0.00315	0.00201	RAM	0.00201	0.57000	0.00115	5.00	RAM	0.00193	0.57000	0.00110	5.00	RAM	0.00184	0.57000	0.00105	0.00403	RAS	0.00403	0.57000	0.00230	10.00	RAS	0.00386	0.57000	0.00220	10.00	RAS	0.00369	0.57000	0.00210	0.02416	Puez	0.02416	0.43500	0.01051	60.00	Puez	0.02318	0.43500	0.01008	60.00	Puez	0.02212	0.43500	0.00962	0.02819	Antrullies	0.02819	0.51000	0.01438	70.00	Antrullies	0.02704	0.51000	0.01379	70.00	Antrullies	0.02580	0.51000	0.01316	0.04169	MonteParei	0.04169	0.41500	0.01730	95.00	MonteParei	0.03670	0.41500	0.01523	161.50	MonteParei	0.05953	0.41500	0.02470	2483.12	TOTAL	1.00		0.45	2588.70	TOTAL	1.00		0.44	2713.00	TOTAL	1.00		0.47	Initial porosity of entire transect					0.45					0.44					0.47																																																																																																																																																																									
54.33	Contrin	0.02188	0.40000	0.00875	45.00	Contrin	0.01738	0.40000	0.00695	38.50	Contrin	0.01419	0.40000	0.00568	300.00	Reitzi	0.12082	0.40000	0.04833	11.00	Reitzi	0.00425	0.40000	0.00170	9.50	Reitzi	0.00350	0.40000	0.00140	300.00	Secendensis	0.12082	0.40000	0.04833	8.00	Secendensis	0.00309	0.40000	0.00124	9.50	Secendensis	0.00350	0.40000	0.00140	200.00	Curtonii	0.08054	0.40000	0.03222	12.00	Curtonii	0.00464	0.40000	0.00185	13.00	Curtonii	0.00479	0.40000	0.00192	30.00	Gredleri	0.01208	0.40000	0.00483	799.00	Gredleri	0.30865	0.40000	0.12346	17.50	Gredleri	0.00645	0.40000	0.00258	20.00	Archelaus	0.00805	0.40000	0.00322	20.00	Archelaus	0.00773	0.40000	0.00309	177.00	Archelaus	0.06524	0.40000	0.02610	100.00	Wengen	0.04027	0.52500	0.02114	100.00	Wengen	0.03863	0.52500	0.02028	723.50	Wengen	0.26668	0.52500	0.14001	40.00	Rabl	0.01611	0.58000	0.00934	40.00	Rabl	0.01545	0.58000	0.00896	40.00	Rabl	0.01474	0.58000	0.00855	100.00	DP1	0.04027	0.40000	0.01611	100.00	DP1	0.03863	0.40000	0.01545	100.00	DP1	0.03686	0.40000	0.01474	0.7048	DP2	0.07048	0.40000	0.02819	175.00	DP2	0.06760	0.40000	0.02704	175.00	DP2	0.06450	0.40000	0.02580	0.1611	DP3	0.01611	0.40000	0.00644	40.00	DP3	0.01545	0.40000	0.00618	40.00	DP3	0.01474	0.40000	0.00590	0.1611	CalGrig1	0.01611	0.60000	0.00967	40.00	CalGrig1	0.01545	0.60000	0.00927	40.00	CalGrig1	0.01474	0.60000	0.00885	0.1410	CalGrig2	0.01410	0.60000	0.00846	35.00	CalGrig2	0.01352	0.60000	0.00811	35.00	CalGrig2	0.01290	0.60000	0.00774	0.44229	CalGrig3	0.04429	0.60000	0.02537	105.00	CalGrig3	0.04056	0.60000	0.02434	105.00	CalGrig3	0.03870	0.60000	0.02322	0.03624	CalGrig4	0.03624	0.60000	0.02175	90.00	CalGrig4	0.03477	0.60000	0.02086	90.00	CalGrig4	0.03317	0.60000	0.01990	0.02819	SanVigilio	0.02819	0.60000	0.01691	70.00	SanVigilio	0.02704	0.60000	0.01622	70.00	SanVigilio	0.02580	0.60000	0.01548	0.00805	CalFila	0.00805	0.60000	0.00483	20.00	CalFila	0.00773	0.60000	0.00464	20.00	CalFila	0.00737	0.60000	0.00442	0.00604	RAM	0.00604	0.57000	0.00344	15.00	RAM	0.00579	0.57000	0.00330	15.00	RAM	0.00553	0.57000	0.00315	0.00201	RAM	0.00201	0.57000	0.00115	5.00	RAM	0.00193	0.57000	0.00110	5.00	RAM	0.00184	0.57000	0.00105	0.00403	RAS	0.00403	0.57000	0.00230	10.00	RAS	0.00386	0.57000	0.00220	10.00	RAS	0.00369	0.57000	0.00210	0.02416	Puez	0.02416	0.43500	0.01051	60.00	Puez	0.02318	0.43500	0.01008	60.00	Puez	0.02212	0.43500	0.00962	0.02819	Antrullies	0.02819	0.51000	0.01438	70.00	Antrullies	0.02704	0.51000	0.01379	70.00	Antrullies	0.02580	0.51000	0.01316	0.04169	MonteParei	0.04169	0.41500	0.01730	95.00	MonteParei	0.03670	0.41500	0.01523	161.50	MonteParei	0.05953	0.41500	0.02470	2483.12	TOTAL	1.00		0.45	2588.70	TOTAL	1.00		0.44	2713.00	TOTAL	1.00		0.47	Initial porosity of entire transect					0.45					0.44					0.47																																																																																																																																																																																								
300.00	Reitzi	0.12082	0.40000	0.04833	11.00	Reitzi	0.00425	0.40000	0.00170	9.50	Reitzi	0.00350	0.40000	0.00140	300.00	Secendensis	0.12082	0.40000	0.04833	8.00	Secendensis	0.00309	0.40000	0.00124	9.50	Secendensis	0.00350	0.40000	0.00140	200.00	Curtonii	0.08054	0.40000	0.03222	12.00	Curtonii	0.00464	0.40000	0.00185	13.00	Curtonii	0.00479	0.40000	0.00192	30.00	Gredleri	0.01208	0.40000	0.00483	799.00	Gredleri	0.30865	0.40000	0.12346	17.50	Gredleri	0.00645	0.40000	0.00258	20.00	Archelaus	0.00805	0.40000	0.00322	20.00	Archelaus	0.00773	0.40000	0.00309	177.00	Archelaus	0.06524	0.40000	0.02610	100.00	Wengen	0.04027	0.52500	0.02114	100.00	Wengen	0.03863	0.52500	0.02028	723.50	Wengen	0.26668	0.52500	0.14001	40.00	Rabl	0.01611	0.58000	0.00934	40.00	Rabl	0.01545	0.58000	0.00896	40.00	Rabl	0.01474	0.58000	0.00855	100.00	DP1	0.04027	0.40000	0.01611	100.00	DP1	0.03863	0.40000	0.01545	100.00	DP1	0.03686	0.40000	0.01474	0.7048	DP2	0.07048	0.40000	0.02819	175.00	DP2	0.06760	0.40000	0.02704	175.00	DP2	0.06450	0.40000	0.02580	0.1611	DP3	0.01611	0.40000	0.00644	40.00	DP3	0.01545	0.40000	0.00618	40.00	DP3	0.01474	0.40000	0.00590	0.1611	CalGrig1	0.01611	0.60000	0.00967	40.00	CalGrig1	0.01545	0.60000	0.00927	40.00	CalGrig1	0.01474	0.60000	0.00885	0.1410	CalGrig2	0.01410	0.60000	0.00846	35.00	CalGrig2	0.01352	0.60000	0.00811	35.00	CalGrig2	0.01290	0.60000	0.00774	0.44229	CalGrig3	0.04429	0.60000	0.02537	105.00	CalGrig3	0.04056	0.60000	0.02434	105.00	CalGrig3	0.03870	0.60000	0.02322	0.03624	CalGrig4	0.03624	0.60000	0.02175	90.00	CalGrig4	0.03477	0.60000	0.02086	90.00	CalGrig4	0.03317	0.60000	0.01990	0.02819	SanVigilio	0.02819	0.60000	0.01691	70.00	SanVigilio	0.02704	0.60000	0.01622	70.00	SanVigilio	0.02580	0.60000	0.01548	0.00805	CalFila	0.00805	0.60000	0.00483	20.00	CalFila	0.00773	0.60000	0.00464	20.00	CalFila	0.00737	0.60000	0.00442	0.00604	RAM	0.00604	0.57000	0.00344	15.00	RAM	0.00579	0.57000	0.00330	15.00	RAM	0.00553	0.57000	0.00315	0.00201	RAM	0.00201	0.57000	0.00115	5.00	RAM	0.00193	0.57000	0.00110	5.00	RAM	0.00184	0.57000	0.00105	0.00403	RAS	0.00403	0.57000	0.00230	10.00	RAS	0.00386	0.57000	0.00220	10.00	RAS	0.00369	0.57000	0.00210	0.02416	Puez	0.02416	0.43500	0.01051	60.00	Puez	0.02318	0.43500	0.01008	60.00	Puez	0.02212	0.43500	0.00962	0.02819	Antrullies	0.02819	0.51000	0.01438	70.00	Antrullies	0.02704	0.51000	0.01379	70.00	Antrullies	0.02580	0.51000	0.01316	0.04169	MonteParei	0.04169	0.41500	0.01730	95.00	MonteParei	0.03670	0.41500	0.01523	161.50	MonteParei	0.05953	0.41500	0.02470	2483.12	TOTAL	1.00		0.45	2588.70	TOTAL	1.00		0.44	2713.00	TOTAL	1.00		0.47	Initial porosity of entire transect					0.45					0.44					0.47																																																																																																																																																																																																							
300.00	Secendensis	0.12082	0.40000	0.04833	8.00	Secendensis	0.00309	0.40000	0.00124	9.50	Secendensis	0.00350	0.40000	0.00140	200.00	Curtonii	0.08054	0.40000	0.03222	12.00	Curtonii	0.00464	0.40000	0.00185	13.00	Curtonii	0.00479	0.40000	0.00192	30.00	Gredleri	0.01208	0.40000	0.00483	799.00	Gredleri	0.30865	0.40000	0.12346	17.50	Gredleri	0.00645	0.40000	0.00258	20.00	Archelaus	0.00805	0.40000	0.00322	20.00	Archelaus	0.00773	0.40000	0.00309	177.00	Archelaus	0.06524	0.40000	0.02610	100.00	Wengen	0.04027	0.52500	0.02114	100.00	Wengen	0.03863	0.52500	0.02028	723.50	Wengen	0.26668	0.52500	0.14001	40.00	Rabl	0.01611	0.58000	0.00934	40.00	Rabl	0.01545	0.58000	0.00896	40.00	Rabl	0.01474	0.58000	0.00855	100.00	DP1	0.04027	0.40000	0.01611	100.00	DP1	0.03863	0.40000	0.01545	100.00	DP1	0.03686	0.40000	0.01474	0.7048	DP2	0.07048	0.40000	0.02819	175.00	DP2	0.06760	0.40000	0.02704	175.00	DP2	0.06450	0.40000	0.02580	0.1611	DP3	0.01611	0.40000	0.00644	40.00	DP3	0.01545	0.40000	0.00618	40.00	DP3	0.01474	0.40000	0.00590	0.1611	CalGrig1	0.01611	0.60000	0.00967	40.00	CalGrig1	0.01545	0.60000	0.00927	40.00	CalGrig1	0.01474	0.60000	0.00885	0.1410	CalGrig2	0.01410	0.60000	0.00846	35.00	CalGrig2	0.01352	0.60000	0.00811	35.00	CalGrig2	0.01290	0.60000	0.00774	0.44229	CalGrig3	0.04429	0.60000	0.02537	105.00	CalGrig3	0.04056	0.60000	0.02434	105.00	CalGrig3	0.03870	0.60000	0.02322	0.03624	CalGrig4	0.03624	0.60000	0.02175	90.00	CalGrig4	0.03477	0.60000	0.02086	90.00	CalGrig4	0.03317	0.60000	0.01990	0.02819	SanVigilio	0.02819	0.60000	0.01691	70.00	SanVigilio	0.02704	0.60000	0.01622	70.00	SanVigilio	0.02580	0.60000	0.01548	0.00805	CalFila	0.00805	0.60000	0.00483	20.00	CalFila	0.00773	0.60000	0.00464	20.00	CalFila	0.00737	0.60000	0.00442	0.00604	RAM	0.00604	0.57000	0.00344	15.00	RAM	0.00579	0.57000	0.00330	15.00	RAM	0.00553	0.57000	0.00315	0.00201	RAM	0.00201	0.57000	0.00115	5.00	RAM	0.00193	0.57000	0.00110	5.00	RAM	0.00184	0.57000	0.00105	0.00403	RAS	0.00403	0.57000	0.00230	10.00	RAS	0.00386	0.57000	0.00220	10.00	RAS	0.00369	0.57000	0.00210	0.02416	Puez	0.02416	0.43500	0.01051	60.00	Puez	0.02318	0.43500	0.01008	60.00	Puez	0.02212	0.43500	0.00962	0.02819	Antrullies	0.02819	0.51000	0.01438	70.00	Antrullies	0.02704	0.51000	0.01379	70.00	Antrullies	0.02580	0.51000	0.01316	0.04169	MonteParei	0.04169	0.41500	0.01730	95.00	MonteParei	0.03670	0.41500	0.01523	161.50	MonteParei	0.05953	0.41500	0.02470	2483.12	TOTAL	1.00		0.45	2588.70	TOTAL	1.00		0.44	2713.00	TOTAL	1.00		0.47	Initial porosity of entire transect					0.45					0.44					0.47																																																																																																																																																																																																																						
200.00	Curtonii	0.08054	0.40000	0.03222	12.00	Curtonii	0.00464	0.40000	0.00185	13.00	Curtonii	0.00479	0.40000	0.00192	30.00	Gredleri	0.01208	0.40000	0.00483	799.00	Gredleri	0.30865	0.40000	0.12346	17.50	Gredleri	0.00645	0.40000	0.00258	20.00	Archelaus	0.00805	0.40000	0.00322	20.00	Archelaus	0.00773	0.40000	0.00309	177.00	Archelaus	0.06524	0.40000	0.02610	100.00	Wengen	0.04027	0.52500	0.02114	100.00	Wengen	0.03863	0.52500	0.02028	723.50	Wengen	0.26668	0.52500	0.14001	40.00	Rabl	0.01611	0.58000	0.00934	40.00	Rabl	0.01545	0.58000	0.00896	40.00	Rabl	0.01474	0.58000	0.00855	100.00	DP1	0.04027	0.40000	0.01611	100.00	DP1	0.03863	0.40000	0.01545	100.00	DP1	0.03686	0.40000	0.01474	0.7048	DP2	0.07048	0.40000	0.02819	175.00	DP2	0.06760	0.40000	0.02704	175.00	DP2	0.06450	0.40000	0.02580	0.1611	DP3	0.01611	0.40000	0.00644	40.00	DP3	0.01545	0.40000	0.00618	40.00	DP3	0.01474	0.40000	0.00590	0.1611	CalGrig1	0.01611	0.60000	0.00967	40.00	CalGrig1	0.01545	0.60000	0.00927	40.00	CalGrig1	0.01474	0.60000	0.00885	0.1410	CalGrig2	0.01410	0.60000	0.00846	35.00	CalGrig2	0.01352	0.60000	0.00811	35.00	CalGrig2	0.01290	0.60000	0.00774	0.44229	CalGrig3	0.04429	0.60000	0.02537	105.00	CalGrig3	0.04056	0.60000	0.02434	105.00	CalGrig3	0.03870	0.60000	0.02322	0.03624	CalGrig4	0.03624	0.60000	0.02175	90.00	CalGrig4	0.03477	0.60000	0.02086	90.00	CalGrig4	0.03317	0.60000	0.01990	0.02819	SanVigilio	0.02819	0.60000	0.01691	70.00	SanVigilio	0.02704	0.60000	0.01622	70.00	SanVigilio	0.02580	0.60000	0.01548	0.00805	CalFila	0.00805	0.60000	0.00483	20.00	CalFila	0.00773	0.60000	0.00464	20.00	CalFila	0.00737	0.60000	0.00442	0.00604	RAM	0.00604	0.57000	0.00344	15.00	RAM	0.00579	0.57000	0.00330	15.00	RAM	0.00553	0.57000	0.00315	0.00201	RAM	0.00201	0.57000	0.00115	5.00	RAM	0.00193	0.57000	0.00110	5.00	RAM	0.00184	0.57000	0.00105	0.00403	RAS	0.00403	0.57000	0.00230	10.00	RAS	0.00386	0.57000	0.00220	10.00	RAS	0.00369	0.57000	0.00210	0.02416	Puez	0.02416	0.43500	0.01051	60.00	Puez	0.02318	0.43500	0.01008	60.00	Puez	0.02212	0.43500	0.00962	0.02819	Antrullies	0.02819	0.51000	0.01438	70.00	Antrullies	0.02704	0.51000	0.01379	70.00	Antrullies	0.02580	0.51000	0.01316	0.04169	MonteParei	0.04169	0.41500	0.01730	95.00	MonteParei	0.03670	0.41500	0.01523	161.50	MonteParei	0.05953	0.41500	0.02470	2483.12	TOTAL	1.00		0.45	2588.70	TOTAL	1.00		0.44	2713.00	TOTAL	1.00		0.47	Initial porosity of entire transect					0.45					0.44					0.47																																																																																																																																																																																																																																					
30.00	Gredleri	0.01208	0.40000	0.00483	799.00	Gredleri	0.30865	0.40000	0.12346	17.50	Gredleri	0.00645	0.40000	0.00258	20.00	Archelaus	0.00805	0.40000	0.00322	20.00	Archelaus	0.00773	0.40000	0.00309	177.00	Archelaus	0.06524	0.40000	0.02610	100.00	Wengen	0.04027	0.52500	0.02114	100.00	Wengen	0.03863	0.52500	0.02028	723.50	Wengen	0.26668	0.52500	0.14001	40.00	Rabl	0.01611	0.58000	0.00934	40.00	Rabl	0.01545	0.58000	0.00896	40.00	Rabl	0.01474	0.58000	0.00855	100.00	DP1	0.04027	0.40000	0.01611	100.00	DP1	0.03863	0.40000	0.01545	100.00	DP1	0.03686	0.40000	0.01474	0.7048	DP2	0.07048	0.40000	0.02819	175.00	DP2	0.06760	0.40000	0.02704	175.00	DP2	0.06450	0.40000	0.02580	0.1611	DP3	0.01611	0.40000	0.00644	40.00	DP3	0.01545	0.40000	0.00618	40.00	DP3	0.01474	0.40000	0.00590	0.1611	CalGrig1	0.01611	0.60000	0.00967	40.00	CalGrig1	0.01545	0.60000	0.00927	40.00	CalGrig1	0.01474	0.60000	0.00885	0.1410	CalGrig2	0.01410	0.60000	0.00846	35.00	CalGrig2	0.01352	0.60000	0.00811	35.00	CalGrig2	0.01290	0.60000	0.00774	0.44229	CalGrig3	0.04429	0.60000	0.02537	105.00	CalGrig3	0.04056	0.60000	0.02434	105.00	CalGrig3	0.03870	0.60000	0.02322	0.03624	CalGrig4	0.03624	0.60000	0.02175	90.00	CalGrig4	0.03477	0.60000	0.02086	90.00	CalGrig4	0.03317	0.60000	0.01990	0.02819	SanVigilio	0.02819	0.60000	0.01691	70.00	SanVigilio	0.02704	0.60000	0.01622	70.00	SanVigilio	0.02580	0.60000	0.01548	0.00805	CalFila	0.00805	0.60000	0.00483	20.00	CalFila	0.00773	0.60000	0.00464	20.00	CalFila	0.00737	0.60000	0.00442	0.00604	RAM	0.00604	0.57000	0.00344	15.00	RAM	0.00579	0.57000	0.00330	15.00	RAM	0.00553	0.57000	0.00315	0.00201	RAM	0.00201	0.57000	0.00115	5.00	RAM	0.00193	0.57000	0.00110	5.00	RAM	0.00184	0.57000	0.00105	0.00403	RAS	0.00403	0.57000	0.00230	10.00	RAS	0.00386	0.57000	0.00220	10.00	RAS	0.00369	0.57000	0.00210	0.02416	Puez	0.02416	0.43500	0.01051	60.00	Puez	0.02318	0.43500	0.01008	60.00	Puez	0.02212	0.43500	0.00962	0.02819	Antrullies	0.02819	0.51000	0.01438	70.00	Antrullies	0.02704	0.51000	0.01379	70.00	Antrullies	0.02580	0.51000	0.01316	0.04169	MonteParei	0.04169	0.41500	0.01730	95.00	MonteParei	0.03670	0.41500	0.01523	161.50	MonteParei	0.05953	0.41500	0.02470	2483.12	TOTAL	1.00		0.45	2588.70	TOTAL	1.00		0.44	2713.00	TOTAL	1.00		0.47	Initial porosity of entire transect					0.45					0.44					0.47																																																																																																																																																																																																																																																				
20.00	Archelaus	0.00805	0.40000	0.00322	20.00	Archelaus	0.00773	0.40000	0.00309	177.00	Archelaus	0.06524	0.40000	0.02610	100.00	Wengen	0.04027	0.52500	0.02114	100.00	Wengen	0.03863	0.52500	0.02028	723.50	Wengen	0.26668	0.52500	0.14001	40.00	Rabl	0.01611	0.58000	0.00934	40.00	Rabl	0.01545	0.58000	0.00896	40.00	Rabl	0.01474	0.58000	0.00855	100.00	DP1	0.04027	0.40000	0.01611	100.00	DP1	0.03863	0.40000	0.01545	100.00	DP1	0.03686	0.40000	0.01474	0.7048	DP2	0.07048	0.40000	0.02819	175.00	DP2	0.06760	0.40000	0.02704	175.00	DP2	0.06450	0.40000	0.02580	0.1611	DP3	0.01611	0.40000	0.00644	40.00	DP3	0.01545	0.40000	0.00618	40.00	DP3	0.01474	0.40000	0.00590	0.1611	CalGrig1	0.01611	0.60000	0.00967	40.00	CalGrig1	0.01545	0.60000	0.00927	40.00	CalGrig1	0.01474	0.60000	0.00885	0.1410	CalGrig2	0.01410	0.60000	0.00846	35.00	CalGrig2	0.01352	0.60000	0.00811	35.00	CalGrig2	0.01290	0.60000	0.00774	0.44229	CalGrig3	0.04429	0.60000	0.02537	105.00	CalGrig3	0.04056	0.60000	0.02434	105.00	CalGrig3	0.03870	0.60000	0.02322	0.03624	CalGrig4	0.03624	0.60000	0.02175	90.00	CalGrig4	0.03477	0.60000	0.02086	90.00	CalGrig4	0.03317	0.60000	0.01990	0.02819	SanVigilio	0.02819	0.60000	0.01691	70.00	SanVigilio	0.02704	0.60000	0.01622	70.00	SanVigilio	0.02580	0.60000	0.01548	0.00805	CalFila	0.00805	0.60000	0.00483	20.00	CalFila	0.00773	0.60000	0.00464	20.00	CalFila	0.00737	0.60000	0.00442	0.00604	RAM	0.00604	0.57000	0.00344	15.00	RAM	0.00579	0.57000	0.00330	15.00	RAM	0.00553	0.57000	0.00315	0.00201	RAM	0.00201	0.57000	0.00115	5.00	RAM	0.00193	0.57000	0.00110	5.00	RAM	0.00184	0.57000	0.00105	0.00403	RAS	0.00403	0.57000	0.00230	10.00	RAS	0.00386	0.57000	0.00220	10.00	RAS	0.00369	0.57000	0.00210	0.02416	Puez	0.02416	0.43500	0.01051	60.00	Puez	0.02318	0.43500	0.01008	60.00	Puez	0.02212	0.43500	0.00962	0.02819	Antrullies	0.02819	0.51000	0.01438	70.00	Antrullies	0.02704	0.51000	0.01379	70.00	Antrullies	0.02580	0.51000	0.01316	0.04169	MonteParei	0.04169	0.41500	0.01730	95.00	MonteParei	0.03670	0.41500	0.01523	161.50	MonteParei	0.05953	0.41500	0.02470	2483.12	TOTAL	1.00		0.45	2588.70	TOTAL	1.00		0.44	2713.00	TOTAL	1.00		0.47	Initial porosity of entire transect					0.45					0.44					0.47																																																																																																																																																																																																																																																																			
100.00	Wengen	0.04027	0.52500	0.02114	100.00	Wengen	0.03863	0.52500	0.02028	723.50	Wengen	0.26668	0.52500	0.14001	40.00	Rabl	0.01611	0.58000	0.00934	40.00	Rabl	0.01545	0.58000	0.00896	40.00	Rabl	0.01474	0.58000	0.00855	100.00	DP1	0.04027	0.40000	0.01611	100.00	DP1	0.03863	0.40000	0.01545	100.00	DP1	0.03686	0.40000	0.01474	0.7048	DP2	0.07048	0.40000	0.02819	175.00	DP2	0.06760	0.40000	0.02704	175.00	DP2	0.06450	0.40000	0.02580	0.1611	DP3	0.01611	0.40000	0.00644	40.00	DP3	0.01545	0.40000	0.00618	40.00	DP3	0.01474	0.40000	0.00590	0.1611	CalGrig1	0.01611	0.60000	0.00967	40.00	CalGrig1	0.01545	0.60000	0.00927	40.00	CalGrig1	0.01474	0.60000	0.00885	0.1410	CalGrig2	0.01410	0.60000	0.00846	35.00	CalGrig2	0.01352	0.60000	0.00811	35.00	CalGrig2	0.01290	0.60000	0.00774	0.44229	CalGrig3	0.04429	0.60000	0.02537	105.00	CalGrig3	0.04056	0.60000	0.02434	105.00	CalGrig3	0.03870	0.60000	0.02322	0.03624	CalGrig4	0.03624	0.60000	0.02175	90.00	CalGrig4	0.03477	0.60000	0.02086	90.00	CalGrig4	0.03317	0.60000	0.01990	0.02819	SanVigilio	0.02819	0.60000	0.01691	70.00	SanVigilio	0.02704	0.60000	0.01622	70.00	SanVigilio	0.02580	0.60000	0.01548	0.00805	CalFila	0.00805	0.60000	0.00483	20.00	CalFila	0.00773	0.60000	0.00464	20.00	CalFila	0.00737	0.60000	0.00442	0.00604	RAM	0.00604	0.57000	0.00344	15.00	RAM	0.00579	0.57000	0.00330	15.00	RAM	0.00553	0.57000	0.00315	0.00201	RAM	0.00201	0.57000	0.00115	5.00	RAM	0.00193	0.57000	0.00110	5.00	RAM	0.00184	0.57000	0.00105	0.00403	RAS	0.00403	0.57000	0.00230	10.00	RAS	0.00386	0.57000	0.00220	10.00	RAS	0.00369	0.57000	0.00210	0.02416	Puez	0.02416	0.43500	0.01051	60.00	Puez	0.02318	0.43500	0.01008	60.00	Puez	0.02212	0.43500	0.00962	0.02819	Antrullies	0.02819	0.51000	0.01438	70.00	Antrullies	0.02704	0.51000	0.01379	70.00	Antrullies	0.02580	0.51000	0.01316	0.04169	MonteParei	0.04169	0.41500	0.01730	95.00	MonteParei	0.03670	0.41500	0.01523	161.50	MonteParei	0.05953	0.41500	0.02470	2483.12	TOTAL	1.00		0.45	2588.70	TOTAL	1.00		0.44	2713.00	TOTAL	1.00		0.47	Initial porosity of entire transect					0.45					0.44					0.47																																																																																																																																																																																																																																																																																		
40.00	Rabl	0.01611	0.58000	0.00934	40.00	Rabl	0.01545	0.58000	0.00896	40.00	Rabl	0.01474	0.58000	0.00855	100.00	DP1	0.04027	0.40000	0.01611	100.00	DP1	0.03863	0.40000	0.01545	100.00	DP1	0.03686	0.40000	0.01474	0.7048	DP2	0.07048	0.40000	0.02819	175.00	DP2	0.06760	0.40000	0.02704	175.00	DP2	0.06450	0.40000	0.02580	0.1611	DP3	0.01611	0.40000	0.00644	40.00	DP3	0.01545	0.40000	0.00618	40.00	DP3	0.01474	0.40000	0.00590	0.1611	CalGrig1	0.01611	0.60000	0.00967	40.00	CalGrig1	0.01545	0.60000	0.00927	40.00	CalGrig1	0.01474	0.60000	0.00885	0.1410	CalGrig2	0.01410	0.60000	0.00846	35.00	CalGrig2	0.01352	0.60000	0.00811	35.00	CalGrig2	0.01290	0.60000	0.00774	0.44229	CalGrig3	0.04429	0.60000	0.02537	105.00	CalGrig3	0.04056	0.60000	0.02434	105.00	CalGrig3	0.03870	0.60000	0.02322	0.03624	CalGrig4	0.03624	0.60000	0.02175	90.00	CalGrig4	0.03477	0.60000	0.02086	90.00	CalGrig4	0.03317	0.60000	0.01990	0.02819	SanVigilio	0.02819	0.60000	0.01691	70.00	SanVigilio	0.02704	0.60000	0.01622	70.00	SanVigilio	0.02580	0.60000	0.01548	0.00805	CalFila	0.00805	0.60000	0.00483	20.00	CalFila	0.00773	0.60000	0.00464	20.00	CalFila	0.00737	0.60000	0.00442	0.00604	RAM	0.00604	0.57000	0.00344	15.00	RAM	0.00579	0.57000	0.00330	15.00	RAM	0.00553	0.57000	0.00315	0.00201	RAM	0.00201	0.57000	0.00115	5.00	RAM	0.00193	0.57000	0.00110	5.00	RAM	0.00184	0.57000	0.00105	0.00403	RAS	0.00403	0.57000	0.00230	10.00	RAS	0.00386	0.57000	0.00220	10.00	RAS	0.00369	0.57000	0.00210	0.02416	Puez	0.02416	0.43500	0.01051	60.00	Puez	0.02318	0.43500	0.01008	60.00	Puez	0.02212	0.43500	0.00962	0.02819	Antrullies	0.02819	0.51000	0.01438	70.00	Antrullies	0.02704	0.51000	0.01379	70.00	Antrullies	0.02580	0.51000	0.01316	0.04169	MonteParei	0.04169	0.41500	0.01730	95.00	MonteParei	0.03670	0.41500	0.01523	161.50	MonteParei	0.05953	0.41500	0.02470	2483.12	TOTAL	1.00		0.45	2588.70	TOTAL	1.00		0.44	2713.00	TOTAL	1.00		0.47	Initial porosity of entire transect					0.45					0.44					0.47																																																																																																																																																																																																																																																																																																	
100.00	DP1	0.04027	0.40000	0.01611	100.00	DP1	0.03863	0.40000	0.01545	100.00	DP1	0.03686	0.40000	0.01474	0.7048	DP2	0.07048	0.40000	0.02819	175.00	DP2	0.06760	0.40000	0.02704	175.00	DP2	0.06450	0.40000	0.02580	0.1611	DP3	0.01611	0.40000	0.00644	40.00	DP3	0.01545	0.40000	0.00618	40.00	DP3	0.01474	0.40000	0.00590	0.1611	CalGrig1	0.01611	0.60000	0.00967	40.00	CalGrig1	0.01545	0.60000	0.00927	40.00	CalGrig1	0.01474	0.60000	0.00885	0.1410	CalGrig2	0.01410	0.60000	0.00846	35.00	CalGrig2	0.01352	0.60000	0.00811	35.00	CalGrig2	0.01290	0.60000	0.00774	0.44229	CalGrig3	0.04429	0.60000	0.02537	105.00	CalGrig3	0.04056	0.60000	0.02434	105.00	CalGrig3	0.03870	0.60000	0.02322	0.03624	CalGrig4	0.03624	0.60000	0.02175	90.00	CalGrig4	0.03477	0.60000	0.02086	90.00	CalGrig4	0.03317	0.60000	0.01990	0.02819	SanVigilio	0.02819	0.60000	0.01691	70.00	SanVigilio	0.02704	0.60000	0.01622	70.00	SanVigilio	0.02580	0.60000	0.01548	0.00805	CalFila	0.00805	0.60000	0.00483	20.00	CalFila	0.00773	0.60000	0.00464	20.00	CalFila	0.00737	0.60000	0.00442	0.00604	RAM	0.00604	0.57000	0.00344	15.00	RAM	0.00579	0.57000	0.00330	15.00	RAM	0.00553	0.57000	0.00315	0.00201	RAM	0.00201	0.57000	0.00115	5.00	RAM	0.00193	0.57000	0.00110	5.00	RAM	0.00184	0.57000	0.00105	0.00403	RAS	0.00403	0.57000	0.00230	10.00	RAS	0.00386	0.57000	0.00220	10.00	RAS	0.00369	0.57000	0.00210	0.02416	Puez	0.02416	0.43500	0.01051	60.00	Puez	0.02318	0.43500	0.01008	60.00	Puez	0.02212	0.43500	0.00962	0.02819	Antrullies	0.02819	0.51000	0.01438	70.00	Antrullies	0.02704	0.51000	0.01379	70.00	Antrullies	0.02580	0.51000	0.01316	0.04169	MonteParei	0.04169	0.41500	0.01730	95.00	MonteParei	0.03670	0.41500	0.01523	161.50	MonteParei	0.05953	0.41500	0.02470	2483.12	TOTAL	1.00		0.45	2588.70	TOTAL	1.00		0.44	2713.00	TOTAL	1.00		0.47	Initial porosity of entire transect					0.45					0.44					0.47																																																																																																																																																																																																																																																																																																																
0.7048	DP2	0.07048	0.40000	0.02819	175.00	DP2	0.06760	0.40000	0.02704	175.00	DP2	0.06450	0.40000	0.02580	0.1611	DP3	0.01611	0.40000	0.00644	40.00	DP3	0.01545	0.40000	0.00618	40.00	DP3	0.01474	0.40000	0.00590	0.1611	CalGrig1	0.01611	0.60000	0.00967	40.00	CalGrig1	0.01545	0.60000	0.00927	40.00	CalGrig1	0.01474	0.60000	0.00885	0.1410	CalGrig2	0.01410	0.60000	0.00846	35.00	CalGrig2	0.01352	0.60000	0.00811	35.00	CalGrig2	0.01290	0.60000	0.00774	0.44229	CalGrig3	0.04429	0.60000	0.02537	105.00	CalGrig3	0.04056	0.60000	0.02434	105.00	CalGrig3	0.03870	0.60000	0.02322	0.03624	CalGrig4	0.03624	0.60000	0.02175	90.00	CalGrig4	0.03477	0.60000	0.02086	90.00	CalGrig4	0.03317	0.60000	0.01990	0.02819	SanVigilio	0.02819	0.60000	0.01691	70.00	SanVigilio	0.02704	0.60000	0.01622	70.00	SanVigilio	0.02580	0.60000	0.01548	0.00805	CalFila	0.00805	0.60000	0.00483	20.00	CalFila	0.00773	0.60000	0.00464	20.00	CalFila	0.00737	0.60000	0.00442	0.00604	RAM	0.00604	0.57000	0.00344	15.00	RAM	0.00579	0.57000	0.00330	15.00	RAM	0.00553	0.57000	0.00315	0.00201	RAM	0.00201	0.57000	0.00115	5.00	RAM	0.00193	0.57000	0.00110	5.00	RAM	0.00184	0.57000	0.00105	0.00403	RAS	0.00403	0.57000	0.00230	10.00	RAS	0.00386	0.57000	0.00220	10.00	RAS	0.00369	0.57000	0.00210	0.02416	Puez	0.02416	0.43500	0.01051	60.00	Puez	0.02318	0.43500	0.01008	60.00	Puez	0.02212	0.43500	0.00962	0.02819	Antrullies	0.02819	0.51000	0.01438	70.00	Antrullies	0.02704	0.51000	0.01379	70.00	Antrullies	0.02580	0.51000	0.01316	0.04169	MonteParei	0.04169	0.41500	0.01730	95.00	MonteParei	0.03670	0.41500	0.01523	161.50	MonteParei	0.05953	0.41500	0.02470	2483.12	TOTAL	1.00		0.45	2588.70	TOTAL	1.00		0.44	2713.00	TOTAL	1.00		0.47	Initial porosity of entire transect					0.45					0.44					0.47																																																																																																																																																																																																																																																																																																																															
0.1611	DP3	0.01611	0.40000	0.00644	40.00	DP3	0.01545	0.40000	0.00618	40.00	DP3	0.01474	0.40000	0.00590	0.1611	CalGrig1	0.01611	0.60000	0.00967	40.00	CalGrig1	0.01545	0.60000	0.00927	40.00	CalGrig1	0.01474	0.60000	0.00885	0.1410	CalGrig2	0.01410	0.60000	0.00846	35.00	CalGrig2	0.01352	0.60000	0.00811	35.00	CalGrig2	0.01290	0.60000	0.00774	0.44229	CalGrig3	0.04429	0.60000	0.02537	105.00	CalGrig3	0.04056	0.60000	0.02434	105.00	CalGrig3	0.03870	0.60000	0.02322	0.03624	CalGrig4	0.03624	0.60000	0.02175	90.00	CalGrig4	0.03477	0.60000	0.02086	90.00	CalGrig4	0.03317	0.60000	0.01990	0.02819	SanVigilio	0.02819	0.60000	0.01691	70.00	SanVigilio	0.02704	0.60000	0.01622	70.00	SanVigilio	0.02580	0.60000	0.01548	0.00805	CalFila	0.00805	0.60000	0.00483	20.00	CalFila	0.00773	0.60000	0.00464	20.00	CalFila	0.00737	0.60000	0.00442	0.00604	RAM	0.00604	0.57000	0.00344	15.00	RAM	0.00579	0.57000	0.00330	15.00	RAM	0.00553	0.57000	0.00315	0.00201	RAM	0.00201	0.57000	0.00115	5.00	RAM	0.00193	0.57000	0.00110	5.00	RAM	0.00184	0.57000	0.00105	0.00403	RAS	0.00403	0.57000	0.00230	10.00	RAS	0.00386	0.57000	0.00220	10.00	RAS	0.00369	0.57000	0.00210	0.02416	Puez	0.02416	0.43500	0.01051	60.00	Puez	0.02318	0.43500	0.01008	60.00	Puez	0.02212	0.43500	0.00962	0.02819	Antrullies	0.02819	0.51000	0.01438	70.00	Antrullies	0.02704	0.51000	0.01379	70.00	Antrullies	0.02580	0.51000	0.01316	0.04169	MonteParei	0.04169	0.41500	0.01730	95.00	MonteParei	0.03670	0.41500	0.01523	161.50	MonteParei	0.05953	0.41500	0.02470	2483.12	TOTAL	1.00		0.45	2588.70	TOTAL	1.00		0.44	2713.00	TOTAL	1.00		0.47	Initial porosity of entire transect					0.45					0.44					0.47																																																																																																																																																																																																																																																																																																																																														
0.1611	CalGrig1	0.01611	0.60000	0.00967	40.00	CalGrig1	0.01545	0.60000	0.00927	40.00	CalGrig1	0.01474	0.60000	0.00885	0.1410	CalGrig2	0.01410	0.60000	0.00846	35.00	CalGrig2	0.01352	0.60000	0.00811	35.00	CalGrig2	0.01290	0.60000	0.00774	0.44229	CalGrig3	0.04429	0.60000	0.02537	105.00	CalGrig3	0.04056	0.60000	0.02434	105.00	CalGrig3	0.03870	0.60000	0.02322	0.03624	CalGrig4	0.03624	0.60000	0.02175	90.00	CalGrig4	0.03477	0.60000	0.02086	90.00	CalGrig4	0.03317	0.60000	0.01990	0.02819	SanVigilio	0.02819	0.60000	0.01691	70.00	SanVigilio	0.02704	0.60000	0.01622	70.00	SanVigilio	0.02580	0.60000	0.01548	0.00805	CalFila	0.00805	0.60000	0.00483	20.00	CalFila	0.00773	0.60000	0.00464	20.00	CalFila	0.00737	0.60000	0.00442	0.00604	RAM	0.00604	0.57000	0.00344	15.00	RAM	0.00579	0.57000	0.00330	15.00	RAM	0.00553	0.57000	0.00315	0.00201	RAM	0.00201	0.57000	0.00115	5.00	RAM	0.00193	0.57000	0.00110	5.00	RAM	0.00184	0.57000	0.00105	0.00403	RAS	0.00403	0.57000	0.00230	10.00	RAS	0.00386	0.57000	0.00220	10.00	RAS	0.00369	0.57000	0.00210	0.02416	Puez	0.02416	0.43500	0.01051	60.00	Puez	0.02318	0.43500	0.01008	60.00	Puez	0.02212	0.43500	0.00962	0.02819	Antrullies	0.02819	0.51000	0.01438	70.00	Antrullies	0.02704	0.51000	0.01379	70.00	Antrullies	0.02580	0.51000	0.01316	0.04169	MonteParei	0.04169	0.41500	0.01730	95.00	MonteParei	0.03670	0.41500	0.01523	161.50	MonteParei	0.05953	0.41500	0.02470	2483.12	TOTAL	1.00		0.45	2588.70	TOTAL	1.00		0.44	2713.00	TOTAL	1.00		0.47	Initial porosity of entire transect					0.45					0.44					0.47																																																																																																																																																																																																																																																																																																																																																													
0.1410	CalGrig2	0.01410	0.60000	0.00846	35.00	CalGrig2	0.01352	0.60000	0.00811	35.00	CalGrig2	0.01290	0.60000	0.00774	0.44229	CalGrig3	0.04429	0.60000	0.02537	105.00	CalGrig3	0.04056	0.60000	0.02434	105.00	CalGrig3	0.03870	0.60000	0.02322	0.03624	CalGrig4	0.03624	0.60000	0.02175	90.00	CalGrig4	0.03477	0.60000	0.02086	90.00	CalGrig4	0.03317	0.60000	0.01990	0.02819	SanVigilio	0.02819	0.60000	0.01691	70.00	SanVigilio	0.02704	0.60000	0.01622	70.00	SanVigilio	0.02580	0.60000	0.01548	0.00805	CalFila	0.00805	0.60000	0.00483	20.00	CalFila	0.00773	0.60000	0.00464	20.00	CalFila	0.00737	0.60000	0.00442	0.00604	RAM	0.00604	0.57000	0.00344	15.00	RAM	0.00579	0.57000	0.00330	15.00	RAM	0.00553	0.57000	0.00315	0.00201	RAM	0.00201	0.57000	0.00115	5.00	RAM	0.00193	0.57000	0.00110	5.00	RAM	0.00184	0.57000	0.00105	0.00403	RAS	0.00403	0.57000	0.00230	10.00	RAS	0.00386	0.57000	0.00220	10.00	RAS	0.00369	0.57000	0.00210	0.02416	Puez	0.02416	0.43500	0.01051	60.00	Puez	0.02318	0.43500	0.01008	60.00	Puez	0.02212	0.43500	0.00962	0.02819	Antrullies	0.02819	0.51000	0.01438	70.00	Antrullies	0.02704	0.51000	0.01379	70.00	Antrullies	0.02580	0.51000	0.01316	0.04169	MonteParei	0.04169	0.41500	0.01730	95.00	MonteParei	0.03670	0.41500	0.01523	161.50	MonteParei	0.05953	0.41500	0.02470	2483.12	TOTAL	1.00		0.45	2588.70	TOTAL	1.00		0.44	2713.00	TOTAL	1.00		0.47	Initial porosity of entire transect					0.45					0.44					0.47																																																																																																																																																																																																																																																																																																																																																																												
0.44229	CalGrig3	0.04429	0.60000	0.02537	105.00	CalGrig3	0.04056	0.60000	0.02434	105.00	CalGrig3	0.03870	0.60000	0.02322	0.03624	CalGrig4	0.03624	0.60000	0.02175	90.00	CalGrig4	0.03477	0.60000	0.02086	90.00	CalGrig4	0.03317	0.60000	0.01990	0.02819	SanVigilio	0.02819	0.60000	0.01691	70.00	SanVigilio	0.02704	0.60000	0.01622	70.00	SanVigilio	0.02580	0.60000	0.01548	0.00805	CalFila	0.00805	0.60000	0.00483	20.00	CalFila	0.00773	0.60000	0.00464	20.00	CalFila	0.00737	0.60000	0.00442	0.00604	RAM	0.00604	0.57000	0.00344	15.00	RAM	0.00579	0.57000	0.00330	15.00	RAM	0.00553	0.57000	0.00315	0.00201	RAM	0.00201	0.57000	0.00115	5.00	RAM	0.00193	0.57000	0.00110	5.00	RAM	0.00184	0.57000	0.00105	0.00403	RAS	0.00403	0.57000	0.00230	10.00	RAS	0.00386	0.57000	0.00220	10.00	RAS	0.00369	0.57000	0.00210	0.02416	Puez	0.02416	0.43500	0.01051	60.00	Puez	0.02318	0.43500	0.01008	60.00	Puez	0.02212	0.43500	0.00962	0.02819	Antrullies	0.02819	0.51000	0.01438	70.00	Antrullies	0.02704	0.51000	0.01379	70.00	Antrullies	0.02580	0.51000	0.01316	0.04169	MonteParei	0.04169	0.41500	0.01730	95.00	MonteParei	0.03670	0.41500	0.01523	161.50	MonteParei	0.05953	0.41500	0.02470	2483.12	TOTAL	1.00		0.45	2588.70	TOTAL	1.00		0.44	2713.00	TOTAL	1.00		0.47	Initial porosity of entire transect					0.45					0.44					0.47																																																																																																																																																																																																																																																																																																																																																																																											
0.03624	CalGrig4	0.03624	0.60000	0.02175	90.00	CalGrig4	0.03477	0.60000	0.02086	90.00	CalGrig4	0.03317	0.60000	0.01990	0.02819	SanVigilio	0.02819	0.60000	0.01691	70.00	SanVigilio	0.02704	0.60000	0.01622	70.00	SanVigilio	0.02580	0.60000	0.01548	0.00805	CalFila	0.00805	0.60000	0.00483	20.00	CalFila	0.00773	0.60000	0.00464	20.00	CalFila	0.00737	0.60000	0.00442	0.00604	RAM	0.00604	0.57000	0.00344	15.00	RAM	0.00579	0.57000	0.00330	15.00	RAM	0.00553	0.57000	0.00315	0.00201	RAM	0.00201	0.57000	0.00115	5.00	RAM	0.00193	0.57000	0.00110	5.00	RAM	0.00184	0.57000	0.00105	0.00403	RAS	0.00403	0.57000	0.00230	10.00	RAS	0.00386	0.57000	0.00220	10.00	RAS	0.00369	0.57000	0.00210	0.02416	Puez	0.02416	0.43500	0.01051	60.00	Puez	0.02318	0.43500	0.01008	60.00	Puez	0.02212	0.43500	0.00962	0.02819	Antrullies	0.02819	0.51000	0.01438	70.00	Antrullies	0.02704	0.51000	0.01379	70.00	Antrullies	0.02580	0.51000	0.01316	0.04169	MonteParei	0.04169	0.41500	0.01730	95.00	MonteParei	0.03670	0.41500	0.01523	161.50	MonteParei	0.05953	0.41500	0.02470	2483.12	TOTAL	1.00		0.45	2588.70	TOTAL	1.00		0.44	2713.00	TOTAL	1.00		0.47	Initial porosity of entire transect					0.45					0.44					0.47																																																																																																																																																																																																																																																																																																																																																																																																										
0.02819	SanVigilio	0.02819	0.60000	0.01691	70.00	SanVigilio	0.02704	0.60000	0.01622	70.00	SanVigilio	0.02580	0.60000	0.01548	0.00805	CalFila	0.00805	0.60000	0.00483	20.00	CalFila	0.00773	0.60000	0.00464	20.00	CalFila	0.00737	0.60000	0.00442	0.00604	RAM	0.00604	0.57000	0.00344	15.00	RAM	0.00579	0.57000	0.00330	15.00	RAM	0.00553	0.57000	0.00315	0.00201	RAM	0.00201	0.57000	0.00115	5.00	RAM	0.00193	0.57000	0.00110	5.00	RAM	0.00184	0.57000	0.00105	0.00403	RAS	0.00403	0.57000	0.00230	10.00	RAS	0.00386	0.57000	0.00220	10.00	RAS	0.00369	0.57000	0.00210	0.02416	Puez	0.02416	0.43500	0.01051	60.00	Puez	0.02318	0.43500	0.01008	60.00	Puez	0.02212	0.43500	0.00962	0.02819	Antrullies	0.02819	0.51000	0.01438	70.00	Antrullies	0.02704	0.51000	0.01379	70.00	Antrullies	0.02580	0.51000	0.01316	0.04169	MonteParei	0.04169	0.41500	0.01730	95.00	MonteParei	0.03670	0.41500	0.01523	161.50	MonteParei	0.05953	0.41500	0.02470	2483.12	TOTAL	1.00		0.45	2588.70	TOTAL	1.00		0.44	2713.00	TOTAL	1.00		0.47	Initial porosity of entire transect					0.45					0.44					0.47																																																																																																																																																																																																																																																																																																																																																																																																																									
0.00805	CalFila	0.00805	0.60000	0.00483	20.00	CalFila	0.00773	0.60000	0.00464	20.00	CalFila	0.00737	0.60000	0.00442	0.00604	RAM	0.00604	0.57000	0.00344	15.00	RAM	0.00579	0.57000	0.00330	15.00	RAM	0.00553	0.57000	0.00315	0.00201	RAM	0.00201	0.57000	0.00115	5.00	RAM	0.00193	0.57000	0.00110	5.00	RAM	0.00184	0.57000	0.00105	0.00403	RAS	0.00403	0.57000	0.00230	10.00	RAS	0.00386	0.57000	0.00220	10.00	RAS	0.00369	0.57000	0.00210	0.02416	Puez	0.02416	0.43500	0.01051	60.00	Puez	0.02318	0.43500	0.01008	60.00	Puez	0.02212	0.43500	0.00962	0.02819	Antrullies	0.02819	0.51000	0.01438	70.00	Antrullies	0.02704	0.51000	0.01379	70.00	Antrullies	0.02580	0.51000	0.01316	0.04169	MonteParei	0.04169	0.41500	0.01730	95.00	MonteParei	0.03670	0.41500	0.01523	161.50	MonteParei	0.05953	0.41500	0.02470	2483.12	TOTAL	1.00		0.45	2588.70	TOTAL	1.00		0.44	2713.00	TOTAL	1.00		0.47	Initial porosity of entire transect					0.45					0.44					0.47																																																																																																																																																																																																																																																																																																																																																																																																																																								
0.00604	RAM	0.00604	0.57000	0.00344	15.00	RAM	0.00579	0.57000	0.00330	15.00	RAM	0.00553	0.57000	0.00315	0.00201	RAM	0.00201	0.57000	0.00115	5.00	RAM	0.00193	0.57000	0.00110	5.00	RAM	0.00184	0.57000	0.00105	0.00403	RAS	0.00403	0.57000	0.00230	10.00	RAS	0.00386	0.57000	0.00220	10.00	RAS	0.00369	0.57000	0.00210	0.02416	Puez	0.02416	0.43500	0.01051	60.00	Puez	0.02318	0.43500	0.01008	60.00	Puez	0.02212	0.43500	0.00962	0.02819	Antrullies	0.02819	0.51000	0.01438	70.00	Antrullies	0.02704	0.51000	0.01379	70.00	Antrullies	0.02580	0.51000	0.01316	0.04169	MonteParei	0.04169	0.41500	0.01730	95.00	MonteParei	0.03670	0.41500	0.01523	161.50	MonteParei	0.05953	0.41500	0.02470	2483.12	TOTAL	1.00		0.45	2588.70	TOTAL	1.00		0.44	2713.00	TOTAL	1.00		0.47	Initial porosity of entire transect					0.45					0.44					0.47																																																																																																																																																																																																																																																																																																																																																																																																																																																							
0.00201	RAM	0.00201	0.57000	0.00115	5.00	RAM	0.00193	0.57000	0.00110	5.00	RAM	0.00184	0.57000	0.00105	0.00403	RAS	0.00403	0.57000	0.00230	10.00	RAS	0.00386	0.57000	0.00220	10.00	RAS	0.00369	0.57000	0.00210	0.02416	Puez	0.02416	0.43500	0.01051	60.00	Puez	0.02318	0.43500	0.01008	60.00	Puez	0.02212	0.43500	0.00962	0.02819	Antrullies	0.02819	0.51000	0.01438	70.00	Antrullies	0.02704	0.51000	0.01379	70.00	Antrullies	0.02580	0.51000	0.01316	0.04169	MonteParei	0.04169	0.41500	0.01730	95.00	MonteParei	0.03670	0.41500	0.01523	161.50	MonteParei	0.05953	0.41500	0.02470	2483.12	TOTAL	1.00		0.45	2588.70	TOTAL	1.00		0.44	2713.00	TOTAL	1.00		0.47	Initial porosity of entire transect					0.45					0.44					0.47																																																																																																																																																																																																																																																																																																																																																																																																																																																																						
0.00403	RAS	0.00403	0.57000	0.00230	10.00	RAS	0.00386	0.57000	0.00220	10.00	RAS	0.00369	0.57000	0.00210	0.02416	Puez	0.02416	0.43500	0.01051	60.00	Puez	0.02318	0.43500	0.01008	60.00	Puez	0.02212	0.43500	0.00962	0.02819	Antrullies	0.02819	0.51000	0.01438	70.00	Antrullies	0.02704	0.51000	0.01379	70.00	Antrullies	0.02580	0.51000	0.01316	0.04169	MonteParei	0.04169	0.41500	0.01730	95.00	MonteParei	0.03670	0.41500	0.01523	161.50	MonteParei	0.05953	0.41500	0.02470	2483.12	TOTAL	1.00		0.45	2588.70	TOTAL	1.00		0.44	2713.00	TOTAL	1.00		0.47	Initial porosity of entire transect					0.45					0.44					0.47																																																																																																																																																																																																																																																																																																																																																																																																																																																																																					
0.02416	Puez	0.02416	0.43500	0.01051	60.00	Puez	0.02318	0.43500	0.01008	60.00	Puez	0.02212	0.43500	0.00962	0.02819	Antrullies	0.02819	0.51000	0.01438	70.00	Antrullies	0.02704	0.51000	0.01379	70.00	Antrullies	0.02580	0.51000	0.01316	0.04169	MonteParei	0.04169	0.41500	0.01730	95.00	MonteParei	0.03670	0.41500	0.01523	161.50	MonteParei	0.05953	0.41500	0.02470	2483.12	TOTAL	1.00		0.45	2588.70	TOTAL	1.00		0.44	2713.00	TOTAL	1.00		0.47	Initial porosity of entire transect					0.45					0.44					0.47																																																																																																																																																																																																																																																																																																																																																																																																																																																																																																				
0.02819	Antrullies	0.02819	0.51000	0.01438	70.00	Antrullies	0.02704	0.51000	0.01379	70.00	Antrullies	0.02580	0.51000	0.01316	0.04169	MonteParei	0.04169	0.41500	0.01730	95.00	MonteParei	0.03670	0.41500	0.01523	161.50	MonteParei	0.05953	0.41500	0.02470	2483.12	TOTAL	1.00		0.45	2588.70	TOTAL	1.00		0.44	2713.00	TOTAL	1.00		0.47	Initial porosity of entire transect					0.45					0.44					0.47																																																																																																																																																																																																																																																																																																																																																																																																																																																																																																																			
0.04169	MonteParei	0.04169	0.41500	0.01730	95.00	MonteParei	0.03670	0.41500	0.01523	161.50	MonteParei	0.05953	0.41500	0.02470	2483.12	TOTAL	1.00		0.45	2588.70	TOTAL	1.00		0.44	2713.00	TOTAL	1.00		0.47	Initial porosity of entire transect					0.45					0.44					0.47																																																																																																																																																																																																																																																																																																																																																																																																																																																																																																																																		
2483.12	TOTAL	1.00		0.45	2588.70	TOTAL	1.00		0.44	2713.00	TOTAL	1.00		0.47																																																																																																																																																																																																																																																																																																																																																																																																																																																																																																																																																																	
Initial porosity of entire transect					0.45					0.44					0.47																																																																																																																																																																																																																																																																																																																																																																																																																																																																																																																																																																

Section B1

section	B1	x base	696128	y base	5133318	x top	8	y top			11	12	13	14	15		
period	stage	fm	mbr	altitude	cum. thick.	ind. thick.	lithology	grain size	carb. class.	sed. char.1	sed. char.2	components1	components2	phys. surf.			
Trassic	Anisian	Schlern		2321	26.2	1.0	lst	coarse >5mm	breccia	debris		clasts					
				2320	25.2	2.0	lst	middle 2-5mm	breccia	debris		clasts					
				2318	23.2	2.0	lst	coarse >5mm	CS	cnr beds							
				2316	21.2	2.1	lst		breccia	debris							
	Anisian	Buchenstein	Plattenkalk	2314	19.1	5.0	hiatus			CS/FIS	cnr beds						
				2309	14.1	2.1	lst		CS/FIS	cnr beds		nor grad					
				2307	12.0	0.6	lst		MS	organics							
				2306	11.4	0.6	lst		FS								
				2306	10.8	3.6	lst		CS	cnr beds		nor grad					
				2302	7.2	1.2	tuff										
				2301	6.0	1.0	lst		MS	hor lam							
				2300	5.0	1.0	tuff										
				2299	4.0	4.0	lst		MS	hor lam							
								2295									

cut-tend capped by microbreccia

cut-tend capped by microbreccia

section	Epircher	x base	695324	y base	5138290	x top	695754	y top	5138298	10	11	12	13	14	15		
period	stage	fm	mbr	altitude	cum. thick.	ind. thick.	lithology	grain size	carb. class.	sed. char.1	sed. char.2	components1	components2	phys. surf.			
Triassic	Scythian	Werfen	Campil	2088	173.4	8.5	silt			sym rip		shells					
				2080	164.9	4.0	hiatus										
				2076	160.9	2.3	marly silt		B&P								
				2074	158.6	2.0	marl, silty		x bed	sero base		ooids		ooids			
				2072	156.6	1.9	silt, marly		B&P	dm beds		ooids		ooids			
				2070	154.7	4.7	silt, marly		cm beds			b clasts		b clasts			
				2065	150.0	3.6	marly silt		cm beds	x bed		ooids		ooids			
				2061	146.4	4.0	marly silt		B&P	cm beds		shells		shells			
				2057	142.4	2.0	marly silt		B&P	cm beds		shells		shells			
				2055	140.4	105.0	hiatus										
				1950	35.4	3.3	shale/silt		cm beds	eva nod							
				1947	32.1	9.9	silt		B&P	eva nod							
				1937	22.2	9.6	lst, silty			WSFS			b clasts		b clasts		
				1928	12.6	3.8	marl						lst nod		b clasts		
				1924	8.8	3.5	lst, marly			MS			B&P				
1920	5.3	3.3	marly lst						hor lam		organics						
1917	2.0	2.0	lst								organics						
1915																	
Permian	Changhsing, Bellerophon		Badiota														

faulting between lower and upper part of section (hiatus is significantly longer)

Section Passo Feudo

section	P.Feudo	x base	697027	y base	5135489	x top	696968	y top		5135210							
1	2	3	4	5	6	7	8	9	10	11	12	13	14	15			
period	stage	fm	mbr	altitude	cum.thick.	ind.thick.	lithology	grain size	carb. class.	sed. char.1	sed. char.2	components1	components2	phys. surf.			
Trassic	Ladinian	Buchenstein	Bänderkalk?	2190	252.0	8.5	lst	WS	cm beds	organics							
			Knollenkalk	folding	243.5	45.5	lst	GS/SPS	lst nod	nor grad							
			Plattenkalk		198.0	7.0	lst	WS/PS	lst nod	dfn beds							
	Anisian	Moena			191.0	13.5	lst	WS	cm beds	organics					Secedensis-zone?		
					177.5	6.0	v. dyke										
					171.5	5.0	breccia	coarse >5mm		ero base	nor grad						
					166.5	6.0	breccia	coarse >5mm		ero base	nor grad						
					160.5	2.0	lst		WS/PS	dfn beds							
					158.5	1.5	lst		WS/PS	dfn beds							
					157.0	2.0	breccia	coarse >5mm		ero base	nor grad						
					155.0	2.0	lst		WS/PS								
					153.0	9.5	cherty lst		WS								
					143.5	5.0	breccia	coarse >5mm		nor grad	nod chert						
	Morbac					138.5	2.5	v. dyke									
						136.0	2.0	lst	MS	dfn beds	organics						
						134.0	2.0	hiatus									
						132.0	6.0	lst. shaly		MS	organics	nod chert					
						126.0	7.0	lst		MS	organics	nod chert					
						119.0	16.0	lst		MS	dfn beds	organics					
						103.0	1.0	cg sst	coarse >5mm		ero base						
Richtthofen								102.0	6.5	lst	GS					ooids	shells
			95.5			4.5	lst	GS	x bed					ooids			
			91.0			2.5	sandy marl		GS	x bed					ooids		
			88.5			1.0	sandy marl		GS						ooids	gastro	
			87.5			15.0	hiatus										
			72.5			1.0	lst		GS								
			71.5			11.0	hiatus										
			60.5			3.0	lst. shaly		GS							ooids	shells
	Werten							57.5	20.0	hiatus							
								37.5	1.0	lst	WS/PS						
					36.5	2.0	dol lst			biot							
					34.5	30.0	hiatus										
					4.5	1.5	lst. shaly		MS	wavy bed							
					3.0	1.0	shaly lst								bl peb		
					2.0	2.0	shale										
Scythian																	

